UNIVERSITY OF NOTTINGHAM

DEPARTMENT OF CIVIL ENGINEERING

OSCILLATORY BOUNDARY LAYER OVER FIXED ROUGH BEDS

by

S.M. BORGHEI, B.Sc.

Thesis submitted to the University of Nottingham for the degree of Doctor of Philosophy, October, 1982.

ABSTRACT

The accurate study of characteristics of the flow under gravity waves has become of prime importance due to the growing demand for structural engineering designs in the coastal environment. Although many investigations have been carried out, the progress of fundamental research was slow due to the lack of an adequate velocity measuring instrument. However in recent years, the development of the Laser Doppler Velocimeter has made it possible to observe the orbital velocity very close to a bed without disturbing the flow. This technique was used in this investigation, in which observations of the oscillatory flow under gravity waves were carried out above smooth, two-dimensional and three-dimensional rough beds.

For the smooth bed case it was found that the velocity profile throughout the depth was well presented by the Stokes second order shear wave equation, except that the theoretical predictions underestimated the observed results, and a linear relationship was obtained for the velocity coefficients between the two sets of values. As for mean velocity the profile was in close agreement with the Longuet-Higgins conduction solution, and it was found to have a negative value (in opposite direction to wave progression) in the bulk of fluid and always positive values within the boundary layer.

The rough beds made little change to the flow in the bulk of fluid. As for inside the boundary layer, the laminar boundary layer was eliminated due to the large size of the rough bed, but for a small size rough bed the flow became laminar at the edge of the boundary layer, and a perturbed laminar boundary layer velocity profile was traceable. However, the two rough beds had similar influences on the flow except for the roughness size and Reynolds number values. Inside the roughness elements of the rough beds vortex formation was clearly observed and the comprehensive range of measurements of these formations are analysed and discussed.

ACKNOWLEDGEMENTS

I am indebted to many people for their invaluable assistance and support in the preparation of this thesis. I acknowledge this debt of gratitude to the following people:-

To Dr. G.B. Parr for his stimulating influence and helpful discussion and suggestions whilst supervising my progress, and for his continual help and direction throughout my work on the project. To Professor R.C. Coates for allowing me the use of the resources of the department and to Dr. F. Rieband for supervising the work.

I would also like to express my gratitude to the following:-

Dr. Williams of the Department of Mechanical Engineering for his assistance and guidance in using the Analogue to Digital Converter of Fourier Analyser Computer.

Mr. J.G. Redfern, the Chief Technican, Mr. J. Moody, Mr. N. Hardy, Mr. J. Leonardi and Mrs. E. Nickeas, staff members of the Civil Engineering laboratories for their assistance.

The staff at the University of Nottingham Computing Centre for their guidance.

The Applied Science Faculty Workshops for manufacturing and repairing the electronic equipment.

The Science Library for making available the references.

Miss S. Close for her skill and limitless patience in typing the manuscript.

Mehran, my brother, for his unselfish help and expertise in the compilation and drawing of figures and diagrams for my thesis.

My colleagues in research especially Dr. N.W. Beech for his discussion.

And, finally, special thanks to my parents for their endless support throughout my education.

CONTENTS

NOTATION

a	wave amplitude
a'	amplitude of water orbit
C	wave celerity
C_1) C_2)	coefficients in equation 6.9
d	mean water depth
f	frequency of light waves
f_D	Doppler frequency
f_s	shift frequency
$f(...)$	a function ...
g	acceleration due to gravity
H	water wave height
K	water wave number, $2\pi/T$
L	water wave length
ℓ	roughness wave length
ℓ_0) ℓ_1) ℓ_2)	harmonic coefficients of second order laminar boundary layer velocity as a Fourier series.
m_1) m_2)	
n	phase number
Re	Reynolds number
r	correlation coefficient
T	wave period
U	horizontal orbital velocity
$\bar{U}$	mass transport velocity

U_c horizontal velocity over crest

U_p perturbed velocity

U_R Ursell parameter

U_T horizontal velocity over trough

U_O horizontal orbital velocity above oscillating plate

$\bar{u}$ mean velocity

u_R horizontal velocity above rough bed

V vertical orbital velocity

X Sleath no., $\beta\kappa/2\pi$

y height above bed

y_s free surface ordinate

Z depth from S.W.L. (-ve)

β boundary layer parameter, $(\sigma/2\nu)^{\frac{1}{2}}$

δ boundary layer thickness, $4.6/\beta$

δ_θ instantaneous boundary layer thickness in separated flow

ε eddy viscosity

ζ orbital horizontal displacement

η orbital vertical displacement

θ angle of intersection for laser light

θ_s phase of separation

λ laser wavelength

κ roughness height

ν kinematic viscosity

μ dynamic viscosity

ϕ velocity potential

ψ stream function

σ wave frequency number, $2\pi/T$

ρ fluid density

τ shear stress

ω angular velocity of water particle in its orbital motion

Notes

suffix ∞ represents kinematics at the edge of boundary layer

circumflex $\hat{}$ represents maximum

circumflex $\check{}$ represents minimum

circumflex $'$ represents velocity in bulk of fluid

ABBREVIATIONS

A.D.C.	Analogue-to-digital convertor
B.E.B.	Beach Erosion Board
B.L.	Boundary Layer
2-D	Two dimension
3-D	Three dimension
L.A.S.	Light-activated switch
L.D.V.	Laser Doppler Velocimeter
M.T.	Mass Transport
P.M.	Photomultiplier
S.D.	Standard Deviation
S.W.G.	Standard-wire-gauge
S.W.L.	Still water level
T.I.	Turbulent intensity

INTRODUCTION

The demand for knowledge of water waves and beach profile during the second World War was the first major turning point in the field of coastal engineering projects. For Civil Engineers however, the growing demand of offshore structure projects such as the oil platforms in the North Sea, the stabilization of submarine pipelines, or the inshore projects such as harbour design, sedimentation in large basins and beach profiles, yield the adaptation of one particular wave theory or another, each of which forms an integral part of many design predictions. Accurate forecasting of wave kinematics stems from a direct understanding of fluid particle velocities and accelerations within a wave motion.

Although many works have been carried out, during the past few decades to examine different wave theories under different conditions, a major obstacle in conducting such experiments has been the lack of satisfactory instrumentation to measure the unsteady velocities of the fluid particles. This problem was an insurmountable one when the particle velocity was to be studied within the viscous boundary layer thickness, considering the thickness is in the order of a few millimetres below laboratory gravity waves or over oscillatory beds.

By developing the 'Laser Doppler Velocimeter' (L.D.V.)

which has the advantages of measuring particle velocity at almost any depth without entering and hence disturbing the flow, and of high accuracy and fast response to an oscillatory flow (high or low speed), studying the flow has come the nearest yet to true flow behaviour. L.D.V. has rapidly become a standard tool in the measurement of fluid velocity, and even though its use in this field is relatively new, tests to obtain a satisfactory theory to support observations of laminar and turbulent oscillatory boundary layer flows, as well as oscillatory flows in the bulk of a fluid are underway.

One of the most convenient, as well as effective, means of predicting surface waves and the orbital velocity in intermediate water waves (for many civil engineering projects) is the use of the Stokes second order theory, except for the mass transport velocity where the practical evidence (Bagnold (1947)) proved contrary to the theory, and instead the Longuet-Higgins conduction solution has been used. However, Beech (1978) showed that if the Stokes equation can be used in the form of a Fourier series at the edge and outside the viscous boundary layer (Longuet-Higgins (1958)), then the same procedure can be applied to the velocity profile inside the viscous boundary layer over smooth and small-sized rough beds.

As a continuation of Beech's work, the present study used a glass plate bed as a hydraulically smooth bed, and

two beds of artificial roughnesses beds. One was a two dimensional rough bed with roughness heights all of 4.65 mm and flat tops, and the other was made of hemispherically shaped roughness elements of 18.95 mm height producing a three dimensional rough bed. On these beds a series of tests have been carried out, using the L.D.V. system, to investigate the following points:-

(i) The validity of Stokes' second order equations for surface wave and orbital velocities, as well as the Longuet-Higgins conduction solution for mass transport velocity.

(ii) The relationship between Stokes' second order equation and the modified equation proposed by Beech in the form of a Fourier series for the laminar boundary layer velocity.

(iii) The comparison of the Stokes second order equation with the factors suggested by Sleath (1970) and Kalkanis (1964) for the 2-D and 3-D rough beds turbulent flow. This comparison enabled an equation for the prediction of velocity profile above a rough bed boundary layer to be proposed.

(iv) The nature of the eddy formation inside the roughness elements of the beds.

(v) The influence of rough beds on orbital and mass transport velocities throughout the whole water depths.

CHAPTER ONE

A REVIEW OF WAVE THEORIES

1.1 INTRODUCTION

An oscillatory boundary layer is formed under the influence of oscillatory flow which can be generated by gravity waves (unsteady free surface flow subjected to gravitational forces). Wind waves, ship waves, tidal waves all are part of the ocean waves which are complicated phenomena and difficult to describe in mathematical terms. However all waves obey some sort of a wave theory. This chapter does not include a full description of all existing wave theories, for that several references are available such as Weigel (1964), Silvester (1974), Le Mehaute (1976), Lighthill (1978) and others, and instead a few more relevant theories with their limits of applicability, especially in reference to laboratory waves are discussed and compared in this section.

1.2 THE CLASSIFICATION OF WAVES

Waves can be differentiated in to several groups and looked upon as each separate family, but the broadest categorization of waves is into long and short waves. For long waves the vertical motion of particles (acceleration, velocity, displacement) are very small compared to horizontal motions and for short waves the vertical motions are taken

into account. Mathematically using the ratio water depth (d) to wave length L, which is called the relative depth, a wave is said to be long when the relative depth is less than 0.05 and short when the ratio is greater than 0.05.

Another group of waves are divided into shallow water waves and deep water waves, the former when the relative depth is less than 0.5 and the latter for relative depth of greater than 0.5.

Combination of these two groups results in a third classification which is more popular and that is dividing the waves into three regions of shallow, intermediate and deep water waves (Fig. 1.1). (McCormic (1973))

1.2.1 Deep Water Waves

A deep water wave occurs when beyond that depth the wave celerity (C) is not affected by depth and is therefore dependent upon wave length (L) and period (T). In this case the water particle motion resulting from wave action is circular and does not extend to the bottom (Fig. 1.2a). An approximation to this condition is given by the relative depth of greater than 0.5, but according to Silvester (1974), a specific ratio of 0.84 is given, but between this value and 0.5 the changes are so slight that the approximation value of 0.5 is acceptable by engineers. At the same time Kamphuis (1972) believes often more practical limits can be set at $d/L > 0.3$.

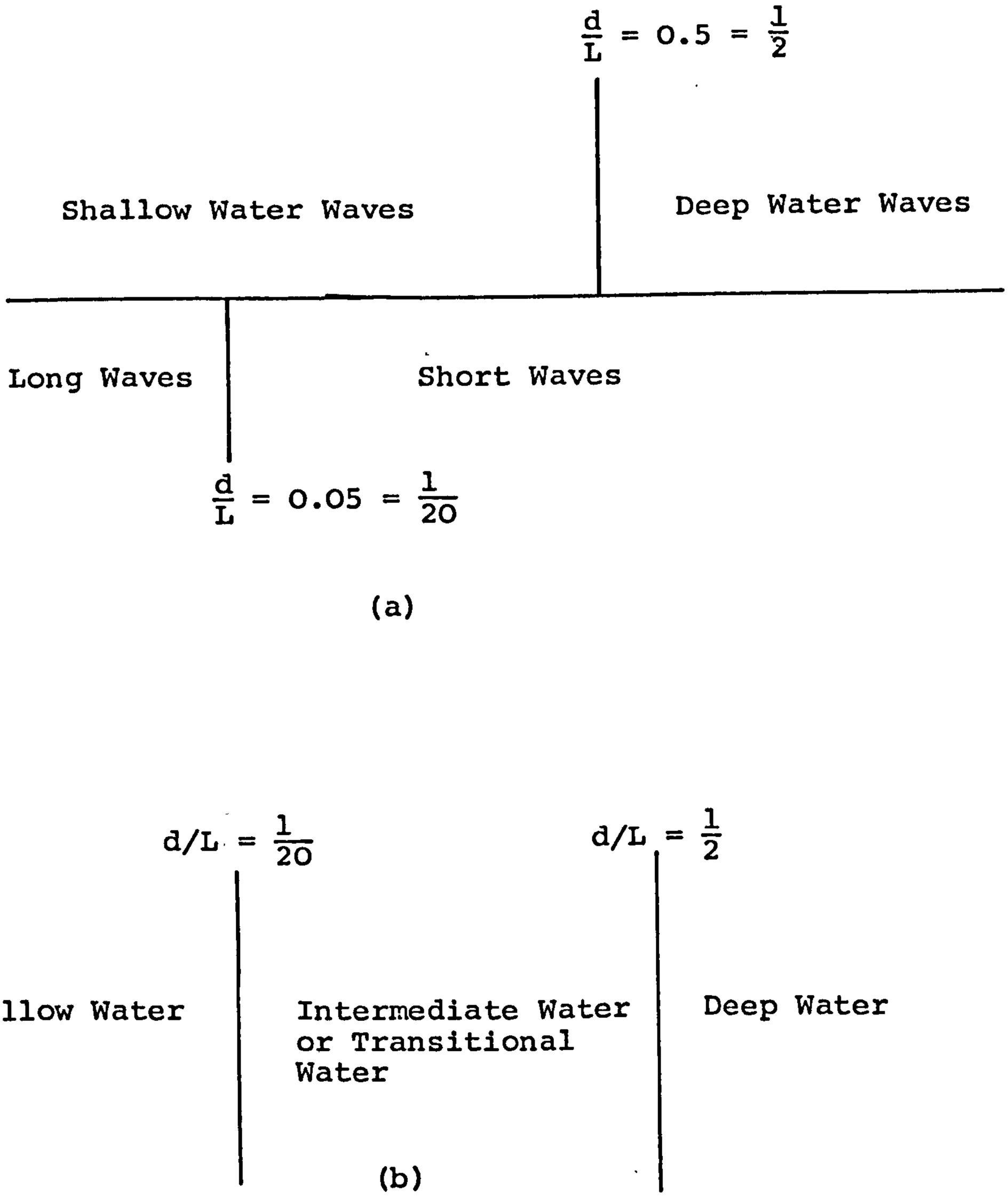

Fig. 1.1 Classification of Waves

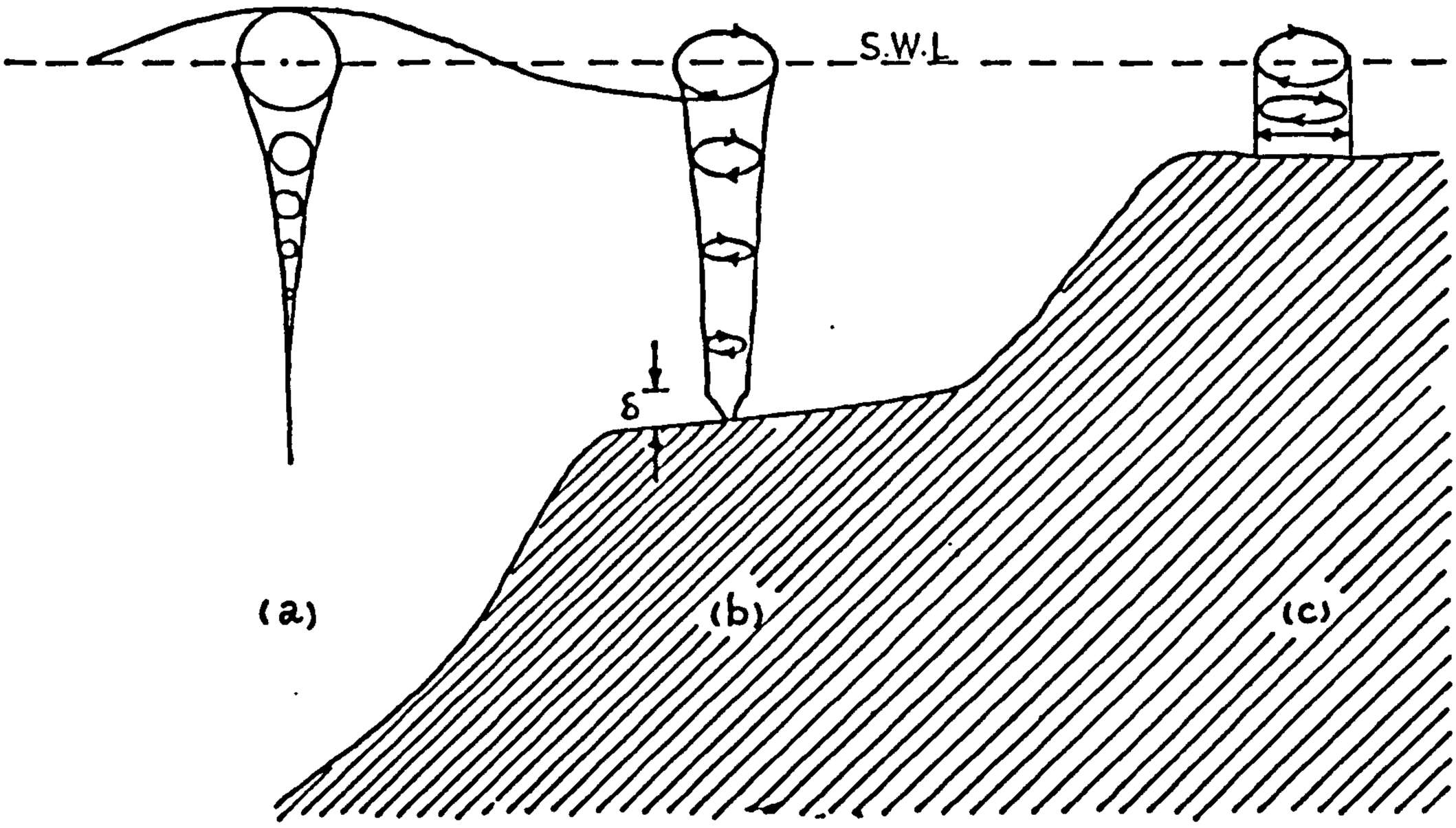

FIG 1.2 DEPTH EFFECTS ON PARTICLE ORBITS
(a) deep water
(b) intermediate depth
(c) shallow depth

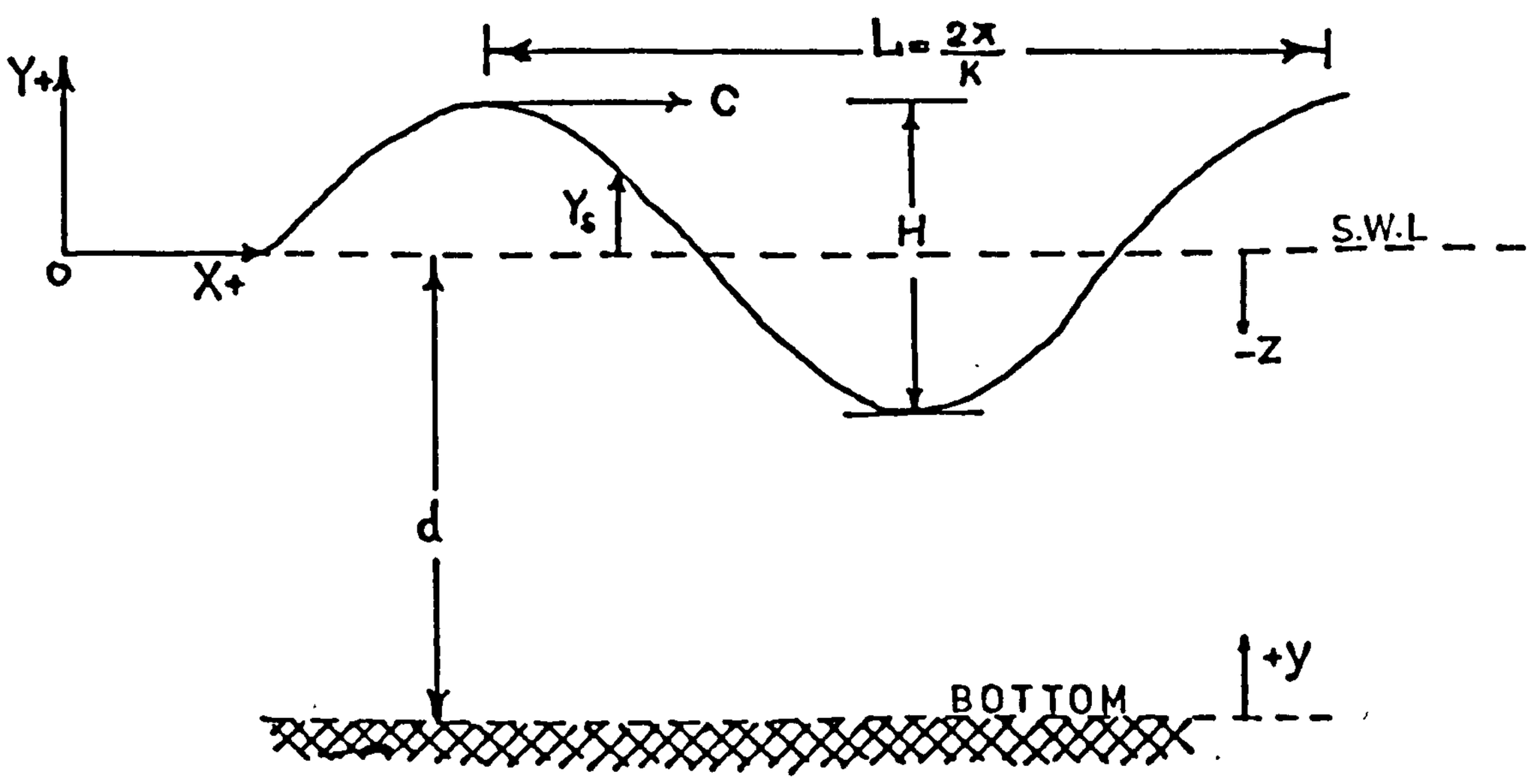

FIG 1.3 A TRAVELLING WAVE

1.2.2 Shallow Water Waves

Unlike the deep water, shallow water is the depth within which the wave celerity depends solely upon depth and is therefore independent of wave period. The water particle path resulting from the wave action is elliptical with the major axis of the ellipse independent of depth (Fig. 1.2c). For shallow water waves also different relative depths are suggested. Wiegel (1964) suggests a 0.04 value (1/25) whilst Eagleson and Dean (1966) has used 0.05 (1/20) for the maximum relative depth of shallow water waves. (viscous boundary layer exists for shallow water too)

1.2.3 Intermediate Depth Water Waves

a

For this case the movement of water particle due to wave action is elliptical, but unlike the shallow water waves, the major and minor axes decrease exponentially with depth and also very close to bed a region of viscous boundary layer exists (Fig. 1.2b). The intermediate water waves exist when $0.05 < d/L < 0.5$.

1.3 WAVE THEORIES CLASSIFICATIONS

Gravity waves are so complicated mathematically that not only a general solution does not exist, but for simplest theories approximations must be made. In fact the main difficulty in the study of water wave motions, is that one of the boundaries (the free surface) is one of the unknowns.

However, the wave theories are generally classified, by the ratio of wave height (H) to wave length (L), as "the small amplitude wave theories" and "the finite amplitude wave theories". Some of the theories are reviewed and compared in the rest of this chapter.

A more comprehensive flowchart of the main characteristics of water waves is presented in Appendix A1, which originally is shown by Le Mehaute (1976).

1.4 LINEAR THEORY

The simplest wave theory is the linear theory which was first presented by Airy (1845) and concerns the first term of the wave series. The theory is based on certain assumptions (Sorensen 1978);

1) The water is homogeneous and incompressible and also surface tension is neglected (except for wave with wavelength less than 30 mm).

2) The flow is irrotational and therefore the velocity potential ϕ must exist and satisfy the Laplace equation:

$$\frac{\partial^2 \phi}{\partial x^2} + \frac{\partial^2 \phi}{\partial y^2} = 0 \qquad (1.1)$$

where x and y are the two directions of flow.

3) The depth of water is uniform and there is no movement at the bed due to wave motion.

4) The wave amplitude is small compared to depth of water and wave length.

Linear theory is also known as 'small amplitude wave theory' and 'Stokes first order theory'.

1.4.1 Progressive Waves

1.4.1.1. Velocity potential and surface ordinate

Using the linear theory assumptions and with the help of Bernoullis' full equation (Wood 1969), the velocity potential for a progressive wave (a wave which progresses across the water surface so that successive crests pass á fixed point) can be written (Lamb 1932a) as;

$$\phi = Pe^{i(\sigma t - Kx)} \qquad (1.2)$$

where P is a function of y, K is wave number ($2\pi/L$) and σ is the wave angular frequency ($2\pi/T$). And the equation for surface ordinate y_s is;

$$Y_s = \frac{H}{2} \text{Cos } (Kx - \sigma t) \qquad (1.3)$$

Fig. 1.3 shows a surface wave moving with velocity C in water depth d. Using the information that vertical velocity (v) at bed (y = O) is zero the real part of the equation 1.2

may be written as;

$$\phi = \frac{gH}{2\sigma} \frac{\text{Cosh } K\ (z+d)}{\text{Cosh } Kd} \text{ Sin } (Kx-\sigma t) \qquad (1.4)$$

where z is zero at surface and -d at bottom.

1.4.1.2 Wave celerity/wave length relation

According to B.E.B. (1942) Report the relationship between the wave celerity, the wave length and wave period which is

$$C = \frac{L}{T} \qquad (1.5)$$

can be used as a definition for waves, though agreement with this equation is not a confirmation of the dynamical theories of waves. Also the relationship between wave velocity C and wave length L is given by Lamb (1932) as;

$$C = \left[\frac{gL}{2\pi} \left(\text{Tanh } \frac{2\pi d}{L}\right)\right]^{\frac{1}{2}} \qquad (1.6)$$

From equations (1.5) and (1.6) the wave length/period relation results;

$$L = \frac{gT^2}{2\pi}\left(\text{Tanh } \frac{2\pi d}{L}\right) \qquad (1.7)$$

This relation is shown graphically in Fig. 1.4 for different values of d and Fig. 1.5 is the specific case of d = 300 mm which was used during this investigation (knowing the period of the wave, the theoretical value of wave length can be calculated from Fig. 1.5). Fig. 1.6 shows

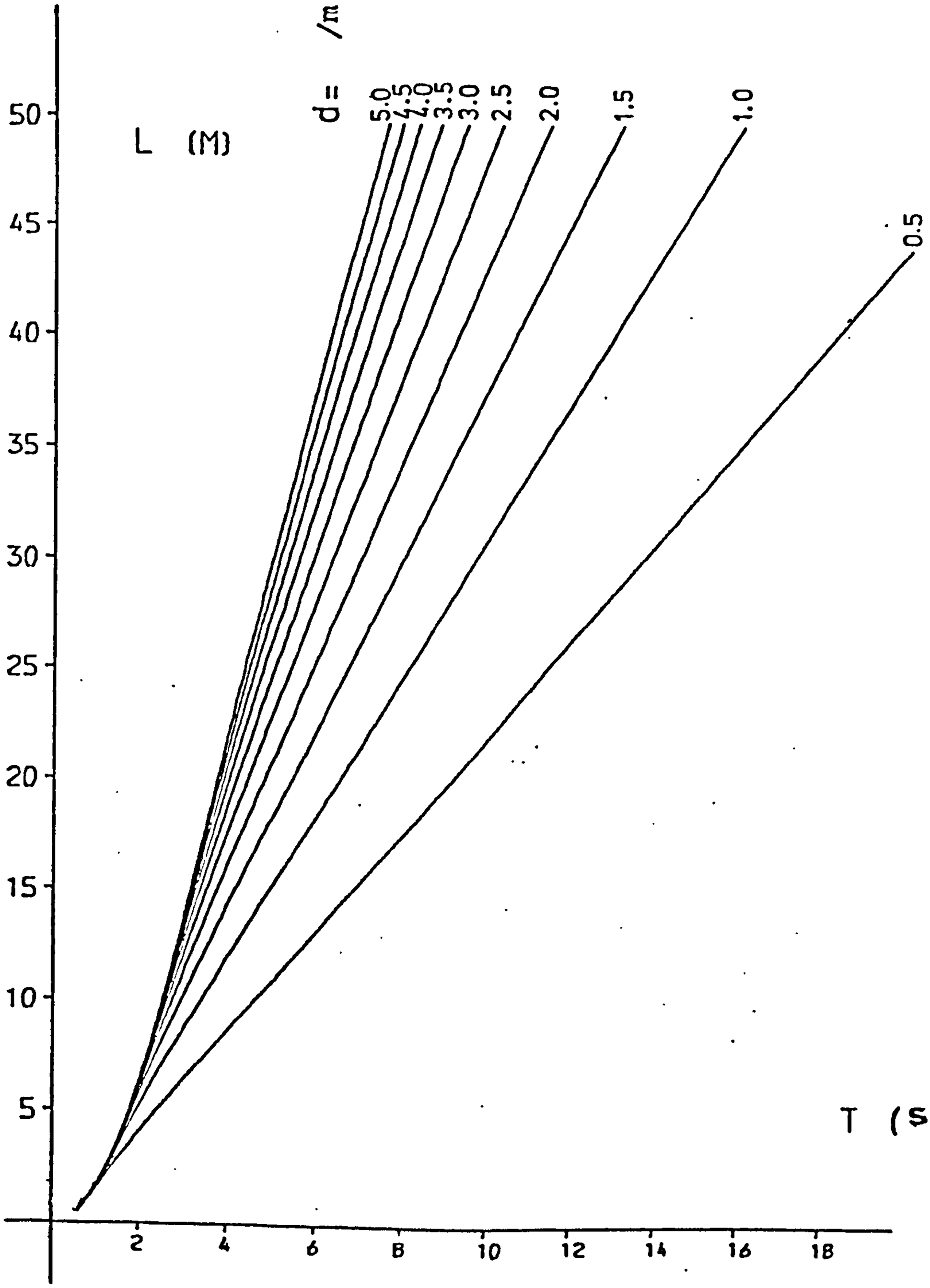

Fig. 1.4. The relation between T (wave period) and L (wave length) for different water depths (d).

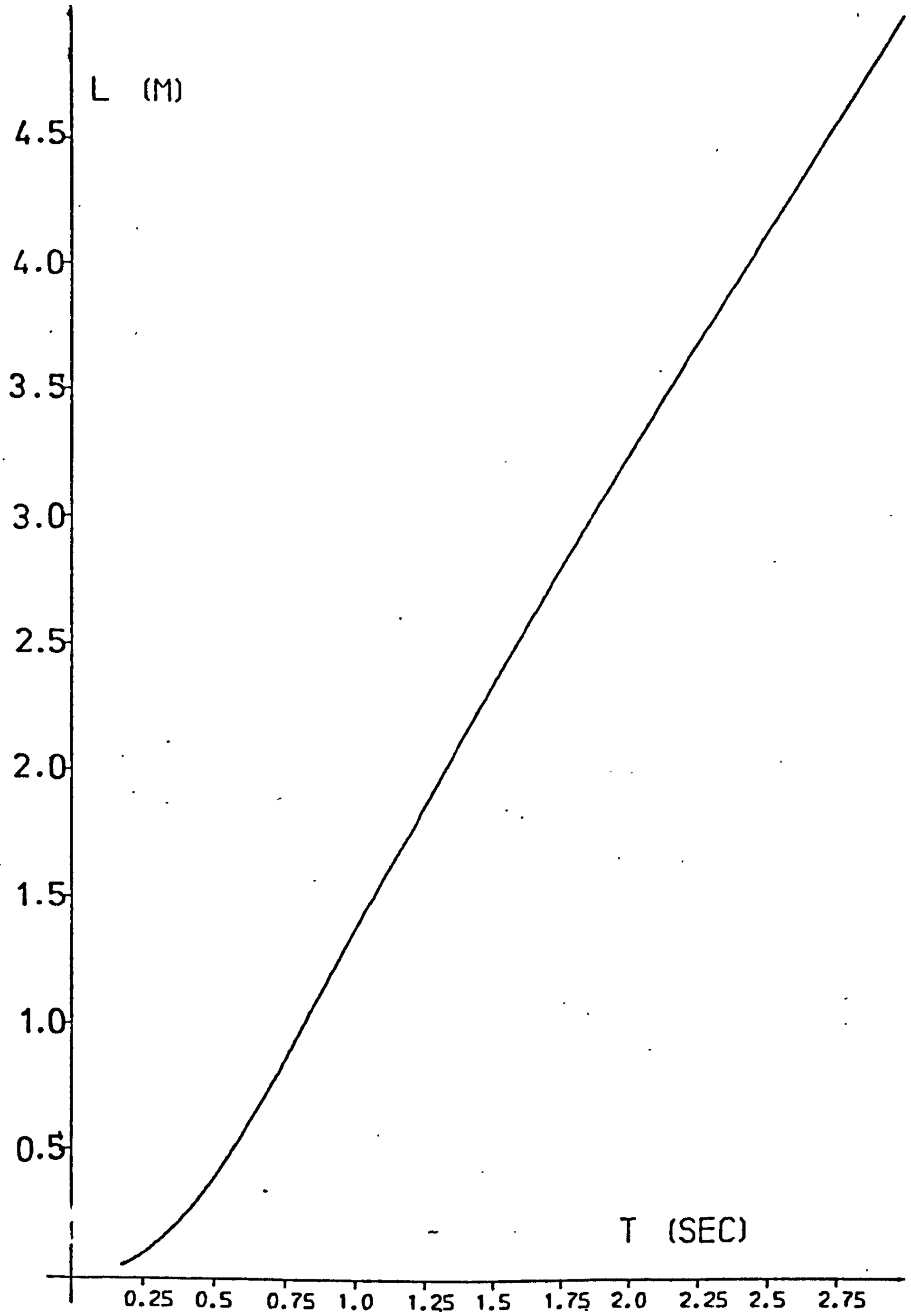

Fig. 1.5 The Relation between T and L for d = 0.3 m.

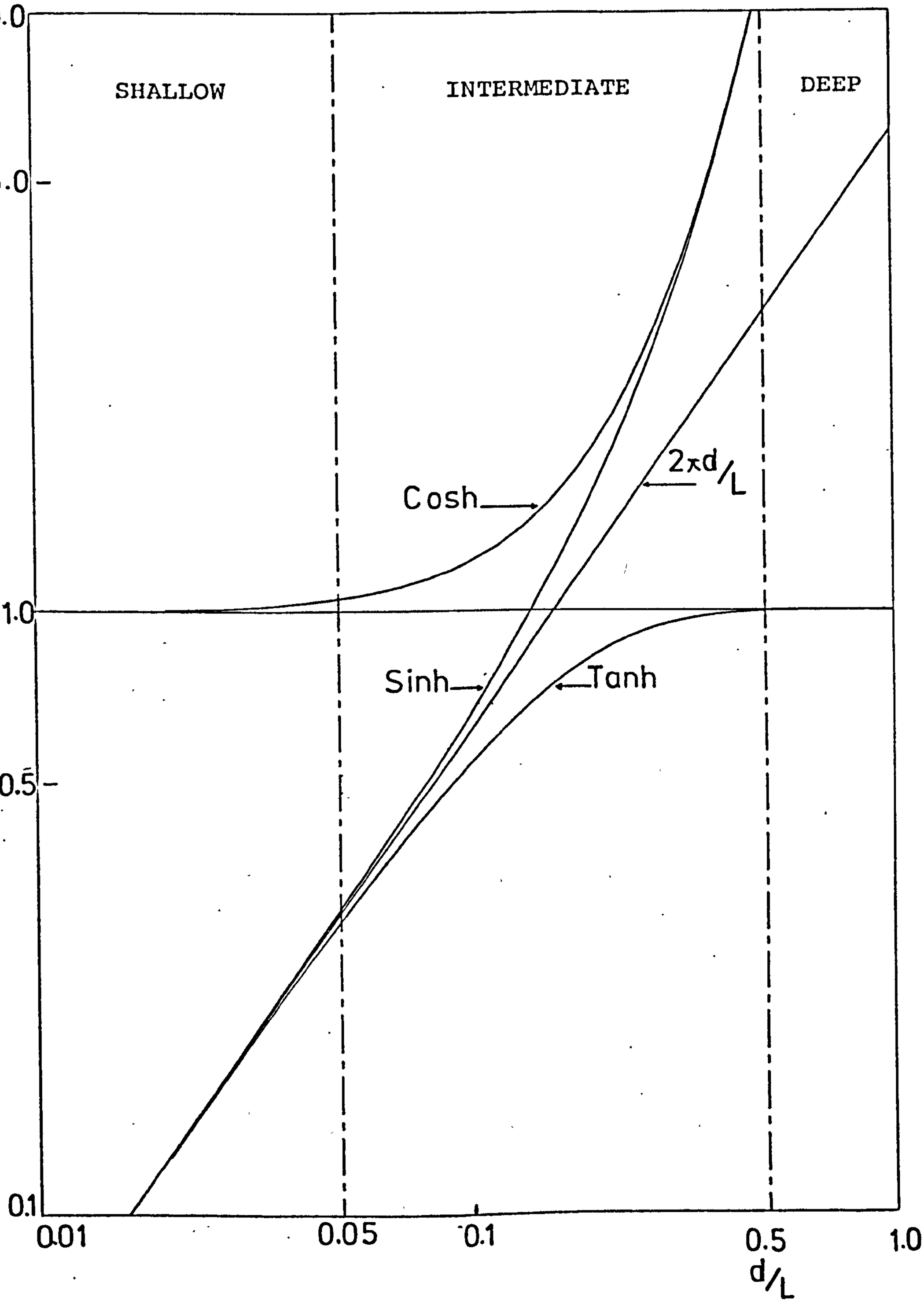

Fig. 1.6 Variations of 2πd/L functions with d/L.

the variation of hyperbolic functions for different relative depth ratio. For deep water d/L is greater than 0.5 and hence Tanh $2\pi d/L$ approaches unity so that equation 1.6 becomes

$$C = \left(\frac{gL}{2\pi}\right)^{\frac{1}{2}} = \frac{gT}{2\pi} \qquad (1.8)$$

and for shallow water $\frac{d}{L}$ is less than 0.05 and Tanh $2\pi d/L$ approaches the value $2\pi d/L$ and hence equation 1.6 changes to:

$$C = (gd)^{\frac{1}{2}} \qquad (1.9)$$

It can be noticed that equation 1.9 is independent of wave length and wave period (see 1.2.2). For the transitional or intermediate region equation 1.6 is unchanged. Also Table 1.1 shows the limiting values of hyperbolic functions for variation of the ratio d/L.

1.4.1.3 Particle motions and displacements for progressive waves

The horizontal (U') and vertical (V') components of water particle velocity are given by $\frac{\partial\phi}{\partial x}$ and $\frac{\partial\phi}{\partial y}$ respectively where ϕ is given by equation 1.4.

Thus:

$$U' = \frac{\partial\phi}{\partial x} = \frac{ga\ K}{\sigma}\ \frac{\text{Cosh } K\ (z+d)}{\text{Cosh } Kd}\ \text{Cos } (Kx-\sigma t) \qquad (1.10)$$

$$V' = \frac{\partial\phi}{\partial y} = \frac{ga\ K}{\sigma}\ \frac{\text{Sinh } K\ (z+d)}{\text{Cosh } Kd}\ \text{Sin } (Kx-\sigma t) \qquad (1.11)$$

Description d/L	Shallow $<\frac{1}{20}$	Intermediate $\frac{1}{20}$ to $\frac{1}{2}$	Deep $>\frac{1}{2}$
Sinh $\frac{2\pi d}{L}$	$\frac{2\pi d}{L}$	$\frac{1}{2}[\exp(\frac{2\pi d}{L})-\exp(\frac{-2\pi d}{L})]$	$\frac{1}{2}\exp(\frac{2\pi d}{L})$
Cosh $\frac{2\pi d}{L}$	1	$\frac{1}{2}[\exp(\frac{2\pi d}{L})+\exp(\frac{-2\pi d}{L})]$	$\frac{1}{2}\exp(\frac{2\pi d}{L})$
Tanh $\frac{2\pi d}{L}$	$\frac{2\pi d}{L}$	$\frac{\exp(\frac{2\pi d}{L})-\exp(\frac{2\pi d}{L})}{\exp(\frac{2\pi d}{L})+\exp(\frac{2\pi d}{L})}$	1

Table 1.1 The Limiting Values of Hyperbolic Functions.

For intermediate water waves substituting for K and σ and using equation 1.7, the velocity components would be:

$$U' = \frac{\pi H}{T} \left[\frac{\text{Cosh } 2\pi\ (z+d)/L}{\text{Sinh } 2\pi d/L}\right] \text{Cos } 2\pi\ \left(\frac{x}{L} - \frac{t}{T}\right) \qquad (1.10a)$$

$$V' = \frac{\pi H}{T} \left[\frac{\text{Sinh } 2\pi\ (z+d)/L}{\text{Sinh } 2\pi d/L}\right] \text{Sin } 2\pi\ \left(\frac{x}{L} - \frac{t}{T}\right) \qquad (1.11a)$$

where $\frac{\pi H}{T}$ is known as the dimension, [ ] as the depth factor and Cos or Sin as the phase. For deep water we therefore have:

$$U' = \frac{\pi H}{T} \exp\ (2\pi z/L) \quad \text{Cos } 2\pi\ \left(\frac{x}{L} - \frac{t}{T}\right) \qquad (1.10b)$$

$$V' = \frac{\pi H}{T} \exp\ (2\pi z/L) \quad \text{Sin } 2\pi\ \left(\frac{x}{L} - \frac{t}{T}\right) \qquad (1.11b)$$

and for shallow water the velocity equations are:

$$U' = \frac{Hg^{\frac{1}{2}}}{2d^{\frac{1}{2}}} \text{Cos } 2\pi\ \left(\frac{x}{L} - \frac{t}{T}\right) \qquad (1.10c)$$

$$V' = \frac{H(z+d)}{Td} \text{Sin } 2\pi\ \left(\frac{x}{T} - \frac{t}{T}\right) \qquad (1.11c)$$

(It is to be noted that equation (1.10c) is independent of z and 1.11c varies linearly with depth and inversely with period).

Also the horizontal displacement is given as:

$$\zeta = -\frac{H}{2} \frac{\text{Cosh } 2\pi\ (z_o + d)/L}{\text{Sinh } 2\pi\ d/L} \text{ sin } 2\pi\ \left(\frac{x_o}{L} - \frac{t}{T}\right) \qquad (1.12a)$$

and vertical displacement as:

$$\eta = \frac{H}{2} \frac{\text{Sinh } 2\pi\ (z_o+d)/L}{\text{Sinh } 2\pi\ d/L} \text{ Cos } 2\pi\ (\frac{x_o}{L} - \frac{t}{T}) \qquad (1.13a)$$

where ζ and η are either side of a mean position x_o and z_o. Equation 1.12a and 1.13a are for the intermediate depth wave with ζ and η representing an ellipse with major axis $H \frac{\text{Cosh } 2\pi\ (z_o+d)/L}{\text{Sinh } 2\pi d/L}$ and focal distance of $\frac{H}{\text{Sinh } 2\pi d/L}$.

For deep water the displacements are:

$$\zeta = -\frac{H}{2} \exp\ (2\pi z_o/L) \quad \text{Sin } 2\pi\ (\frac{x_o}{L} - \frac{t}{T}) \qquad (1.12b)$$

$$\eta = \frac{H}{2} \exp\ (2\pi z_o/L) \quad \text{Cos } 2\pi\ (\frac{x_o}{L} - \frac{t}{T}) \qquad (1.13b)$$

where the path is a circle with radius $\frac{1}{2}H \exp\ (2\pi z_o/L)$ which reduces exponentially with depth. And for shallow water the equations are:

$$\zeta = \frac{HTg^{\frac{1}{2}}}{4\pi d^{\frac{1}{2}}} \text{ Sin } 2\pi\ (\frac{x_o}{L} - \frac{t}{T}) \qquad (1.12c)$$

$$\eta = \frac{H(z_o+d)}{2d} \text{ Cos } 2\pi\ (\frac{x_o}{L} - \frac{t}{T}) \qquad (1.13c)$$

The amplitude of horizontal motion is uniform throughout the depth ($HL/2\pi d$) and the vertical oscillation varies with depth and is zero at bed.

1.4.2 Standing Wave

1.4.2.1 Velocity potential and surface ordinate

The simplest description for the velocity potential of standing waves (whose crests occur at certain fixed points

at successive intervals) is that ϕ is a simple harmonic function of horizontal displacement x. Therefore according to Lamb (1932b) the function is in the form of:

$$\phi = (P \text{ Sin } Kx)e^{i(\sigma t)} \qquad (1.14)$$

where P is only function of y and the surface profile, which is the production of two progressive waves travelling in directly opposite directions, is given by:

$$y_s = \frac{H}{2} \text{ Sin } (Kx) \text{ Sin } (\sigma t) \qquad (1.15)$$

and the real part of equation 1.14 can be written as the potential function:

$$\phi = \frac{gH}{2\sigma} \frac{\text{Cosh } K(z+d)}{\text{Cosh } Kd} \text{ Sin Kx Cos } \sigma t \qquad (1.16)$$

1.4.2.2 Particle motion and displacements

In the same way as for a progressive wave, the particle motion equations may be derived from the potential function (equation 1.16) as:

$$U' = \frac{\pi H}{T} \frac{\text{Cosh } 2\pi (z+d)/L}{\text{Sinh } 2\pi d/L} \text{ Cos Kx Cos } \sigma t \qquad (1.17a)$$

$$V' = \frac{\pi H}{T} \frac{\text{Sinh } 2\pi (z+d)/L}{\text{Sinh } 2\pi d/L} \text{ Sin Kx Cos } \sigma t \qquad (1.18a)$$

The above equations can be simplified for deep water waves as:

$$U' = \frac{\pi H}{T} \exp (2\pi z/L) \text{ cos Kx Cos } \sigma t \qquad (1.17b)$$

$$V' = \frac{\pi H}{T} \exp\ (2\pi z/L)\ \text{Sin}\ Kx\ \text{Cos}\ \sigma t \qquad (1.18b)$$

and for shallow water waves:

$$U' = \frac{HL}{2Td}\ \text{Cos}\ Kx\ \text{Cos}\ \sigma t \qquad (1.17c)$$

$$V' = \frac{H}{Td}\ (z+d)\ \text{Sin}\ Kx\ \text{Cos}\ \sigma t \qquad (1.18c)$$

Similarly the displacements are given as:

$$\zeta = \frac{H}{2}\ \frac{\text{Cosh}\ 2\pi\ (z_o+d)/L}{\text{Sinh}\ 2\pi\ d/L}\ \text{Cos}\ Kx_o\ \text{Sin}\ \sigma t \qquad (1.19a)$$

$$\eta = \frac{H}{2}\ \frac{\text{Sin}\ 2\pi\ (z_o+d)/L}{\text{Sinh}\ \frac{2\pi d}{L}}\ \text{Sin}\ Kx_o\ \text{Sin}\ \sigma t \qquad (1.20a)$$

which for deep water simplify to:

$$\zeta = \frac{H}{2} \exp\ (2\pi Z_o/L)\ \text{Cos}\ Kx_o\ \text{Sin}\ \sigma t \qquad (1.19b)$$

$$\eta = \frac{H}{2} \exp\ (2\pi z_o/L)\ \text{Sin}\ Kx_o\ \text{Sin}\ \sigma t \qquad (1.20b)$$

and for shallow water

$$\zeta = \frac{HL}{4\pi d}\ \text{Cos}\ Kx_o\ \text{Sin}\ \sigma t \qquad (1.19c)$$

$$\eta = \frac{H}{2d}\ (z_o+d)\ \text{Sin}\ Kx_o\ \text{Sin}\ \sigma t \qquad (1.20c)$$

1.5 FINITE AMPLITUDE WAVES

1.5.1 Stokes Second Order Theory

Gerstner (1802) was first to suggest a theory for deep water waves on the assumption of vorticity and excluding any progressive movement of particles. Stokes (1847) analysed the second order theory under no vorticity but

accepting the wave current condition.

His conclusions were that:

"The expression for the velocity of propagation is independent of the height of the waves to a second order approximation with respect to the form of the waves, the elevations are no longer similar to the depressions as is the case to a first approximation, but the elevations are narrower than the hollows, and the height of the former exceeds the depth of the latter.

There is one result of a second approximation which may possibly be of practical importance. It appears that the forward motion of the particles is not altogether compensated by their backward motion; so that, in addition to their motion of oscillation, the particles have a progressive motion in the direction of propagation of the waves."

1.5.1.1 Velocity potential and surface ordinate

The velocity potential to the second approximation is given by Stokes as:

$$\phi = \frac{HL}{2T} \frac{\text{Cosh } 2\pi\ (z+d)/L}{\text{Sinh } 2\pi d/L} \text{ Sin } 2\pi\ (\frac{x}{L} - \frac{t}{T})$$

$$+ \frac{3\pi H^2}{16T} \frac{\text{Cosh } 4\pi(z+d)/L}{\text{Sinh}^4\ 2\pi d/L} \text{Sin } 4\pi \left(\frac{x}{L} - \frac{t}{T}\right) \qquad (1.21)$$

To the second approximation the equations of wave velocity and wave length are unchanged ($C^2 = \frac{gL}{2\pi}$ Tanh $2\pi d/L$, $L = \frac{gT^2}{2\pi}$ Tanh $2\pi d/L$).

The surface profile is then given by:

$$y_s = \frac{H}{2} \text{Cos } 2\pi \left(\frac{x}{L} - \frac{t}{T}\right) + \frac{\pi H^2}{8L} \frac{\text{Cosh } 2\pi d/L\ (2 + \text{Cosh } 4\pi d/L)}{\text{Sinh}^3\ 2\pi d/L}$$

$$\cdot \text{Cos } 4\pi \left(\frac{x}{L} - \frac{t}{T}\right) \qquad (1.22)$$

1.5.1.2 Particle motions and displacements

The components of water particle velocities at any place x, y in the fluid is given by,

$$U' = \frac{\pi H}{T} \frac{\text{Cosh } 2\pi\ (z + d)/L}{\text{Sinh } 2\pi d/L} \text{Cos } 2\pi \left(\frac{x}{L} - \frac{t}{T}\right)$$

$$+ \frac{3}{4} \left(\frac{\pi H}{T}\right) \left(\frac{\pi H}{L}\right) \frac{\text{Cosh } 4\pi\ (z + d)/L}{\text{Sinh}^4\ 2\pi d/L} \text{Cos } 4\pi \left(\frac{x}{L} - \frac{t}{T}\right) \qquad (1.23)$$

$$V' = \frac{\pi H}{T} \frac{\text{Sinh } 2\pi\ (z+d)/L}{\text{Sinh } 2\pi d/L} \text{Sin } 2\pi \left(\frac{x}{L} - \frac{t}{T}\right)$$

$$+ \frac{3}{4} \left(\frac{\pi H}{T}\right) \left(\frac{\pi H}{L}\right) \frac{\text{Sinh } 4\pi\ (z+d)/L}{\text{Sinh}^4\ 2\pi d/L} \text{Sin } 4\pi \left(\frac{x}{L} - \frac{t}{T}\right) \qquad (1.24)$$

Also the equations for displacements are:

$$\zeta = -\frac{H}{2} \frac{\text{Cosh } 2\pi\ (z_o+d)/L}{\text{Sinh } 2\pi d/L} \text{Sin } 2\pi \left(\frac{x_o}{L} - \frac{t}{T}\right)$$

$$+ \frac{\pi H^2}{8L \text{sinh}^2 2\pi d/L} \left[1 - \frac{3\text{Cosh } 4\pi\ (z_o+d)/L}{2\text{Sinh}^2\ 2\pi d/L}\right] \text{Sin } 4\pi \left(\frac{x_o}{L} - \frac{t}{T}\right)$$

$$+ \frac{\pi H^2}{4L} \left[\frac{\text{Cosh } 4\pi \ (z_o/d)/L}{\text{Sinh}^2 \ 2\pi d/L} \right] \frac{2\pi t}{T} \qquad (1.25)$$

$$\eta = \frac{H}{2} \frac{\text{Sinh } 2\pi \ (z_o+d)/L}{\text{Sinh } 2\pi d/L} \ \text{Cos } 2\pi \ (\frac{x_o}{L} - \frac{t}{T})$$

$$+ \frac{3\pi H^2}{16L} \frac{\text{Sinh } 4\pi \ (z_o+d)/L}{\text{Sinh}^4 \ 2\pi d/L} \ \text{Cos } 4\pi \ (\frac{x_o}{L} - \frac{t}{T})$$

$$+ \frac{\pi H^2}{8L} \frac{\text{Sinh } 4\pi \ (z_o+d)/L}{\text{Sinh}^2 \ 2\pi d/L} \qquad (1.26)$$

1.5.1.3 Mass Transport

The net movement forward (or backward) each period T at a given depth z_o is given by the third term in equation 1.25 by substituting t = T and then dividing by T. This result is known as the mass transport velocity which is given by:

$$\bar{U}' = \frac{1}{2} \ (\frac{\pi H}{T}) \ (\frac{\pi H}{L}) \ \frac{\text{Cosh } 4\pi \ (z_o+d)/L}{\text{Sinh}^2 \ 2\pi d/L} \qquad (1.27)$$

Stokes assumed that no net motion occurs throughout the complete depth of water and therefore added a constant to the right hand side of the above equation (Raudkivi 1976) which becomes:

$$\bar{U}' = \frac{1}{2} \ (\frac{\pi H}{T}) \ (\frac{\pi H}{L}) \ \frac{\text{Cosh } 4\pi (z_o+d)/L}{\text{Sinh}^2 \ 2\pi d/L} - \frac{\pi H^2}{4Td} \ \text{Coth } 2\pi d/L \qquad (1.28)$$

and for deep water waves

$$\bar{U}'_o = (\frac{\pi H}{T}) \ (\frac{\pi H}{L}) \ (\exp 4\pi \ z/L - L/4\pi d) \qquad (1.29)$$

Equations 1.28 and 1.29 neglect the viscous effects and

therefore are not applicable inside the viscous boundary layer and interior of fluid.

1.5.2 Stokes Third and Higher Order Theories

Stokes has developed the potential function linear theory in the form of a series of terms cos $2\pi n$ $(\frac{x}{L} - \frac{t}{T})$ where n = 1, 2, 3 .... . Since then it has been the work of many investigators (Wilton (1914), Hurt (1953), De (1955), Skyelbreia (1959)). For example the third approximation to the surface profile is given as:

$$Y_s = \frac{H}{2} \text{Cos } 2\pi \left(\frac{x}{L} - \frac{t}{T}\right) + \frac{\pi H^2}{4L} f_2 \text{ Cos } 4\pi \left(\frac{x}{L} - \frac{t}{T}\right)$$

$$+ \frac{\pi^2 H^3}{8L^2} f_3 \text{ Cos } 6\pi \left(\frac{x}{L} - \frac{t}{T}\right) \qquad (1.30)$$

where f_2 and f_3 are functions of d/L (Wiegel 1964). And for wave velocity the relationship is:

$$C^2 = \frac{gL}{2} \text{ Tanh } 2\pi d/L \left(1 + \frac{\pi H^2}{4L} \frac{8 + \text{Cosh } 8\pi d/L}{8 \text{ Sinh}^4 2\pi d/L}\right) \qquad (1.31)$$

particle displacements and velocity equations are also given by Wiegel.

For fourth order and so on the term Cos 8π (x/L - t/T) and .... are added and more complicated wave velocity and other dynamic equations are introduced (Kinsman (1965)).

Whatever be the order of approximation, as Stokes stated, there is a common factor among these theories that:

"The wave will be symmetrical with respect to vertical planes through their ridges, as also with respect to vertical planes through their lowest points".

1.5.3 Introduction and Significance of Ursell Parameter

The linear theory is valid for waves of small amplitude and small wave steepness. But ocean waves are not small in amplitude for deep region and the wave steepness is distorted in shallow water. Stokes pointed out that for the linear theory to be valid, in addition to the conditions of small wave steepness, the ratio $L^2H/2d^3$ must be small too. This ratio is the result of the amplitudes of the two terms of equation 1.21. After simple calculations the ratio of the amplitude of second order term to the amplitude of the first order term becomes

$$\frac{3}{16}\,\frac{1}{(2\pi)^2}\,\frac{H}{L}\,\left(\frac{L}{d}\right)^3$$

The non linearity of the waves, is measured by the parameter known as Ursell parameter (Chakrabarti (1980));

$$U_R = \frac{H}{L}\left(\frac{L}{d}\right)^3 \qquad (1.32)$$

The Ursell number of less than 1 describes the deep water waves, the Ursell number of greater than 20 is for shallow water waves. But in principle more and more terms of the power series would be required in order to keep the same relative accuracy as the Ursell parameter increases.

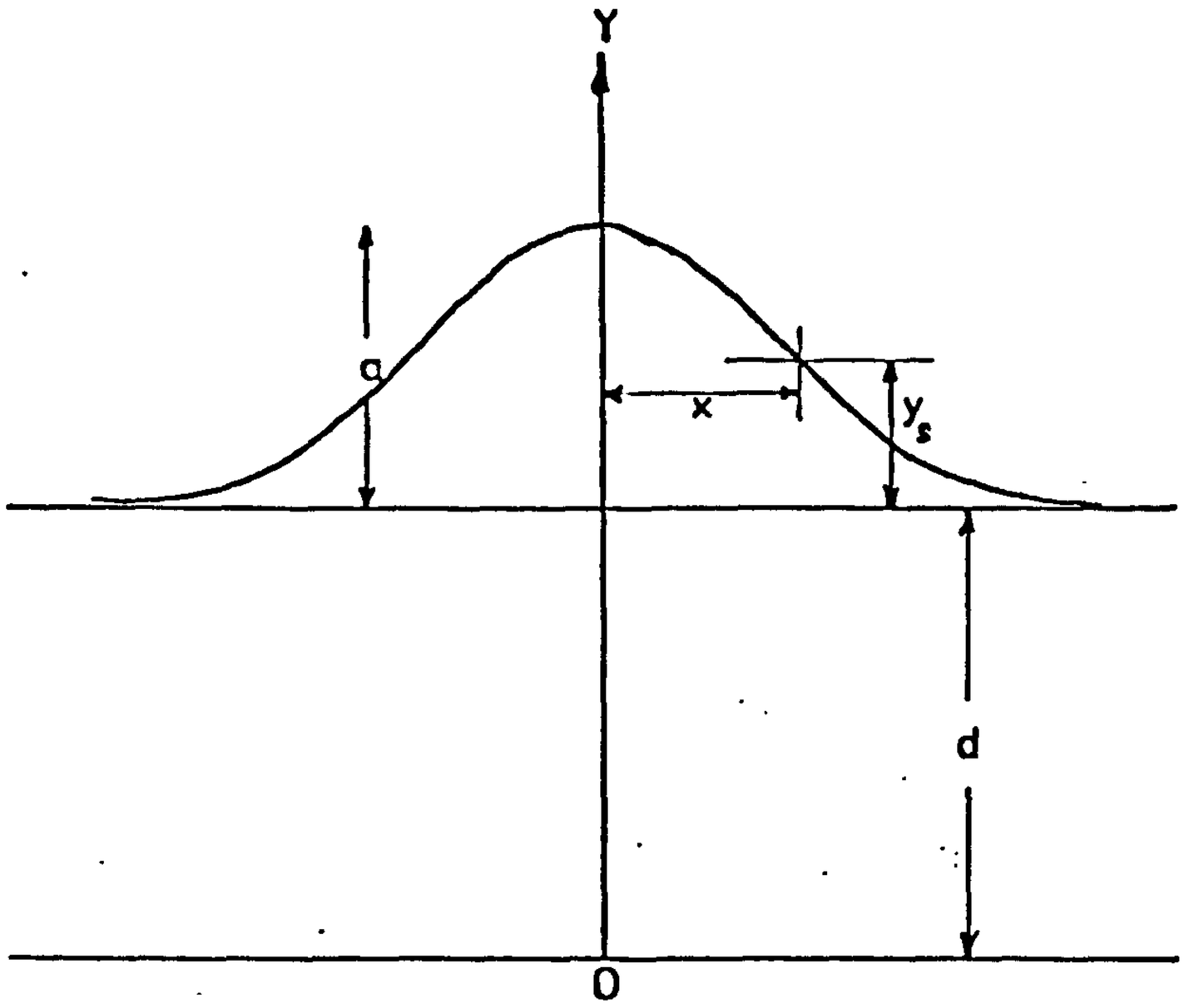

FIG 1.7 CNOIDAL WAVE PROFILE

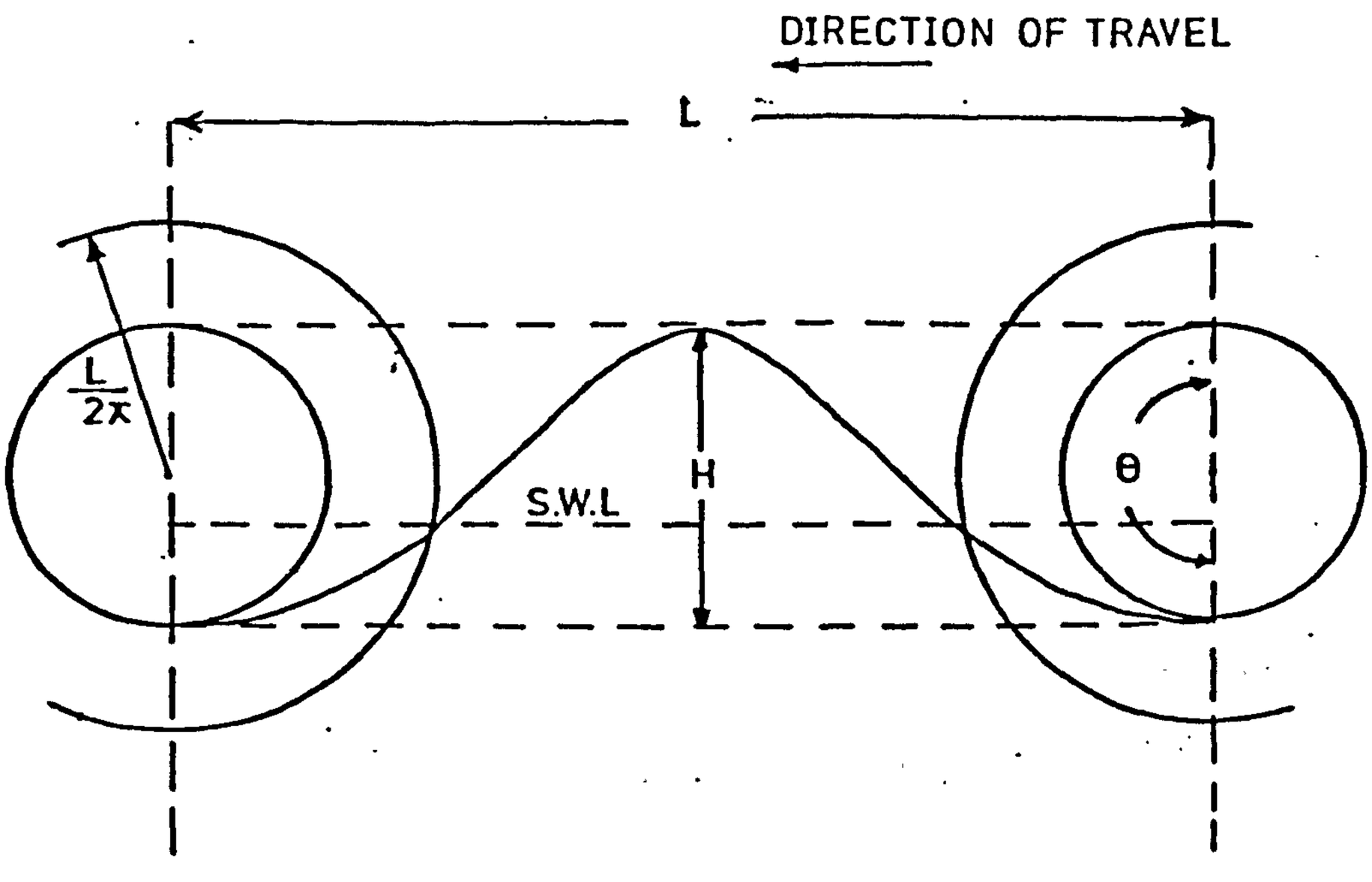

FIG 1.8 TROCHOI DIAL WAVE

1.6 CNOIDAL WAVES

Keulegan (1950) and De (1955) argued that Stokes theories are valid for deep water (when $d/L > 1/8$), but for shallower water the cnoidal wave theory appears to be more satisfactory. The theory was first developed by Korteweg and De Vries (1895) and since it has attracted many investigators (Keller (1948), Wehausen (1963)). The computations are based upon the equation for a stationary wave;

$$b/2 \ (dy_s/dx)^2 = y_s \ (a-y_s) \ (K+y_s) \qquad (1.33)$$

(- here y-axis moves with the wave)

where b and K are constants and a represents the vertical height of crest above trough, then y_s and x are the vertical and horizontal coordinates of water surface (Fig. 1.7). Where the origin is situated at the level of the wave trough, then the surface wave equation becomes:

$$y_s = a \ C_n^2 \left[\frac{(K+a)^{\frac{1}{2}} \cdot x}{(2b)^{\frac{1}{2}}} \right] \qquad (1.34)$$

Where $C_n(u)$ denotes the Jacobian elliptic function of U and modulus here being $a^{\frac{1}{2}}/(a+K)^{\frac{1}{2}}$. This theory has been fully covered in Wiegel together with the particle velocity equations and displacements. Also higher order theories for cnoidal wave representation are discussed by Laitone (1960) and Silvester (1974).

1.7 SOLITARY WAVE

A solitary wave is the special case of a cnoidal wave

when the wave length becomes infinite and the trough becomes asymptotic to still water level (S.W.L.). A solitary wave is a progressive wave relative to the body of water, whose motion is unaffected by preceding of following crests. The general surface equation is given by:

$$y_s = a\ \mathrm{Sech}^2\ x/2b \qquad (1.35)$$

where a is the crest height above S.W.L. and b is given by:

$$b = d\ \left(\frac{d + a}{3a}\right)^{\frac{1}{2}} \qquad (1.36)$$

Also the celerity of the wave is given by:

$$C = g^{\frac{1}{2}}\ (d + a)^{\frac{1}{2}} \qquad (1.37)$$

The velocity functions and displacement equations are given by Wiegel, Silvester and Wood (1969).

1.8 TROCHOIDAL WAVE THEORY

The trochoidal wave theory for deep water waves was developed by Gerstner (1802). The surface of the wave is the path of a point on a disc whose circumference rotates along a straight line (Fig. 1.8). For an angle of rotation θ, the surface profile below crest level is:

$$y_s = H/2\ (1-\cos\ \theta) \qquad (1.38)$$

and the horizontal distance from the origin at a crest is given by:

$$x = L\ \left(1 - \frac{\theta}{2\pi} + \frac{H}{2L}\ \mathrm{Sin}\ \theta\right) \qquad (1.39)$$

With the positions of crest and trough from S.W.L. as:

$$\left.\begin{aligned}\text{height of crest} &= H/2 + \pi H^2/4L \\ \text{depth of trough} &= H/2 - \pi H^2/4L\end{aligned}\right\} \qquad (1.40)$$

The wave velocity equation for deep water is equivalent to that for Airy wave:

$$C^2 = gL/2\pi$$

and the water particles, for deep water waves, describe circular orbits while for shallow water the particles have elliptical orbits. A full summary of trochoidal theory is given by B.E.B. (1942) and Wiegel (1964).

1.9 COMPARISON OF THE WAVE THEORIES

One of the basic assumptions in this sort of investigation is the application of a suitable analytical wave theory. The theories have been briefly presented above; each has practical limitations, advantages and disadvantages, and is suitable for special conditions (as dictated by the wave amplitude to water depth ratio (H/d) which classifies the finite or infinite amplitude wave or by the water depth to wavelength ratio (d/L) which defines the wave classifications)

The trochoidal theory is an example which is used by engineers because of its exactness (Wiegel). While cnoidal theory is suitable in place of Stokes theories for shallower water and greater wave period (T > 6 sec), the Stokes second

and third order predict the mass transport, as well as being a good approximation to practical cases of small period, finite amplitude and intermediate water waves.

In a theoretical comparison of progressive waves (see p. 122) Dean (1970) concludes that linear theory and cnoidal first are good approximations for shallow water while linear and Stokes third order theories are more suitable for intermediate and deep water regions. On the practical side, the tests carried out by Le Mehaute et al. (1968) suggest that for waves in deep and shallow water, linear theory predicts velocities at the bed with good accuracy and at still water level cnoidal first is a better approximation in shallower water. Tests by Chakrabarti (1980) prove that for waves between 1.4 sec. and 3.25 sec. period the best estimate is Stokes third while the linear theory also compares well for waves of up to 3.5 sec. period. Isaacson (1978) has shown that both Stokes and cnoidal wave theories will predict the mass transport velocity near the sea bed, but the cnoidal theory is a better fit when

$$H/d > 350\ (d/gT^2)^{3/2} \qquad (1.41)$$

and H/d is limited by wave breaking.

A tabulated comparison of the above six theories is shown in Table 1.2. For this study, however, Stokes second order has been chosen as the suitable theory, and the comparison of the theory with data is presented in Chapter 5.

Wave Theories	ADVANTAGES	DISADVANTAGES	Limits;
Linear	Simple Mathematics	Small amplitude only	$\frac{L^2H}{2d^3} << \frac{16\pi^2}{3}$ or $\frac{H}{L} < \frac{1}{50}$
Stokes II	Accuracy for small period - Mass transport applicable in intermediate zone		T < 4 sec.
Stokes III	"	Complicated formulae	"
Cnoidal	Applicable for shallow water	Complicated formulae	$\frac{d}{L} < \frac{1}{8}$
Solitary	Special case of cnoidal	Not oscillatory	"
Trochoidal	Exactness	Rotational	

Table 1.2. Comparison of Some Wave Theories.

CHAPTER TWO

REVIEW OF THE OSCILLATORY BOUNDARY LAYER

2.1 INTRODUCTION

A comprehensive study and comparison of different wave theories, together with the equations for surface wave profile and orbital paths has been made in Chapter One. However, because for wave theories the assumption is zero viscosity, the orbital velocity equations would be acceptable up to a depth close to the bed where the influence of viscosity becomes effective. The present chapter contains a review to this layer (better known as oscillatory boundary layer), which includes the boundary layer thickness definition, laminar and turbulence for oscillatory flow with the relevant Reynolds number values suggested by previous works, the velocity equations for smooth and rough beds, the mass transport equation, separation at boundary layer, shear stresses on the bed due to surface wave, the effect of roughness in the boundary layer theories and Reynolds number values and definitions.

2.2 STOKES SHEAR WAVE EQUATION

Stokes (1851) in his memoir on pendulums pioneered the problem of an oscillating plane boundary in an infinite fluid known as the "Shear Wave" solution, which later was extended by Lord Rayleigh (1911).

Among many others to investigate the above problem was Lamb (1932), who approached the problem for an infinite and semi infinite plane, the latter being closely related to the oscillatory boundary layer problem. By choosing suitable axes, Lamb (1932 c) obtained that because the plate has infinite length (or fluid is extended to infinity) the derivatives of velocity with respect to the axes parallel to plate movement (x direction) must be zero ($\frac{\partial u}{\partial x} = 0$) hence $\frac{\partial v}{\partial y} = 0$ from the continuity equation ($\frac{\partial u}{\partial x} + \frac{\partial v}{\partial y} = 0$), and also v is zero at the boundary. Now with having constant pressure everywhere the Navier-Stokes equation can be written as;

$$\frac{\partial u}{\partial t} = \nu \frac{\partial^2 u}{\partial y^2} \qquad (2.1)$$

where ν is the kinematic viscosity of the fluid.

Equation 2.1 is a linear equation with the plate oscillating in its own plane (simple harmonic motion). Assuming a time factor of $e^{i(\sigma t+\varepsilon)}$ where $\sigma = \frac{2\pi}{T}$ (T is the period) and boundary conditions of

$$\left.\begin{aligned} u &= 0 \text{ at } y = \infty \\ u &= u_o(t) \text{ at } y = 0 \end{aligned}\right) \qquad (2.2)$$

The solution to equation 2.1 is

$$u = Ae^{(1+i)\beta y} + Be^{-(1+i)\beta y} \qquad (2.3)$$

where β is the boundary layer parameters and;

$$\beta = \left(\frac{\sigma}{2\nu}\right)^{\frac{1}{2}} \qquad (2.4)$$

Solving equation 2.1 for a fluid which is bounded by a fixed rigid plane ($y = 0$) and under a horizontal force acting uniformly on the mass of water with the boundary conditions of;

$$\left.\begin{aligned} U &= 0 \text{ at } y = 0 \\ U &= U_\infty \cos(\sigma t) \text{ at } y = \infty \end{aligned}\right\} \qquad (2.5)$$

where δ is the thickness of viscous boundary layer and suffix "∞" represents the flow just outside the boundary layer and taking only the real part of the equation, the solution (for equation 2.1) will be (Lamb 1932 c);

$$U = U_\infty [\cos(\sigma t) - e^{-\beta y}\cos(\sigma t - \beta y)] \qquad (2.6)$$

while equation 2.6 is for horizontal velocity in a viscous boundary layer above a fixed bed and under oscillating fluid (or gravity wave), for an oscillating plate the equation can be obtained (Schlichting 1968) as;

$$U = U_o e^{-\beta y} \cos(\sigma t - \beta y) \qquad (2.7)$$

where U_o is the maximum velocity of the plate.

Figs. 2.1 and 2.2 represent the two equations (2.6 and 2.7) for eight equal intervals in one period.

2.3 BOUNDARY LAYER THICKNESS

Obviously the thickness of the boundary layer depends

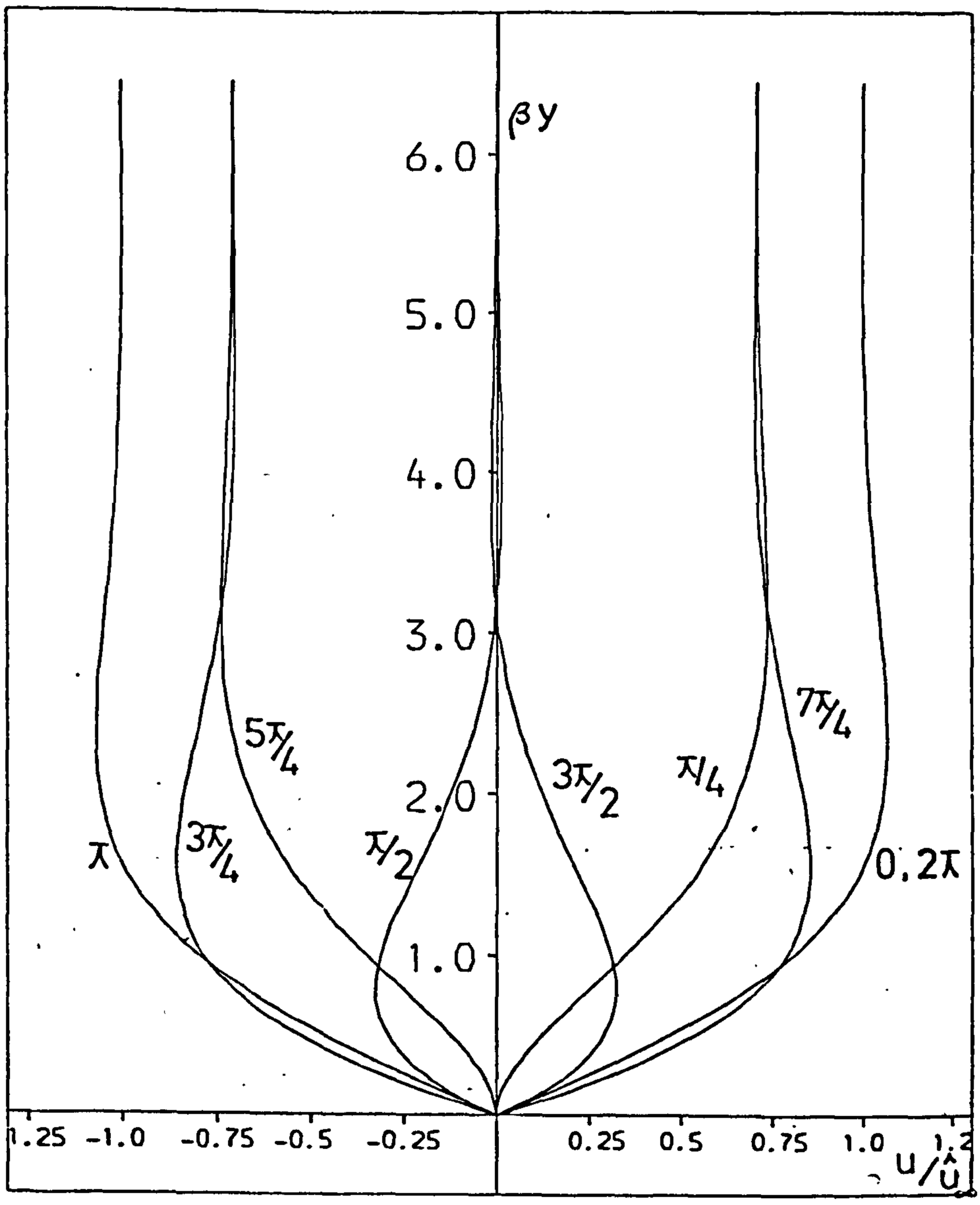

Fig. 2.1. Laminar Boundary Layer Velocity distribution under gravity waves (Eq. 2.6).

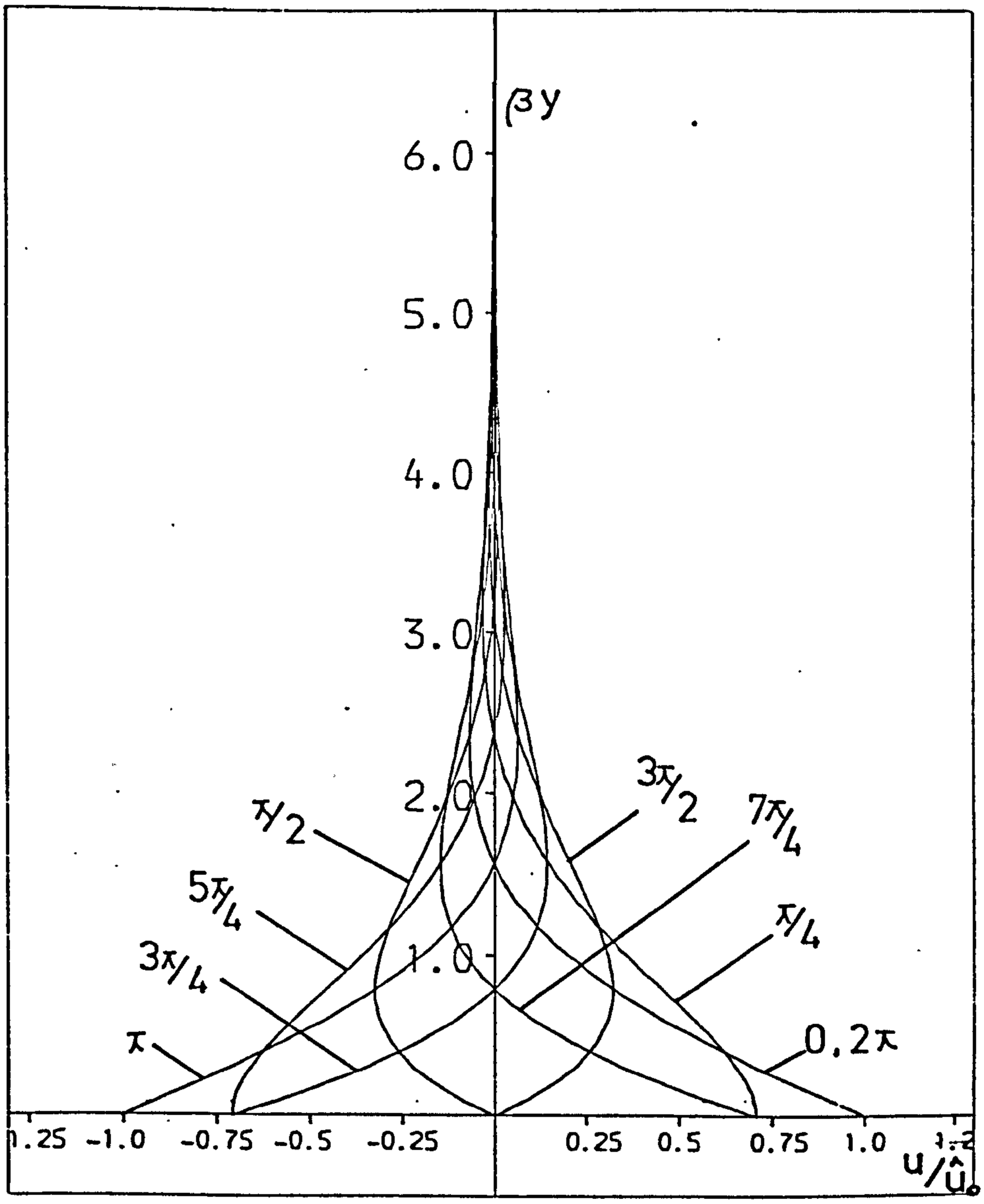

Fig. 2.2 Laminar Boundary Layer Velocity distribution above an oscillatory bed. (Eq. 2.7).

on the influence of viscosity from the bed. Examining equations 2.6 and 2.7 the influence of $e^{-\beta y}$ is rapidly decreasing with increasing of βy and it reduces to one percent when $\beta y = 4.6$. Taking the limit of y as δ (the boundary layer thickness) we will have;

$$\beta\delta = 4.6$$

or
$$\delta = \frac{4.6}{\beta} = \frac{4.6}{(\sigma/2\nu)^{\frac{1}{2}}} = 6.5 \left(\frac{\nu}{\sigma}\right)^{\frac{1}{2}} \qquad (2.8)$$

This equation is accepted by many investigators as viscous boundary layer thickness (Li (1954), Manohar (1955), Brebner et al. (1966)). While some others (Eagleson (1959), Lamb (1932)) believe that one wave-length ($2\pi/\beta$) is a more proper definition for the vertical range of boundary layer thickness, for which the effect of bed shear is then reduced to 0.2 per cent. However Jonsson (1966) argues that for the velocity inside boundary layer to have the same value as the velocity outside the boundary layer it requires that βy be equal to $\pi/2$ and in this case the boundary layer thickness becomes $\pi/2\beta$. Fig. 2.3 shows the maximum velocity profile in the boundary and Fig. 2.4 shows the velocity phase variation for maximum velocity within the boundary layer.

It is conclusive that the boundary layer thickness is proportional only to (wave period)$^{\frac{1}{2}}$ (from equation 2.8, $\delta = 2.59(\nu T)^{\frac{1}{2}}$). Taking a value of 10^{-6} m^2/s for kinematic

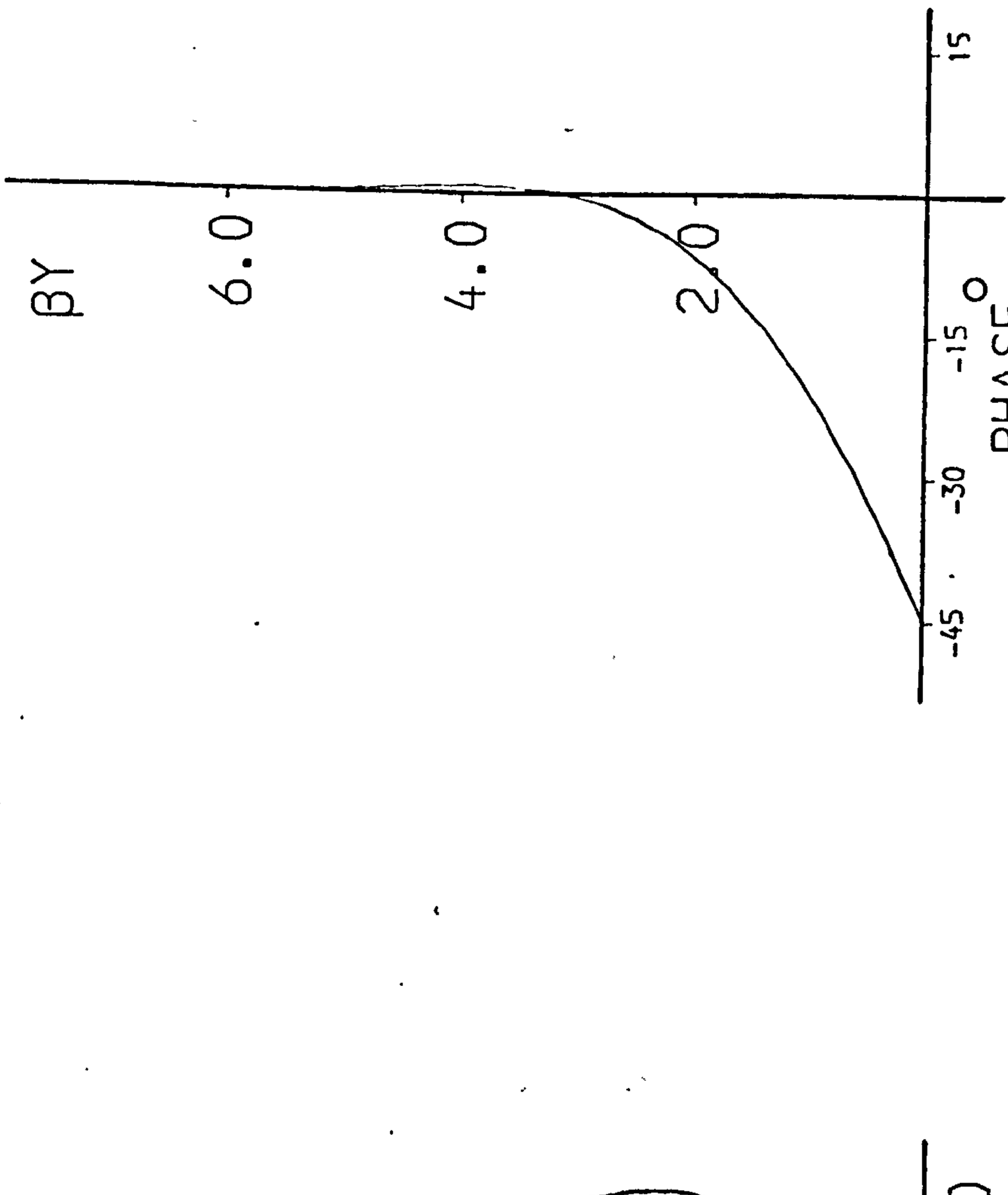

Figure 2.4 Velocity Maxima Phase Profile (Eq. 2.6).

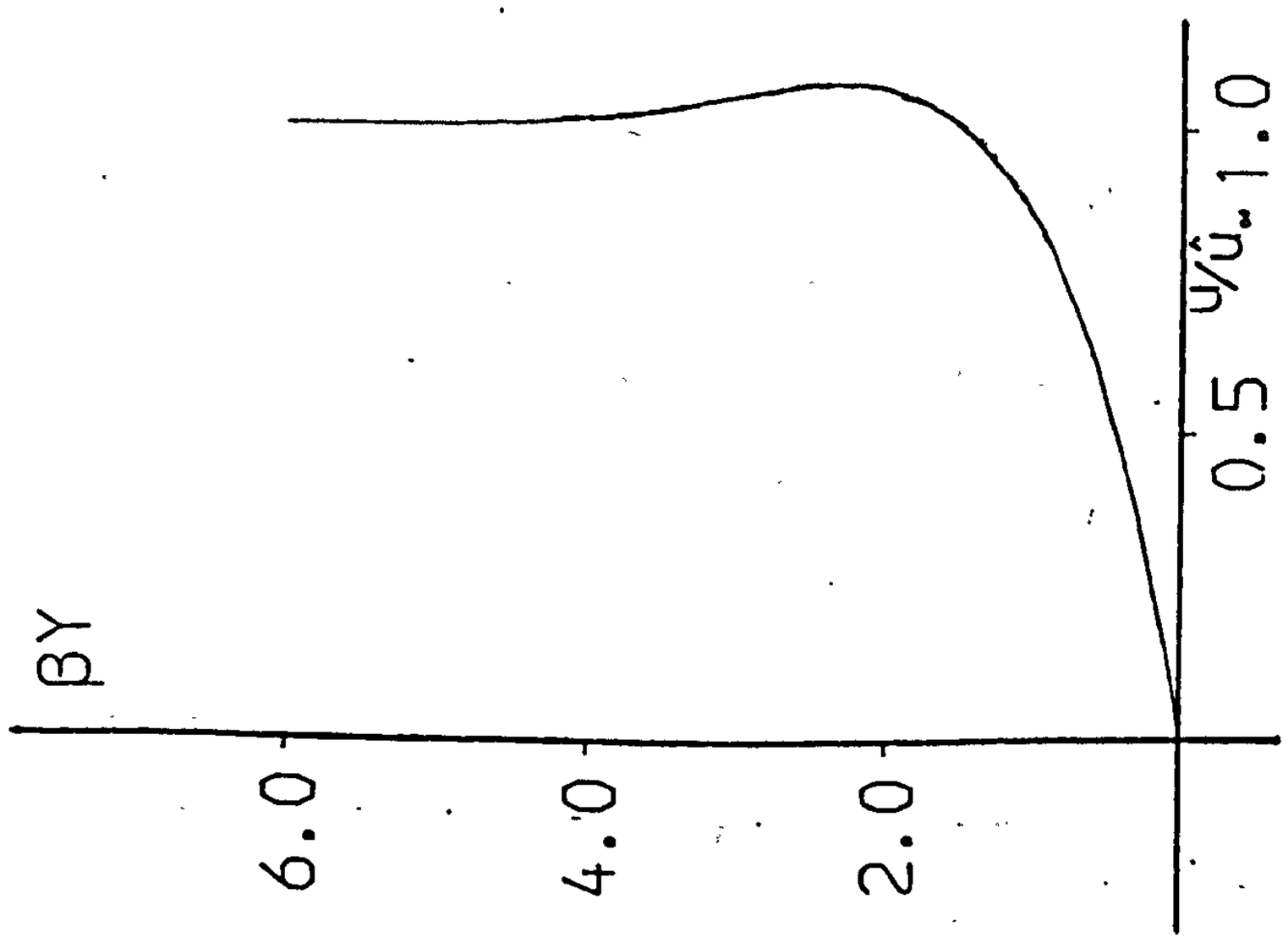

Figure 2.3 Velocity Maxima Profile (Eq. 2.6).

viscosity of water the boundary layer thickness varies between 2 mm and 500 mm for wave periods of 1 second to 12 hours (which is a tidal wave). The laboratory waves of up to 10 sec. period produce a boundary layer thickness of up to 10 mm.

From Fig. 2.3 it appears that equation 2.8 is an adequate definition for boundary layer thickness and this will be used throughout this thesis.

2.4 BOUNDARY LAYER EQUATIONS UNDER LAMINAR AND TURBULENT CONDITIONS

2.4.1 Laminar and Turbulent Flow in Oscillatory Flow

To discuss the boundary layer equations under laminar and turbulent conditions, the first step would be to understand what is meant by these terms.

While the definition of the terms 'laminar' and 'turbulent' have been made descriptively and by observation on dye introduced into the flow (Reynolds (1883)), these terms can also be defined mathematically by consideration of the ratio of inertia to viscous forces known as "Reynolds Number".

Though many books and reports have been published investigating the states of laminar and turbulent flows for oscillatory flow cases still the question of how and under what condition transition from laminar to turbulent occurs

remains one of considerable dispute, especially when the problem of hydraulically rough surface is added.

Li (1954) reports that,

> "Two different types of mechanisms exist. (1) Sufficiently large disturbance which break down into individual eddies, and (2) a discontinuity becomes unstable and rolls up into individual eddies. While the first case is similar to the breakdown of a surface wave, the second case can be demonstrated by the unstable character of a vortex-sheet of ideal flow".

(The latter statement means that in a plane vortex-sheet with a small sinusoidal disturbance vorticity occurs which becomes more and more concentrated in the rolled-up portion, and then breaks down to small eddies). He adds,

> "On the other hand the formation of the eddies does not necessarily represent the beginning of turbulence. Flow becomes turbulent only when the eddies move away from the location of origin".

Manohar's (1955) description of laminar and turbulent flow is that;

"In laminar flow, the entire region of flow is divided into an orderly series of fluid laminar or layers conforming generally to the configuration of the boundary, and turbulence is a random of fluid masses which mix continually with other similar fluid masses in the same fluid".

This view is also shared by Kalkanis (1957) that in a turbulent case the molecular exchange of momentum gives way to momentum or vorticity exchange of large masses of fluid which move temporarily as a unit and then mix with other masses.

Visual observation has been widely used by many other investigators to define the flow, but as Sleath (1970, 1974a) point out, the disturbance of the dye cloud, might be caused by the formation of vortices around individual roughness element, and does not necessarily mean the start of transitional flow. So the next section examines the critical Reynolds number for the occurrence of laminar and turbulent flow.

2.4.2 Critical Reynolds Number and the Effect of Roughness

The transition from laminar to turbulent boundary layer occurs on the increasing of the inertia forces relative to friction forces. Reynolds number which is the ratio of these forces can be used to represent the laminar and turbulent

boundary layer characterisation. For a representative Re, the kinematic viscosity of water (ν) is easily found by knowing the temperature (from the empirical Poiseulle equation), but for a characteristic length and velocity different views exist. According to Einstein (1972);

> "The characteristic values must be chosen by logical arguments, but if too many variables of the same dimension are involved it may become necessary to determine the proper variable empirically. The critical value of the Reynolds number must always be found by experiment".

Li (1954) using an oscillating plate for his experiment suggests that for a smooth boundary the critical Reynolds number at which the transition takes place is 800 providing; (- also see Table 2.1)

$$(Re)_l = \omega^{\frac{1}{2}} d_1 / \nu^{\frac{1}{2}} \qquad (2.9)$$

where ω is the angular velocity and d_1 is the total displacement of the oscillatory plate in feet, and ν is the kinematic viscosity ($ft^2/sec.$). For a rough boundary the Reynolds number is found from;

$$(Re)_{Rl} = \frac{\omega d_1 \kappa}{\nu} \qquad (2.10)$$

where κ is the roughness height. For two dimensional roughness, Li suggests that when $\frac{\delta}{\kappa}$ is less than 2.6 the bed behaves hydraulically rough and for $\frac{\delta}{\kappa}$ greater than 6.8 it is hydraulically smooth. While for three dimensional roughness when $\frac{\delta}{\kappa}$ is less than 18.5 it is taken as hydraulically

rough and for $\frac{\delta}{\kappa}$ greater than 30 it is smooth, where δ is the height of laminar boundary layer.

Manohar (1955) also suggests that the ratio of δ to the height of the element for roughness (κ) has three cases. First when $\delta >>> \kappa$ which then the Reynolds number is defined as $\frac{U_o \delta}{\nu}$ when U_o is the maximum velocity of oscillatory bottom, or;

$$(Re)_{R1} = \frac{\omega^{\frac{1}{2}} a'}{\nu^{\frac{1}{2}}} \qquad (2.11)$$

where a' is the length of semi major axis of the orbit of water particle near or at bottom and ω is the angular velocity of the water particles in its orbital motion. Second case is when $\delta >> \kappa$ then the Reynolds number will be $\frac{\omega a' \kappa}{\nu}$, and thirdly when $\delta > \kappa$ which for Reynolds number κ is replaced by a function of κ;

$$(Re)_{R2} = \frac{\omega a' f(\kappa)}{\nu} \qquad (2.12)$$

and $f(\kappa)$ is to be determined experimentally. Manohar using an oscillatory plate found that the critical value of Re in the smooth case is 400, for 3-D roughness is 104 and for fully turbulent is 1.78×10^4 providing $f(\kappa)$ is equal to $\kappa^{0.2}$ and verifying Li's results (Note that for $f(\kappa) = \kappa^{0.2}$ the Re would not be dimensionless anymore i.e. not Reynolds number anymore but just a ratio).

Vincent (1957) using the ratio given by Li (eq. 2.10)

found a constant Re for each roughness. The results for transiton or "Setting Off", Re values are found to be a fifth of the values suggested by Li for rough beds. He also found that for $\frac{\delta}{\kappa} > 30$ the bed still behaves as the rough beds. However Vincent used a wave channel instead of the oscillating plate used by Li and Manohar, where in this case ω is $\frac{2\pi}{T}$, T being the wave period and d_1 is the total travel of a fluid particle in the immediate vicinity of the bed (or $d_1 = \frac{H}{\text{Sinh } 2\pi h/L}$; in which H is the wave height and h and L are water depth and wave length respectively).

Eagleson (1959) obtained that the laminar boundary layer exists at least up to a value of 3×10^4 for Re where;

$$(\text{Re})_1^2 = \frac{U_\infty{}^2 T}{4\nu}$$

By taking the boundary layer thickness $(1/\beta)$ as the characteristic length for Reynolds number, Brebner and Collins (1961) rewrite Re as;

$$(\text{Re})_2 = \frac{U_\infty}{\nu\beta} = (\frac{\pi}{\nu})^{\frac{1}{2}} \frac{H}{T^{\frac{1}{2}} \text{SinhKd}} \qquad (2.13)$$

from which turbulence will occur when;

$$\left(\frac{H}{\sqrt{T}}\right)_{crit} \geq \text{Re}_{crit} (\frac{\nu}{\pi})^{\frac{1}{2}} \text{ Sinh Kd}$$

while Kalkanis (1964) believes that,

> "in a practical application it is not important to know the exact value of the Re_{crit} as to be able to predict with sufficient confidence that under the existing conditions the flow regime in the boundary is not laminar and consequently that the theoretical laminar solution is no more applicable. This type of information can be obtained by experimental methods".

His results of Re_{crit} number for turbulent flow are different to those of Li and Manohar, and states;

> "Re_{crit} as defined for the transition regime may well be extended to cover the rough case too. This implies that in Li's and Manohar's experiments the flow in this region was already unstable before it could be established as such from observations".

Johnsson's (1980) conclusions are different to his earlier statements (1966). For smooth bed case he suggests that a Reynold number of about ten times higher than his previous estimated value is to be taken for a fully developed turbulence. As for rough beds he suggests the limits are still vague and for present Sleath's (Table 2.1) and Kajuira's results are more appropriate for practical uses.

Where Jonsson (1966) using a wave channel found that for smooth turbulence Re_{crit} is 250 and for a rough turbulent the value is 500. $(Re = \frac{U_\infty \delta}{\nu},\ \delta = \frac{\pi}{\sqrt{2}})$

Brebner et al. (1966) completing the work of Brebner and Collins (1961) found that when $\frac{\kappa}{\delta}$ approaching zero the bed is smooth and Re_{crit} $(\frac{U_\infty \delta}{\nu})$ is 160, and for $\frac{\kappa}{\delta}$ approaching unity the bed is hydraulically rough and critical $(Re)_{R1}$ $(\frac{U_\infty \kappa}{\nu})$ is 110. So for $0 < \frac{\kappa}{\delta} < 1$ the bed could behave hydraulically rough or smooth. It is concluded that when Re is greater than 160 the flow is turbulent and below 110 it is laminar $(\delta = \frac{1}{\beta})$.

Results from the oscillatory plate work of Einstein (1972), he suggests that the Re_{crit} for smooth bed is 1.7×10^5 where $(Re)_1^2 = a'^2\omega/\nu$, ω and a being the angular velocity and amplitude of the moving plate. For two dimensional and three dimensional roughness the critical $(Re)_{R1}$ $(\frac{\kappa a'\omega}{\nu}$, κ is the Roughness element) are 640 and 104 providing

$$\frac{a'}{\kappa} < \begin{cases} 266 \text{ for 2-D roughness} \\ \\ 1630 \text{ for 3-D roughness} \end{cases}$$

all other cases behave hydraulically smooth.

Riedel et al. (1972) using a wave tunnel concluded that for a smooth boundary the critical Reynold No.

($\frac{U_\infty a_\infty}{\nu}$, where a_∞ is the orbital amplitude just outside the boundary layer) for transition is between 9×10^3 and 6×10^5.

While most of the critical Reynold numbers given have been evaluated visually by the effect of dye, Sleath (1974a) explains that the onset of mixing of dye with fluid does not necessarily mean the occurrence of the turbulence especially when it comes to roughnesses such as grains, for sometimes on the lee of larger grains a wake of dye appears which could be mistaken for transition. For large scale roughness ($\frac{\beta}{\kappa'} = 5$) he found that for Reynolds number ($\kappa' = \frac{2\pi}{\ell}$) ($\frac{U_\infty \ell}{\nu}$ where ℓ is the bed roughness wavelength) of 800, the first signs of vortex formation appears and when it is 4000 the vortex is fully mixed throughout the cycle. In the case of small scale roughness ($\frac{\beta}{\kappa'} = 0.3$), however, he states that at high Re the flow is unstable and with decreasing Re the flow changes gradually to one in which the fluid moves in closed recirculating cells with negligible mixing from one cell to the next. By introducing the two ratios of $\frac{\beta}{\kappa'}$ (where $\kappa' = \frac{2\pi}{\ell}$) and $\frac{U_\infty \kappa'}{\omega}$ (where ω is the angular frequency of water waves) a fully developed mixing curve for two dimensional roughness (some three dimensional roughness as well) is introduced in the form of

$$\frac{U_\infty \kappa'}{\omega} = 100 \left(\frac{\beta}{\kappa'}\right)^{-1.29} \qquad (2.14)$$

where $0.03 < \frac{\beta}{\kappa'} < 5$. Equation 2.14 well agrees with the

work of previous investigators (Li, Manohar, Vincent).

Knight (1978) rewrites equation 2.14 in the form;

$$\frac{U}{\sqrt{\omega\nu}} = \frac{241}{(\beta D)^{0.29}} \qquad (2.15)$$

where D is the mean grain size (which is equivalent to the roughness wavelength) with the limits of $0.19 < \beta D < 31$. Sleath (1975), by assuming 5 per cent fluctuations of root mean square of velocity as the transition state to turbulent from laminar, introduced a new relationship for rippled 2-D roughness in the form (Sleath 1975 notation):-

$$\left[\left(\frac{U_\infty L}{\nu}\right)\left(\frac{h}{L}\right)^{1.16} - 108.2\right]\left[\frac{a}{L}\left(\frac{h}{L}\right)^{1.16} - 0.042\right] = 0.58 \qquad (2.16)$$

which tends towards $\left(\frac{a}{L}\right)\left(\frac{h}{L}\right)^{1.16}$ at large $\frac{U_\infty L}{\nu}\left(\frac{h}{L}\right)^{1.16}$ (for large βL) and vice versa (small βL).

Meanwhile George and Sleath (1978) conclude that,

"For oscillatory flow over a rough bed there is a range of Reynolds numbers for which the flow remains laminar, in the strict sense of that term, but in which the velocity profile is significantly different from that over a smooth bed. It has usually been assumed in the past that the flow regime at the sea bed is either fully developed turbulence or that the velocity distribution for laminar flow over a smooth bed applies. It is clear from the present work that a third regime which may be called "rough laminar" may also be important."

The state of transition, as presented by the authors mentioned above, has been interpreted differently in mathematical forms. But that which all of the statements have in common is that the conditions of transition is very complicated and dependent on the type of roughness. There is the problem of different types of two dimensional roughness as well as the problem of 2-D and 3-D roughness. Also the value of Re is defined by different physical parameters as well as the different results which have been obtained. However in the case of a smooth boundary it seems that $(Re)_3 = \frac{\hat{U}_\infty \delta}{\nu}$ is more popular and logical, whilst in the case of rough boundary the height of roughness would be a good characteristic length for Reynolds number, of the form $\frac{U_\infty \kappa}{\nu}$. Also the ratio of roughness height to the roughness wavelength should be taken into account. Again Vincent suggests that the results from oscillatory plate and wave channel have some discrepancies, while Sleath believes that the two different methods are still very much comparable.

Values for Reynolds numbers which have been studied in this section are shown in Table 2.1. The author takes the Reynolds number of the form of $\frac{\hat{U}_\infty \delta}{\nu}$ for smooth boundary and $\frac{\hat{U}_\infty \kappa}{\nu}$ (κ being the roughness height) in the case of rough beds having considered the κ/ℓ ratio (ℓ is the roughness wavelength).

Table 2.1 Critical Re Suggested by Different Investigators

	Bed		
	Hyd. Smooth	Hyd. Rough	Limitations
Li (1954)	$(Re)_1 = 400$	$(Re)_{R1}$	$\frac{\delta}{\kappa} < \begin{matrix}(2.6 - 2D \\ (18.5 - 3D\end{matrix}$
Manohar (1955)	$(Re)_1 = 400$	$104 < (Re)_{R1} < 1.78\times10^4$ (3-D)	$\begin{matrix}6.8) \\ 30)\end{matrix} < \frac{\delta}{\kappa} < \begin{matrix}(2.6 & 2\text{-}D \\ (18.5 & 3\text{-}D\end{matrix}$
Kalkanis (1969) Einstein (1972)	$(Re)_1 = 400$	$\begin{matrix}640) \\ 104)\end{matrix} < (Re)_{R_1} < \begin{matrix}(2.52\times10^4 \\ (1.78\times10^4\end{matrix}$	- 2-D - 3-D
Brebner & Collins (1961) Brebner et al. (1966)	$(Re)_2 = 160$	$(Re)_{R_1} = 110$	$0 < \beta\kappa < 1$ Smooth - Rough
Sleath (1974a)		$800 < \frac{U_\infty \kappa'}{\nu} < 4000$	$\kappa' = 2\pi/\ell$ $.03 < \frac{\beta'}{\kappa} < 5.0$ $\frac{U_\infty \kappa'}{\omega} = 100 \left(\frac{\beta'}{\kappa}\right)^{-1.29}$

$(Re)_1 = \frac{\omega^{\frac{1}{2}} a'}{\nu^{\frac{1}{2}}}$ $\quad (Re)_2 = \frac{U}{\beta\nu}$ $\quad (Re)_{R1} = \frac{\omega a \kappa}{\nu}$

$(Re)_1 = 1.25\ (Re)_2$

2.5 THE BOUNDARY LAYER VELOCITY EQUATION

2.5.1 Laminar Flow

For the laminar flow case, equation 2.6

$$U = U_\infty \left[\mathrm{Cos}\ (\sigma t) - e^{-\beta Y}\ \mathrm{Cos}\ (\sigma t - \beta y)\right]$$

which is known as the "Lamb Solution", is used for the velocity in the boundary layer beneath the wave (while equation 2.7 is used for the oscillatory plate condition), and is the basis for the equation in turbulent flow.

Another solution for laminar flow known as "Agnew's Solution"

(Knight (1978)). The velocity equation in this case is in the form:

$$U = U_\infty \mathrm{Cos}\ (\sigma t - \phi) = V_1 \mathrm{Cos}\sigma t - W_1 \mathrm{Sin}\sigma t \qquad (2.17)$$

and by substituting this equation into Navier-Stokes equation (eq. 2.1). The coefficients V_1 and W_1 can be obtained.

2.5.2 Turbulent Flow

Manohar (1955) suggests that by introducing eddy viscosity (ε) instead of kinematic viscosity, the boundary layer equation for turbulent flow can be written as

$$U = U_\infty \left[\mathrm{Cos}\ (\sigma t) - e^{-\beta' Y}\ \mathrm{cos}\ (\sigma t - \beta' y)\right] \qquad (2.18)$$

where $\beta' = \left(\frac{\sigma}{2\varepsilon}\right)^{\frac{1}{2}}$ (while $\beta = \left(\frac{\sigma}{2\nu}\right)^{\frac{1}{2}}$).

Kalkanis (1957, 1964) proposed an equation for the velocity distribution in turbulent flow in the form:

$$U = U_\infty [\mathrm{Cos}(\sigma t) - f_1(y)\ \mathrm{Cos}\ (\sigma t - f_2(y))] \qquad (2.19)$$

in which $f_1(y)$ and $f_2(y)$ are functions of y alone and are determined experimentally for different flows. In Table 2.2 are given the values for $f_1(y)$ and $f_2(y)$ in cases of 2-D and 3-D roughness. However these equations are valid only over a specific range. Kalkanis (1964) says:

> "These equations do not satisfy the boundary condition at the wall (y = 0) which is not a very serious limitation since it can be easily circumvented by assuming the formation of a laminar sublayer as in a steady mean flow."

Einstein (1972) accepting the above equations, found experimentally that only the ranges given in Table 2.3 are acceptable for the values of Table 2.2.

Kamphuis accepting equation 2.19 proposed different values for $f_1(y)$ and $f_2(y)$ as follows:

$$f_1(y) = \tfrac{1}{2}\, e^{\frac{-267}{Re}(\beta y)}$$

$$f_2(y) = \tfrac{1}{2}\,(\beta y)^{2/3}$$

where $Re = \frac{U_\infty \kappa}{\nu}$, κ is the roughness height.

Sleath (1970) proposed an equation for velocity distribution somewhat similar to equation 2.19, but instead of

Type of rough bed	$f_1(y)$	$f_2(y)$
2-D	$e^{-\frac{y}{a\beta\ell}} \times 10^3$	$0.5(\beta y)^{2/3}$
3-D	$0.5\ e^{-133\ \frac{y}{a\beta\ell}}$	$0.5(\beta y)^{2/3}$

Table 2.2 The f Values of Eq. 2.19 (after Kalkanis)

Type of rough bed	ℓ/mm	a'/m	ω/rad s^{-1}
2-D	1.19-31.70	.032-0.61	0.174-10.4
3-D	0.27-13.81	.032-0.61	0.169-5.82

Table 2.3 The Limits of the f Values (after Einstein)

$f_1(y)$ and $f_2(y)$ the equation is written as:

$$U = U_\infty \left[\mathrm{Cos}(\sigma t) - e^{-\beta y/X} \mathrm{Cos}\ (\sigma t - \beta y/X)\right] \qquad (2.20)$$

in which X is a constant for any given test and is determined by trial and error. The range of X, for his experiments, was found to be between 1.0 to 1.8. For X = 1.0 the flow represents laminar criteria. He suggests that the relationship between X and $\frac{U_o \kappa^2 \beta}{\nu}$ is in the form;

$$X = 1 + 0.00815 \left(\frac{U_o \kappa^2 \beta}{\nu} - 115\right)^{0.78} \qquad (2.21)$$

The value of 115 for $\frac{U_o \kappa^2 \beta}{\nu}$ is given by Sleath as the critical value at which the vortex formation perturbs the velocity distribution. Equation 2.21 was used by Keiller and Sleath (1976) to compare the theoretical and measured values of X. Comparing the two sets of values it was concluded that the theoretical values give lesser values than the measured ones. So for large $\beta\kappa$ a new equation for X is introduced in the form;

$$X = \mathrm{Cost}.\beta\kappa$$

which is nearly the same as that given by Sleath (1974b) for two dimensional bed shape ($X = \beta\kappa/2\pi$).

Therefore it can be concluded that for a turbulent flow the velocity distribution equation is of the form of equation 2.19, with the values of $f_1(y)$ and $f_2(y)$ chosen from those given by Kalkanis or Sleath.

2.6 MASS TRANSPORT

Stokes (1851) was the first to study the generation by surface waves of the second order drift in a direction parallel to the waves. He assumed the fluid to be non viscous and irrotational. However, for mass transport viscosity cannot be neglected in the boundary layer region. Observation by Bagnold (1947) in a wave tunnel of mass transport velocity were made over 10 waves by inserting grains of dye impregnated with fluorescein, showed that the result was opposite to what Stokes' theory predicts. He found that the mass transport at the top was weak and in the opposite direction to the wave progression (or backwards), while at the bottom a strong drift existed in the wave direction (or forwards). Where viscous effects might not be important for wave vel-ocity and period equations, it has great effects within the boundary layer since it is the velocity gradient which gives rise to rotational motion. Longuet-Higgins (1953) proposed that this vorticity will spread beyond the boundary layer in two ways - by viscous diffusion, which is similar to the diffusion of heat in a solid, and diffusion by convection with the mass transport velocity itself; these are called "conduction" and "convection" respectively. In the conduction approach the convective inertia terms of the Navier-Stokes relationship are neglected and in terms of the stream function (ψ) the equation of conduction is:

$$(\frac{\partial}{\partial t} - \nu\nabla^2)\nabla^2\psi = 0$$

For the convection solution the viscous friction terms of the Navier-Stokes relationship are neglected and the stream function equation is;

$$(\frac{\partial}{\partial t} + U\frac{\partial}{\partial x} + v\frac{\partial}{\partial y})\nabla^2\psi = 0$$

However the convection solution for a progressive wave is indeterminate , and the conduction solution is applicable when the ratio $\frac{a}{\delta}$ (a is the wave amplitude and δ the boundary layer thickness) is small. Since δ is only of the order of a few millimeters (for wave period between 1 and 10 seconds) the applicability of the conduction solution is very limited as well. However it is expected that the conduction equation should be applicable for laminar flow within and just outside the boundary layer. The Longuet-Higgins mass transport equation within the viscous boundary layer under a progressive wave is;

$$\bar{U} = \frac{a^2\sigma K}{4\ \mathrm{Sinh}^2 Kd}\ f\ (\beta y) \qquad (2.23)$$

where

$$f(\beta y) = 5 - 8e^{-\beta y}\ \mathrm{Cos}\ \beta y + 3e^{-2\beta y} \qquad (2.24)$$

Equation 2.23 always has a positive value, with a maximum of 1.391 $\frac{a^2\sigma K}{\mathrm{Sinh}^2 Kh}$ when $\beta y = 2.306$, and as βy approaches infinity (the limit of the boundary layer thickness), f (βy)

approaches the limit of 5 and mass transport just outside the boundary layer is;

$$\bar{U}_\infty = \frac{5a^2\sigma K}{4\ \mathrm{Sinh}^2 Kd} \qquad (2.25)$$

and the equation of the mean velocity in the boundary layer by Longuet-Higgins (Beech (1978)) is given as; (Appendix D)

$$\bar{u} = \frac{a^2\sigma K}{2\ \mathrm{Sinh}^2 Kd} \left[1 - e^{-\beta y}\mathrm{Cos}(\beta y) + \tfrac{1}{2}\left(1 - 2e^{-\beta y}\mathrm{Cos}(\beta y) + e^{-2\beta y}\right)\right.$$

$$\left. -\beta y e^{-\beta y}\mathrm{Cos}(\beta y) - (\beta y - 1)e^{-\beta y}\mathrm{Sin}(\beta y)\right] \qquad (2.26)$$

which tends to the value of $\frac{3a^2\sigma K}{4\ \mathrm{Sinh}^2 Kd}$ as βy approaches the boundary layer limit, and a maximum of 0.87 $\frac{a^2\sigma K}{\mathrm{Sinh}^2 Kd}$ at βy equal to 2.79. Although equation 2.23 is known to be for laminar flow, Longuet-Higgins (1958) proves that for turbulent but steady boundary layers the flow may be well-approximated by the laminar velocity profile, providing that in the outer part of the layer the kinematic viscosity is replaced by the eddy viscosity. This has been observed by Russell and Osorio (1958), for which the Longuet-Higgins theory well-predicts the mass transport for all values of Kd while the flow was nearly always turbulent, but it is not clear what is meant by turbulent flow in terms of Re. On the other hand, Collins (Sleath (1975)) suggests that transition at the bed starts when the results start to disagree with Longuet-Higgins theory. Also Brebner and Collins (1961) believe that the theory works as long as the flow is not turbulent and when the Reynolds no. is less than 160.

The conduction solution in the interior of the fluid, by Longuet-Higgins, is given as;

$$\bar{U}' = \frac{a^2\sigma K}{4\ \mathrm{Sinh}^2 Kd}\ [2\ \mathrm{Cosh}\ (2Kd(\beta y-1)) + 3 + Kd\ \mathrm{Sinh}\ 2Kd(3(\beta y)^2$$

$$- 4(\beta y) + 1) + 3\ (\frac{\mathrm{Sinh}\ 2Kd}{2Kd} + \frac{3}{2})\ ((\beta y)^2 - 1)] \qquad (2.27)$$

Equation (2.27) and also Stokes mass transport equation have been compared with theoretical results by Russell and Osorio, and they seem to agree with their experimental results (a comparison of the two theories for mass transport with the observed data for this investigation are shown in Chapter 5, Fig. 5.3b). Meanwhile Sleath (1972) says that;(for boundary layer only)

> "discrepancies between the previous theory and experiment are shown to be due to neglect of the higher-order terms and not to the influence of turbulence."

He has studied the motion in the viscous boundary layer up to the fourth order.

2.7 ROUGHNESS EFFECT TO MASS TRANSPORT VELOCITY

Because almost no natural bed is known to be completely smooth, it is of necessity to study the topic of mass transport due to roughness effects. But the vortices which form in a rough boundary make the observation and recording of the velocity more difficult. Measurements which have been made

so for (see 2.4.2.) conclude that the larger the size of roughness the sooner the flow becomes turbulent. Sleath (1974b, 1973) compared the experimental results of Brebner et al. (1966) with the numerical result. The observation was,

"In all cases the effect of bottom roughness, as $u_\infty/(\omega\nu)^{\frac{1}{2}} \rightarrow 0$, was to increase the mass-transport velocity. The increase was most marked for the roughest bed where the mass-transport velocity was approximately double that for a smooth bed. For the finer beds of sand the increase was very much smaller. The theory also shows the mass transport velocity to be increased by bed roughness."

Sleath believes similar effect could occur with sand beds where the theory is for 2-D rough bed, and makes the statement that higher order terms in the M.T. velocity equation could reduce the mass transport velocity.

2.8 FLOW SEPARATION WITHIN THE BOUNDARY LAYER

So far boundary layer flow, has always implied non-separated constant flow and a constant thickness was assumed. Lhermitte (1958) observed that twice in a wave period a regrowth of separation occurs in the laminar boundary layer. The profile of the velocity in boundary layer, from equation 2.6, is shown in Fig. 2.5b. This shows that on two occasions the velocity changes sign. This occurs at about $\pi/4$ and

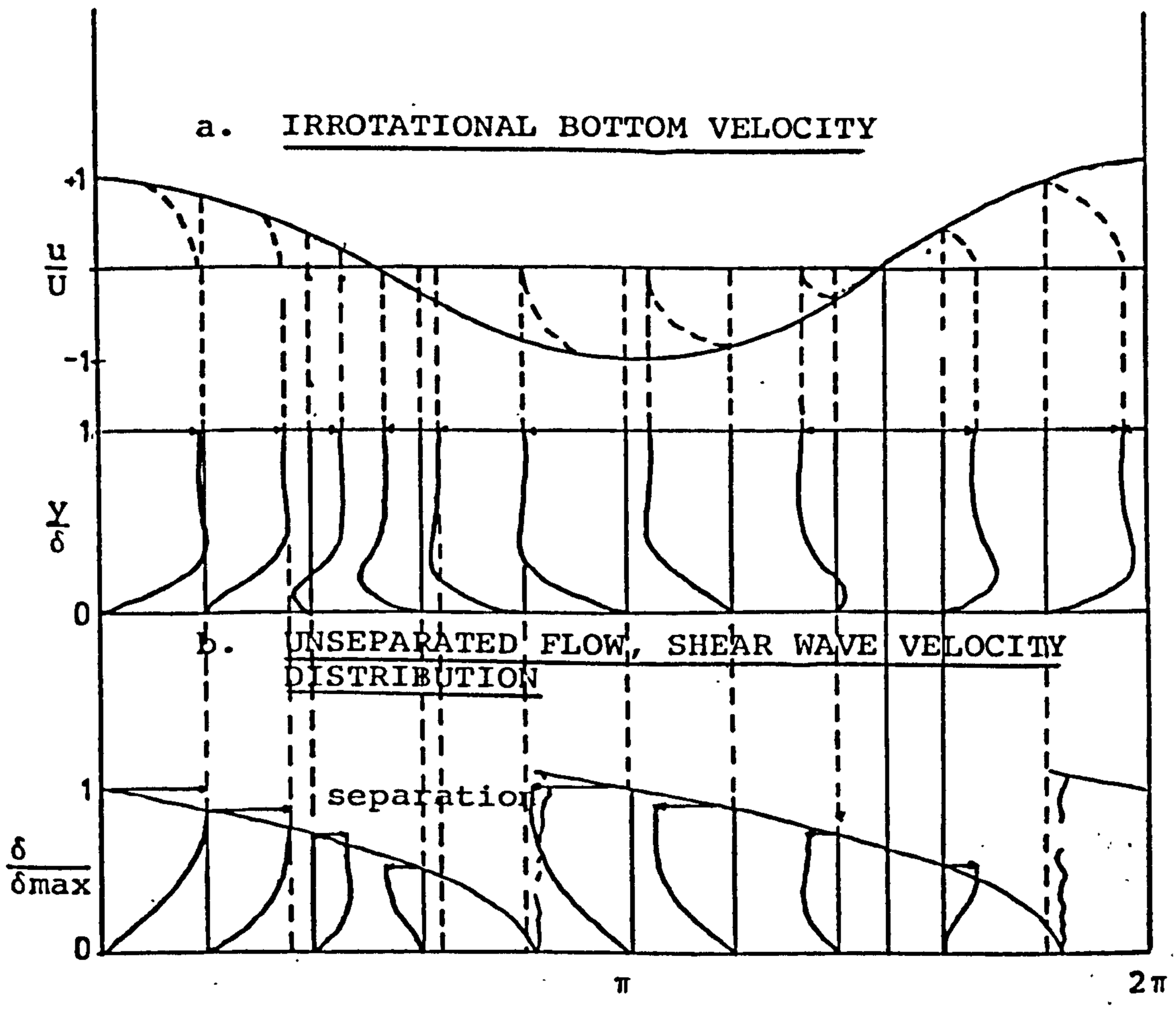

c. Karman-Polhausen Velocity Distribution

Fig. 2.5 Velocity Distribution in Boundary Layer for Separated and Unseparated Flow.

$5\pi/4$ which indicates that the separation occurs near these phase angles.

The velocity distribution within this assumed laminar boundary layer was first determined by the Karman-Polhausen technique (Schlichting 1968). The instantaneous velocity u is in the form of

$$\frac{u}{U} = f(\eta) = a\eta + b\eta^2 + c\eta^3 + d\eta^4 + S \qquad (2.28)$$

where $\eta = \frac{y}{\delta(\theta)}$, $\delta(\theta)$ being the instantaneous boundary layer thickness and the value of η is $0 \leq \eta \leq 1$. with the boundary conditions of;

$$\left.\begin{array}{lll} u = 0 & y = 0 & \frac{\partial u}{\partial y} = 0 \\ u = U & y = \delta & \frac{\partial^2 u}{\partial y^2} = 0 \end{array}\right\} \quad \text{at } y = \delta$$

and neglecting the vertical velocity, the equation 2.28 becomes (Eagleson (1959))

$$\frac{u}{U} = 1 - (1-\eta)^3(1-\eta) - \frac{\delta^2(\theta)}{\nu T}\,\frac{\pi \tan(\theta)}{3}\,\eta(1-\eta)^3 \qquad (2.29)$$

Equation 2.29 is plotted in Fig. 2.5c, which shows separation at

$$\theta' = 2.64 \text{ and } 2.64 + \pi \text{ rad}$$

which is different from the shear wave velocity distribution for separated flow which appears at about $\eta/4$ and $5\eta/4$.

2.9 BOUNDARY SHEAR STRESSES

Boundary shear stresses is one of the topics on which not much work has been done. One of the reasons could be the lack of knowledge about turbulent boundary layers where shear stresses become more important. Amongst the previous workers, Eagleson (1959) has found that the measured shear stresses were many times larger than the theoretical values predicted by the shear wave solution in which;

$$\tau_o = \mu \left(\frac{\partial u}{\partial y}\right)_{y=o} \qquad (2.32)$$

τ_o being the shear stress at bed. For his solution for unseparated flow the shear wave velocity distribution from equations 2.32 and 2.6 is;

$$\tau_o = \mu\beta U \ (\mathrm{Sin}\theta + \mathrm{Cos}\theta) \qquad (2.33)$$

with the limits of integration being $3\pi/4$ and $-\pi/4$ giving the average shear stress under an entire wave as;

$$\bar{\tau}_o = \frac{1}{\pi} \int_{-\pi/4}^{3\pi/4} \tau_o \, d\theta = 0.9 \ \mu\beta U \qquad (2.34)$$

and for separated flow (Eagleson);

$$\tau_o = 0.29\mu\beta U(1.83\alpha^{-\frac{1}{2}}\mathrm{Cos}\alpha - \alpha^{-\frac{1}{2}}\mathrm{Sin}\alpha - \alpha^{\frac{1}{2}}\mathrm{Cos}\alpha - 1.83\alpha^{\frac{1}{2}}\mathrm{Sin}\alpha) \qquad (2.35)$$

for $0<\alpha\leq\pi$ $\qquad \alpha = 1.07-\theta$

with an average of 0.29 $\mu\beta U$ for the shear stress.

By introducing f, the wave friction factor (or resistance coefficient) in the form of

$$f = \frac{2\hat{\tau}_o}{\rho \hat{U}_\infty^2}$$

(where $\hat{\tau}_o$ (max. shear stress) and $\hat{U}_\infty$ (max. velocity at boundary) are out of phase), a new group of equations have been suggested in terms of f.

Kajiura (1968) for smooth turbulent and rough bed, gives the relationship as;

for smooth: $$\frac{1}{8.1\sqrt{f}} + \text{Log}\ \frac{1}{\sqrt{f}} = -0.135 + \text{Log}\ \sqrt{Re} \qquad (2.36)$$

where $Re = \frac{U_\infty a_\infty}{\nu}$

(a_∞ is the orbital amplitude just outside the boundary layer).

for rough: $$\frac{1}{4.05\sqrt{f}} + \text{Log}\ \frac{1}{4\sqrt{f}} = -0.254 + \text{Log}\ \left(\frac{u}{\sigma\kappa}\right) \qquad (2.37)$$

where κ is the roughness size.

Jonsson (1963) deduced a similar equation as;

$$\frac{1}{4\sqrt{f}} + \text{Log}\ \frac{1}{4\sqrt{f}} = -0.08 + \text{Log}\ \left(\frac{u}{\sigma\kappa}\right) \qquad (2.38)$$

while the curve which fits experimental values, by Riedel et al. (1972), has an equation in the form:-

$$\frac{1}{4.95\sqrt{f}} + \text{Log}\ \frac{1}{4\sqrt{f}} = 0.122 + \text{Log}\ \left(\frac{u}{\sigma\kappa}\right) \qquad (2.39)$$

with a much simpler approximation for the limit of

$0.1 < \frac{u}{\sigma\kappa} < 25$

where

$$f = 0.25\ \left(\frac{\alpha\kappa}{u_\infty}\right)^{0.77} \qquad (2.40)$$

Also similar equations have been given by Kamphuis (1975);

$$\frac{1}{4\sqrt{f}} + \text{Log}\ \frac{1}{4\sqrt{f}} = -0.35 + \frac{4}{3}\ \text{Log}\ \left(\frac{u_\infty}{\sigma\kappa}\right) \qquad (2.41)$$

which is valid in the region $5 < \frac{u}{\sigma\kappa} < 5\text{x}10^3$, and an approximation to equation 2.41 when $\frac{u}{\sigma\kappa} < 100$,

$$\text{and} \quad f = 0.4\ \left(\frac{\sigma\kappa}{u}\right)^{0.75} \qquad (2.42)$$

The experimental study of boundary shear, whilst being a topic which requires investigation, was considered to fall outside the range of the present work.

CHAPTER THREE

INSTRUMENTATION

3.1 INTRODUCTION

The content of this chapter is divided into two major parts. The first part covers the wave channel and wave probe instruments, and the second part is a brief study of "Laser Doppler Velocimeter" (L.D.V. the flow measuring equipment).

3.2 WAVE CHANNEL AND WAVE MEASURING INSTRUMENTS

3.2.1 General

A basic study of boundary layer and shear stress due to wave action, requires a simple harmonic oscillation between the fluid and the bed. So far three methods of obtaining this effect have been used; (i) The oscillating bed under a body of water within the confines of a flume (Bagnold (1946), Kalkanis (1964), Li (1954), Manohar (1955)), (ii) Water tunnel or U-tube type in which the body of water is driven by air pressure on the water surface (or a piston inside the water) and simple harmonic oscillations of the fluid are produced in a working section (Jonsson (1963), Carstens and Neilson (1976)), (iii) The wave channel, in which a block of water above a fixed bed is oscillating (Chakrabarti (1980), Beech (1978)), for which more information is available by Riedel et al. (1972). Each method

has its advantages which are listed in Table 3.1. For this investigation the third method (wave channel) has been selected.

3.2.2 The Wave Channel

3.2.2.1 The Channel

The wave tank with a wave generator at one end and wave breaker at the other end, was originally manufactured by Armfield Engineering Limited. Excluding the two ends, the possible working area of the channel has 5.7 m length with 0.3 m width and 0.5 m depth. The transparent glass walls of the channel produces good visual inspection ability as well as a smooth boundary on the sides. The tank is mounted rigidly on the top of a steel structure which can adjust the inclination of the whole length of the tank (Fig. 3.1).

3.2.2.2 Wave Generator

At the upper end of the channel a 0.6 m x 0.3 m flap is connected by a rod to a variable pitch cam on a pully which is run by the driving motor (Fig. 3.2). The angular velocity of the motor is adjustable to the required wave period (within the possible range); the full details of the wave generator are given by Beech (1978).

3.2.2.3 Wave Breaker

An aluminium frame was designed as a wedge shape (a

	ADVANTAGES
Oscillatory bed	1. High speed studies for oscillatory flow. 2. Quickly settles.
U-Tube	1. Very good simple harmonic oscillation at working section.
Wave channel	1. Close to real wave situation. 2. For mass transport velocity studies.

Table 3.1. The advantages of different methods for oscillatory flow studies.

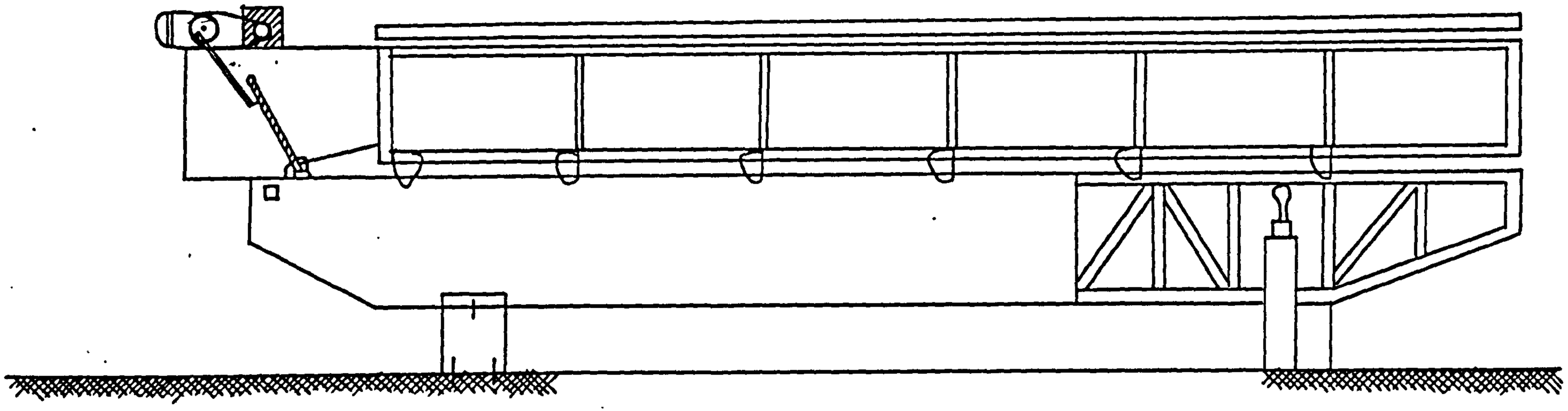

FIG 3.1 THE WAVE CHANNEL

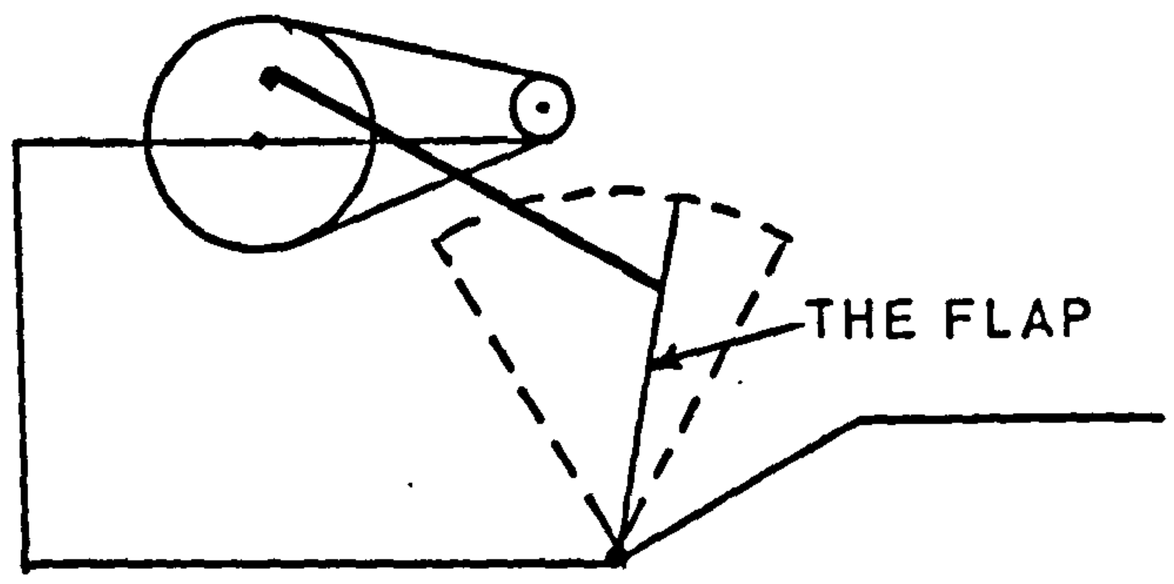

FIG 3.2 THE WAVE GENERATOR

triangle and quadratic prism which are joined at the base, Fig. 3.3), and was filled by expanded aluminum mesh (Explofoil) for its wave energy absorption property.

The mechanism of this is very simple. As the wave approaches the wedge some of the wave passes through it and some will be reflected. Because the wave hits it non-normal incidence therefore the part which is reflected will be in an angle also (Fig. 3.4), and because the incident angle is large, the reflected wave continues towards the down-stream of the channel and goes through the same process again until it reaches the second part of the wedge, which lets the wave pass through only absorbing most of the wave energy. The measured oscillation of the water beyond the wave breaker was about 15% of the incident amplitude. Now considering that the reflected wave from the end of the tank had to go through the same procedure but in reverse, then the actual reflected wave had an amplitude of less than 2.5% of the incident wave. The results and discussion of the tests which have been carried out on the effectiveness of the wave breaker and working section area are shown in Appendix B.

3.2.3 Wave Celerity Probe

Two identical probes were used to measure the wave characteristics (period and wave length). Plate 3.1a shows one of the probes with the timer and the control box (the

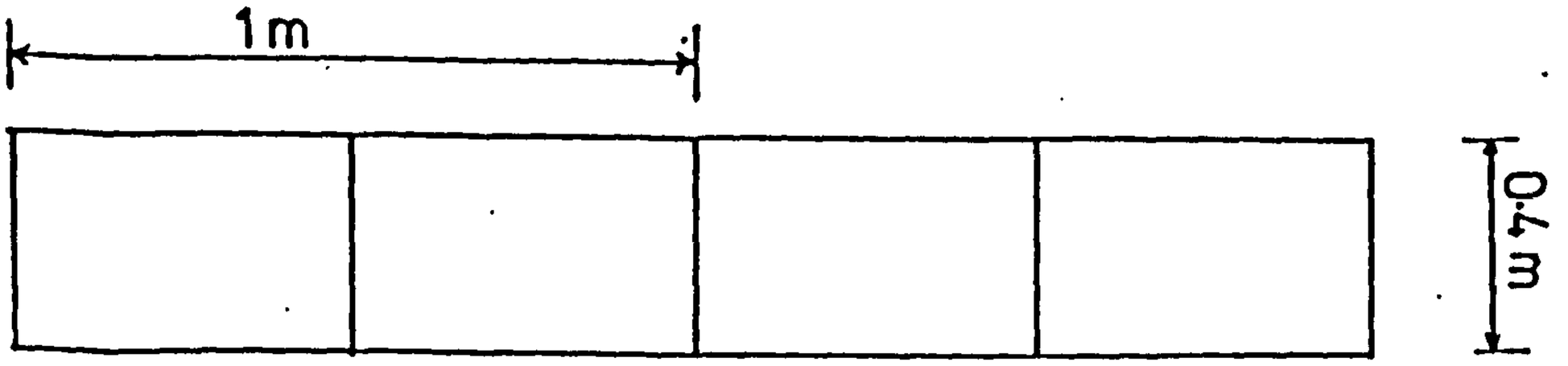

(a) side view

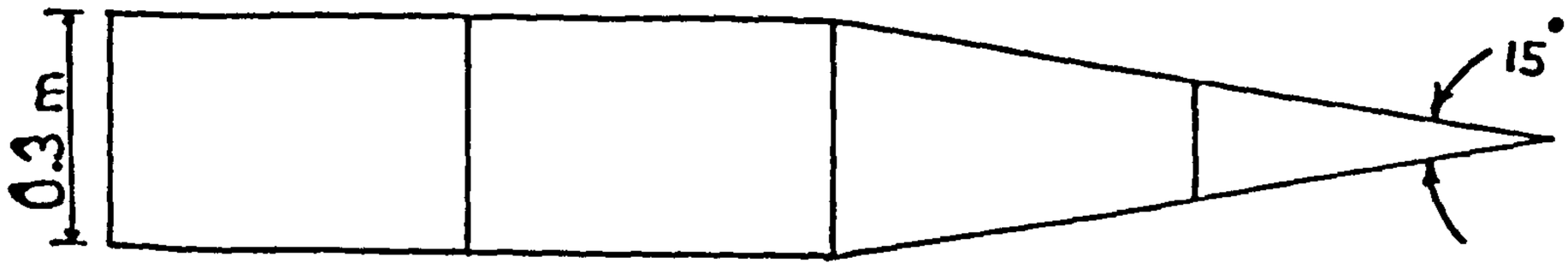

(b) plan view

FIG 3.3 WAVE BREAKER

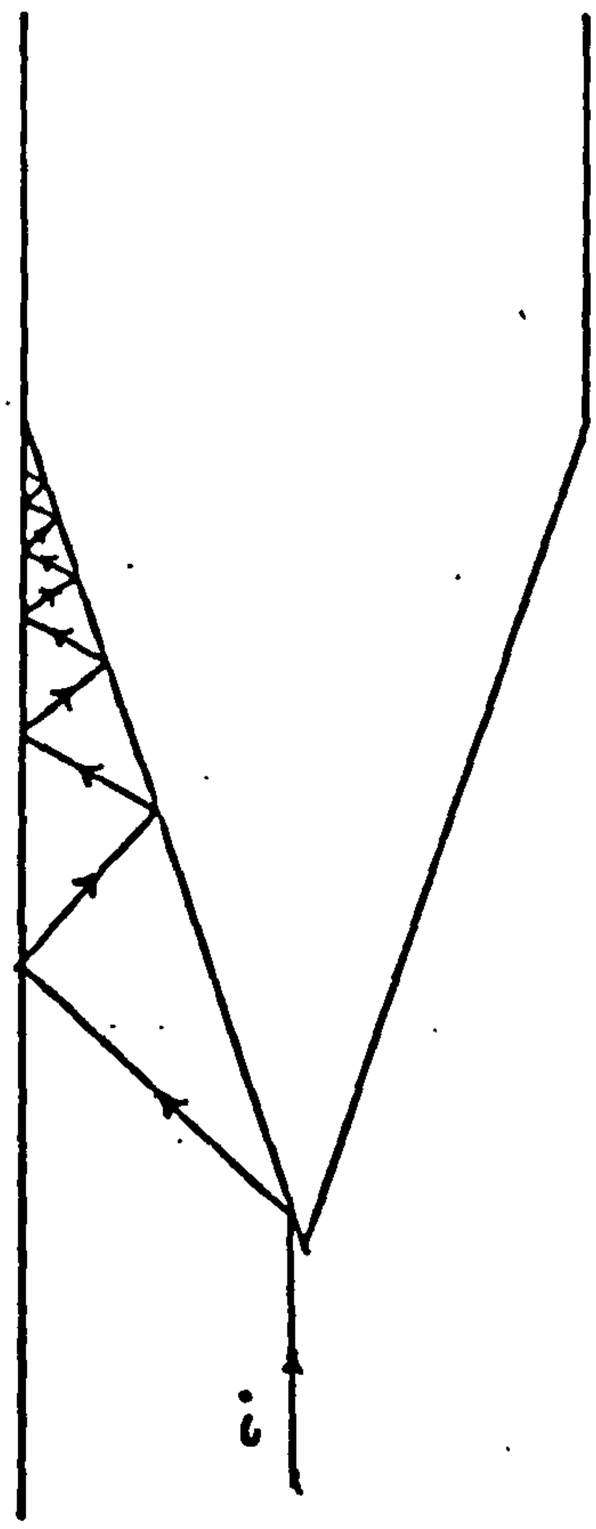

FIG 3.4 WAVE DIFFRACTION

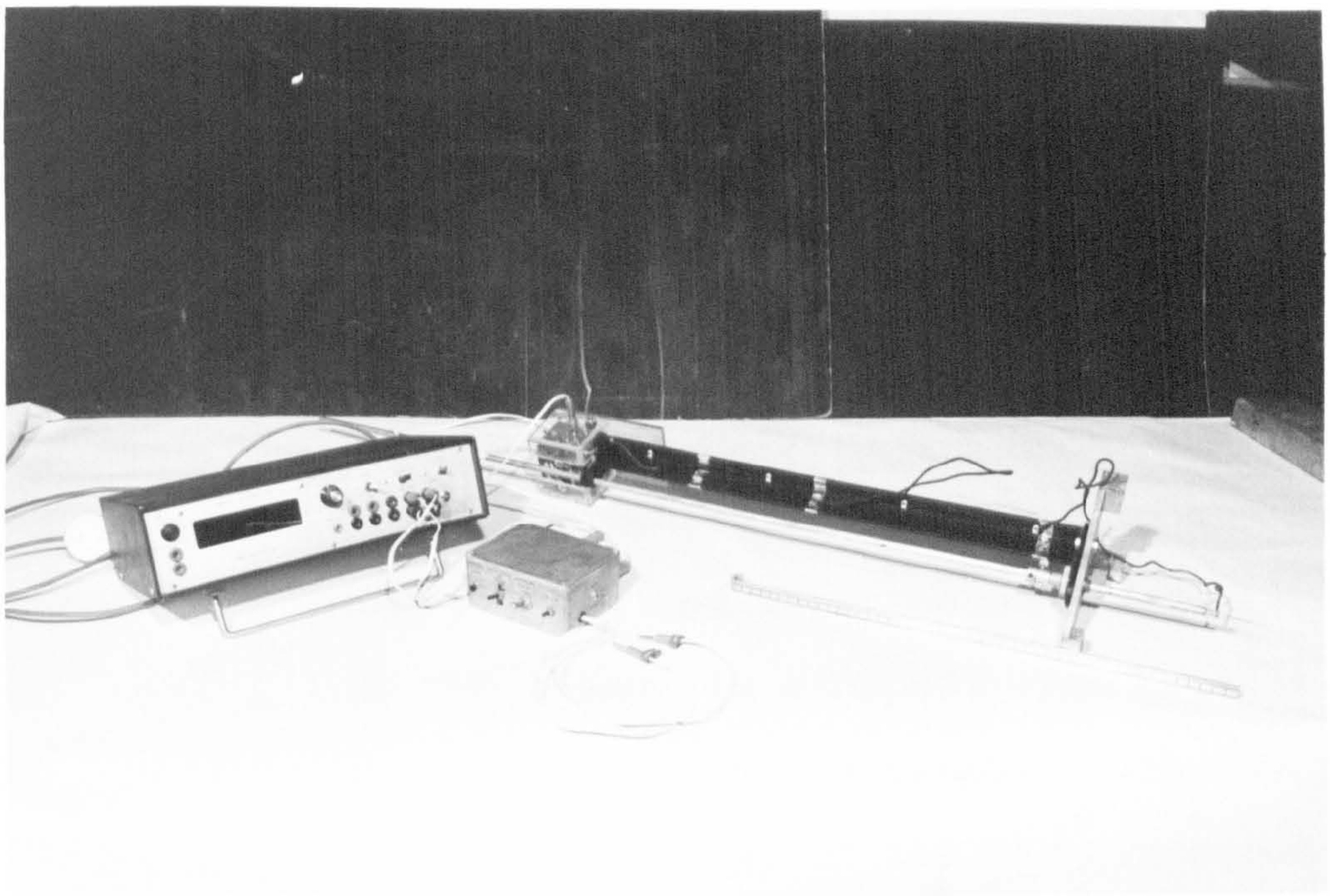

3.1(a) Wave Celerity Probe and Tim er.

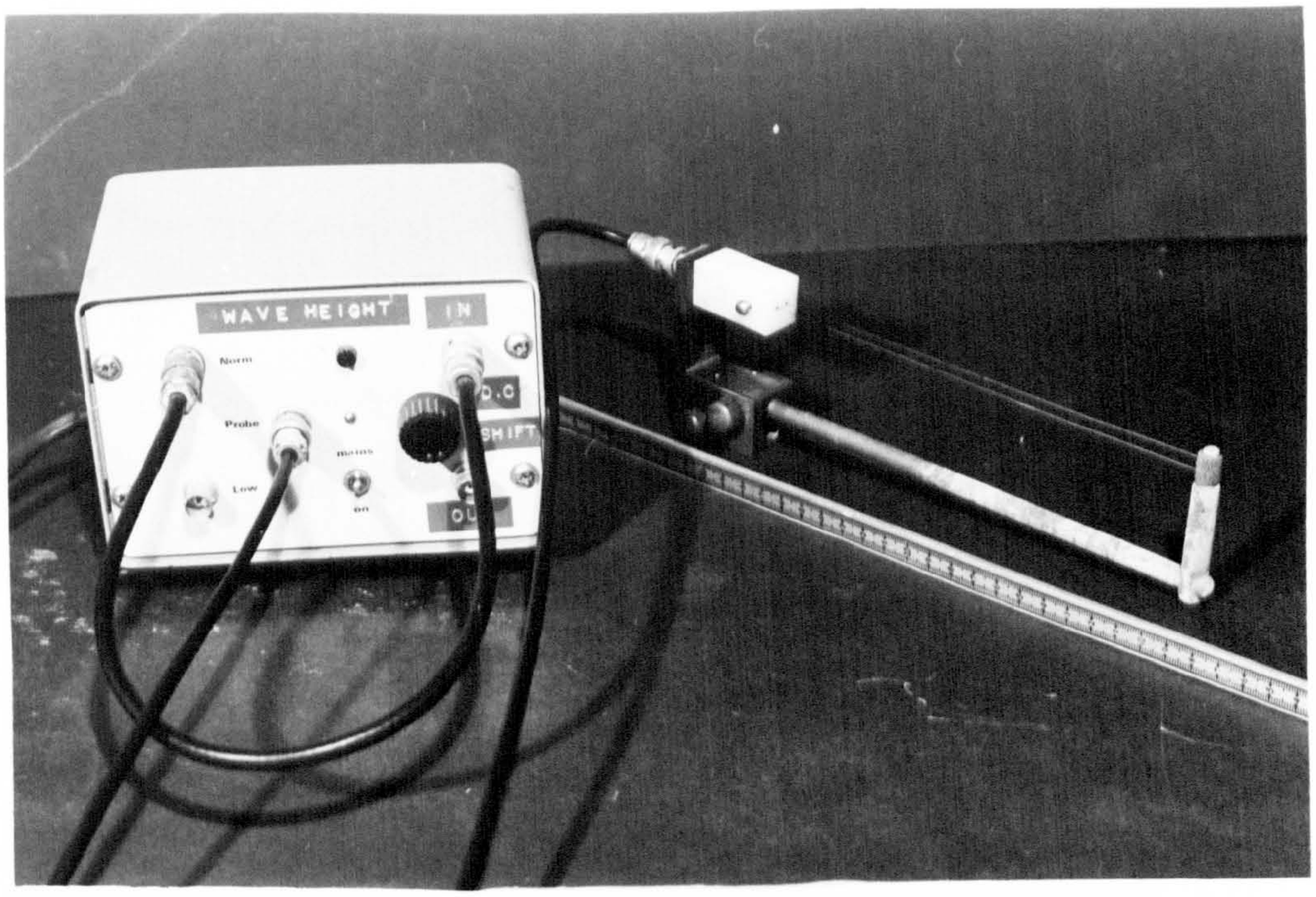

3.1(b) Wave Surface Probe and D.C. Shift.

Plate 3.1 Wave Probes

principle and construction of the probes are fully explained by Beech (1978)).

Fig. 3.5 shows the mode of operation of the two probes in order to measure the velocity of the wave. When the wave touches the first probe, which is connected to the START switch, timing is started and when the same wave touches the second probe the timing is stopped. The transit time between the probes is shown on the timer. With the probes being 1 m apart, the reciprocal of the time recorded is the wave speed.

If the START and STOP switches are connected to the same probe, then the time recorded would be the period of the wave. Knowing this and the velocity, the wave length can be determined (L = C.T).

3.2.4 Wave Surface Probe

The surface profile of the wave was observed using a standard wire gauge in a closed loop form. Control was by use of an electronic circuit, the output of which was fed into a D.C. shift facility and amplifiers for output signal conditioning.(Plate 3.1b).

Fig. 3.6 shows the probe in operation. Because of the dielectric behaviour of the coating of the wire sandwiched between its copper core and water, it forms a capacitor the impedance of which is proportional to the submergence

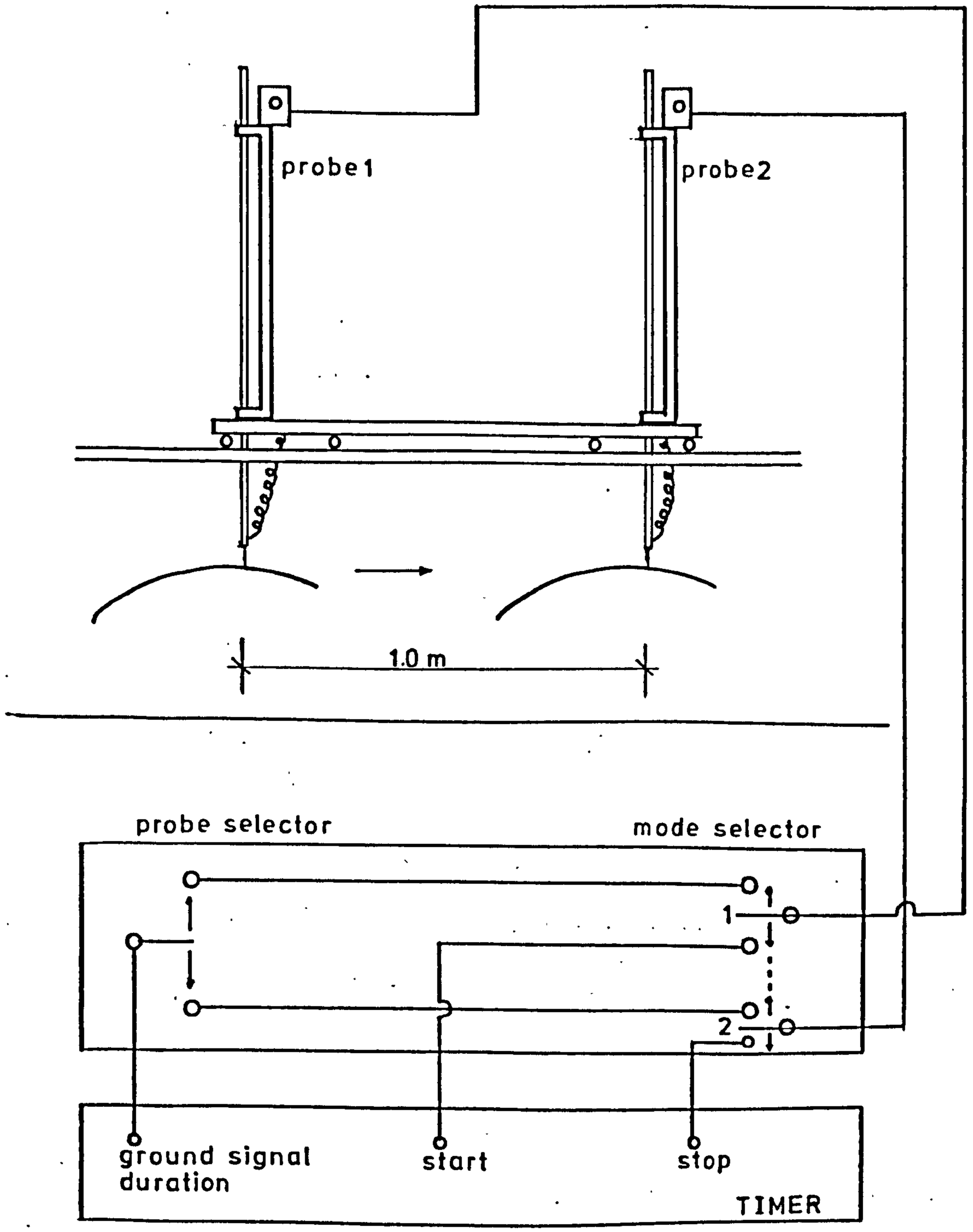

FIG 3.5 WAVE CELERITY PROBES

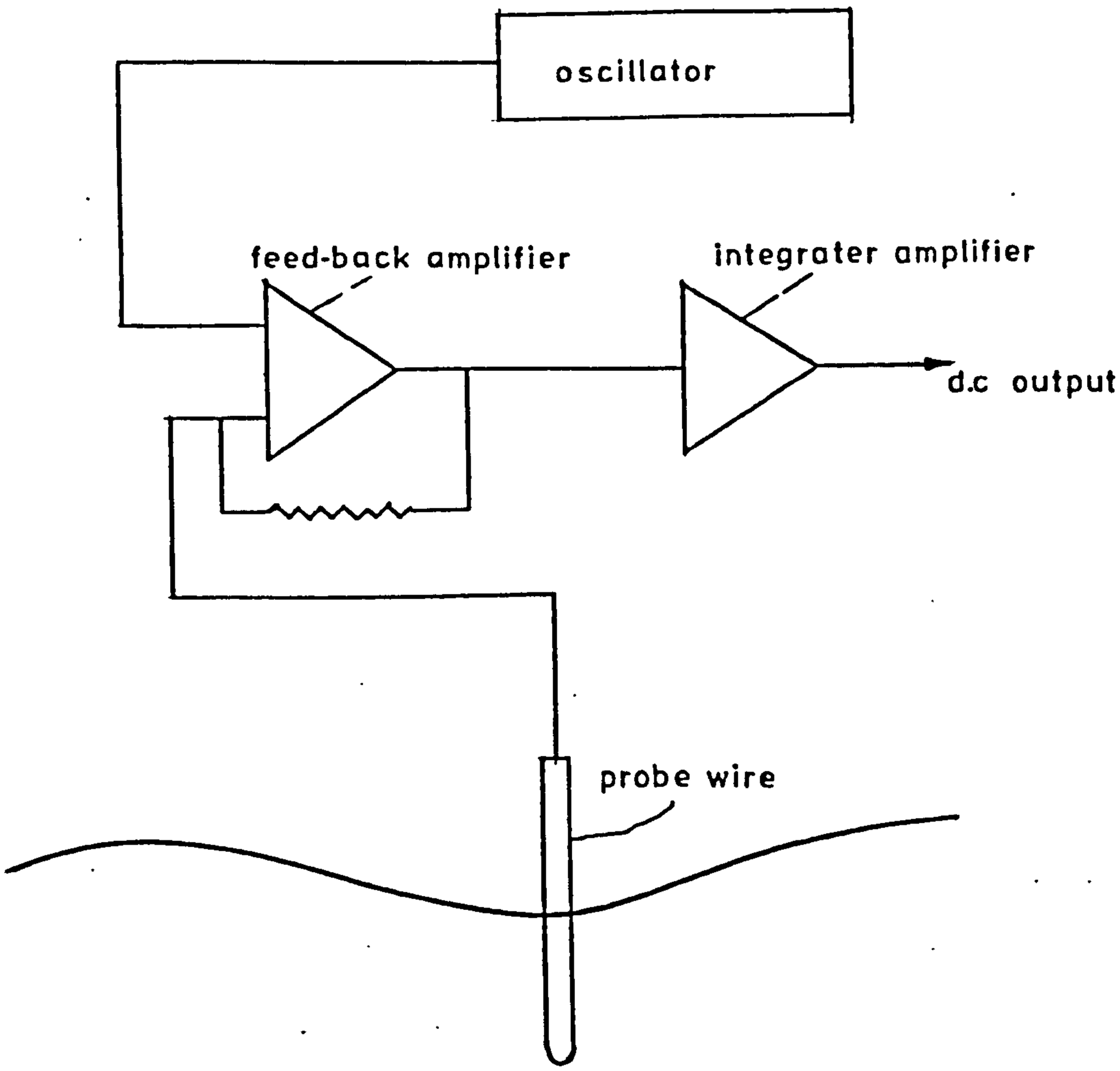

FIG 3.6 WAVE SURFACE PROBE

in the water. Therefore the impedance of the wire is compared with that of a resistor in a feed-back circuit and an integrator stage converts the combined signal to single analogue fluctuating output d.c. voltage (as before Beech (1978) has discussed the principle of the equipment in full detail).

3.2.5 Tests on the Channel

Many tests have been performed by Beech (1978) into the applicability and accuracy of the wave surface probe and satisfactory results have been achieved. Also some preliminary tests on the wave channel, the attenuation of wave, wave settling time and various other performance characteristics testing have been done which are discussed by Beech (1978).

3.3 THE FLOW MEASUREMENT EQUIPMENT

3.3.1 General

Measurements of fluid velocities have been made by many investigators using conventional methods such as pitot tubes, hot films or other methods such as tension wire (Sleath (1970)), hydrogen bubble technique (Horkawa and Watanabe (1969), electrolytic measurements (Boyer (1956)), electromagnetic flow measurements (Shercliff (1962)). But the main disadvantage of all of these methods is either the disturbing of the water by the measuring instruments so

altering the flow pattern, or the poor response of these methods to low velocities of water especially in oscillating conditions when the response should be quick.

The disadvantages of the above techniques desired the development of an instrument which does not require the insertion of a probe or wire into the fluid as well as high resolution and the advantage of measuring very low velocities.

Therefore in the past few years the interest in the possibility of underwater measurement using laser techniques has increased and sophisticated instruments and systems in conjunction with this attitude have been developed. Laser Doppler Systems for measuring fluid velocity have been subject to many investigators (Blake and Jespersen (1972), Manning, (1973)), and many authors (Richards (1977), Watrasiewicz & Rudd (1976), Drain (1980)). However, because the subject of the Laser Doppler Velocimeter (L.D.V.) is a very important issue for this study, a brief theory of L.D.V. is presented here, as well as the ancillary instrumentation associated with it.

3.3.2 The Laser Doppler System

3.3.2.1 Laser

Light Amplification by Stimulated Emission of Radiation (laser), produces light beams with power densities many millions of times greater than ordinary light, with wave oscillation of 10^{14} per second and wavelength of 10^{-5} m

(10 μm) and highly monochromatic. Apart from this the laser is remarkable for being "coherent", which means that it is composed of regular and continuous waves, like those emitted at much lower frequencies by radiotransmitters (Fishlock (1967)).

3.3.2.2 Doppler Effect

When the relative distance between an observer and a second source gets less, the observer encounters waves more frequently (higher noise pitch); if the relative distance is getting larger then the effect is less frequent waves (lower noise pitch). The phenomenon of frequency change in propagation of waves (sound or light), due to relative movement of the source is called 'Doppler' effect (the everyday examples are passing trains or fast cars which have a drop in the noise pitch as they pass an observer).

A laser beam, because of being highly coherent, can be used in velocity measurements based on the Doppler effect.

3.3.2.3 Principle of Laser Doppler Velocimeter

Laser Doppler velocimeter (L.D.V.), which is one of the systems discussed by Greated (1971), measures the frequency shift of light scattered by a moving particle in a fluid (unless special precautions have been taken, all fluids contain small impurity particles such as specks of

dust, air, bubbles or algae. DISA L.D.V. makes use of contaminants whose dimensions are between 1 μ and 10 μ (DISA instruction manual)). If this particle is moving with a velocity of v and is picked up by a beam of laser light frequency f_o and wavelength λ_o along the unit vector $\hat{e}_o$, a stationary observer receiving scattered light along $\hat{e}_s$ will only receive light of frequency f_s (Fig. 3.7). The relationship between f_s and v can be shown to be (Lennet (1972))

$$f_s = f_o + \frac{v}{\lambda_o} (\hat{e}_s - \hat{e}_o) \tag{3.1}$$

or the Doppler frequency shift which is

$$f_D = \frac{v}{\lambda_o} (\hat{e}_s - \hat{e}_o) \tag{3.2}$$

But, because the Doppler frequency shift is somewhere between 10^5 and 10^8 Hz (Richards (1977)) and the frequency of the laser light is of the order of 10^{14} Hz, a direct measurement of the frequency of scattered light is almost impossible, since it requires an instrument with a very high resolution (better than 10^{-6}%), which is why the most important part of a laser Doppler velocimeter is its optical arrangements, and hence the different settings or modes of operation are introduced. The most popular modes of operation are; (a) reference beam, (b) single-beam or virtual fringe model and (c) dual beam or fringe beam (Fig. 3.8). Different modes of operation (including these three) have been

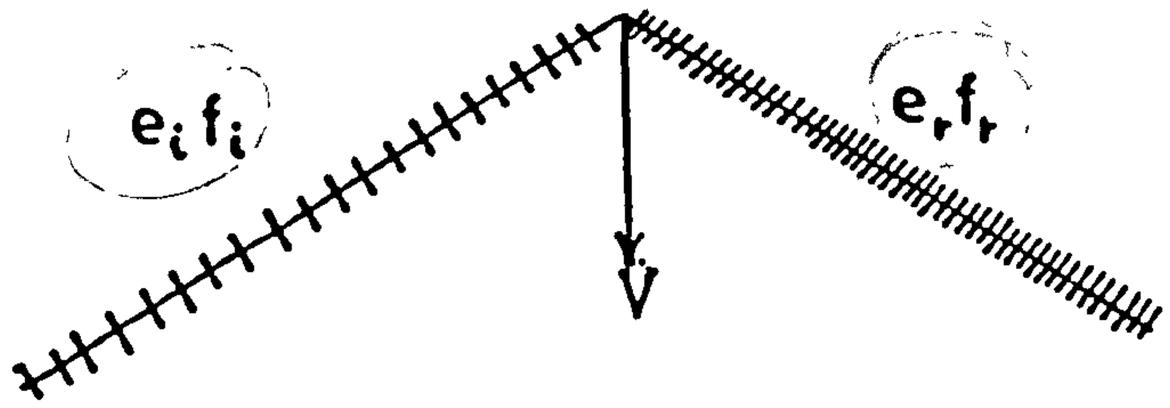

FIG 3.7 DOPPLER EFFECT

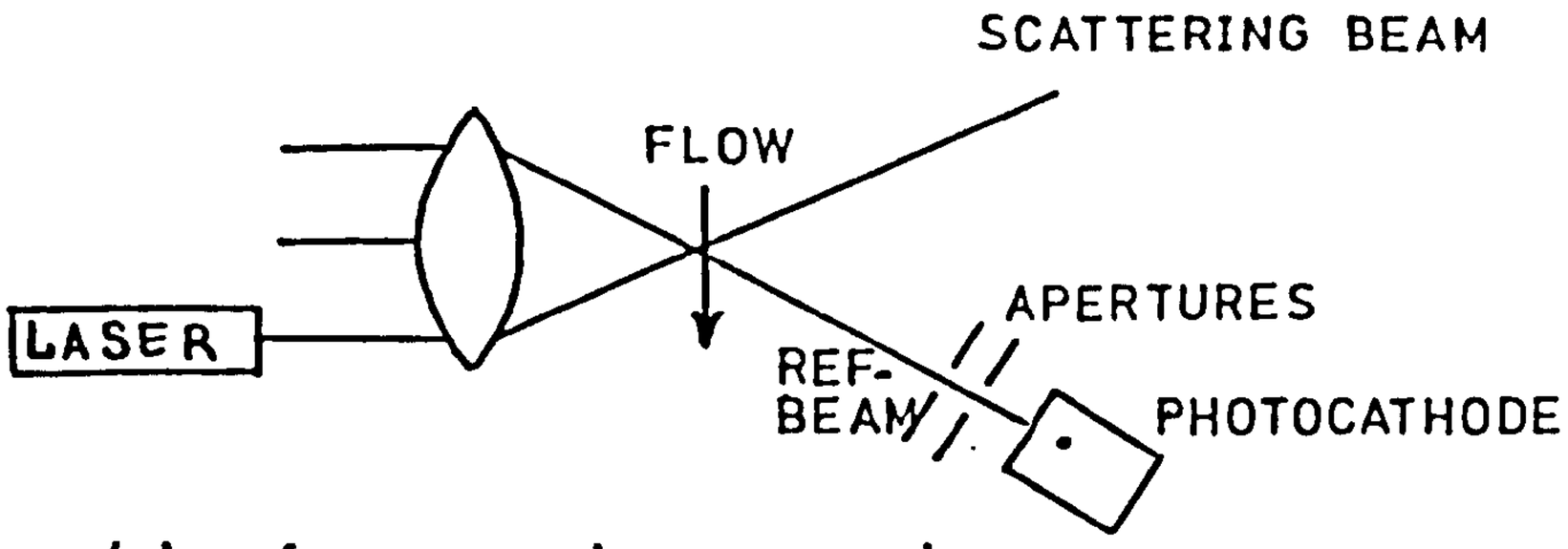

(a) reference - beam mode

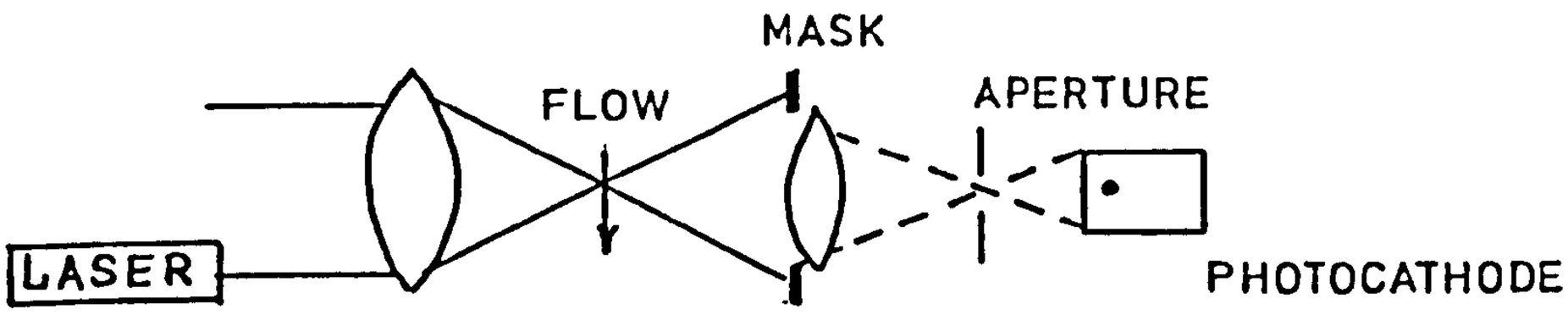

(b) fringe - dual beam mode

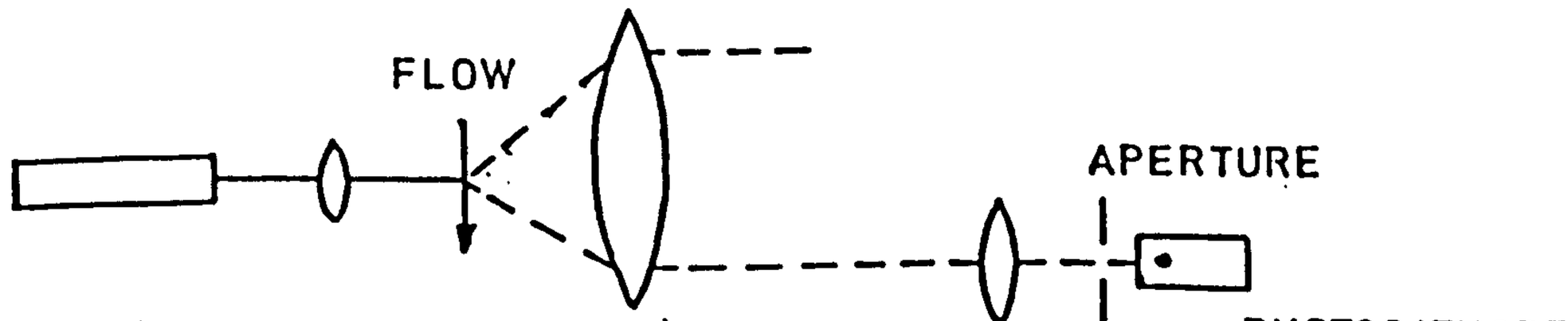

(c) single - beam mode

FIG 3.8 OPTICAL ARRANGEMENT

discussed in full detail by Drain (1980), Watrasiewiez and Rudd (1976), DISA (instruction manual) and many more. The most popular mode for laboratory measurements is the dual beam or fringe mode which is easy to operate and therefore of more practical use.

In this case two beams of equal intensity illuminate the moving particle (Fig. 3.9) and therefore equation 3.2 can be written for both beams (Blake (1972)) as;

$$f_{D1} = \frac{v}{\lambda_o} (\hat{e}_s - \hat{e}_{o1})$$

$$f_{D2} = \frac{v}{\lambda_o} (\hat{e}_s - \hat{e}_{o2})$$

and the combination of the two is therefore independent of the viewing direction $\hat{e}_s$

$$f_D = f_{D1} - f_{D2} = \frac{v}{\lambda} (\hat{e}_{o2} - \hat{e}_{o1})$$

If the angle between the two beams is θ and the angle between the normal to the fringe planes and the direction of the moving particle is α, then;

$$f_D = \frac{2v \ \mathrm{Sin}\ \theta/2 \ \ \mathrm{Cos}\alpha}{\lambda_o} \qquad (3.3)$$

or if $\alpha = 0$, then;

$$f_D = \frac{2v \ \mathrm{Sin}\ \theta/2}{\lambda_o} \qquad (3.4)$$

Now, considering the region of intersection of the two beams, a measuring volume which includes sets of fringes is produced

(Fig. 3.10). This volume which is known as the probe volume (Drain (1980)) as well, is the volume within which a scatter centre will produce photodetector signals larger than $1/e^2$ of those produced by a scatter centre located in the centre of the volume (Fig. 3.11).

The probe volume consists of fringes with spacing d which is given by;

$$d = \frac{\lambda/2}{\sin\ \theta/2} \qquad (3.5)$$

where λ is the wavelength of the laser light. Now if we consider a particle crossing these fringes, it will block off a lot of light in passing a bright fringe and only a little light in a dark fringe. Therefore, if the transmitted light is collected, it fluctuates at the rate at which the particle crosses the fringes. This will modulate the light at a frequency of v/d where v is the particle velocity crossing the probe volume. Thus the frequency shift is given by;

$$f = \frac{2v\ \sin\ \theta/2}{\lambda}$$

which is the same value as obtained for doppler shift f_D.

3.3.3 Some Remarks about L.D.V.

3.3.3.1 Measurements in Liquid Flow

The derived formula for L.D.V. (equation 3.4) is valid for measurements in air (or vacuum). For measurements in

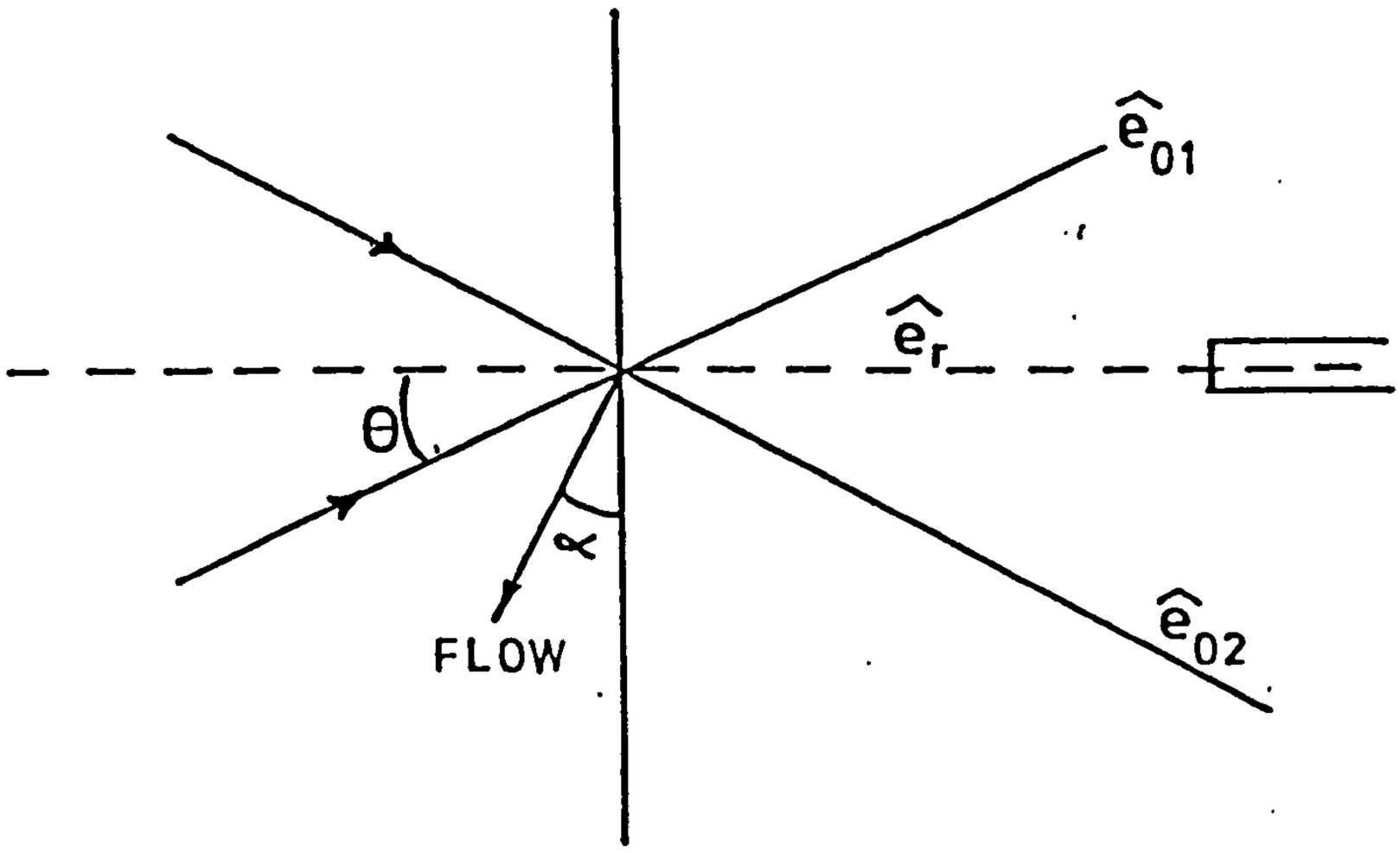

FIG 3.9 DUAL BEAM MODE

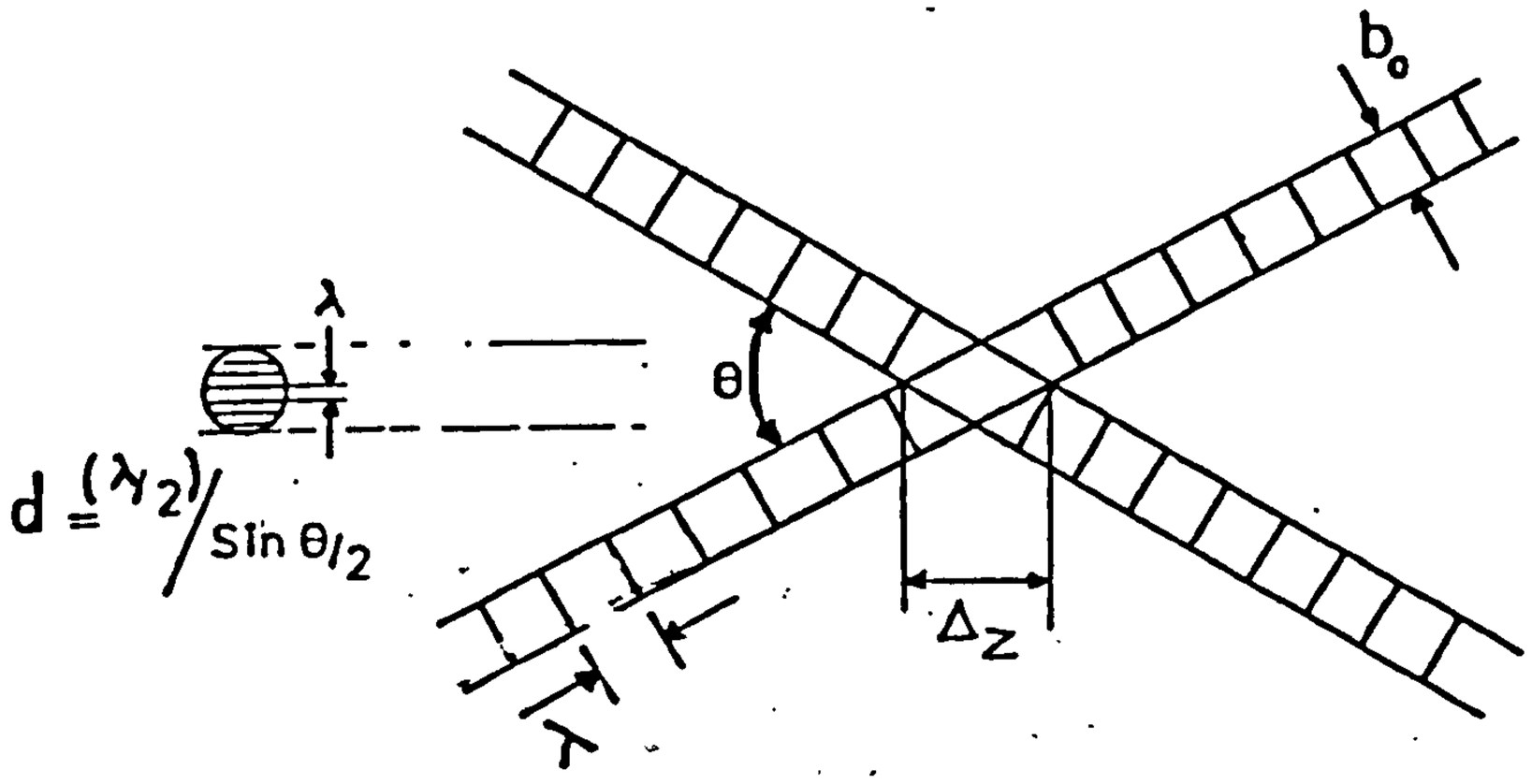

FIG 3.10 FRINGES PRODUCED BY DUAL BEAM

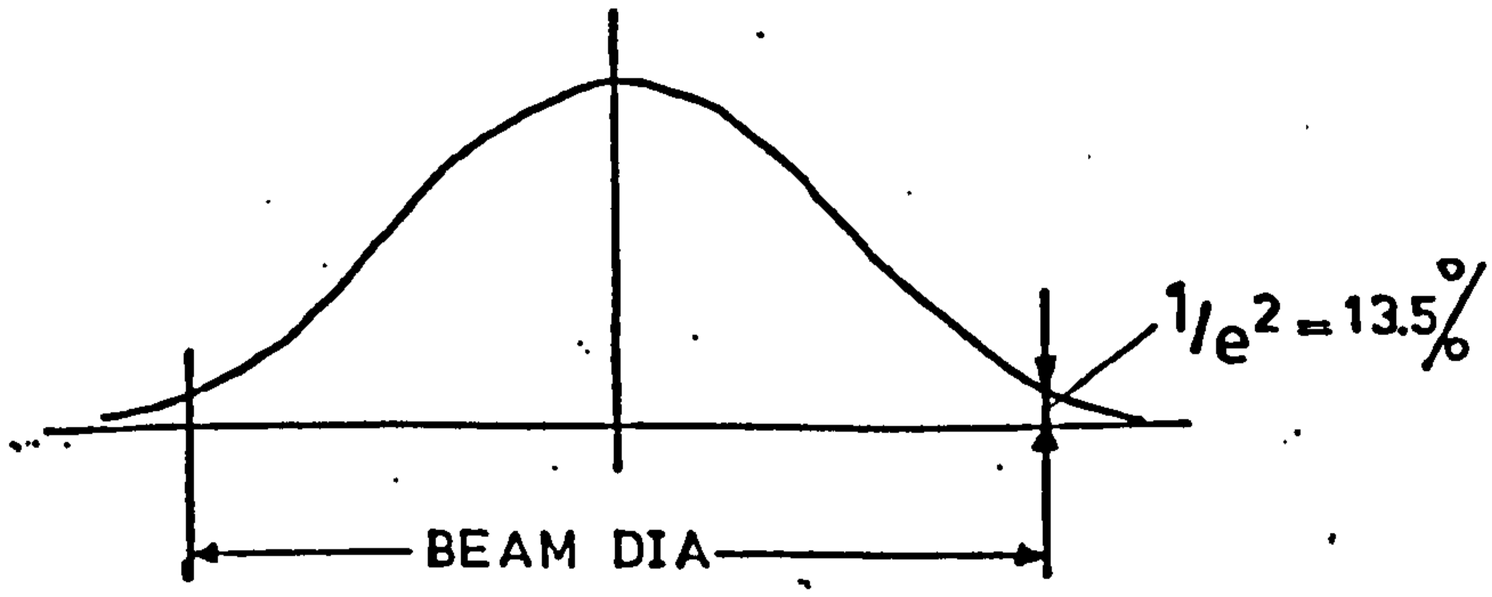

FIG 3.11 GAUSSIN LIGHT INTENSITY DISTRIBUTION

liquid with refractive index n_ℓ the laws of refraction should be included.

If λ_ℓ and λ are the wavelengths of laser light in a liquid and air, then;

$$\left.\begin{aligned} \lambda_\ell &= \frac{n}{n_\ell}\,\lambda \\ \text{and} \qquad \text{Sin}\ \theta_\ell/2 &= \frac{n}{n_\ell}\ \text{Sin}\ \theta/2 \end{aligned}\right\} \qquad (3.6)$$

where θ_ℓ and θ are the angles of intersection of the beams in the liquid and in air (Fig. 3.12).

Therefore $$\frac{\lambda}{\text{Sin}\ \theta/2} = \frac{\lambda_\ell}{\text{Sin}\ \theta_\ell/2}$$

and hence equation 3.4 can be written as;

$$f_D = \frac{2v\ \text{Sin}\ \theta_\ell/2}{\lambda_\ell} = \frac{2v\ \text{Sin}\ \theta/2}{\lambda}$$

3.3.3.2 Measurement of Flow Direction

A fundamental problem in L.D.V., for beating or fringe modes of operation, is the discrimination of the velocity direction, because the Doppler frequency is the difference of two frequencies and it is not possible to tell which one is higher. Therefore a change in sign of velocity produces no difference in frequency. In some applications the direction of the flow is either known or the optics could be orientated to give the positive direction, or it is always the same. But the problem especially arises for oscillatory

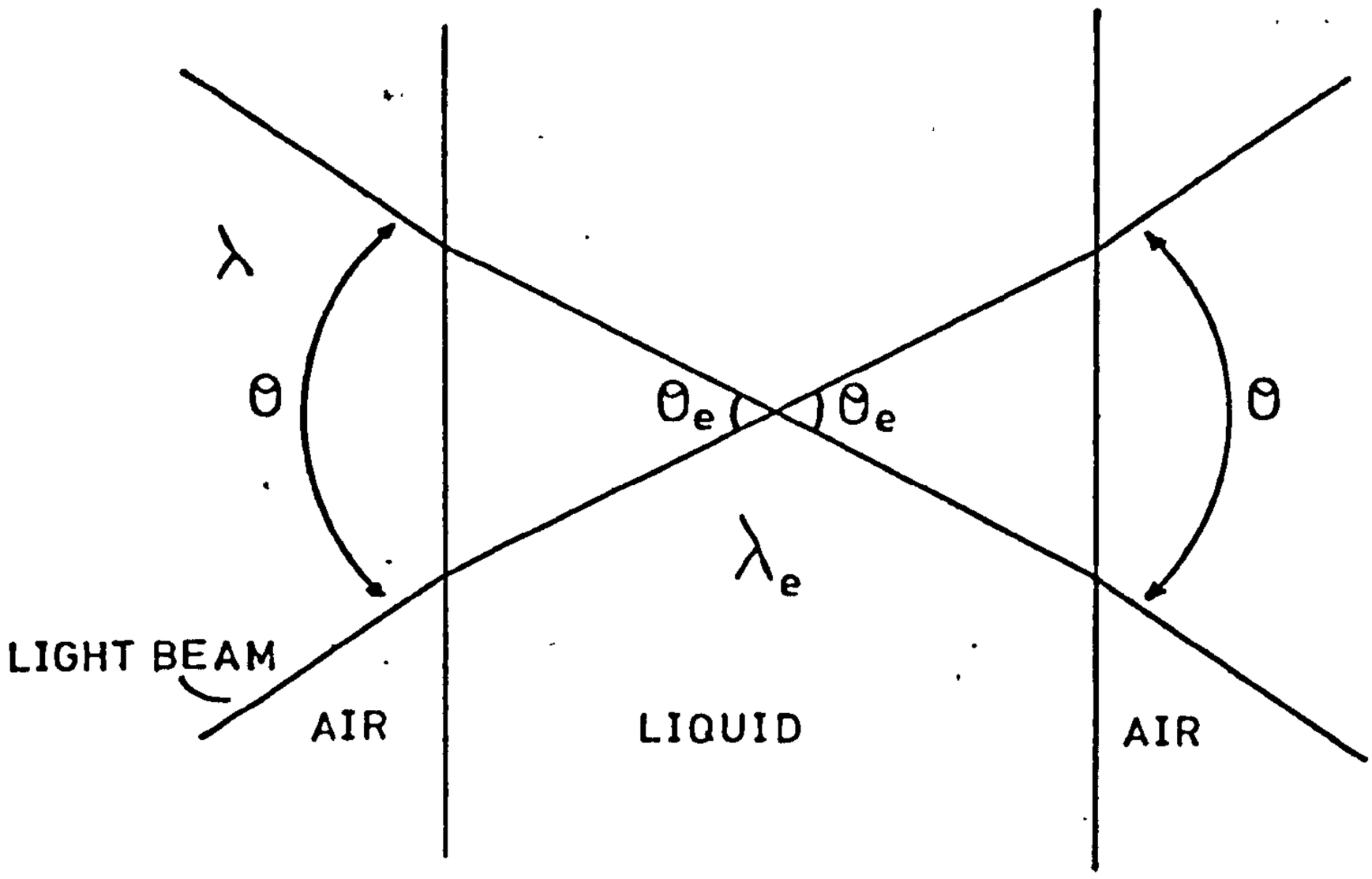

FIG 3.12 REFRACTION OF LIGHT IN THE LIQUID.

flow in which the direction of the velocity rapidly changes and therefore a negative velocity requires a negative frequency (since $v = \frac{f_D \lambda}{2 \text{ Sin } \theta/2}$ and λ and Sin $\theta/2$ are positive therefore f_D must be negative for negative v).

But there are techniques to overcome this problem. Probably the most commonly used technique for directional discrimation involves shifting the frequency of the light beam (Drain (1980)). If the laser light frequency is f and the Doppler frequency f_D then the frequency of the scattered light is $f - f_D$ or $f + f_D$ (depending on the direction of flow),

But if the frequency of the light is increased by f_s where $f_s > f_D$, then the corresponding beat frequency on the velocimeter would be $f_s - f_D$ or $f_s + f_D$ which is greater than zero. Hence knowing the value of the shift frequency and taking that value for zero velocity, positive and negative values of velocity can be recorded.

3.3.3.3 The Advantages and Disadvantages of L.D.V.

Since the first measurements of fluid velocity by Yeh and Commins in 1964 using the Doppler shift of laser light many investigators have been using L.D.V. more and more for accurate measurements (according to Greated (1971), the instantaneous velocity can be measured up to an accuracy of

5% and still this can be improved by time averaging of velocity records).

L.D.V. is a field still in rapid development and the presently available equipment is by no means perfect. Even so L.D.V. has many advantages over other conventional methods, as well as some disadvantages. Notwithstanding the advantages and disadvantages given by Drain (1980), table 3.2, L.D.V. is the best system for measuring the oscillatory viscous boundary layer since it facilitates the measurement of velocity very close to the bed (0.5 mm from bed).

3.3.4 The Equipment

A 10 mW Helium-Neon laser model 3225H-PCS supplied by DISA was mounted on a steel plate (Fig. 3.13) screwed to the optics (the DISA optical system included beam splitter type 55LO2 and frequency shift adaptor type 55LO2). The whole instrument was placed on a DISA optical bench for horizontal distance adjustments (if necessary), which was fixed on a traverse assembly (Beech (1978)). The vertical movement of the assembly, and therefore laser optics, was controllable to an accuracy of 0.02 mm (Plate 3.2). The scattered light was then collected on the side of the channel opposite to the laser by a DISA photomultiplier type 55L10, and with the help of a High Voltage supply source to the photomultiplier (the supply voltage was about 1.1 KV), the Doppler shift frequency was detected and directed to a DISA Doppler signal processor (including

ADVANTAGES	DISADVANTAGES
1. Does not disturb the flow.	1. Medium must be transparent.
2. High spatial resolution.(depending on the diameter of the beam and angle of intersection.)	2. Needs scattering particles: artificial seeding may be necessary.
3. Fast response	3. Optical access is required: windows may have to be installed.
4. Response is linear and easily calibrated.	4. Expensive signal processing equipment may be required in difficult situations where the signal to noise ratio is poor.
5. Directional discrimination possible.	5. Not well suited for measurements of total flow as this requires a tedious investigation over a cross section.
6. Operation not usually seriously affected by temperature.	

Table 3.2. Velocity Measurement by L.D.V. (after Drain).

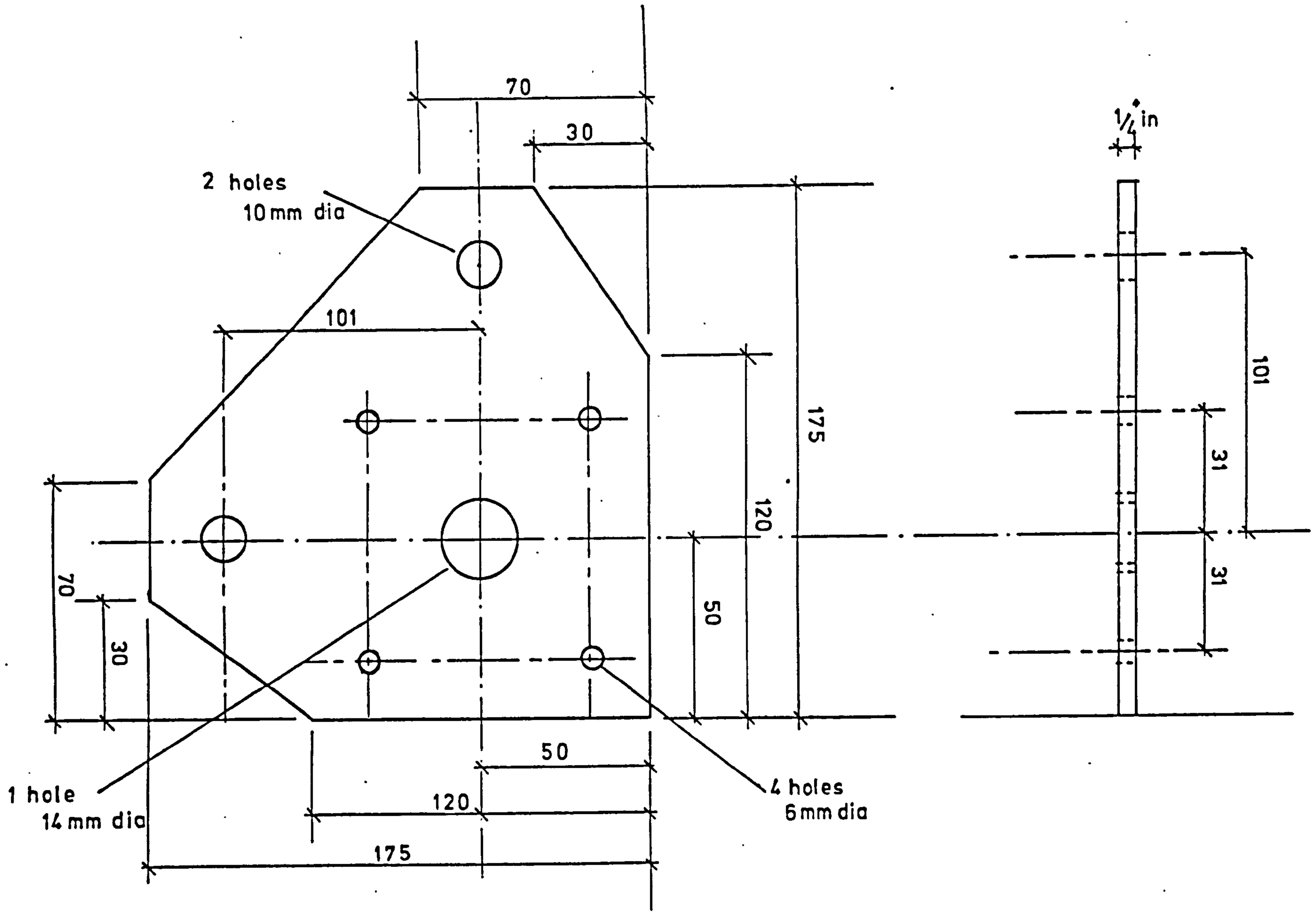

Figure 3.13 Steel Plate Joining the Laser to the Optics.

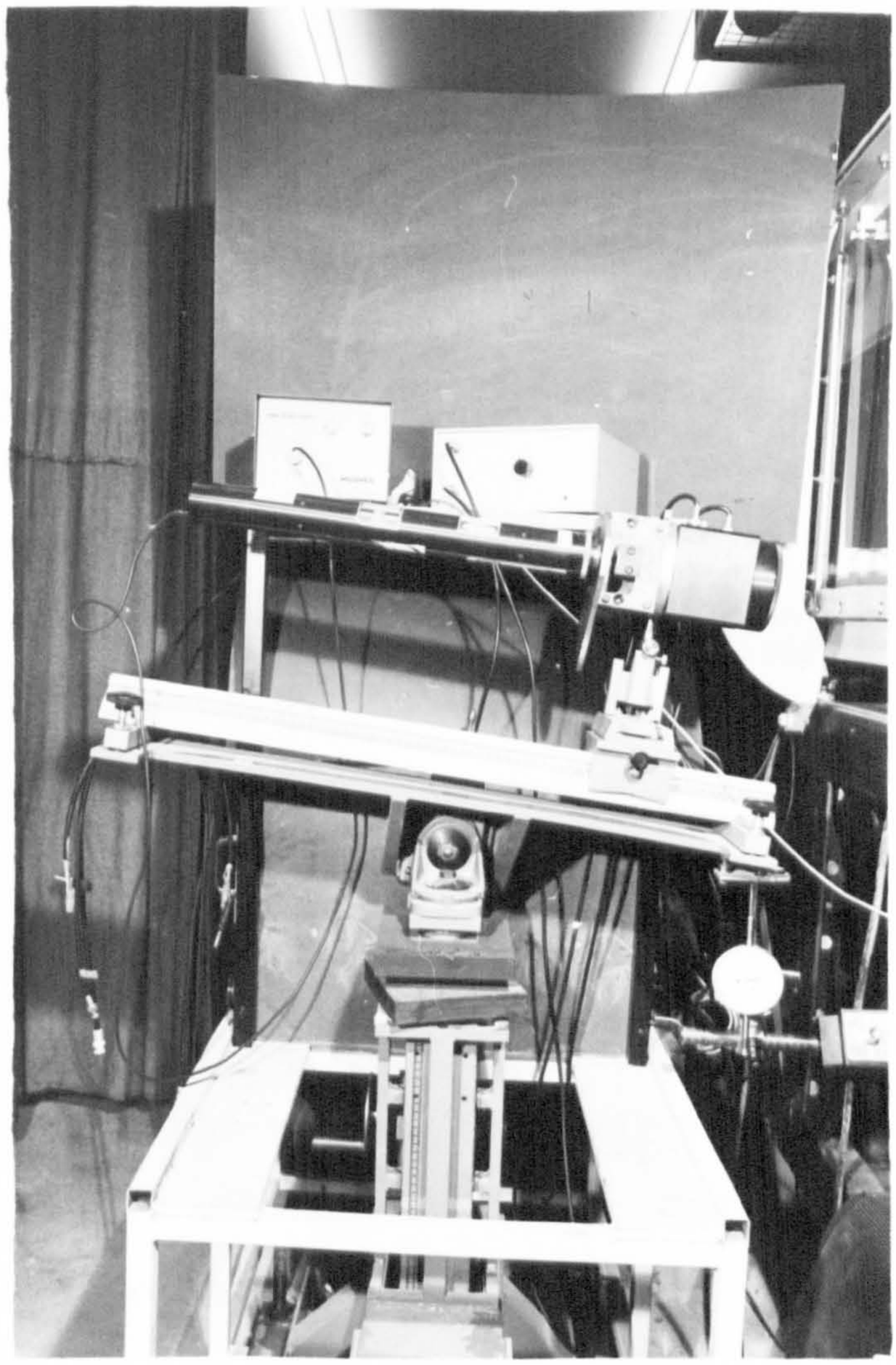

3.2(a) The Laser and Optics

3.2(b) The Photomultiplier

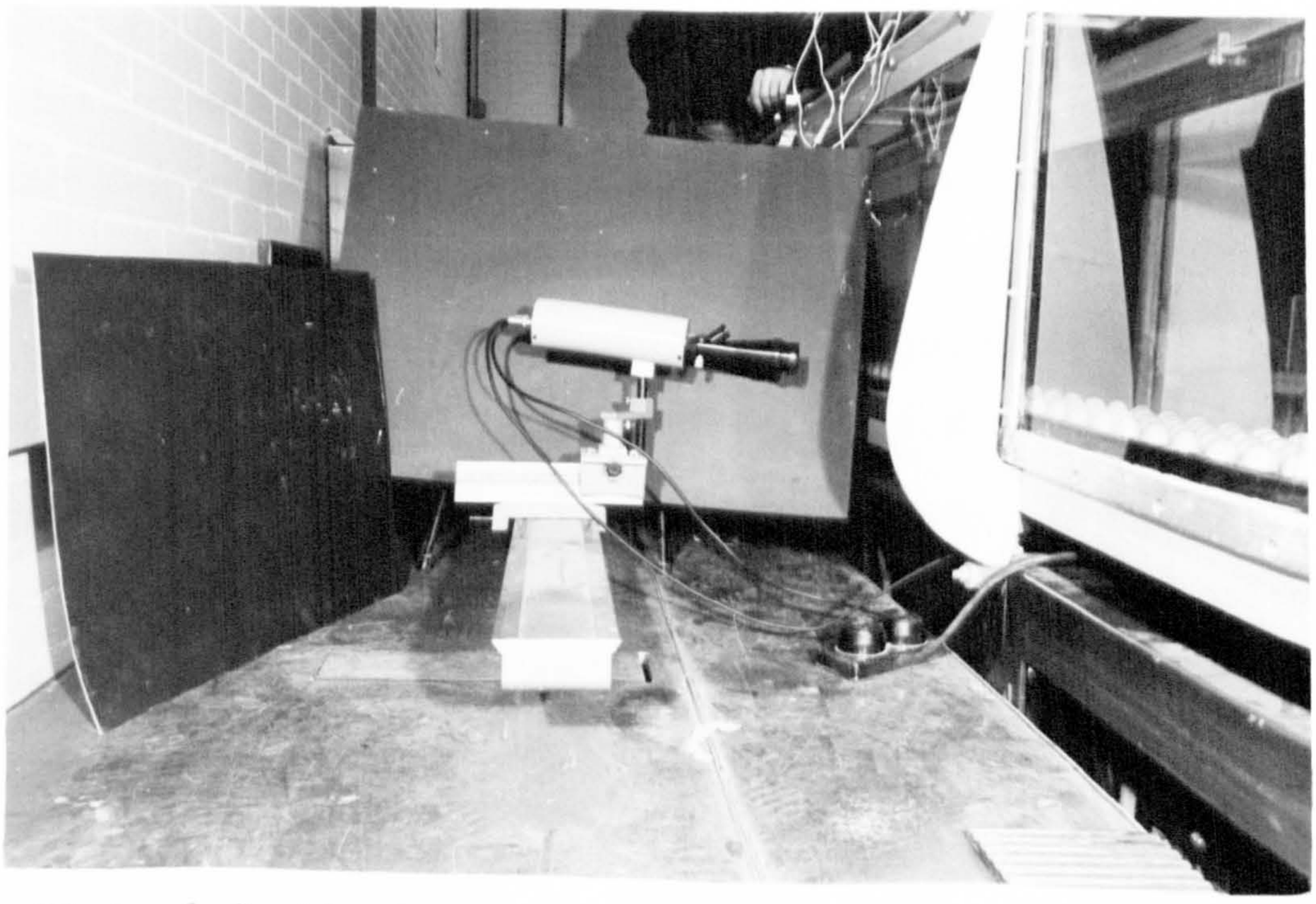

Plate 3.2 The L.D.V.

preamplifer model 55L30, Frequency Tracker model 55L35 and then meter unit type 55L40). A full description of the application of DISA instruments is available in the DISA instruction manual.

A previously determined calibration factor (Section 3.3.5) of the signal processor was used to convert the output voltage into the Doppler frequency (and hence the velocity, since $f_d \alpha v$). The analogue output from the velocimeterwas recorded on a Bell and Howell tape recorder/ reproducer (see Chapter 4 for full description of the tape recorder), and with the use of an Analogue to Digital Convertor (ADC) the signal was converted to digital form and then analysed on the computer. Fig. 3.14 shows the operation system.

3.3.5 Calibration of the Velocimeter

As previously stated, one of the advantages of L.D.V. is the linear response and ease of calibrating the equipment. To calibrate the velocimeter some extra equipment, such as sinusoidal signal generator with a range of output frequency up to 500 KHz and a frequency meter unit, were used. Because the values of the horizontal and vertical velocities in the bulk of fluid varied greatly, the equipment had to be calibrated for four different ranges (15 KHz, 50 KHz, 150 KHz and 500 KHz) on the frequency tracker. The lower value in this range was for observing the vertical velocity component close to the bed and the upper value for the

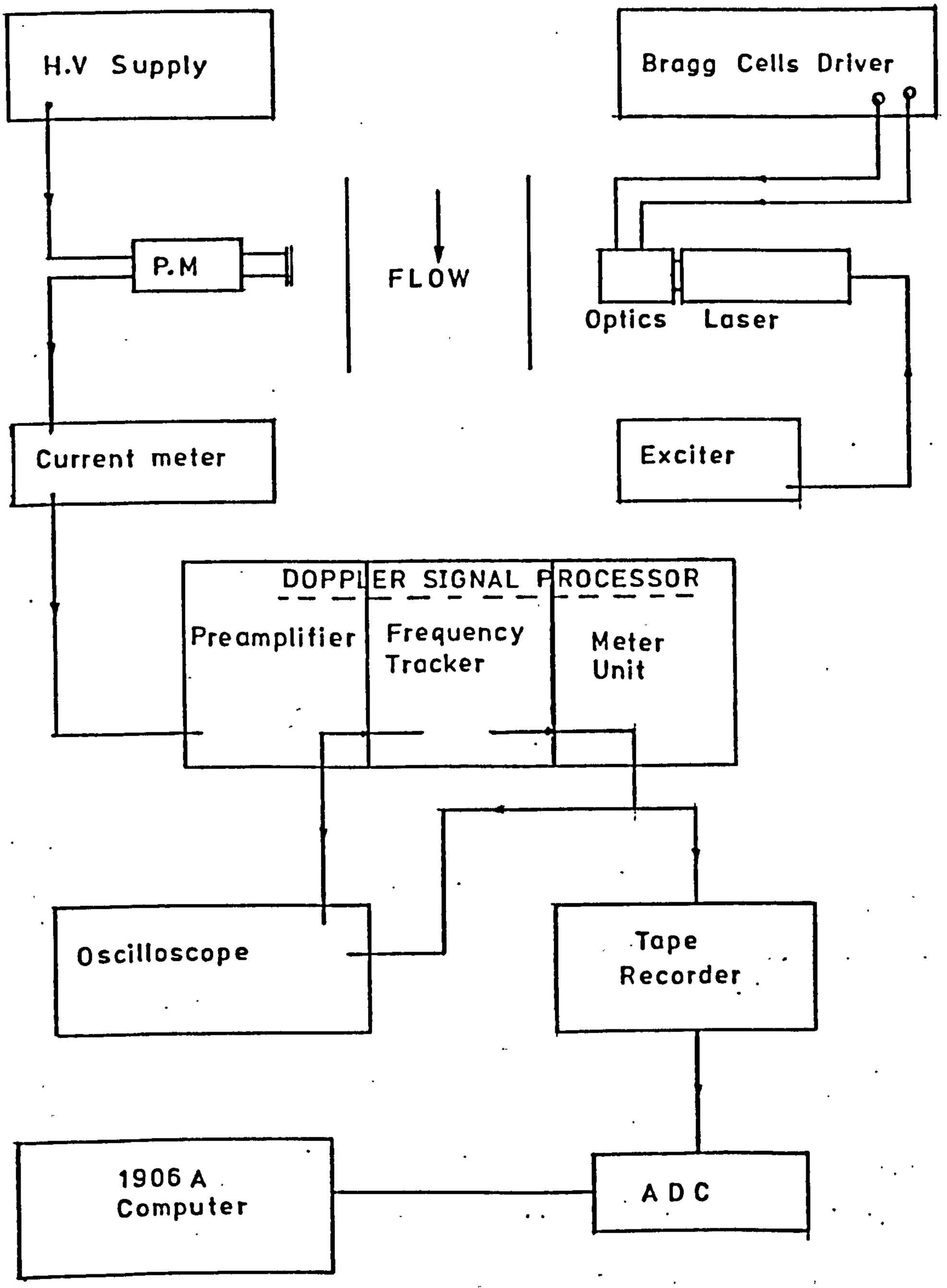

FIG 3.14 THE OPERATION SYSTEM

horizontal velocity close to the surface of the wave for a period of 1.4 second.

In order to calibrate the velocimeter a known frequency had to be fed into the frequency tracker (by-passing the preamplifier) and the output voltage from the meter unit recorded. For ranges of 15 KHz and 150 KHz, thirteen input frequencies (with steps of 1 KHz for 15 KHz range and 10 KHz for 150 KHz range) were fed in and for 50 KHz and 500 KHz ranges, nine input frequencies (with intervals of 5 and 50 KHz for 50 and 500 KHz ranges respectively) were used. The linear regression analysis of relationship between the frequency inputs and voltage outputs, indicate highly correlated calibration factors for the four frequency ranges. Fig. 3.15 shows this relationship between input and output when maximum frequency range is 150 KHz. However, there is no need to include the other three graphs, since the appropriate equivalent of the four observed values had only a maximum discrepancy of less than 2%, which is also a proof for linearity of the velocimeter.

3.3.6 Velocity Measurements

The velocity of water particles were measured in the horizontal and vertical directions. Because the laser tube was mounted on the optical system which could rotate clockwise or anticlockwise in a plane parallel to the horizontal flow direction (the bisector of the laser beam was perpendicular to the horizontal flow direction), then the reallignment

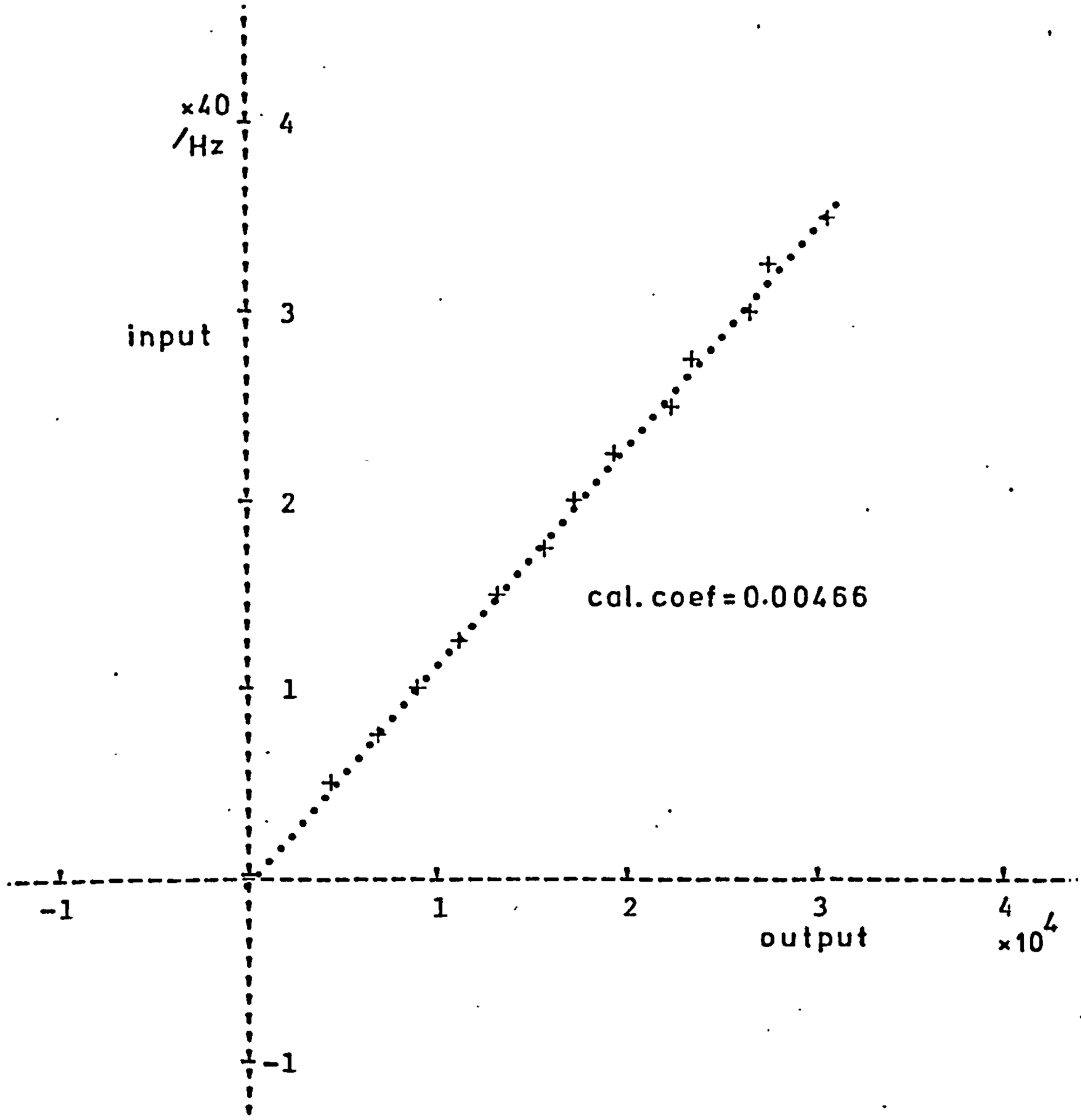

Figure 3.15 A Sample of the Calibration Curve for the L.D.V.

of the optics from horizontal velocity measurements to vertical velocity measurements was not necessary, and therefore the vertical velocity could be measured immediately after the measurement of velocity in horizontal direction had been made.

3.3.6.1 Horizontal Velocity Measurements

There were three separate zones in which measurement of the horizontal velocity was important: (a) in the main bulk of fluid, beyond any effect of the viscous boundary layer, (b) inside and just outside the viscous boundary layer and (c) the horizontal velocity of the turbulent area below the roughness height.

For all these measurements the frequency tracker range was set at 150 KHz and frequency shift at 75 KHz, except when occasionally the range had to be increased to 500 KHz and a frequency shift of 250 KHz (for velocity near the surface wave at low wave period).

3.3.6.2 Vertical Velocity Measurements

Because of a practical limitation to the laser system, the vertical velocity was measured in the bulk of fluid and just outside the viscous boundary layer (the signal quality from below the roughness height and inside viscous boundary layer positions for photomultiplier was poor due to the reflected light from roughness element or smooth bed). A

minor problem arose for measuring the vertical velocity, since the laser beams had to be tilted a few degrees in order to be able to measure the vertical velocity (Fig. 3.16). Hence the actual direction of measured vertical velocity was also tilted to the same degree. However as the angle was small (4 degrees) error in measurement was small since, Cos 4^{o} is close to unity (see Eq. 3.3).

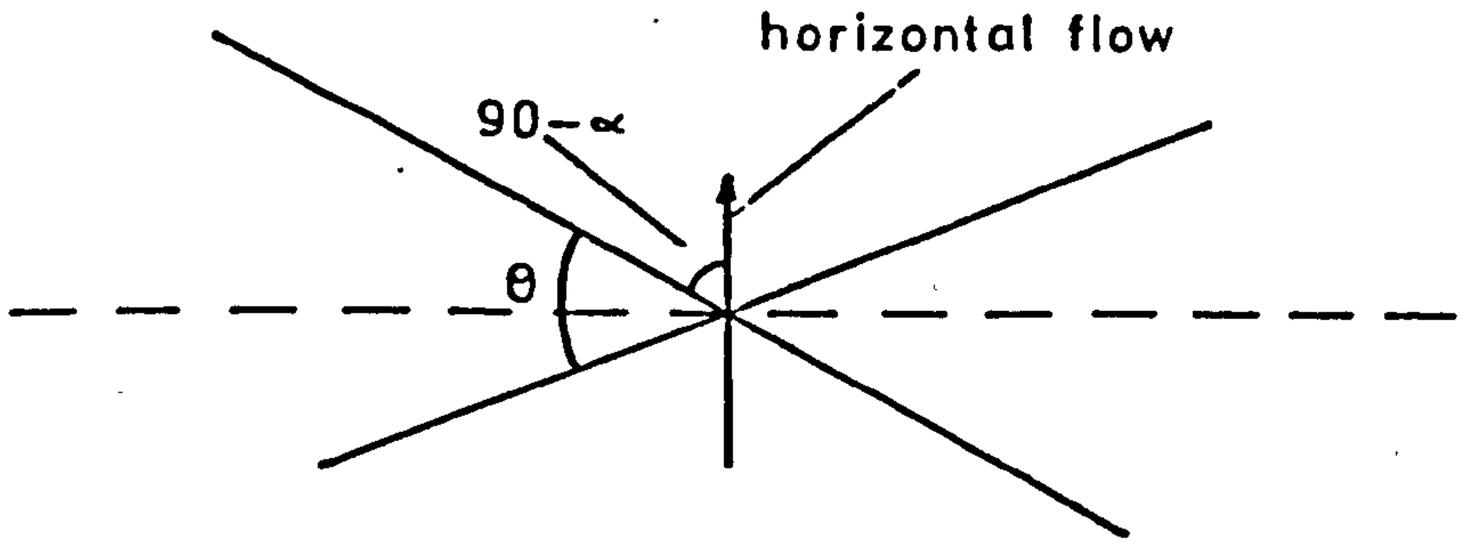

(a) horizontal case.

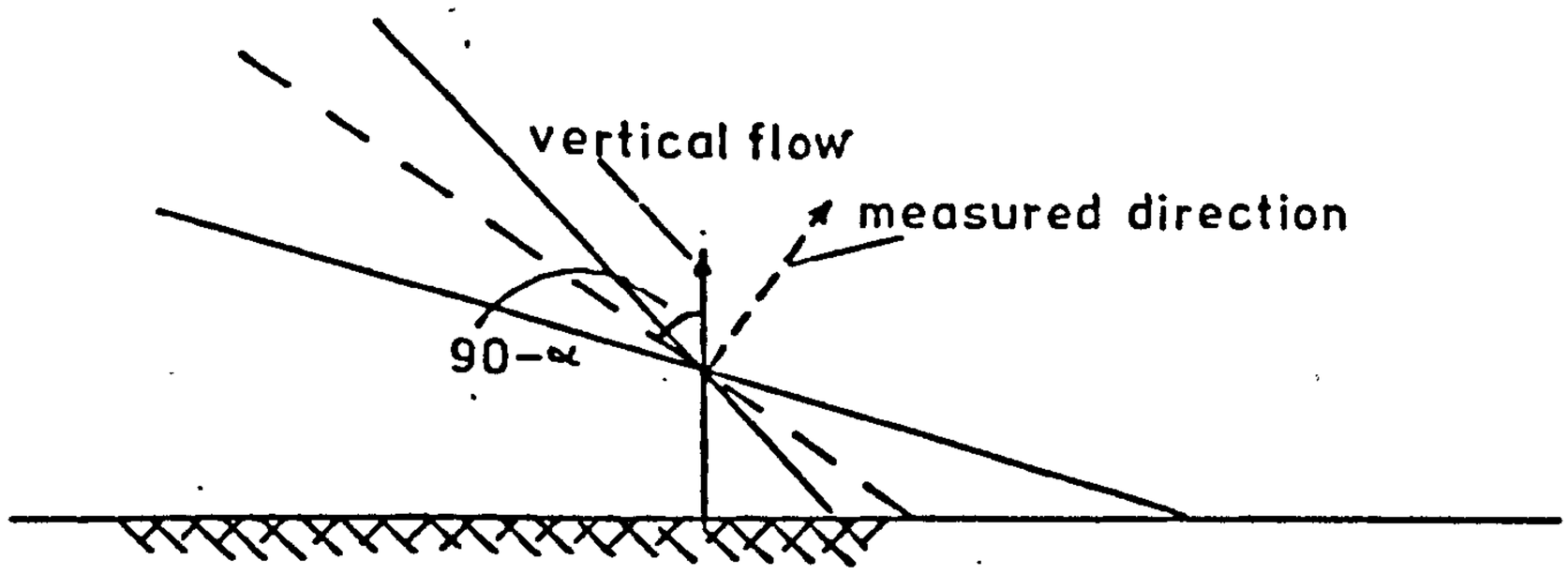

(b) exaggerated vertical case.

FIG 3.16 THE INTERSECTION OF FLOW DIRECTION AND BISECTOR OF THE BEAMS.

CHAPTER FOUR

EXPERIMENTAL METHODS, DATA COLLECTION AND ANALYSIS

4.1 INTRODUCTION

The flow was studied under gravity waves over three different textures; (a) smooth bed, (b) two dimensional roughness and (c) three dimensional roughness. The procedure and data collection system form the content of the first part of this chapter with the method of data analysis in the second part.

4.2 PROCEDURE AND DATA COLLECTION

The following section explains the reasons for selecting certain values of the variable, such as 'water depth', and the methods of collecting data.

4.2.1 Water Depth and Wave Period

The two most important variables for this investigation are water depth (d) and wave period (T). Throughout the experiment the depth of water was fixed at 0.3 m (the value was found by Beech (1978) to produce the most favourable wave conditions below the 2.5 sec. period). When regular rough beds were used, for the sake of simplicity the water depth was measured from the trough of the roughness. (Or two approaches can be made for non-sinusoidal roughness shapes;

(a) taking the mid point between the trough and crest of the roughness as bed datum,

(b) flatten the roughness elements on the bed and take the new bed height as datum.

However, either of the methods does not change the outcome of the results and with the present roughness heights being small, the changes for the water depth is as small as 1 per cent).

As for the wave periods, Beech's results, which have been presented for wave periods between 1.2 to 2.3 sec. at 0.1 sec. intervals, show little change in the wave characteristics from one wave period to the next. Thus with a minimum wave period of 1.3 sec. and maximum of 2.3 sec. (without distortion of the wave profile), resulting in gradual changes of wave characteristics, five wave periods were here selected from 1.4 to 2.2 sec. at steps of 0.2 sec. for smooth and two dimensional rough beds, and for three dimensional rough bed the two periods of 1.4 and 2.2 sec. were used.

4.2.2 Smooth Bed

Smooth finish glass was used to represent hydraulically smooth bed. For this part the surface wave profile, the mass transport velocity in the bulk of fluid and the velocity in the viscous boundary layer were measured.

4.2.2.1 Surface Wave Profile

Before starting the wave generator, the wave probe was calibrated by measuring the output at different submerged

depths of the probe.

After adjusting the wave generator for the required wave period, ten minutes was allowed for the wave-settling time before any data collection was done, as well as checking on the fluctuation of the wave period from time to time at constant speed of wave generator.

The surface wave profile at different periods was measured only when the boundary at the bed was smooth. No attempt was made to measure the surface wave for different bed roughness since these did not influence the surface wave profile (see Chapter Five).

4.2.2.2. Flow Measurements in the Bulk of Fluid

The depth outside the viscous boundary layer to surface wave is known as the bulk of fluid. At eleven depths, in the bulk of fluid, with intervals of 22.5 mm, measurements were made of the horizontal and vertical velocities under gravity waves. The significance of these results was in the comparison of them with the Stokes second order theory and Longuet-Higgins mass transport equation (Chapter 5 for results and discussion).

4.2.2.3 Velocity at the Edge of the Viscous Boundary Layer

The depths just outside the viscous boundary layer to a few multiples of the boundary layer thickness (δ) above it was the region within which horizontal and vertical velocity

profiles (u_∞, v_∞), free of the bed shear affect, were measured.

The free surface wave results and the u_∞ and v_∞ values enable a comparison to be made between Stokes second order predictions and actual results; more about the importance of u_∞ and v_∞ is discussed in Chapters 5 and 6.

4.2.2.4 Velocity in the Viscous Boundary Layer

It is shown by Eagleson (1959), that the vertical velocity in this region is very small and it was also found to be beyond the practical abilities of the instruments used for this investigation. The velocity was measured only in the horizontal direction for the viscous boundary layer, from 0.5 mm to 5 mm above bed (which is greater than the boundary layer thickness of 4.3 mm at 2.2 sec. wave period) at intervals of 0.1 mm up to 1 mm height and 0.25 mm from 1 to 5 mm height from bed.

4.2.3 Rough Beds

4.2.3.1 The Geometry of the Rough Beds

Two textures were used to represent two dimensional (Fig. 4.1) and three dimensional (Fig. 4.2) rough beds (or 2-D and 3-D rough beds respectively). The square shape rubber matting with roughness height of 4.65 mm for 2-D rough bed and the half ping-pong balls equally spaced at 5 in a row with roughness height of 18.95 mm for 3-D rough

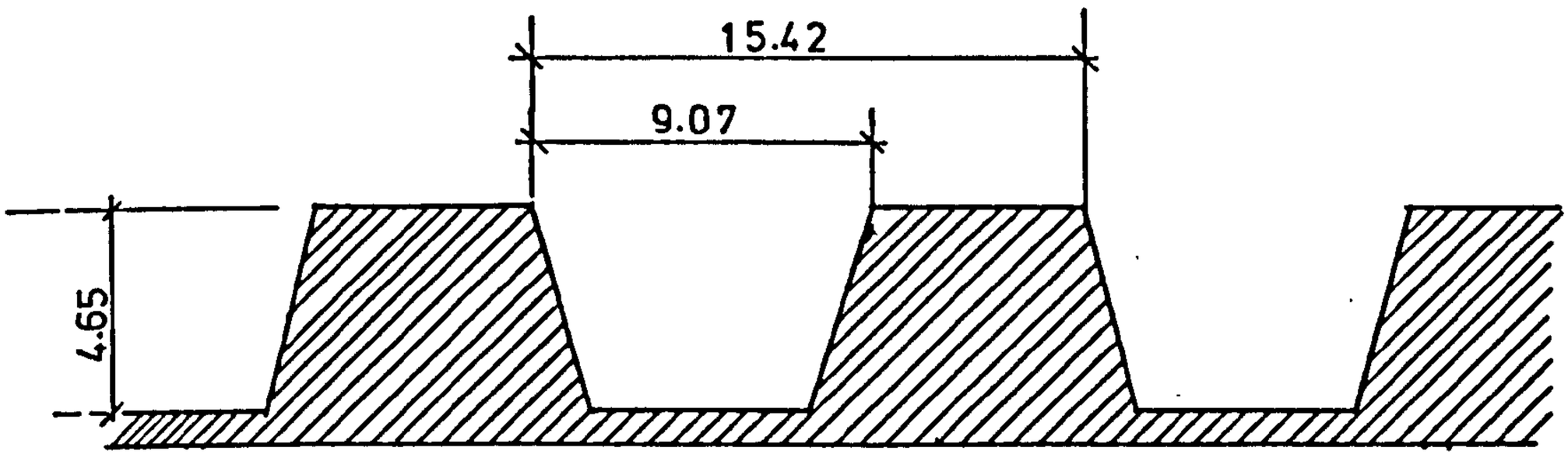

FIG 4.1 2-D ROUGH BED DIMENSIONS (mm).

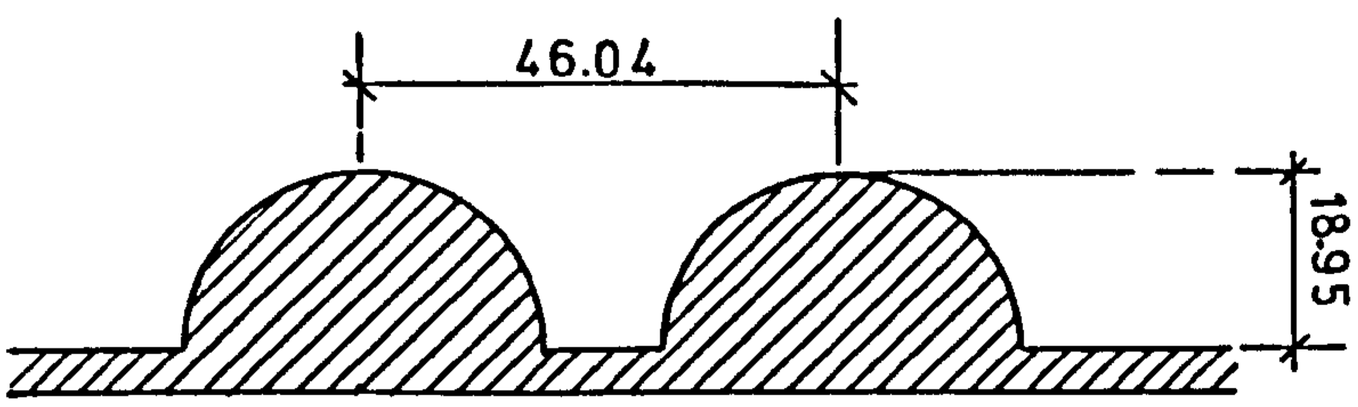

(a) side view

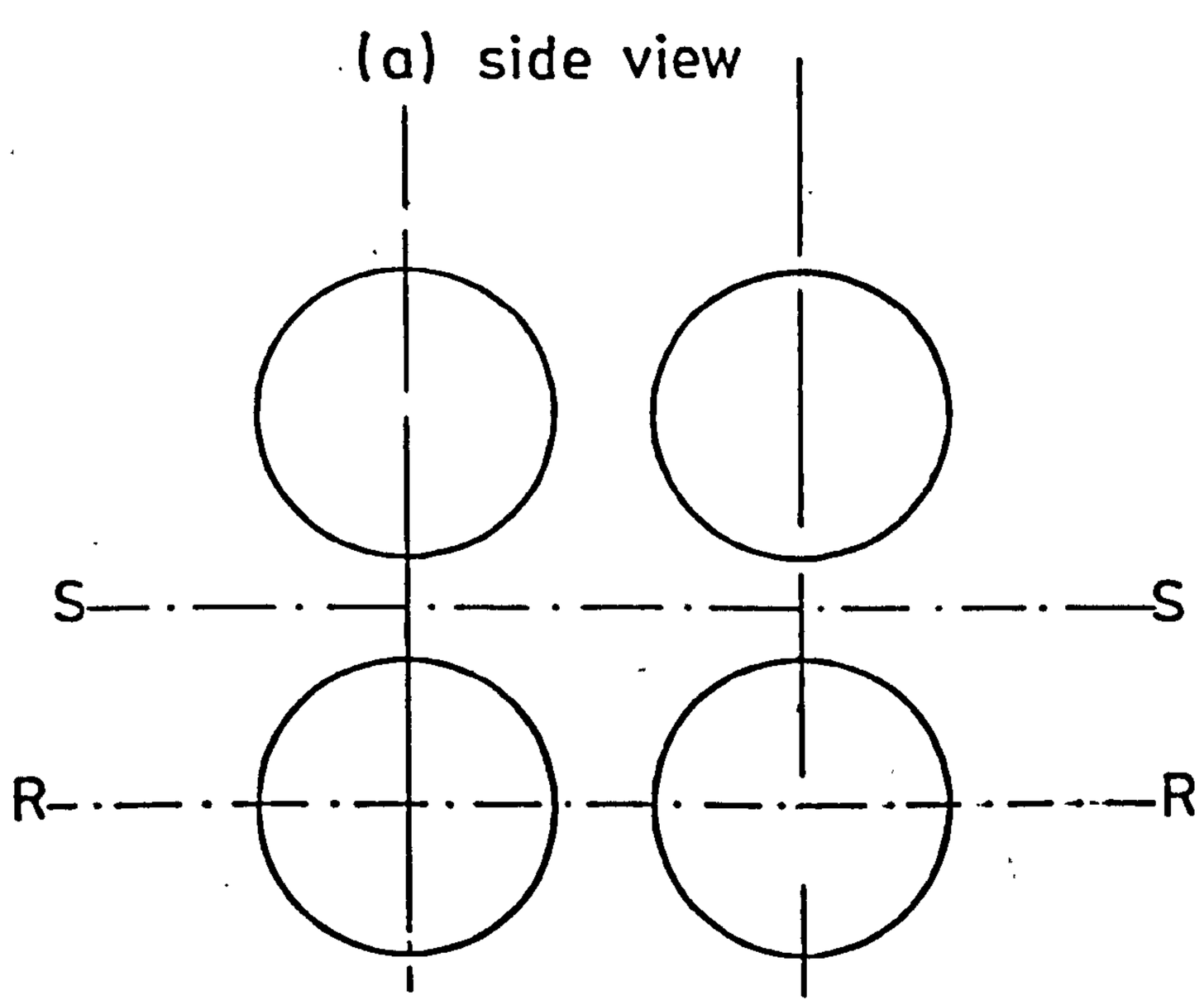

(b) plan view

FIG 4.2 3-D ROUGH BED DIMENSIONS (mm).

bed; for the latter two sets of data were collected at vertical sections RR and SS on Fig. 4.2b. The data for the relevant sections are referred to as 3-DR and 3-DS.

4.2.3.2 Velocity Inside the Roughness Elements

For the 2-D rough bed, from 0.5 mm to 4.5 mm above the trough and at intervals of 0.25 mm, the horizontal velocity was recorded at each point over five cycles for the five wave periods (1.4 to 2.2 sec.).

As for 3-D rough bed the collected data was from 0.5 mm to 18.5 mm above the trough, and at intervals of 1 mm over three wave cycles for two wave periods (1.4 and 2.2 sec.). Because of the practical limitations of the laser doppler system, it was almost impossible to measure any vertical velocity for 2-D rough bed and very poor response from any data collected for the 3-D rough bed.

4.2.3.3 The Sampling Location

Computational limitations made it impossible to collect more data at each point in order to have a fuller understanding of the vortex formation inside and outside the roughness elements. Instead four typical points, two inside the roughness at 0.5 mm above the trough and just under the crest of the roughness peaks (4.5 mm above bed for 2-D and 18.5 mm above bed for 3-D rough bed), and two points outside the roughness at 1.5 mm and 5 mm above the crest of the

roughness peaks, were chosen for taking horizontal velocity over 45 and 30 wave cycles.

4.2.3.4. The Viscous Boundary Layer Velocity

For the sake of argument, it was assumed that the viscous boundary layer over rough beds develops outside the roughness element. Therefore taking the datum level at the top of the roughness crest, the velocity was measured over the trough and crest of the roughness from zero and 0.5 mm respectively to 10 mm above the crest at intervals of 0.25 mm up to 5 mm and 0.5 mm for the remaining depth.

4.2.3.5 Velocity Outside the Boundary Layer

Assuming that a region of viscous boundary layer exists over the rough bed, the depth from 5 mm up to a few multiples of the boundary layer thickness would be the depth for measuring the horizontal and vertical velocities just outside the boundary layer. The significance of these results would be to understand the effect of the roughness on the flow of the bulk of fluid (Chaper 5 for results and discussion).

4.3 DATA ANALYSIS, METHODS AND UNITS

This section deals with the method of data handling, and facilitates understanding. Figs. 4.3 and 4.4 summarize these methods. Reference to these may be helpful.

4.3.1 Data Tape

A multi track magnetic tape record/reproducer by Bell

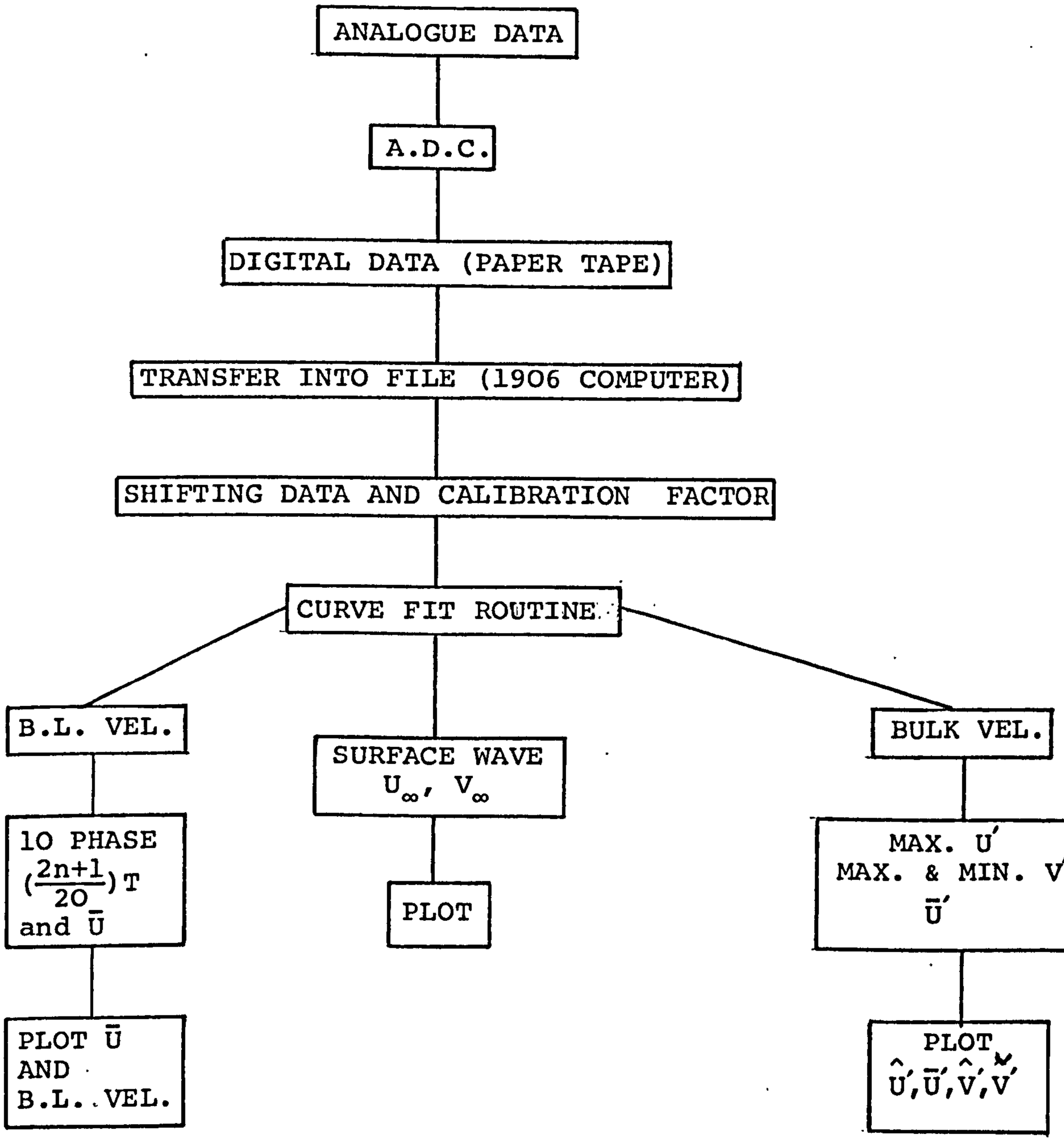

Fig. 4.3 Data Analyses Outlet for Surface Wave, B.L. Vel., M.T. Vel., U_∞, V_∞

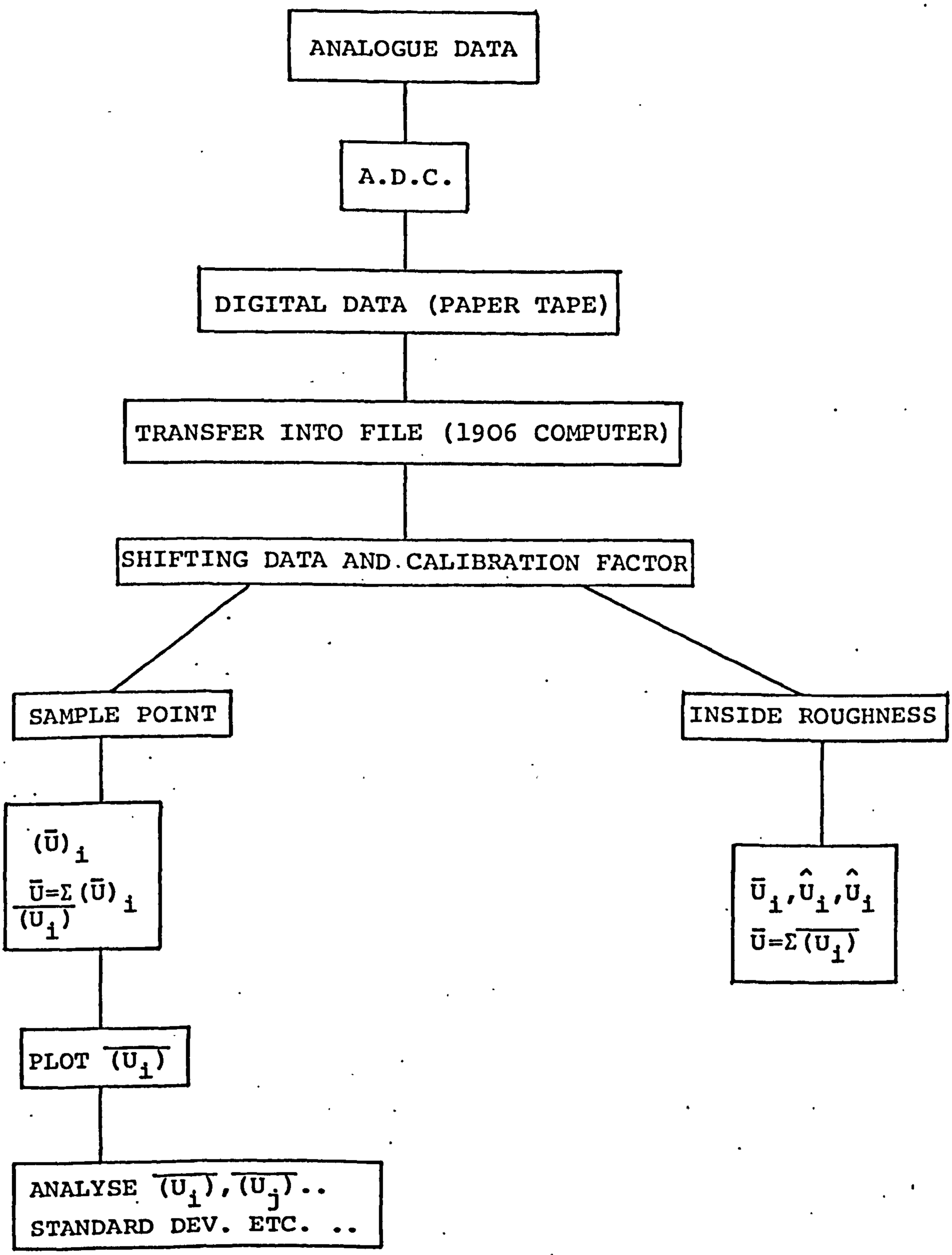

Fig. 4.4 Data Analysis Outlet for Collected Data Below Roughness Height and Sampling Points.

and Howell, type VR3300, was used for recording output data from the laser doppler velocimeter and the wave celerity probe. This is an F.M. analogue recorder and the operation procedures are given in the manufacturer's manuals.

Three of the channels were used for L.D.V. signal, wave probe signal and timing disc pulse generator signal (section 4.3.2). Beside these three channels, a voice-logging unit (microphone, speaker, record/reproduce electronics) used an edge track. In order to optimise the response of the reading of the tapes by the analogue-to-digital convertor, the output of the disc pulse generator from the FM reproduce amplifier of the tape deck was amplified from about 1.4 V to about 5.0 V.

4.3.2 The Timing Disc Pulse Generator

A circular disc was assembled via a shaft on part of the wave generator mechanism, which introduced the same cyclic rotational period to the disc as to the wave generator, and hence to the wave (plate 4.1). It ensured that all the recorded data had the same phase interval of sampling of 120 equal intervals of the period.(on the assumption that the speed of the motor is not fluctuating)

It consisted of an aluminum disc with 120 equally spaced slots around the periphery, the reference slot being longer than the others. As the disc revolved the longer slot passed a light-activated switch on a light-tight box (Fig. 4.5), which introduced an electrical pulse or phase marker and the second light activated switch (L.A.S.), staggered slightly

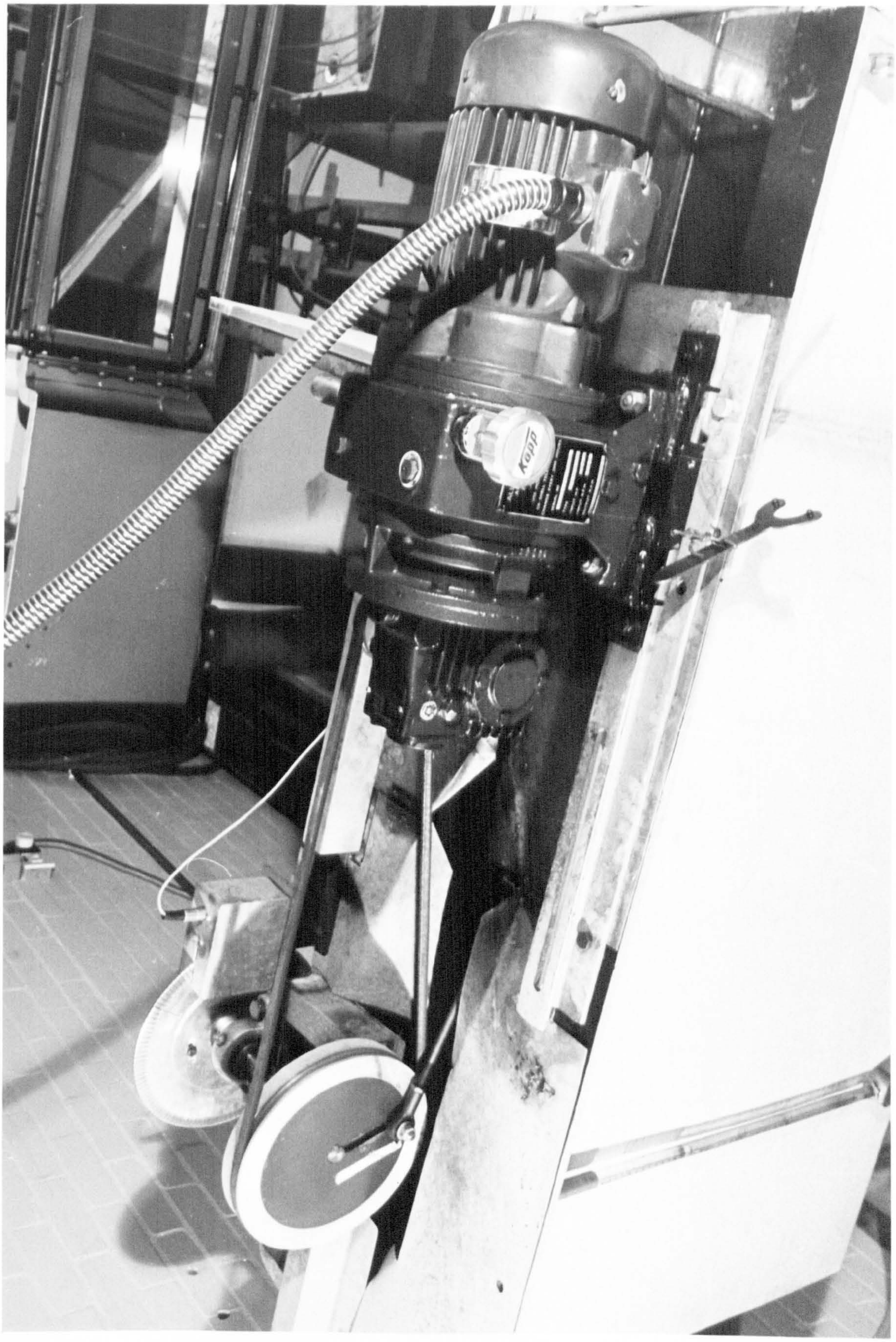

Plate 4.1 The Time Disc Pulse Generator and the Wave Generator

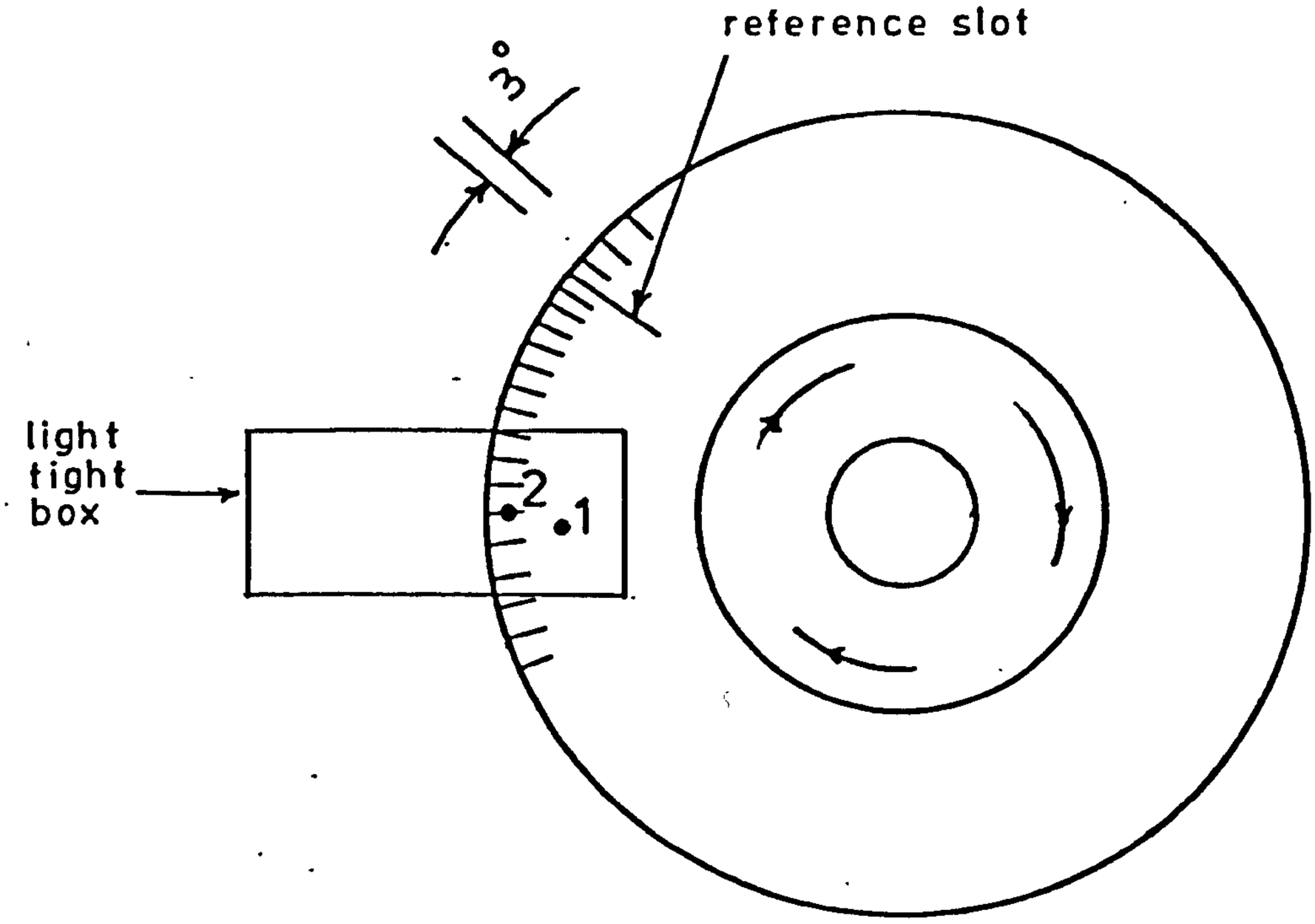

FIG 4.5 THE TIMING DISC.

from the first, developed a rapid square wave signal or the timing pulse. The supplied voltage for driving the unit was about 5 volts.

When the control unit was switched to 'START', then the electric pulse would start sampling when the phase marker passes L.A.S. and a small lamp on the control unit comes on. The sampling continued until the unit was switched to 'STOP' and the phase marker passed the L.A.S. A special time delay was built into the system to allow one more timing pulse after the 'STOP' command, which caused 121 pulses instead of 120 to be recorded. The first and last pulse had the same phase position within the wave cycle.

4.3.3. The Analogue to Digital Convertor (A.D.C.)

The data on magnetic tape in analogue form was converted into digits by using an A.D.C. The A.D.C. (Hewlett-Packard model 5466A) was part of a Fourier Analyser Computer (Hewlett-Packard model 5451B). The digital data was then presented on paper tape.

4.3.4 The 1906A Computer Software

Data on paper tape were transferred to the main computer to form data files (a sample of data at this stage is shown in Fig. 4.6), and different FORTRAN programs were introduced for data analysis.

All the programs used have not been presented here, but

```
SF      1       0      47    6554
(       0)   17330   17586   16754   17074   17842   17714   17010   16498
(       8)   16562   16690   16434   15986   16818   17074   16754   17010
(      16)   16370   15154   15346   16498   16498   16498   16626   15922
(      24)   16114   17074   18994   19826   19890   20146   19122   19570
(      32)   20594   23282   24306   26162   26674   25714   24626   24562
(      40)   24946   25906   24562   22962   21362   19890   18482   17394
(      48)   16946   16882   17906   19250   20210   20786   21874   22450
(      56)   21746   21298   20914   20030   19570   17650   17010   17522
(      64)   17266   16434   15858   16626   16370   16178   16818   17074
(      72)   16754   16818   17074   17074   17138   16434   16946   17394
(      80)   16562   15858   15218   14898   15794   16818   16946   17266
(      88)   18034   18034   18610   19314   19058   18290   16306   15986
(      96)   15730   16690   17842   19058   19762   22386   22002   19890
(     104)   18738   18418   18418   18866   18994   17394   17202   16626
(     112)   17138   17906   18162   18738   18546   20146   20658   20082
(     120)   20978   20146   18738   17522   16754   16690   16562   17074
```

Figure 4.6 A Sample of Data after Conversion to Digital

Appendix C shows some of the programs and subroutines used for analysis. The most important routine, used for programs handling data for establishing wave profiles, boundary layer velocities, mass transport velocities and horizontal and vertical velocities outside the boundary layers, was the curve fitting routine introduced from computer library known as NAG (Nottingham Algorithms Group) library.

4.3.4.1 The Curve Fitting Routine

Since the analogue data could be affected by spurious electrical and magnetic signals (noise) which could produce random errors in the perceived experimental data, smoothing out of the recorded data signals was necessary. By using a curve fitting routine from NAG library, a weighted least square approximation to the set of data points by a cubic spline was computed.

The smoothness and closeness requirements are conflicting for this routine and a balance had to be struck for the right number of coefficient for the fitting function (the smoothness requirement was looked-after by keeping down the number of coefficient and if the number was high, the fit would have been closer to the data). So the 121 data points for each period (whether from the wave celerity probe or the laser doppler velocimeter) were divided into 30 equal intervals of 5 data points each (the last data point from each set was the first data point for the next set) and the

smoothing process was applied. Equal weights were used for the routine. (The theory of the routine in full is available in the Nottingham University Computing Centre Library).

A typical output using this routine is shown in Fig. 4.7. It is to be noted that as long as the residual of the fit is very small compared to the original data then the fit is valid.

4.3.5 Data Shifting

Because of the arbitrary phase shift of the data, depending on the period of the wave, the first step in the data analysing was to shift back the data to be in phase with the predictions from the Stokes second order equations. An interesting phenomenon was that the shifting phase for the surface wave and the velocity data for the same wave period were different (different phase shift from the wave surface probe and the laser doppler velocimeter). But because the difference was constant for all the periods it was assumed that one of the pieces of equipment was delaying the output and causing a phase lag. However, since it did not have any effect on the data, different and compensating phase shiftings were used.

4.3.6 Boundary Layer Velocity

The data for the boundary layer velocity, after being shifted and smoothed, was transferred into a data matrix

J	KNOT K(J+2)	B-SPLINE COEFF C(J)
2	0.00000000E 00	0.45038775E 00
3	0.13000000E 01	0.99062178E 00
4	0.18000000E 01	0.10369829E 01
5	0.31000000E 01	0.89568200E-01
6	0.43000000E 01	-0.99541716E 00
7	0.50000000E 01	-0.10467582E 01
8	0.62831900E 01	-0.44212183E 00

CUBIC SPLINE APPROXIMATION AND RESIDUALS

	ABSCISSA	APPROXIMATION	RESIDUAL
1	0.00000000000E 00	-0.17396706 90E-02	-0.1739670690E-02
	0.13090000000E 00	0.1327429197E 00	
2	0.26180000000E 00	0.2621957978E 00	0.3375797798E-02
	0.39270000000E 00	0.3853584067E 00	
3	0.52360000000E 00	0.5009701897E 00	0.9701897070E-03
	0.65450000000E 00	0.6077705899E 00	
4	0.78540000000E 00	0.7044990506E 00	-0.2610949443E-02
	0.91630000000E 00	0.7898950148E 00	
5	0.10472000000E 01	0.8626979258E 00	-0.3332074186E-02
	0.11781000000E 01	0.9216472268E 00	
6	0.13090000000E 01	0.9654823924E 00	-0.4476076065E-03
	0.14390000000E 01	0.9930605599E 00	

Figure 4.7 A Sample of Output After Calling the Curve Fitting Routine

with 121 columns (121 is the number of data points in each period). Ten equal phase positions were selected to represent the typical boundary layer throughout one period ($(\frac{2n-1}{20})T$, n=1, 2, ...). A sample of the output is shown in Fig. 4.8. This process was carried out for smooth bed, 2-D rough bed over crest and trough of roughness and 3-D (R and S) rough bed over crest and trough (Chapter 6 for results).

4.3.7 Velocity Outside Boundary Layer

Horizontal and vertical observed velocities (for all types of bed) were shifted and smoothed, and the results were sketched together with the predicted values by Stokes second order equations for comparison (see Chapter 5 for results).

4.3.8 Velocity in the Bulk of Fluid

From the smoothed data, the average of horizontal velocity has been compared with the Stokes and Longuet-Higgins predictions (the theoretical vertical velocity mean is zero). Also profiles of the horizontal velocity maxima, and maxima and minima for vertical velocity throughout the depth have been examined with the Stokes second order profiles (Chapter 5 for results).

4.3.9 Velocity Inside the Roughness Elements

Since the flow in this region was disordered and vortices

HEIGHT FROM BED MM	VELOCITY IN MM/S AT 1T/20	3T/20	5T/20	7T/20	9T/20	11T/20	13T/20	15T/20	17T/20	19T/20	YAVERAGE
5.00	241.64	135.21	-16.00	-136.19	-196.16	-188.30	-130.58	-14.28	125.51	232.23	7.94
4.75	240.68	136.61	-14.86	-135.95	-194.36	-182.37	-126.56	-14.24	130.65	240.91	10.93
4.50	243.88	133.17	-18.56	-137.18	-192.86	-181.81	-123.68	-4.42	137.09	243.28	11.85
4.25	252.07	147.42	-3.01	-126.58	-187.13	-181.50	-126.71	-15.94	125.74	237.58	14.34
4.00	255.10	153.20	3.35	-119.07	-179.64	-177.35	-129.58	-15.77	123.03	238.33	17.74
3.75	246.17	143.35	-2.89	-126.33	-183.54	-180.63	-126.93	-13.36	130.84	236.70	14.23
3.50	245.79	149.85	1.36	-124.09	-187.87	-184.67	-138.80	-24.46	116.93	224.97	10.83
3.25	260.37	174.32	26.22	-107.95	-178.66	-186.69	-142.89	-38.44	102.45	225.12	15.42
3.00	258.38	157.75	1.83	-124.14	-186.08	-182.66	-128.12	-16.15	123.76	241.57	16.50
2.75	256.25	147.25	-6.62	-128.09	-183.83	-177.25	-124.86	-9.05	135.80	250.02	18.46
2.50	263.67	161.83	11.90	-115.22	-178.28	-179.42	-133.02	-20.50	126.65	248.09	21.19
2.25	264.89	160.97	6.37	-123.91	-189.63	-185.02	-126.65	-15.27	134.23	254.12	20.09
2.00	263.27	152.69	-0.15	-126.52	-188.21	-180.16	-121.31	1.13	144.94	263.42	22.82
1.75	265.56	149.72	-6.48	-134.63	-196.36	-184.84	-117.34	7.93	154.92	269.42	22.63
1.50	273.21	161.04	1.22	-126.82	-189.57	-182.34	-127.52	-4.68	149.71	268.61	24.93
1.25	247.17	133.95	-23.01	-146.69	-198.93	-179.19	-102.82	25.25	172.30	274.64	23.11
1.00	248.38	119.09	-37.68	-155.19	-198.76	-168.91	-95.03	37.88	181.15	270.58	22.03
0.90	250.57	131.92	-22.49	-148.31	-195.39	-173.28	-104.76	21.04	168.99	265.38	22.22
0.80	243.51	127.54	-31.19	-141.06	-195.47	-166.67	-90.88	30.59	168.14	262.73	22.02
0.70	224.42	101.60	-46.78	-145.25	-174.68	-137.37	-68.00	53.77	178.03	248.16	25.28
0.60	226.36	114.08	-21.84	-135.74	-172.88	-150.03	-80.37	29.88	159.98	237.68	22.76
0.50	187.01	81.74	-42.33	-143.58	-168.54	-112.49	-44.09	55.81	179.38	230.71	24.77

Figure 4.8 Sample of the Output Boundary Layer Velocity Profile at 10 Phases.

occurred, use of the curve-fitting routine and velocity profile were not fruitful in analysing the data. Instead the mean velocity over 5 cycles and the mean velocity for each cycle of the 5 cycle sample (or 3 cycle sampled for 3-D rough bed) throughout the roughness depth were found (Fig. 4.9) and with a series of the significance tests (Section 7.3), the level of significance of the 5 or 3 sample population with respect to the result of sampling locations (45 or 30 cycle samples) were calculated.

4.3.10 Analysis of the Data from Sampling Locations

Data for the sampling locations were analysed in two stages.

(a) The mean velocity at each cycle was measured and the statistical analysis of the normal distribution and standard deviation was carried out for the 45 (or 30) mean velocities.

(b) The turbulence intensity was calculated from the mean profile of the velocity over 45 cycles. Also by selecting three arbitrary phase positions in the period the type of distribution and the value of standard deviation of the 45 cycle sample (or 30 cycle for 3-D rough bed) were calculated.

This type of analysis was carried out to establish the reproducibility of the results which gave an indication of how representative the results in the velocity fluctuation zones are.

Y (MM)	1ST PERIOD VAVE	2ND PERIOD VAVE	3RD PERIOD VAVE	4TH PERIOD VAVE	5TH PERIOD VAVE	FOR 5 PERIOD VAVE
0,50	-4,9	3,2	3,6	3,6	1,9	1,5
0,75	8,6	4,9	12,1	1,8	-0,3	5,4
1,00	3,3	3,2	7,1	3,8	2,1	3,9
1,25	0,0	2,2	6,0	-0,2	5,7	2,9
1,50	4,7	-1,2	1,4	2,2	2,5	1,9
1,75	1,1	3,0	22,1	-2,2	-0,4	4,7
2,00	4,6	-2,4	0,5	17,4	4,3	4,9
2,25	19,0	-6,0	-2,8	-1,1	-5,0	0,8
2,50	-0,8	1,1	-10,0	-0,7	6,3	-0,8
2,75	7,0	-6,5	-0,7	4,1	7,0	2,2
3,00	7,9	10,8	6,0	-3,6	2,6	4,7
3,25	8,2	46,1	3,0	10,2	3,9	14,3
3,50	5,7	-2,2	3,2	14,2	2,6	4,7
3,75	2,4	16,9	3,1	9,1	-0,5	6,2
4,00	10,8	23,9	1,2	5,2	6,4	9,5
4,25	1,6	-2,6	7,5	1,2	5,9	2,7
4,50	5,9	11,1	11,9	-1,3	5,8	6,7

Figure 4.9 Sample of the Output Mean Velocity Below the Roughness Height.

CHAPTER FIVE

RESULTS AND ANALYSIS OF WAVE PROFILE AND ORBITAL VELOCITIES

5.1 Introduction

This chapter is the first of three on presentation and discussion of the data collected in this investigation. The contents include discussion of the surface wave profile data, the horizontal and vertical orbital velocities in the bulk of the fluid (that is outside the viscous boundary layer) and a full comparison of experimental data with Stokes second order predictions (in the case of mass transport velocity in the bulk of fluid, the Longuet-Higgins prediction as well). Also consideration of the effect of rough beds on the velocity outside the viscous boundary layer is included in this chapter.

5.2 The Classification of Generated Waves

5.2.1 Relative Depth

In section 1.2 classification of waves which are known from the ratio of water depth (d) to wavelength (L) has been discussed ($d/L > 0.5$ deep water waves, $d/L < 0.05$ shallow water waves). The values of relative depth together with other wave parameters are shown in Table 5.1.

Since the d/L values ranged from 0.154 for 1.3 sec. wave period to 0.081 for 2.3 sec. wave period, thus the class of these waves, according to the above definition, are intermediate water waves. Because the differences between the

T/s	H/mm	L/m		d/L	U_R $[\frac{H}{L}(\frac{L}{d})^3]$	H/d	$350(\frac{d}{gT^2})^{3/2}$
		Measured	Calculated				
1.3	76.4	1.95	1.96	0.154	11.0	0.26	0.85
1.4	75.4	2.23	2.15	0.135	13.0	0.25	0.68
1.5	69.2	2.28	2.34	0.132	14.0	0.23	0.56
1.6	66.8	2.42	2.53	0.124	15.8	0.22	0.46
1.7	69.2	2.62	2.71	0.115	18.8	0.23	0.38
1.8	59.0	2.81	2.89	0.107	18.6	0.20	0.32
1.9	57.4	3.01	3.08	0.100	20.0	0.19	0.27
2.0	59.6	3.32	3.26	0.090	23.4	0.20	0.23
2.1	61.4	3.47	3.44	0.086	27.0	0.20	0.20
2.2	51.8	3.55	3.62	0.085	25.2	0.17	0.18
2.3	44.2	3.70	3.79	0.081	23.6	0.15	0.15

Table 5.1 The Characteristics of Generated Waves (d = 0.3 m)

theoretical and measured values of wave-length (theoretical values are calculated from Eq. 1.7) have a maximum of only 4% (for wave period of 1.6 second), then it can be assumed that the relative depth values qualify the generated waves as intermediate type.

5.2.2 Ursell Parameter

On the other hand it has been shown (section 1.5.3) that the Ursell parameter is another factor which specifies the classification of waves (U_R < 1 deep water waves, U_R > 20 shallow water waves). Ursell parameters of 11.0 to 27.0 exist for the data presented in Table 5.1. Up to 1.9 second wave period an U_R of less than 20 occurs and hence predicts intermediate water wave zone, and above 1.9 sec. period with U_R of greater than 20 the waves are in the shallow water region with maximum of 27.0 which occurs at 2.1 sec. wave period. Also when the wave period is 1.9 sec., U_R is 20 which is taken in the intermediate zone.

While the relative depth values group the waves as intermediate, Ursell parameter differentiates between waves of above 2.0 sec. period as shallow water and those of less than 2.0 sec. period (intermediate waves). Whether the former or latter parameter is a better approach to classify the waves is arguable, since not much practical evidence exists. However one way would be to accept both limitation values, then for this case, waves over 1.9 sec. period are in the shallow

water region and 1.9 sec. period and under are part of the intermediate water waves. Also the values of 0.5 and 0.05 for relative depth and 1 and 20 for Ursell parameter are shown in Fig. 5.1 which is after Le Mehaute (1976).

This clearly shows that for much lesser values than 0.5 for d/L the Ursell parameter is still less than unity. This means while the former is the condition for intermediate waves the latter accepts the deep water zone. Also when U_R is greater than 20 which is the shallow water region, the relative depth is any value between 0.03 and 0.3 (where H/T^2 is from 3×10^{-4} to 2×10^{-1} m s^{-2}) which is well above the mid-value for intermediate waves.

Evidently the Ursell parameter being proportional to the wave height (H- which classifies waves as finite and infinite -sec. 1.3) as well as water depth and wave-length, can be a better wave classifier, but as it was stated before the relation between the two parameters needs much better evidence on the practical side which is lacking at the present time.

5.2.3 Limitations of Wave Theories

Beside Table 1.2, presented in Chapter One for comparison of wave theories, Le Mehaute (1976) presents the wave theories limitations in the form of Fig. 5.1, which is the relationship between H/T^2 and d/T^2.

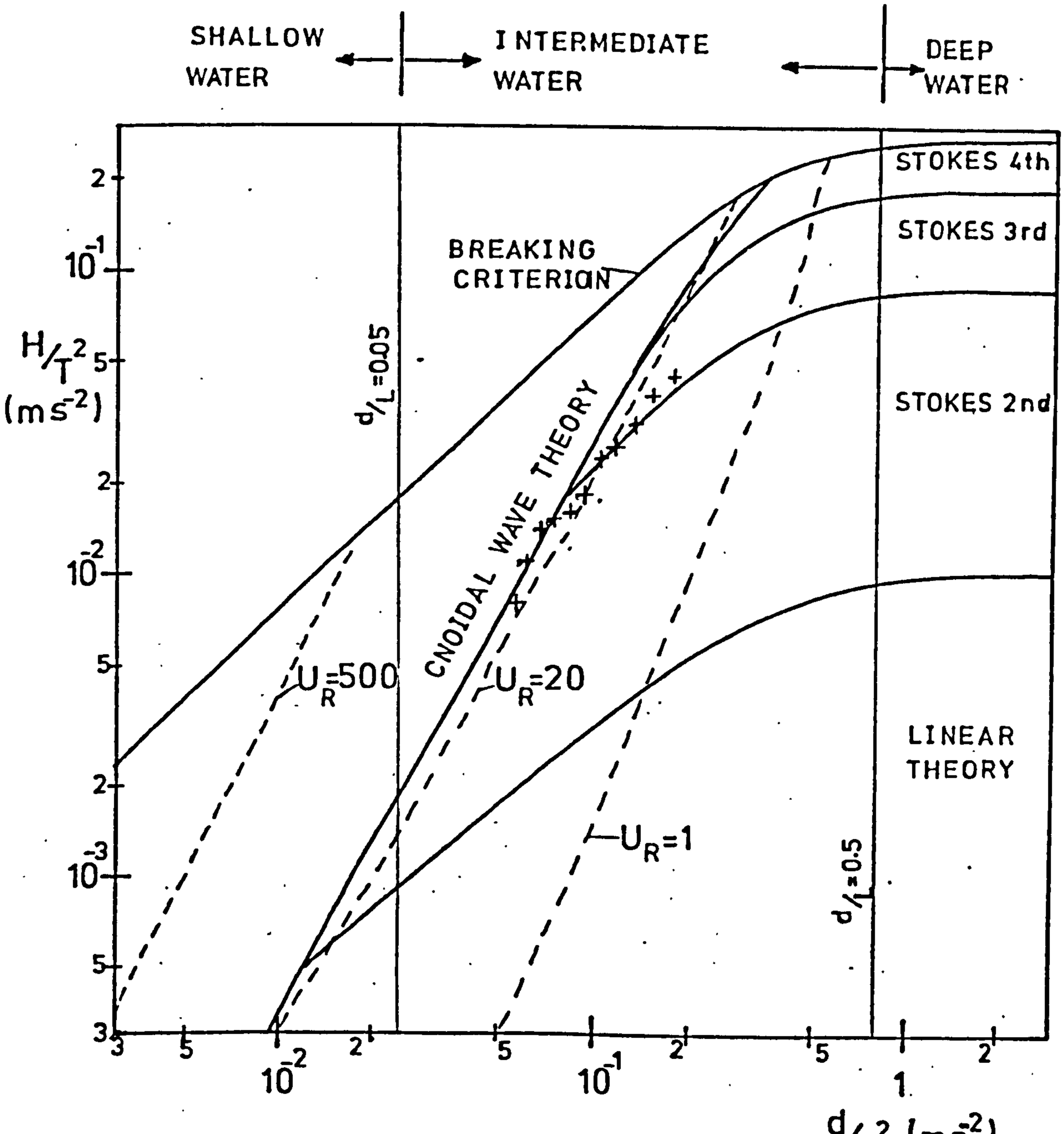

Fig. 5.1. Limits of validity of different wave theories (after Le Mehaute (1976)), and the observed data.

Most data points shown on the graph lie on the border between Stokes second and third order line, while for lower frequency waves the limits of Cnoidal and Stokes second order is covered by the data. Stokes second order just satisfies the data values, and it also covers all the periods and is suitable for intermediate water waves as well, then it is the convenient theory. Also according to Isaacson (eq. 1.41), since the values of H/d are always less than 350 $(\frac{d}{gT^2})^{1.5}$ (Table 5.1), therefore Stokes theory well predicts the mass transport near the bed too.

5.3 Data of Surface Wave Profile

The collected data for surface profiles together with the Stokes second order theory predictions (eq. 1.22) are presented in Fig. 5.2. The data could be differentiated by two groups. First those waves for which the trough is in phase with the theory, and includes periods of 1.4, 1.5, 2.1, 2.2 and 2.3 seconds. These waves have profiles the same shape as the theory (having the same phase for maxima and minima as the predicted graphs). Among the five waves, the 1.5 sec. period wave has the best correlation with the theory, while the 1.4 sec. period wave has also a good correlation with the prediction but it looks as though the whole curve is shifted downwards with respect to the x axis. For the other three period waves (2.1, 2.2 and 2.3 sec.), the shape of the trough is flatter than the theory curves which causes a sharper crest than the Stokes theory too.

Fig. 5.2 Surface Wave Profile

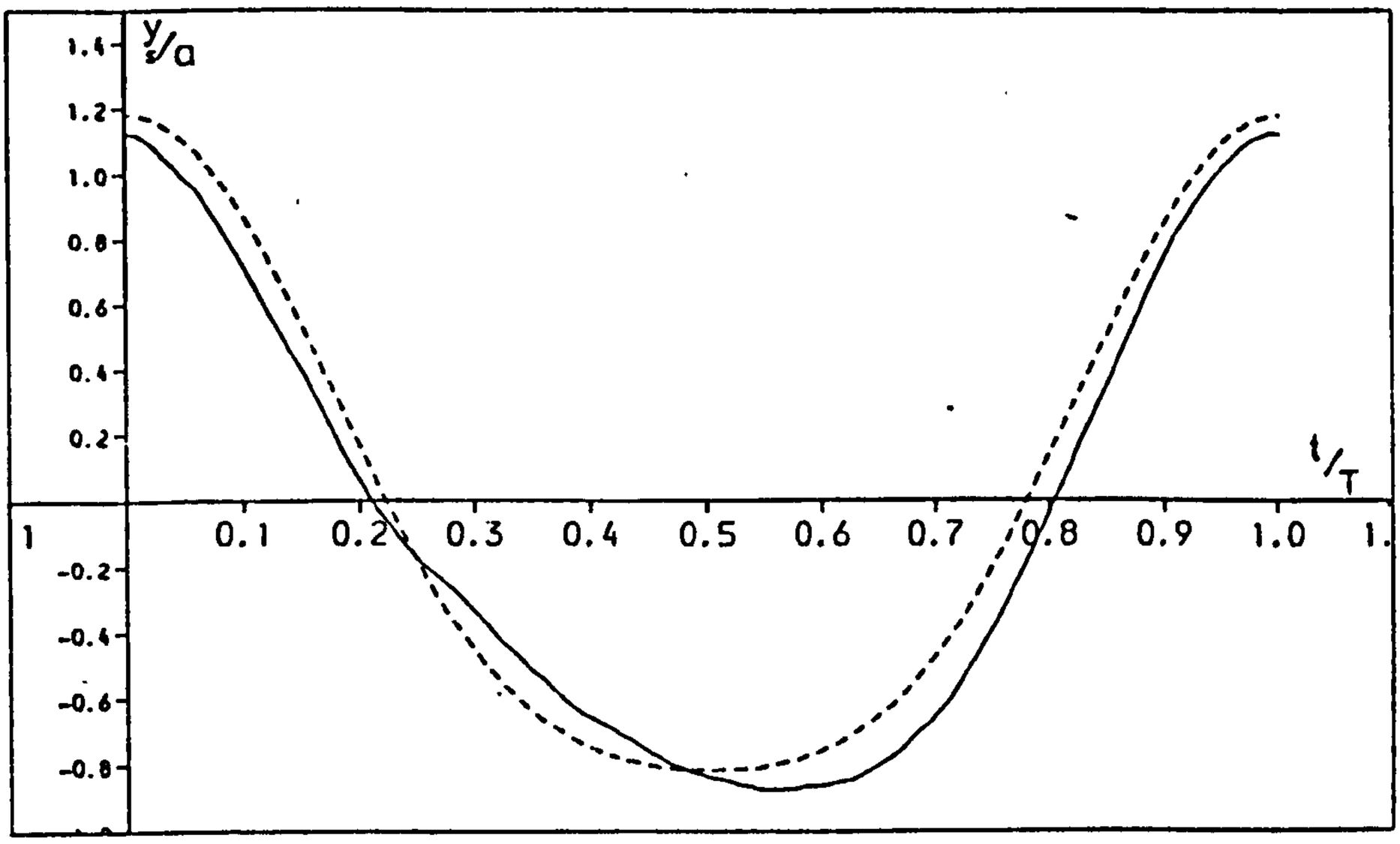

(i) T=1.3 s a=38.2 mm

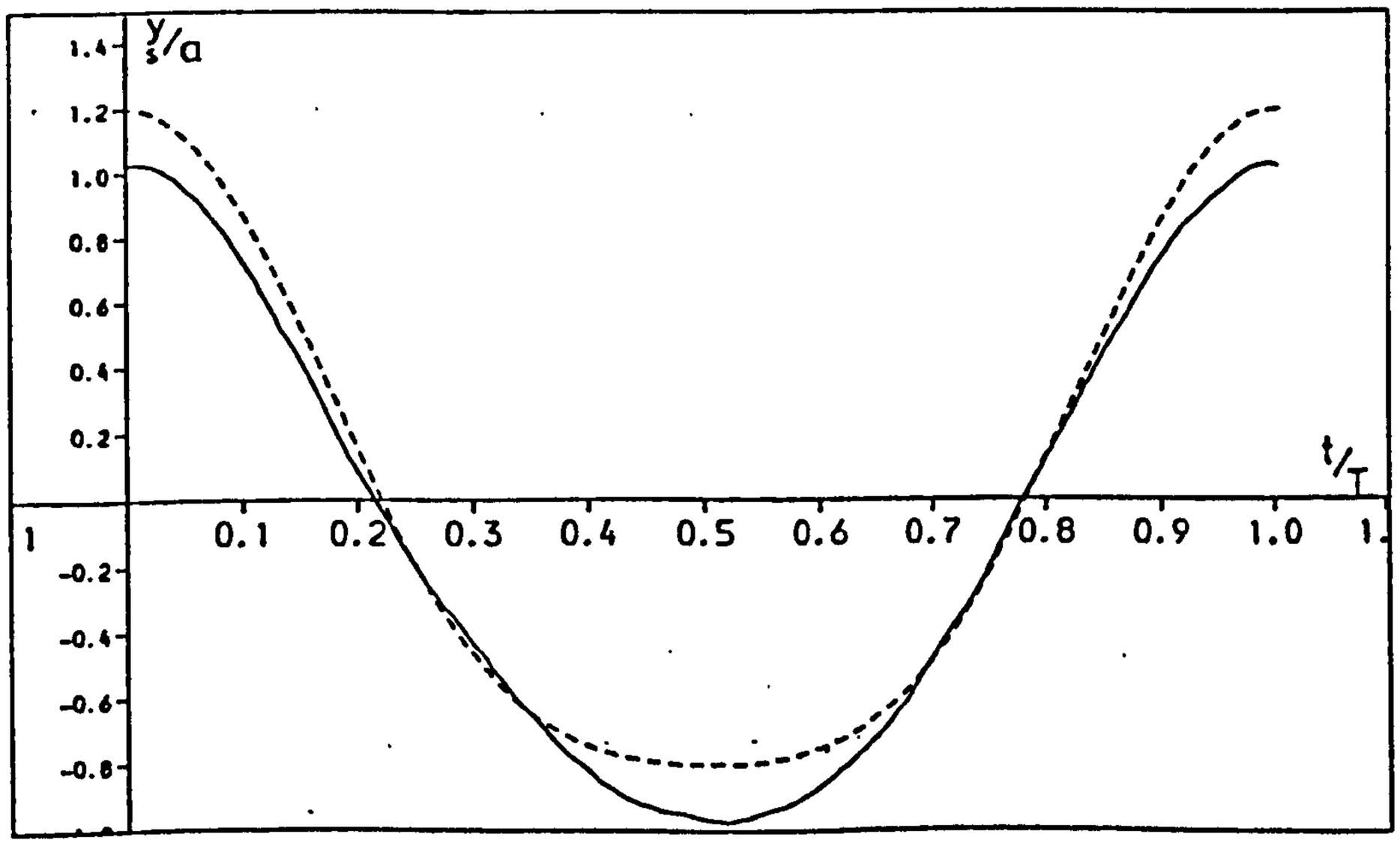

(ii) T=1.4 s , a=37.7 mm

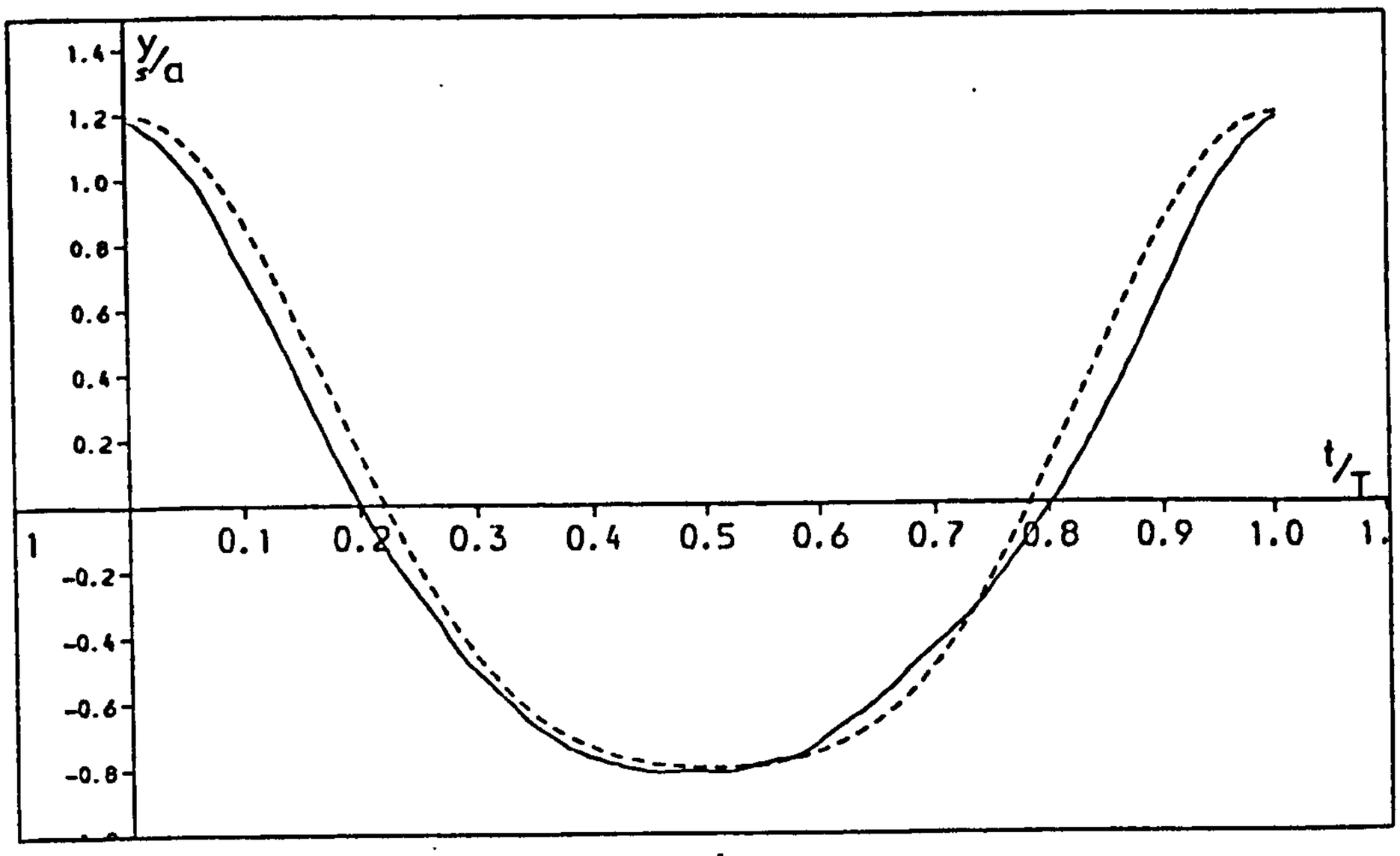

(iii) T=1.5s , a=34.6 mm

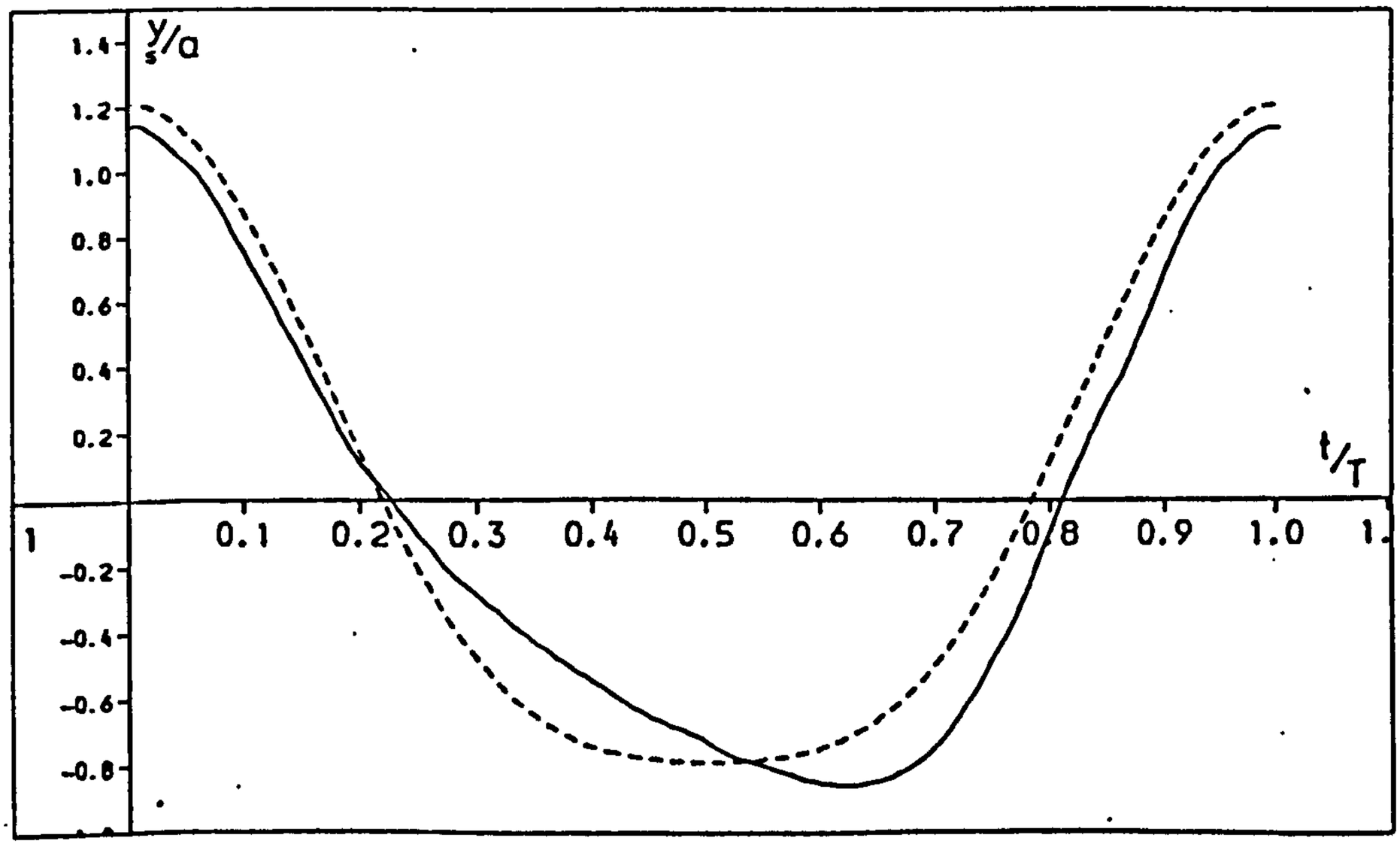

(iv) T=1.6s , a=33.4 mm

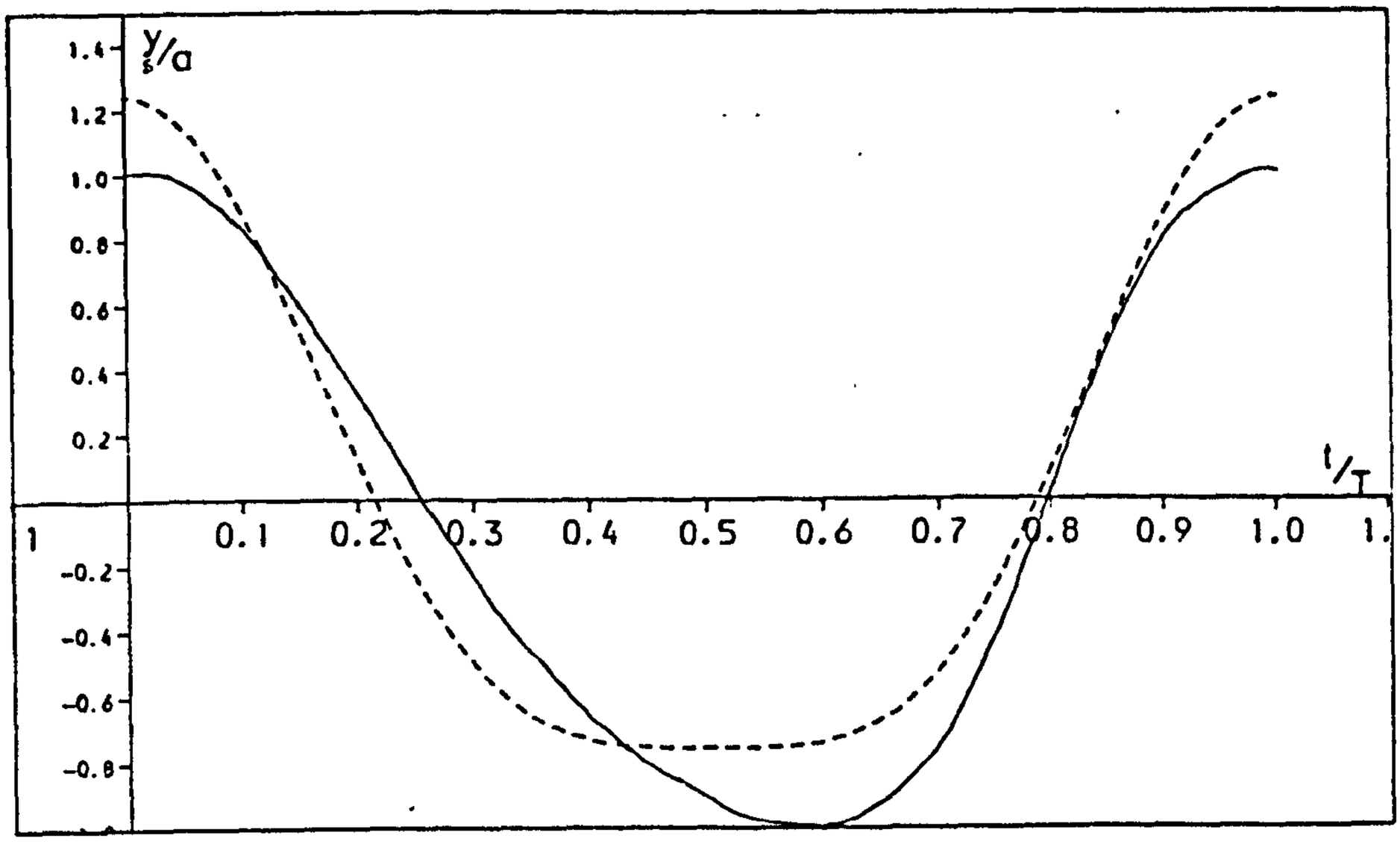

(v) T=1.7s , a=34.6 mm

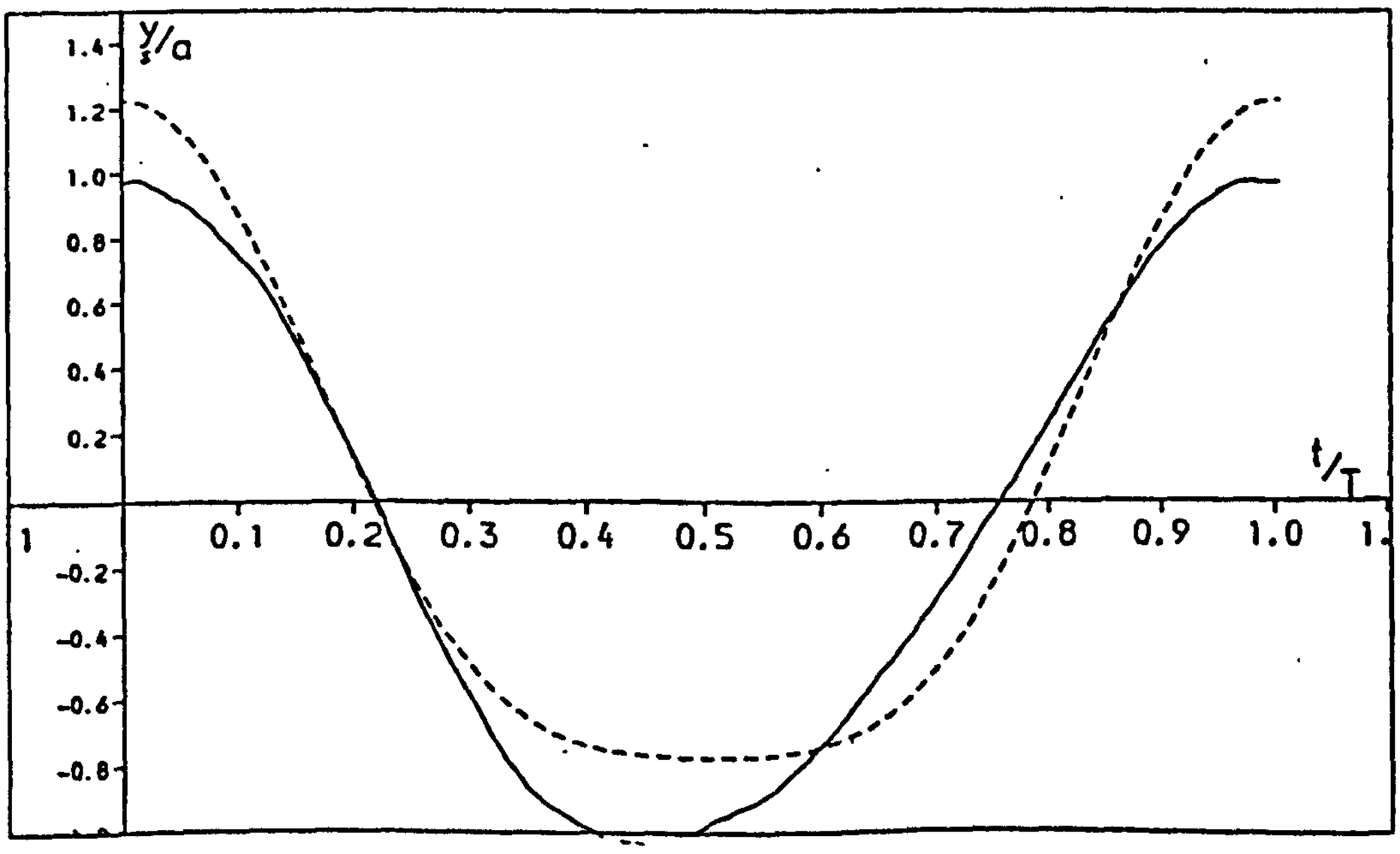

(vi) T=1.8s , a=29.5 mm

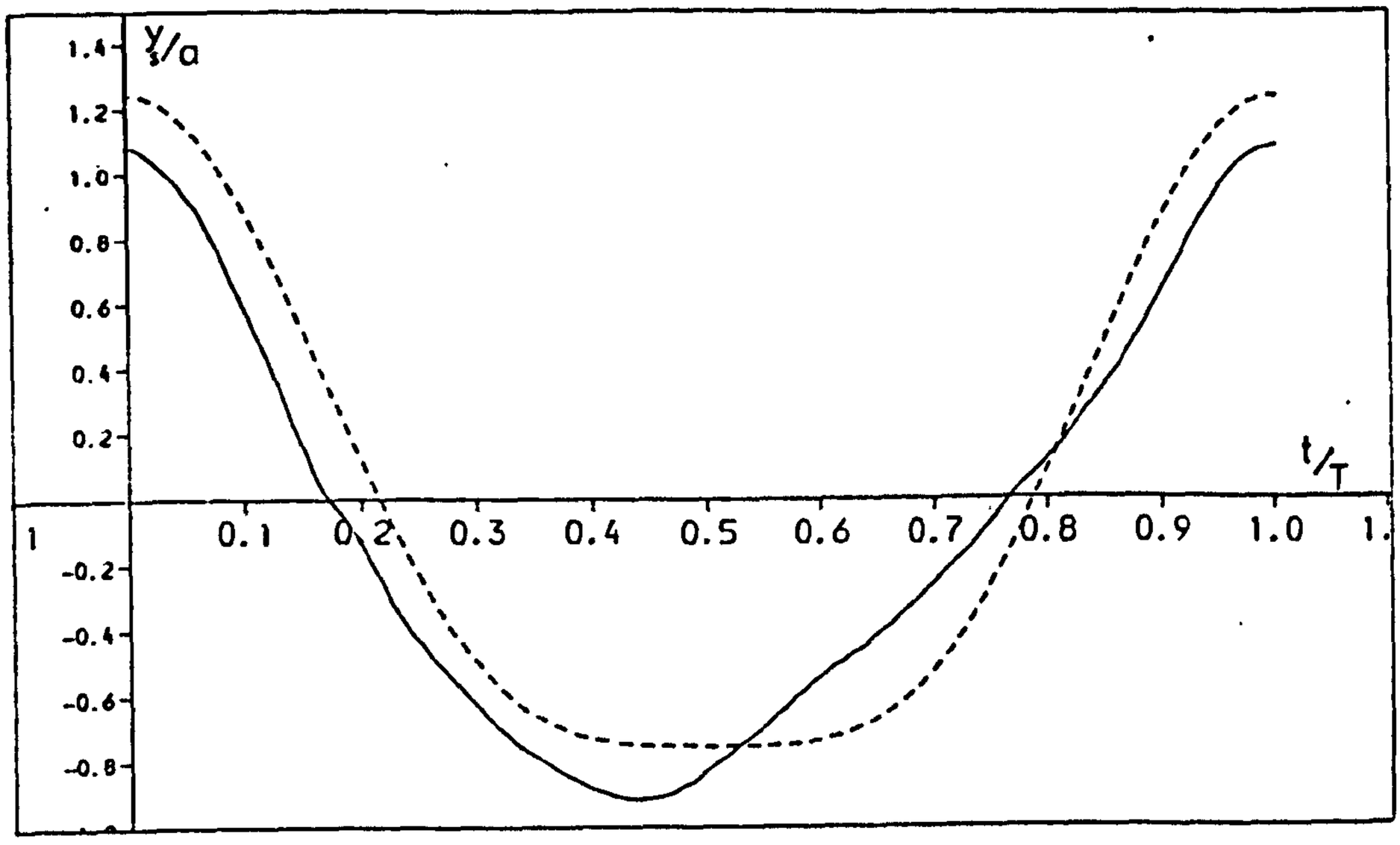

(vii) T=1.9s , a=28.7 mm

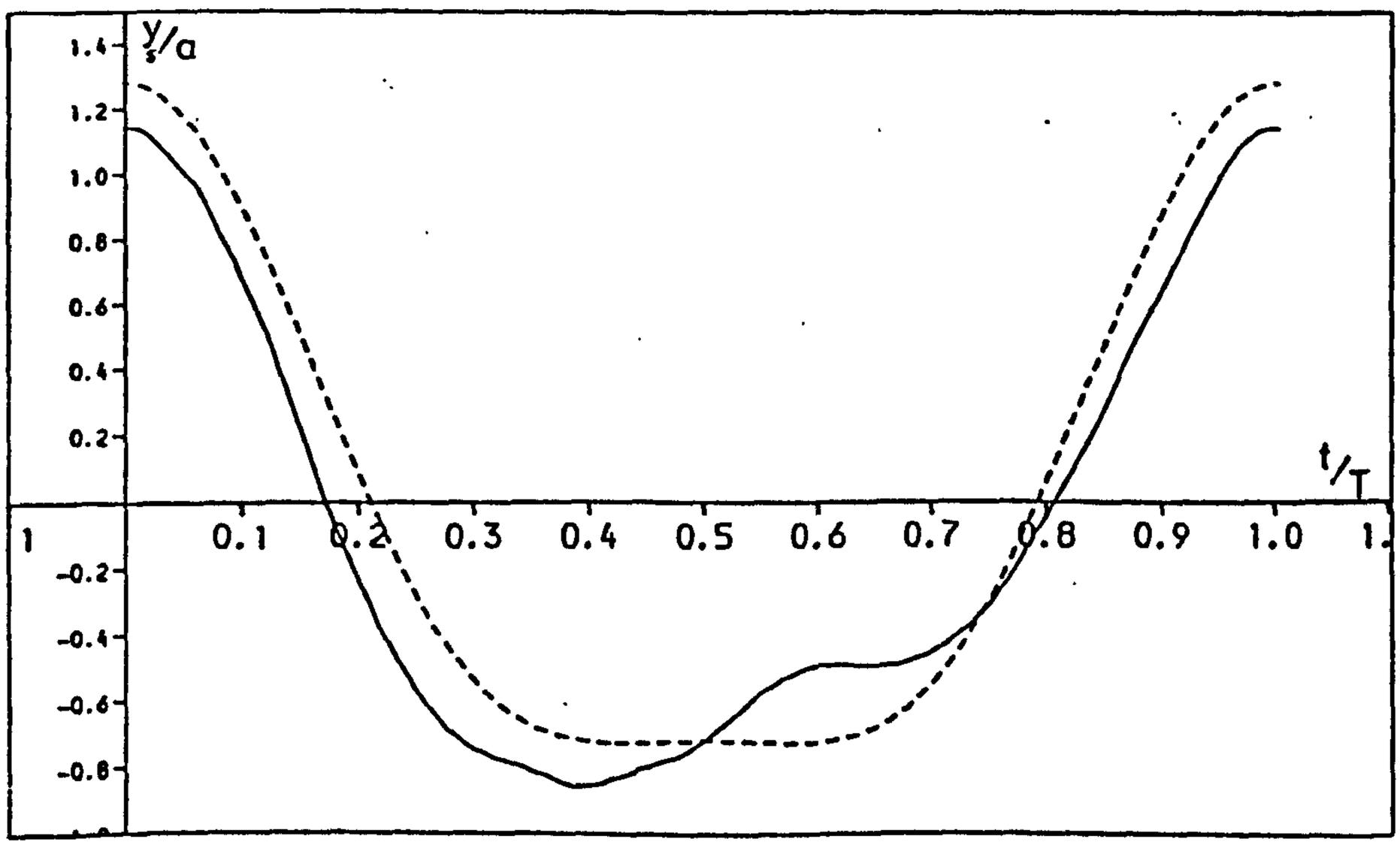

(viii) T=2.0s , a=29.8 mm

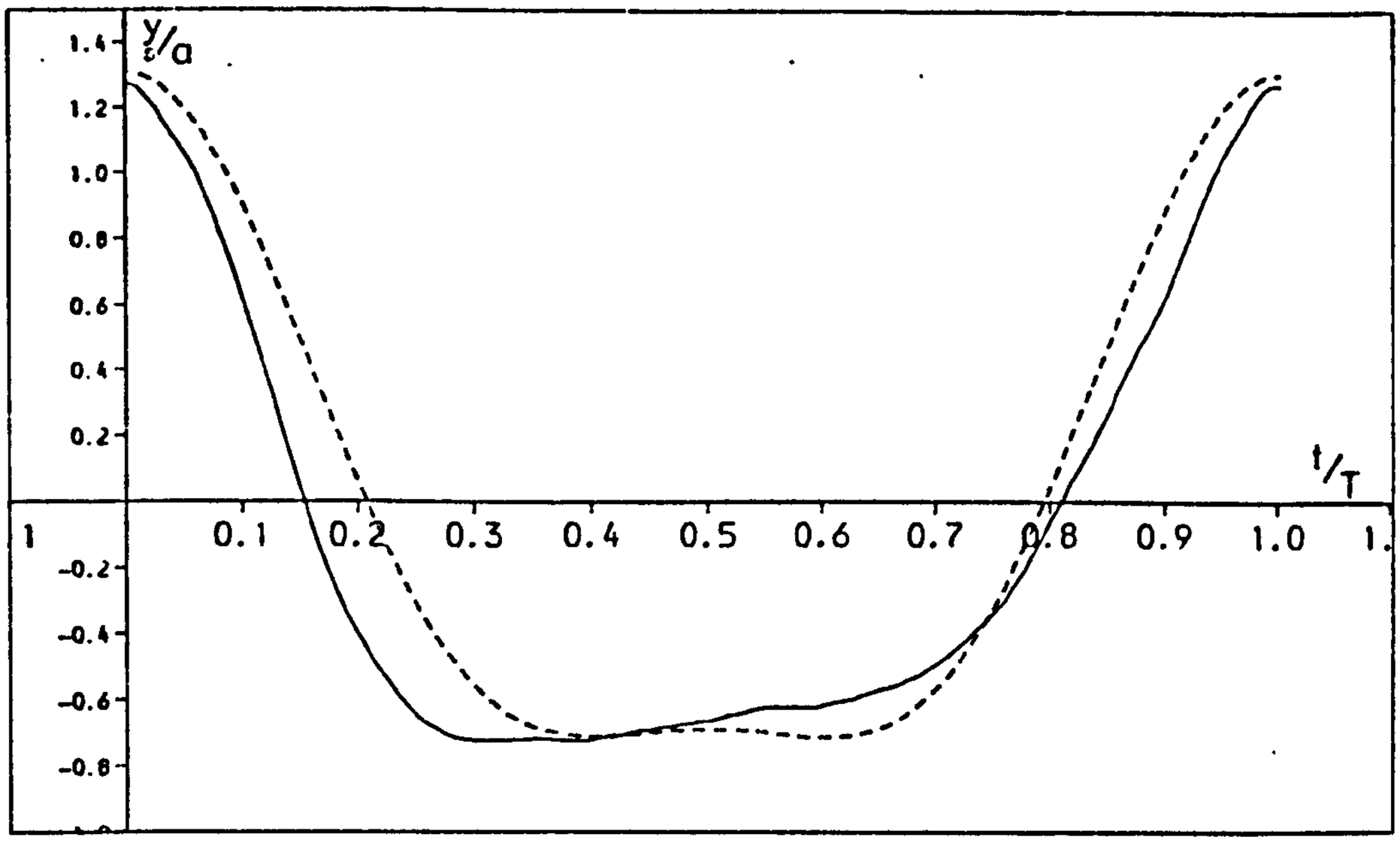

(ix) T=2.1s , a=30.7 mm

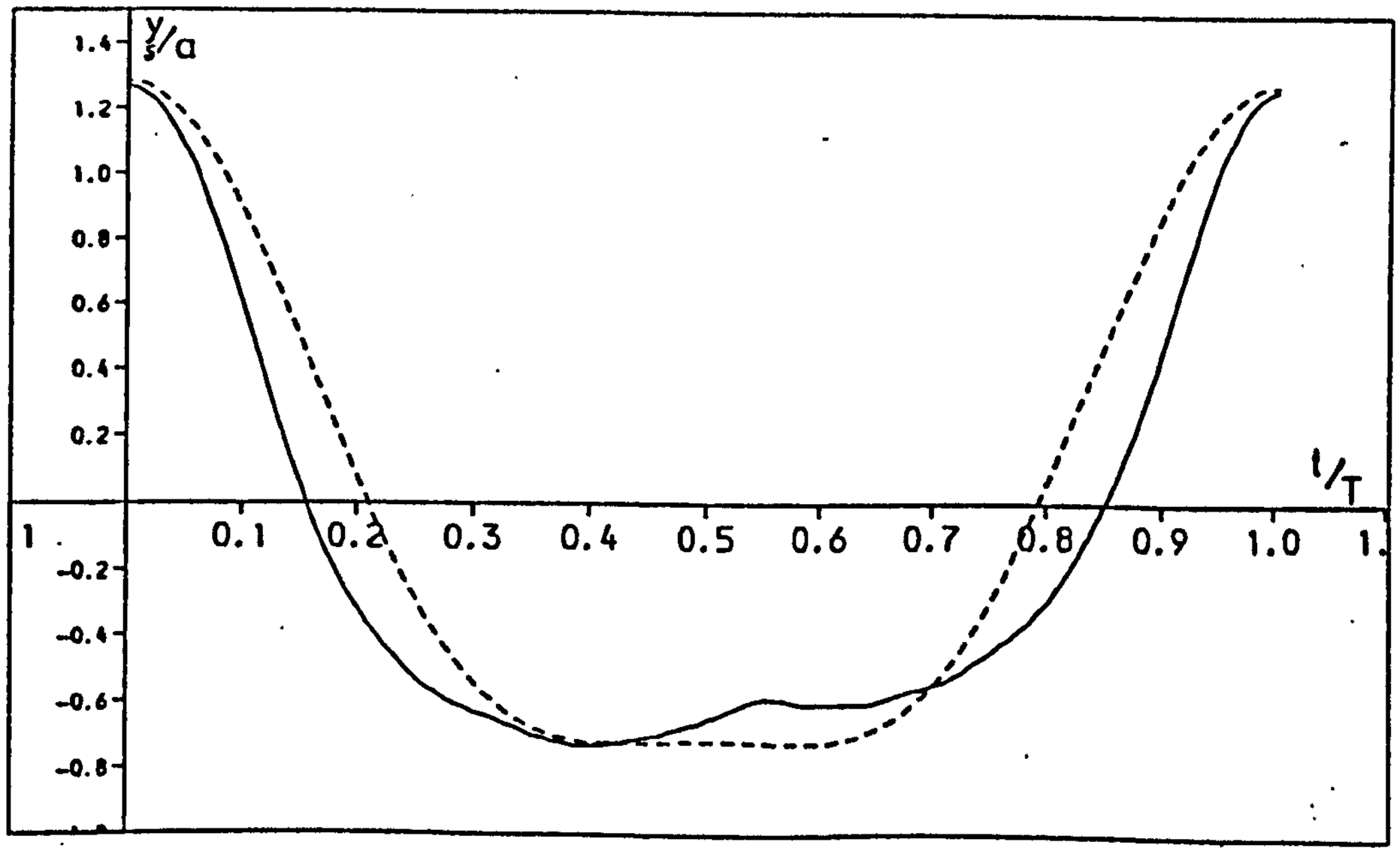

(x) T=2.2s , a=25.9 mm

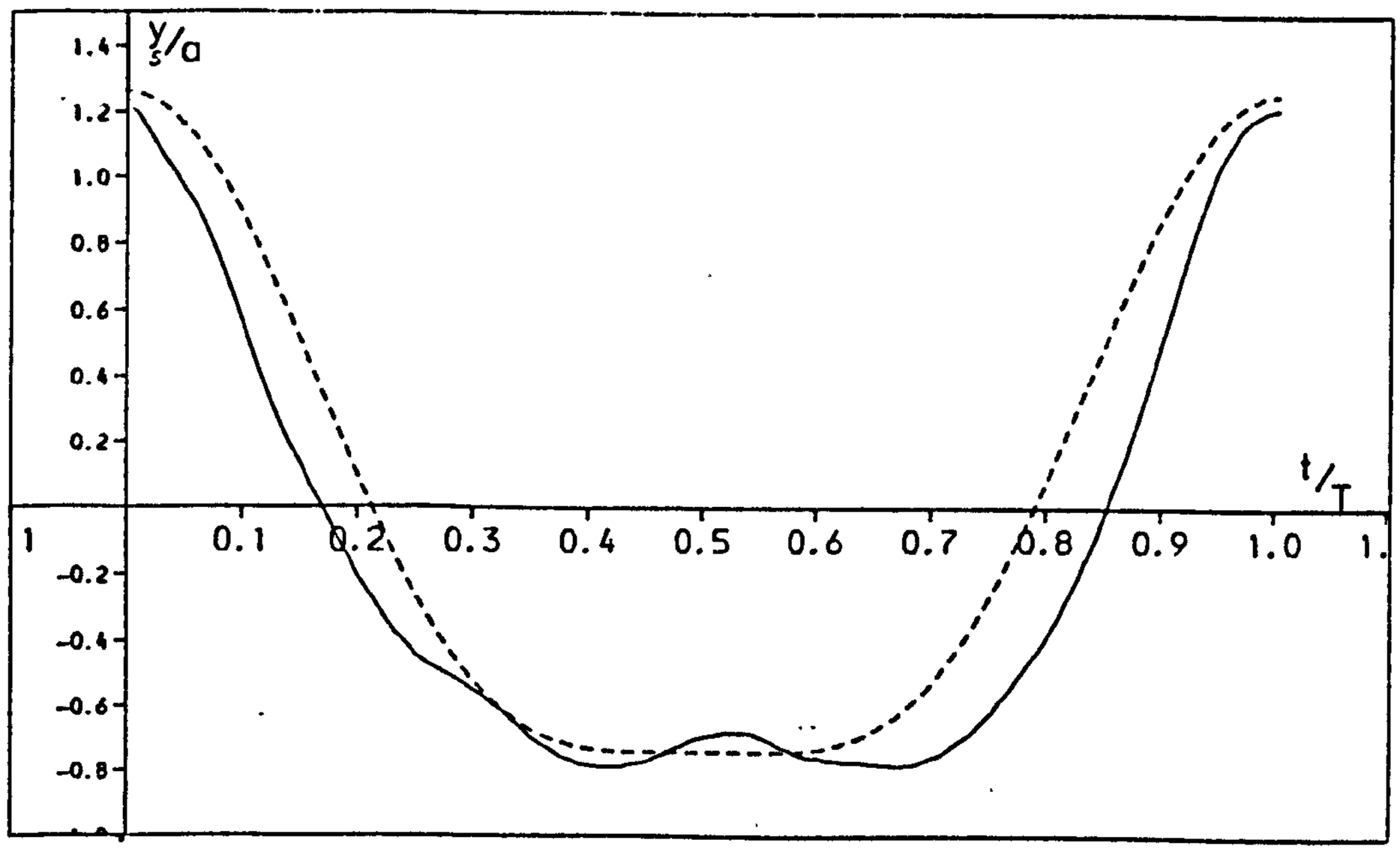

(xi) T=2.3s , a=22.1 mm

The second group of waves (1.3, 1.6, 1.7, 1.8, 1.9 and 2.0 second period) have different phases for occurrences of troughs to those of the theory predictions. For three of the waves (1.3, 1.6 and 1.7 sec.) the trough occurs after the theory (t greater than T/2) while for the rest the trough is in front of the Stokes curve. Also except for 1.3 and 1.6 sec. period waves, the wave profile is shifted with respect to the x axis. Wave 'set up' and 'set down' have not been considered in the above discussion

Since the data for all waves was collected over three cycles, with a very close agreement between the individual cycles with each other, the sources of mis-fit between data and theory are either due to the origin of the generated waves and the measuring instruments or the assumption of the theory. This is discussed further later in this chapter. However Fig. 5.2 clearly shows that for most of the priods (except 1.7, 1.8, 1.9 and 2.0 sec.) a good agreement exists between data and Stokes second order prediction.

5.4 Orbital Velocity in the Bulk of Fluid

As mentioned before (Chapter Four) eleven depths at equal intervals of 22.5 mm from just outside the viscous boundary layer were the sampling positions of the orbital velocities (horizontal and vertical) representing the bulk of fluid, for collecting the data. (Unlike the last section the rest of the results are presented for only five wave periods from 1.4 to 2.2 second at intervals of 0.2 second.

Since the eleven periods of 0.1 sec. interval do not contribute much more to the collected information than that from five wave periods).

Two approaches exist to compare the data for orbital velocities with the Stokes prediction. One is to compare the profile with the predictions of theory (eqs. 1.23 and 1.24), and the second option is to compare some characteristics of data at each depth and period with the Stokes prediction and present a sample of the profile as well.

However, because the data was collected without any change of circumstance, the author believes that the second option is equally as effective as the first with the advantage of cutting short the repetition analysis. Therefore the typical point for the analysis of orbital velocity profiles is just outside the viscous boundary layer, and the characteristics of horizontal velocity (maxima and mean) and vertical velocity (maxima and minima - since theoretically the mean velocity is zero) are analysed and compared with the prediction curves from Stokes second order and also Longuet-Higgins (as for horizontal mean or mass transport velocity).

5.4.1 Velocity Maxima and Minima

Fig. 5.3a represents the results for maximum horizontal velocity and maximum and minimum vertical velocity with the Stokes theory (eq. 1.23 and 1.24). The obvious observation

5.3(a) Max. and Min. Profiles

---- Theoretical max. and min. vertical velocity Eq. 1.24

—— Theoretical max. horizontal velocity Eq. 1.23

5.3(b) Mass Transport Velocity

—— Stokes Theory Eq. 1.28

---- Longuet-Higgins Conduction Solution Eq. 2.27.

M.T. vel.

.—.—. L-Higgins Mean Vel.

Data

▽ max. vertical vel.

△ min. vertical vel.

✕ max. horizontal vel.

◊ mean vel.

$\hat{U}'$, $\hat{V}'$ theoretical values

Fig. 5.3 Velocity of Water Particle Orbits in the Bulk of Fluid. Smooth Bed

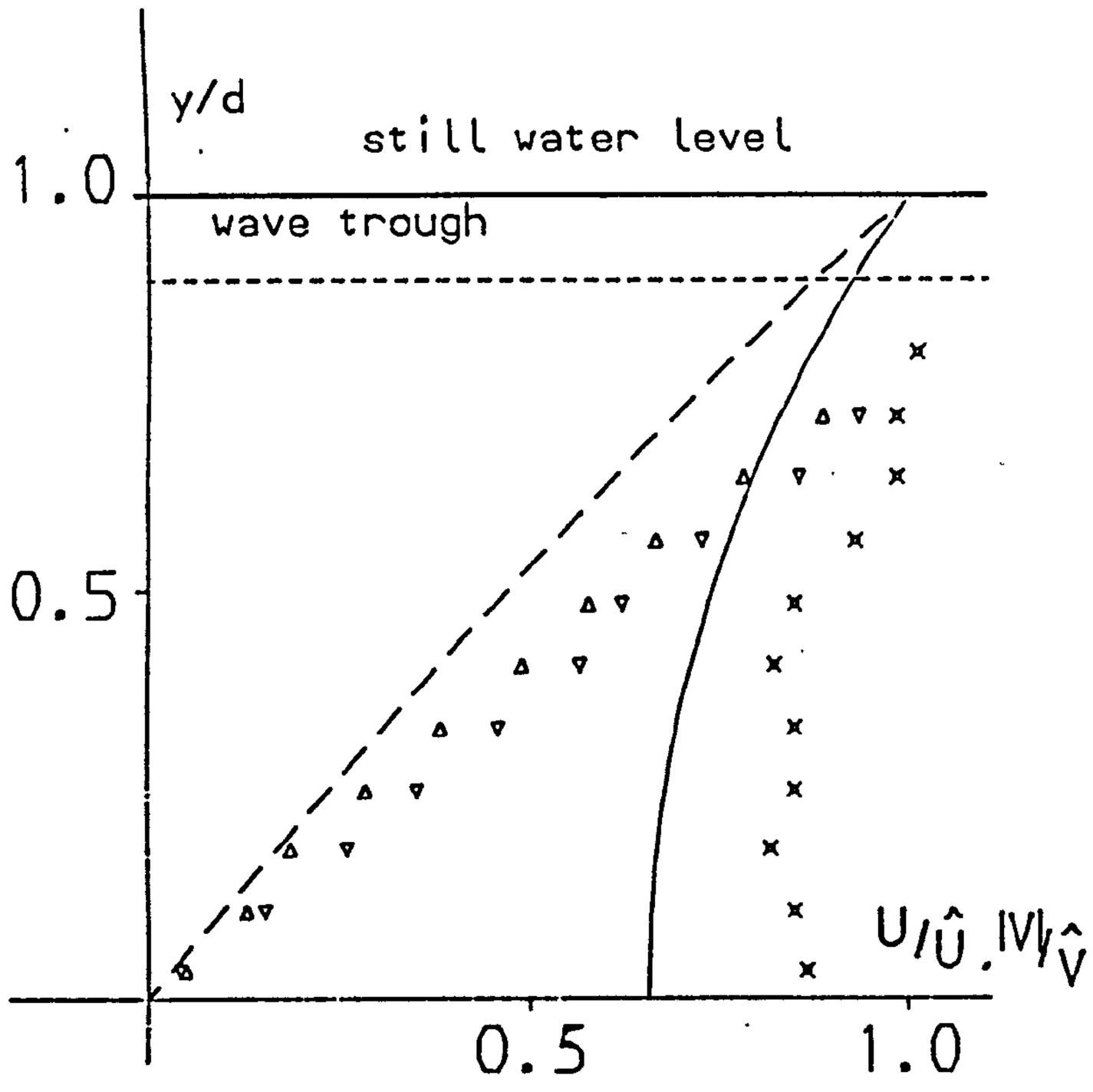

(a)

Û = 283.3 mm/s

V̂ = 173.2 mm/s

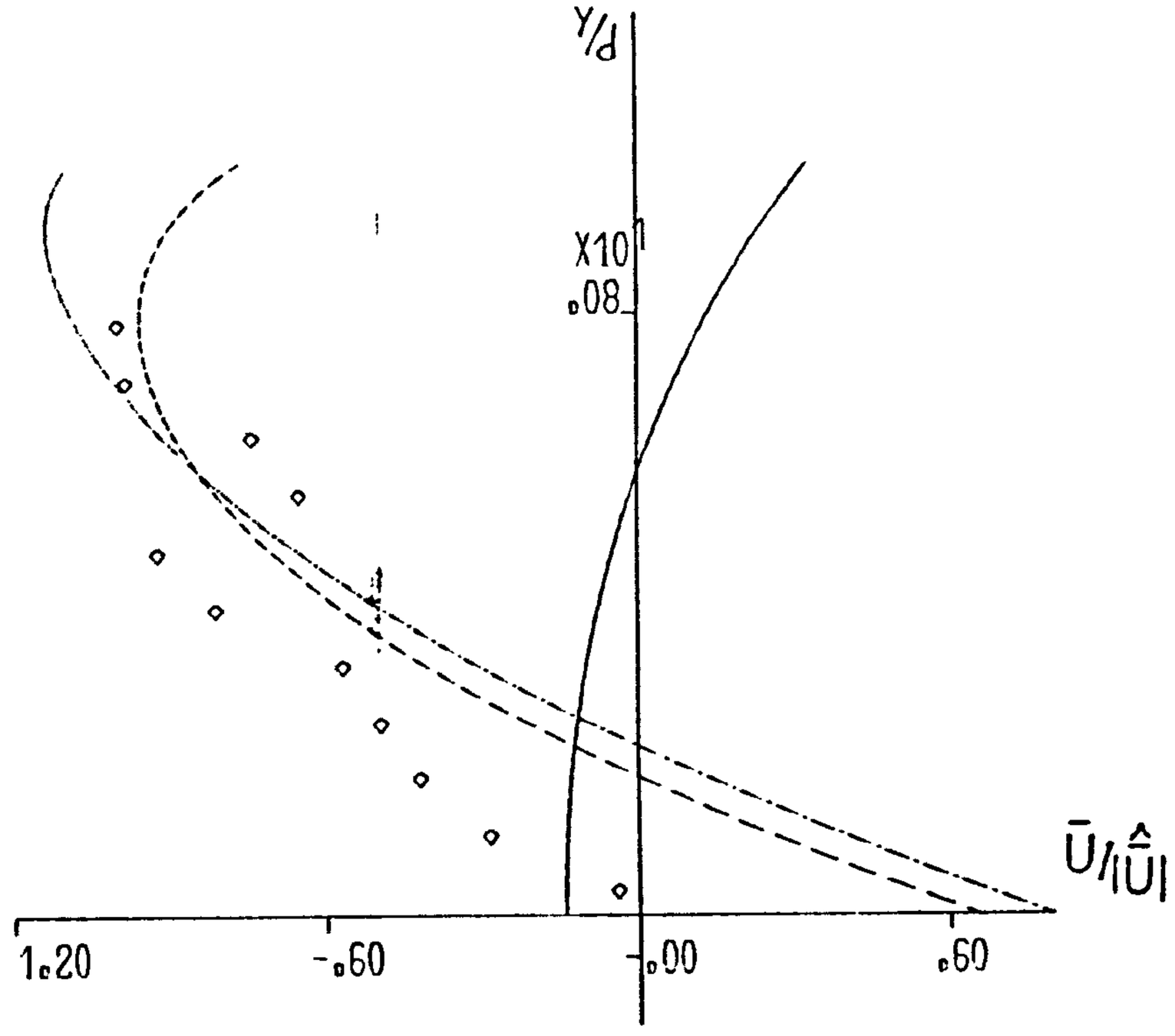

(b)

|Û| = 38.1 mm/s

(i) T = 1.4 s

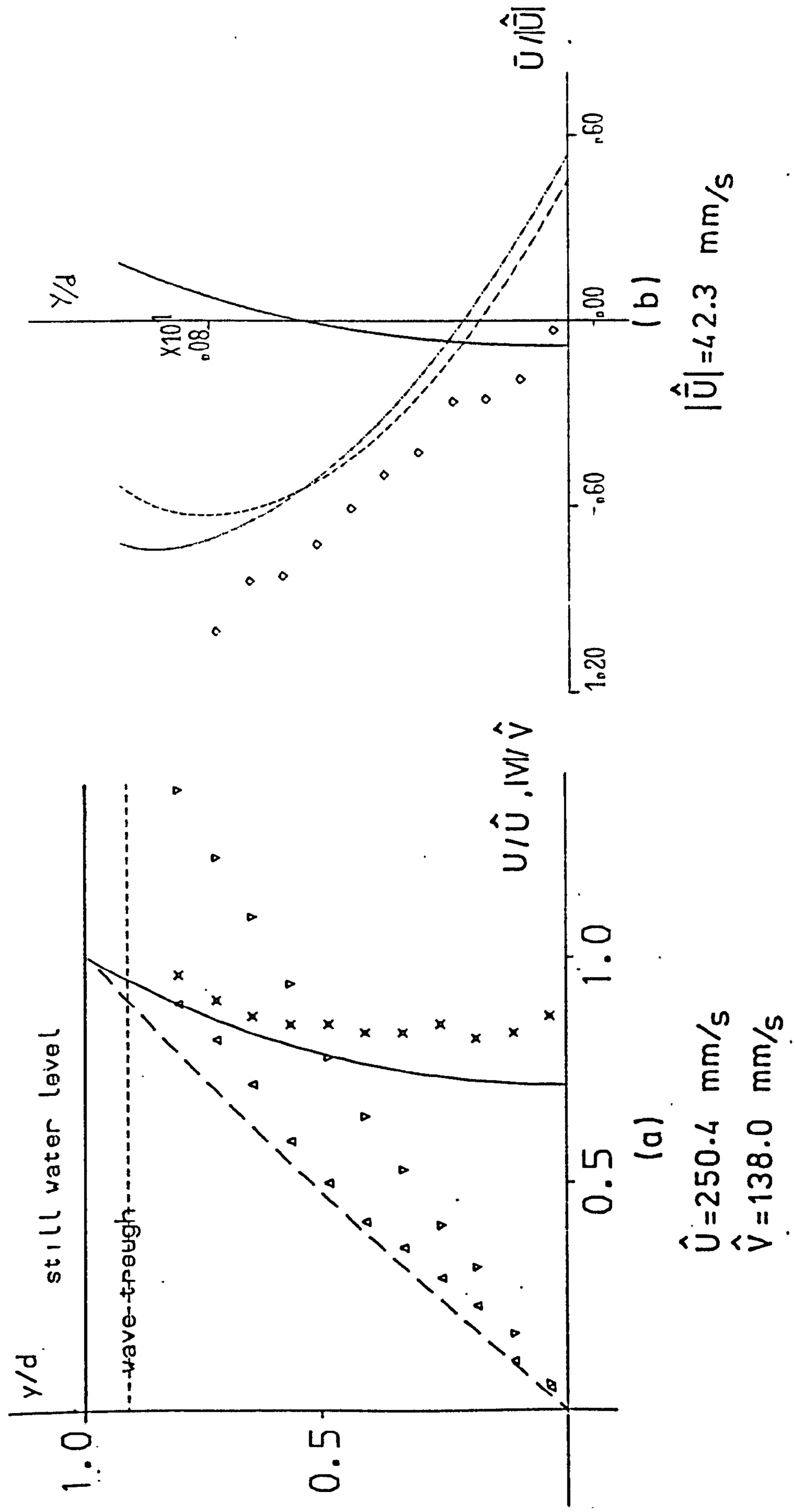
Ū/|Ū|
Y/d
X10
.08
.00
.60
-.60
1.20
(b)
|Ū|=42.3 mm/s
U/Û , V/V̂
0.5
1.0
(a)
Û=250.4 mm/s
V̂=138.0 mm/s
(iii) T=1.6 s
still water level
wave-trough
y/d
1.0
0.5

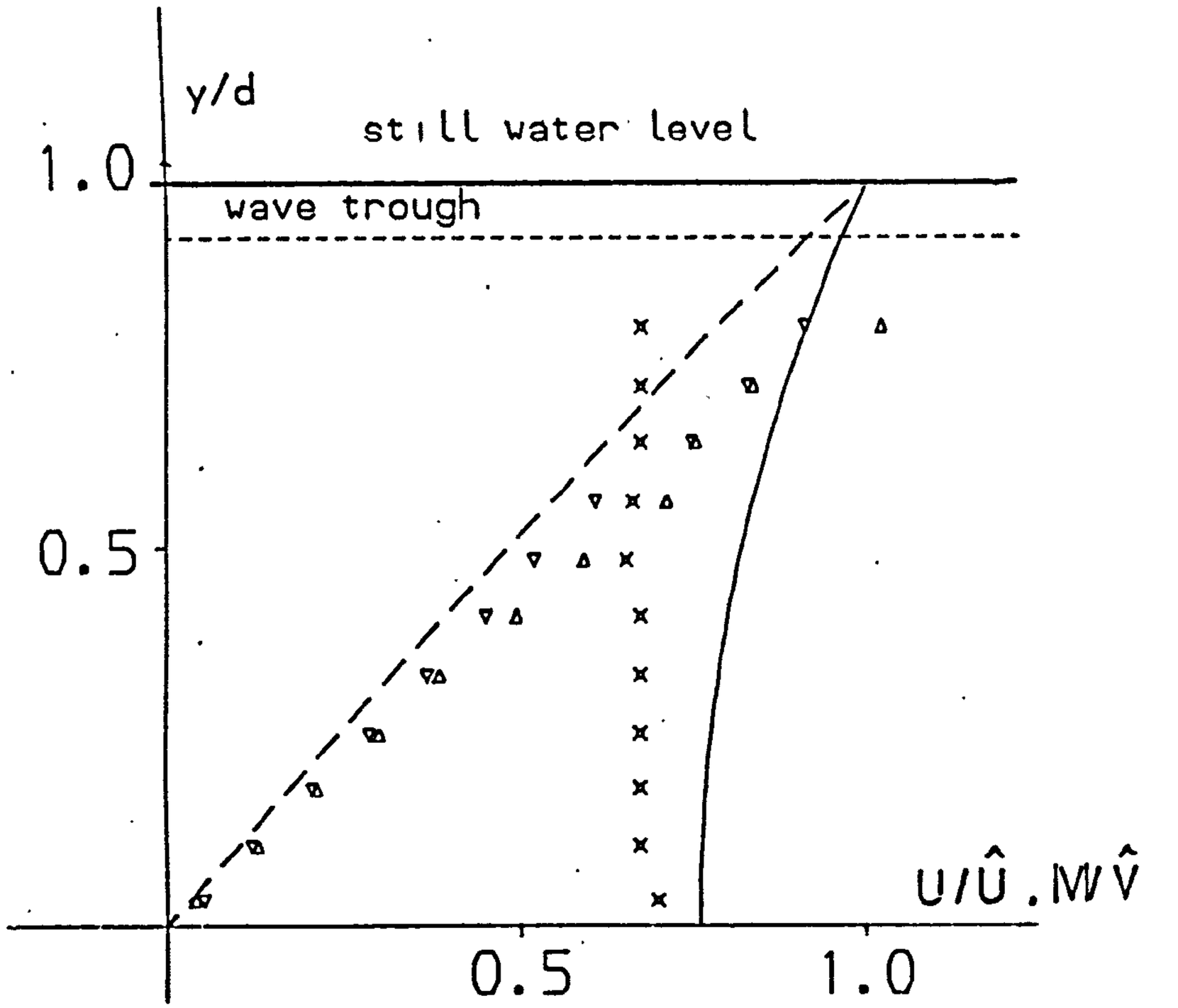

(a)

$\hat{U}$=221.0 mm/s

$\hat{V}$=112.5 mm/s

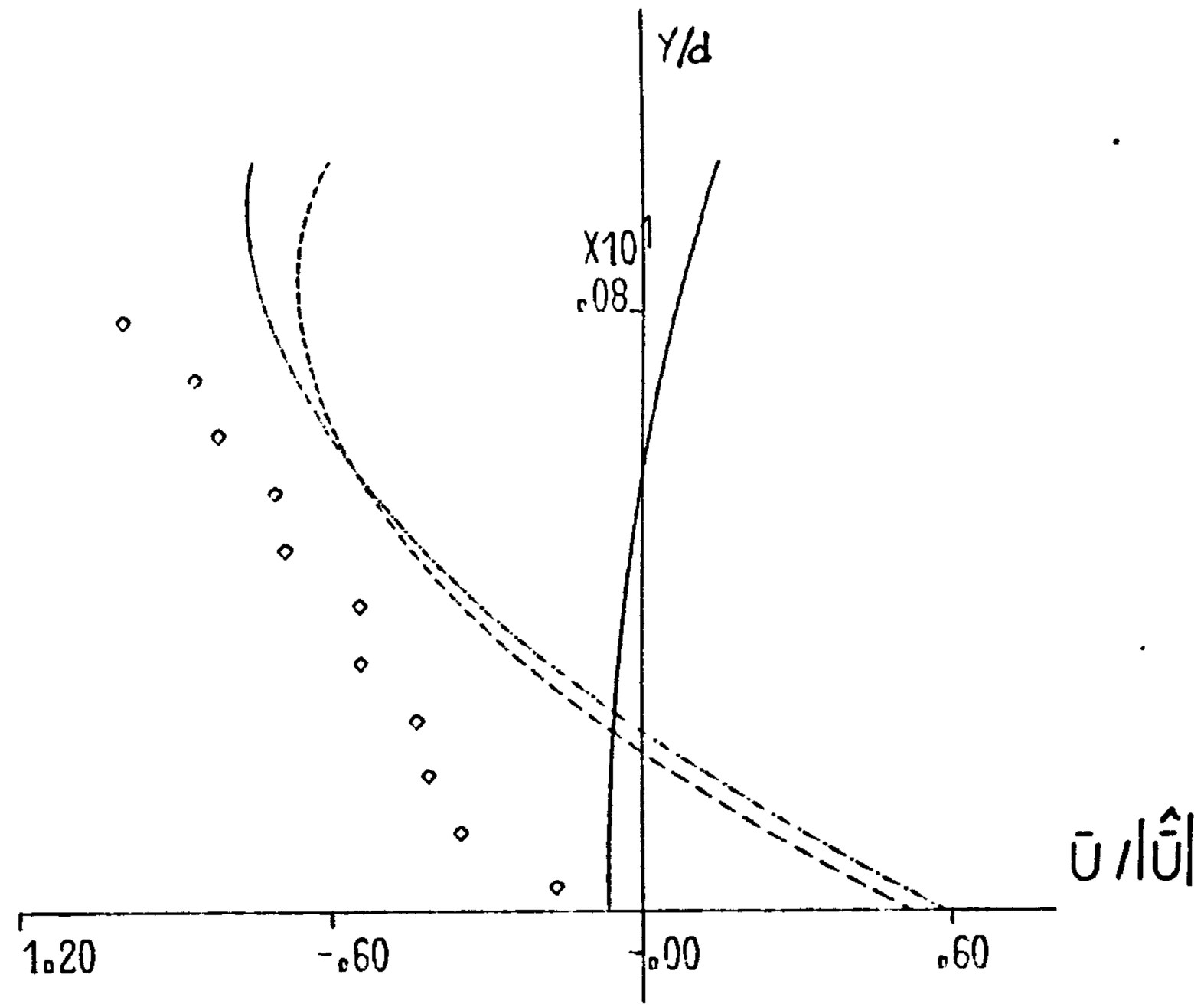

(b)

$|\hat{U}|$=31.3 mm/s

(iii) T=1.8 s

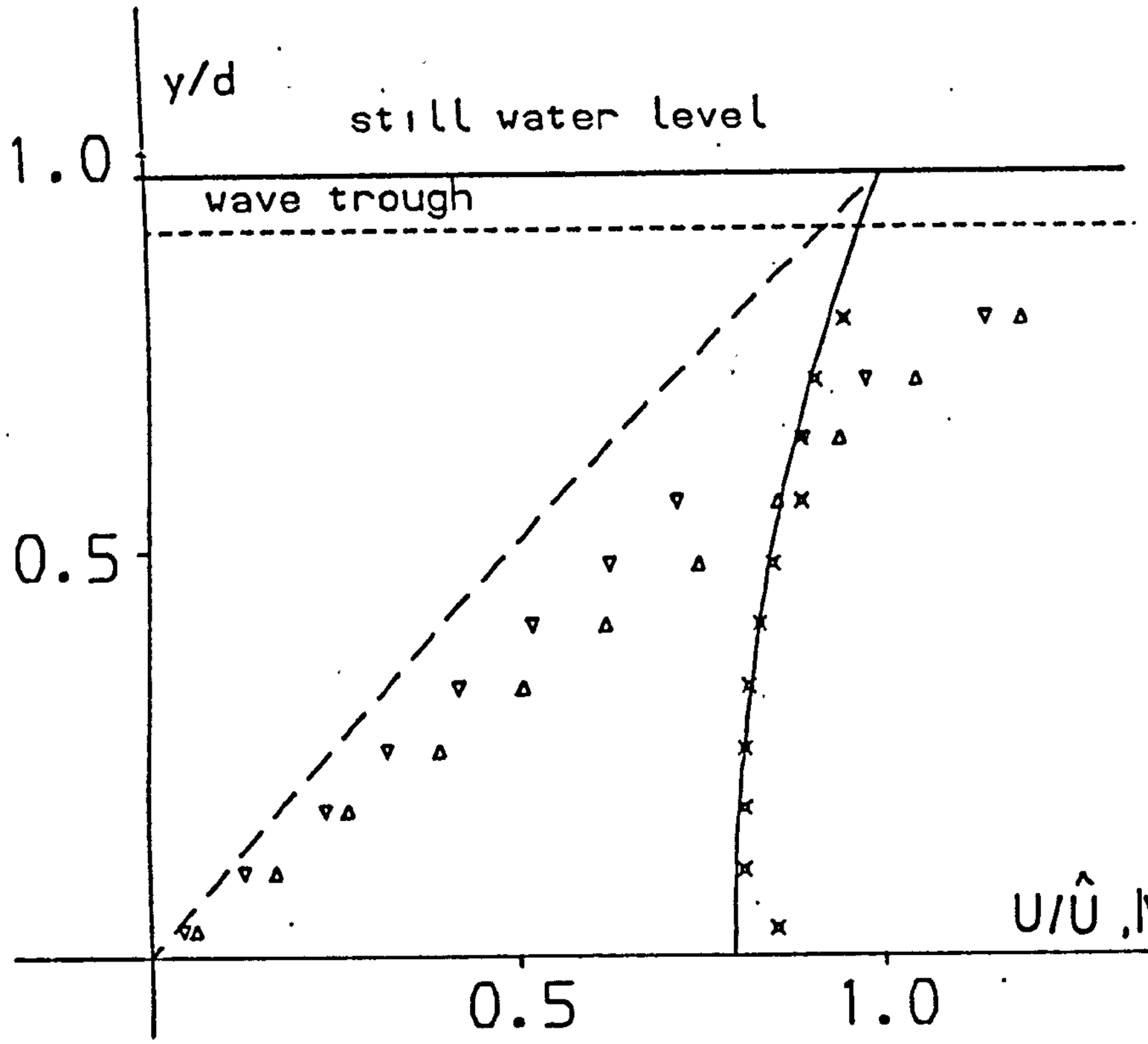

(a)

$\hat{U}$ = 230.1 mm/s

$\hat{V}$ = 110.0 mm/s

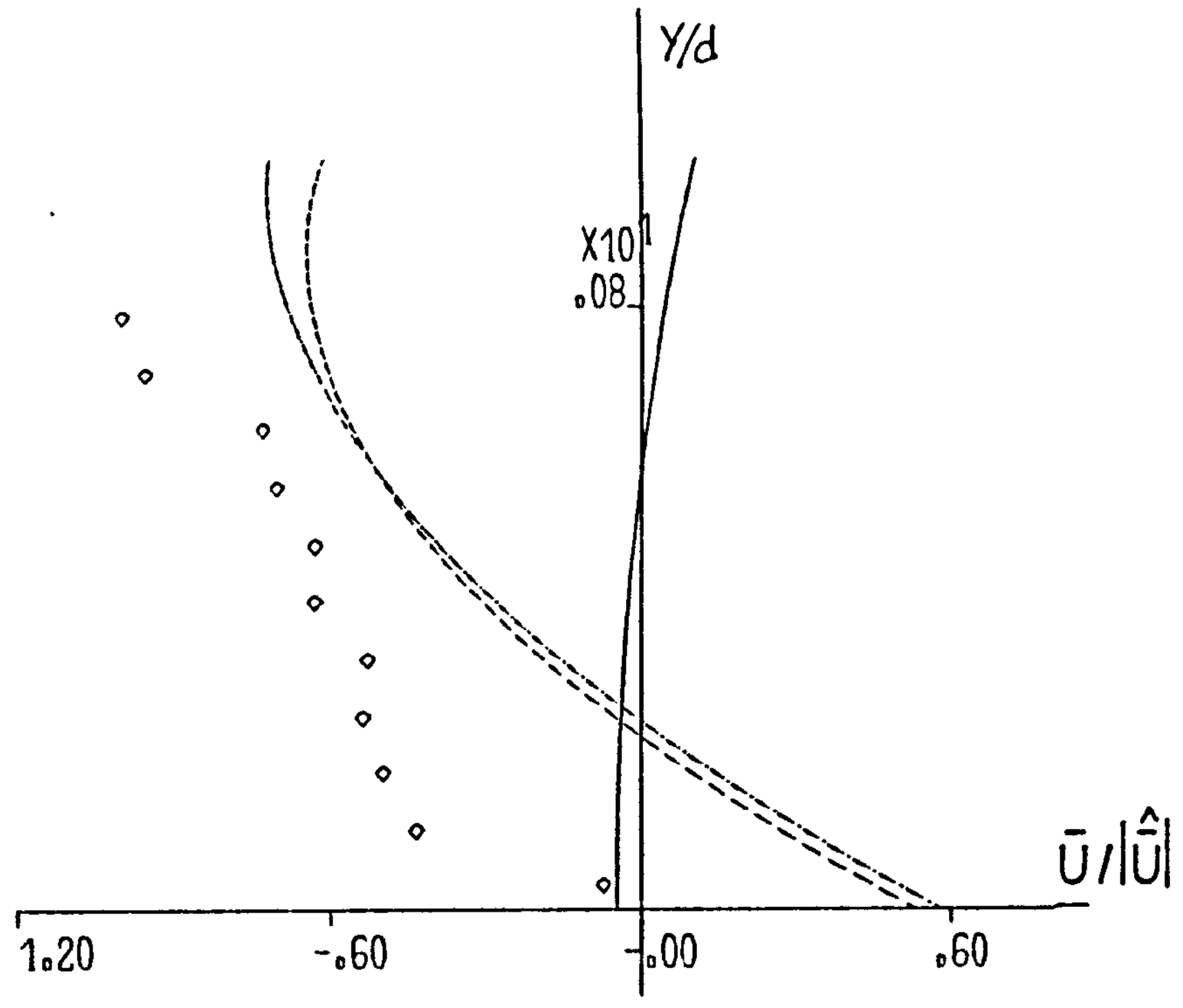

(b)

$|\hat{U}|$ = 34.5 mm/s

(iv) T = 2.0 s

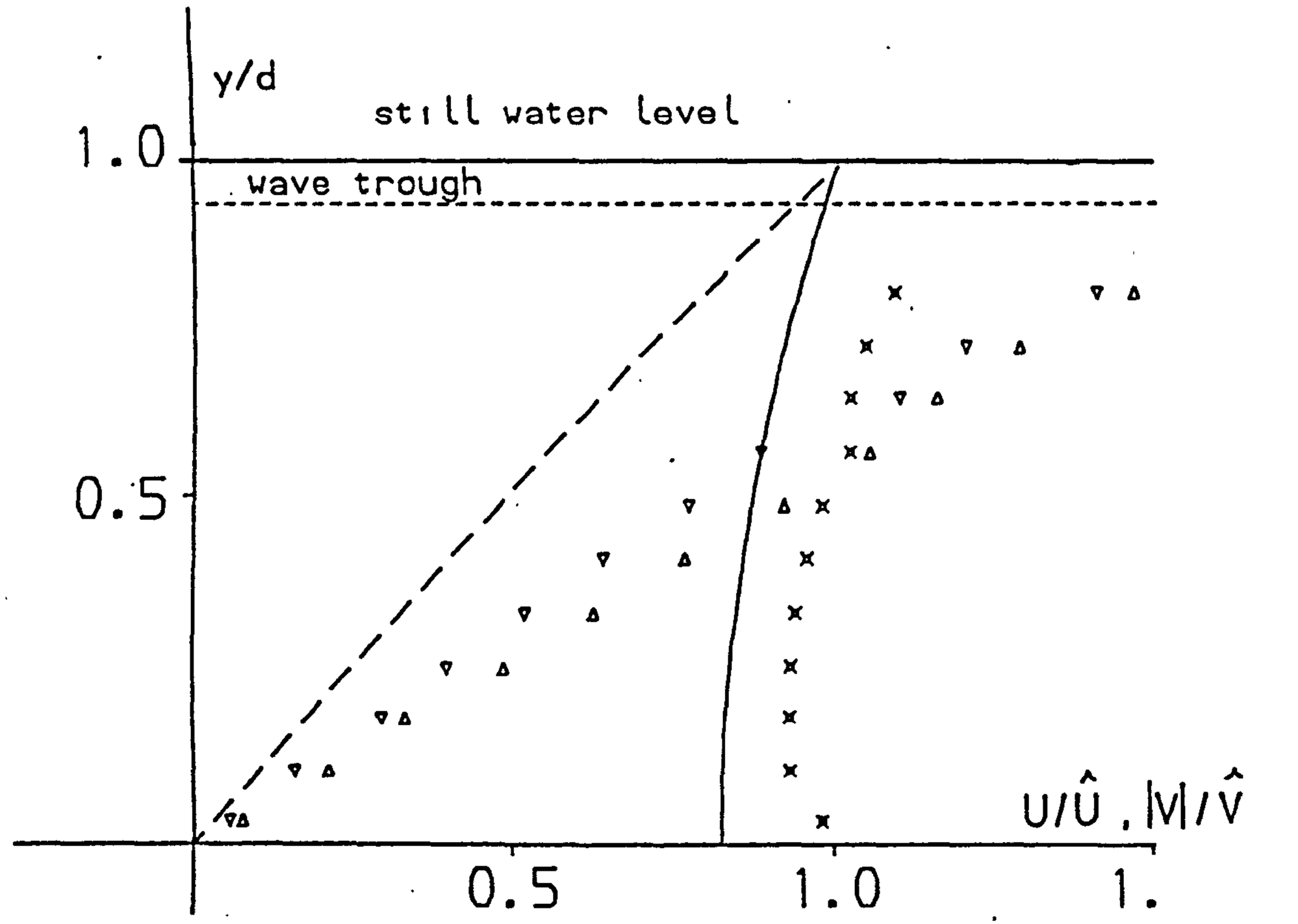

(a)

$\hat{U}$ =199.9 mm/s

V =89.3 mm/s

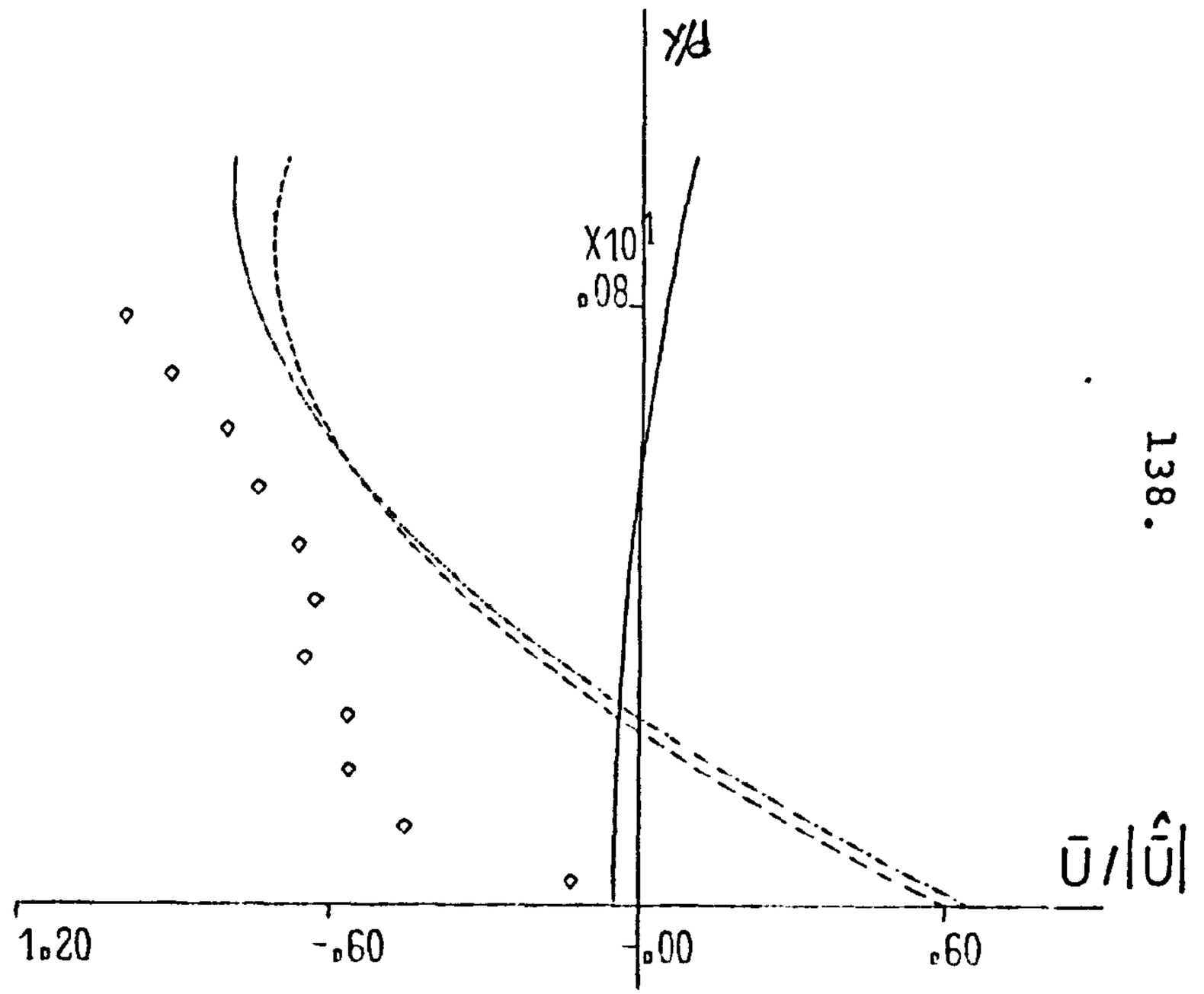

(b)

$|\hat{U}|$ =22.5 mm/s

(v) T= 2.2 s

from all the graphs is that for vertical velocity maxima, measured values are always greater than the prediction curve (for 1.6 and 2.2 sec. wave periods it is up to 100%). For minimum values of vertical velocity too the data is always greater than theoretical curve (again for 2.2 sec. wave it is almost twice the theoretical value). This surely suggests that the theory does not produce a good prediction and under-estimates the collected values by a large amount.

On the other hand the maximum horizontal velocity values are better predicted by Stokes theory. Except for the 1.8 sec. wave period, for which the data has lesser values than theoretical curve, and for 2.0 sec. wave period for which the points are on the calculated curve the other three periods' data values are greater than the prediction values. But overall the correlation is good and the theory is acceptable for horizontal velocity.

5.4.2 Drift Velocity

Fig. 5.3a shows a backward drift (opposite direction to the wave progression) throughout the depth for all the periods (except very close to bed for 1.6 sec. wave period), which is contradictory to the Stokes prediction (eq. 1.23). However, this was not a surprise since it was shown by Bagnold (1947) that the mass transport velocity is different to Stokes second order theory, and Longuet-Higgins (1953) also showed theoretically that the mass transport velocity is

different from the prediction theory by Stokes for a perfect non-viscous fluid. The Longuet-Higgins prediction theory (eq. 2.27) is a reasonable fit to the results, considering that the theory is for mass transport velocity whilst the data is the mean velocity values (see Appendix D), nevertheless in all the graphs the theory has larger values than the data (for lower wave periods the difference is less).

5.4.3 Velocity Outside the Viscous Boundary Layer

5.4.3.1 Horizontal Velocity

Graphs (a) of Fig. 5.4 show the profile of the horizontal velocity data (30 points in each period) together with the predicted theory. The first impression from the graphs is the good agreement between the collected and the theoretical profiles. Although for 1.4 and 1.6 sec. waves the data has larger (or smaller for negative velocity) value of up to 30 per cent and for 2.0 and 2.2 sec. waves a secondary inflexion point exists in the trough, also for 1.8 sec. wave the minimum (or trough of the curve) value of data occurs before the theoretical value, but in general the misfits are very small and the theory is a good prediction for horizontal velocity.

5.4.3.2 Vertical Velocity

Generally in the (b) graphs of Fig. 5.4 the recorded result for vertical velocity has greater values than the theoretical

- Stokes Theory Eq. 1.23

• Data

5.4(a) Horizontal Velocity

- Stokes Theory Eq. 1.24

• Data

5.4(b) Vertical Velocity

Fig. 5.4 Velocity Profile Outside the Viscous Boundary Layer(Smooth bed)

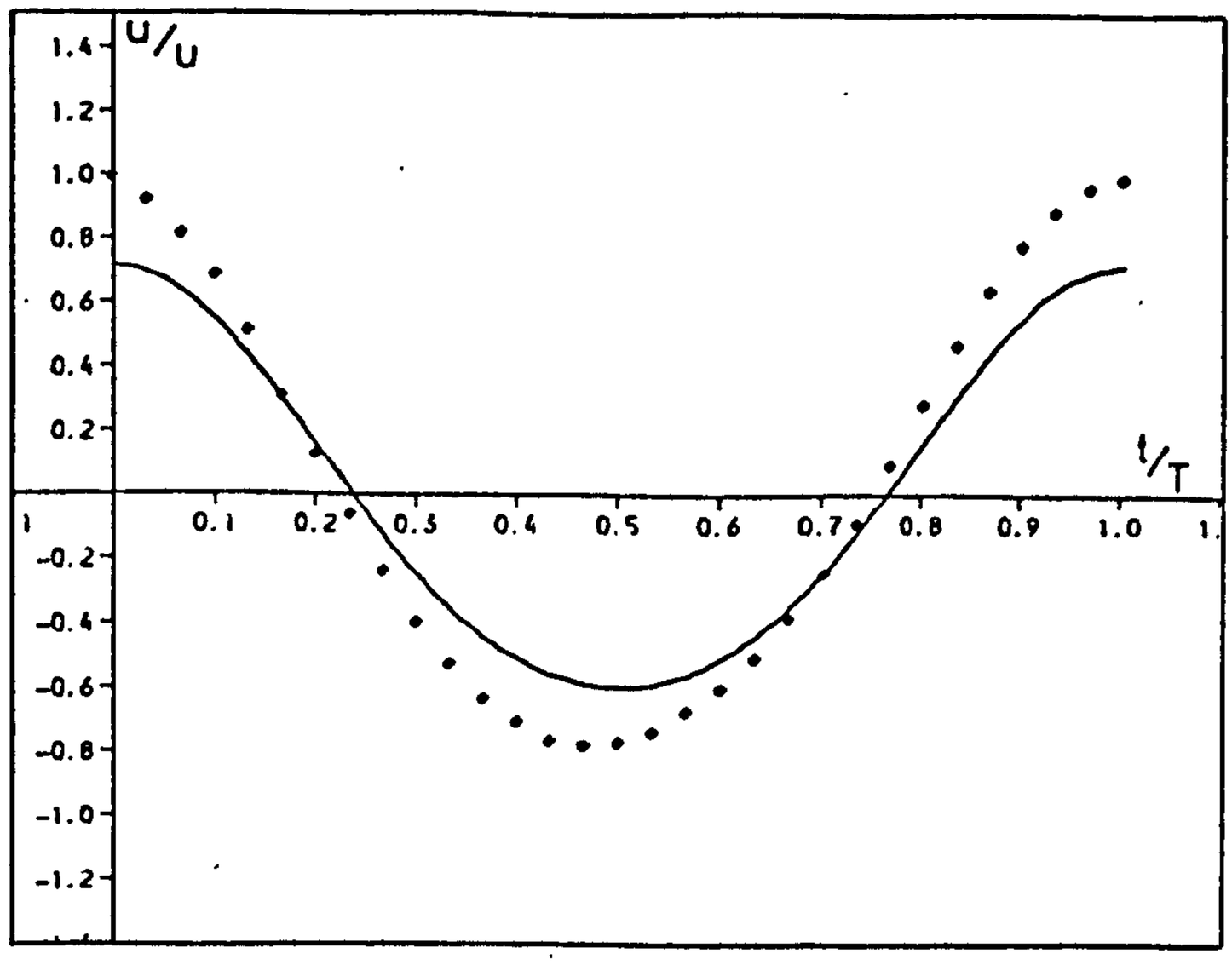

(a) $\hat{u}$=260.4 mm/s

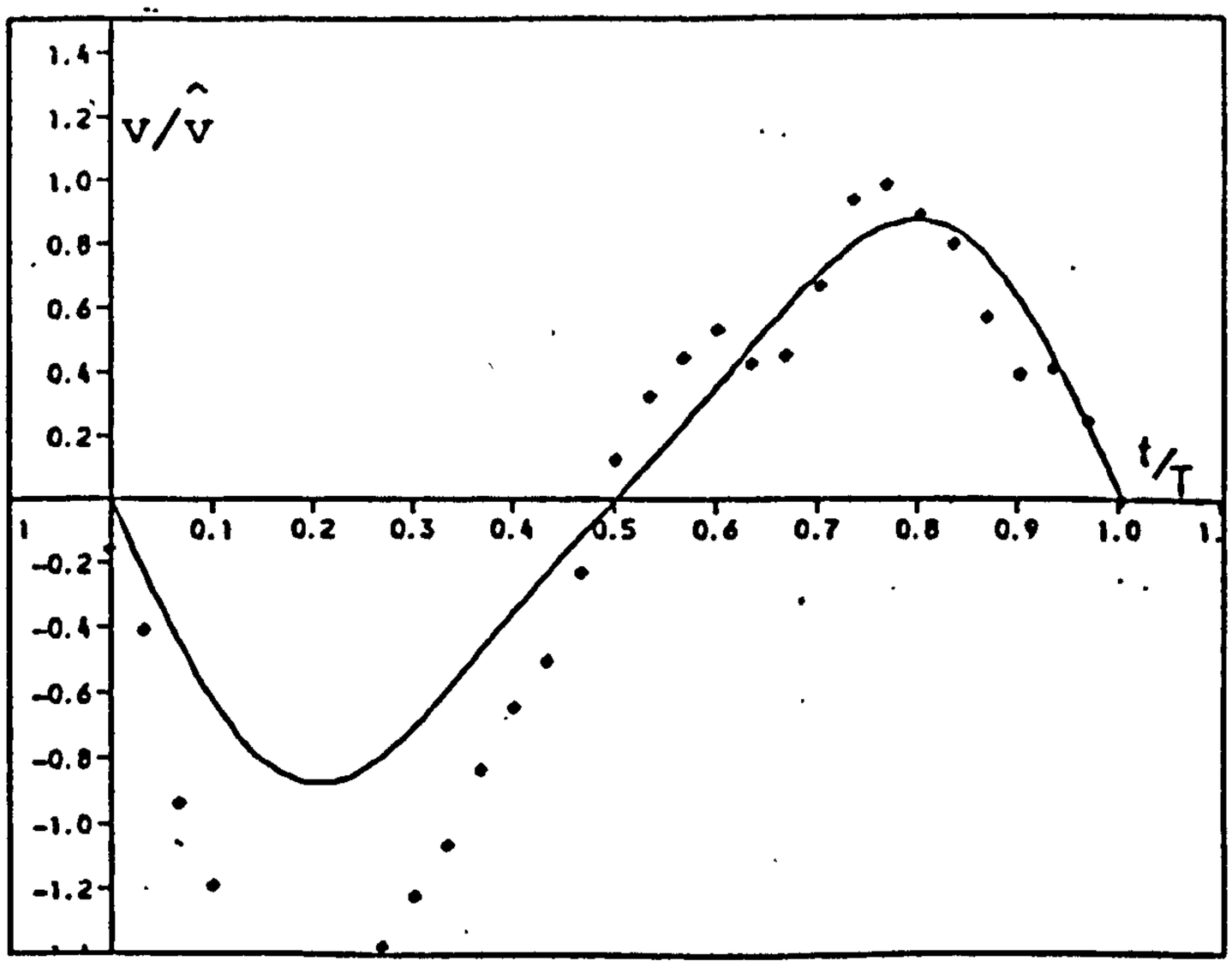

(b) $\hat{v}$= 6.0 mm/s

(i) T=1.4 s

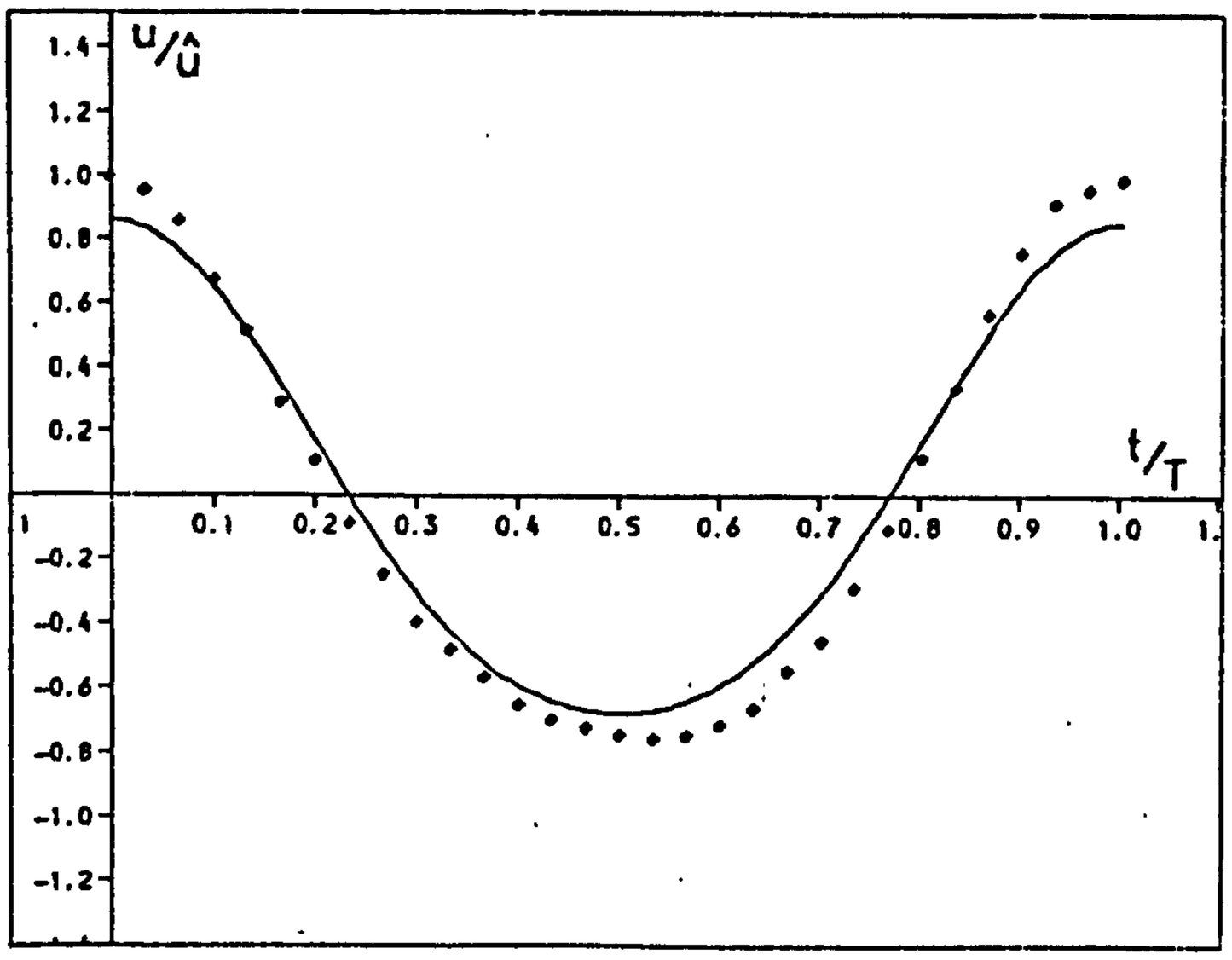

(a) $\hat{u}$=209.5 mm/s

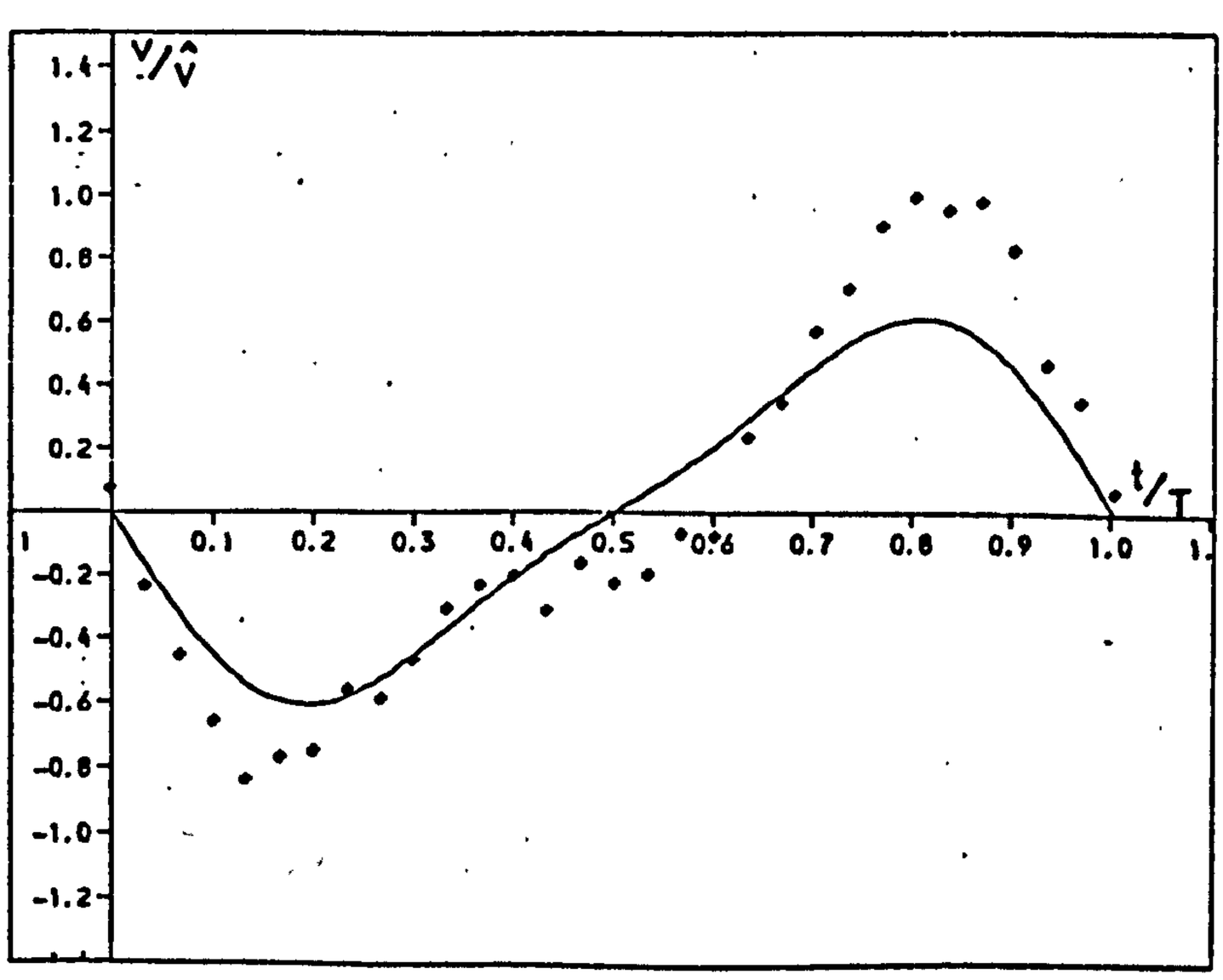

(b) $\hat{v}$=7.1 mm/s

(ii) T=1.6 s

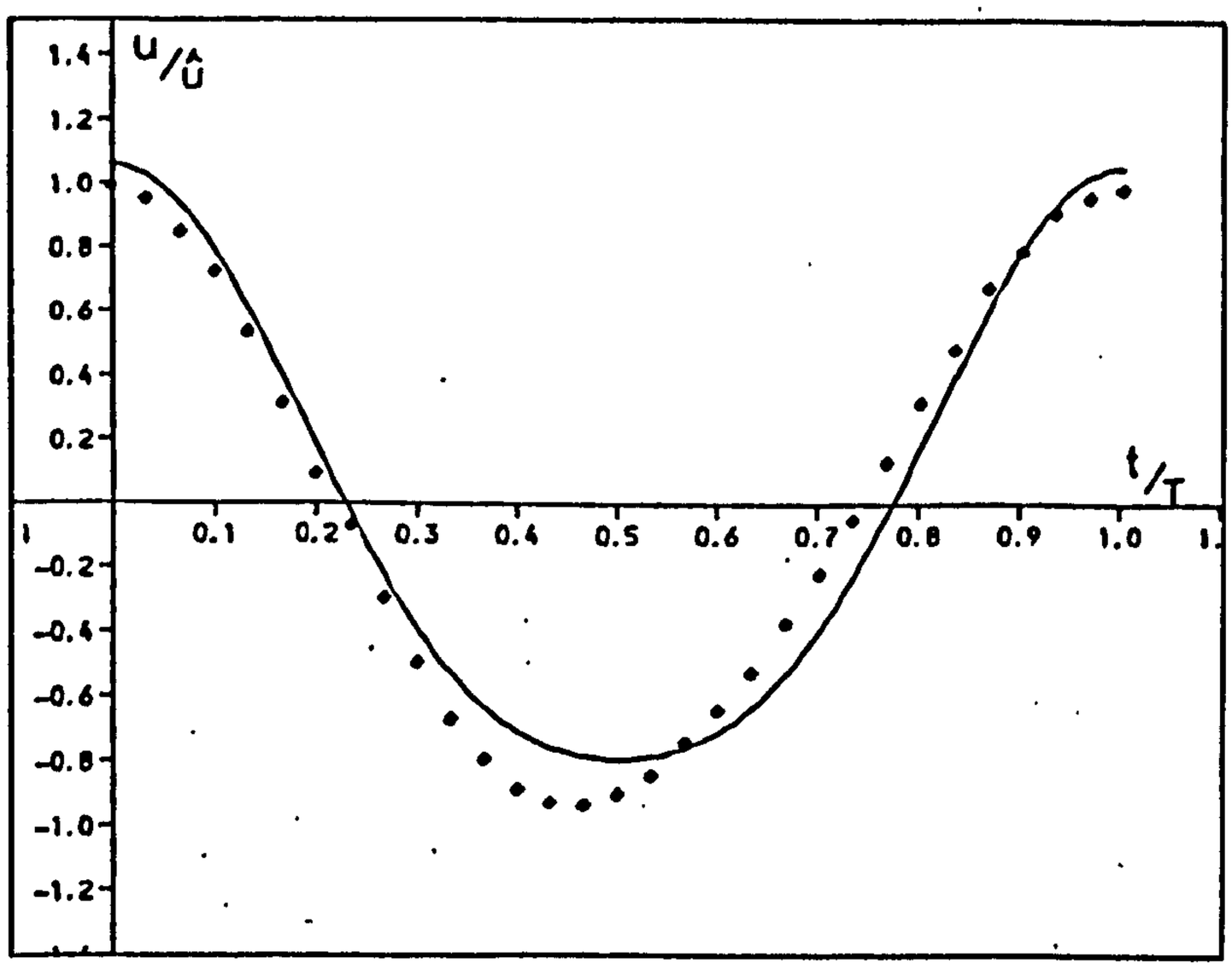

(a) $\hat{u}$=159.6 mm/s

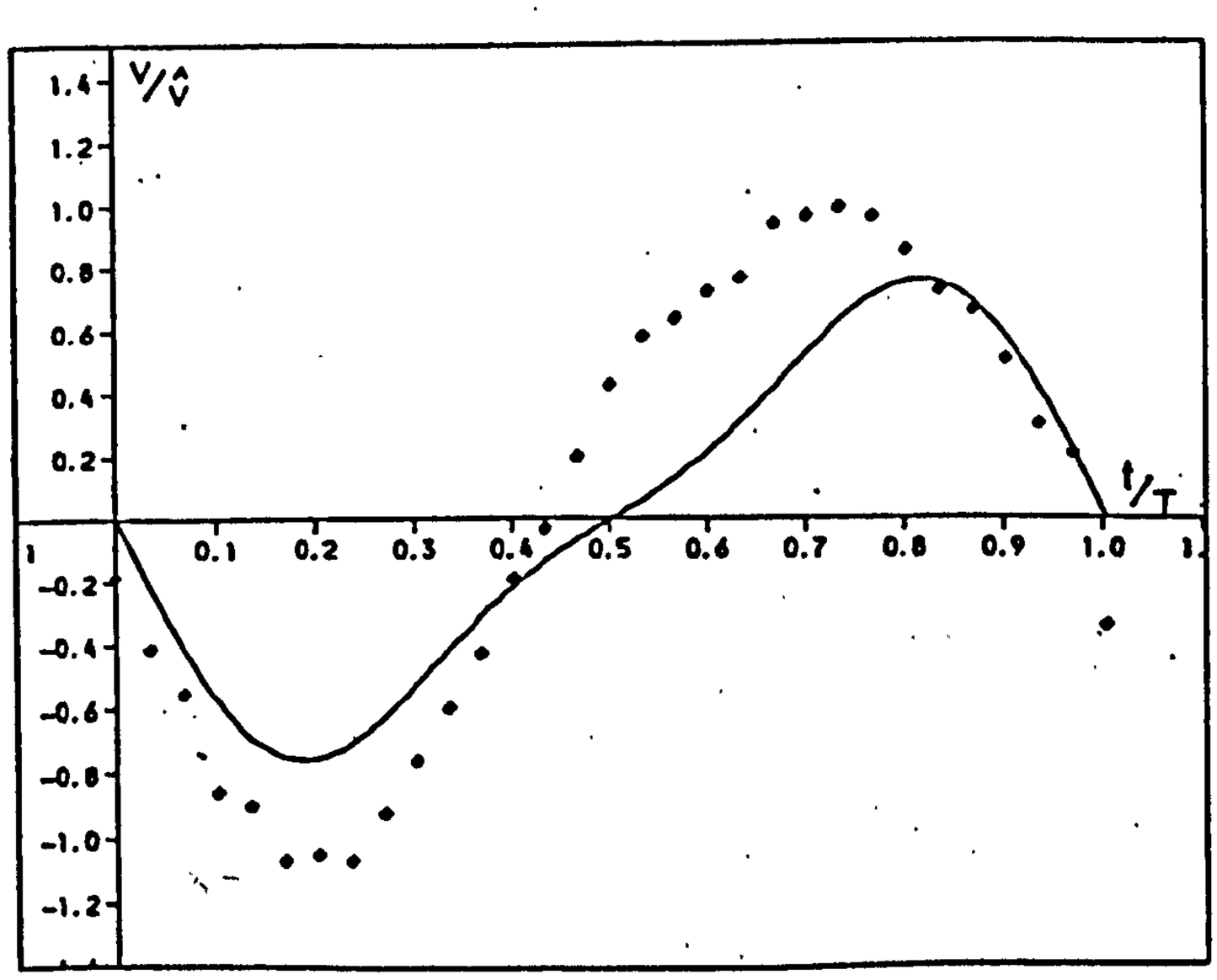

(b) $\hat{v}$=4.8 mm/s

(iii) T=1.8 s

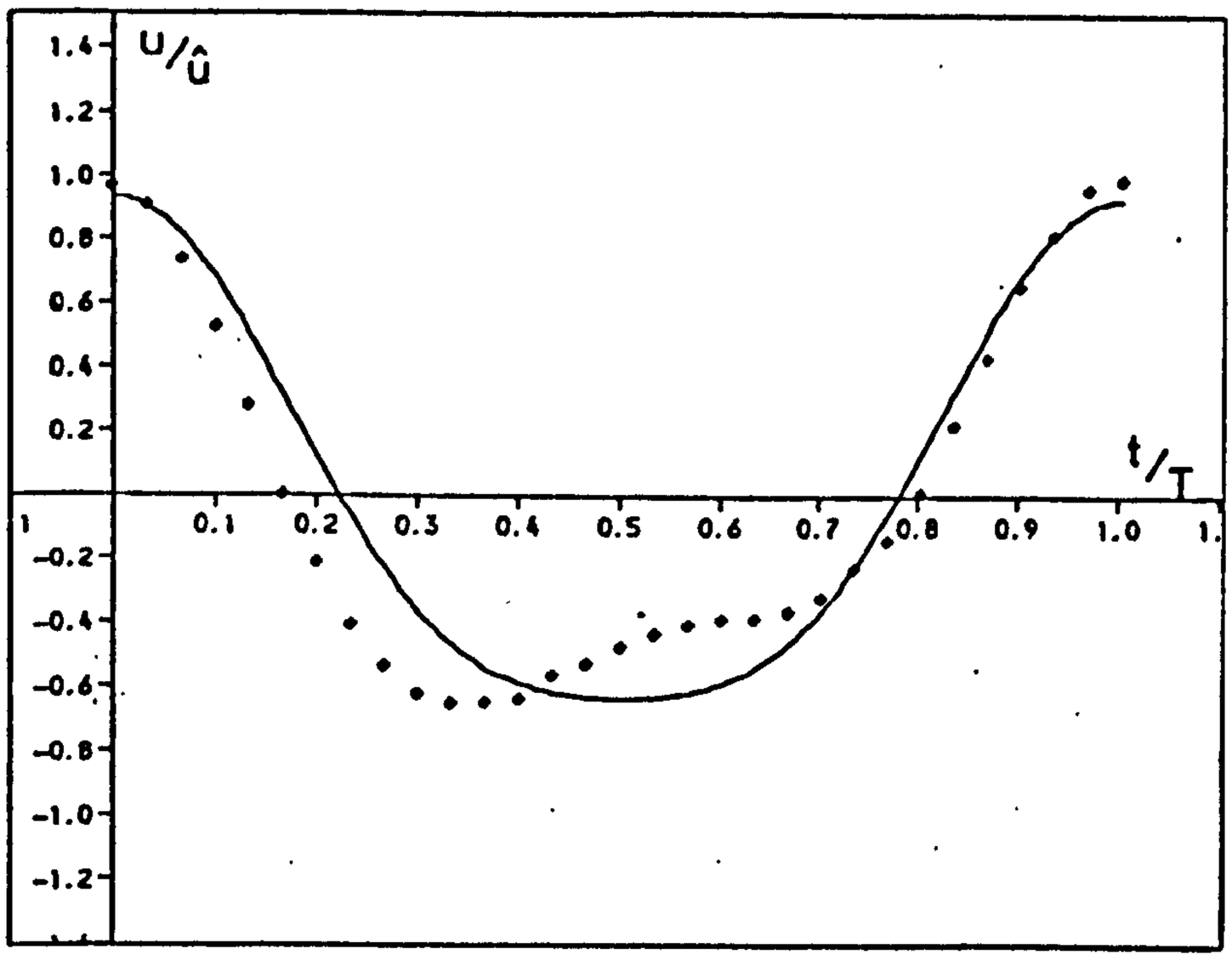

(a) $\hat{u}$=195.6 mm/s

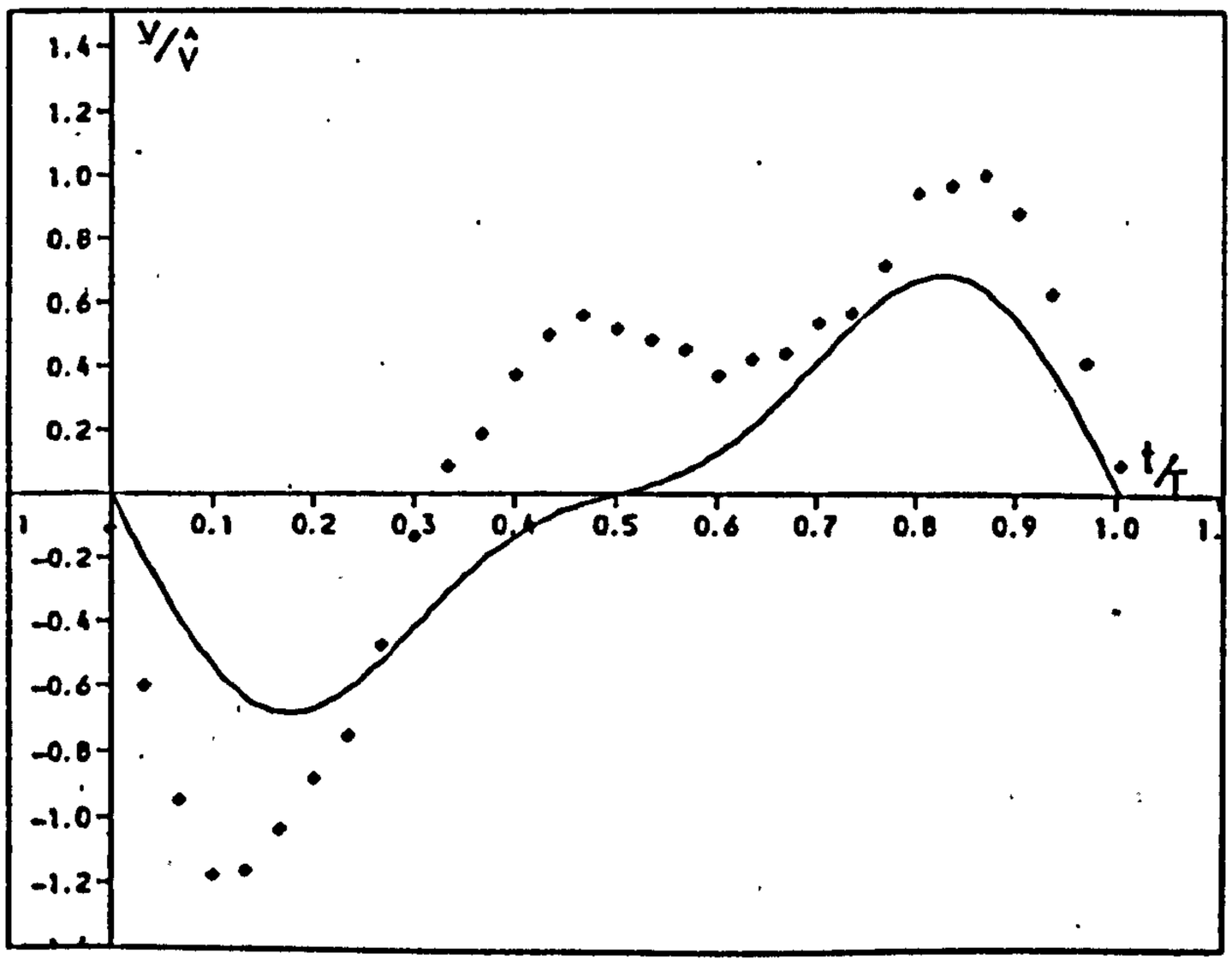

(b) $\hat{v}$=5.2 mm/s

(iv) T=2.0 s

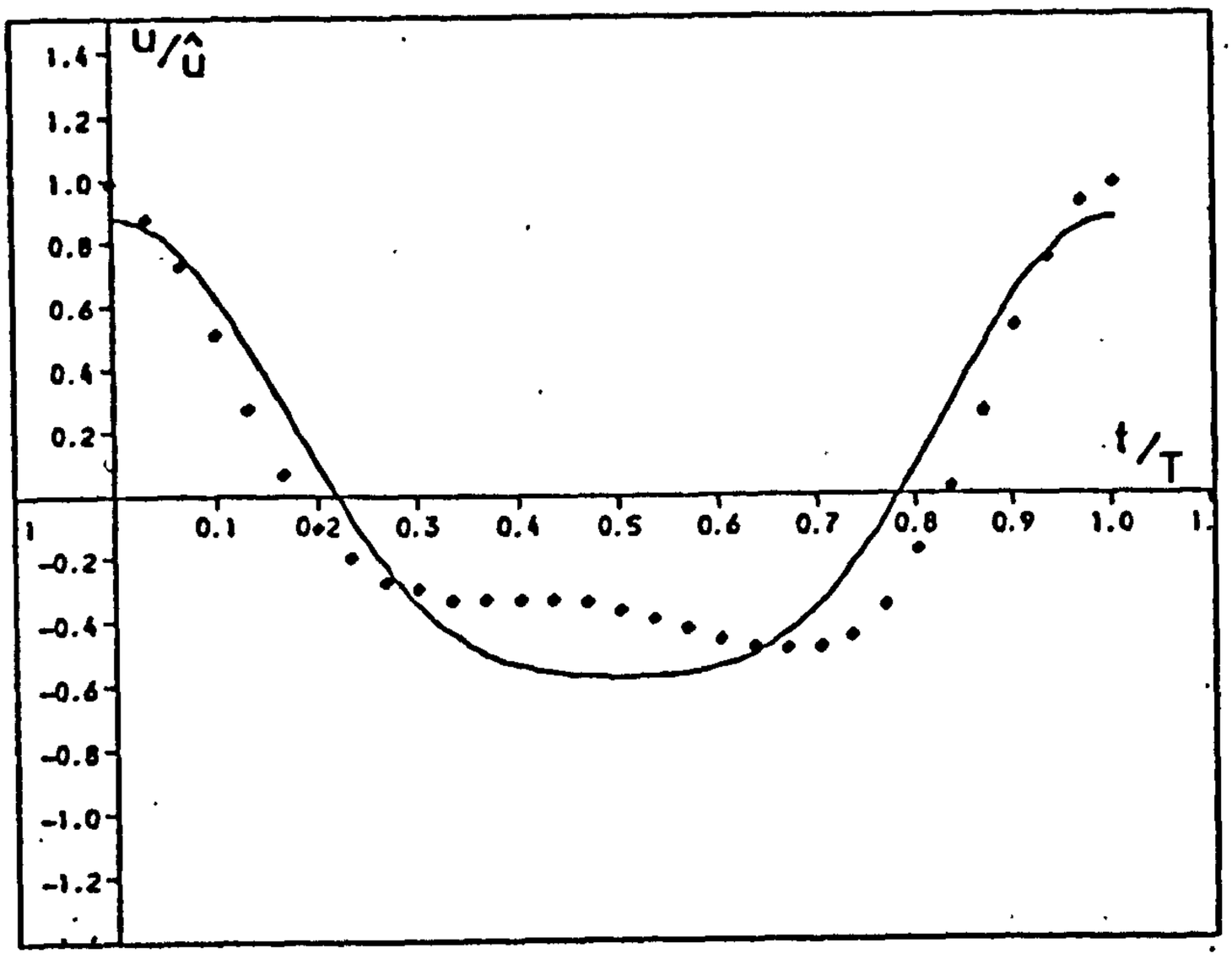

(a) $\hat{u}$=187.8 mm/s

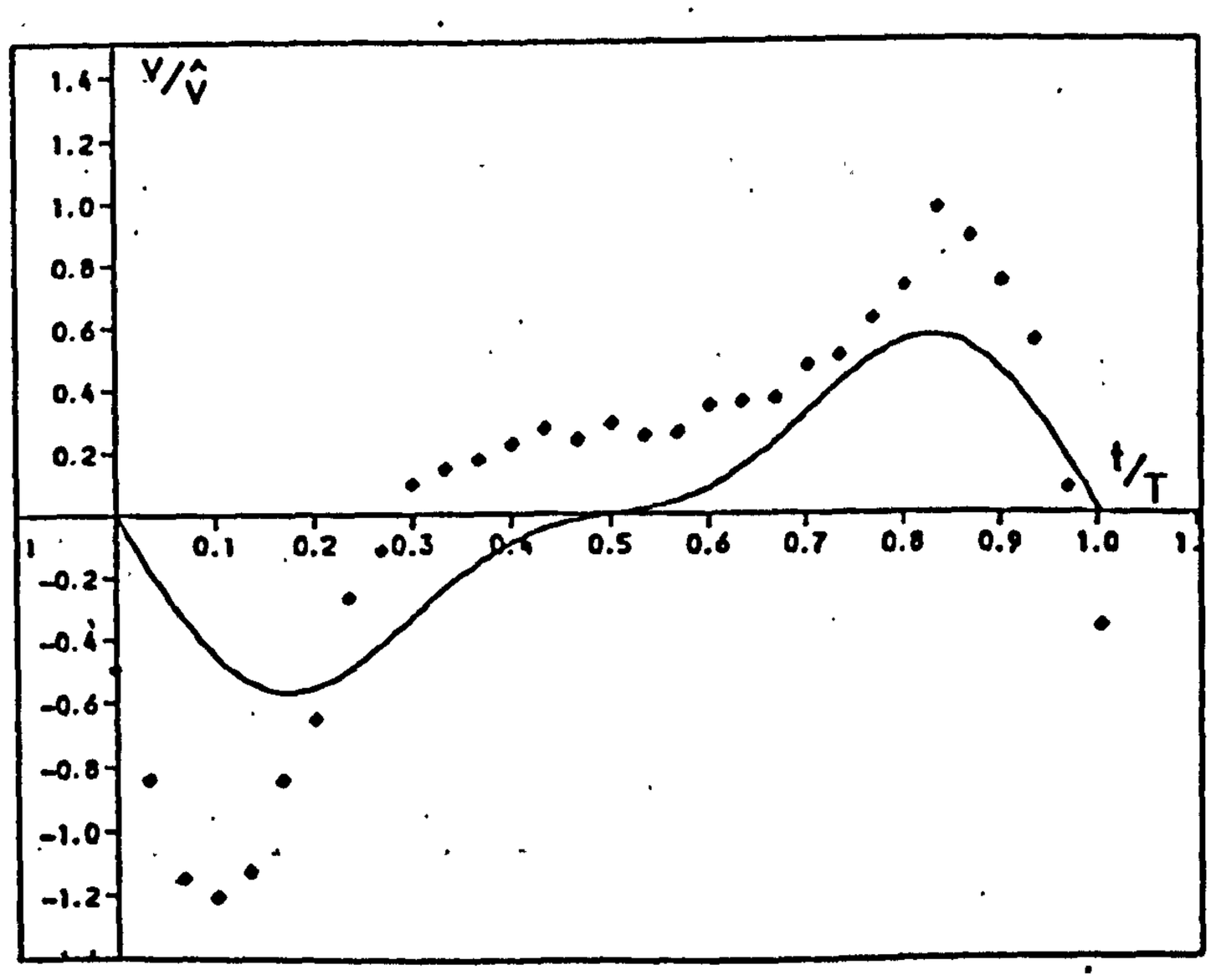

(b) $\hat{v}$= 5.1 mm/s

(v) T= 2.2 s

prediction values. For some periods the trough to crest height is almost twice that of the theoretical curve. However, the profile of the results is of the expected shape and accepting that the vertical velocity close to the bed has small values (relative to the horizontal velocity), then the possibility of greater percentage of error occurs especially when the reflected laser light from the glass bed interferes with the collected light and produces a weaker response from the photomultiplier.alsothe collection point is above the edge of B.L. which results in larger observed values.

5.5 Results and Stokes Second Order Predictions

A general comparison between the experimental data obtained and Stokes second order predictions yield the following conclusions;

The results from Figs. 5.3 and 5.4 point to the general conclusion that the profiles of the observed velocities are the same as those from the Stokes predictions (especially for higher frequency waves). But the magnitudes of the velocities maxima and minima from the collected data are greater than the calculated results (the difference for horizontal velocity at most is 30% and for vertical velocity it gets as high as twice the theoretical value).

Nevertheless the surface wave has a profile with low correlation with the theoretical one. Beside the greater complexity of the realistic surface wave equations, the differences arise from the limitation of the measuring

instruments. Although the wave probe has proved to be a highly reliable tool for measuring the surface wave profile (Beech 1978), there are however two disadvantages using the probe;

(a) The probe enters the water to measure the water level and disturbs the wave profile. (Though for the laser doppler velocimeter the collection of data is without interfering with the velocity of water particles, still disadvantages and limitations exist which are discussed in Chapter Three).

(b) Beech showed that the probe has to be cured for a long period to produce a steady output throughout the test duration. He concluded that even if the time of the test is long (say two hours), voltage output would not remain steady. This can result in a few millimetres shift in the profile (depending on the duration of the test) with respect to the initial output of the still water level (s.w.l.).

Also the reflected wave from downstream of the channel and the imperfection of the wave due to the shortness of the channel have some effect. At the same time, the method of analysis and collecting data could be improved to obtain more accurate results (suggestions are discussed in Chapter 8).

For high period wave a more important factor exists,

which is that the type of waves, which according to the Ursell parameter values qualify as lying in the shallow water zone, are not acceptable as such by the Stokes second order predictions.

More about the second order theory is discussed in Chapters 6 and 8. Nevertheless considering all these factors, for all periods, Stokes predictions are in good correlation with data for orbital horizontal velocity and surface wave profiles. Also good predictions are made of the profile (but not the magnitude) of the vertical velocity.

5.6 Influence of Roughness on the Orbital Motions in the Bulk of Fluid

The two textures with dimensions shown in Chapter 4, were used as two and three dimensional artifically roughened beds. There is no doubt that the roughness elements influence the flow and introduce vortices, but the question is to what depth do these eddies exist? Since this section presents the discussion of velocity in the bulk of fluid (the velocity over the smooth and rough bed within the viscous boundary layer is covered in the next chapter), it is reasonable to first investigate the effect of roughness on the velocity just outside the boundary layer, and then consider the effects at observations points as the surface is approached. Then if the effect becomes negligible at some depth, beyond that depth the roughness can be assumed to have no effect on the flow.

5.6.1 Two-Dimensional Rough Bed

5.6.1.1 Horizontal Velocity

Fig. 5.5a shows the profile of horizontal velocities together with the Stokes prediction for the two-dimensional rough bed. Certainly the graphs show a good agreement between measured data and Stokes curve. The important features of the graphs are that no fluctuations of data due to the roughness elements are apparent. Some differences exist but these are not from the roughness effect since similar misfits appear for the data collected over the smooth bed, and can be presumed to be experimental observation scatter.

5.6.1.2 Vertical Velocity

The second set of graphs in Fig. 5.5b shows that fluctuation exists for vertical velocity except for the 1.4 sec. period wave. Beside the explanation put forward in the last section, since the magnitude of vertical velocity is small by comparison with horizontal velocity, any small vortex is likely to be significant in perturbing the vertical velocity while its effect is probably negligible on the horizontal velocity. But beyond the boundary layer thickness the vertical velocity increases and the effect of roughness becomes small and can be neglected.

5.6.2 Three Dimensional Rough Bed

Results for 3-D rough bed were taken for two periods

- Stokes Theory Eq. 1.23

• Data

5.5(a) Horizontal Velocity

- Stokes Theory Eq. 1.24

• Data

5.5(b) Vertical Velocity

Fig. 5.5 Velocity Profile Outside the Viscous Boundary Layer - 2-D Rough Bed.

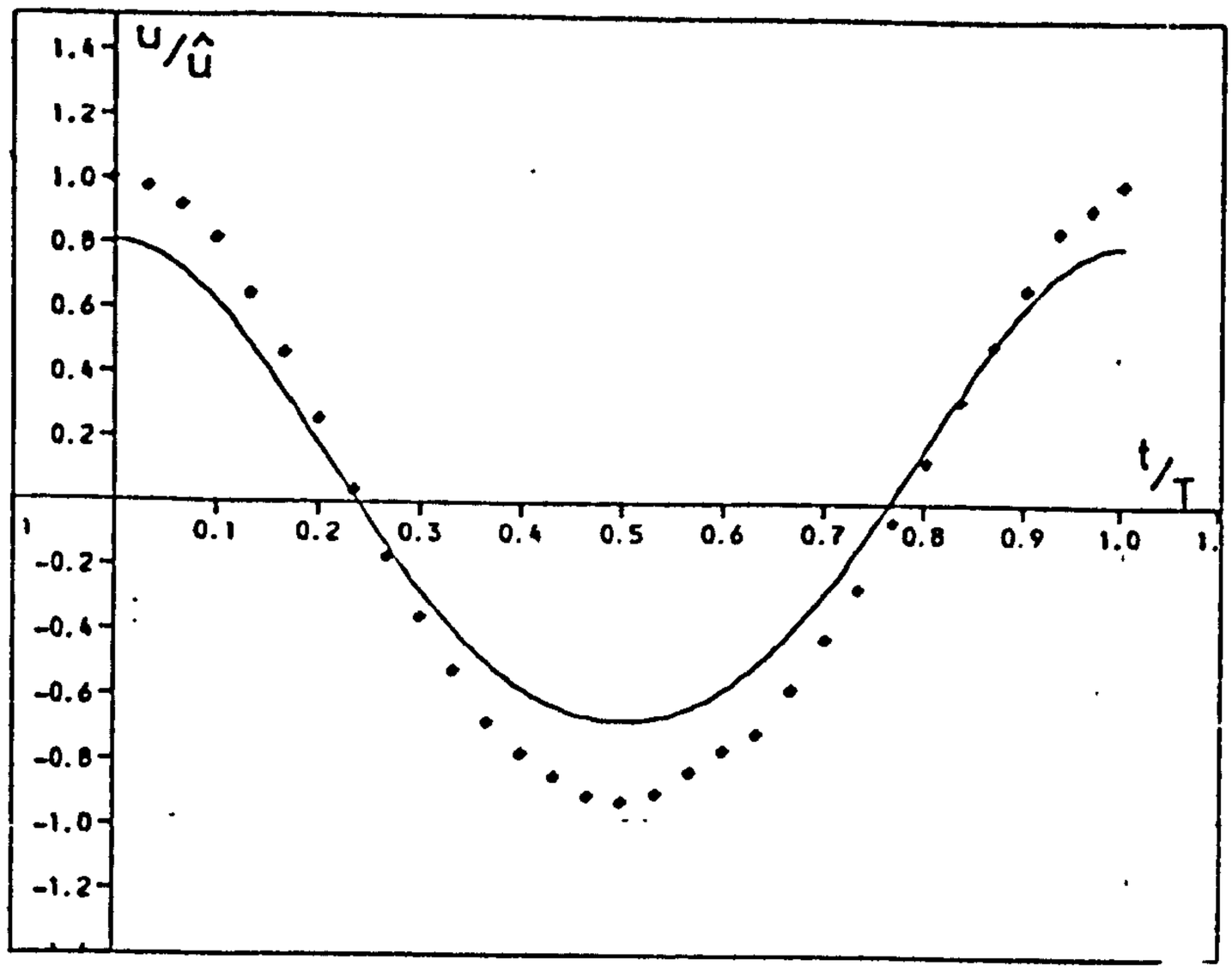

(a) $\hat{u}$=231.3 mm/s

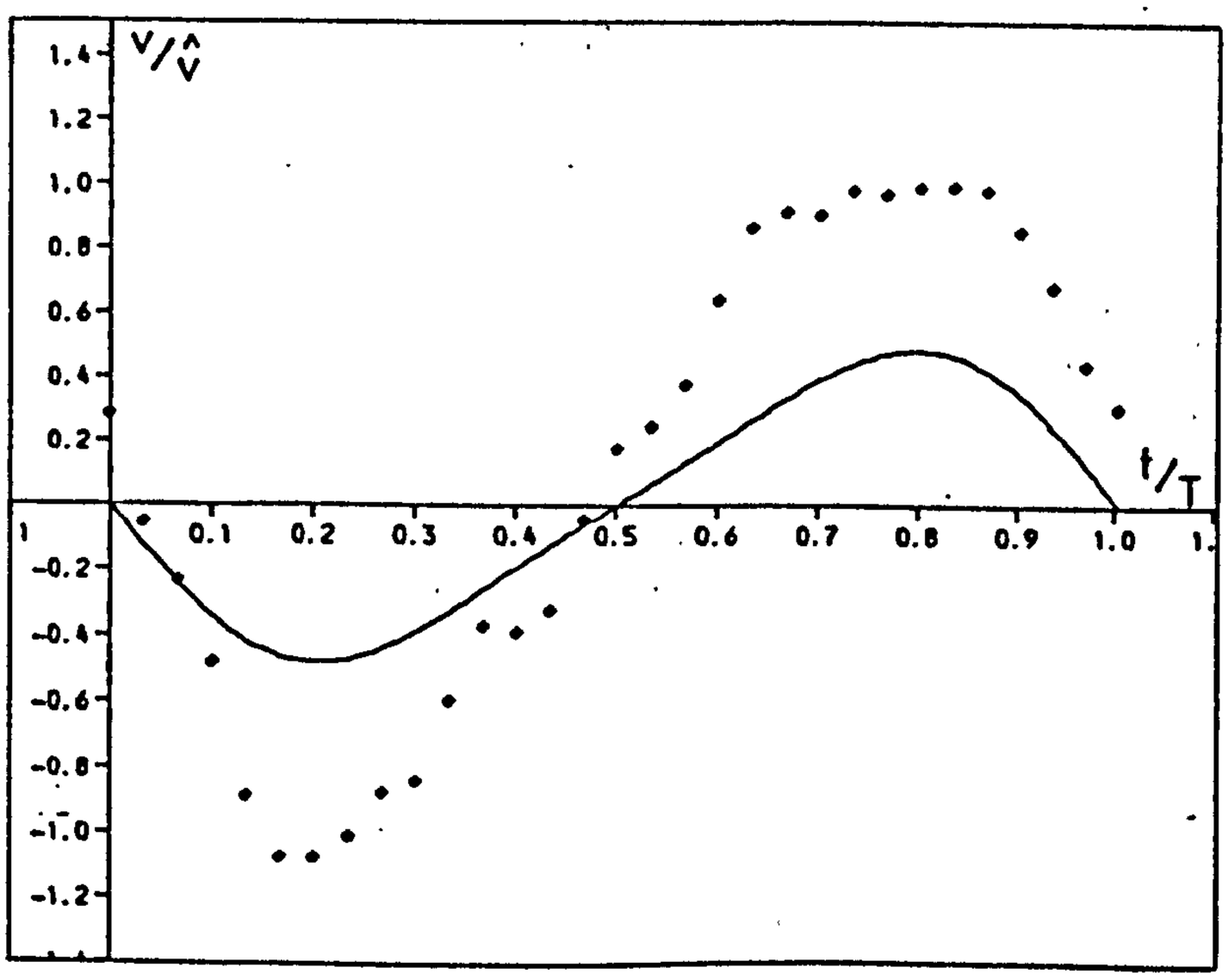

(b) $\hat{v}$=10.9 mm/s

(i) T=1.4s

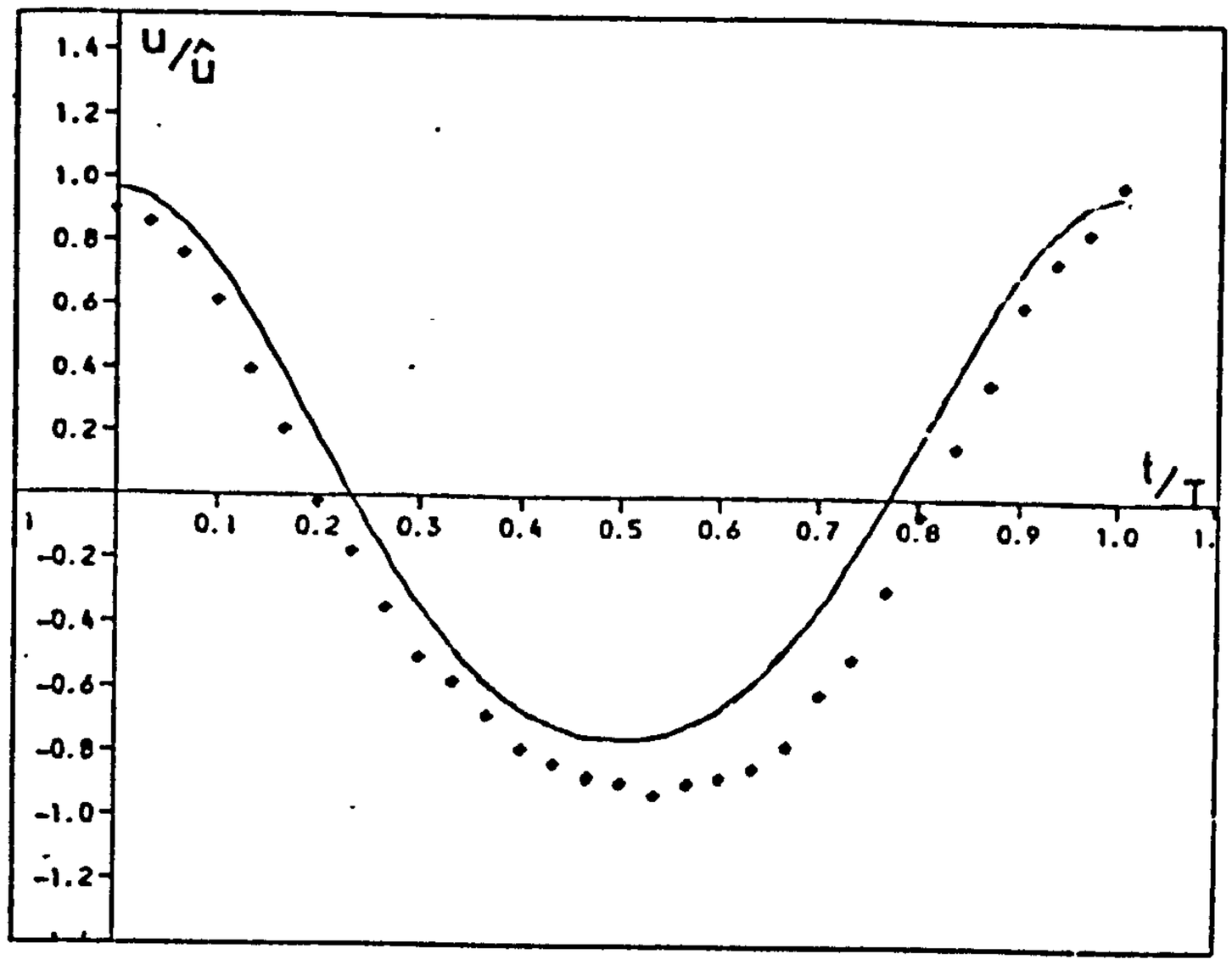

(a) $\hat{u}$=187.3 mm/s

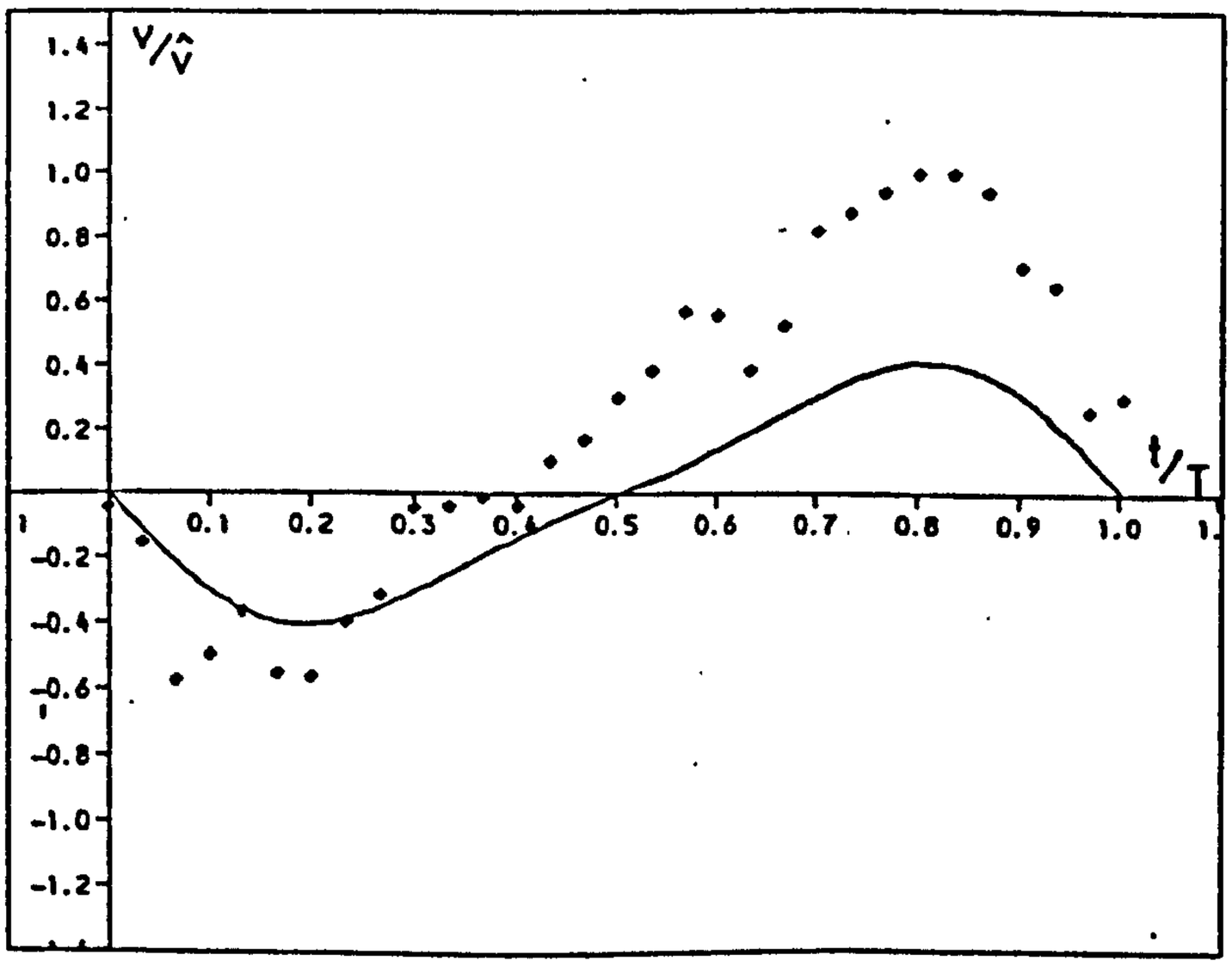

(b) $\hat{v}$=10.7 mm/s

(ii) T=1.6 s

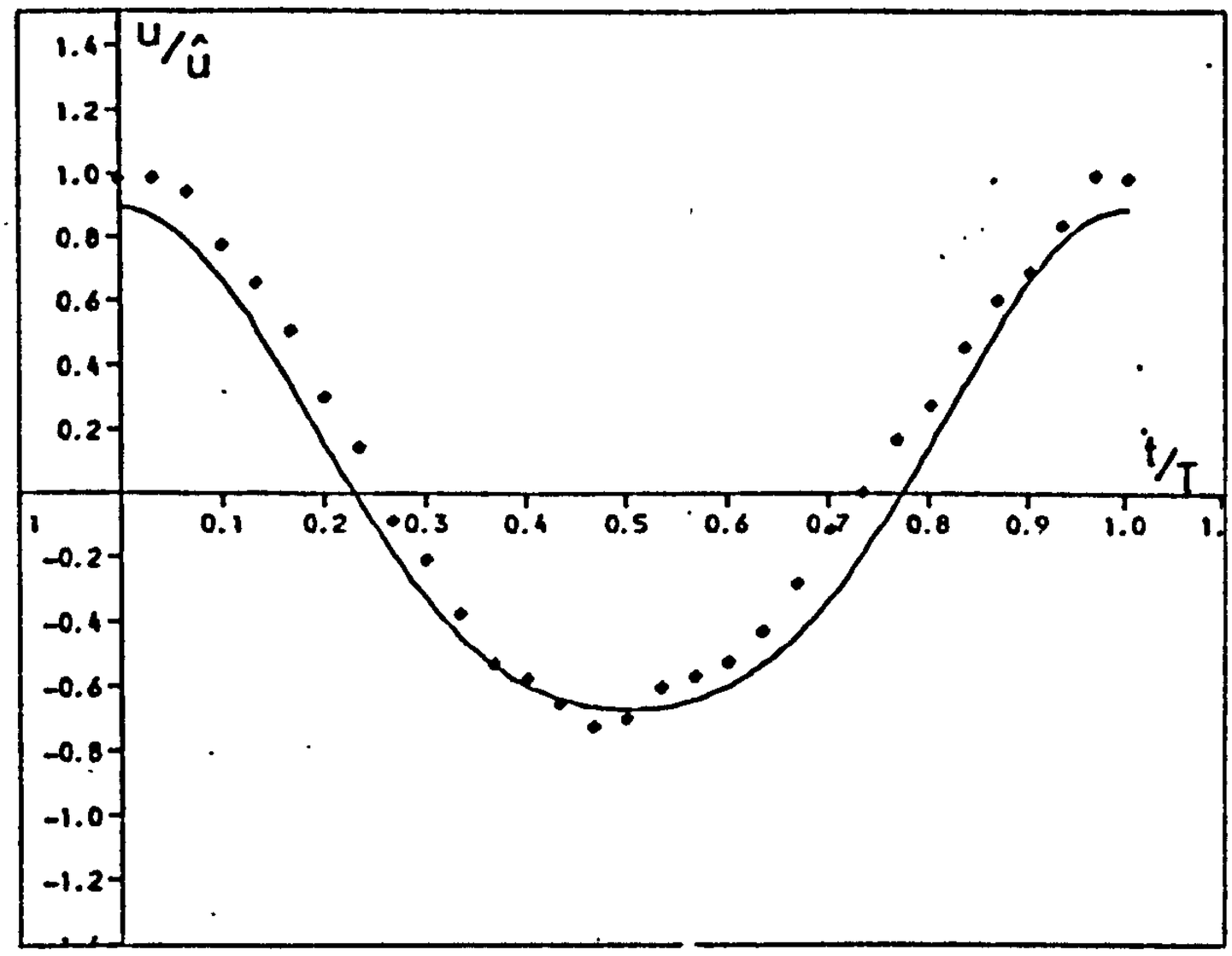

(a) $\hat{u}$=188·9 mm/s

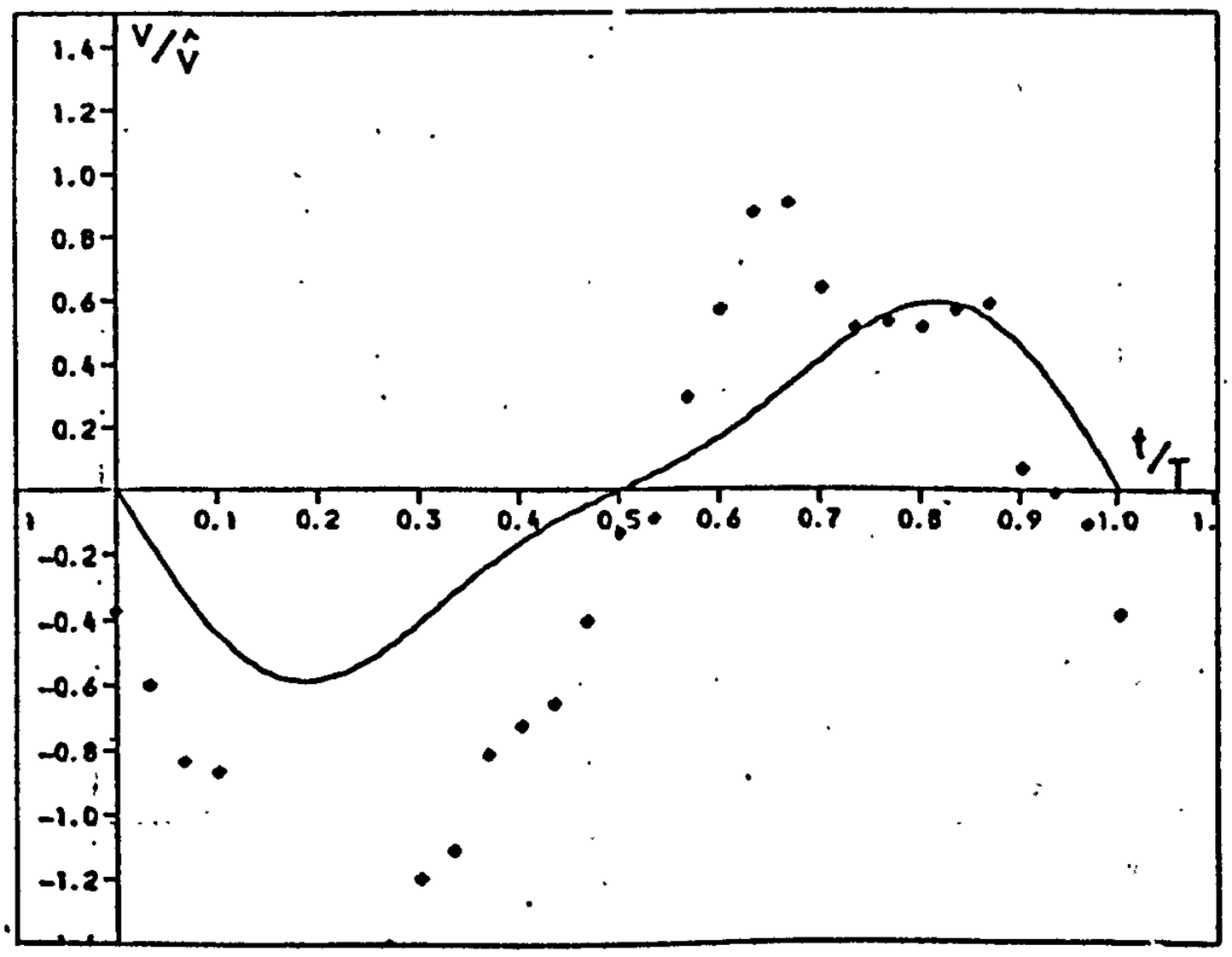

(b) $\hat{v}$=6.1 mm/s

(iii) T=1.8 s

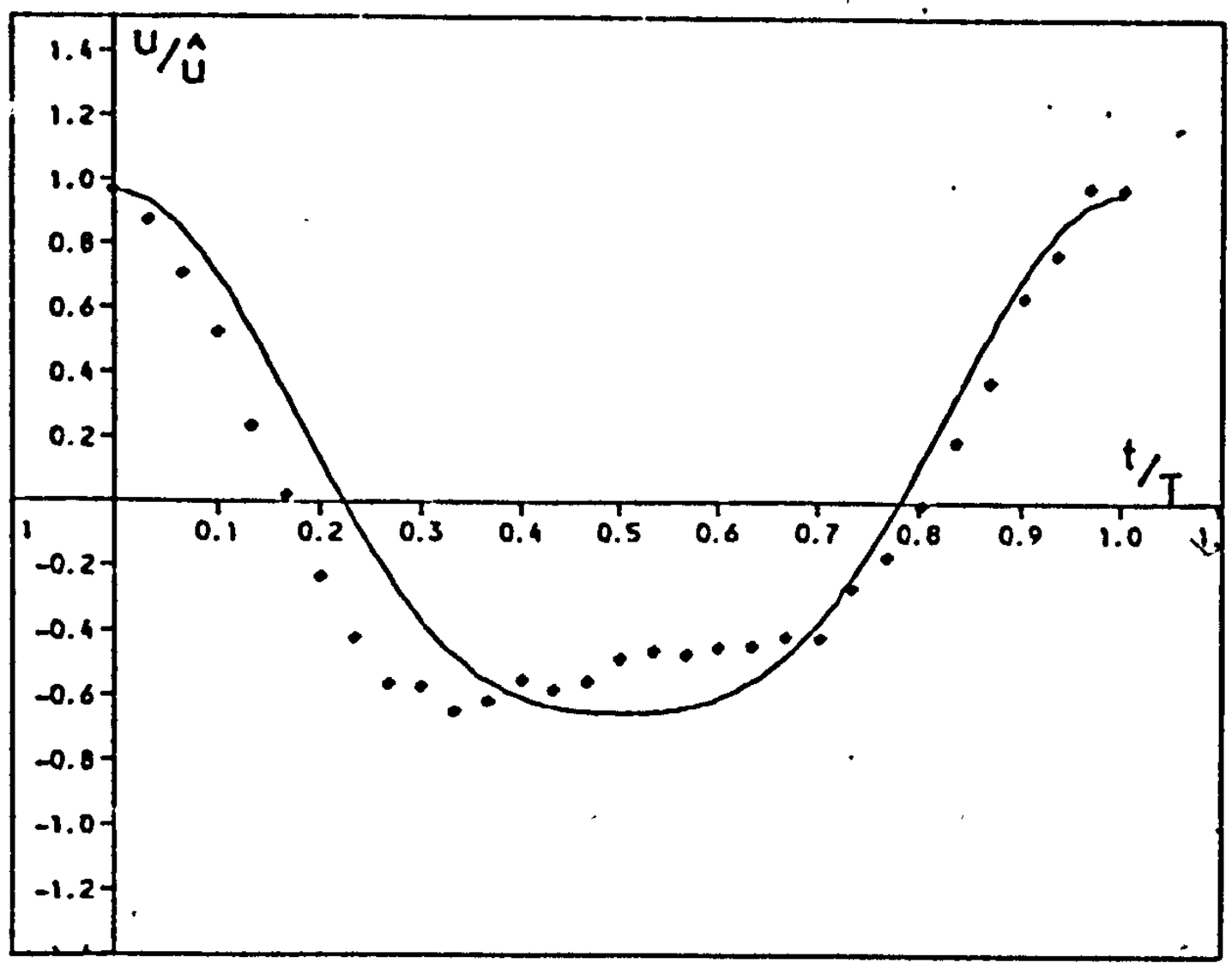

(a) $\hat{u}$=189.7 mm/s

(b) $\hat{v}$=6.1 mm/s

(iv) T=2.0s

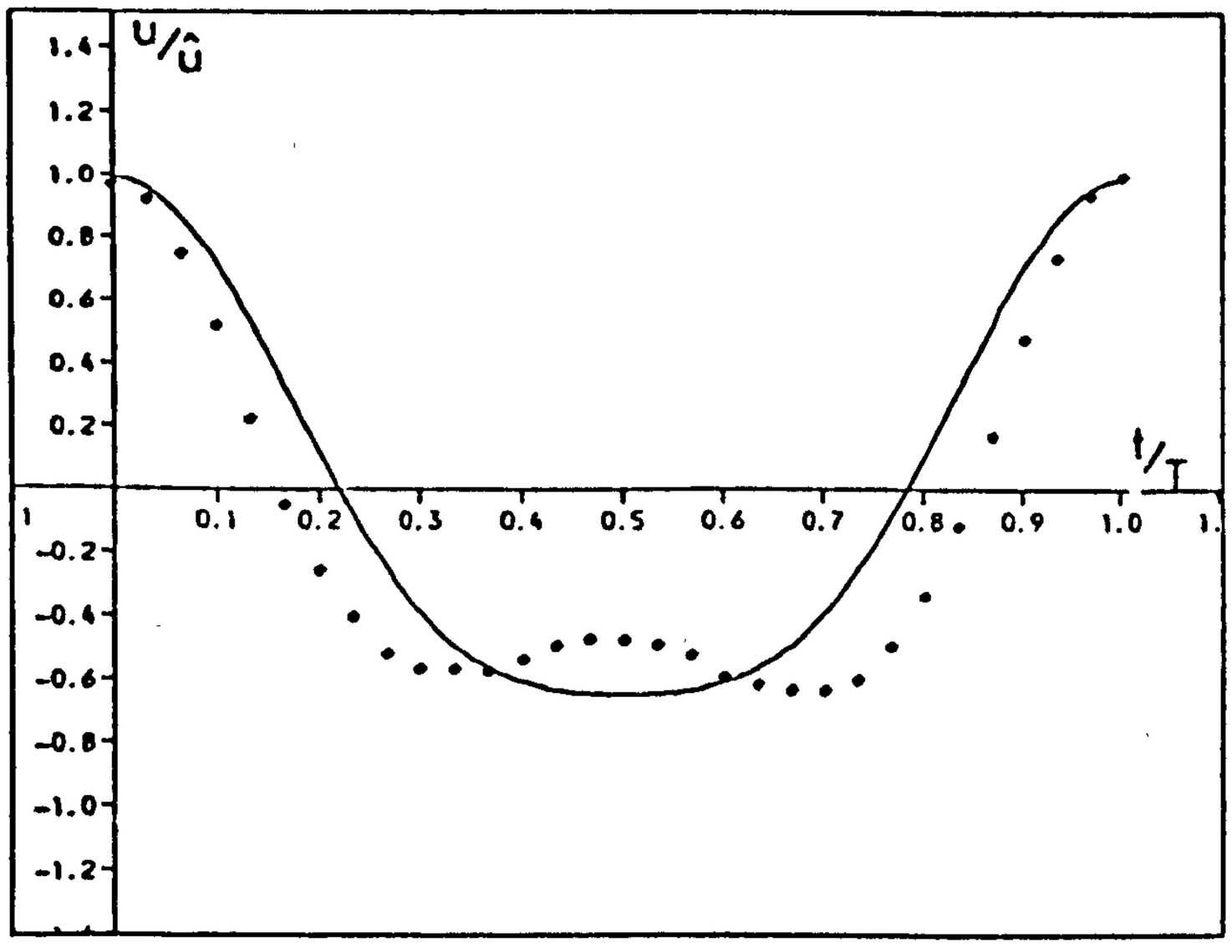

(a) $\hat{u}$=166.9 mm/s

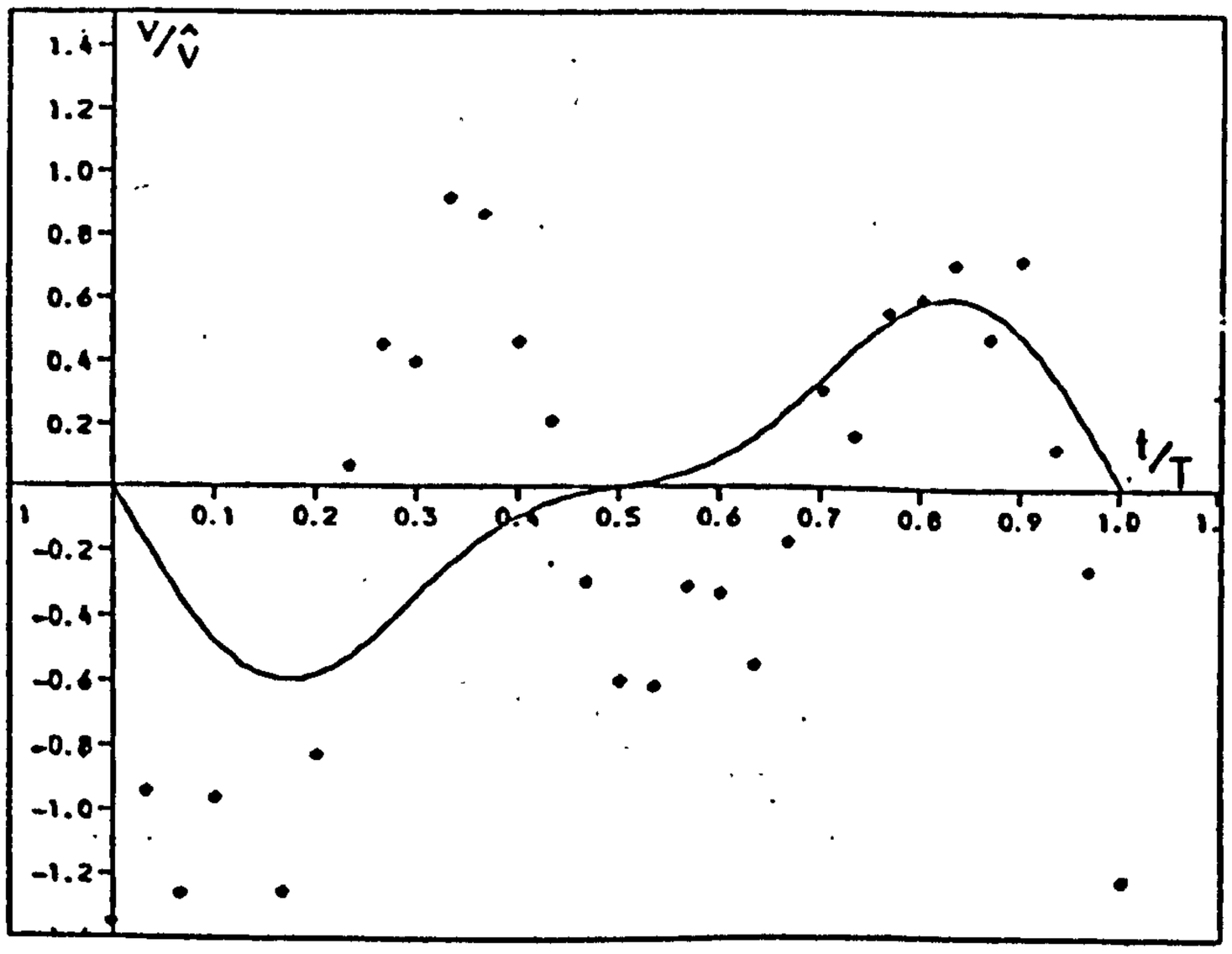

(b) $\hat{v}$=4.9 mm/s

(v) T=2.2 s

(1.4 and 2.2 sec.) and at two locations on the XY plane (the two locations are shown in Fig. 4.2, and referred to as 3-DR and 3-DS).

5.6.2.1 Horizontal Velocity

Figs. 5.6a and 5.7a are the results for horizontal velocity together with the Stokes predictions. Again no rapid fluctuation of speed exist for either set of results and so the roughness effect is negligible and the velocity profiles are the same as those for smooth and 2-D rough beds.

5.6.2.2 Vertical Velocity

For vertical velocity, again, not intense fluction occurs for 1.4 sec. wave (Figs. 5.6b and 5.7b) although some discrepancies do exist, but for the 2.2 sec. wave the fluctuation is more apparent. Here, also, the same argument applies as for the 2-D rough bed.

5.6.3 Results over Rough Beds

It is clear that the roughness textures which are used for this investigation as artificial 2-D and 3-D rough beds, although creating some disorder in the bulk of fluid, only generate very small intensity of fluctuations as shown by the experimental evidence, and also the eddies very quickly disappear in the bulk of fluid towards the free surface. Thus it can be assumed that for the existing conditions there is no influence outside the boundary layer thickness from the

- Stokes Theory Eq. 1.23

• Data

5.6(a) Horizontal Velocity

- Stokes Theory Eq. 1.24

• Data

5.6(b) Vertical Velocity

Fig. 5.6. Velocity Profile Outside the Viscous Boundary Layer - 3-DS Rough Bed.

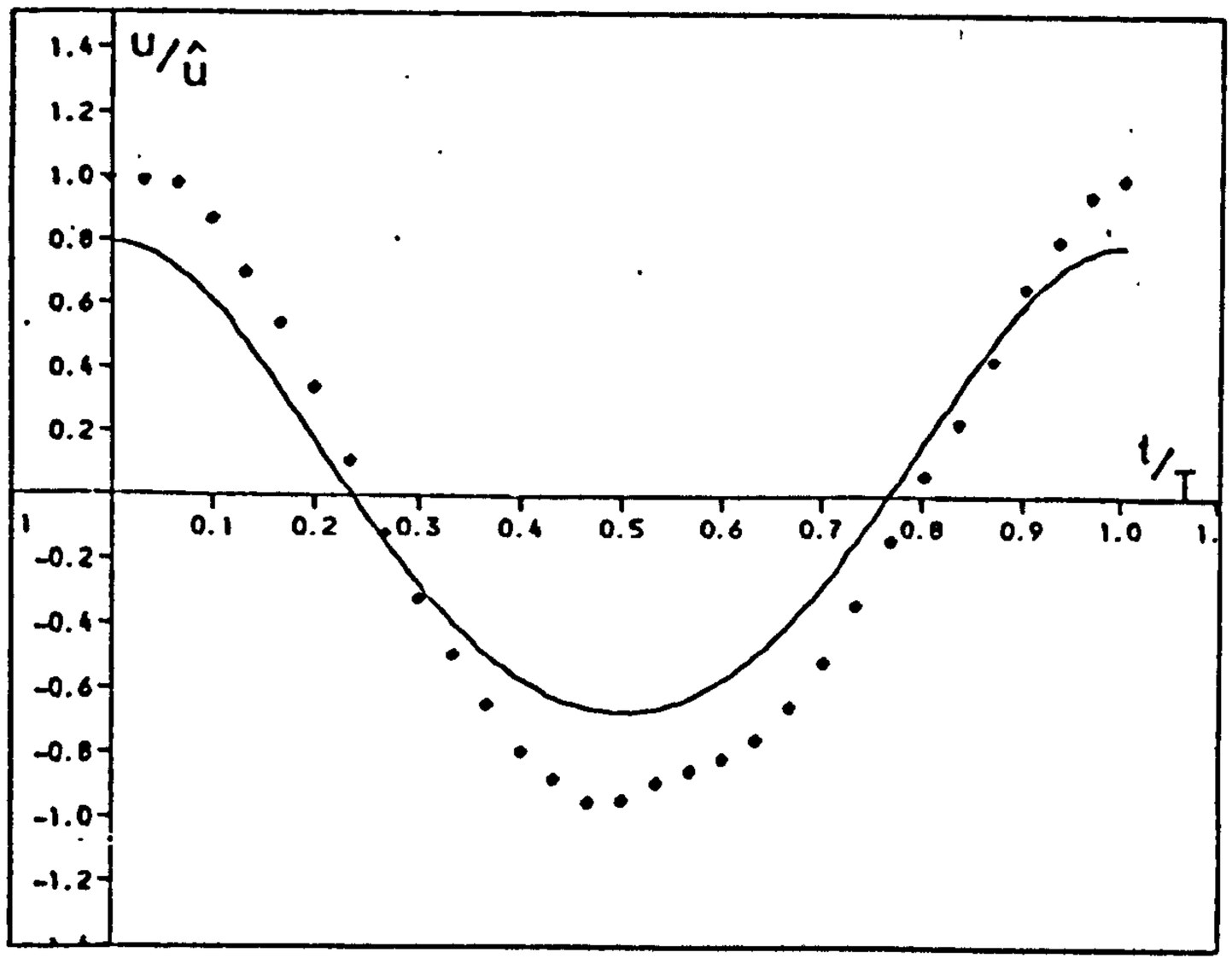

(a) $\hat{u}$=234.4 mm/s

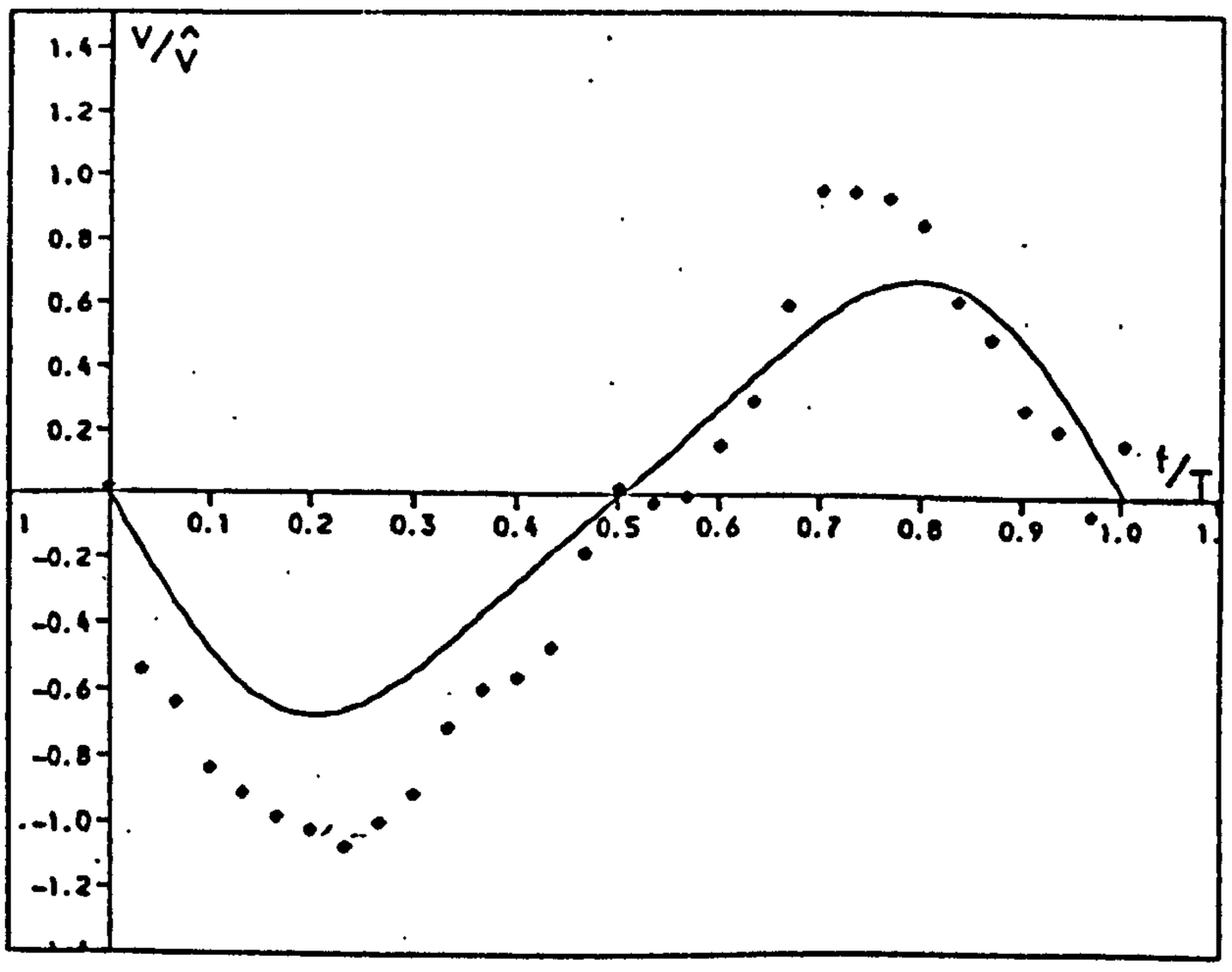

(b) $\hat{v}$=7.8 mm/s

(i) T=1.4 s

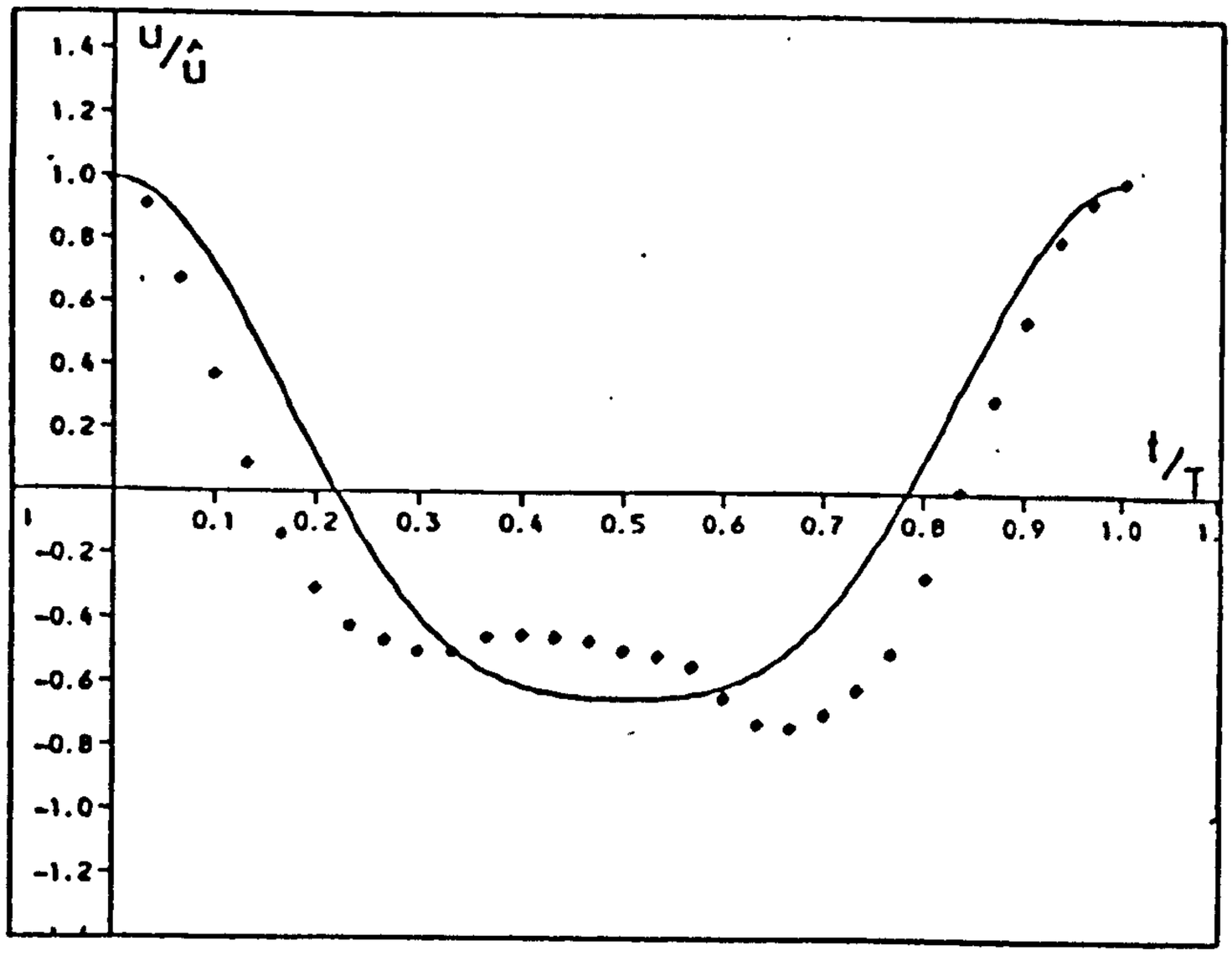

(a) $\hat{u} = 166.0$ mm/s

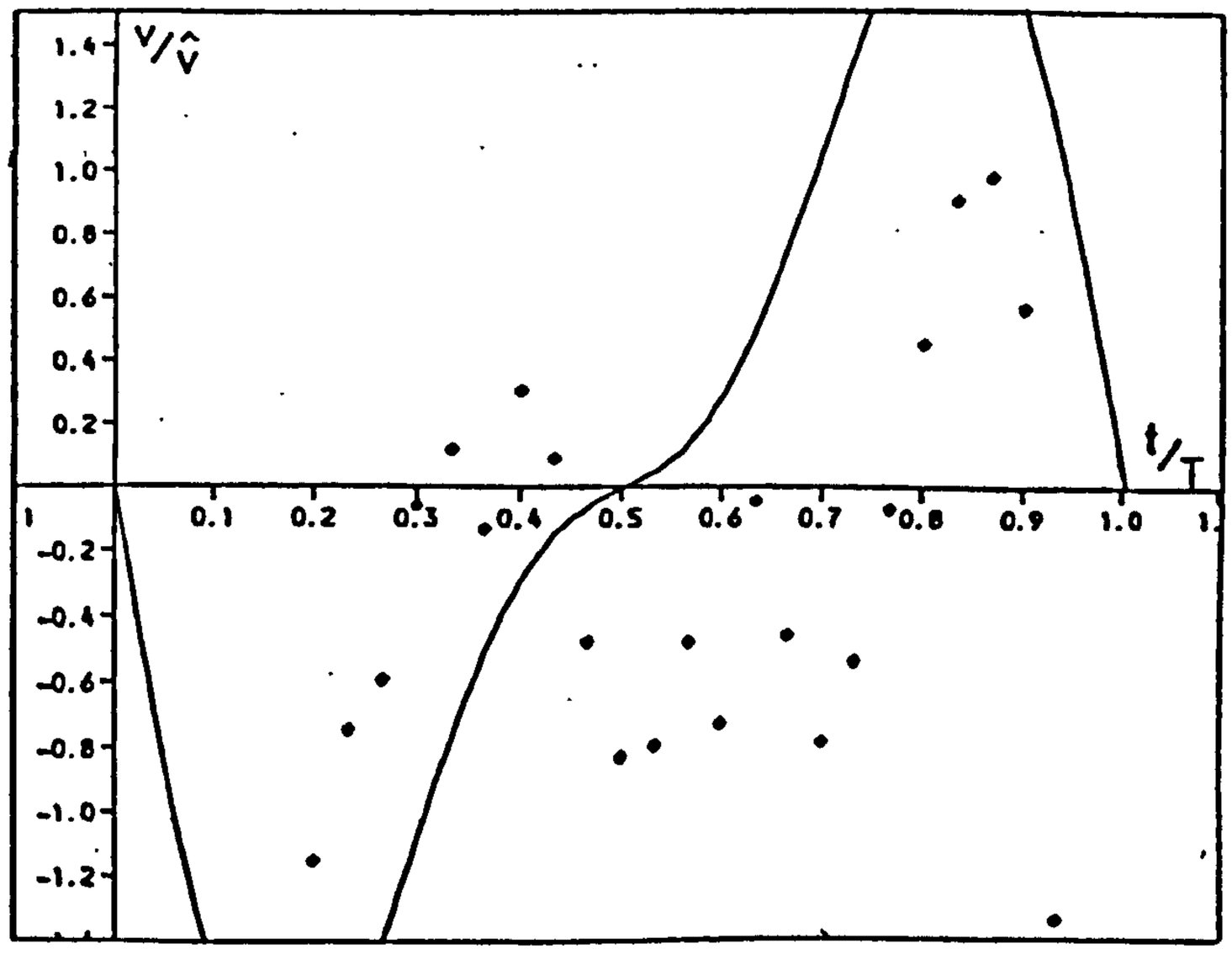

(b) $\hat{v} = 1.5$ mm/s

(ii) T=2.2 s

- Stokes Theory Eq. 1.23

• Data

5.7(a) Horizontal Velocity

- Stokes Theory Eq. 1.24

• Data

5.7(b) Vertical Velocity

Fig. 5.7 Velocity Profile Outside the Viscous Boundary Layer - 3-DR Rough Bed.

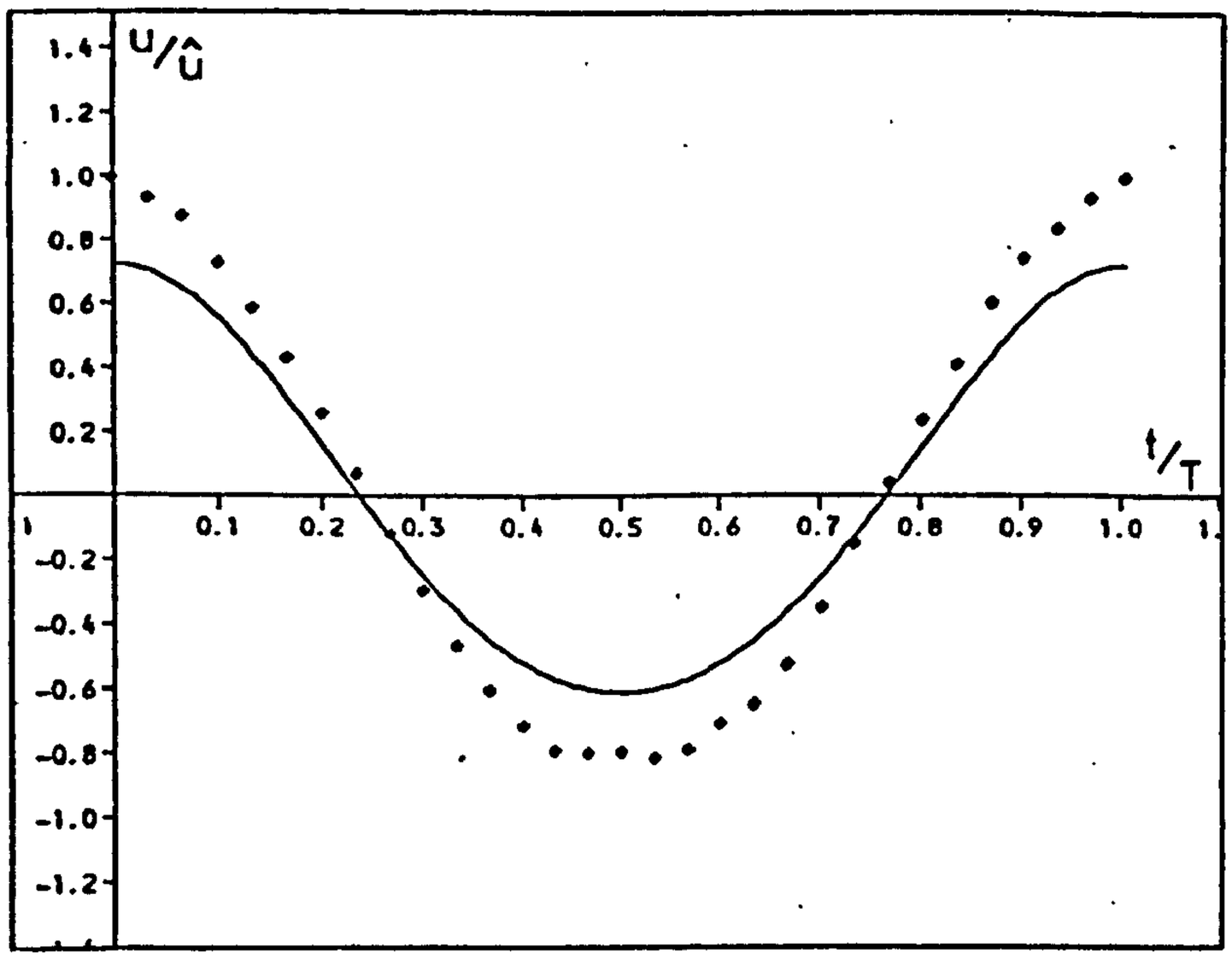

(a) $\hat{u}$=257.2 mm/s

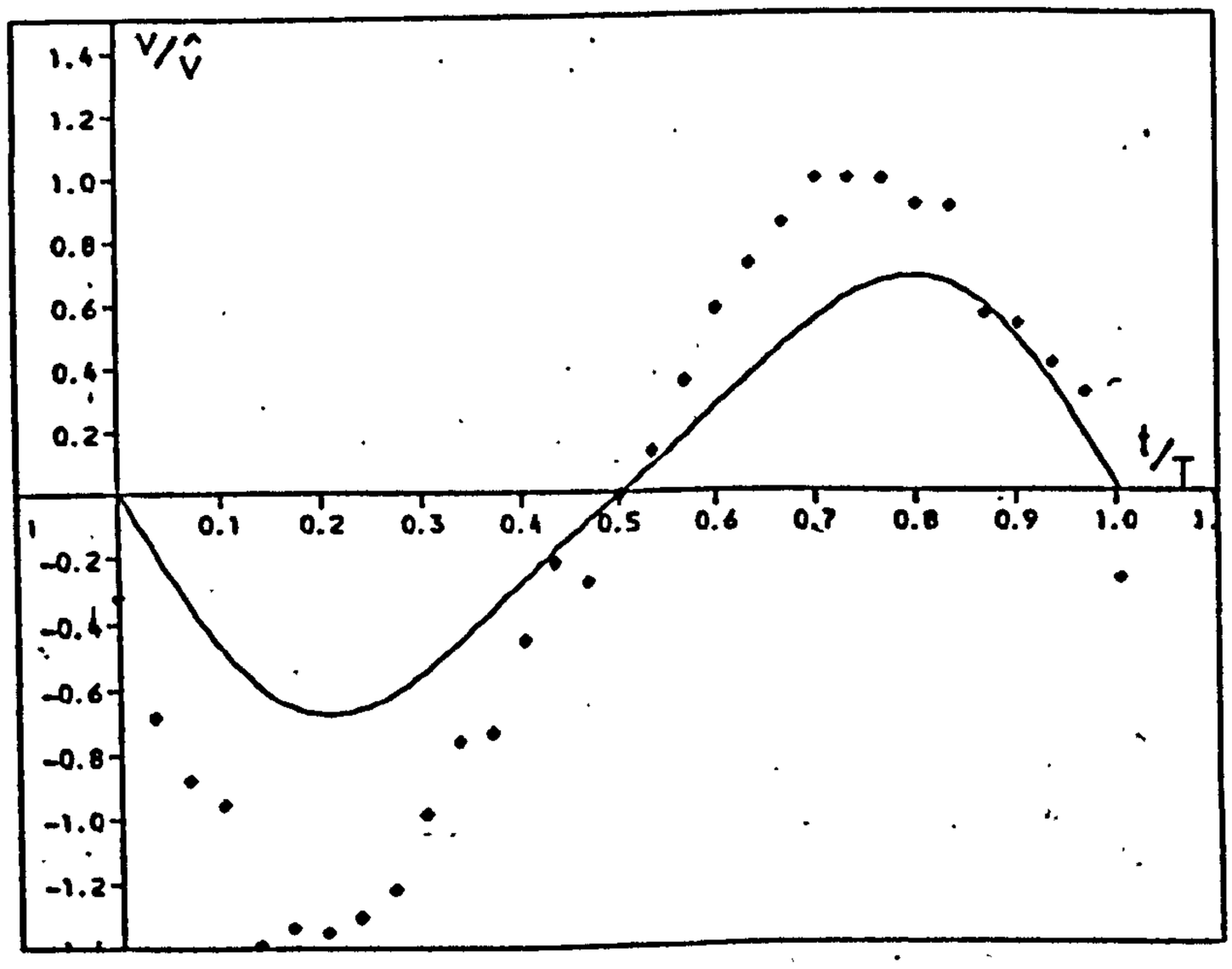

(b) $\hat{v}$=7.8 mm/s

(i) T=1.4s

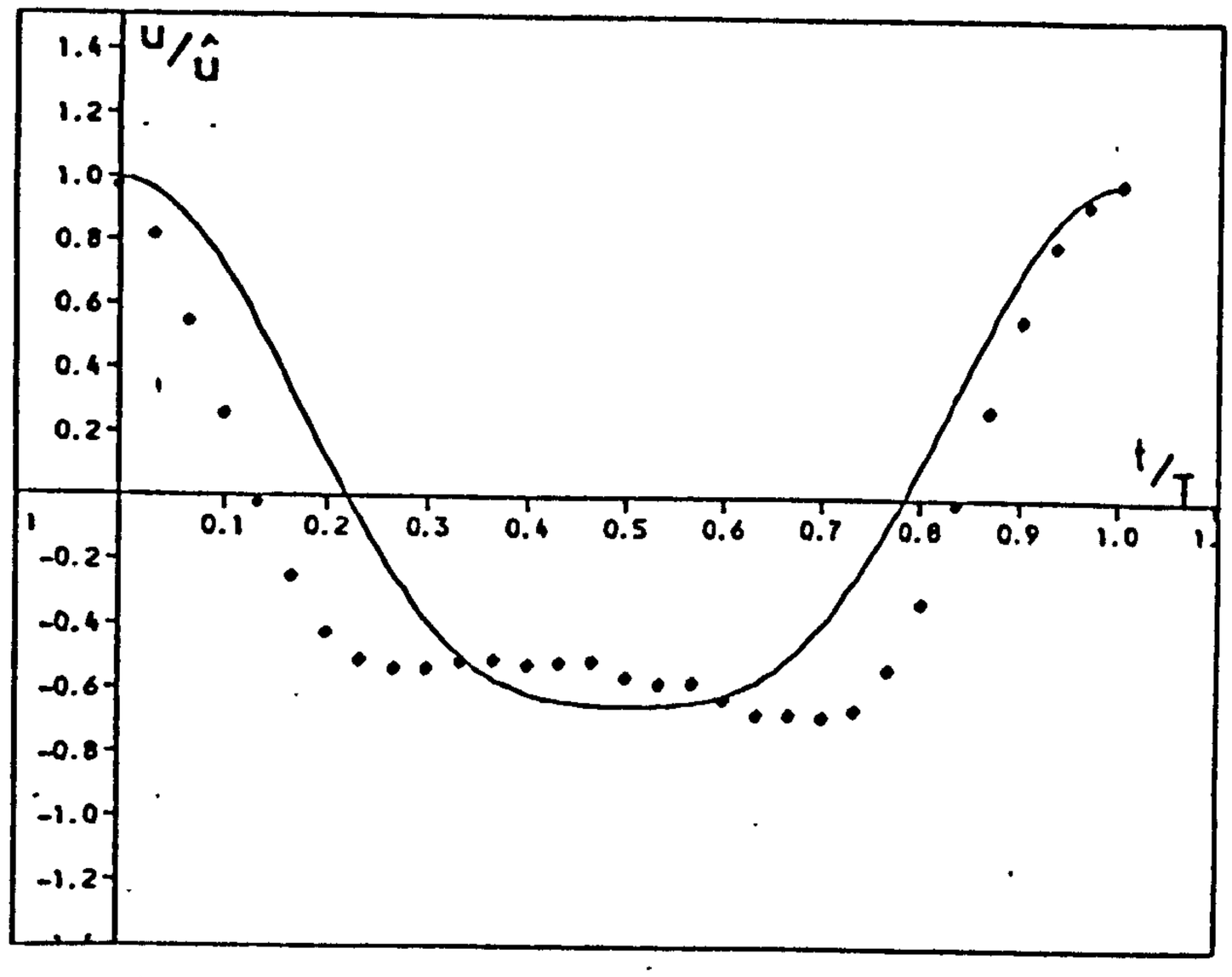

(a) $\hat{u}$=165.2 mm/s

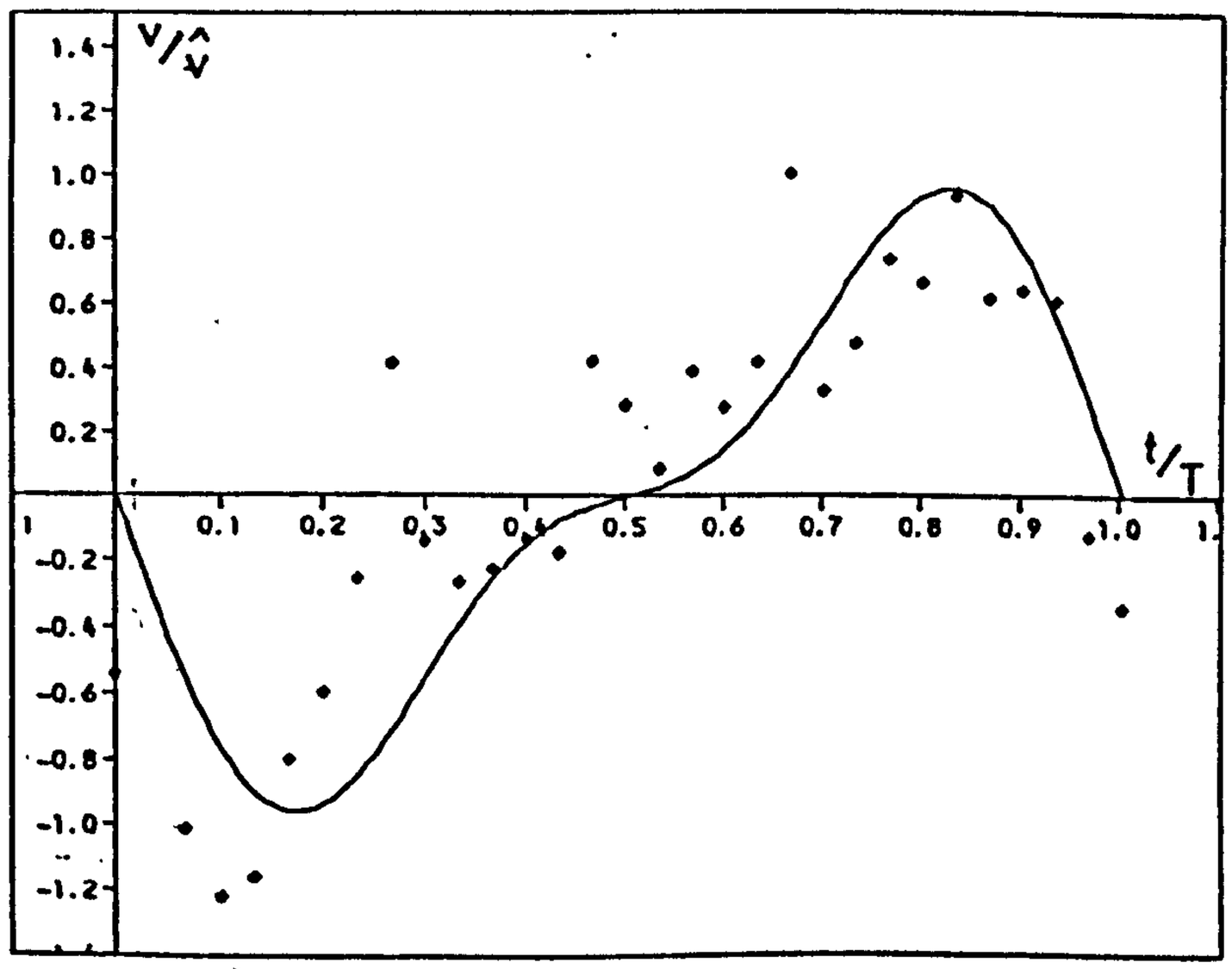

(b) v=3.0 mm/s

(ii) T= 2.2 s

roughness elements (the thickness influenced by the rough beds is taken from the top of the roughness to few multiples of the boundary layer thickness over the smooth bed).

5.7 Concluding Remarks

1. The relative depth lies between 0.154 and 0.086 (intermediate water waves), while the Ursell parameter values of more than 20 have been obtained for wave periods of 2.0 s and more. This means for the higher periods the waves lie in shallow water zone while any value below is indicative of intermediate water waves.

2. The surface wave profile and Stokes second order equation are highly correlated considering the discrepancies caused by the wave probe for all the wave periods.

3. The velocity profiles (horizontal and vertical) at the edge and outside the viscous boundary layer are well predicted by the Stokes second order equations, but the collected data values are higher.

4. Outside the boundary layer thickness the mean velocity is always negative (in opposite direction to wave progression) and Longuet-Higgins conduction solution closely predicts the data profile for intermediate water waves except that the theoretical values are an over-estimate of the data values.

5. At a very small distance from the rough bed (depending on the roughness size), the influence of roughness elements becomes negligible.

CHAPTER SIX

BOUNDARY LAYER VELOCITY OVER SMOOTH AND ROUGH BEDS

6.1 Introduction

Stokes 2nd order equation for velocity outside the viscous boundary layer has been compared with the observed data in Chapter Five. The comparison of Stokes prediction and second order shear wave equation with the velocity data inside the viscous boundary layer over smooth, two dimensional and three dimensional rough beds form the content of this chapter.

First the results of the smooth bed are compared with the suggested theories and later in the chapter, the collected data for rough beds are analysed (for the two sets - over crest and trough of roughness). Then the influence of roughness elements on the boundary layer velocity is studied by considering the differences of velocity profile over rough and smooth beds, and also the predicted theories (e.g. Kalkanis, Sleath and Beech equations) are examined for the observed results.

6.2 Smooth Bed

6.2.1 Boundary Layer Velocity Profile

The profile of the velocity in the viscous boundary layer thickness for five periods, at intervals of T/10 for ten

phases starting with t_1 = T/20, is shown in Fig. 6.1(a). The data points are joined by curved lines which do not represent the actual velocity profile, but help to illustrate that when the flow is not laminar anymore, the fluctuation of the points intensify the random pattern of the line (a good example of this is clearly illustrated for the velocity profile over rough beds Figs. 6.8 and 6.14). For the smooth bed case, when the period of the wave is greater than 1.4 sec. a fairly smooth profile of velocity exists which indicates a laminar flow, but for 1.4 sec. wave period a perturbation emerges in the velocity profile. However for this wave period the disorder within the boundary layer velocity is weak and the individual profile for each phase is traceable, and hence indicates the existence of the laminar flow. This can also be concluded from the observed Reynolds number $(\frac{U_\infty \delta}{\nu})$ values from Table 6.1. The values vary between just over 800 for 1.4 second wave period to about 586 for 1.8 second wave period (the Re value for 2.2 second wave is 704). The equivalent critical Reynolds number from Table 2.1 (well accepted by many investigators, Li, Manohar ...) is about 1500 which is well above the maximum observed value for 1.4 second wave period.

Hence the flow for our condition is in the state of laminar and equations for laminar flow can

◇ Data

——— Mass Transport) Longuet-Higgins

- - - - Mean Velocity)

6.1(a) Velocity Profile for the Ten Equal Phases in the Period

6.1(b) Mean Velocity

Fig. 6.1 Boundary Layer Velocity Profile over Smooth Bed.

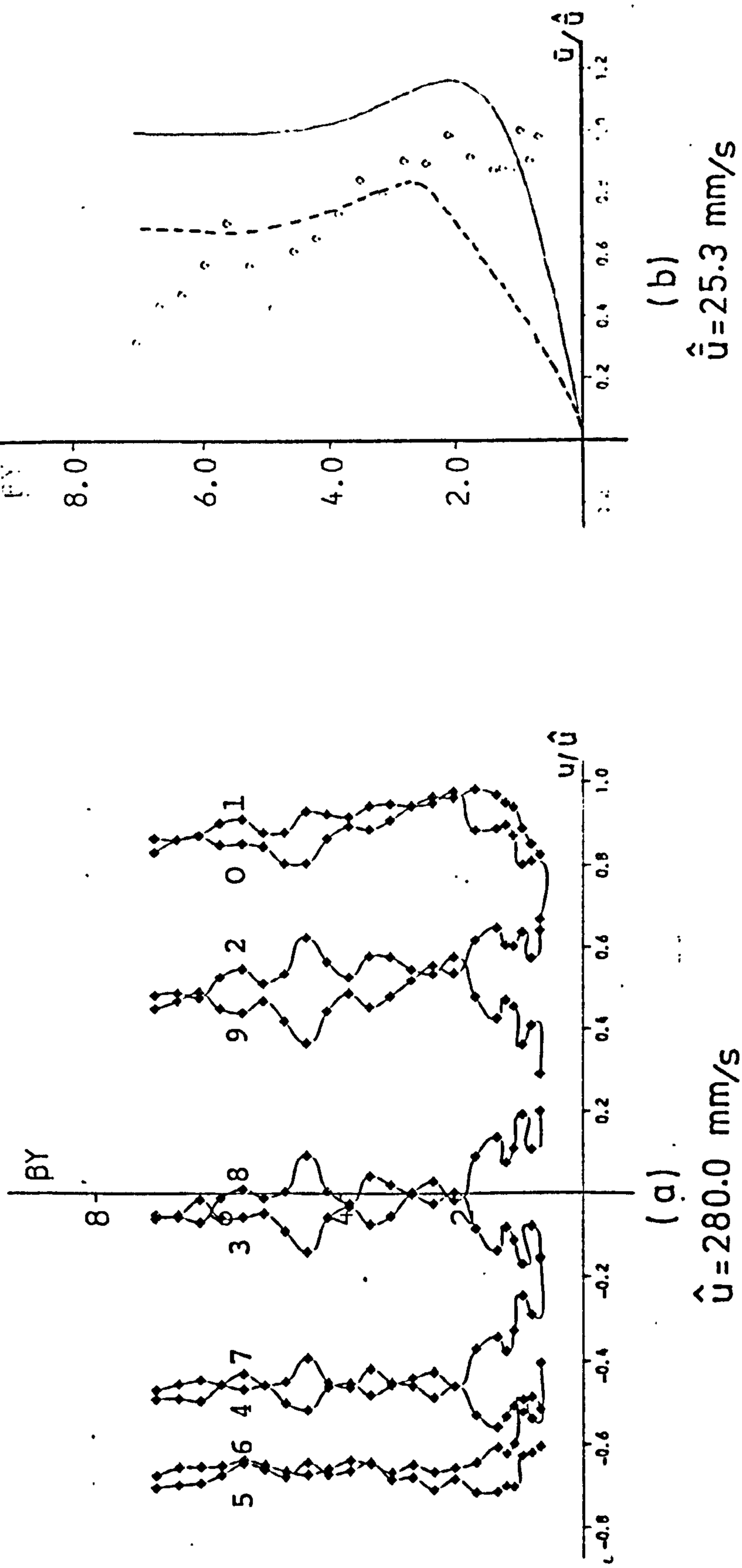
BY
8
0
1
9
2
3
8
4
2
7
6
5
U/Û
1.0
0.8
0.6
0.4
0.2
-0.2
-0.4
-0.6
-0.8
(a)
Û=280.0 mm/s
(b)
Û=25.3 mm/s
(i) T=1.4 s

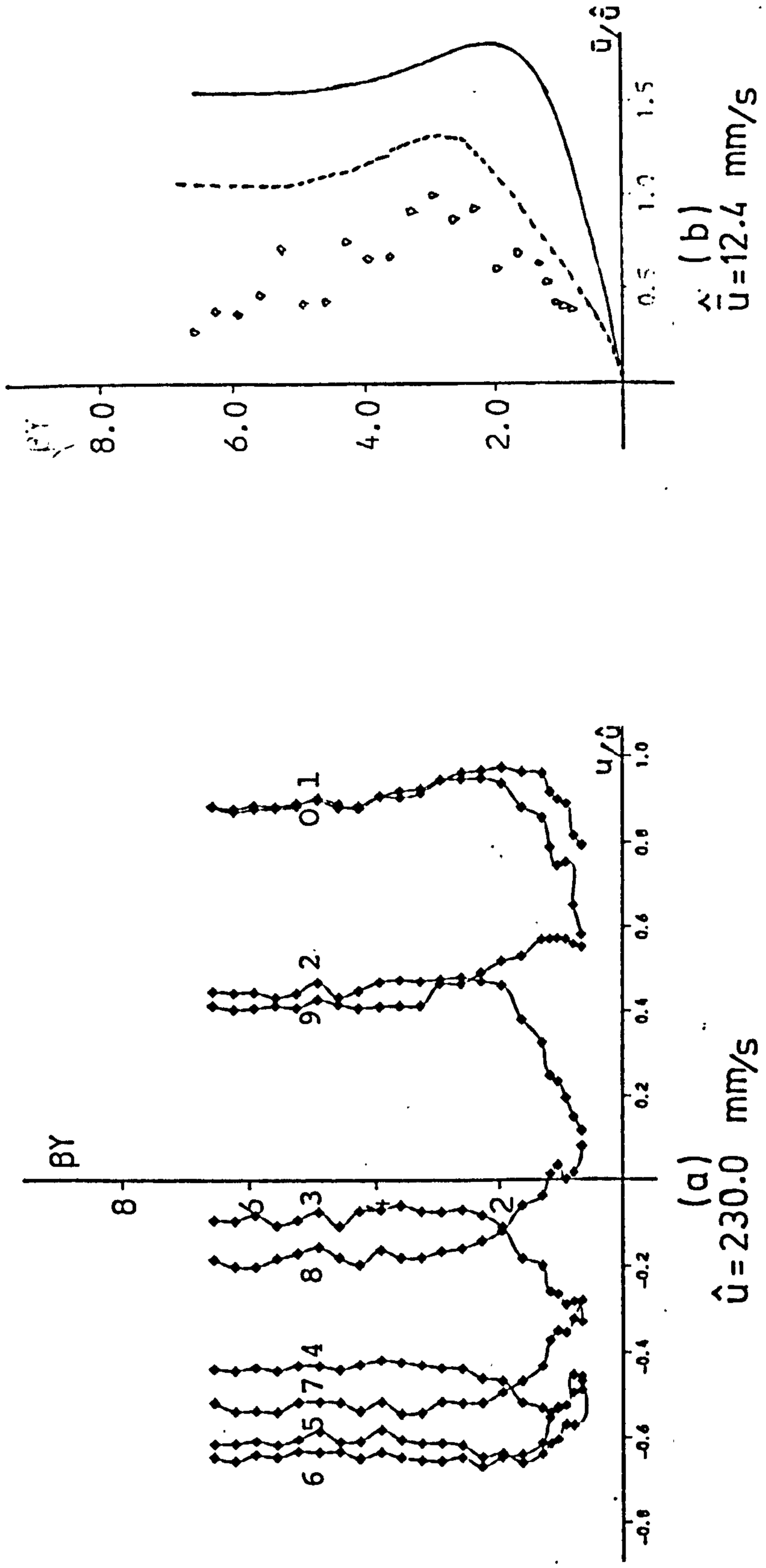
u/û
1.5
1.0
0.5
(b)
û=12.4 mm/s
8.0
6.0
4.0
2.0
BY
8
6
4
2
(a)
û=230.0 mm/s
u/û
1.0
0.8
0.6
0.4
0.2
-0.2
-0.4
-0.6
-0.8
1
2
3
4
5
6
7
8
9
0
(ii) T=1.6 s

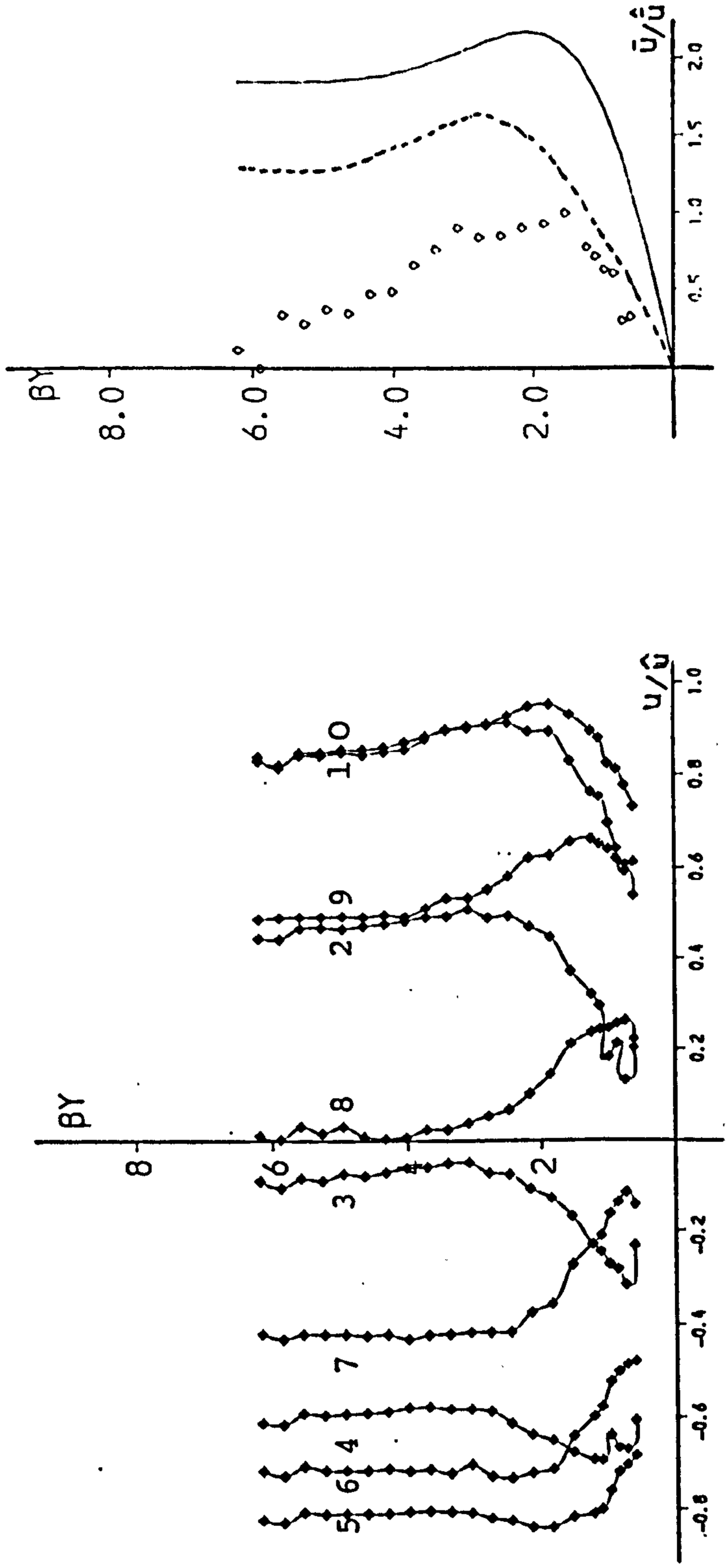
BY
8.0
6.0
4.0
2.0
ū/û
2.0
1.5
1.0
0.5
(b)
û=8.8 mm/s
(iii) T=1.8 s
BY
10
9
8
7
6
5
4
3
2
ū/û
1.0
0.8
0.6
0.4
0.2
-0.2
-0.4
-0.6
-0.8
(a)
û=180.0mm/s

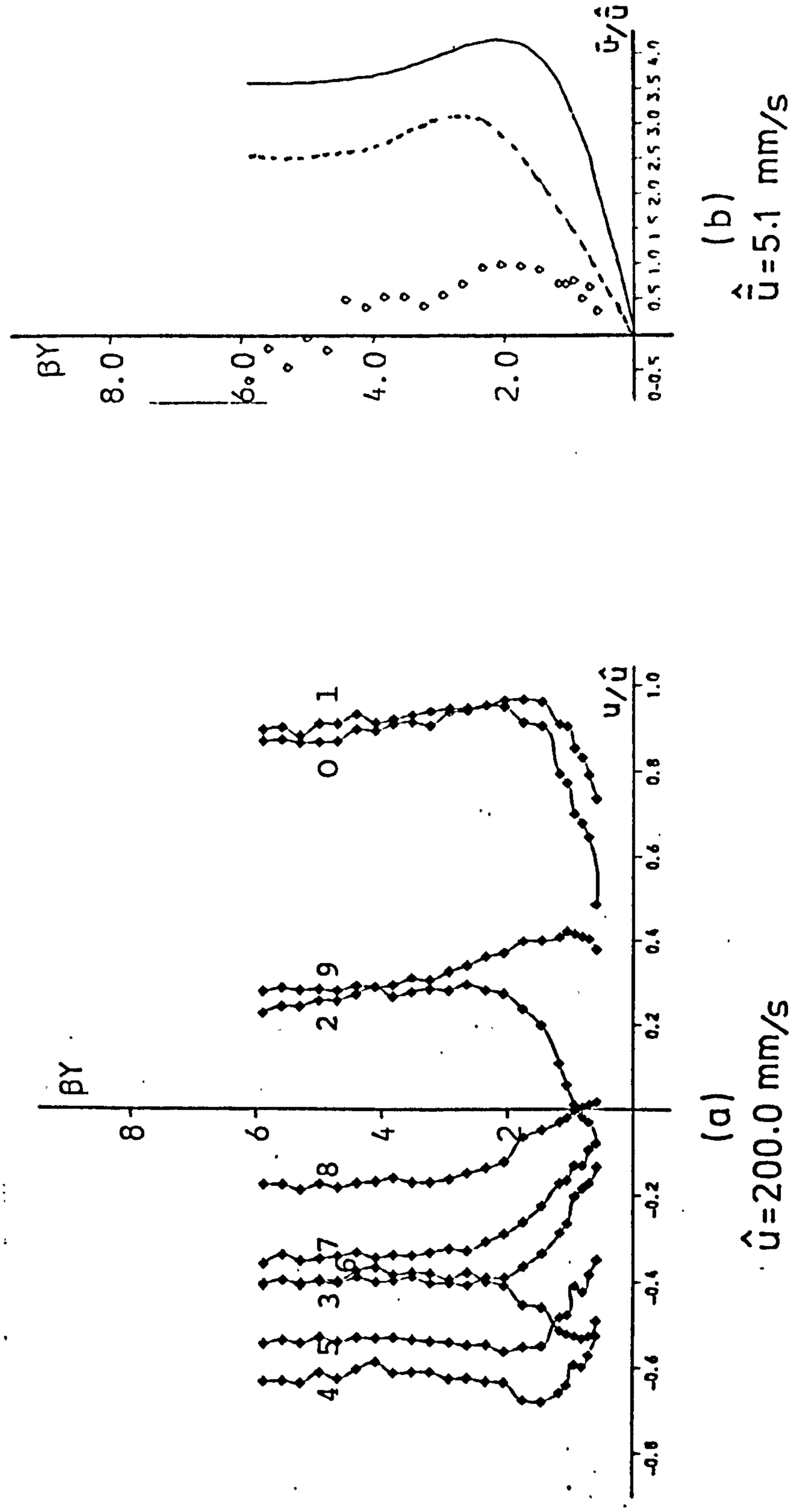
BY
8.0
6.0
4.0
2.0
ū/Û
0.5
1.0
1.5
2.0
2.5
3.0
3.5
4.0
(b)
<U=5.1 mm/s
T=2.0 s
BY
8
6
4
2
u/Û
0.2
0.4
0.6
0.8
1.0
-0.2
-0.4
-0.6
-0.8
1
0
9
2
8
7
6
3
5
4
(a)
Û=200.0 mm/s
(iv)

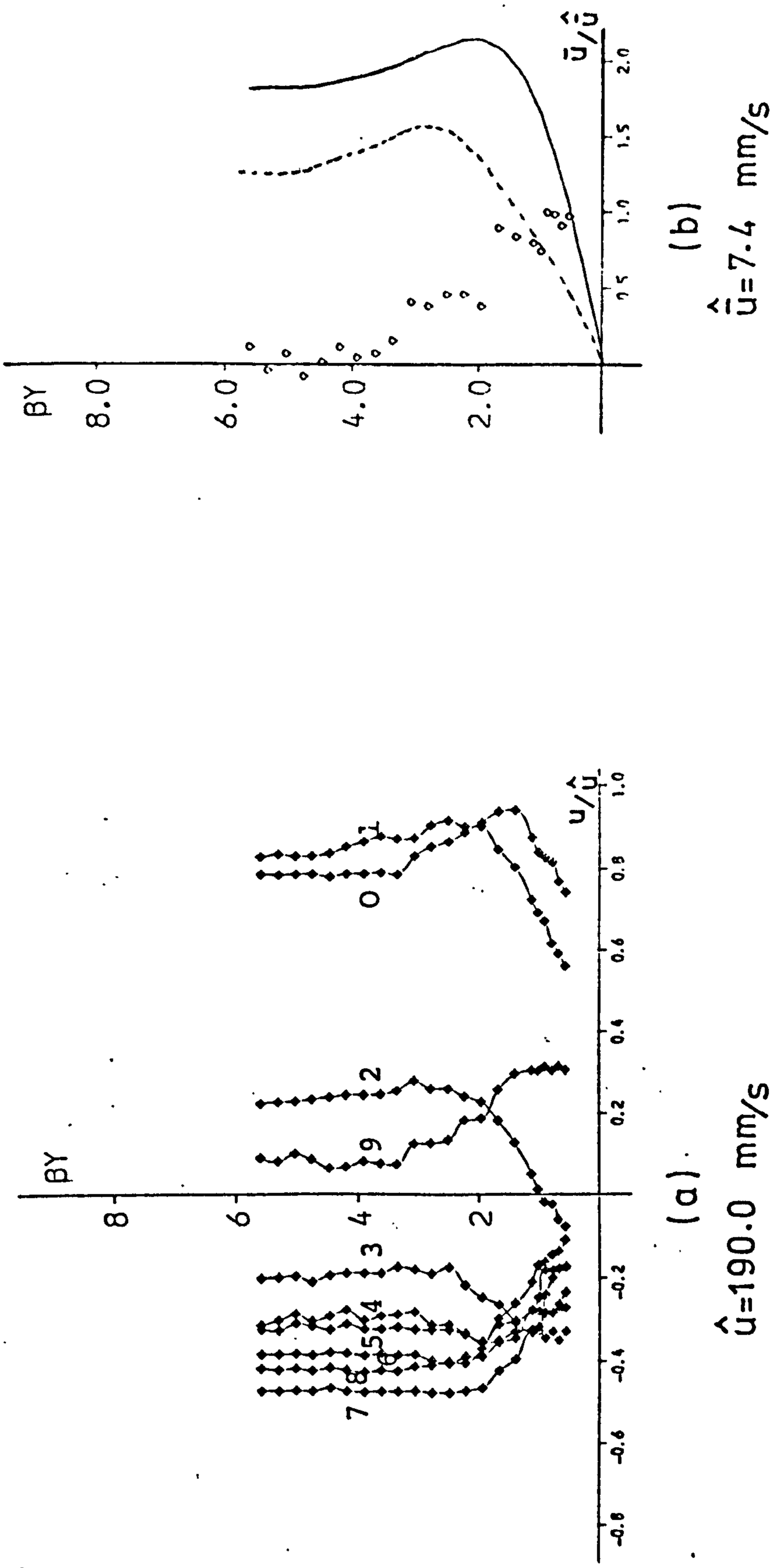
BY
8.0
6.0
4.0
2.0
U/Û
2.0
1.5
1.0
(b)
Û=7.4 mm/s
T= 2.2 s
(a)
Û=190.0 mm/s
1
2
3
4
5
6
7
8
9
0
0.2
0.4
0.6
0.8
1.0
-0.2
-0.4
-0.6
-0.8

T/s	$Re = \frac{\hat{U}_\infty \delta}{\nu}$
1.4	809
1.6	693
1.8	586
2.0	692
2.2	704

Table 6.1. Reynolds No. values for flow over smooth bed.

be applied for comparison with the results.

Fig. 6.2 shows the velocity maxima and theoretical value of velocity maxima phase profile (from Eq. 2.6) and the observed data (for three wave periods). A high correlation occurs for velocity maxima profile and data (Fig. 6.2b) but less correlation of velocity maxima phase profile and data when the depth is below 2.5 (Fig. 6.2a), and this discrepancy is greater for 2.2 sec. wave period. Generally one effect which has influence on all the data points is the weakness of the data collection technique, since for each full period, only 120 velocity readings (and other data points) are taken at equispaced phases of 3 degree intervals throughout the wave cycle (this is to do with the spacing of the slots on the timing disc).

The recorded phases, are the phases of velocity maxima observed but not 'the velocity maxima'. The observed value can fluctuate by up to 3 degrees from the true value and the disagreement can increase by having more than one velocity maxima phase (for example if 3 adjacent phases have the same value for velocity maxima then the recorded phase can fluctuate by up to 6 degrees and so on). Considering all the disadvantages of the method the data and theoretical line (which is a first order equation) are in good agreement for the 1.4 and 1.8 sec. wave periods.

However from Fig. 6.1(a) a clear conclusion arises that the velocity profiles are not symmetrical with respect to the βy axis, which means that first order equation theory

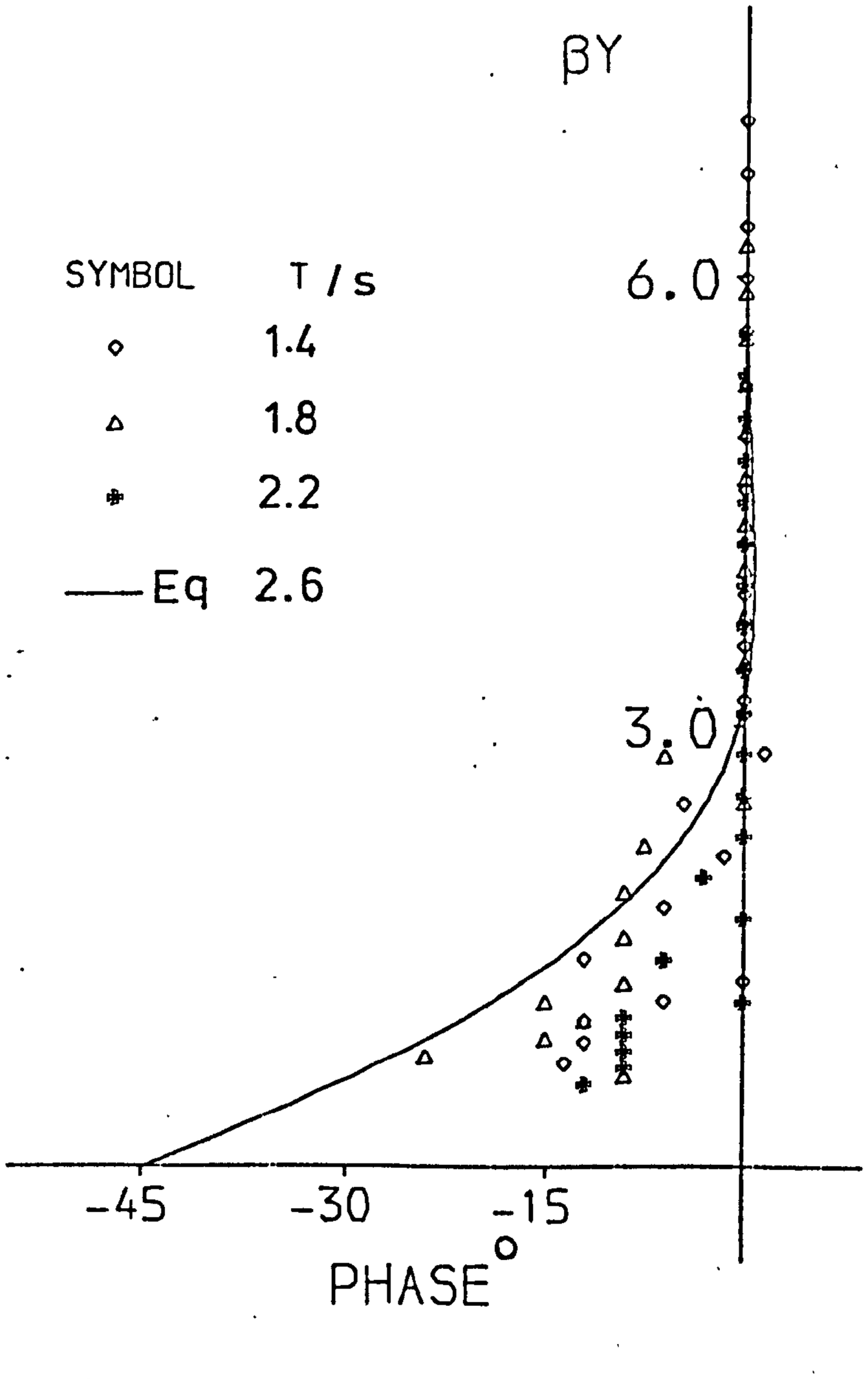

Fig. 6.2(a) Phase of Velocity Maxima within Boundary Layer.

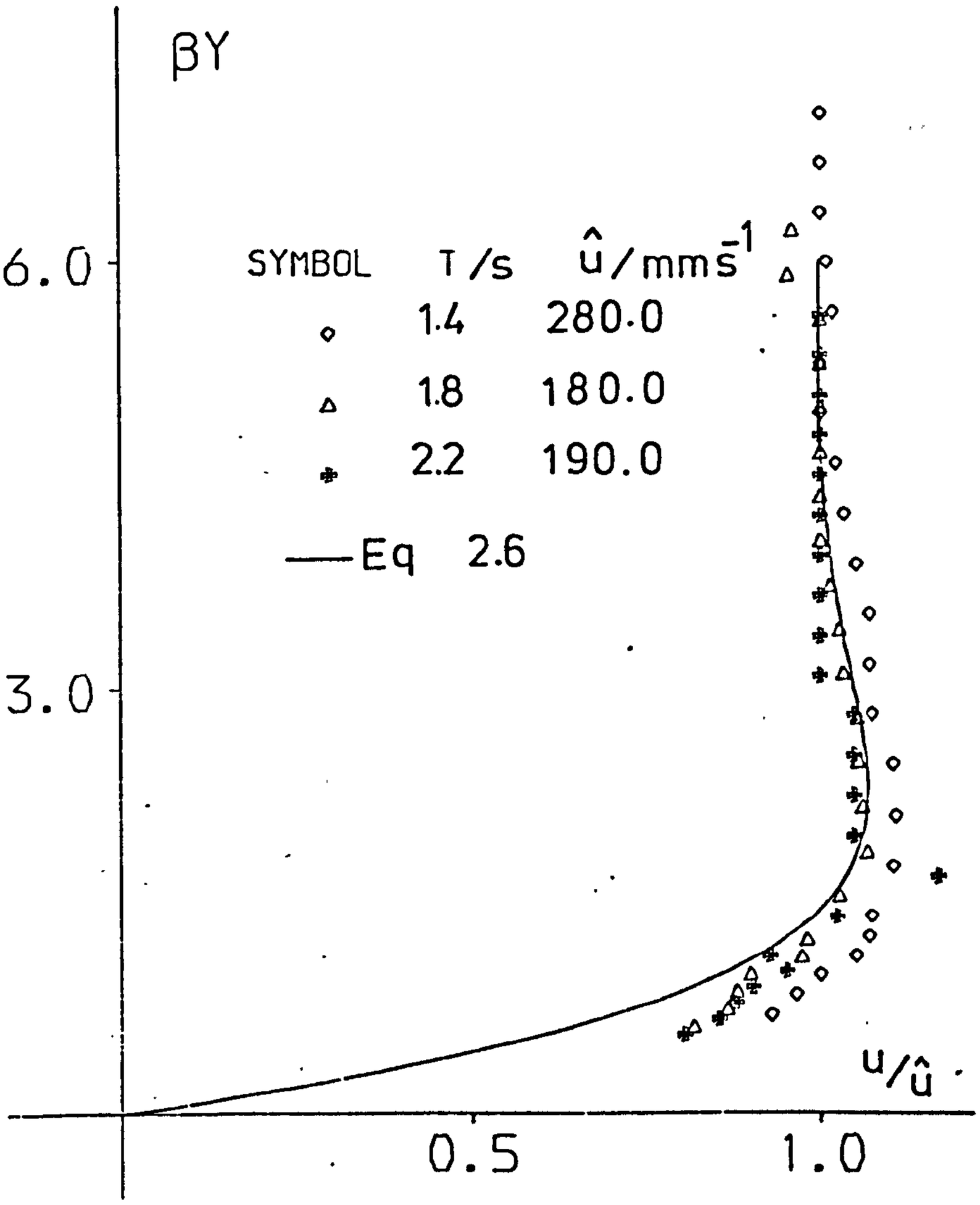

Fig. 6.2(b) Velocity Maxima Profile within Boundary Layer

for boundary layer velocity is not adequate when the wave has a finite amplitude. It is certain now that higher order terms should be added to Lamb's solution for the velocity profile within the boundary layer over a smooth bed (eq. 2.6). Hence a first approach to the velocity profile representation is by the second approximation of Lamb's equation in the form:

$$U = U_1 \left[\mathrm{Cos}(\sigma t) - f_1(y)\ \mathrm{Cos}\ (\sigma t - f_2(y))\right]$$

$$+ U_2 \left[\mathrm{Cos2}\ (\sigma t) - f_3(y)\ \mathrm{Cos2}\ (\sigma t - f_4(y))\right] \qquad (6.1)$$

The first assumption for the values of U_1 and U_2 would be equivalent to the values from Stokes shear wave equation (1.23), which are;

$$\left.\begin{aligned} U_1 &= \frac{\pi H}{T\ \mathrm{Sinh}Kd} \\ U_2 &= \frac{3}{4}\ \frac{(\pi H)^2}{LT\ \mathrm{Sinh}^4 Kd} \end{aligned}\right\} \qquad (6.2)$$

and the f(y) values from equation 2.6;

$$\left.\begin{aligned} f_1(y) = f_3(y) &= e^{-\beta y} \\ f_2(y) = f_4(y) &= \beta y \end{aligned}\right\} \qquad (6.3)$$

Comparison of combined equations 6.1, 6.2 and 6.3 and the observed data, Fig. 6.3 (for 1.4 and 2.2 sec. wave period, and the first five phases) yields the same conclusion about the velocity profile at the edge of the boundary layer (Fig. 5.4a). That is, for example, at a period of 1.4 sec. the modulus of velocity recorded is up to a third greater

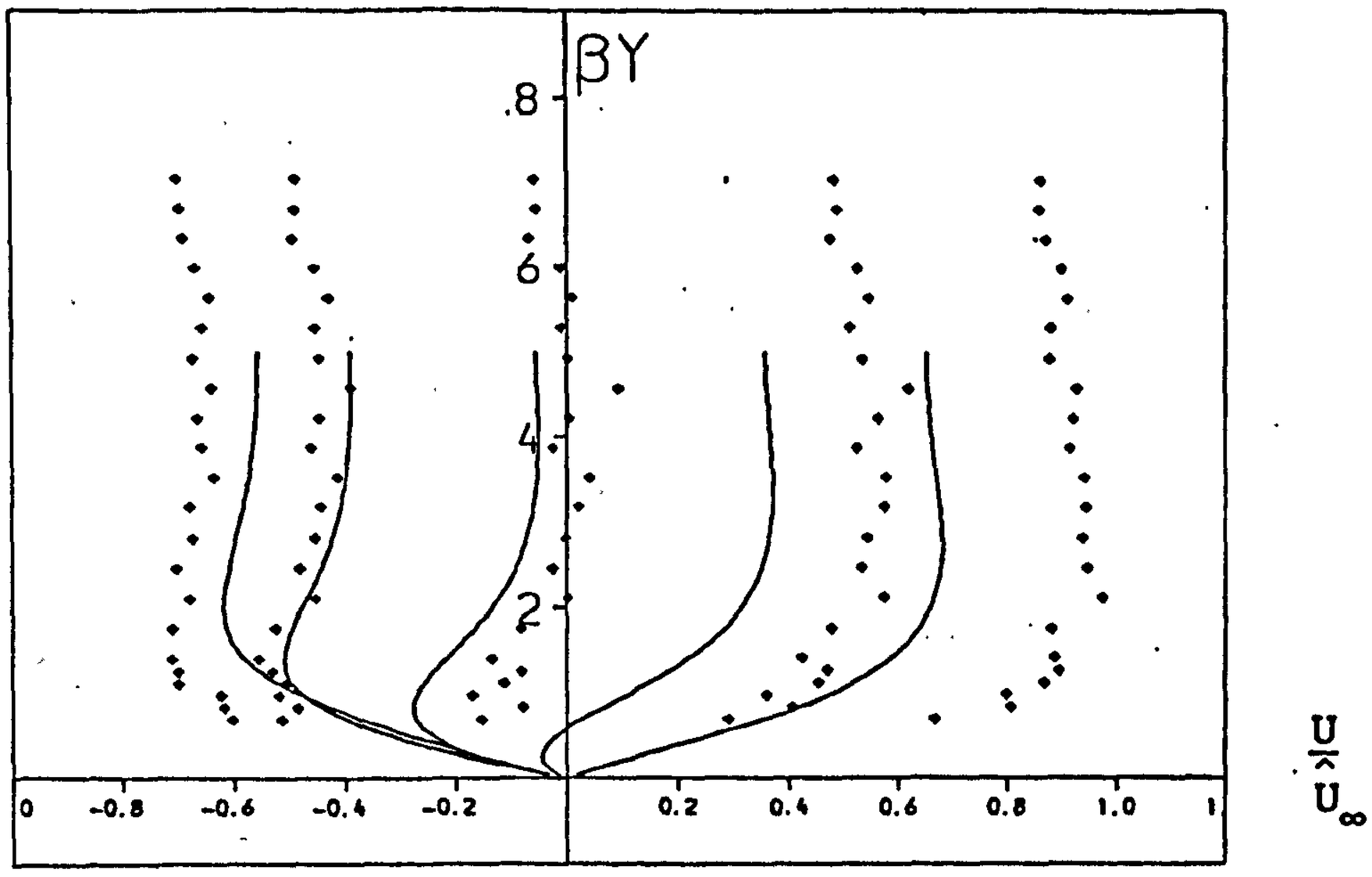

(a) T = 1.4 s, $\hat{U}_\infty$ = 280 mm/s

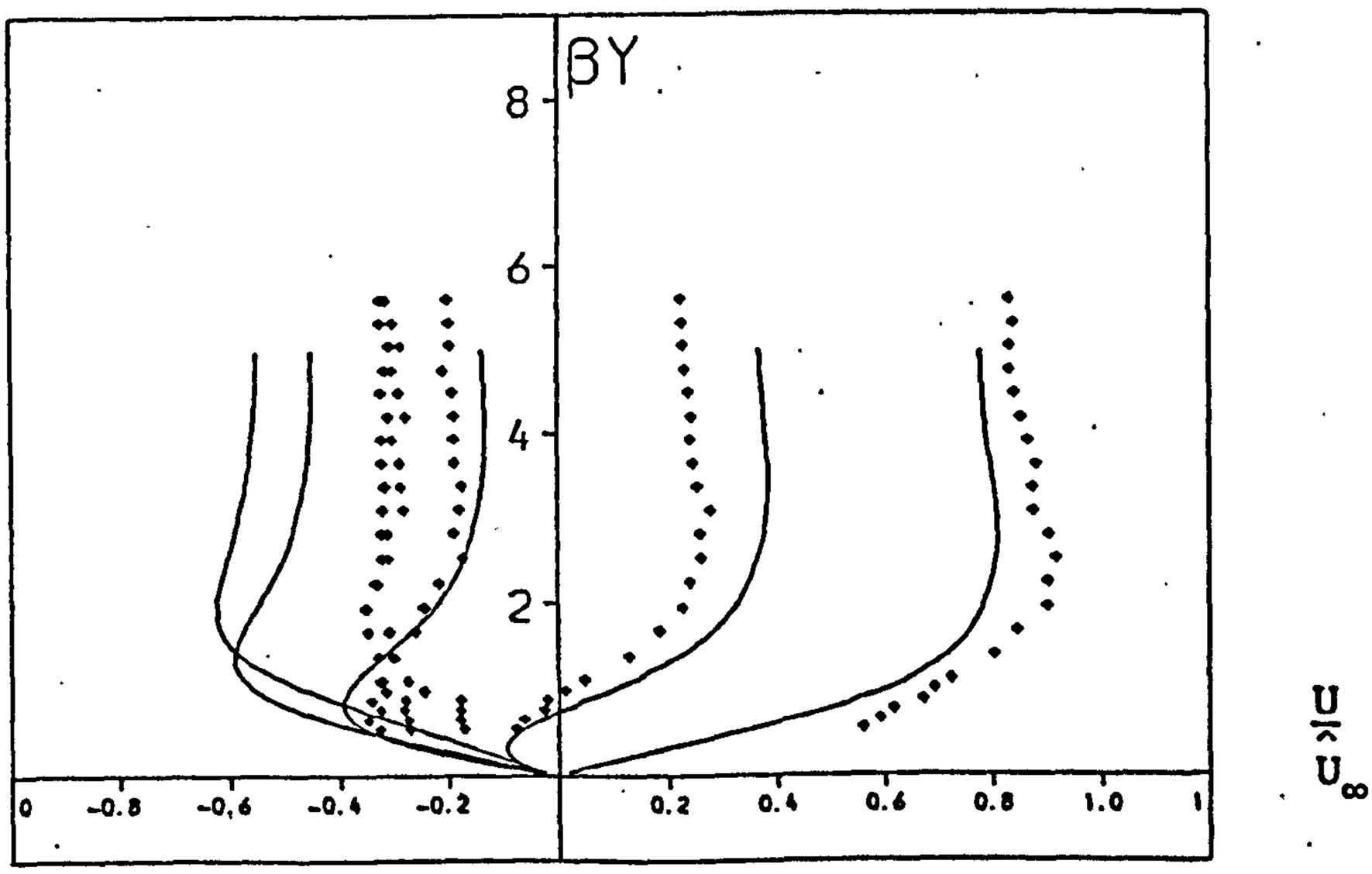

(b) T = 2.2 s, $\hat{U}_\infty$ = 180 mm/s

Fig. 6.3 Velocity Profile for Laminar Flow (Eq. 6.1, ♦ Data)

(To be compared with Beech's solution, all harmonics, Fig. 6.4 and even harmonics Fig. 6.5)

than the theoretical values. For 2.2 sec. wave period the negative observed velocity is less than the prediction values and the positive recorded velocity has almost the same value as the theory. In fact it is fair to assume that, if the Stokes second order is a good prediction for orbital velocity in the bulk of fluid, then equations 6.1, 6.2 and 6.3 are acceptable theoretical predictions for boundary layer velocity. As for other profiles it was noted (velocity and wave surface) that for wave periods of greater than 2.0 sec. inclusive, the Stokes second order theory is not a good prediction anymore since the waves are in the shallow water zone.

Following from this, work has been done by Beech (1978) who, has developed the shear wave equation of Stokes in the form of a Fourier series having the odd and even terms. The equation suggested is in the form;

$$U = \ell_o + \sum_{1}^{\infty} \ell_n \left[\text{Cos } n\ (\sigma t) - \bar{e}^{\sqrt{n\beta}y} \text{ Cos } n\ (\sigma t - \sqrt{n\beta}y)\right]$$

$$+ \sum_{1}^{\infty} m_n \left[\text{Sin } n\ (\sigma t) - \bar{e}^{\sqrt{n\beta}y} \text{ Sin } n\ (\sigma t - \sqrt{n\beta}y)\right] \quad (6.4)$$

where ℓ_o is the mean velocity and for second order equation the values of ℓ_o, ℓ_1, ℓ_2, m_1 and m_2 can be found theoretically (Heading 1970) or experimentally from the data available.

The values of Table 6.2, which have been found from the velocity profile at the edge of the boundary layer (i.e. results of Fig. 5.4a) using the harmonic analysis method proposed by Heading, are used in Eq. 6.4 to plot the theoretical values with the observed data (Fig. 6.4) having the

T/s	ℓ_o	ℓ_1	ℓ_2	m_1	m_2
	/mm s^{-1}				
1.4	5.9	224.7	22.9	-21.5	0.2
1.6	-11.1	181.4	32.5	1.7	-7.7
1.8	-5.8	149.5	9.7	-20.8	6.0
2.0	-17.2	134.7	57.1	-28.3	5.2
2.2	-7.2	110.9	58.4	11.9	-7.1

Table 6.2. The harmonic coefficients of the Fourier series (Eq. 6.4).

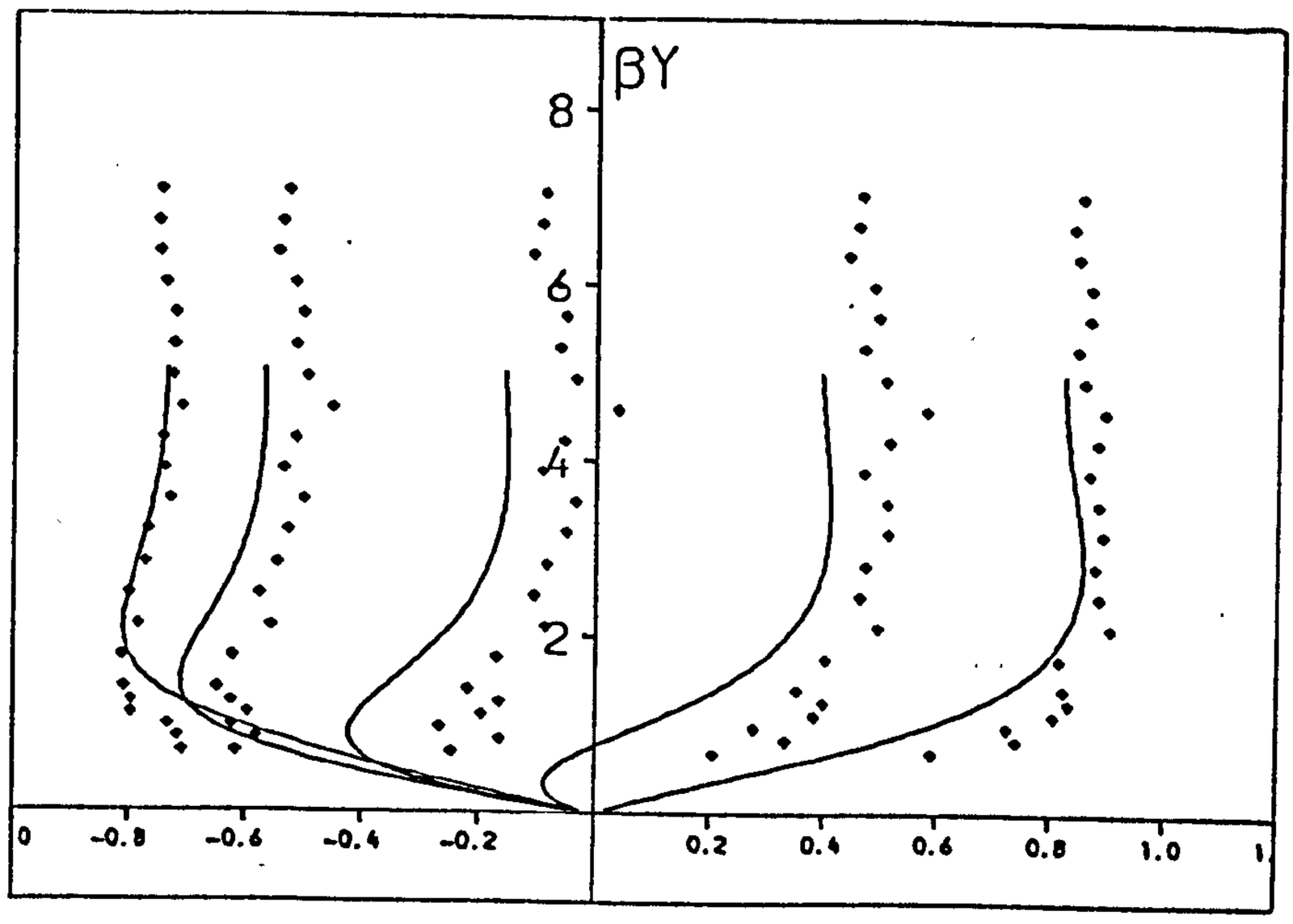

(a) $T = 1.4$ s, $\hat{U}_\infty = 280$ mm/s

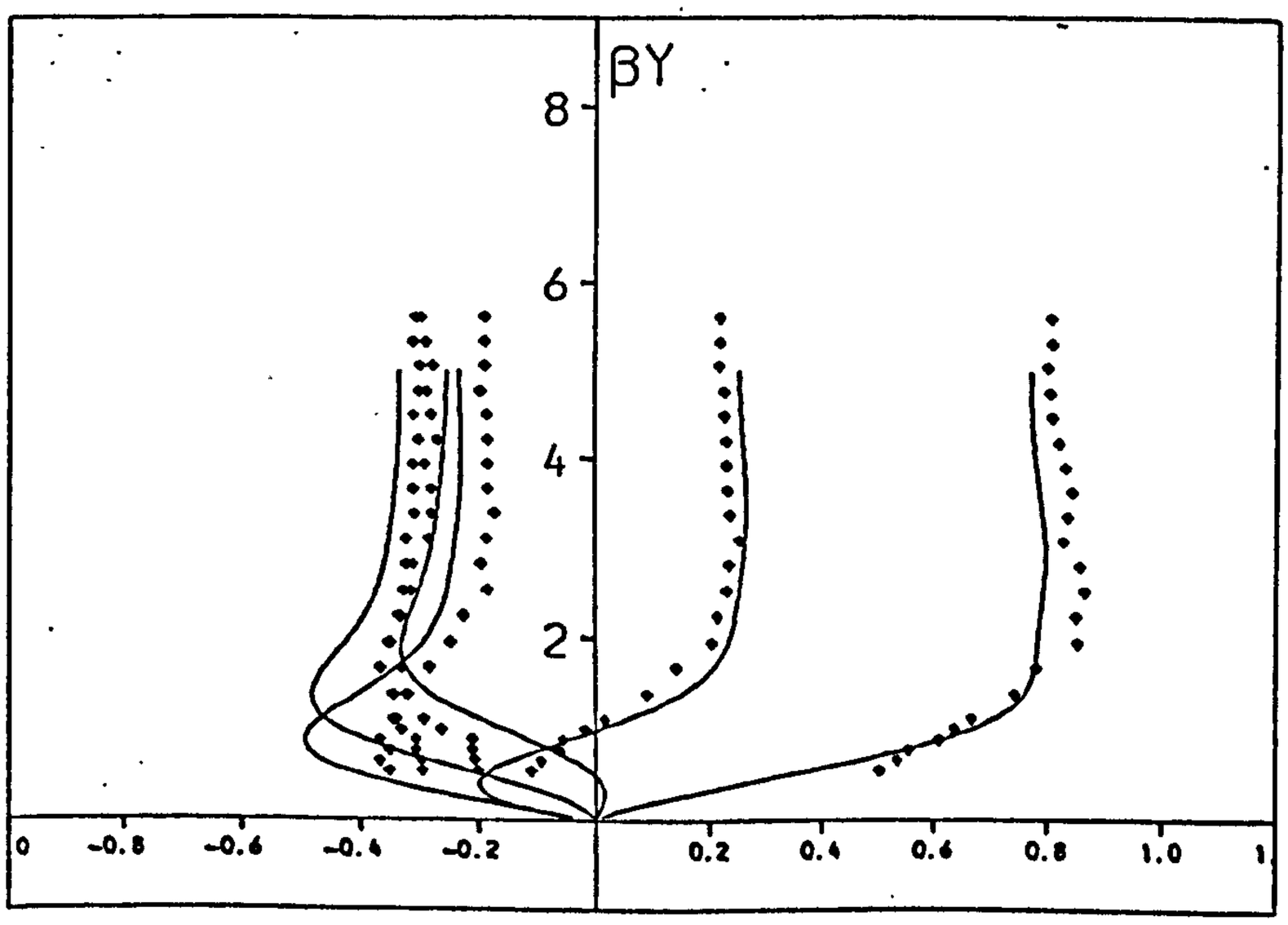

(b) $T = 2.2$ s, $\hat{U}_\infty = 180$ mm/s

Fig. 6.4 Boundary Layer Velocity Profile for Smooth Bed (Eq. 6.4, ♦ Data)

(To be compared with Beech's solution, even harmonics, Fig. 6.5).

abscissa of the graph $\frac{U-\bar{U}}{U_\infty-\bar{U}_\infty}$ instead of $\frac{U}{U_\infty}$ (Beech 1978). A high correlation results for the wave periods of up to 2.0 sec. between the theory and data and a lesser agreement is noticeable for 2.0 and 2.2 sec. wave periods from Fig. 6.4 (the reason has been discussed before). Hence it is conclusive that Beech's equation for waves in the intermediate water zone is a good prediction of the boundary layer velocity for smooth bed. However, the disadvantages of this method are that, unless the profile of the velocity at the boundary layer limit is known the theory cannot be used. So the ideal technique would be to find a factor (or factors) for relating the coefficients U_1 and U_2 from equation 6.2 (which can be calculated by knowing the characteristics of wave and the water depth) to the coefficients of the Fourier series.

Because equation 6.1 contains only the 'Cos' terms, while equation 6.4 has the 'Sin' terms as well, to compare the two sets of coefficients it would be reasonable to eliminate the odd harmonics of Eq. 6.4 and transfer ℓ_o (or $\bar{U}$) to the other side of the equation. Then we have;

$$U-\bar{U} = \ell_1 \left[\text{Cos } \sigma t - e^{-\beta y} \text{ Cos } (\sigma t - \beta y)\right] + \ell_2 \left[\text{Cos2 } \sigma t - e^{-\sqrt{2}\beta y} \text{ Cos } 2 (\sigma t - \sqrt{2}\beta y)\right] \quad (6.5)$$

Plotting the velocity profiles from the above equation with the values of ℓ_1 and ℓ_2 from Table 6.2 with the collected data (Fig. 6.5), a very good agreement occurs. (There was

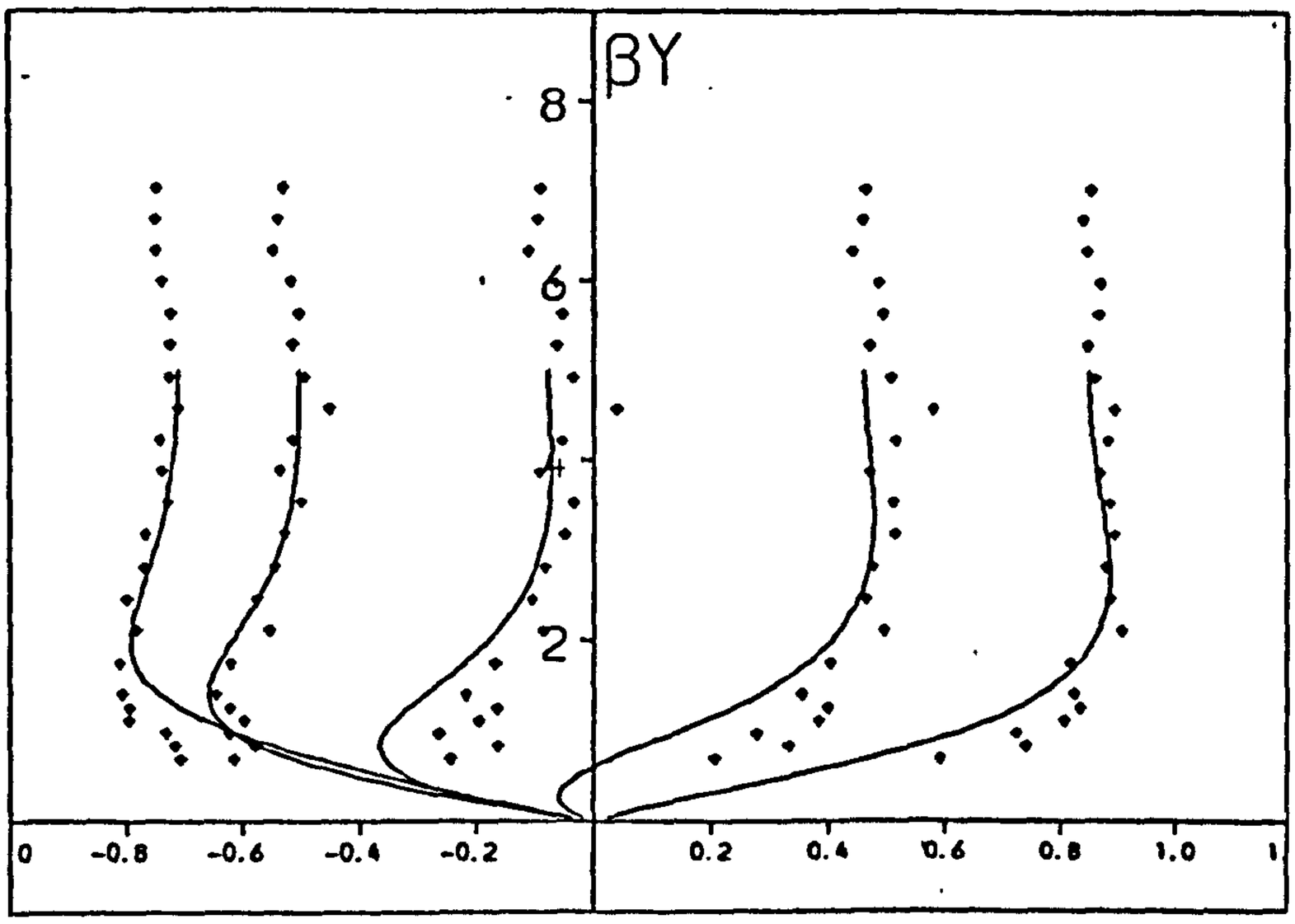

(a) T = 1.4 s, $\hat{U}_\infty$ = 280 mm/s

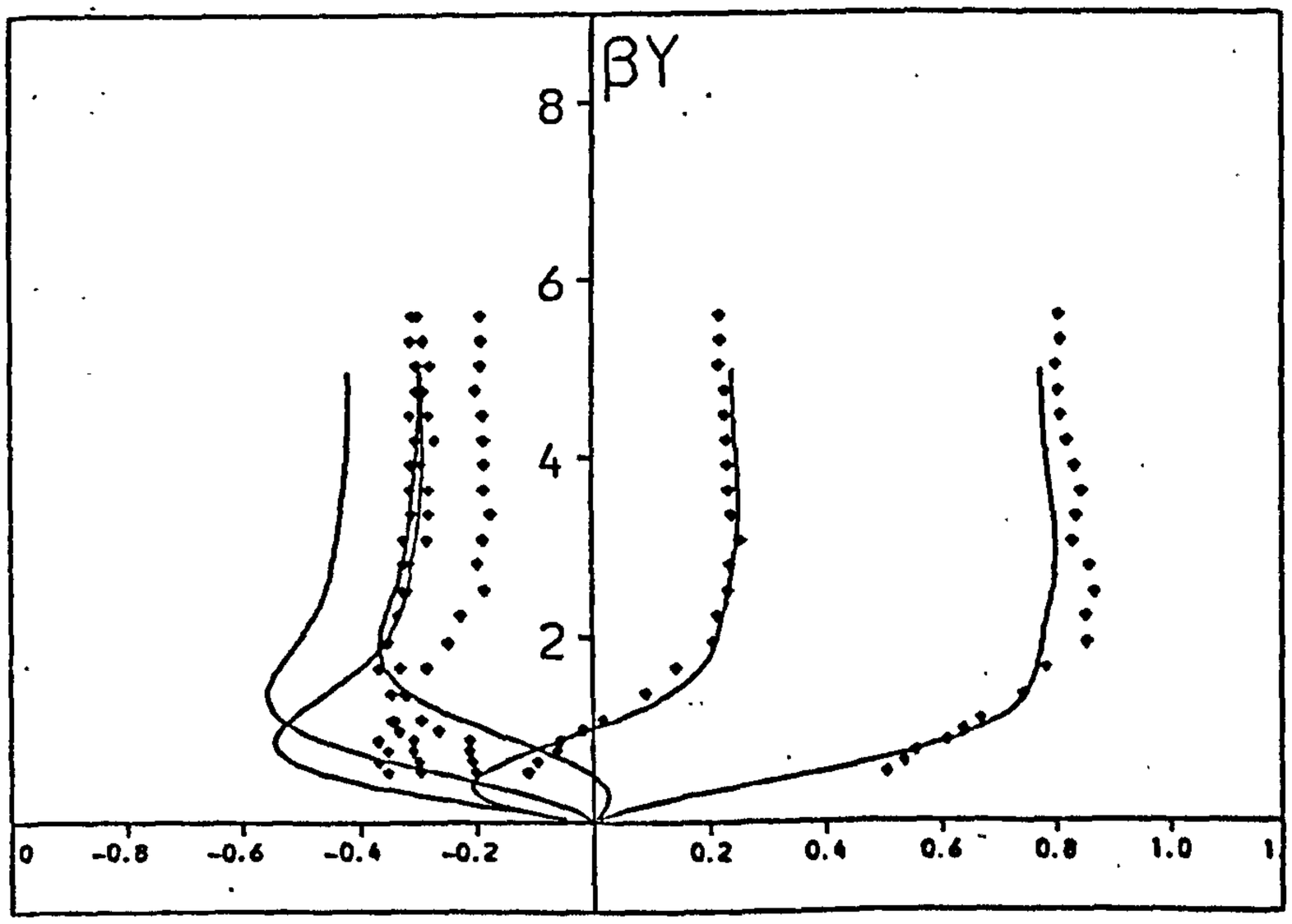

(b) T = 2.2 s , $\hat{U}_\infty$ = 180 mm/s

Fig. 6.5 Boundary Layer Velocity Profile for Smooth Bed (Eq. 6.5, ♦ Data)

(c.f. with Fig. 6.4 - all harmonics)

no reason to present all the wave periods and instead only the lowest and highest frequencies are shown. It can be concluded that the profiles of the 1.6 and 1.8 sec. waves behave like the 1.4 sec. wave period one and the 2.0 and 2.2 sec. wave periods have a very close profile for the theory and data). There is little difference between Figs. 6.4 and 6.5 which proves that the odd harmonics of the Fourier series do not have much effect on the theory and can be neglected.

Calculating the theoretical values of U_1 and U_2 from equation 6.2 and plotting the ratios ℓ_1/U_1 and ℓ_2/U_2 versus the period of the present and Beech's data, Fig. 6.6 is then presented. Passing the best straight line through the data points (separate regression analysis has been done for the five data points observed for this investigation and the data from Beech's observation - except the last three periods which somehow does not fit into the rest of the data), the equations for the two relationships are;

$$\left.\begin{aligned} \frac{\ell_1}{U_1} &= a_o T + a_1 \\ \frac{\ell_2}{U_2} &= b_o T + b_1 \end{aligned}\right\} \quad (\ell/u = K\ (\to 1) \text{ for small } T) \tag{6.6}$$

where the coefficients for the present investigation are;

$$\left.\begin{aligned} a_o &= -0.58 \\ a_1 &= 2.09 \end{aligned}\right\} \tag{6.7(a)}$$

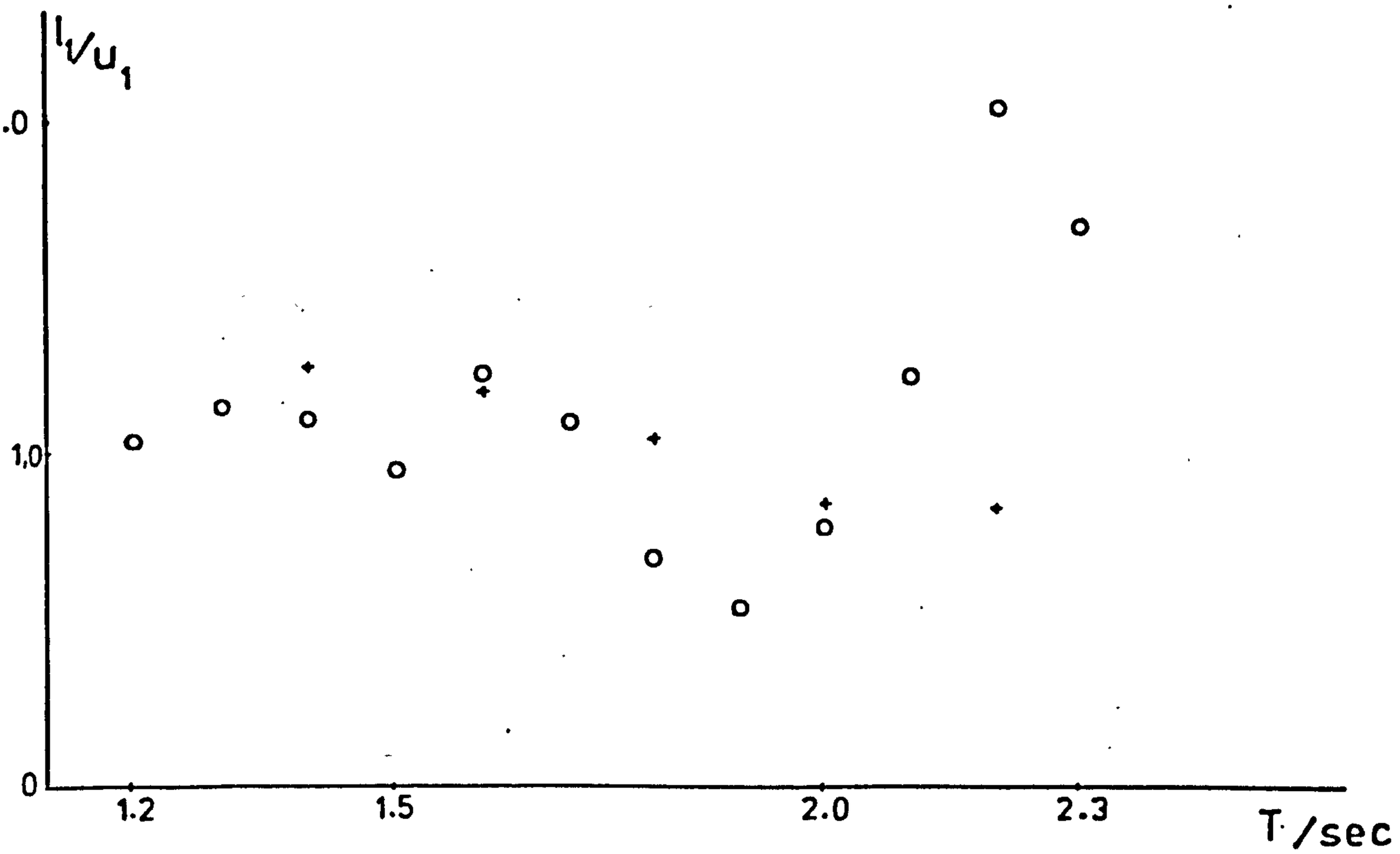

(a) l_1/u_1 v wave period

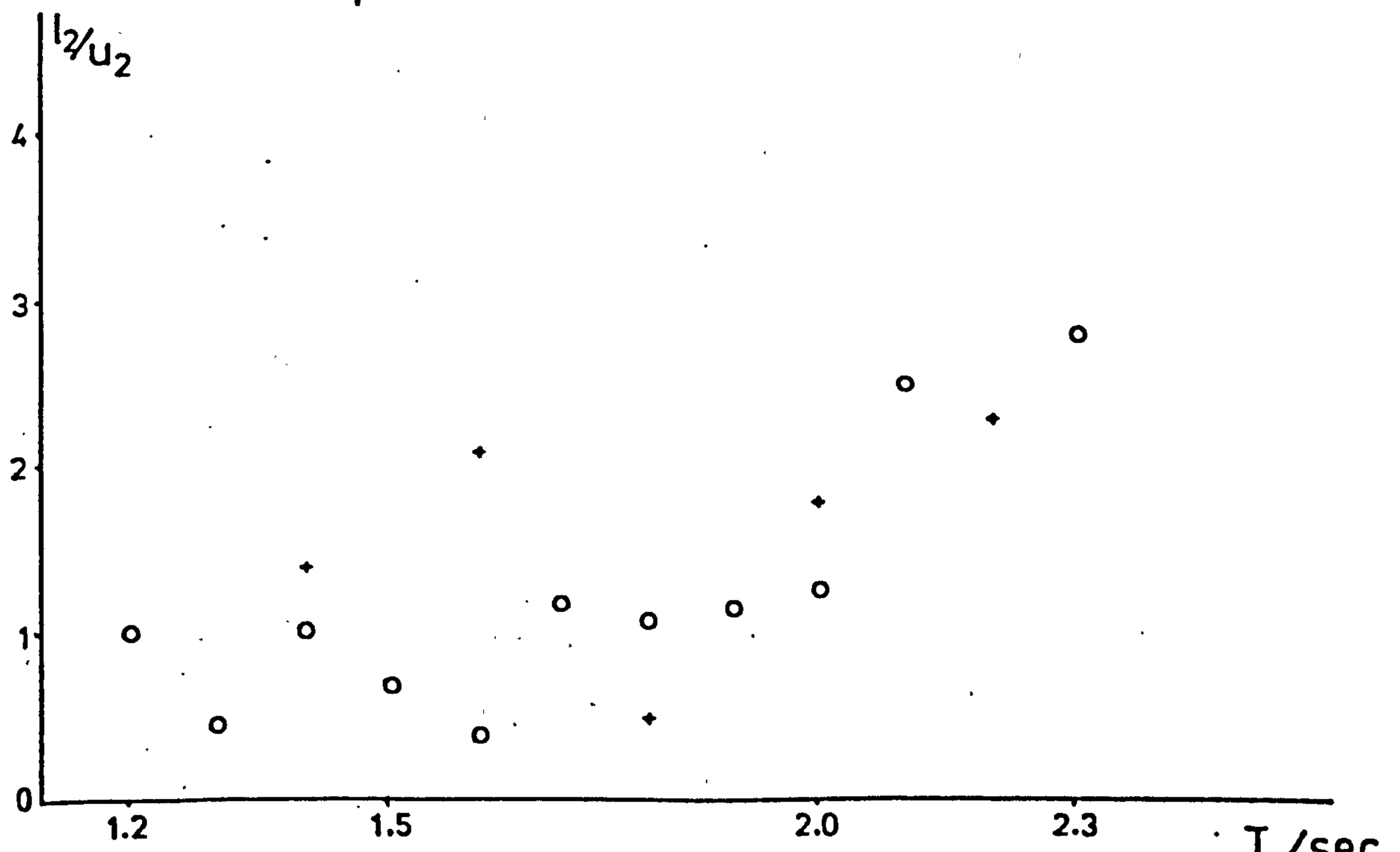

(b) l_2/u_2 v wave period

+ present data

o Beech's data

FIG 6.6 THE RELATIONSHIP BETWEEN l_1, l_2, u_1 AND u_2 FOR DIFFERENT WAVE PERIODS.

$$\left.\begin{aligned} b_o &= 0.75 \\ b_1 &= 0.27 \end{aligned}\right) \qquad (6.7(b))$$

and for Beech's observation are;

$$\left.\begin{aligned} a_o &= -0.58 \\ a_1 &= 1.88 \end{aligned}\right) \qquad (6.8(a))$$

$$\left.\begin{aligned} b_o &= 0.62 \\ b_1 &= -\ 0.08 \end{aligned}\right) \qquad (6.8(b))$$

The close agreement of equations 6.7(a) and 6.8(a) show a significant meaning to the equation 6.5 in relating to the values of ℓ_1 and U_1. In fact a single equation can be assumed for ℓ_1 and U_1 since a high correlation exists. However, this can not be said for ℓ_2/U_2 relationship, since some disagreement between the two sets of results has occurred.

Also the values of velocity maxima phase from equation 6.5 has been found by iteration technique to the nearest 0.25 of a degree. A profile for wave periods of 1.4 and 2.2 sec. is shown in Fig. 6.7, with the collected data. A highly correlated result is observed unlike the profile from the first order equation. However, since the velocity maxima profile does not change much from the profile of first order (Fig. 6.2b), the profile for velocity maxima is not presented for second order equations.

Therefore, now it can be said with confidence that equation 6.5 is a good theoretical prediction for the set of results observed for this investigation as well as those of

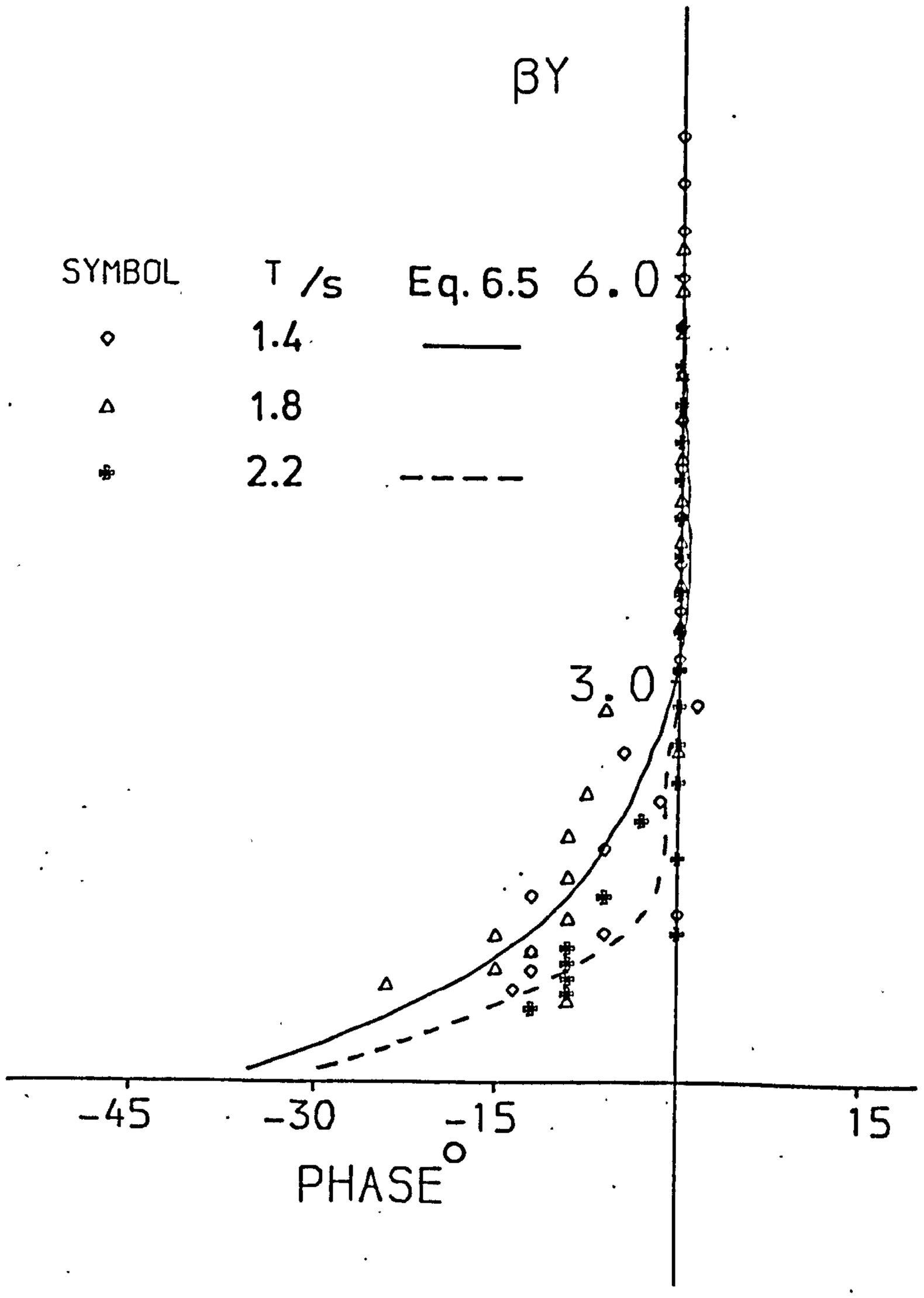

Figure 6.7. Phase of Velocity Maxima from Eq. 6.5.

Beech's, with the values of ℓ_1 and ℓ_2 to be found from the relationship with U_1 and U_2 from equations 6.6 and 6.7.

6.2.2 Mean Velocity

Fig. 6.1b illustrates the observed mean velocity values with the Longuet-Higgins predictions of mass transport velocity (Eq. 2.23) and mean velocity (Eq. 2.26). According to the definition in Appendix D, the average velocity here is the mean velocity rather than the mass transport velocity, and a good agreement is observable between the theoretical mean values and observed data, except for 1.4 sec. wave period.

At high values of βy the data points get closer to zero mean velocity and as the wave period increases the mean velocity has negative value, which is not as suggested by the theory, but it is convincing that the mean velocity close to the bed is always positive.

The magnitude of the observed mean velocity values from 1.4 sec. wave period suddenly drops to less than half that value for 1.6 sec. wave period and a dramatic drop is observed for a wave of 2.0 sec. period. One reason for this variance is that the observation error as a fraction of the mean velocity result is much greater than that of the same magnitude error for the maximum velocity, and the origin of the error is the same. For example while a 5 mm/s fluctuation

introduces less than 2% difference for the boundary layer velocity maxima, the error is at least as large as 20% for mean velocity. In fact the result for the mean velocity within the boundary layer is similar to that for the bulk of fluid.

So, while the mean velocity is always positive inside the boundary layer, its magnitude is less than the predicted values of Longuet-Higgins (except for 1.4 sec. wave period). And at higher wave periods the mean velocity has a reverse direction to the wave propagation above the bed (as it was seen for the mean velocity in the bulk of fluid Fig. 5.3b).

6.3 Rough Beds and the Boundary Layer Velocity Profile

6.3.1 Two Dimensional Rough Bed

The bottom of the trough roughness was taken as zero height and the boundary layer thickness was assumed to start from the top of the roughness crest.

The velocity profile over the roughness up to 10 mm above the top of roughness element (which is well greater than the boundary layer thickness) for two periods of 1.4 and 2.2 seconds are illustrated in Fig. 6.8. (For other wave periods the boundary layer velocity profile are available but it did not seem to contribute much to the understanding of the behaviour of flow by presenting other than these two). The right hand side graphs (Fig. 6.8b) are the velocity over the trough and the left hand side graphs

6.8(a) Over Crest of Roughness

6.8(b) Over Trough of Roughness

Fig. 6.8 Boundary Layer Velocity Profile for 2-D Rough Bed (10 phases in a cycle).

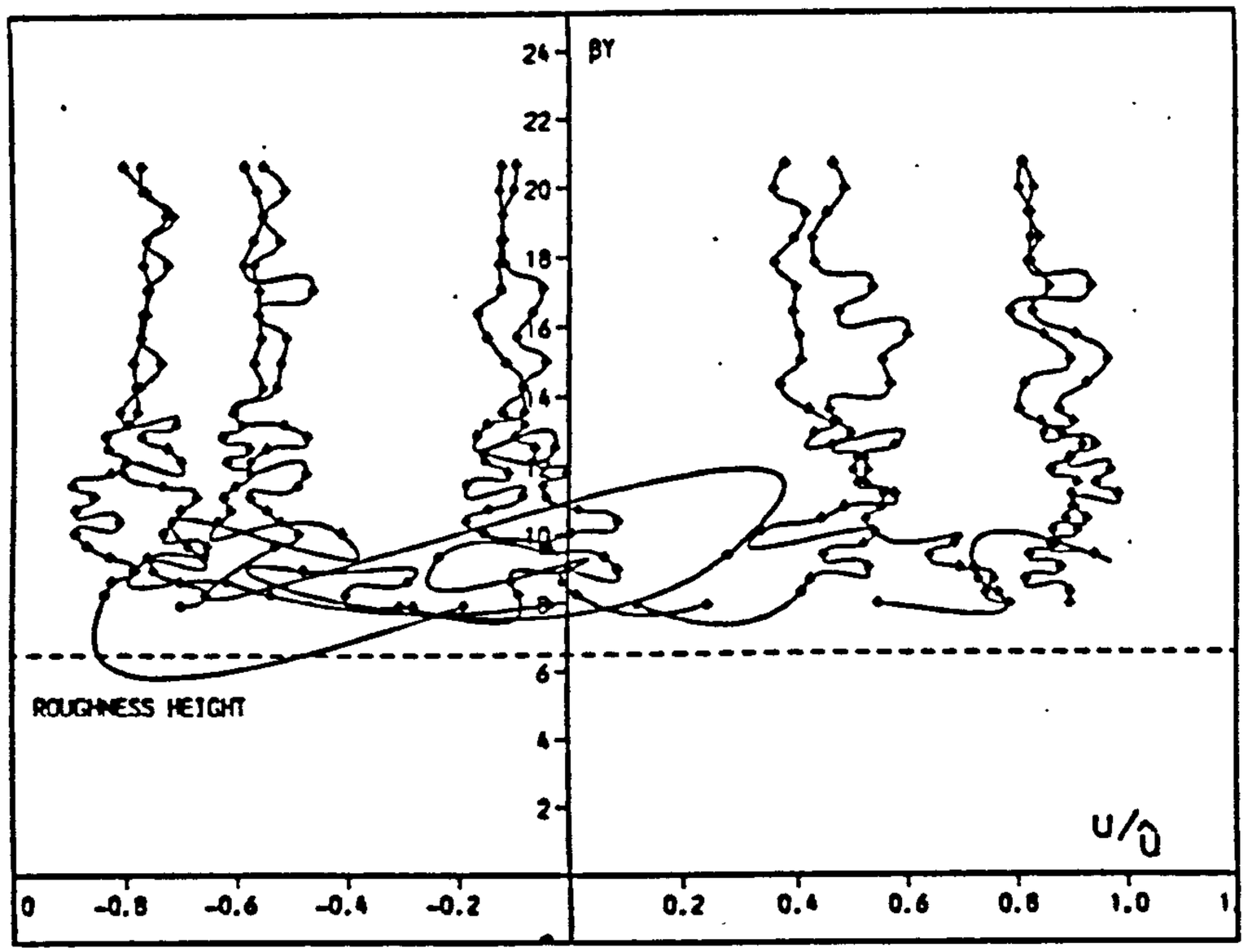

(a)

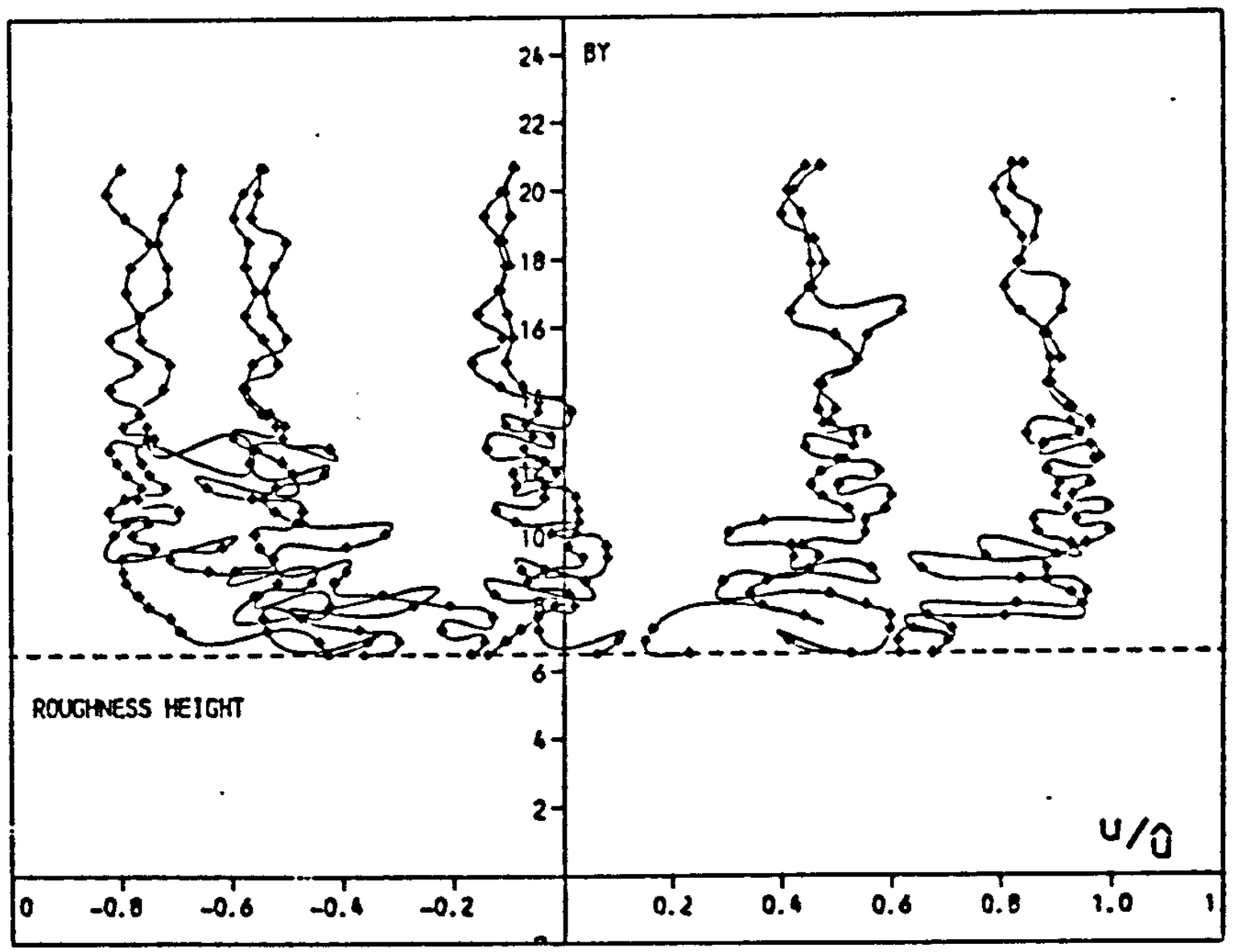

(b)

T=1.4 s
$\hat{u}$=280.0 mm/s

(i)

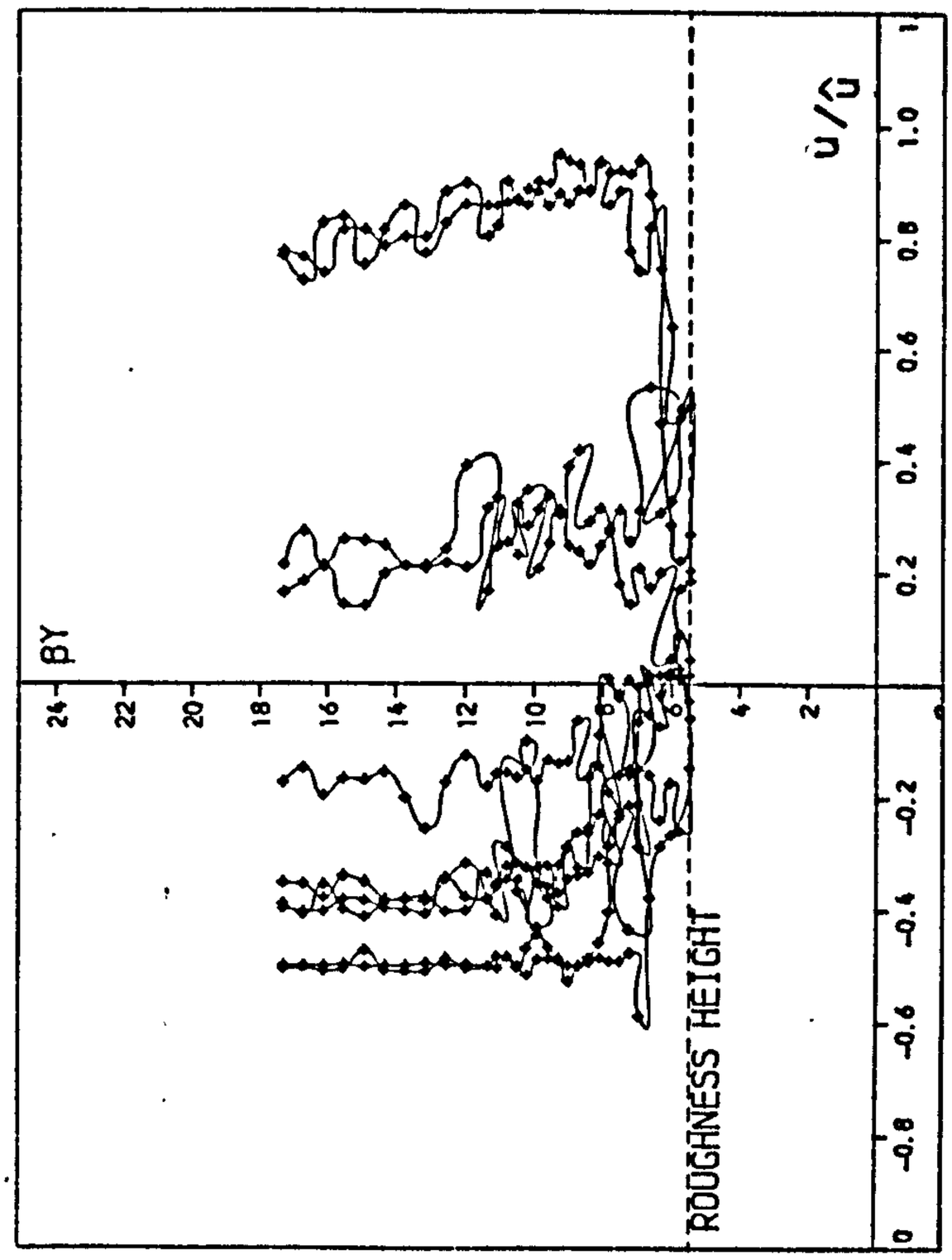

(b)

T=2.2 s
Û=205.0 mm/s

(ii)

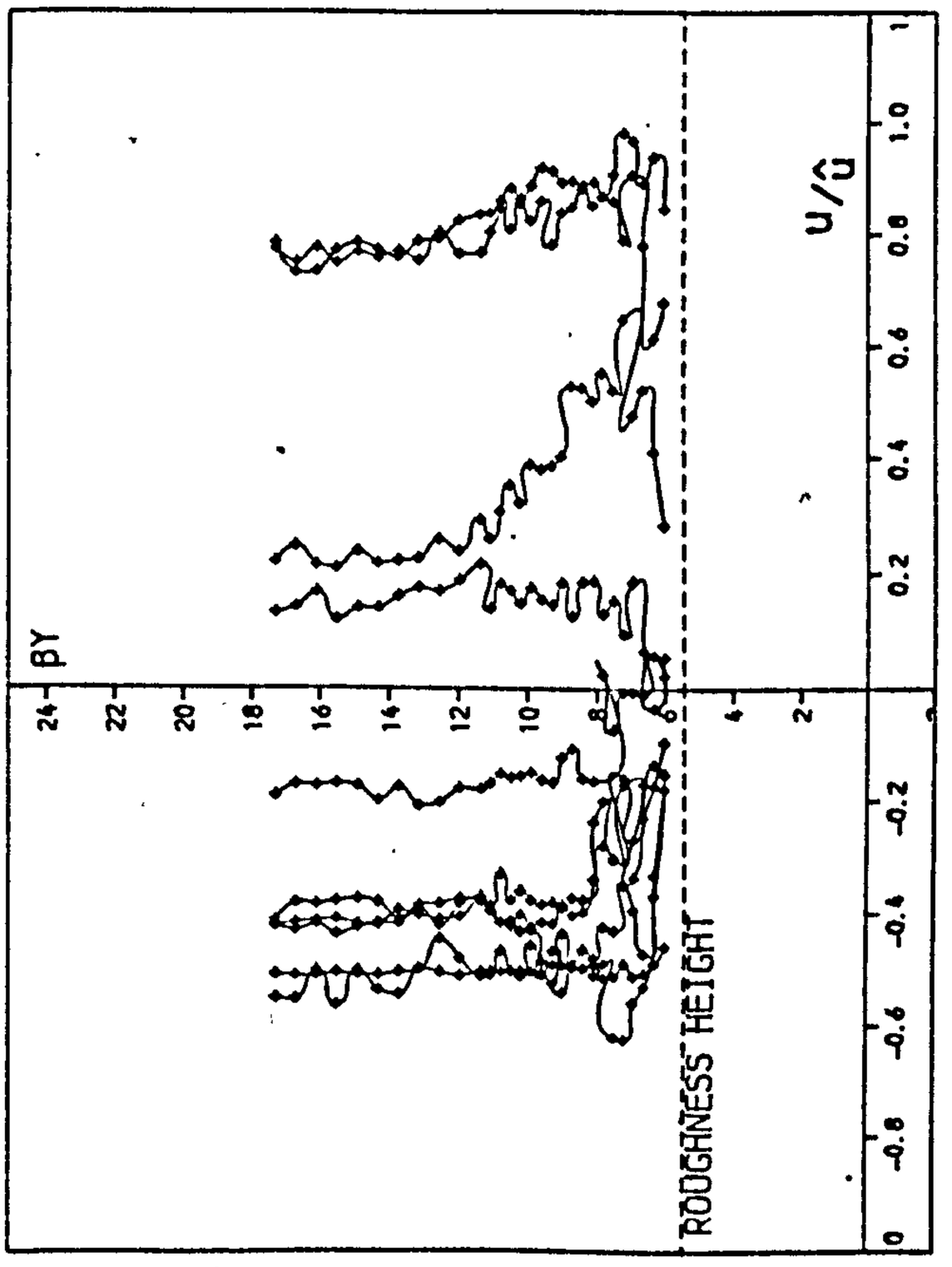

(a)

(Fig. 6.8a) are the profile of velocity over the crest of roughness (both values are recorded at exactly mid-point of the trough or crest).

It has been mentioned (see 6.2.1) that the line connecting the data points (for each phase) does not show the actual velocity profile but it is very useful for showing the existence of velocity fluctuations. The graphs clearly indicate that the flow close to the roughness height is not laminar anymore and as the height increases the profiles become more smooth and laminar flow reappears. And it happens at lower depths for the 2.2 sec. wave period than for the 1.4 sec. wave period, since the magnitude of the velocity is greater for the latter than the former.

Before studying the influence of roughness on the velocity profile, it is obvious that the velocity profile over trough and crest need: to be compared. Although some conclusion can be achieved from Fig. 6.8, one precise method is to compare velocities at the individual phase position separately, as in Fig. 6.9 for the 1.8 second wave period.

A more comprehensive way is to study the relationship of complete profile of velocity at each depth over trough and crest of roughness. Fig. 6.10 shows the relationship of the two velocities at 6 different heights at the same phase at each position for 1.8 sec. wave period. The extent of correlation between the two variables is indicated by the correlation coefficient given in Fig. 6.10; a complete

6.9(a) - Over Trough

6.9(b) - Over Crest

Fig. 6.9 A Sample of Boundary Layer Velocity Profiles for each phase in a cycle (T = 1.8 s) for 2-D Rough Bed ($t_n = \frac{(2n-1)}{20}$ T).

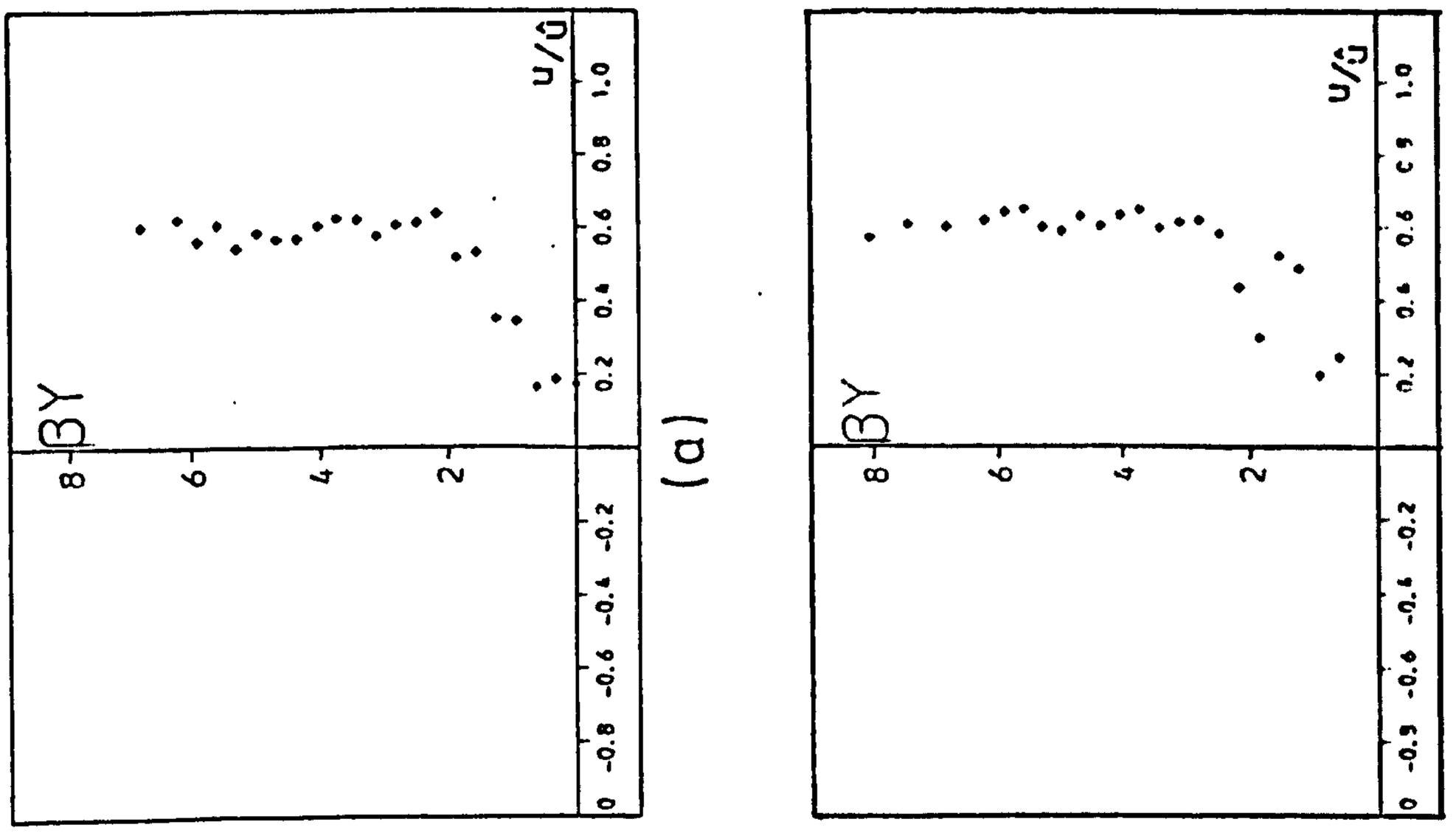
βY
U/Û
(a)
(b)
(ii) t_2

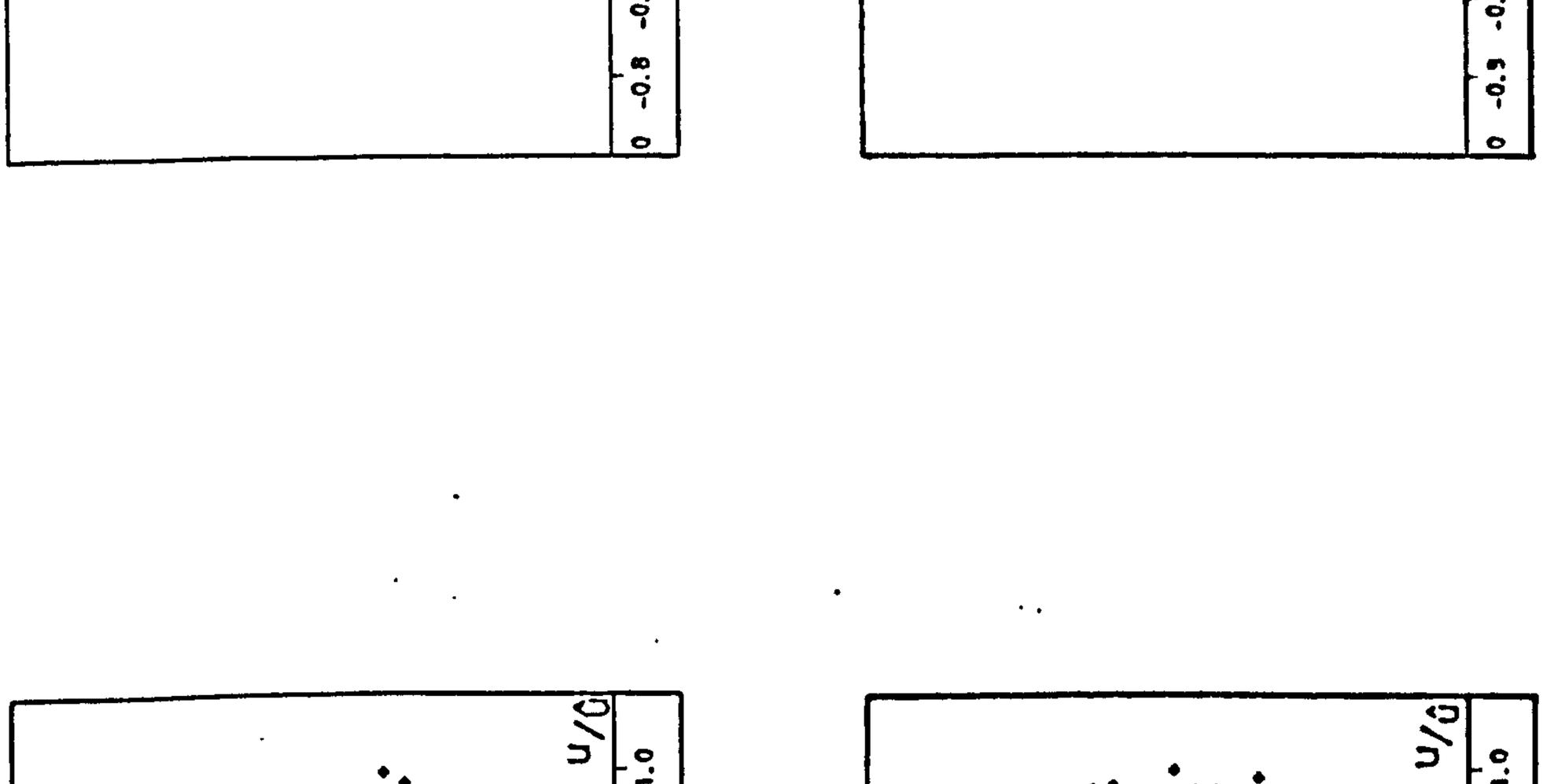
βY
U/Û
(a)
(b)
(i) t_1

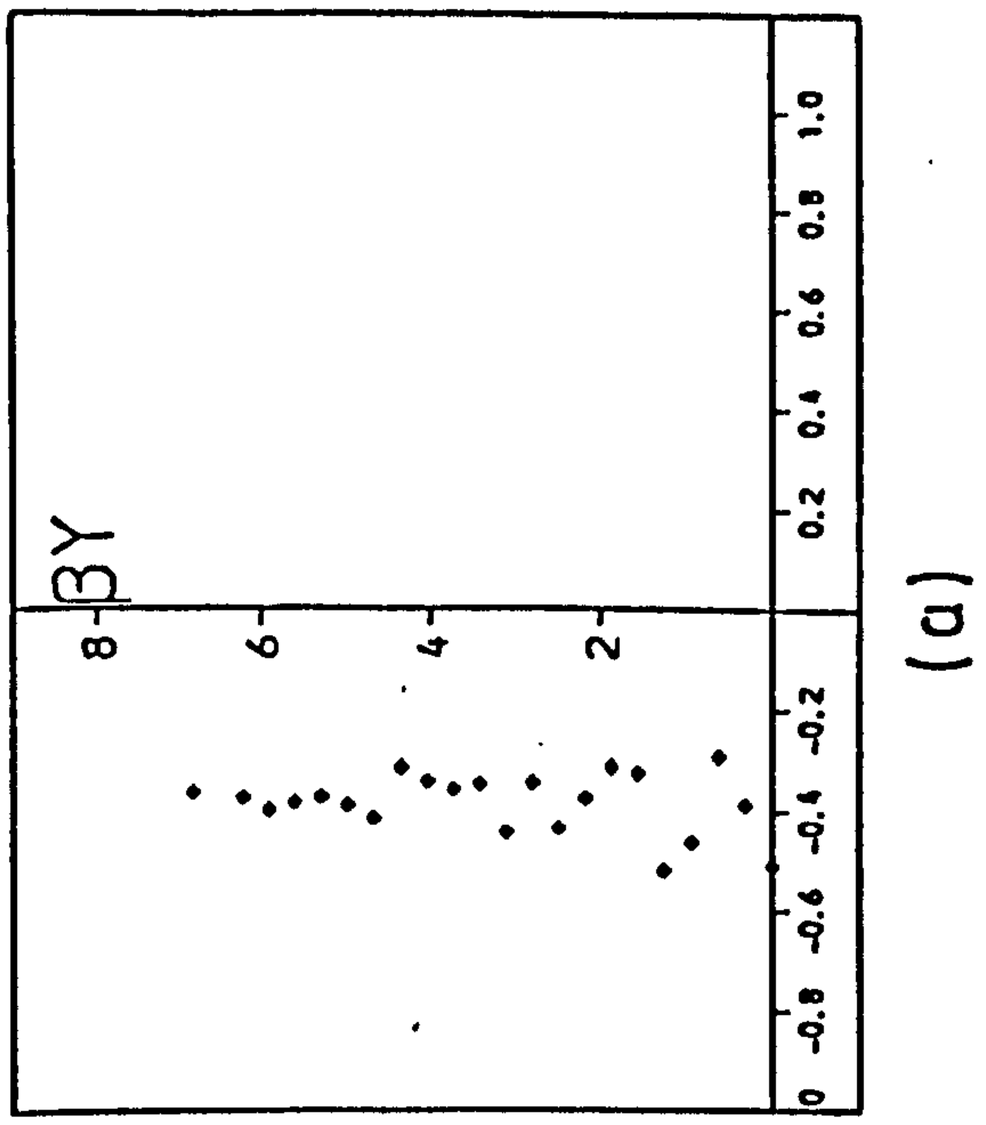

(a)

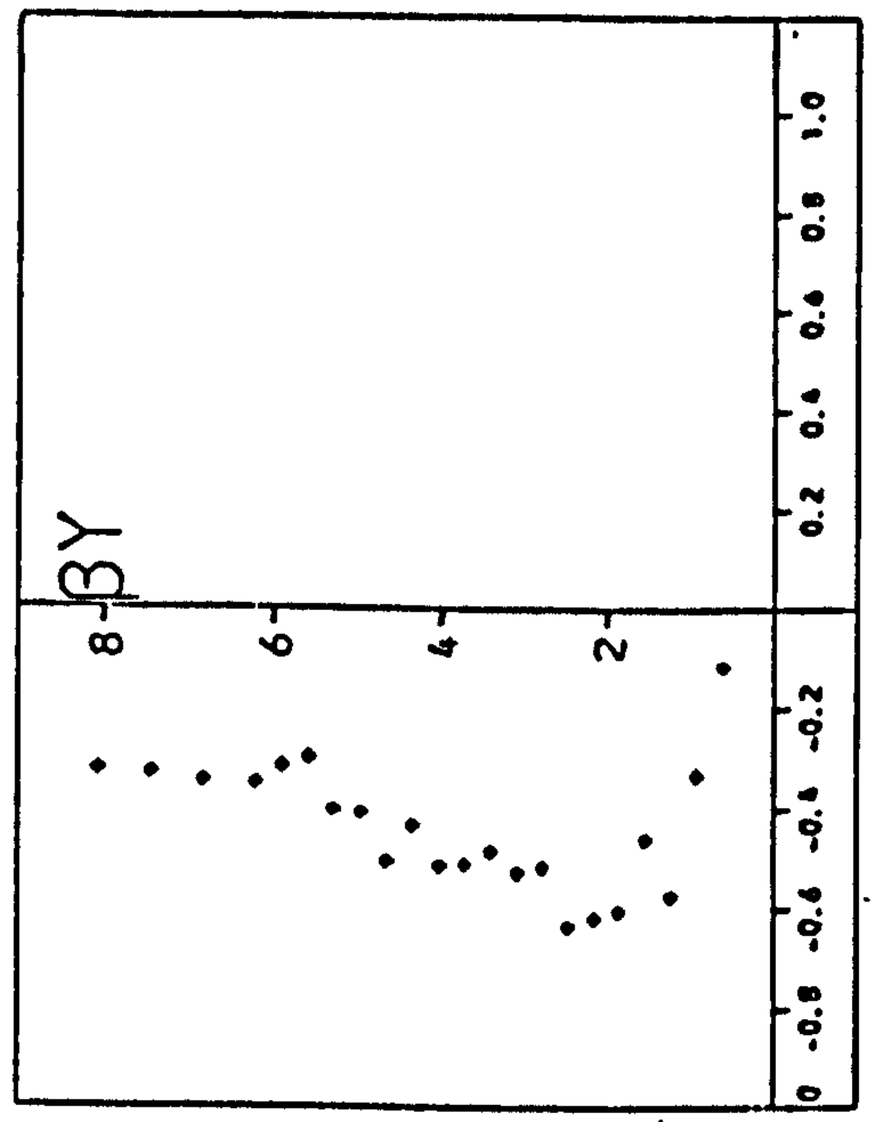

(b)

(iv) t_4

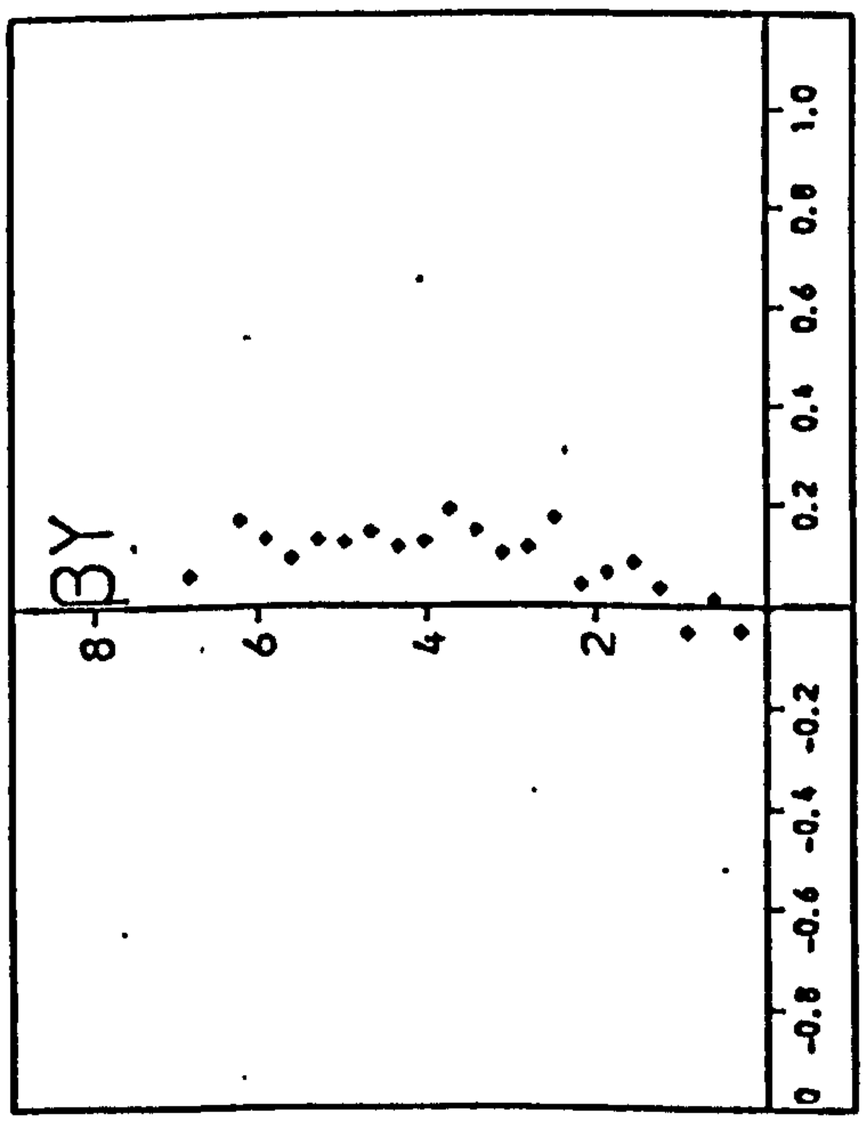

(a)

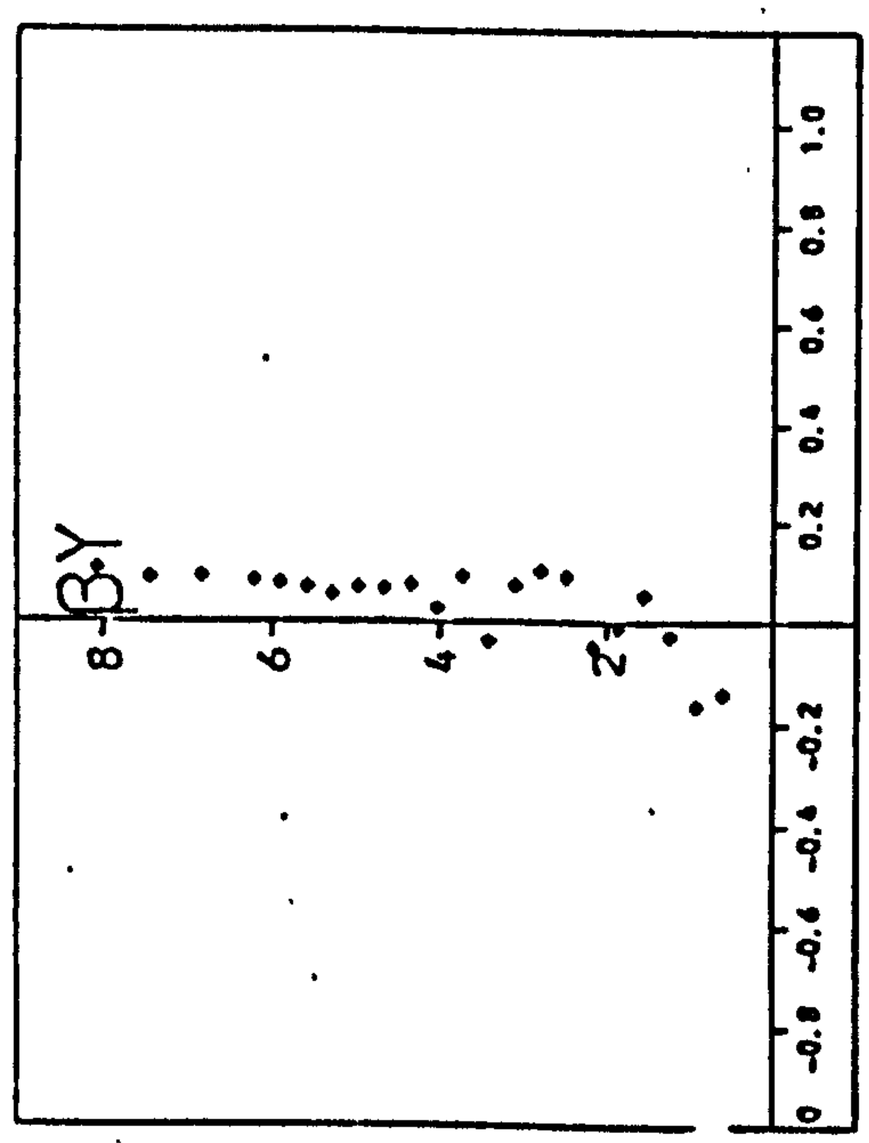

(b)

(iii) t_3

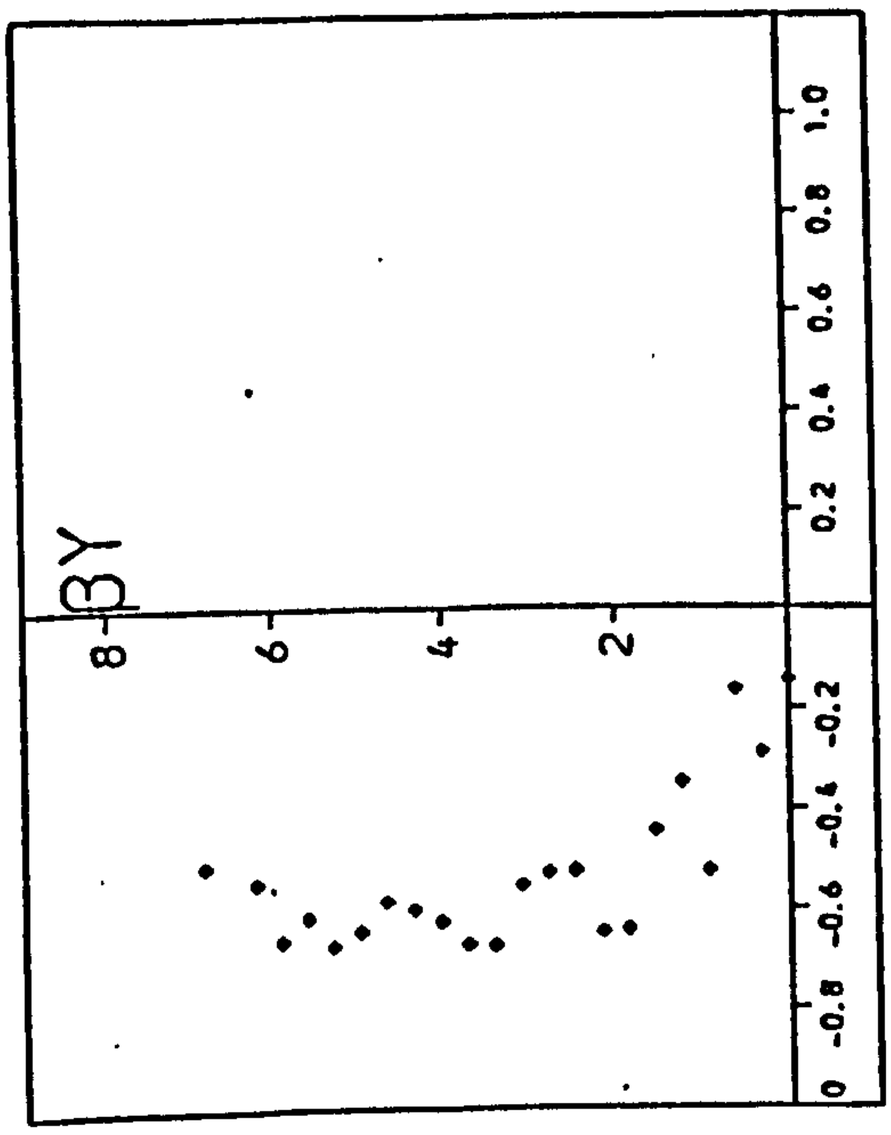
BY
8
6
4
2
0.2
0.4
0.6
0.8
1.0
-0.2
-0.4
-0.6
-0.8
0
(a)

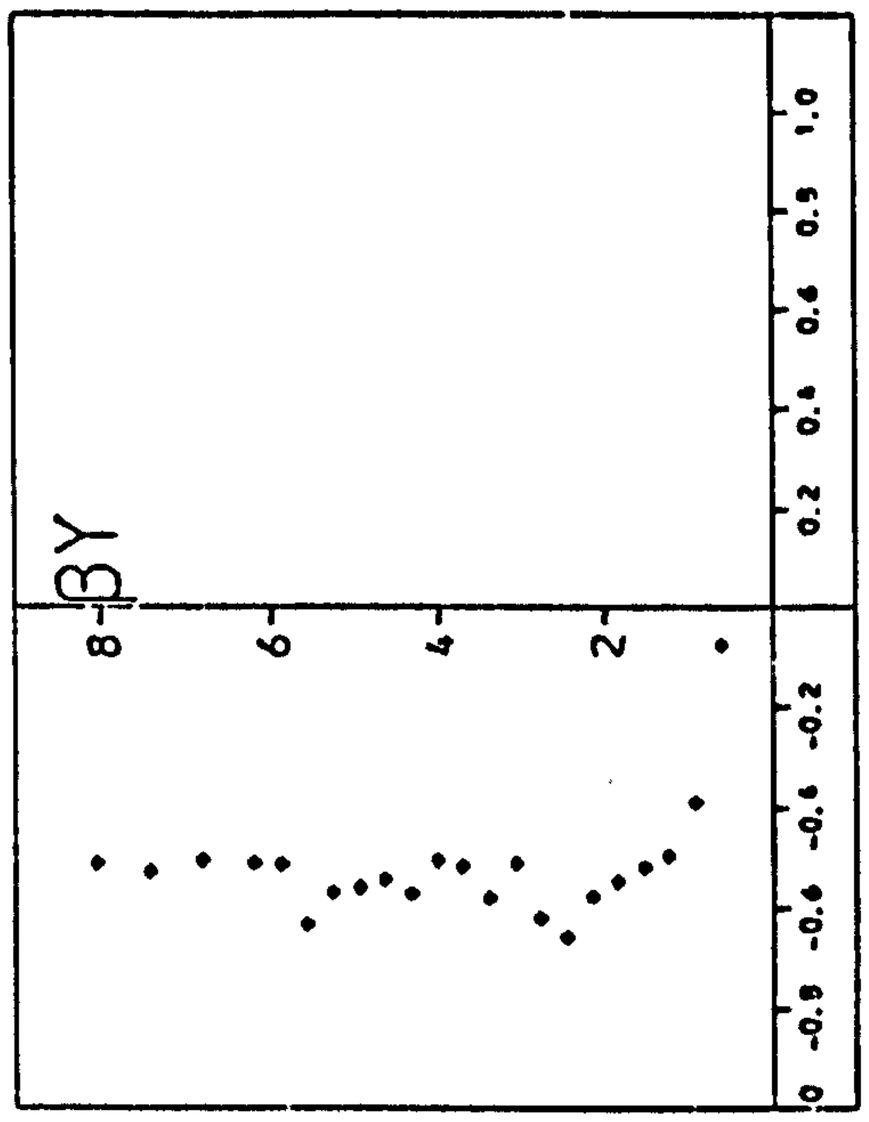
BY
8
6
4
2
0.2
0.4
0.6
0.8
1.0
-0.2
-0.4
-0.6
-0.8
0
(b)

(vi) t_6

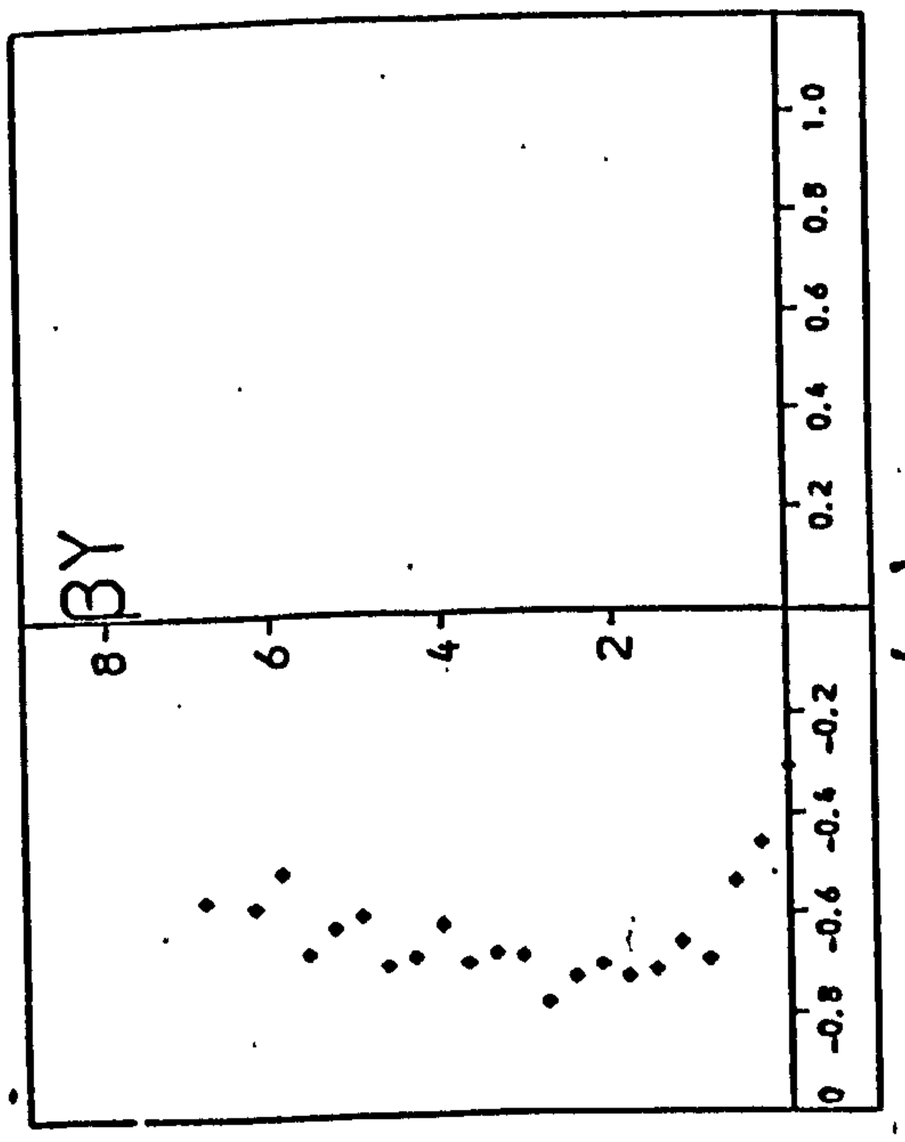
BY
8
6
4
2
0.2
0.4
0.6
0.8
1.0
-0.2
-0.4
-0.6
-0.8
0
(a)

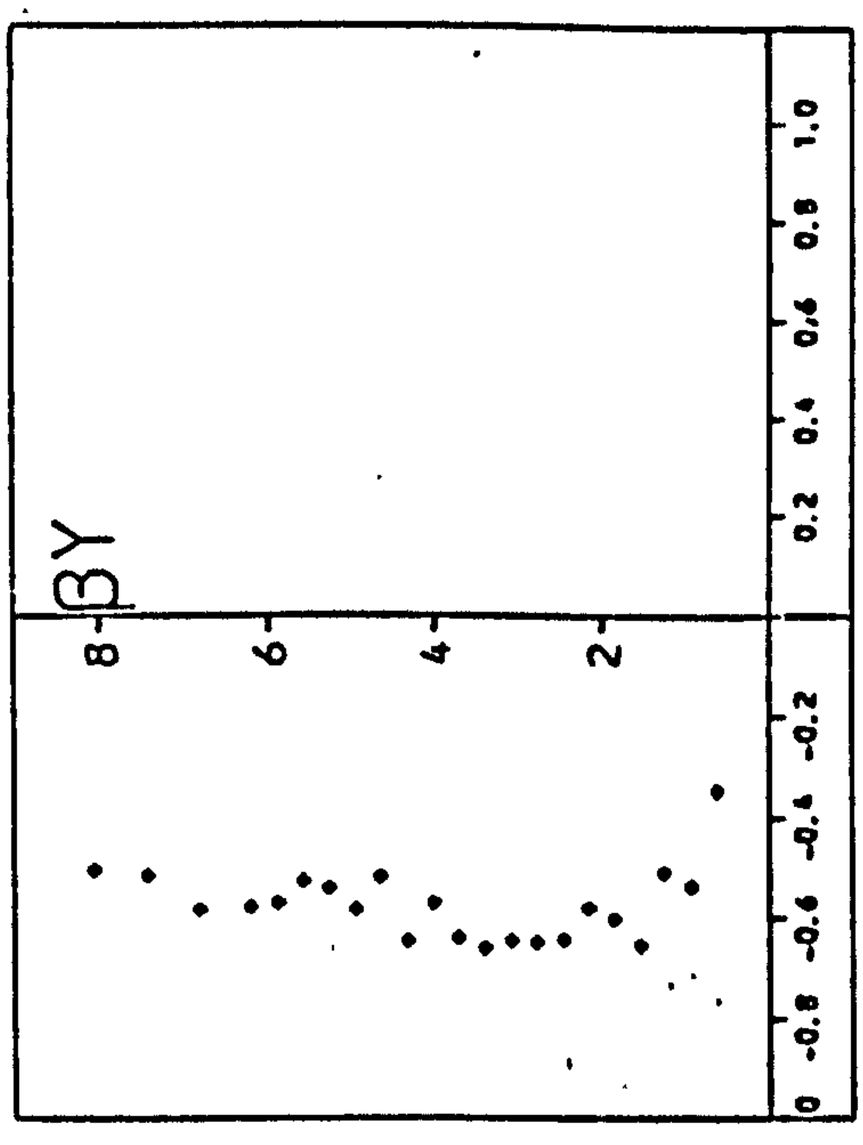
BY
8
6
4
2
0.2
0.4
0.6
0.8
1.0
-0.2
-0.4
-0.6
-0.8
0
(b)

(v) t_5

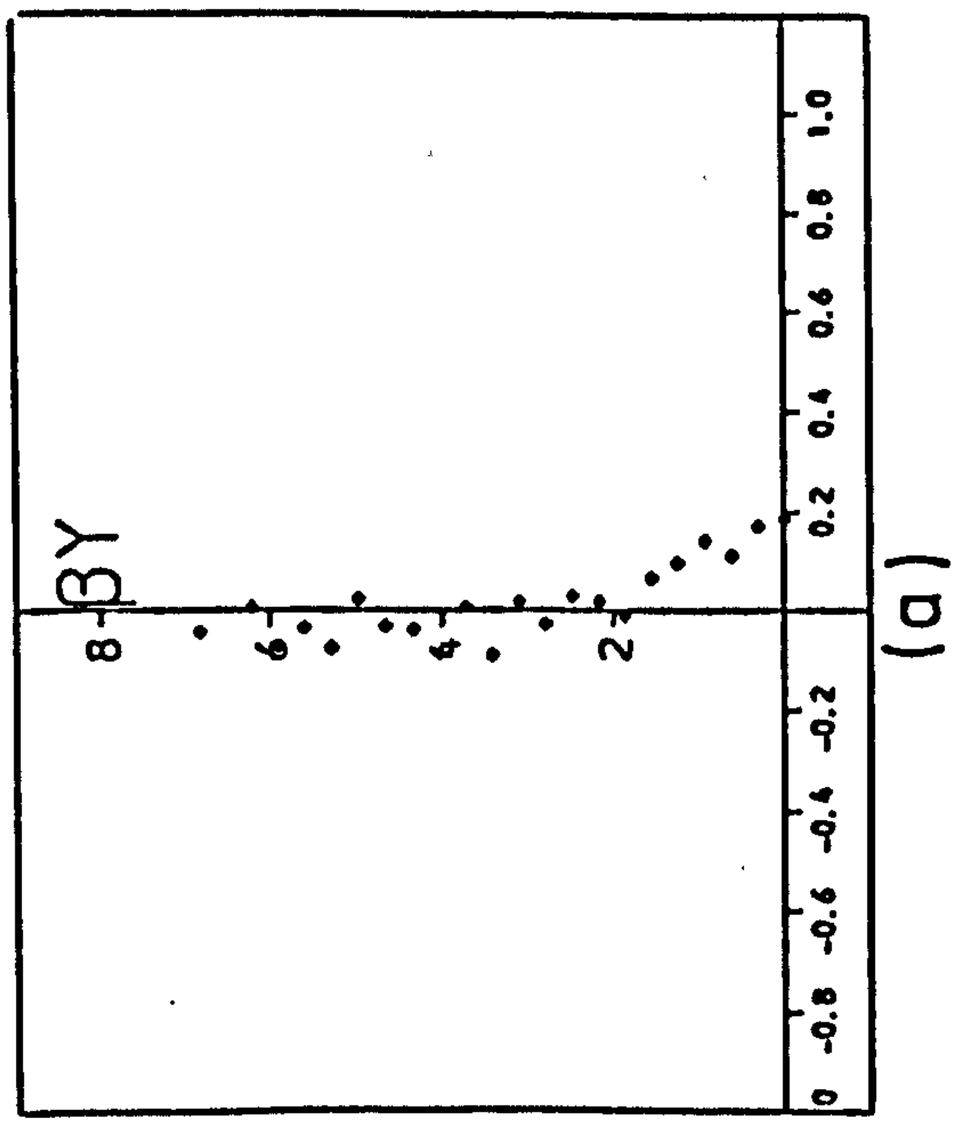
βY
8
6
4
2
0.2
0.4
0.6
0.8
1.0
-0.2
-0.4
-0.6
-0.8
0
(a)
(b)
(viii) t_8

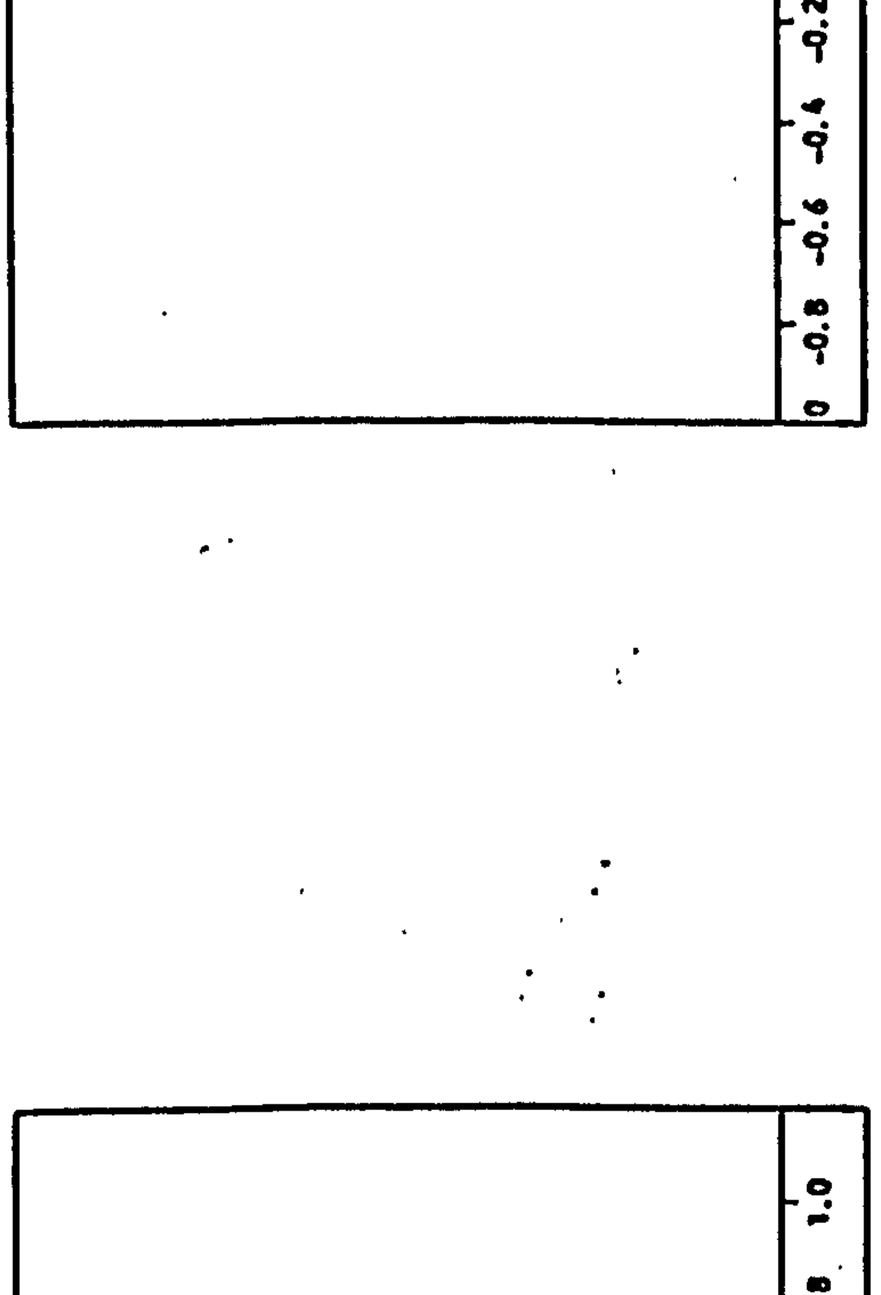
βY
8
6
4
2
0.2
0.4
0.6
0.8
1.0
-0.2
-0.4
-0.6
-0.8
0
(a)
(b)
(viii) t_7

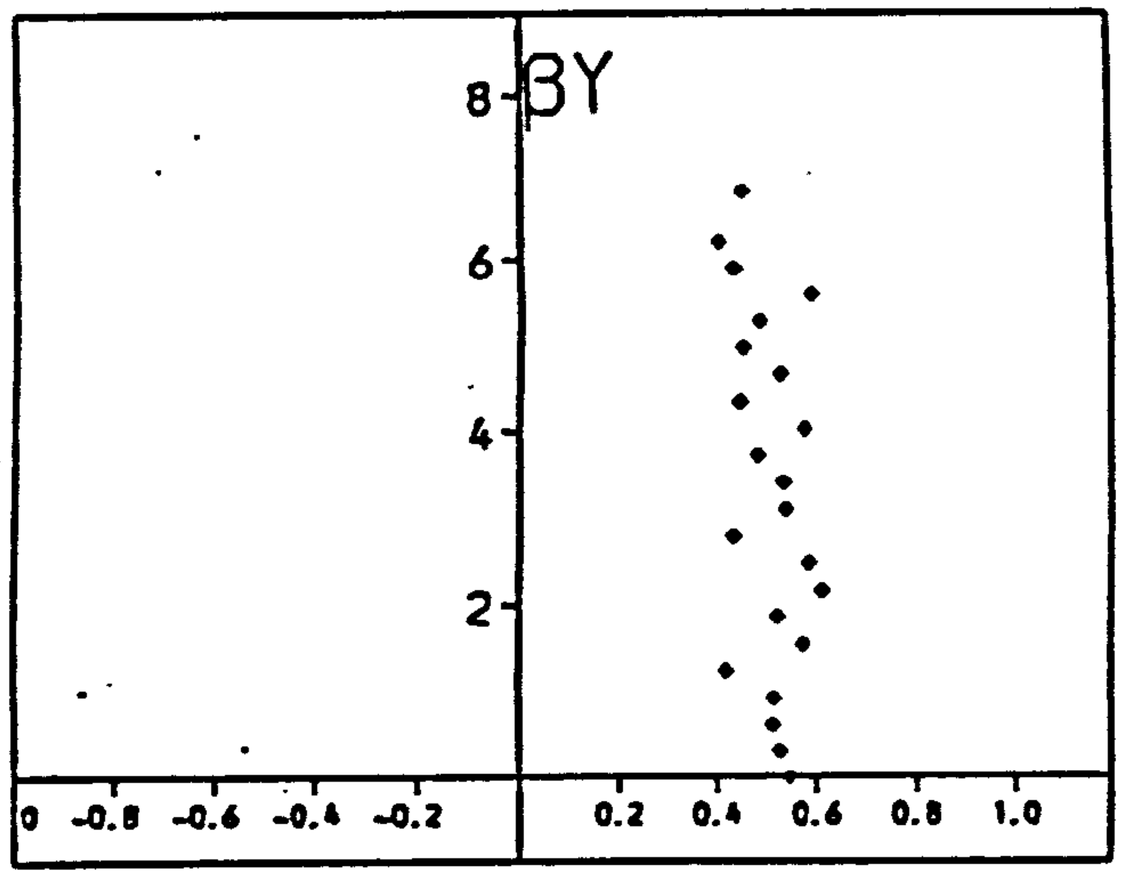

(a)

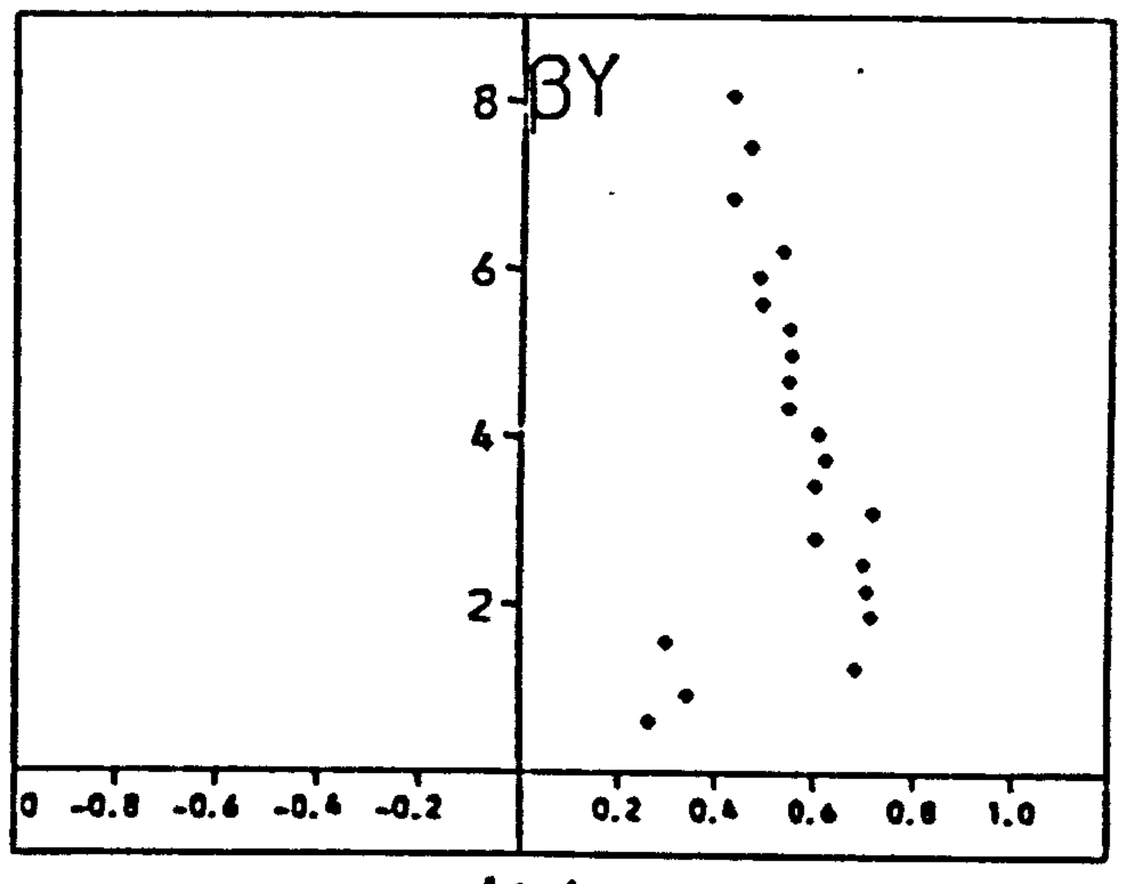

(b)

(ix) t_9

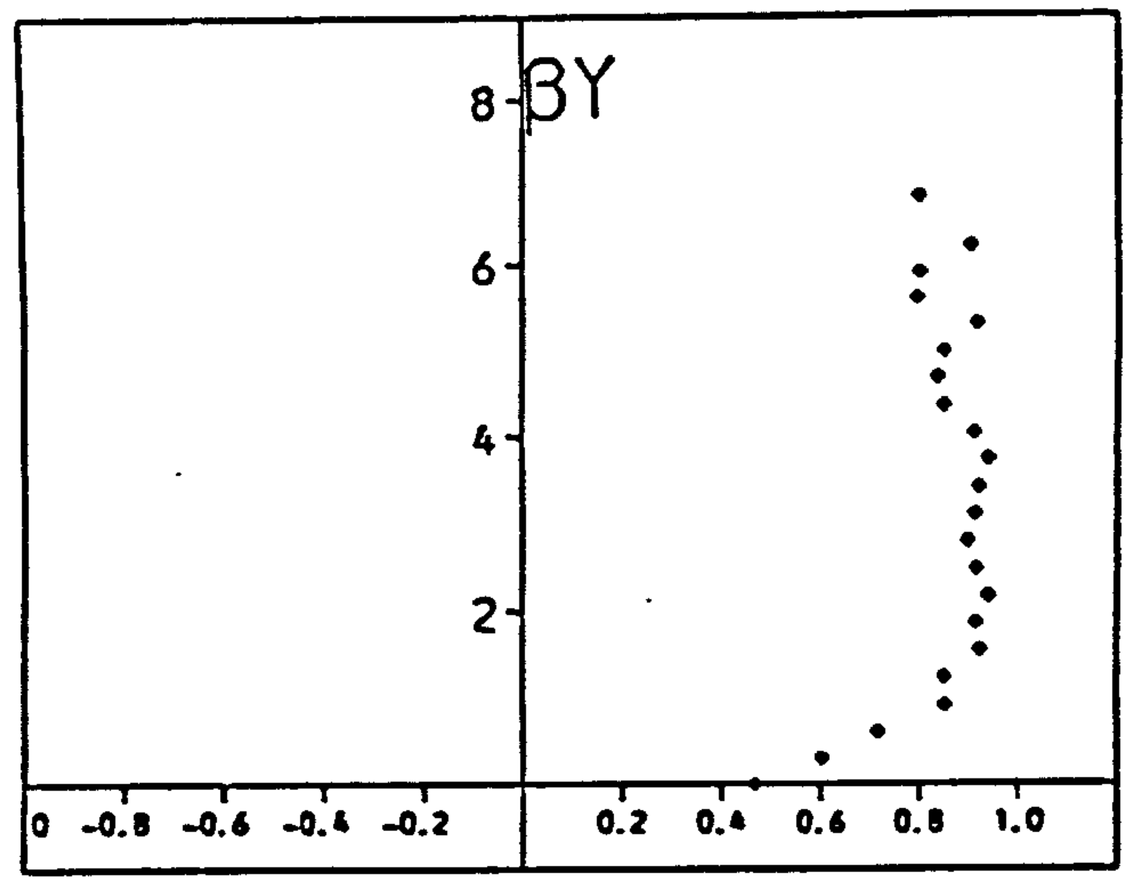

(a)

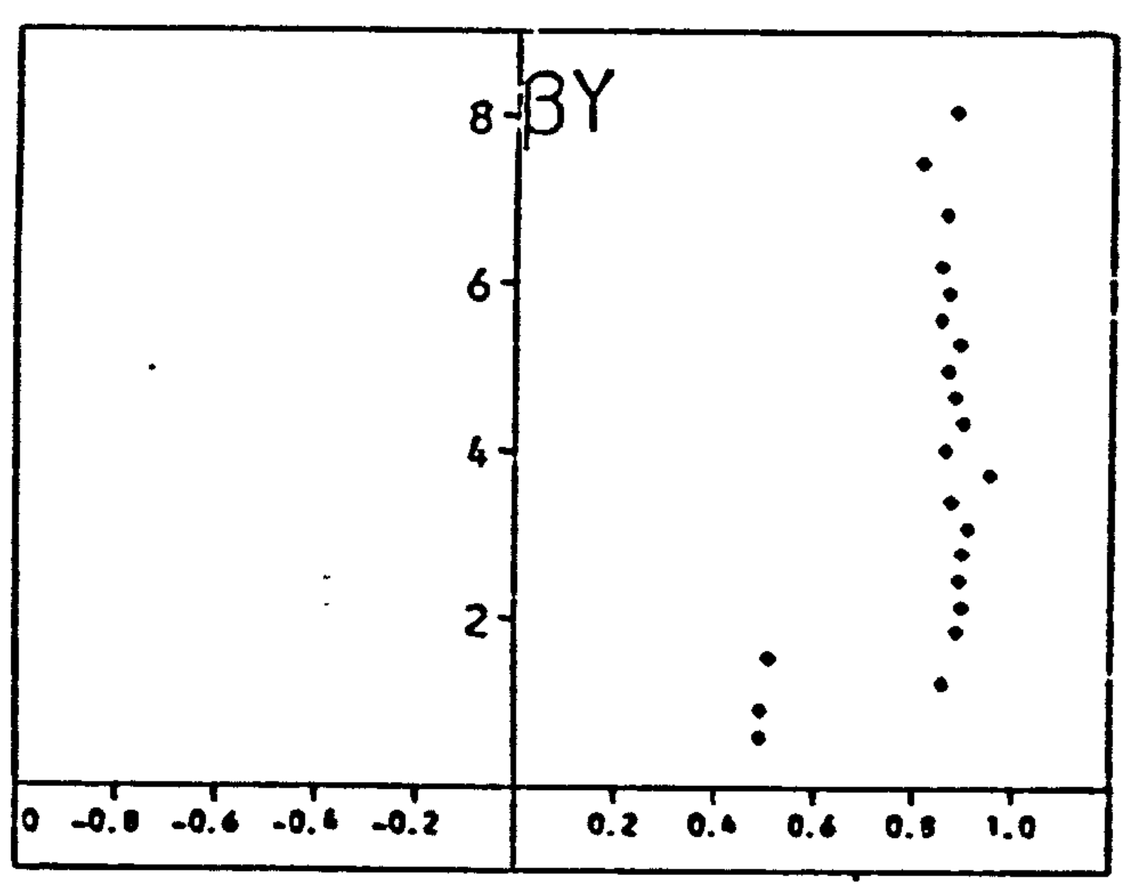

(b)

(x) t_{10}

U_t = Velocity over Trough

U_c = Velocity over Crest

r = Correlation Coefficient

Fig. 6.10 An Example of Correlation of Boundary Layer Velocities over Trough with that over Crest at Different Depths.

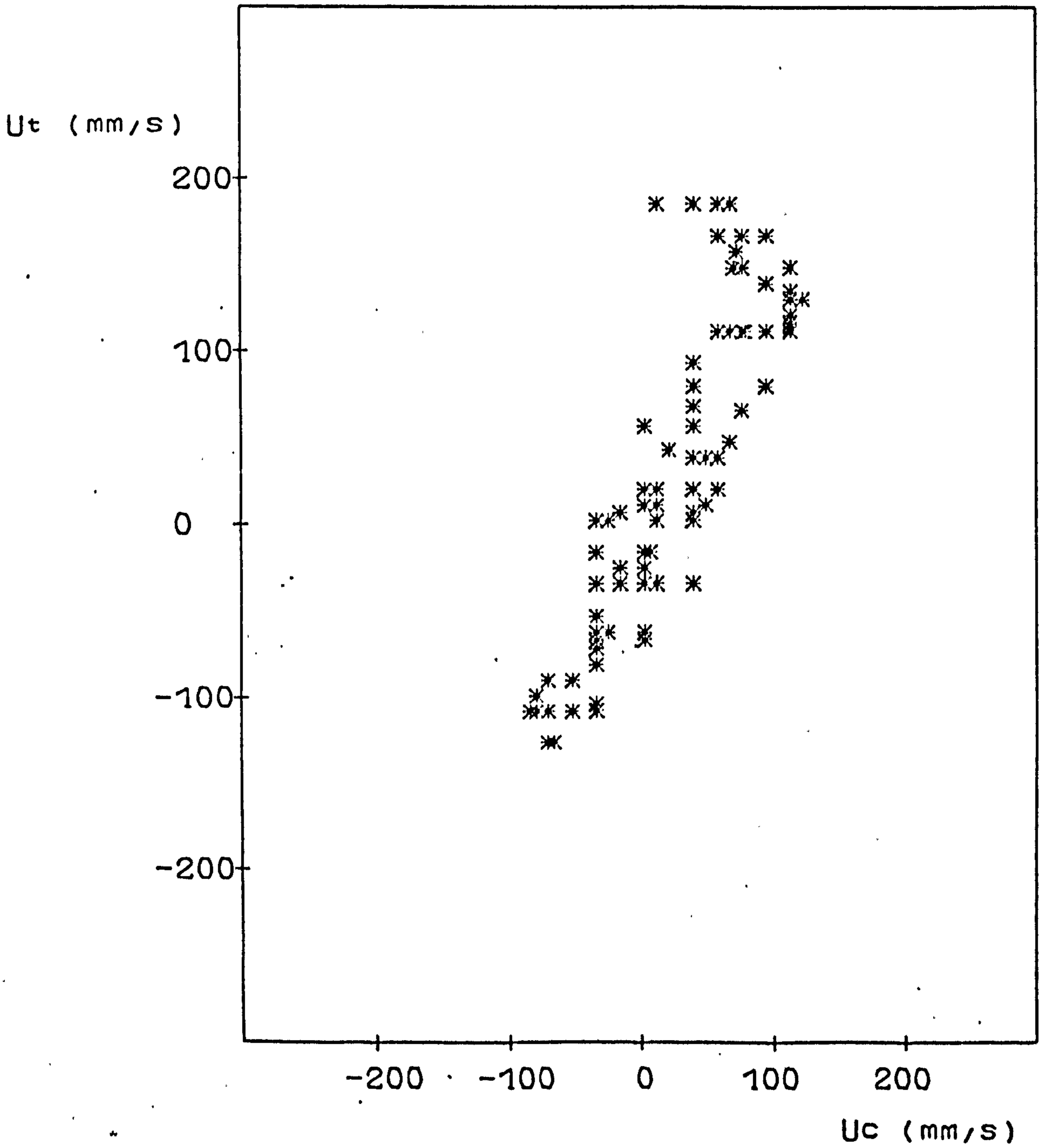

(i) y = 0.5 mm
r = 0.852

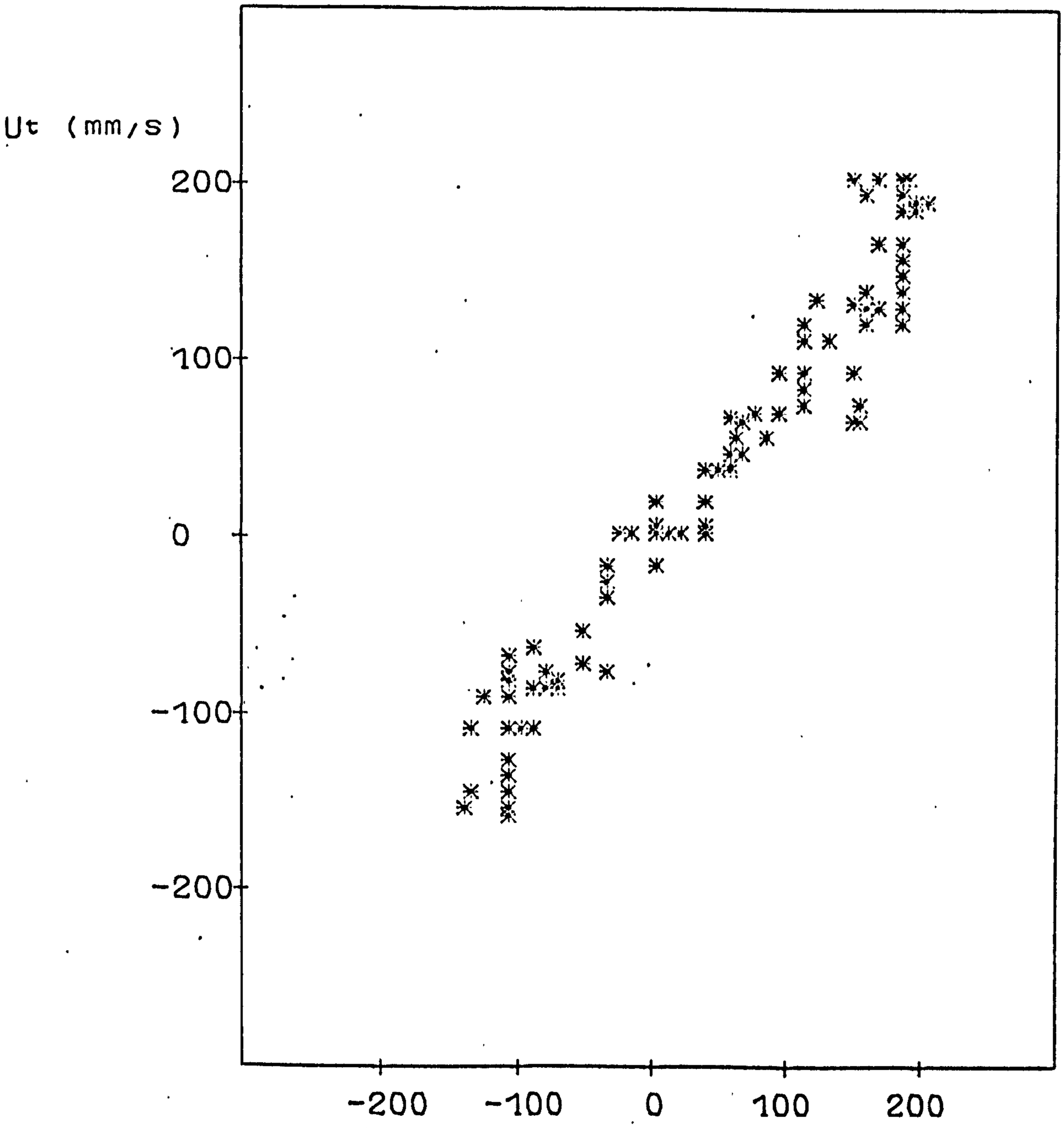

(ii) y=1.0 mm
r=0.973

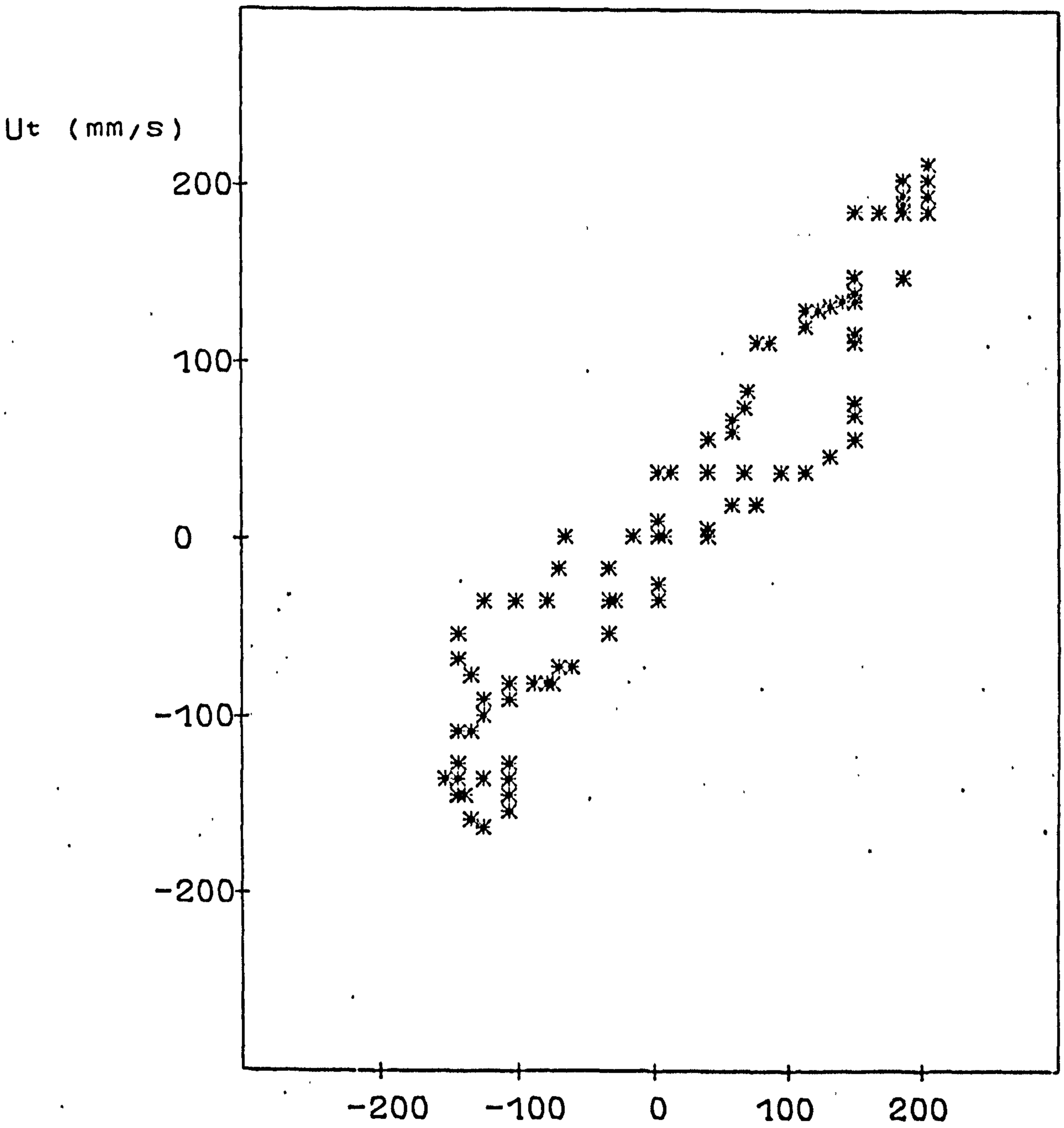

(iii) y=2.0 mm
r=0.967

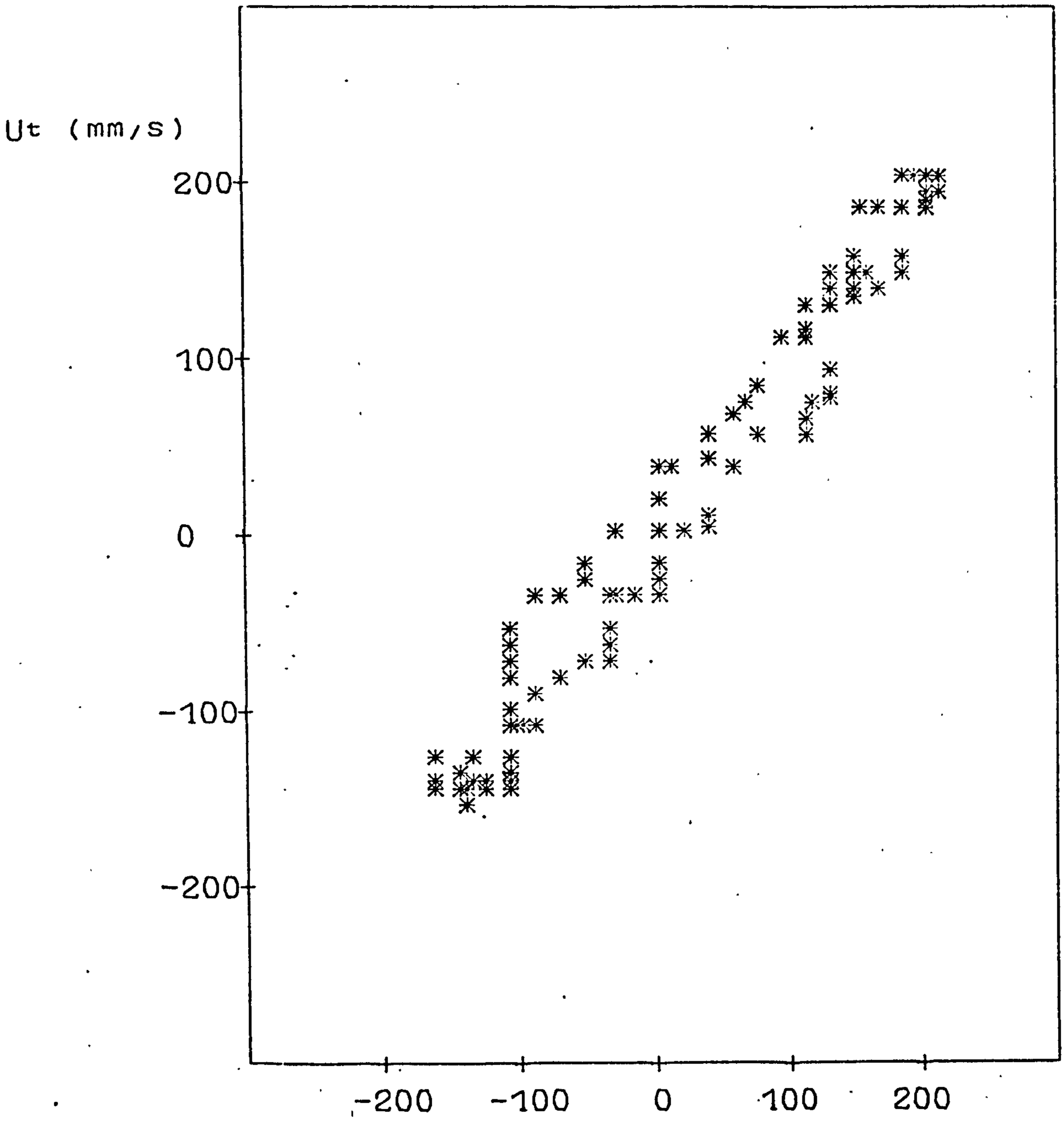

(iv) y=3,0 mm

r=0.983

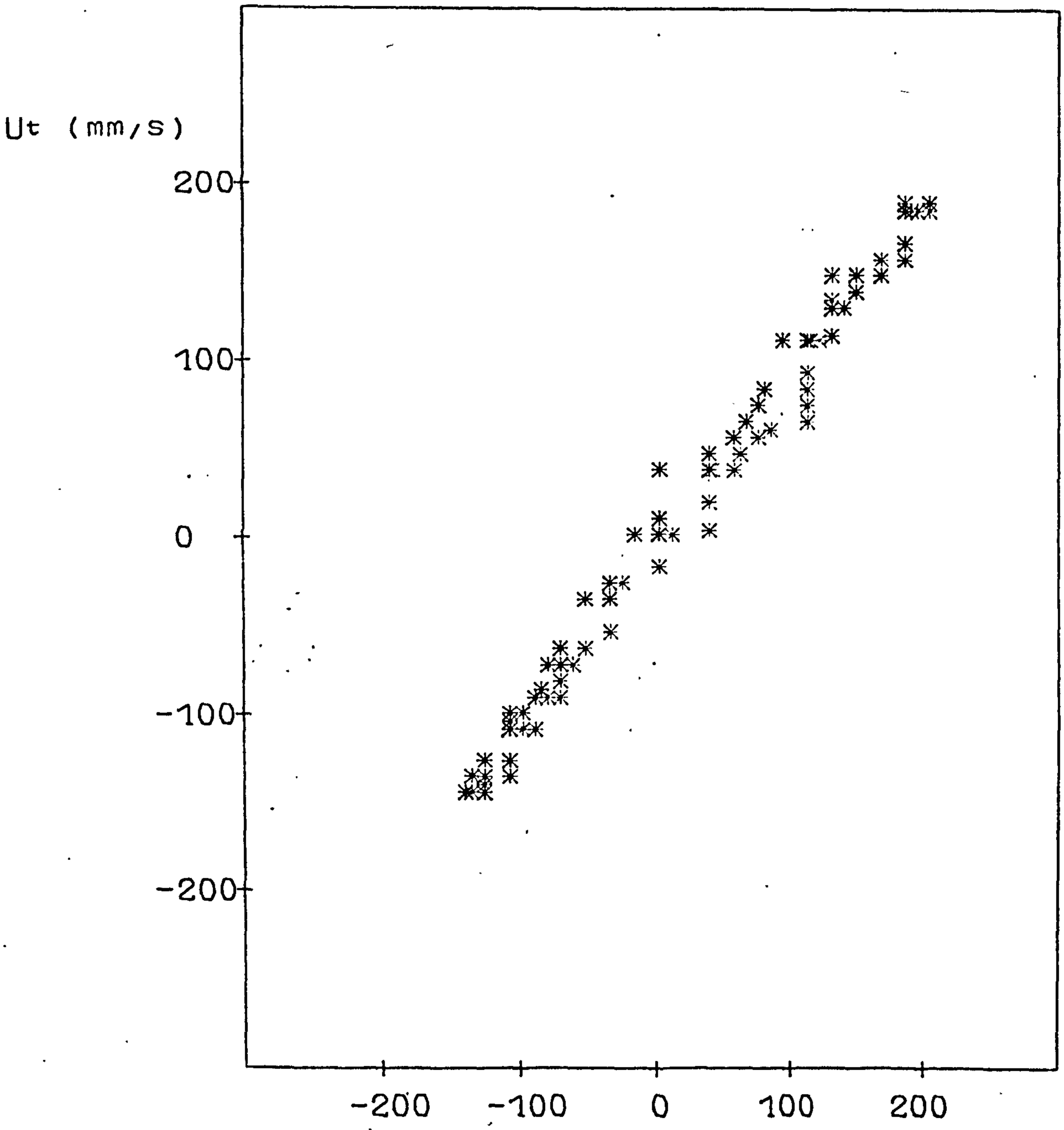

(v) y=4.0 mm

r=0.995

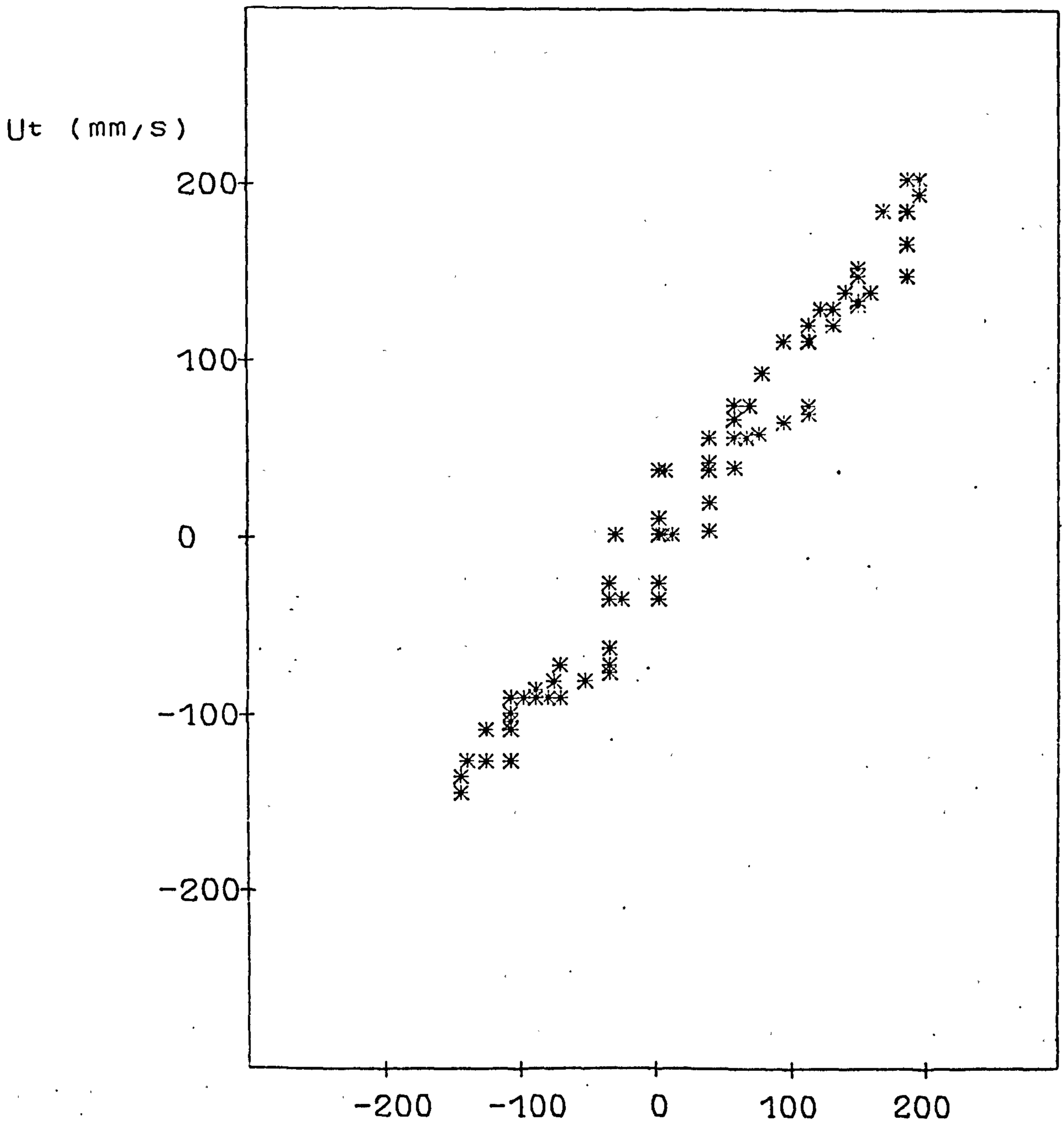

(vi) y=5.0 mm
r=0.991

definition of the correlation coefficient is given in Appendix E.

A closer look at Fig. 6.10 gives a better understanding of the coefficient. For example at 0.5 mm height, there is a scattered relationship between the two velocities and as the height increases the values seem to be less relatively perturbed with the correlation coefficient increasing from 0.85 to 0.995 which represent a highly correlated variation.

The correlation coefficients (r) for the entire depth of the velocity profile observed for the boundary layer for each wave period are shown in Fig. 6.11. (At this stage it is assumed that the boundary layer thickness, δ, is the same as that for a smooth boundary). Although this coefficient does not define the state of flow (laminar or turbulent), it does give a good impression that for correlation coefficients of greater than 0.99 a uniform flow exists and indicates that the vortex formations due to roughness element do not influence the flow anymore. For 1.4 sec. and 1.6 sec. wave periods this value occurs at a height (βy) of greater than 5 and for other wave periods it occurs at a height of less than 4, completing the conclusion from Fig. 6.8, which shows a turbulent flow up to a depth of 12 or 14 (about 5 mm above the top of the roughness).

Because the correlation coefficient, here, describes the state of two fluctuating velocities, without having

Fig. 6.11 Coefficient of Correlation of Boundary Layer Velocity over Trough and Crest of 2-D Rough Bed at Different Heights.

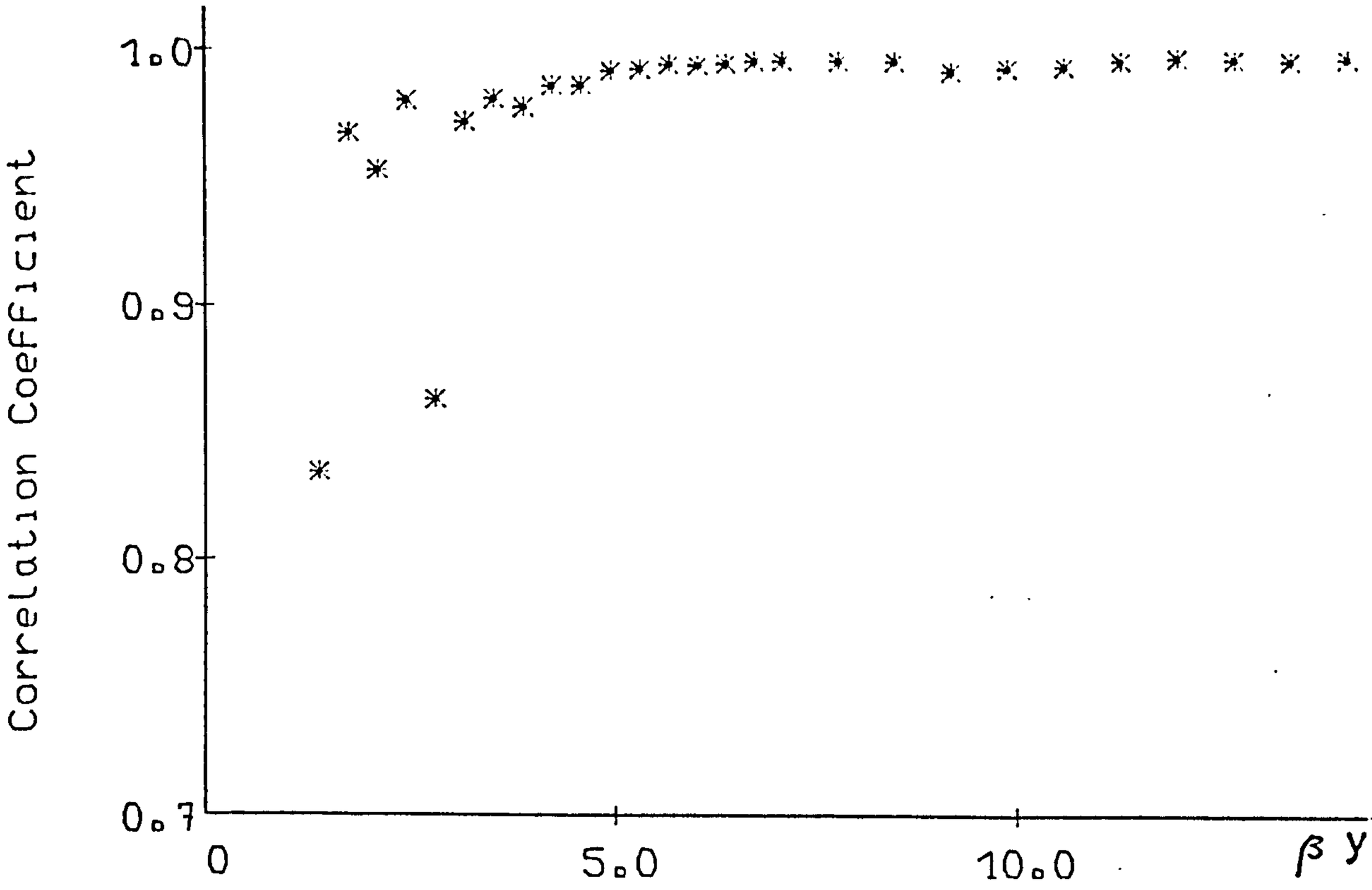

(i) T = 1.4 s

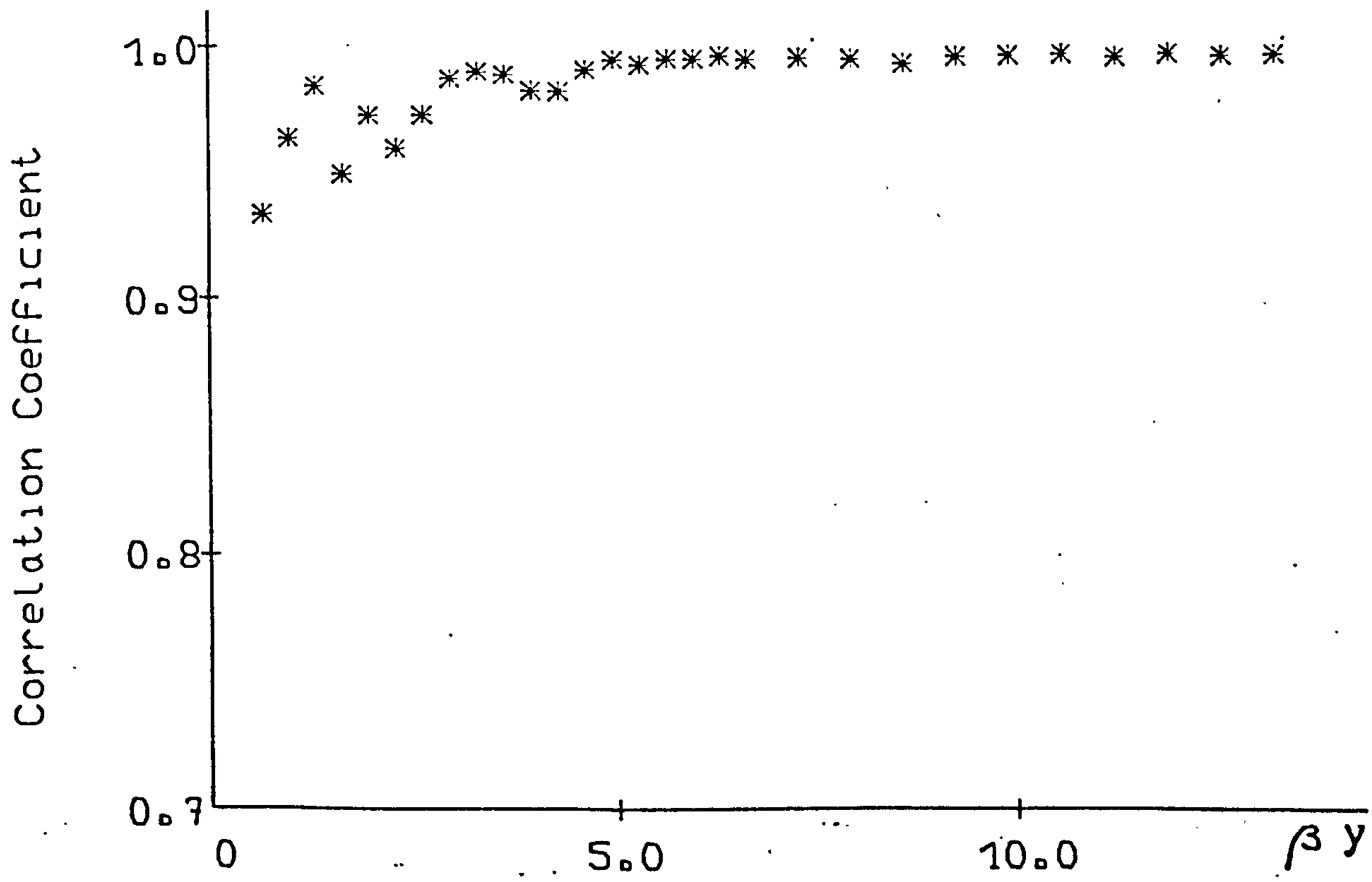

(ii) T = 1.6 s

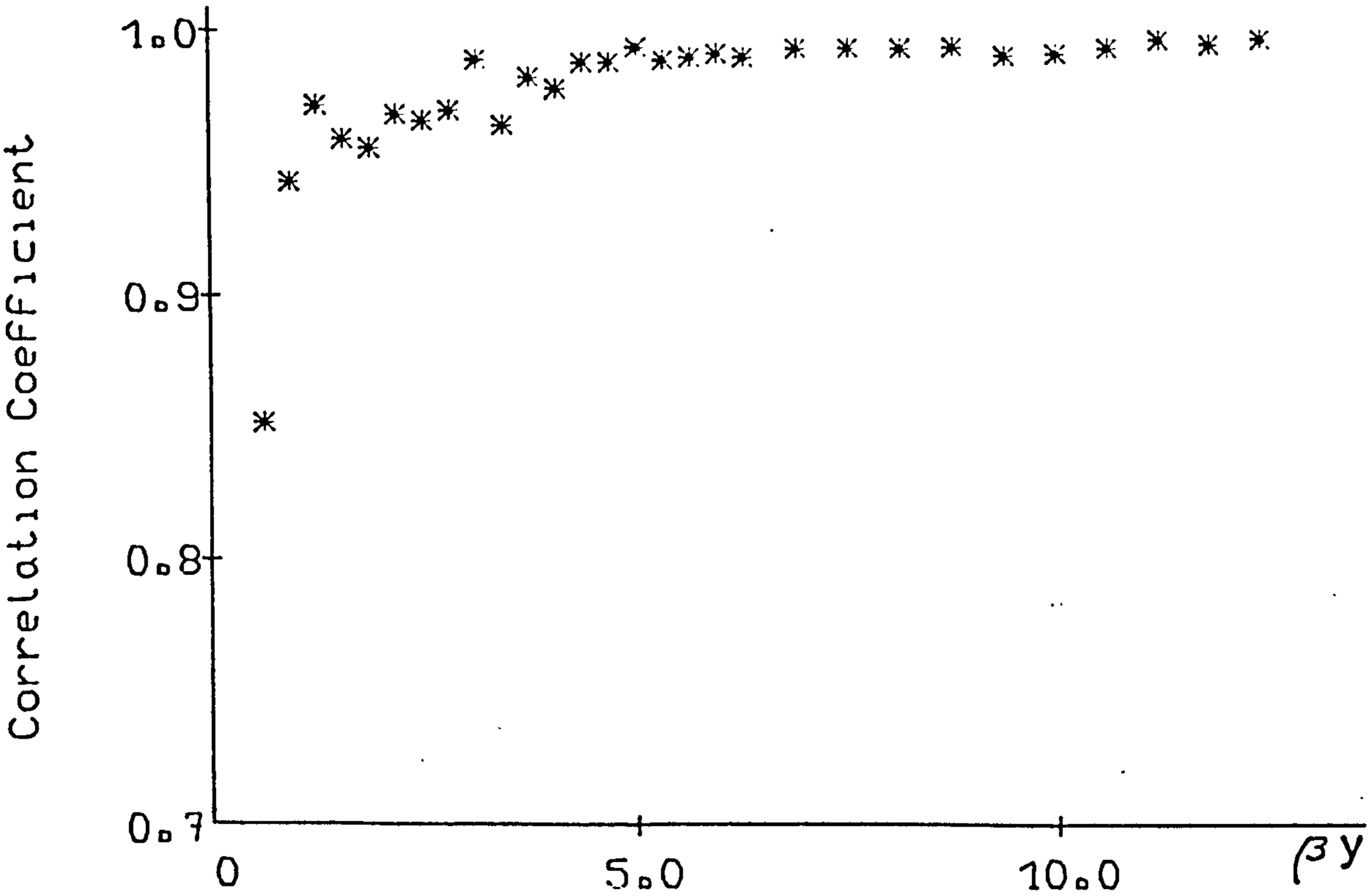

(iii) T=1.8 s

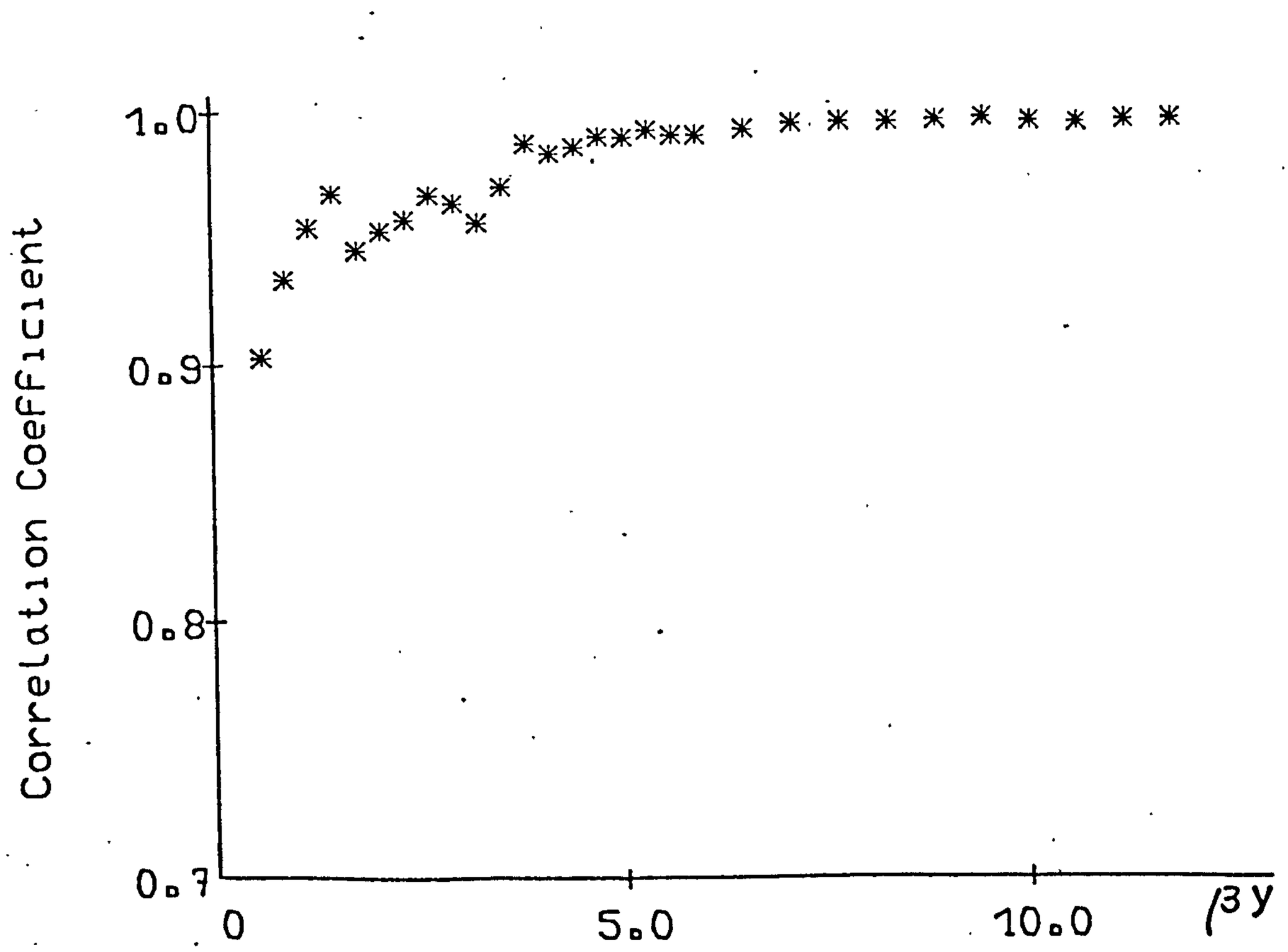

(iv) T=2.0 s

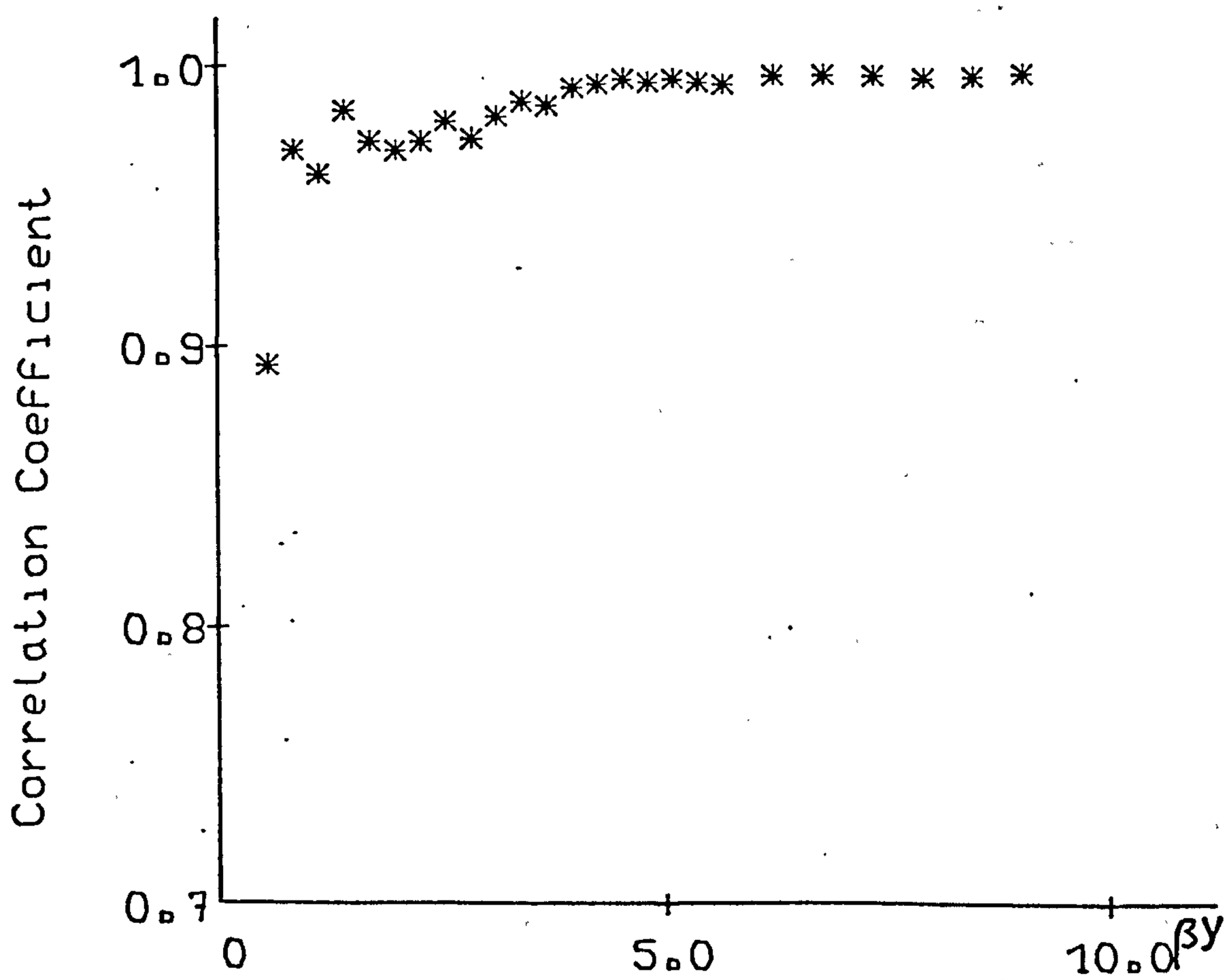

(v) T=2.2 s

better knowledge of one of them, it would be wrong to draw a full conclusion from these results. Instead if one of the conditions is chosen and the velocity profile is compared with the equivalent effect over a smooth bed, the effect of roughness element on the flow can be studied in detail. This has been done in the next section (Section 6.4).

Nevertheless, if it is assumed that the flow over the smooth bed is almost laminar, then by observing the velocity at each depth over many wave passages, the degree of turbulence for the flow can be analysed. Since this technique requires an unlimited time on the analysis side of the problem, a convenient, and to some degree, effective approach is to analyse the velocity profile over a continuous passage of waves at some typical heights. If the choice is at two heights, the immediate positions would be one in the region of poor correlation and one in the region of a higher correlation taken as follows.

Hence, one height within the boundary layer thickness (1.5 mm above the roughness top) and the other position just outside or at the edge of the boundary layer (5 mm above the roughness top) were taken for observing the velocity profile over 45 continuous waves at each period (45 is an arbitrary number assumed to show a population sample). Fig. 6.12 shows samples of the cyclic variation of the velocity averaged over 45 waves with the range of fluctuation of velocity for twenty equal phase positions at the two heights (for 1.4 sec. and 2.2 sec. wave period).

(i)

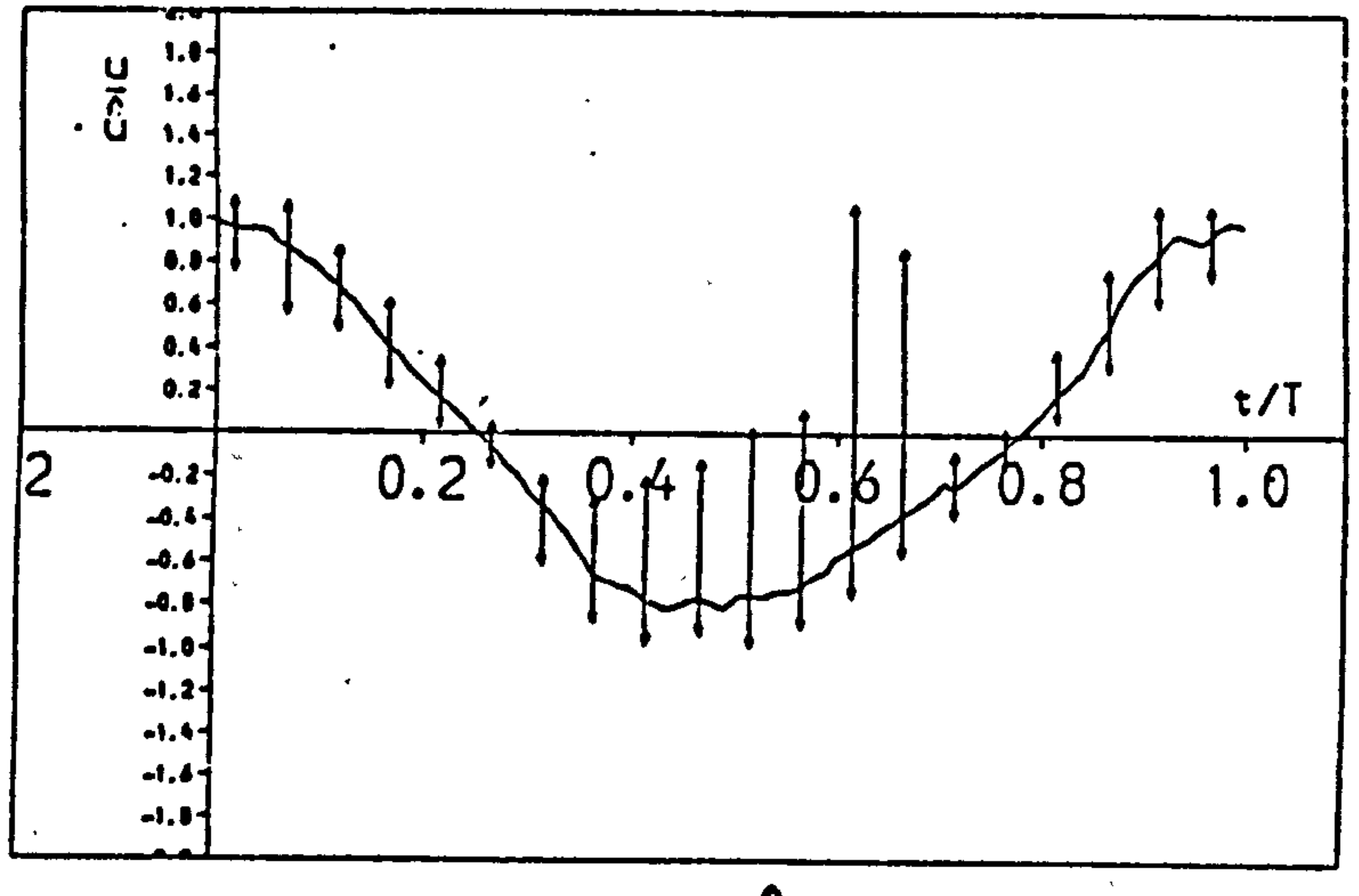

Y=6.1 MM T=1.4 SEC $\hat{U}$=243.8 mm/s

(a)

(ii)

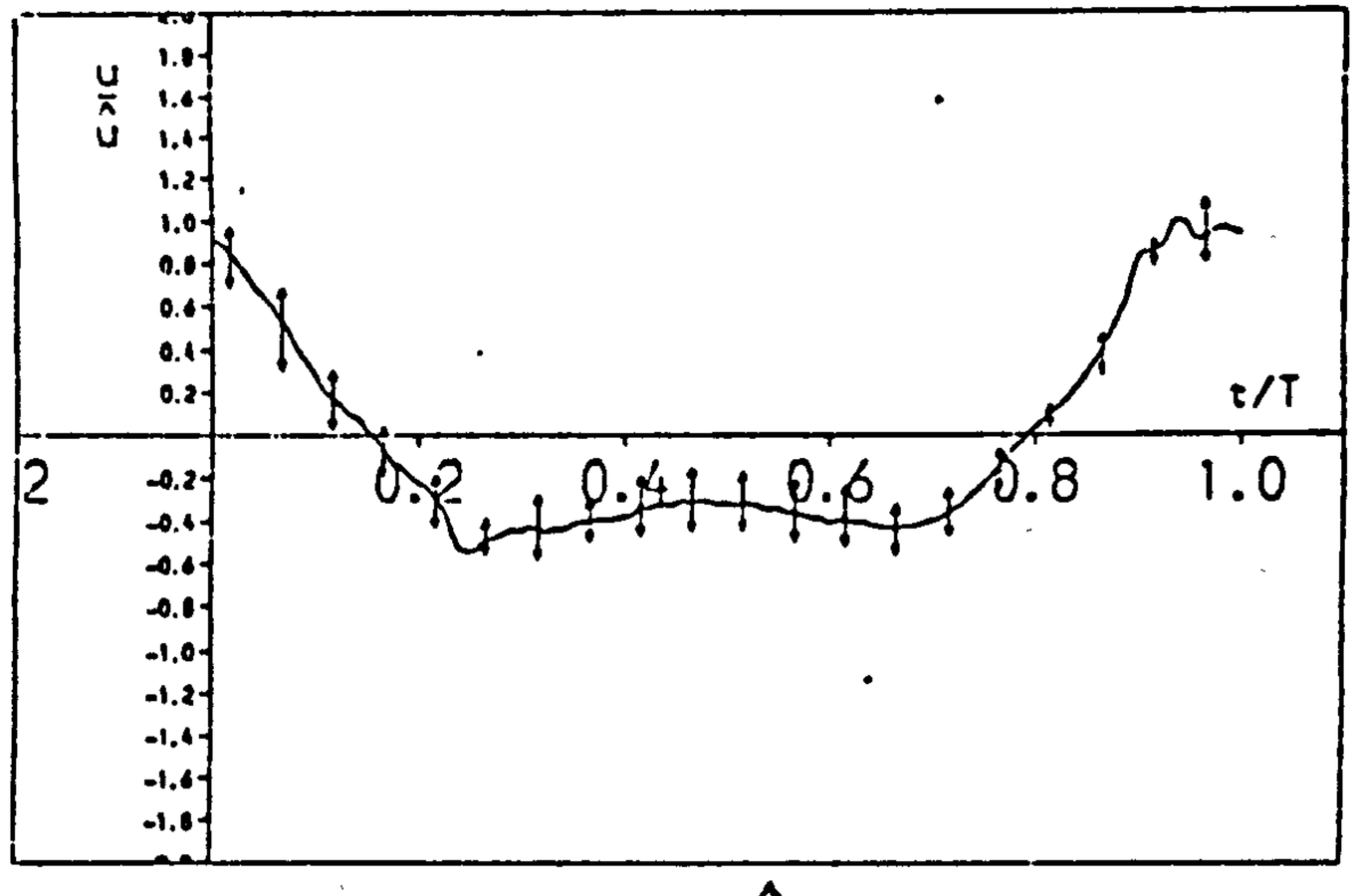

Y=6.1 MM T=2.2 SEC $\hat{U}$=200.9 mm/s

(a)

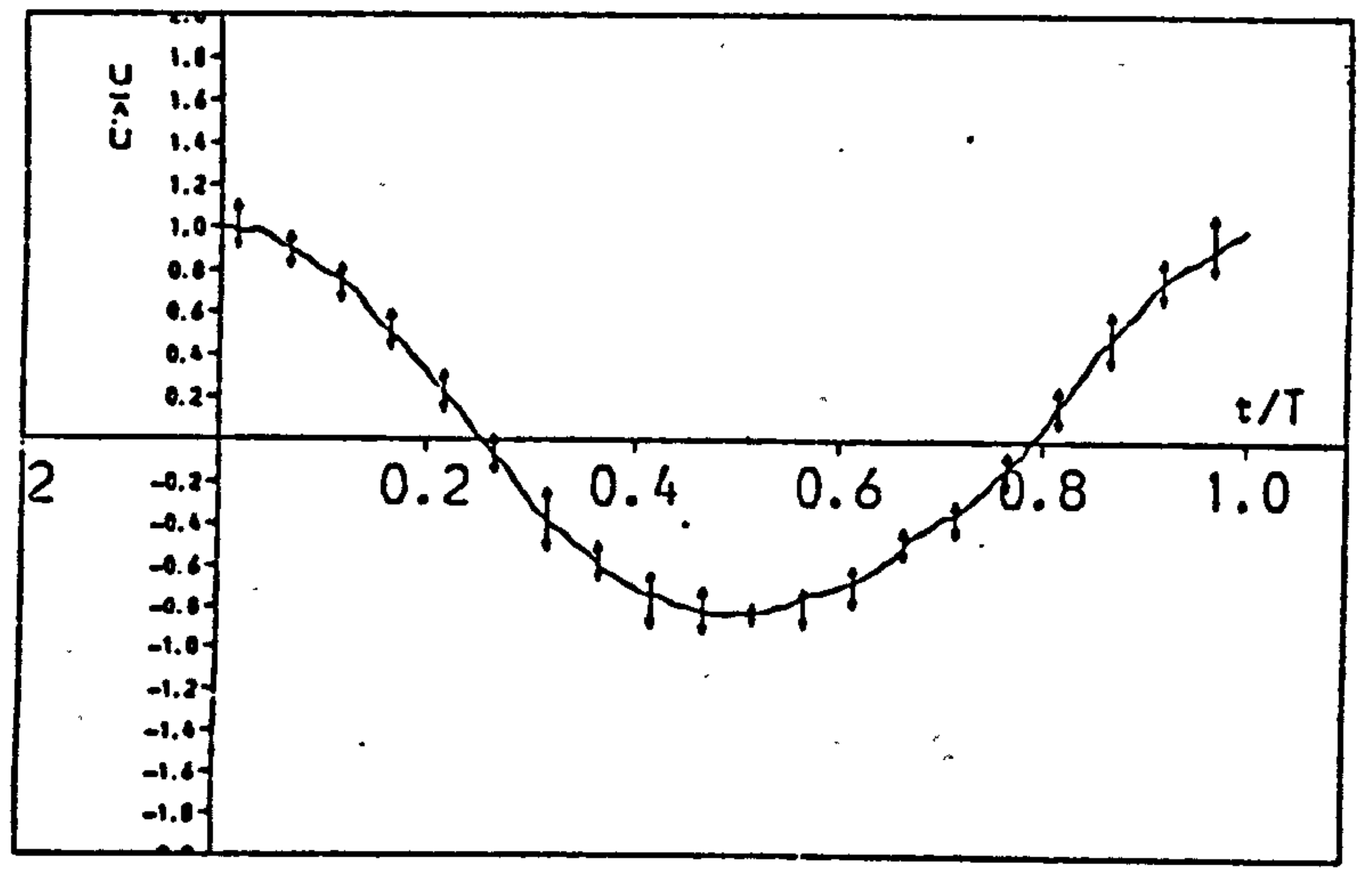

Y=9.6 MM T=1.4 SEC $\hat{U}$=250.3 mm/s

(b)

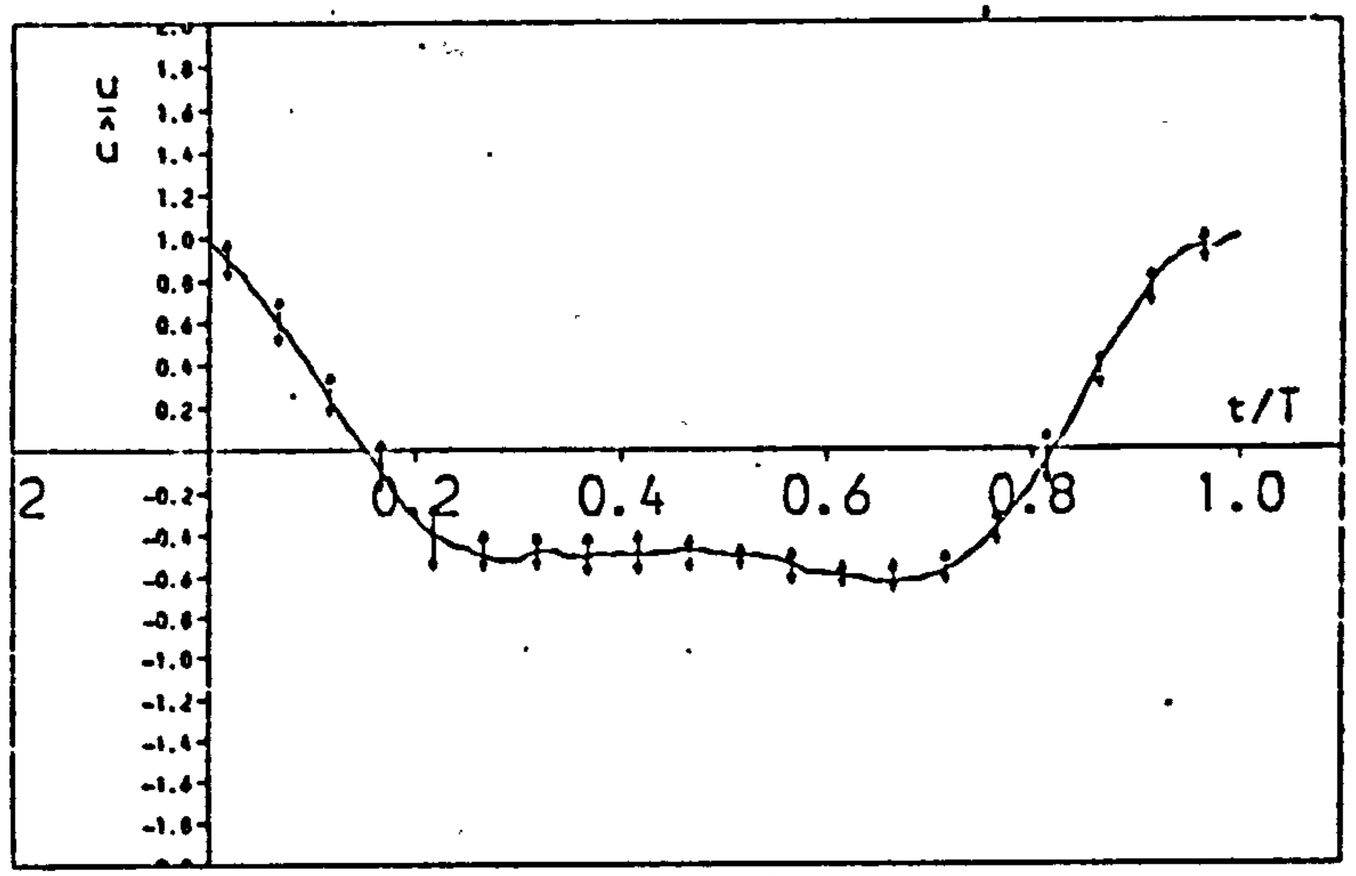

Y=9.6 MM T=2.2 SEC $\hat{U}$=178.6 mm/s

(b)

Fig. 6.12 The Mean Cyclic Variation of Velocity over 45 Waves at Two Heights Over the 2-D Rough Bed.

Three arbitrary phases (out of 120) together with the mean velocity for each cycle over 45 waves are taken as a sample velocity and presented in the form of probability graphs in Fig. 6.13 (the three arbitrary phases are kept constant for the coming analyses - 3-D rough bed - as well as the analyses in Chapter Seven). The velocity at each phase is analysed for evaluating the form of the distribution, together with the mean and standard deviation (a full description of the statistical terms is made in Appendix E).

If the distribution is found to be normal, then by knowing the mean and standard deviation (S.D.), assumptions on the flow pattern can be made. From studying carefully the graphs of Fig. 6.13, the first impression is that the distribution rarely appears to be normal (for both heights). The author suspects that this effect is due to the sharpness of the roughness elements edges which disorders the eddies produced by the roughnesses even more.

On the other hand since the standard deviation values and the range of the data points (Fig. 6.13 - 0.0 to 1.0 represent the range of data), for all the graphs have a lesser value for larger height sampling location than the lower location, indicates a more turbulent flow close to the roughness top, and as the height gets larger the fluctuation decreases rapidly which is as expected.

Interesting observations from Fig. 6.13 are that all the (d) graphs (which are the mean velocity over 45 cycles - the other graphs are the arbitrary phases within the period for

*	1.5 mm height over rough bed
o	5.0 mm height over rough bed
SD	Standard Deviation
0.0-1.0	The range of the Data

Fig. 6.13 The velocity distribution for 3 arbitrary phases (a, b, c) and mean velocity (d) over 45 cycles over 2-D rough bed.

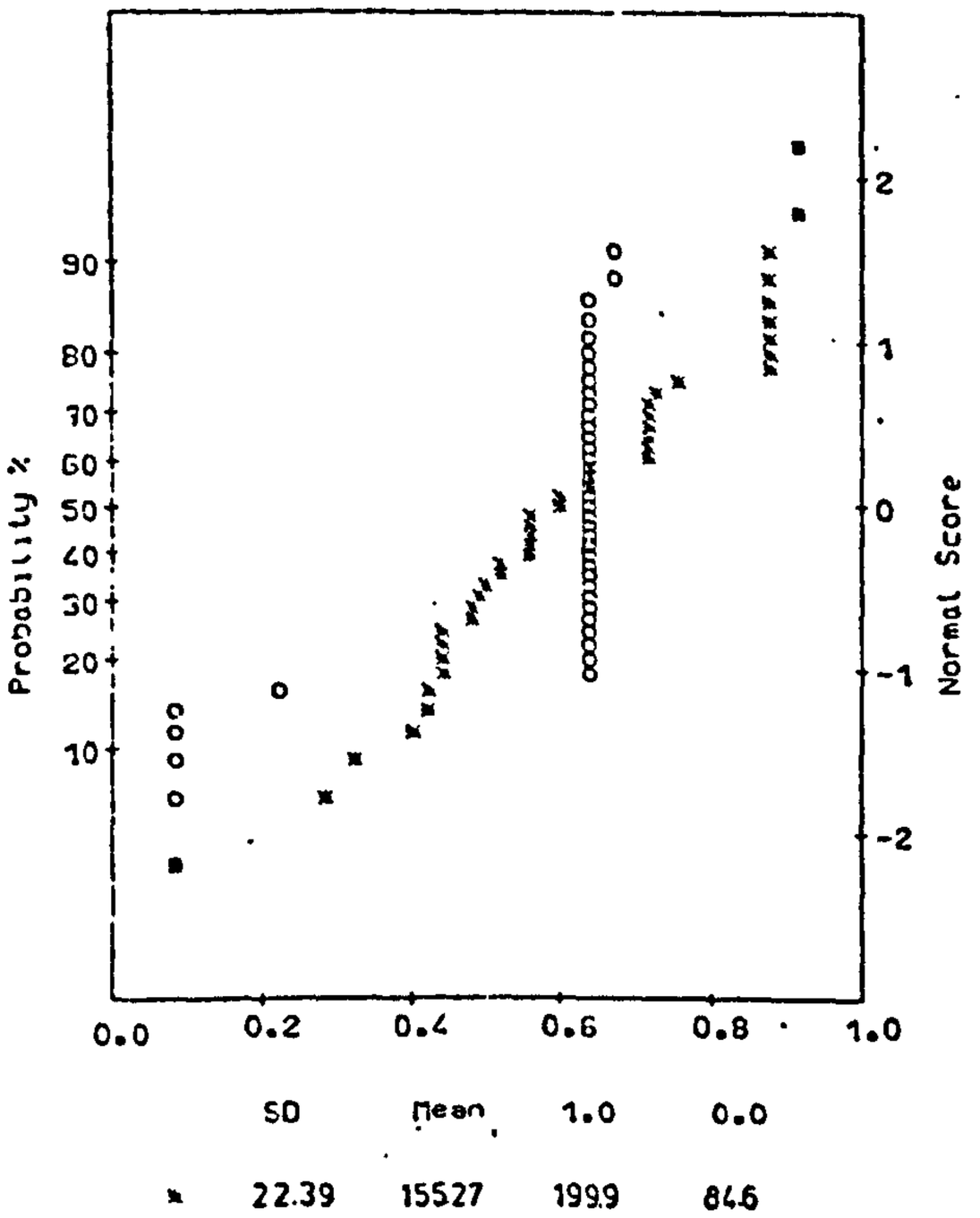

	SD	Mean	1.0	0.0
x	22.39	155.27	199.9	84.6
o	6.67	183.73	197.7	164.6

(a)

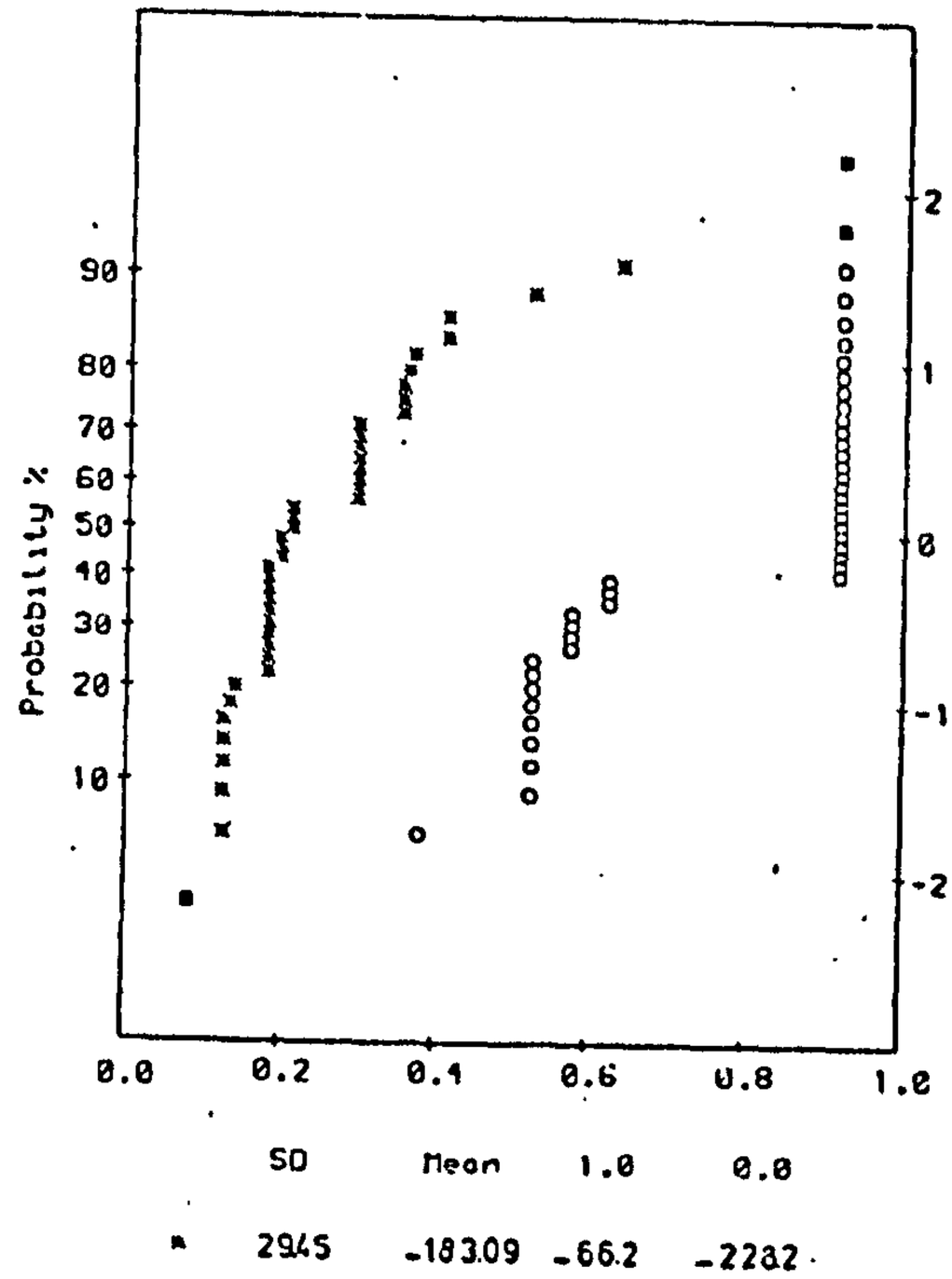

	SD	Mean	1.0	0.0
x	29.45	-183.09	-66.2	-223.2
o	9.88	-187.72	-176.5	-223.2

(b)

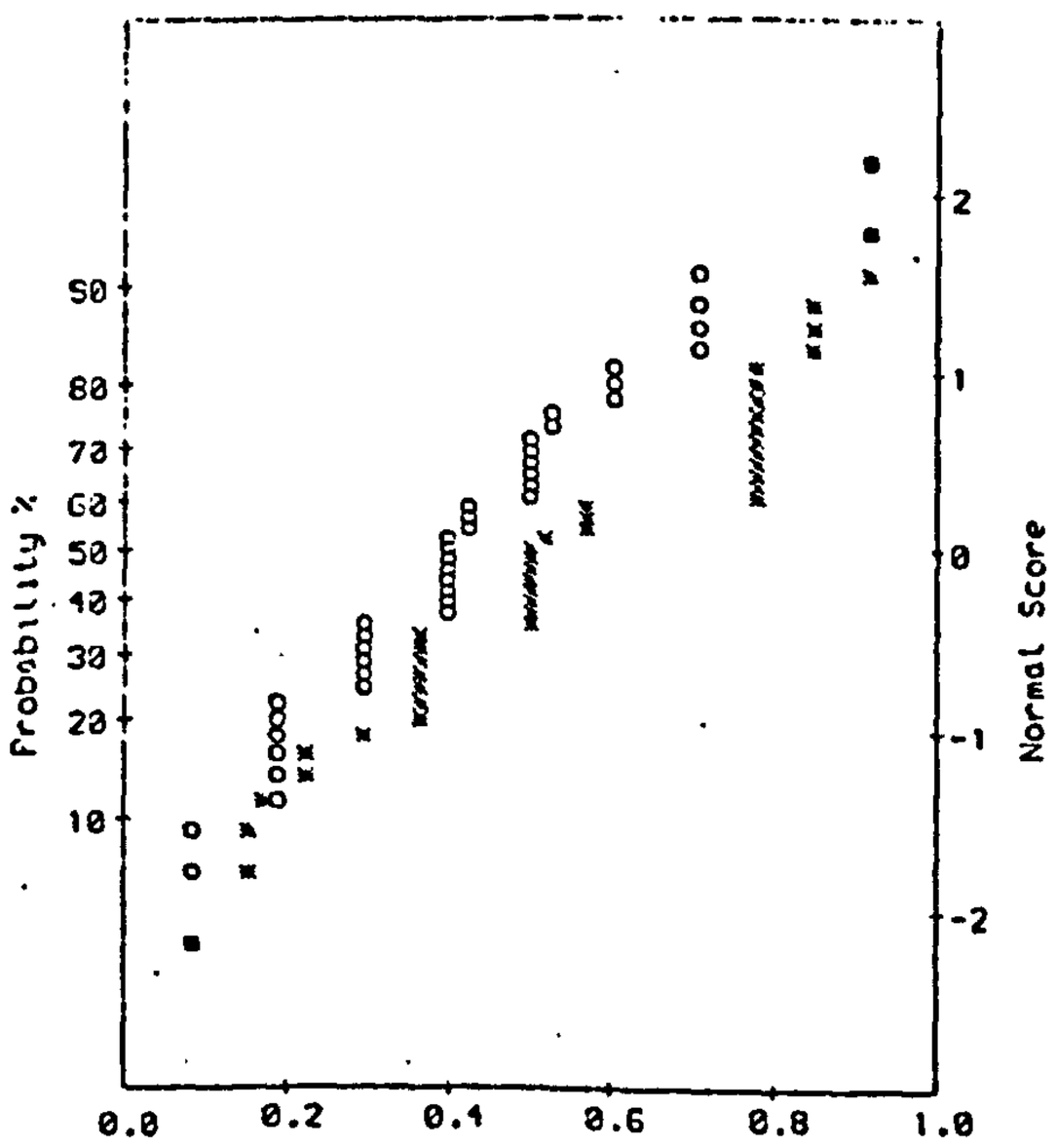

	SD	Mean	1.0	0.0
x	15.98	-48.58	-19.3	-85.2
o	8.98	-74.04	-48.6	-92.5

(c)

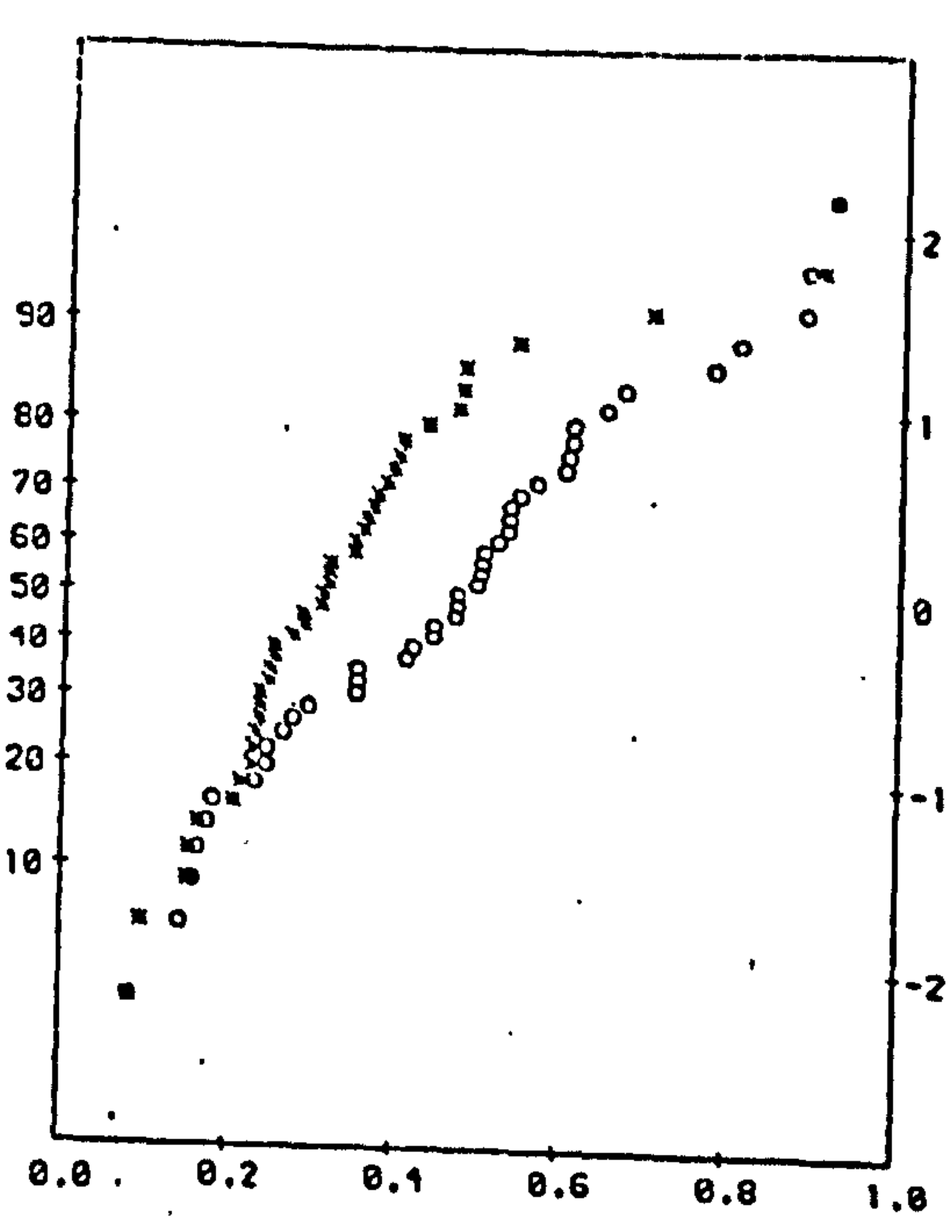

	SD	Mean	1.0	0.0
x	9.82	4.12	41.5	-14.8
o	2.92	0.81	8.3	-5.6

(d)

(i) T = 1.4 s

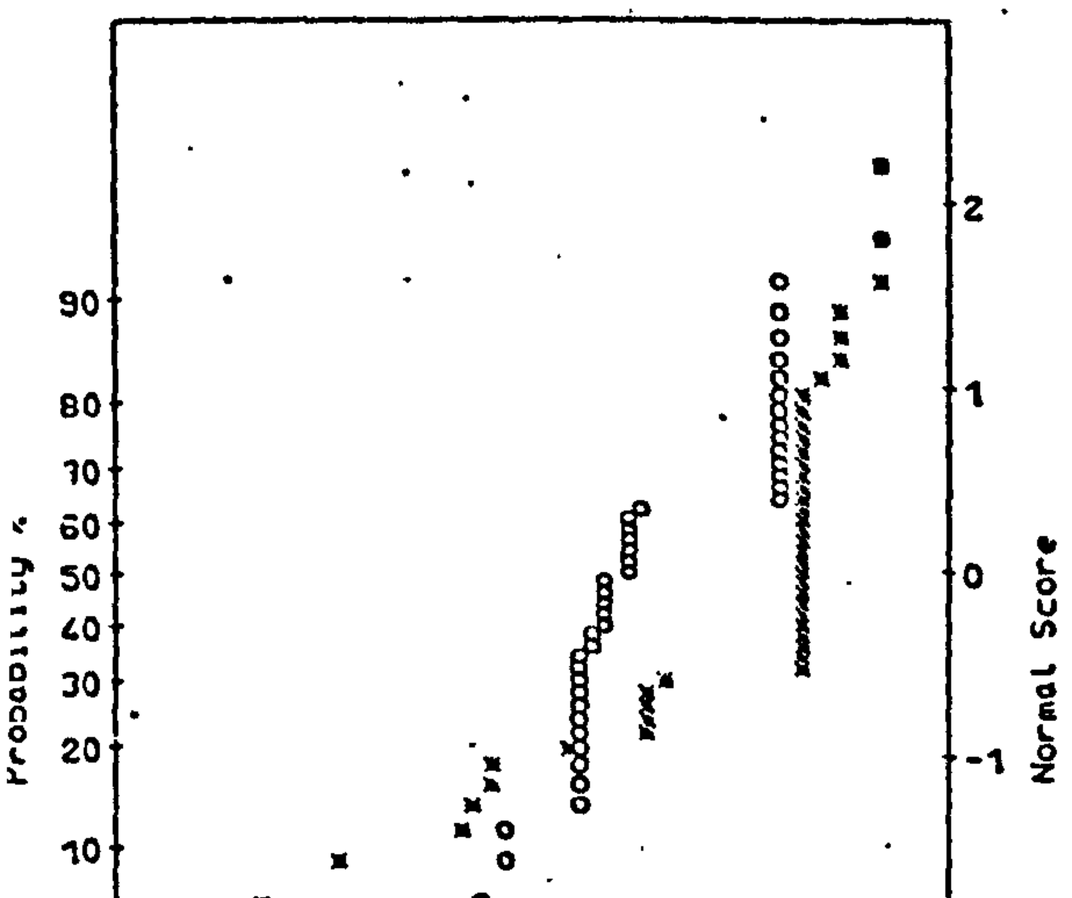

	SD	Mean	1.0	0.0
x	19.7	103.21	129.8	31.1
o	11.6	100.82	128.0	51.2

(a)

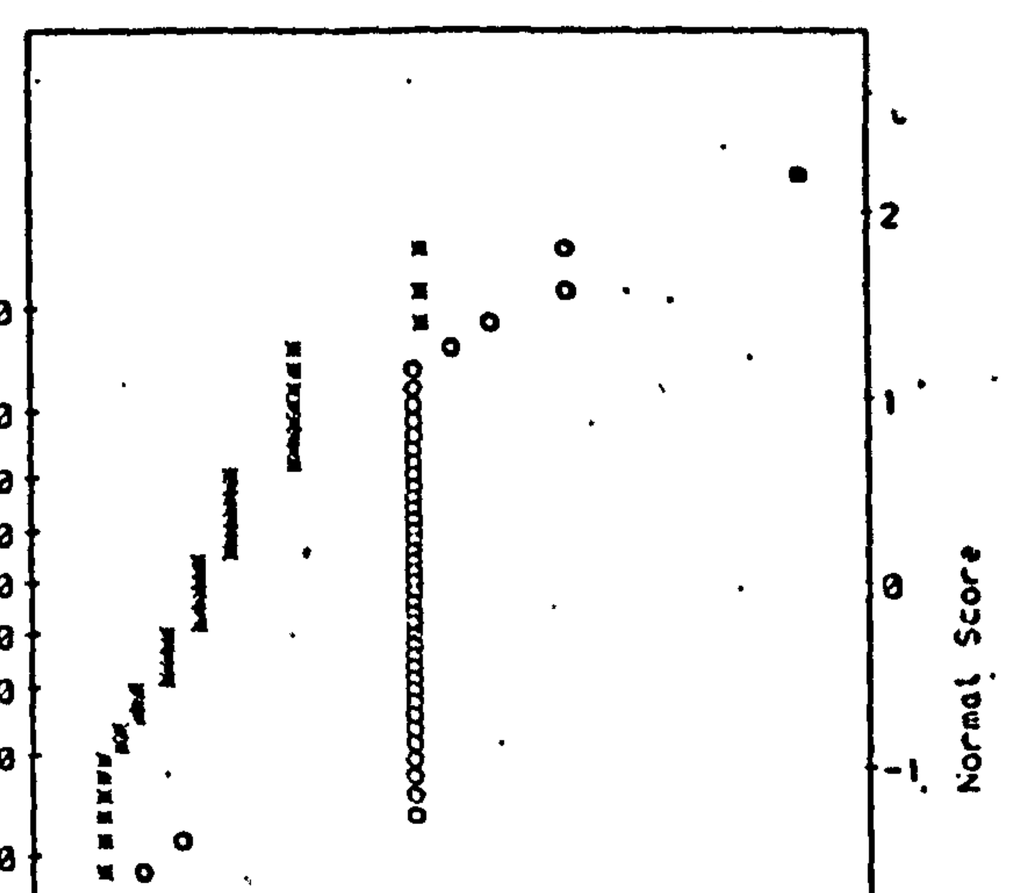

	SD	Mean	1.0	0.0
x	17.81	-135.9	-42.2	-163.0
o	3.22	-162.3	-148.5	-173.3

(b)

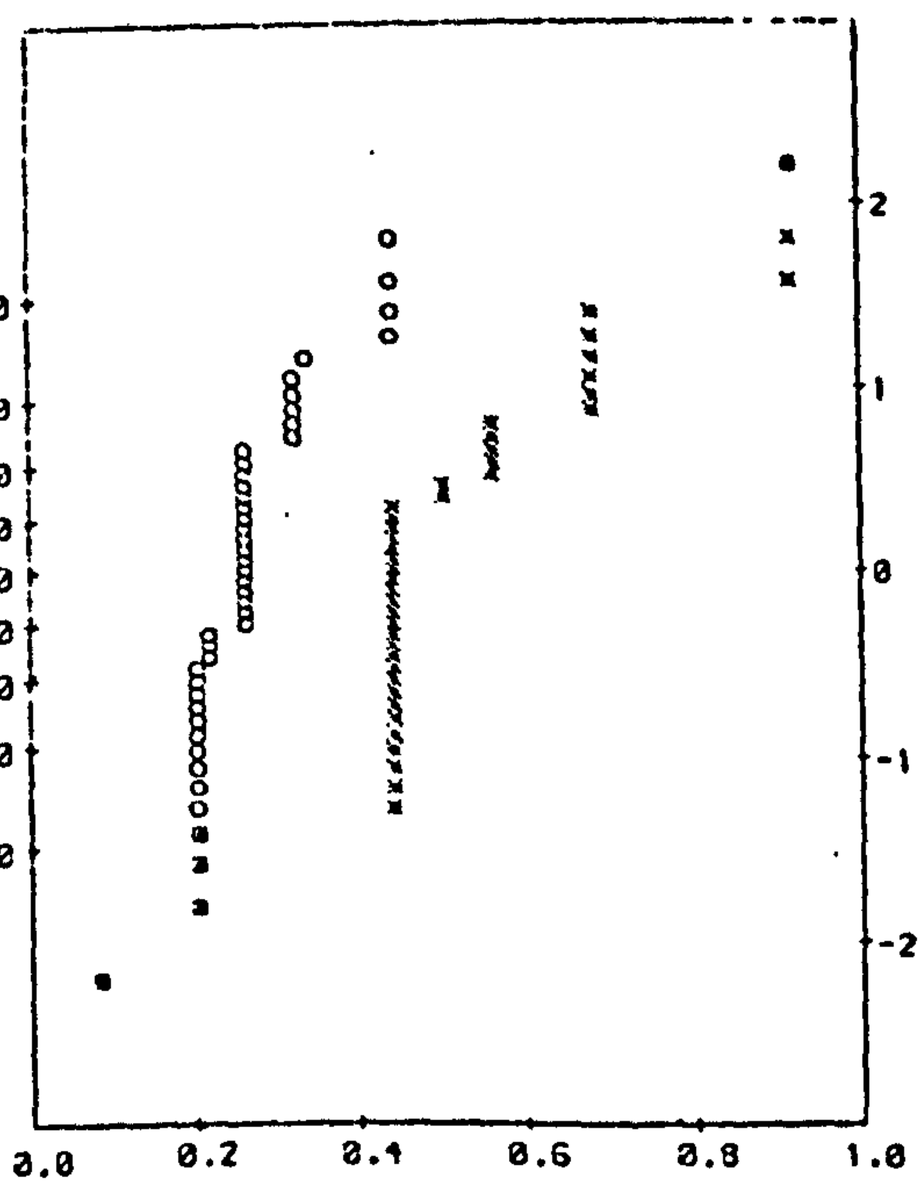

	SD	Mean	1.0	0.0
x	12.99	-29.67	-9.1	-67.8
o	9.37	-64.84	-9.2	-86.1

(c)

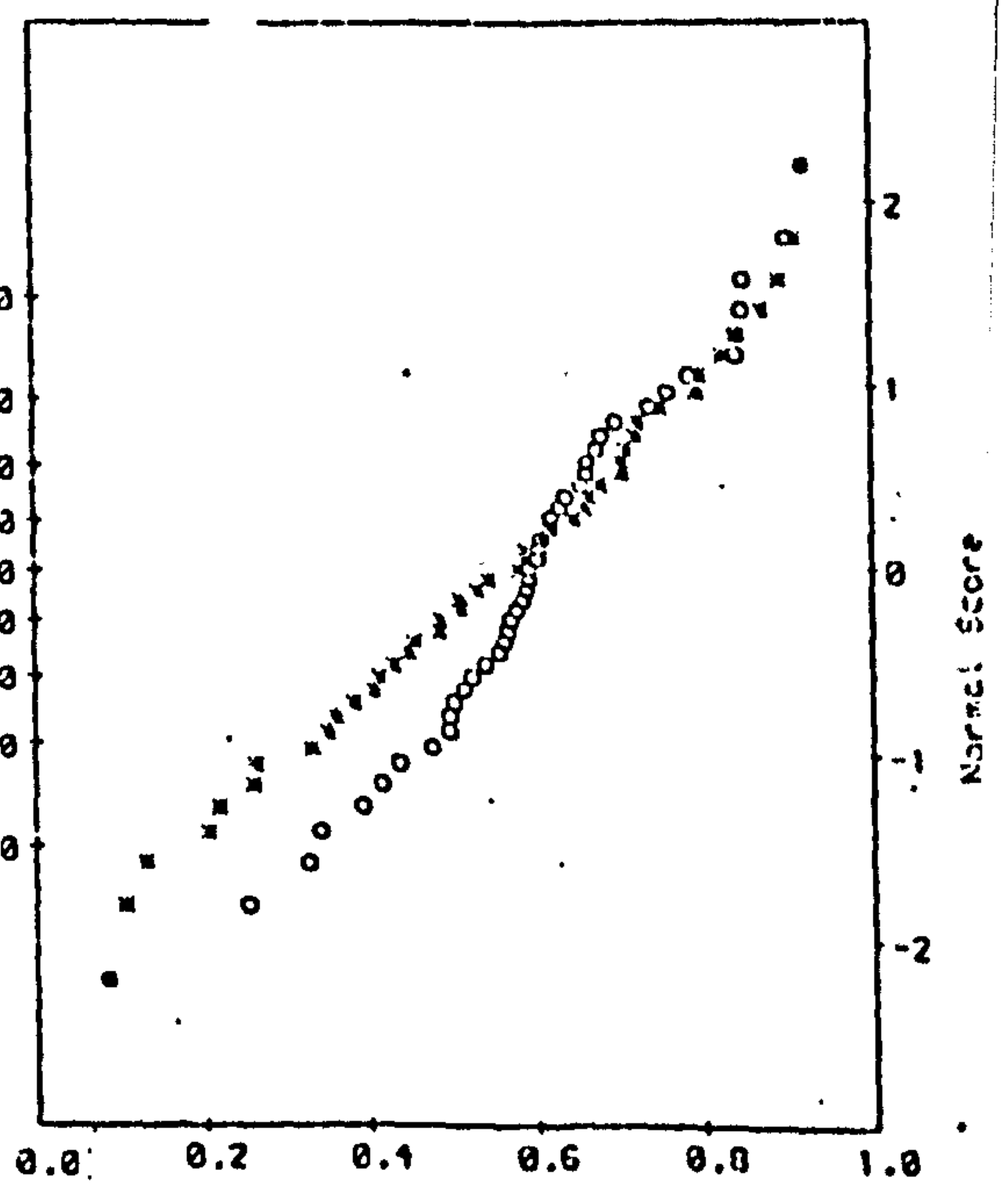

	SD	Mean	1.0	0.0
x	4.3	5.7	14.4	-4.7
o	2.2	-9.6	-4.4	-17.2

(d)

(ii) T = 1.6 s

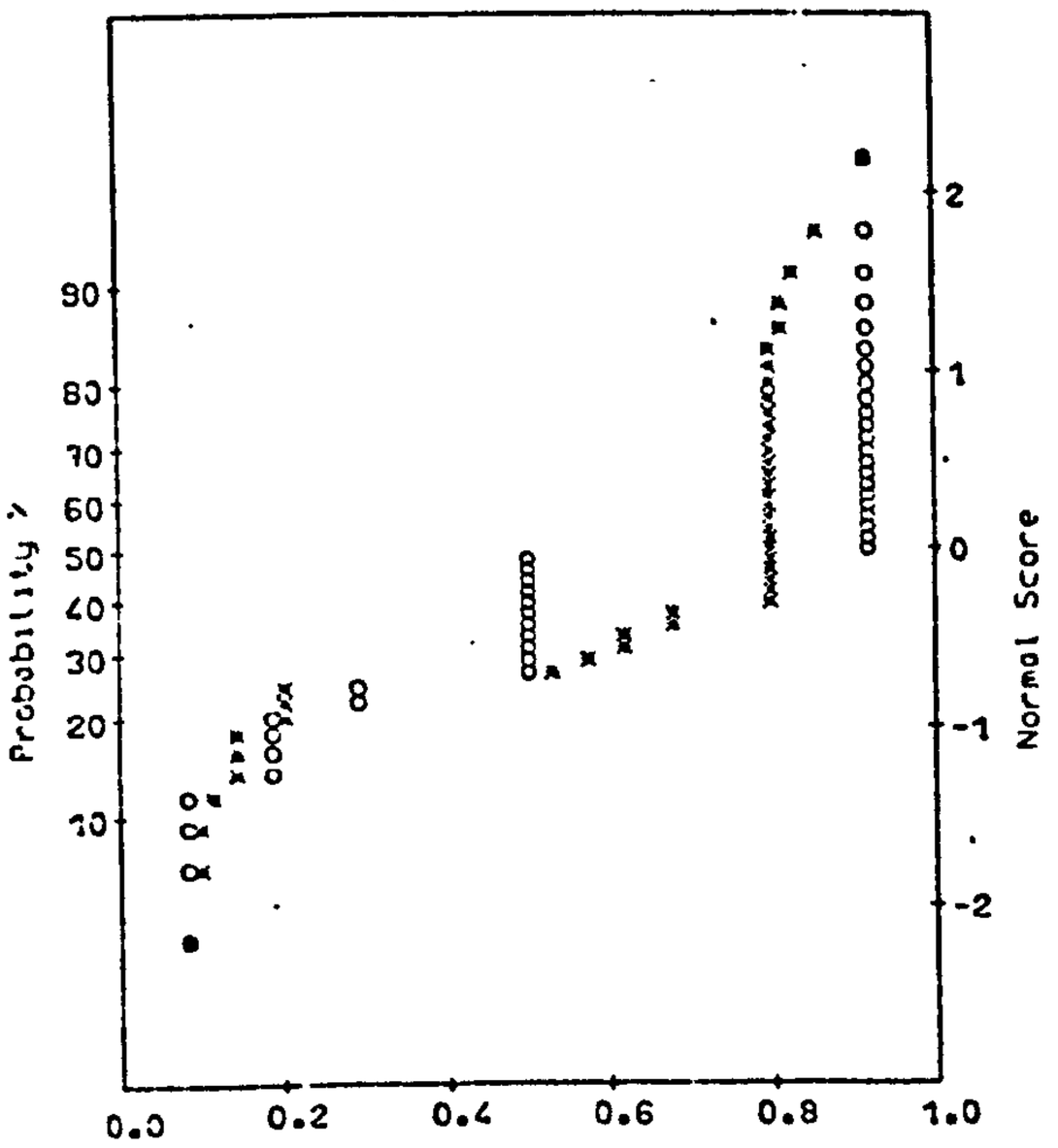

	SD	Mean	1.0	0.0
x	42.9	86.0	143.6	-10.1
o	6.9	124.6	132.6	110.7

(a)

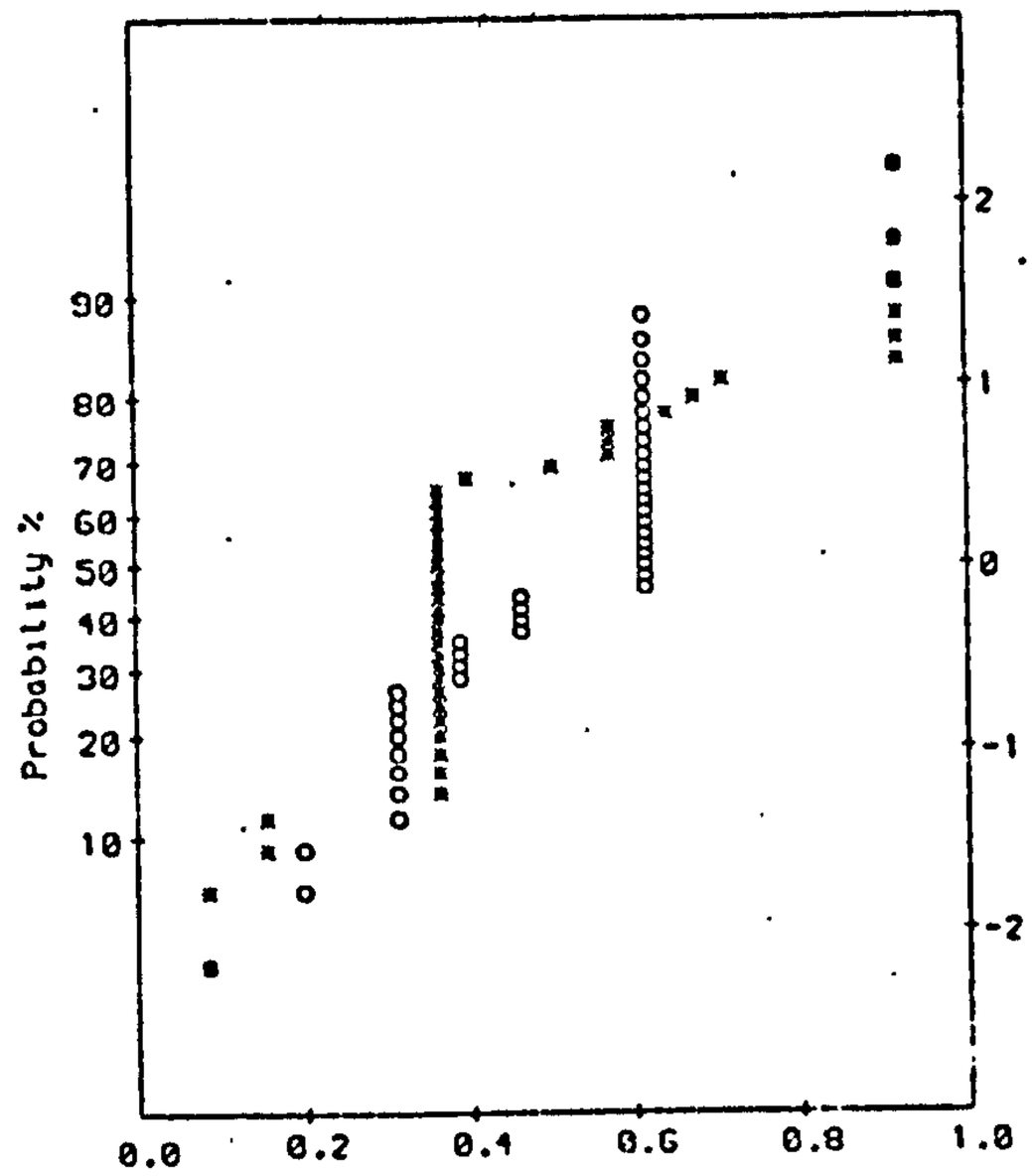

	SD	Mean	1.0	0.0
x	29.8	-94.6	-22.9	154.8
o	11.4	-131.6	-102.2	162.5

(b)

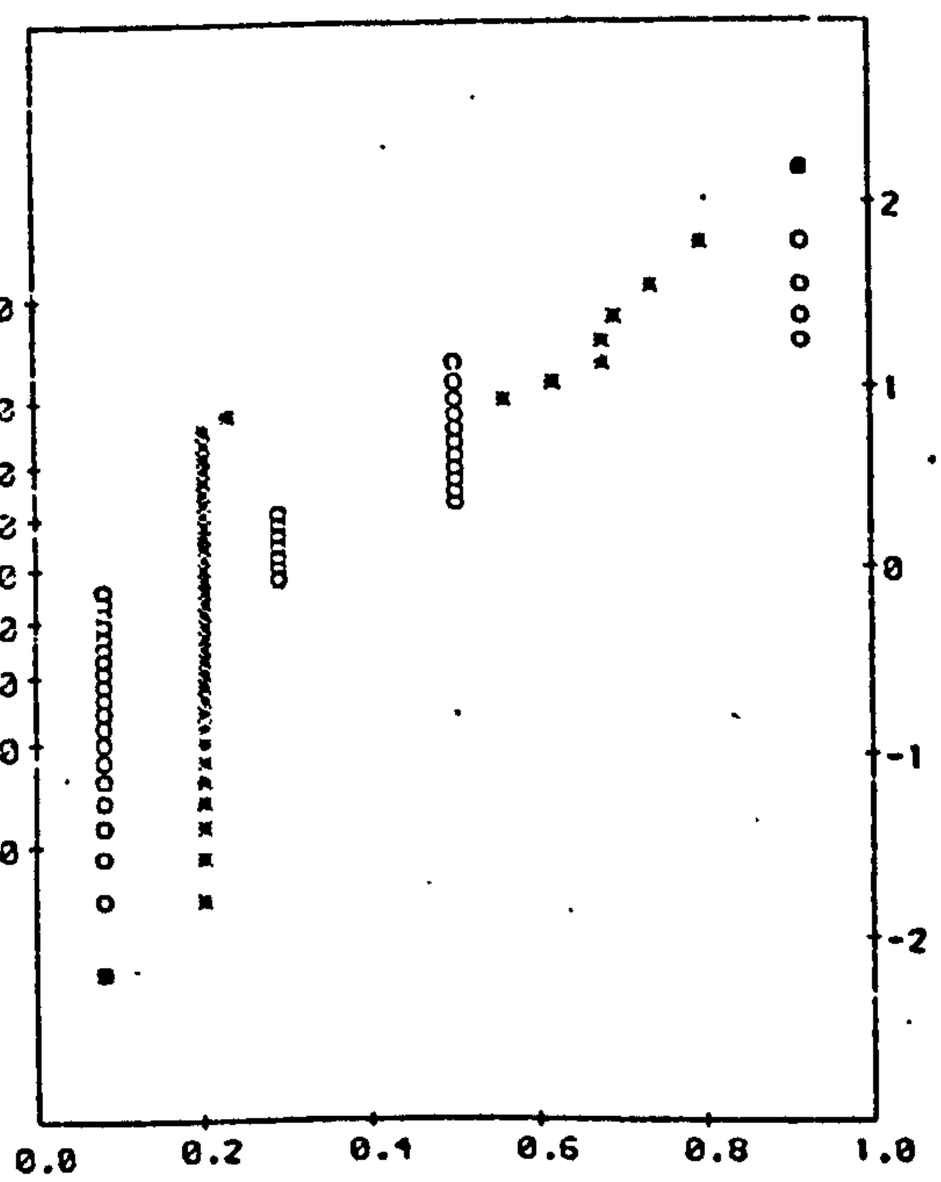

	SD	Mean	1.0	0.0
x	31.8	16.9	125.3	-28.4
o	6.1	-28.7	-13.8	-35.7

(c)

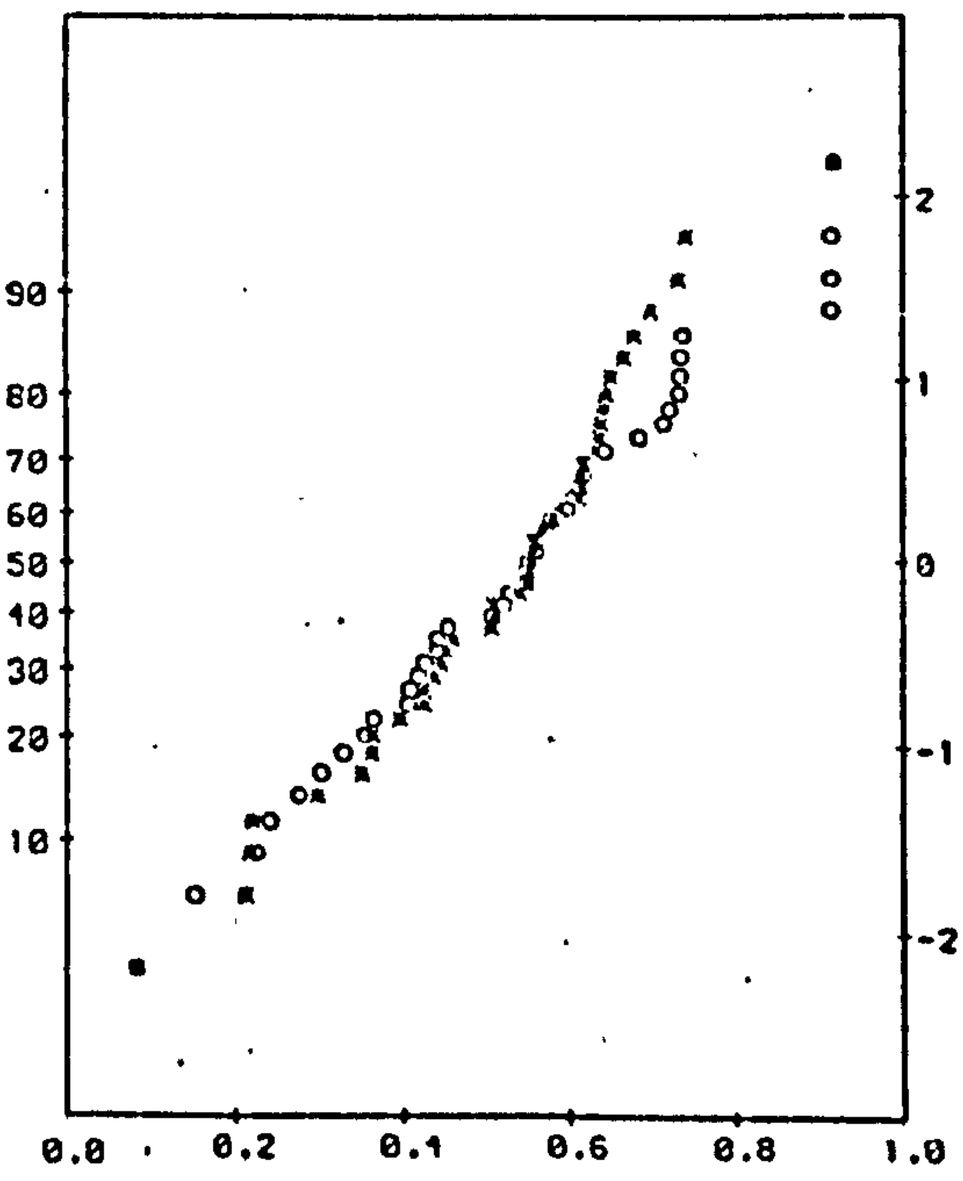

	SD	Mean	1.0	0.0
x	3.0	11.8	20.5	2.3
o	1.8	9.4	13.6	4.5

(d)

(iii) T = 1.8 s

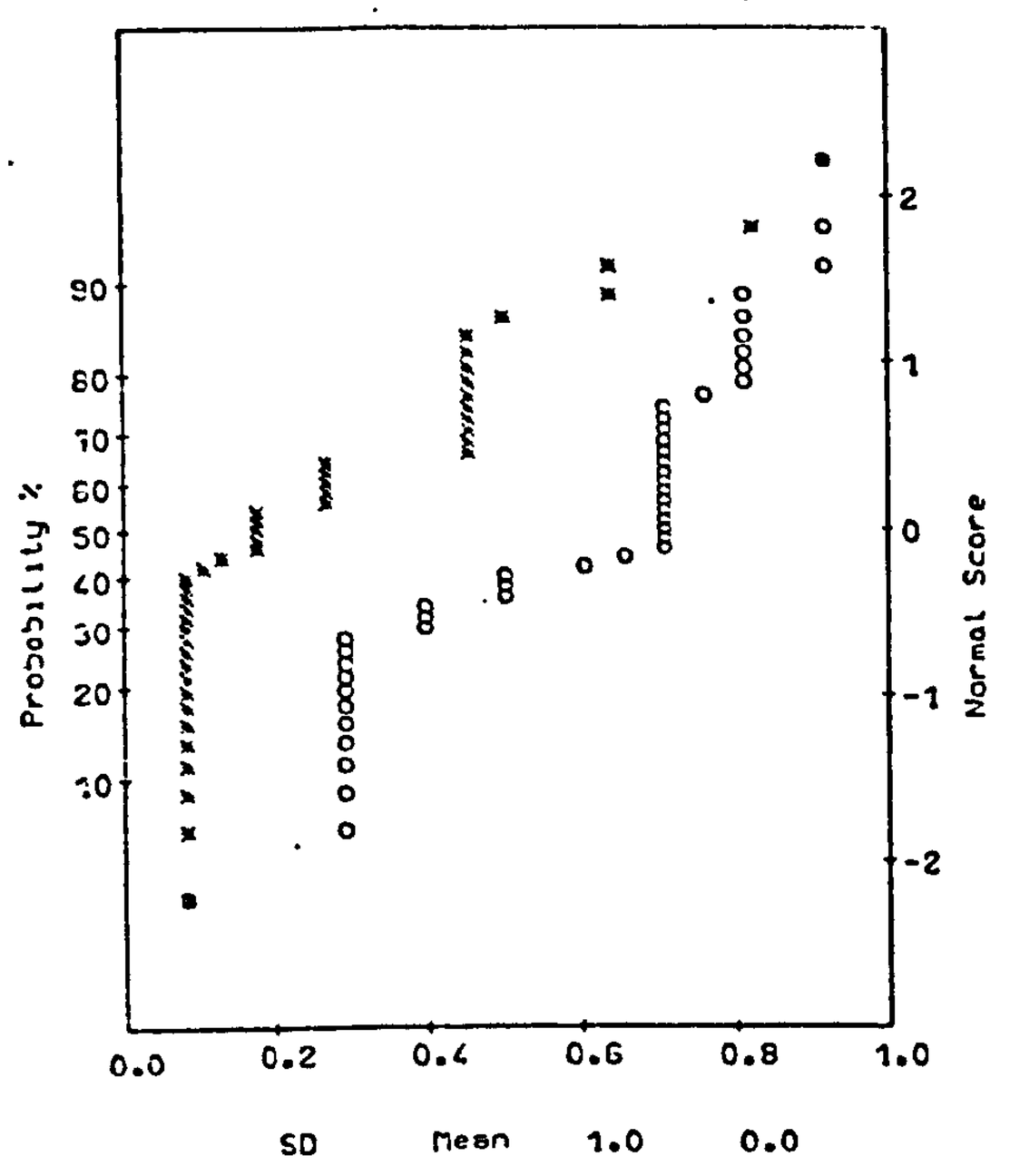

▪	10.8	48.4	84.6	35.2
o	5.0	73.1	82.3	60.4

(a)

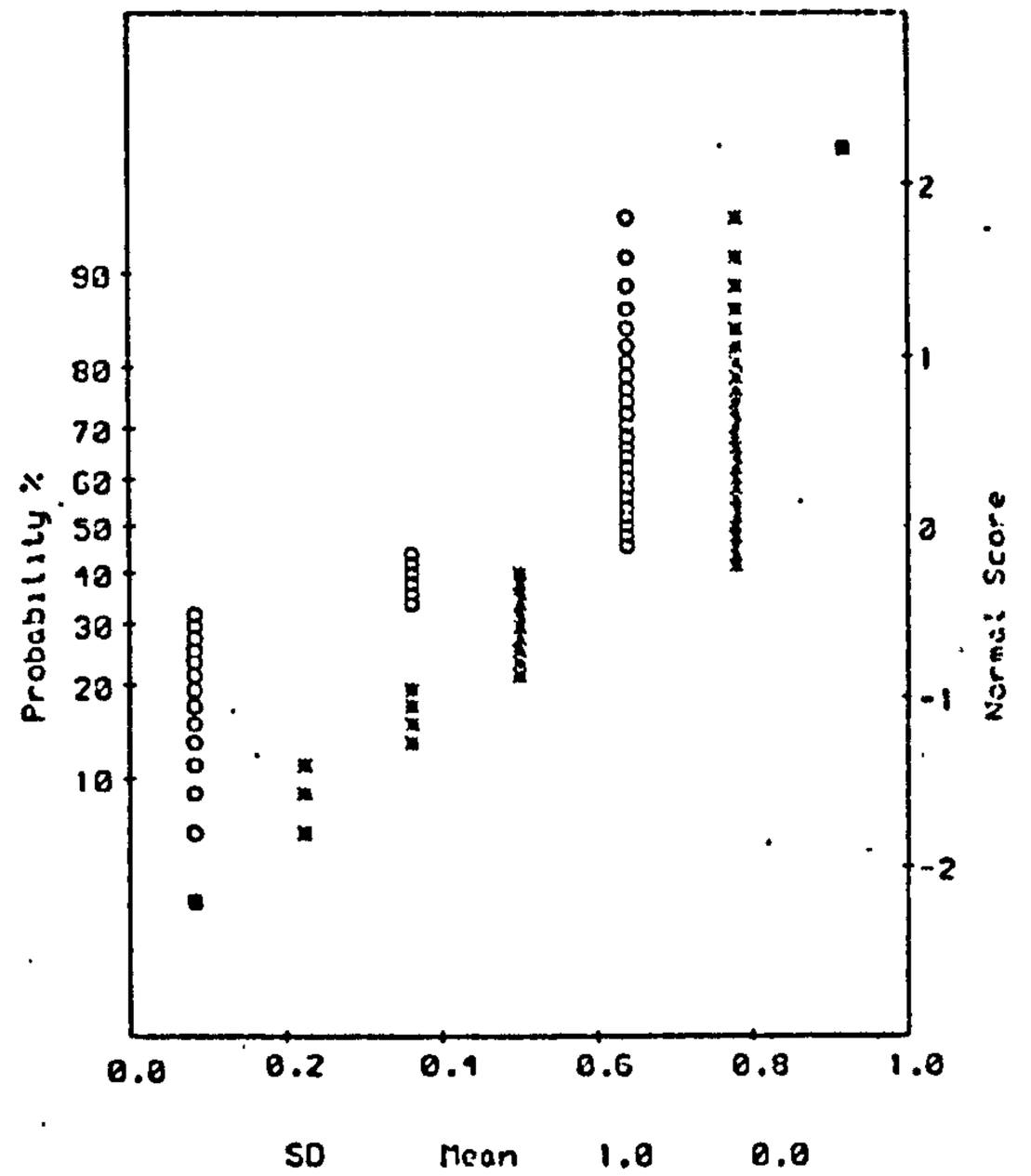

x	13.7	-43.7	-19.3	-85.2
o	4.3	-83.1	-73.7	-90.3

(b)

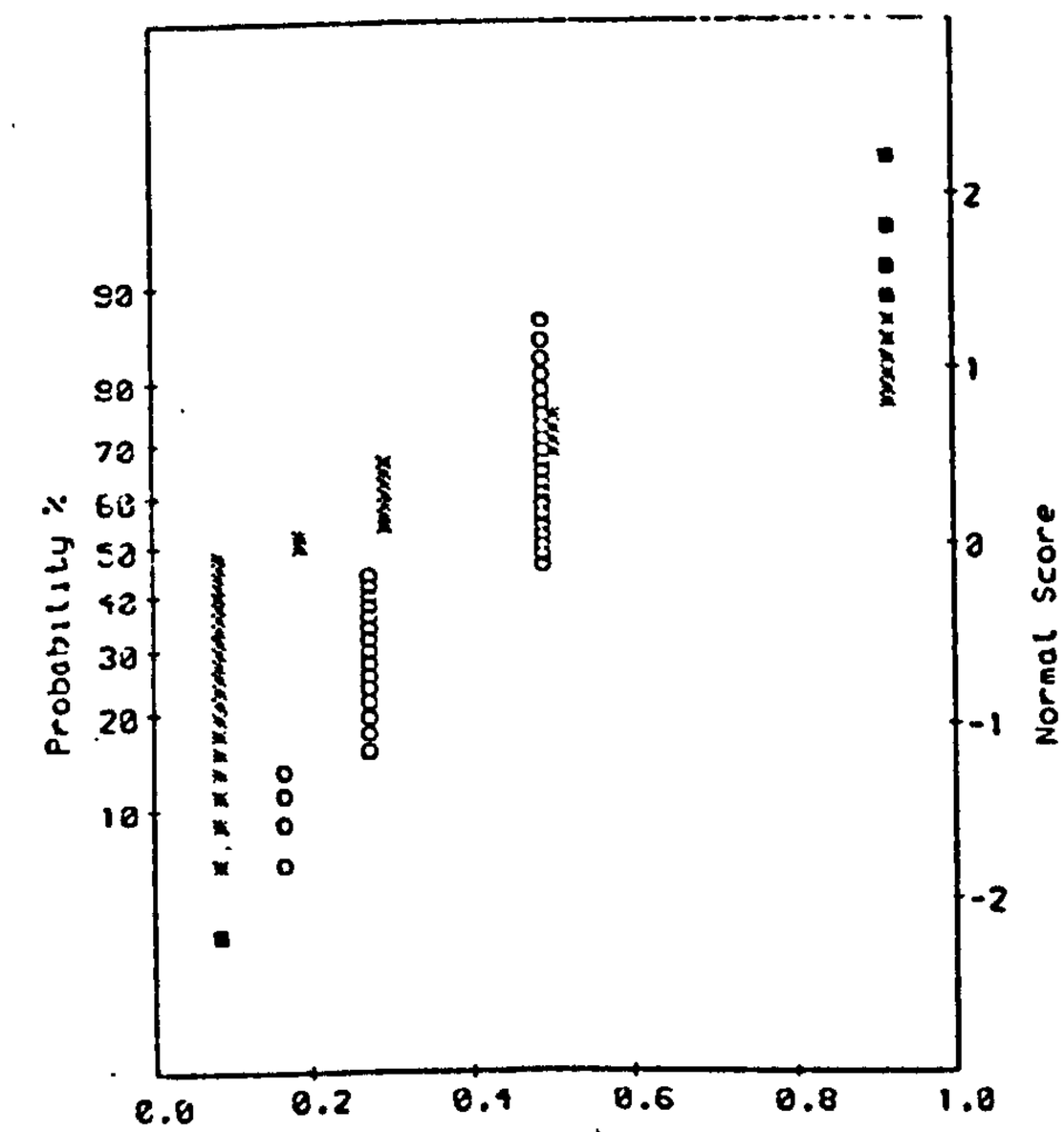

x	14.7	-22.6	6.4	-37.6
o	8.6	-55.3	-30.3	-73.0

(c)

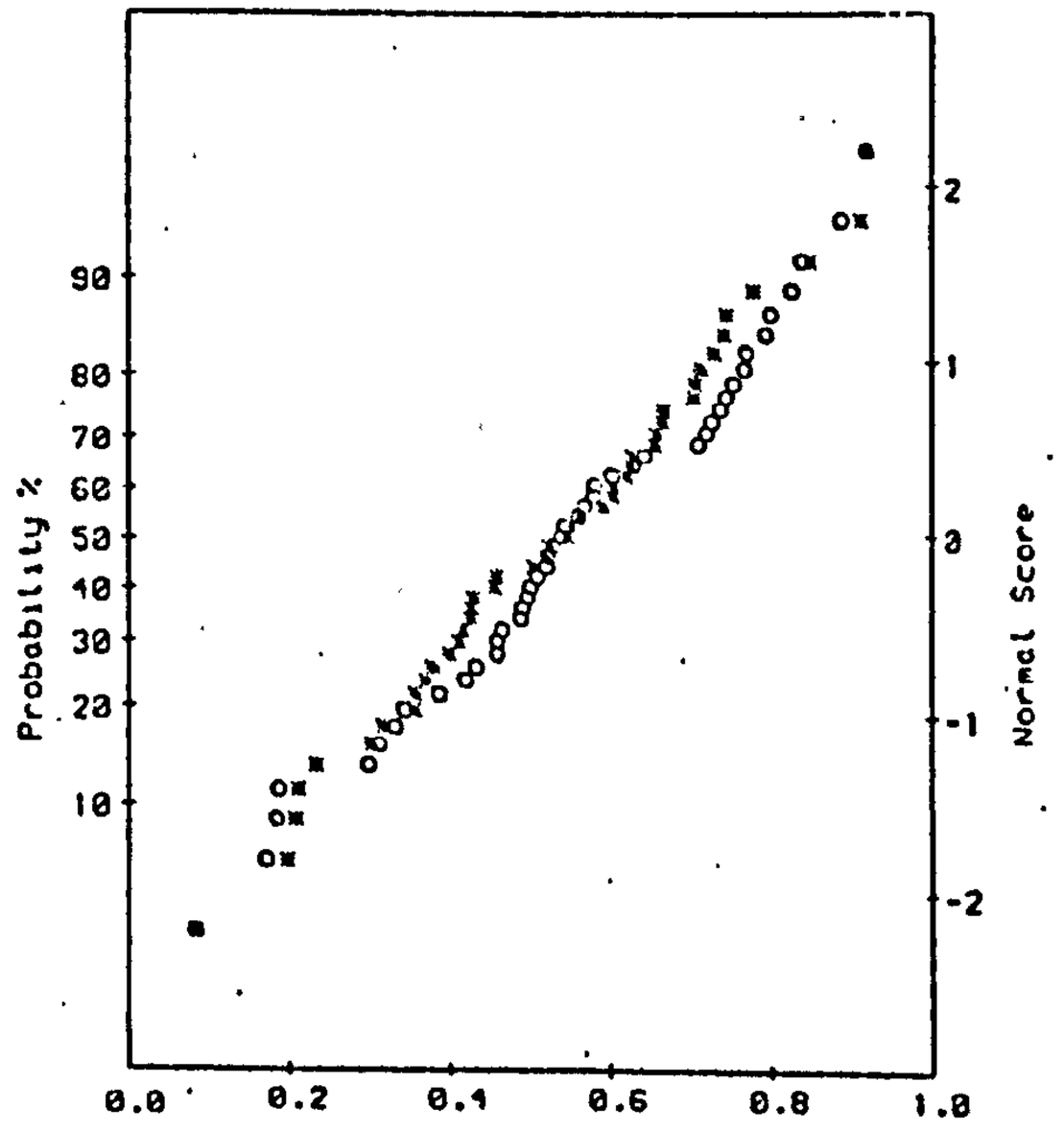

x	4.0	9.5	19.2	-1.4
o	1.8	-7.6	-3.7	-12.3

(d)

(iv) T = 2.0 s

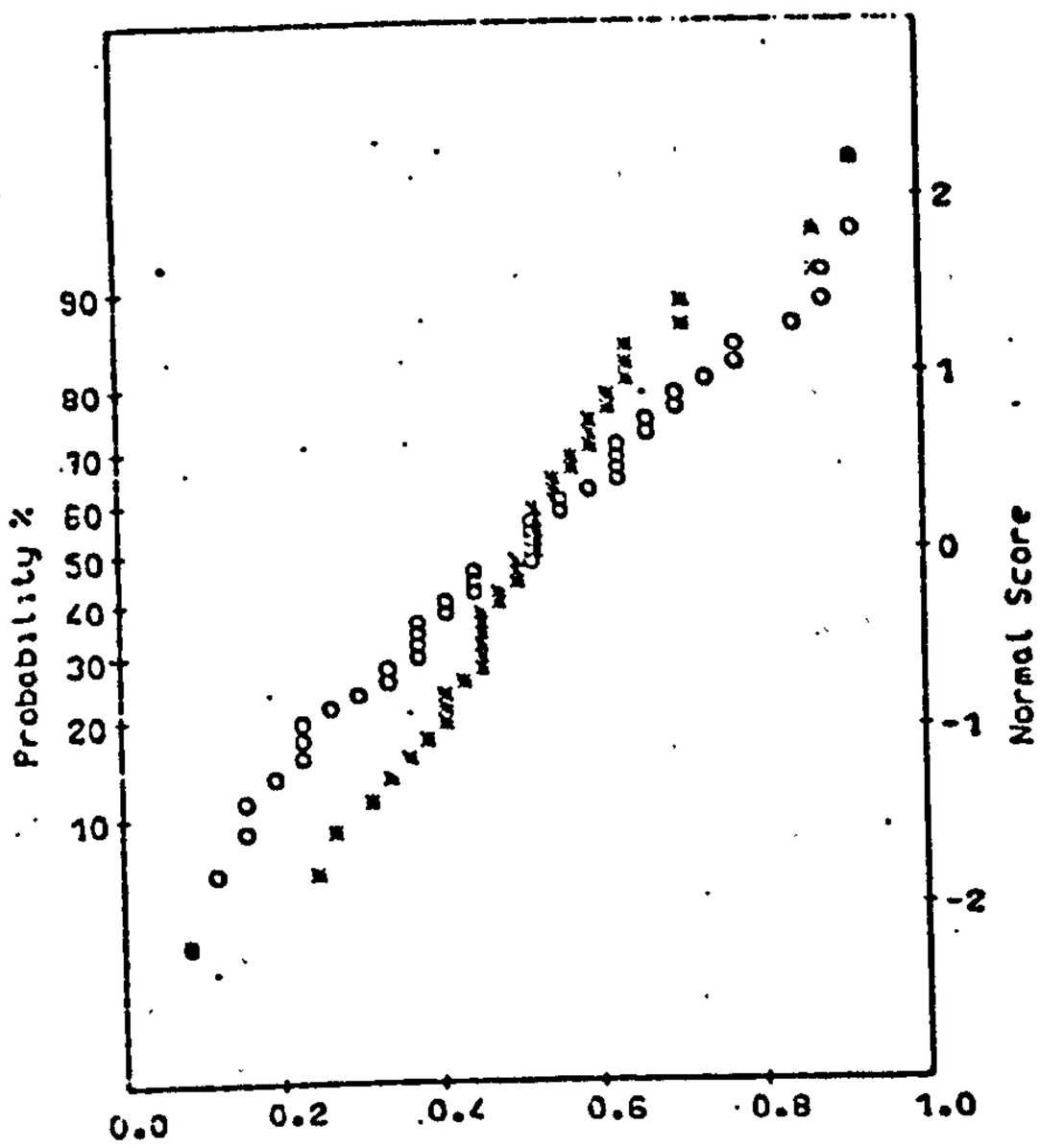

	SD	Mean	1.0	0.0
x	7.8	27.8	51.7	2.3
o	7.2	34.4	50.2	18.7

(a)

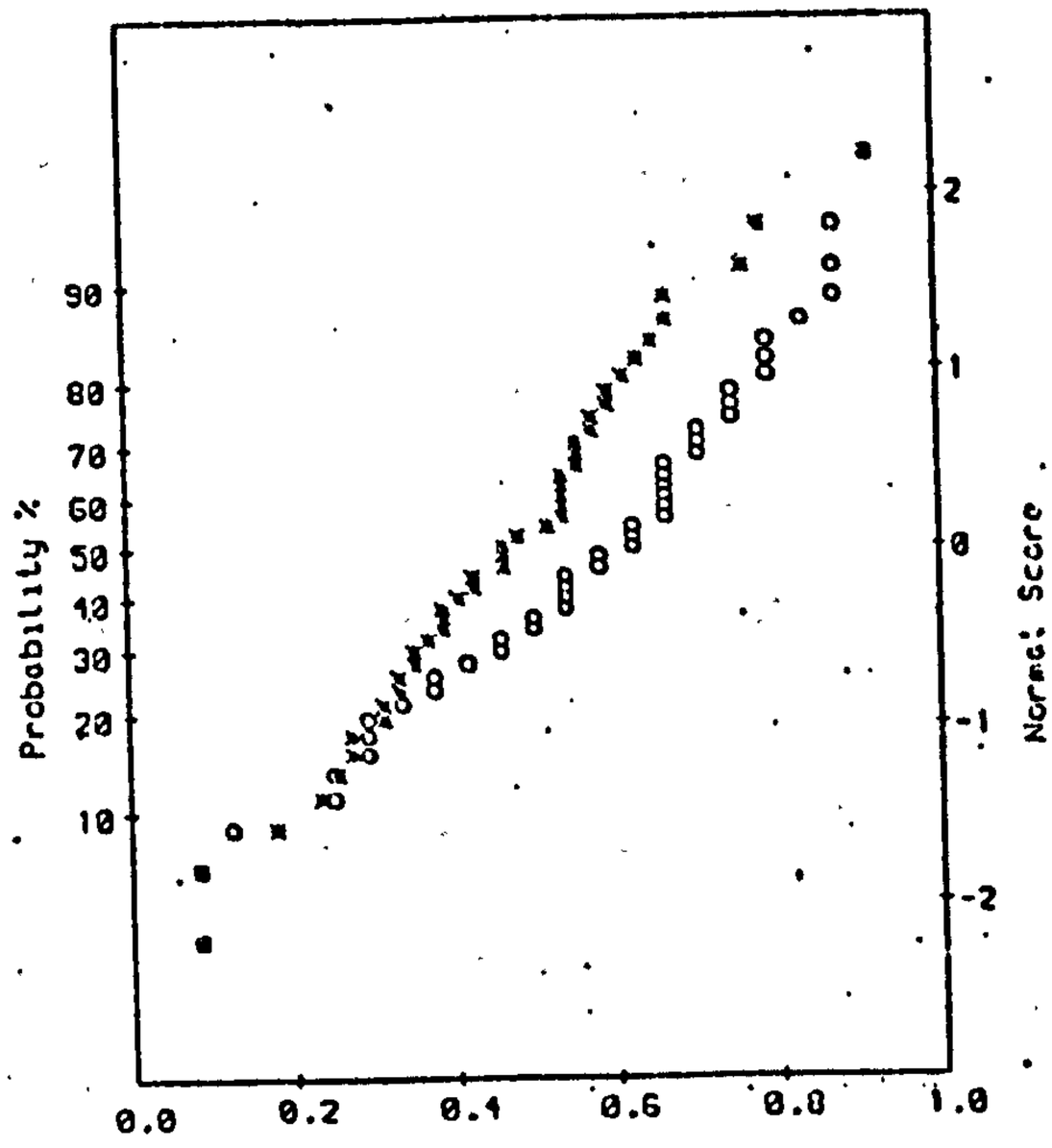

	SD	Mean	1.0	0.0
x	10.7	-71.2	-39.	-99.3
o	6.1	-95.9	-84.0	-111.5

(b)

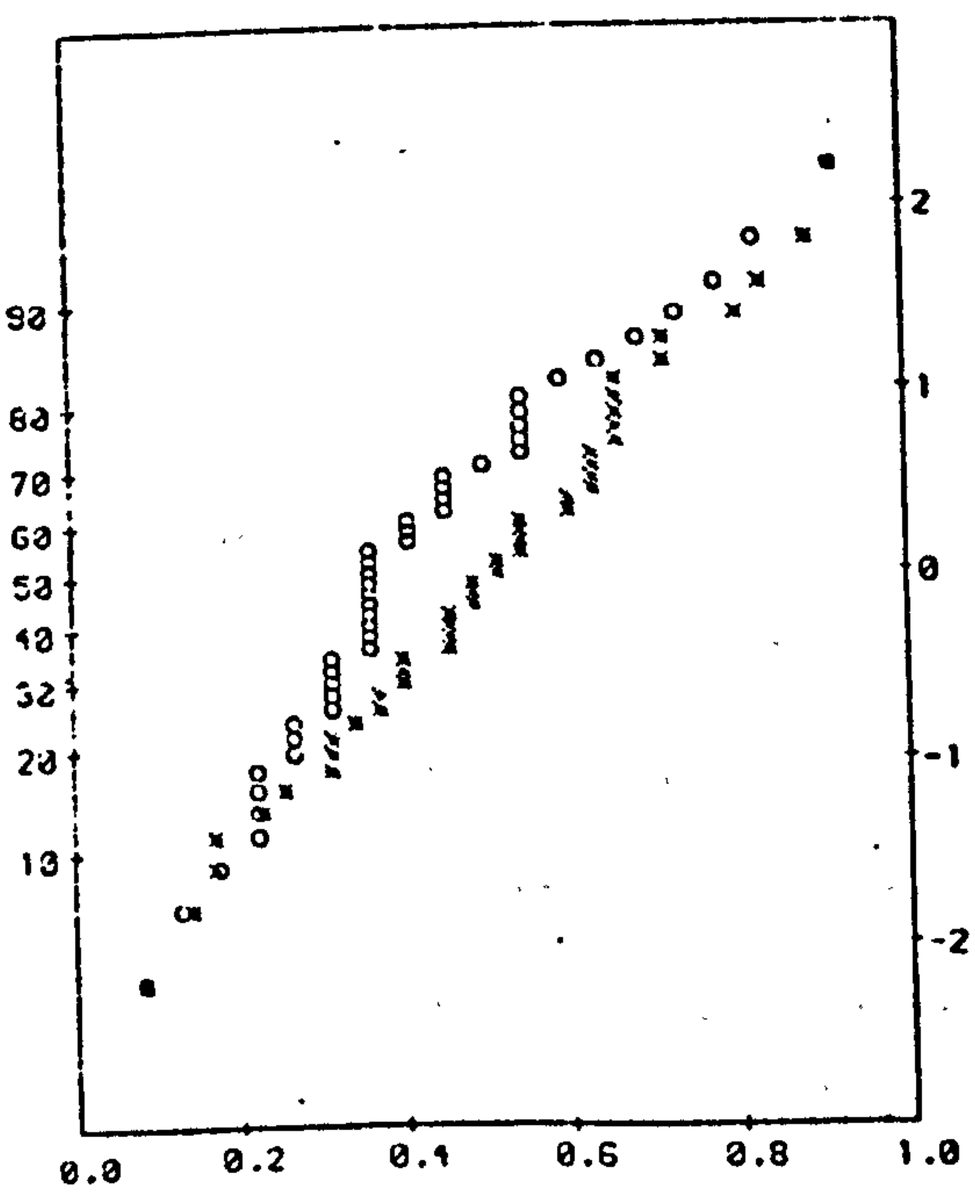

	SD	Mean	1.0	0.0
x	7.8	-62.7	-42.9	-82.7
o	4.5	-92.9	-78.5	-103.3

(c)

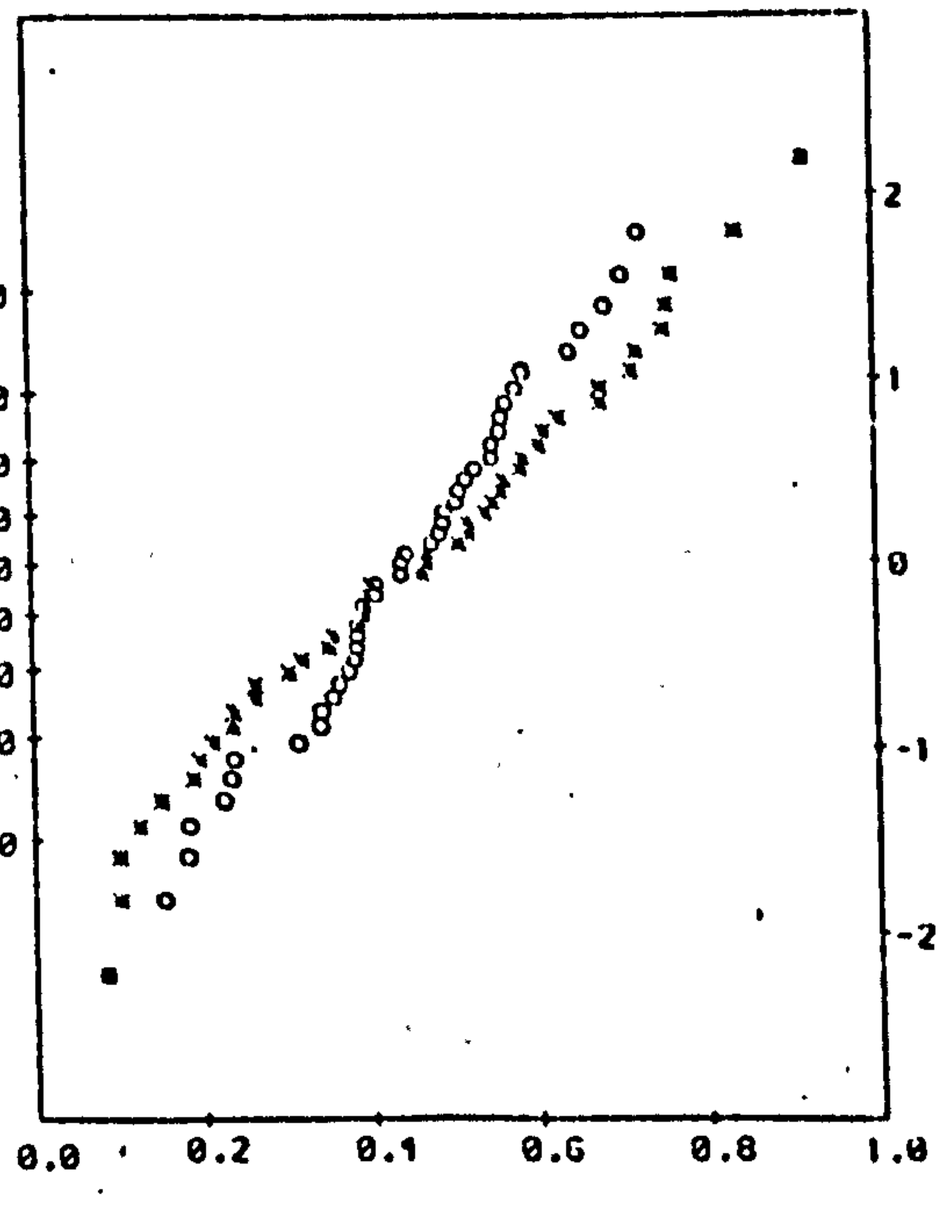

	SD	Mean	1.0	0.0
x	2.8	-3.3	3.8	-9.2
o	2.7	-18.7	-9.6	-25.9

(d)

(v) T = 2.2 s

cyclic variation of the velocity) are normally distributed for both positions, also that for 2.2 second wave period all the graphs show a normal distribution relationship. Since the mean velocities are averaged over 121 points, any error due to randomness is minimised so that a distribution closer approximating to normal results. But for the 2.2 sec. wave period, the only differences from the results from other period waves are the magnitudes of velocity and therefore the type of wave. Also the standard deviation values which for 2.2 sec. wave are less than all other waves, show that a less perturbed situation occurred for this period which is why the distribution approximates more closely to normal than for the others.

Calculating the turbulence intensity (T.I.) of these profiles for each period may help to understand better this problem. Knowing that;

$$T.I. = \frac{\overline{(U')^2}^{\frac{1}{2}}}{\bar{U}} \times 100$$

where U' is the difference of instantaneous velocity from mean velocity and $\bar{U}$ is the mean velocity. For sinusoidal waves the problem arises in the taking of suitable $\bar{U}$ and U' values. However if the mean velocity is taken when it is the maximum value the choice of U' is between that where $\bar{U}$ is taken or where U' has its maximum value for that period. Observing Fig. 6.12 makes this problem more clear especially

for the profile at lower height (1.5 mm above roughness) than at higher height (5 mm above roughness), and therefore maximum value of $\sqrt{\overline{U'^2}}$ if used for evaluating the turbulent intensity.

The "observed" values of T.I. (stress on the observed values) are tabulated (Table 6.3), showing a turbulence intensity of about 6 per cent in the 5 mm high region (at the edge of the boundary layer) which is just greater than the limit of 5 per cent (Sleath (1976)) for the onset of transition to turbulent flow. Hence the region is in a state of weak turbulence and as the wave period increases the intensity decreases.

But for the height within the boundary layer, the observed T.I. values are not related for different periods and no clear conclusion can be reached and so it needs more precise observation and especially a more comprehensive analyses technique to clearly discuss the flow.

The conclusion to be drawn from Figs. 6.12 and 6.13 and Table 6.3 is that the two dimensional roughness of 4.65 mm height has a greater effect on the flow inside the boundary layer while outside it the turbulence intensity decreases rapidly and very quickly the flow is as normal as over the smooth bed (as shown in Chapter Five). The comparison of boundary layer velocity over smooth and 2-D rough bed is discussed in Section 6.4.

T/sec	T.I. %		Re = $\frac{U_\infty \kappa}{\nu}$
	1.5 mm	5 mm	
1.4	12	4	1152
1.6	10	6	946
1.8	24	6	741
2.0	7	5	823
2.2	5	4	782

Table 6.3. Re and T.I. values for 2-D rough bed.

6.3.2 Three Dimensional Rough Bed

For the two wave periods of 1.4 sec. and 2.2 sec., the boundary layer velocity for two sections (S and R, which have been shown diagrammatically in section 4.2) over three dimensional rough bed have been observed. The data include the velocity over trough and crest (for 3-DS the equivalent height of crest) for each period (Fig. 6.14).

The curved lines which join the data points show clearly a fluctuation which is higher in two areas than in any others. The first one is the immediate vicinity of the roughness top up to about double thickness of δ for all the graphs in Fig. 6.14 and with more intensity over the trough of the roughness element, and the second is the 3-DS region in which the fluctuation is intensified relative to the 3-DR results.

As has been shown for the last section the correlation coefficient values illustrate this observation with more confidence (Fig. 6.15). The coefficients are the result of two sets of comparison. One set (as for 2-D rough bed) is from the correlation of sets of results over the same section (3-DR or 3-DS) and the other set shows the correlation over troughs (3-DR and 3-DS) or crest (R and S) at each period.

The correlation coefficients for R are very close to the observed values for two dimensional rough bed, that is above the fluctuation within the boundary layer thickness (and in this case slighly beyond the boundary layer thickness

6.14(a) Over Crest of Roughness.

6.14(b) Over Trough of Roughness

Fig. 6.14 Boundary Layer Velocity Profile for 3-D Rough Bed (10 phases in a cycle).

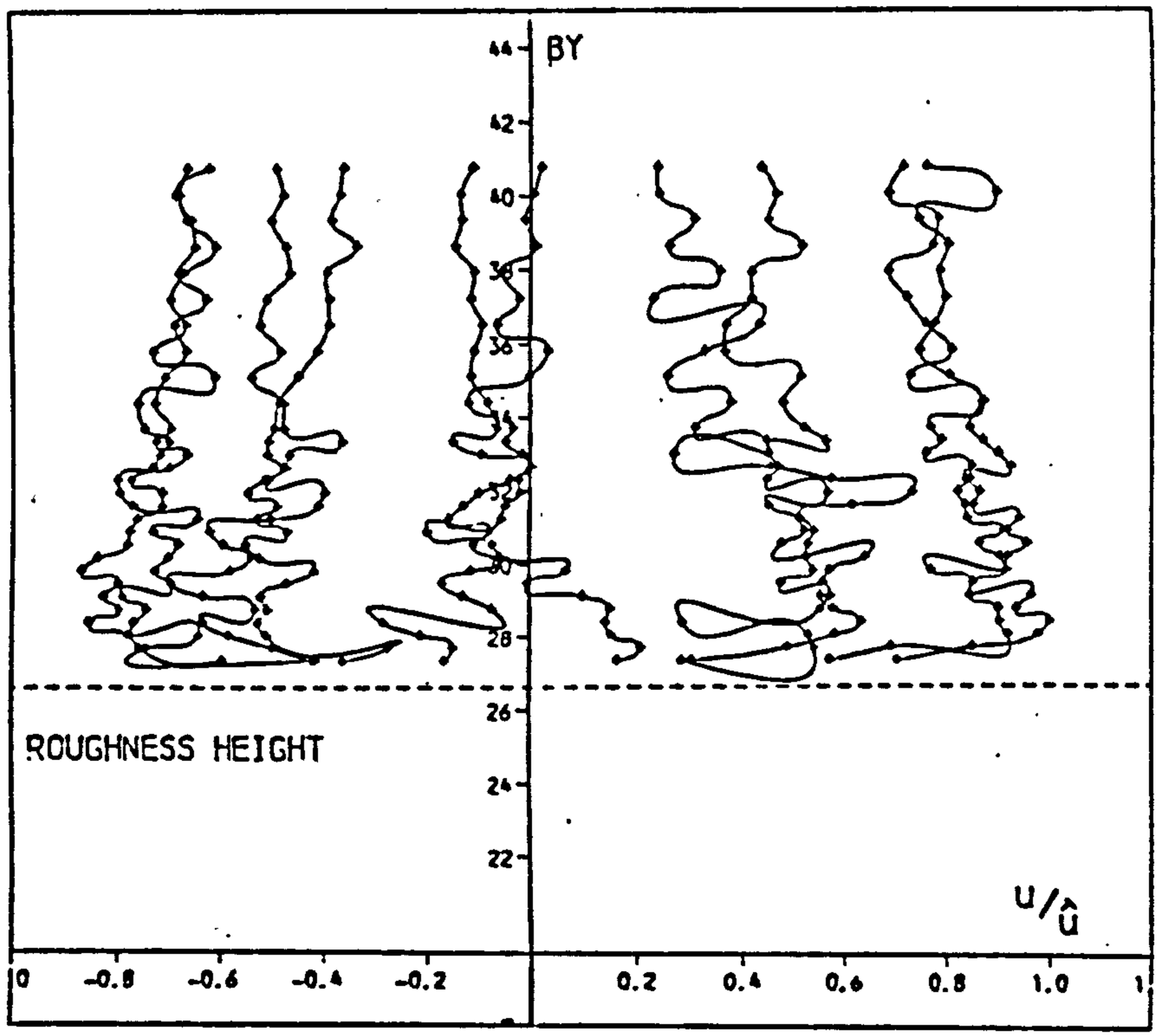

(a)

$\hat{u}$=346.0 mm/s

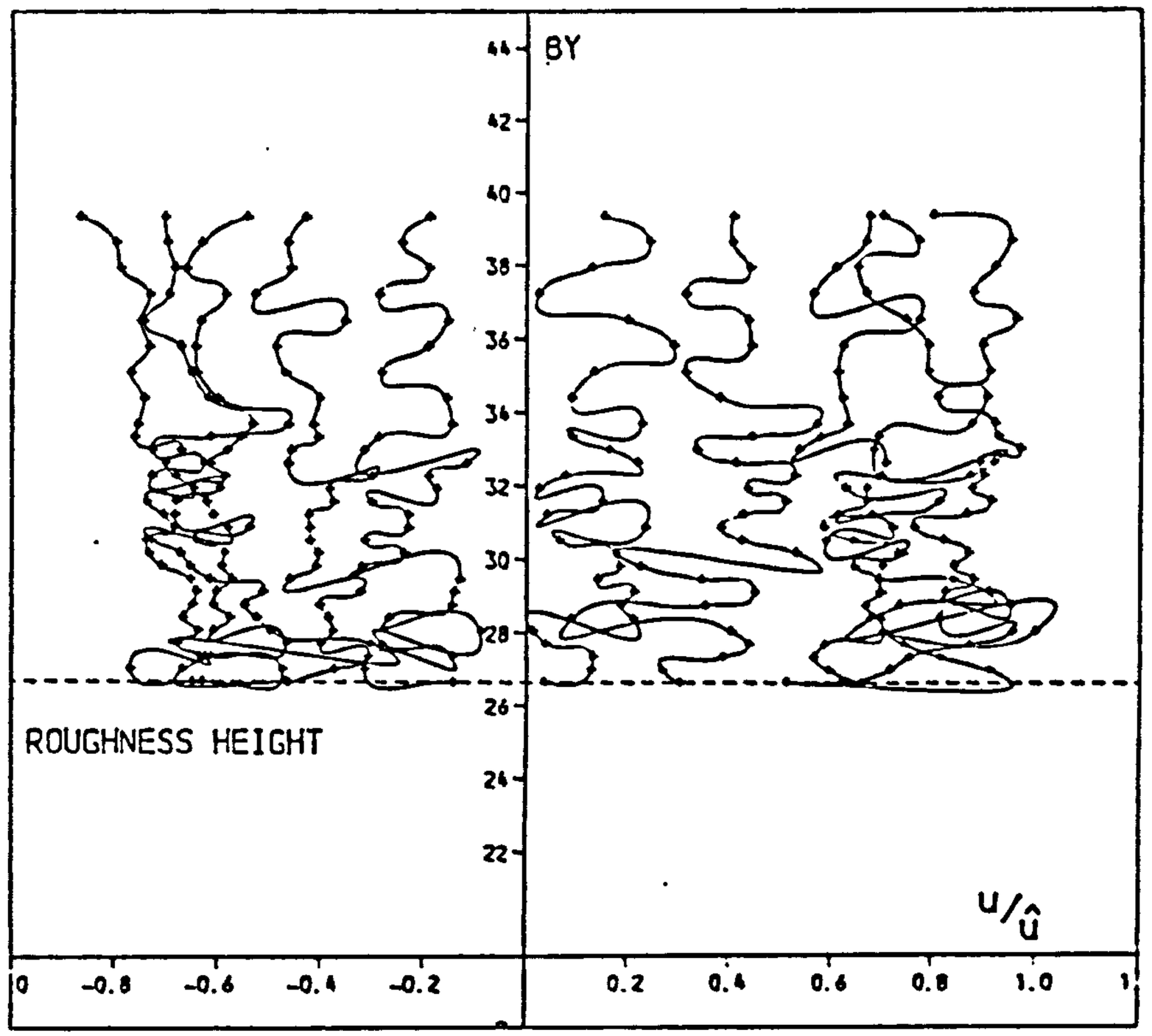

(b)

$\hat{u}$=262.0 mm/s

(i) T=1.4s , position R

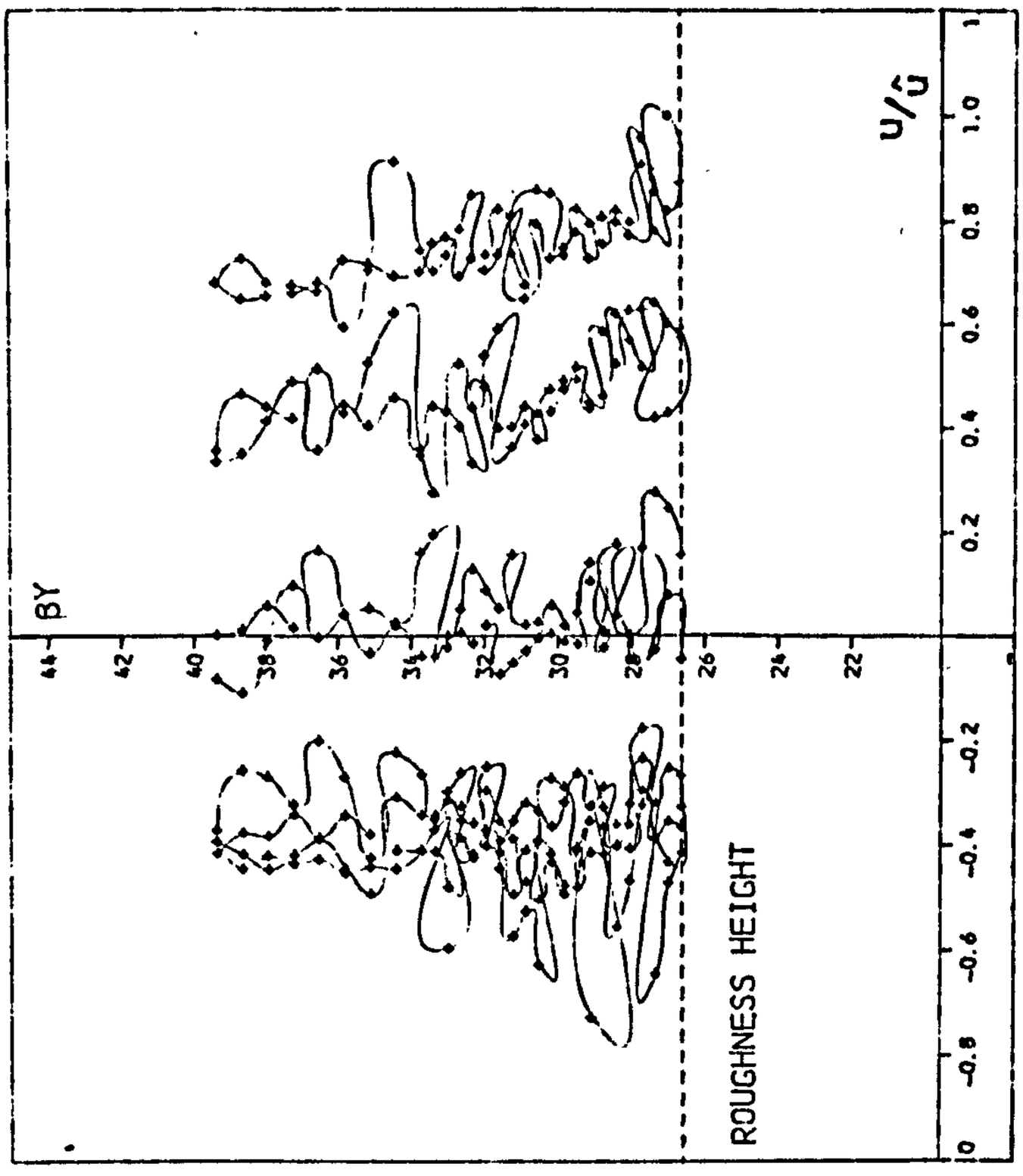

(b) $\hat{u}$=382.0 mm/s

(ii) T=1.4 s , position S

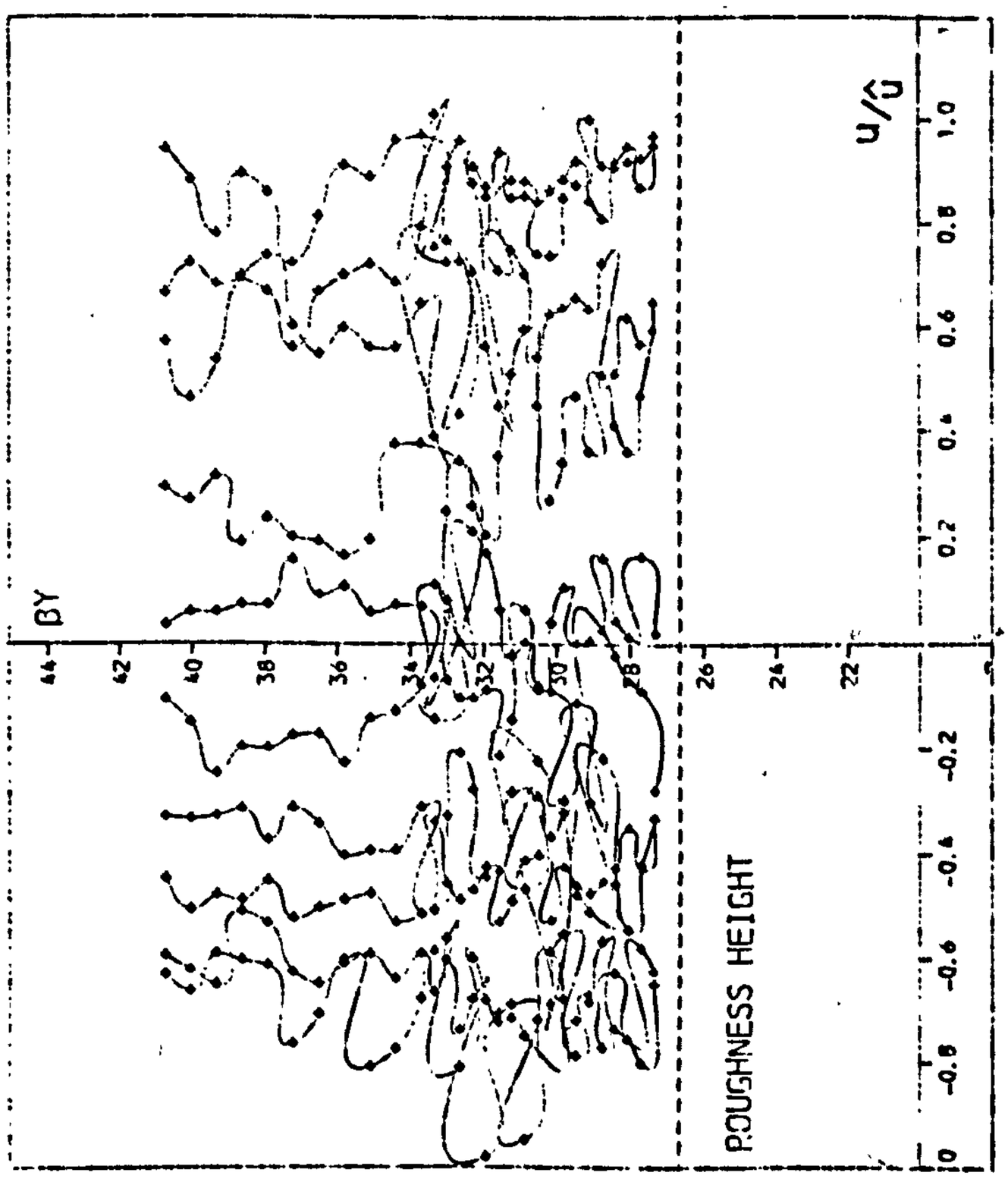

(a) $\hat{u}$=326.0 mm/s

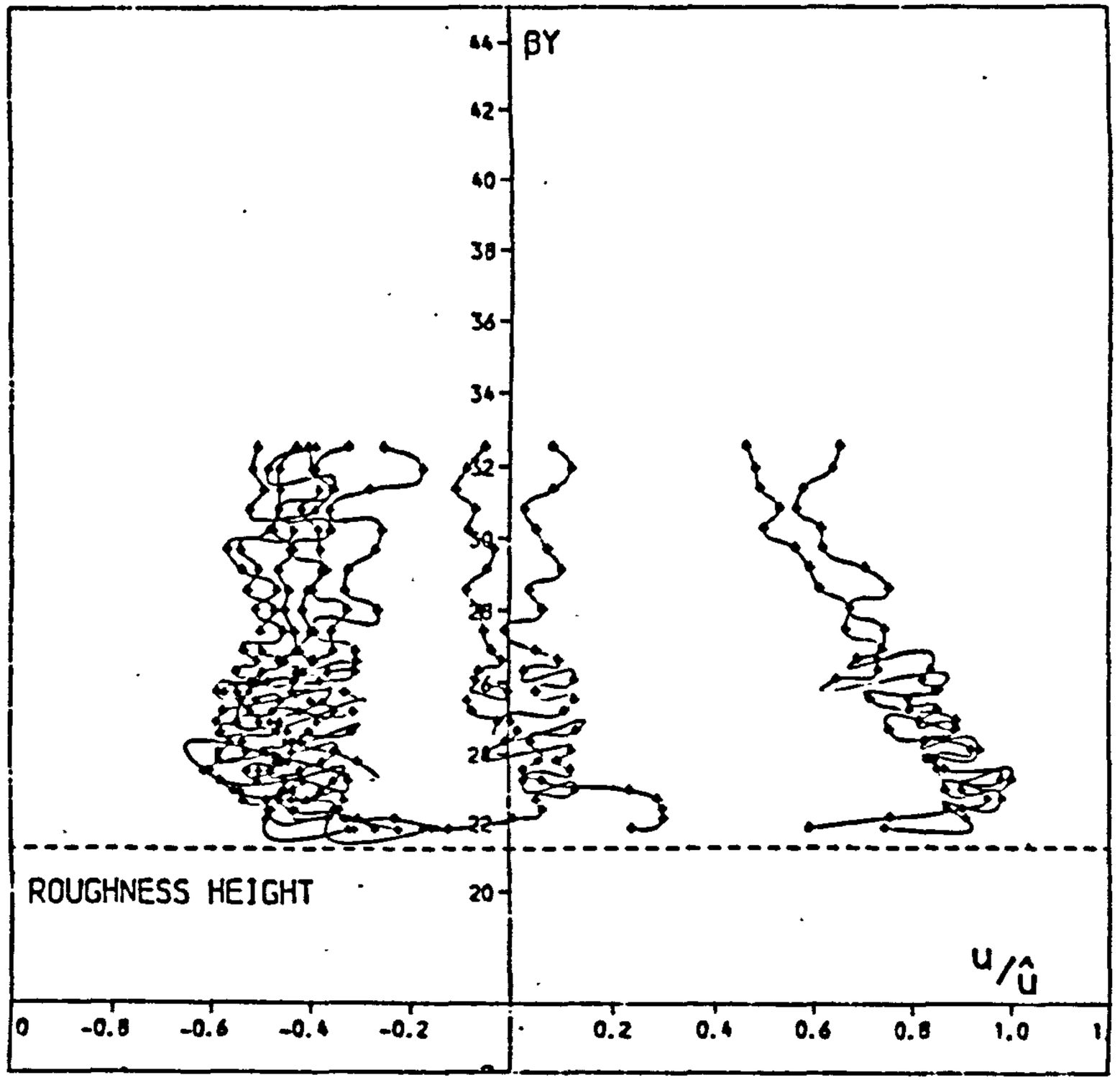

(a)

$\hat{u}$=240.0 mm/s

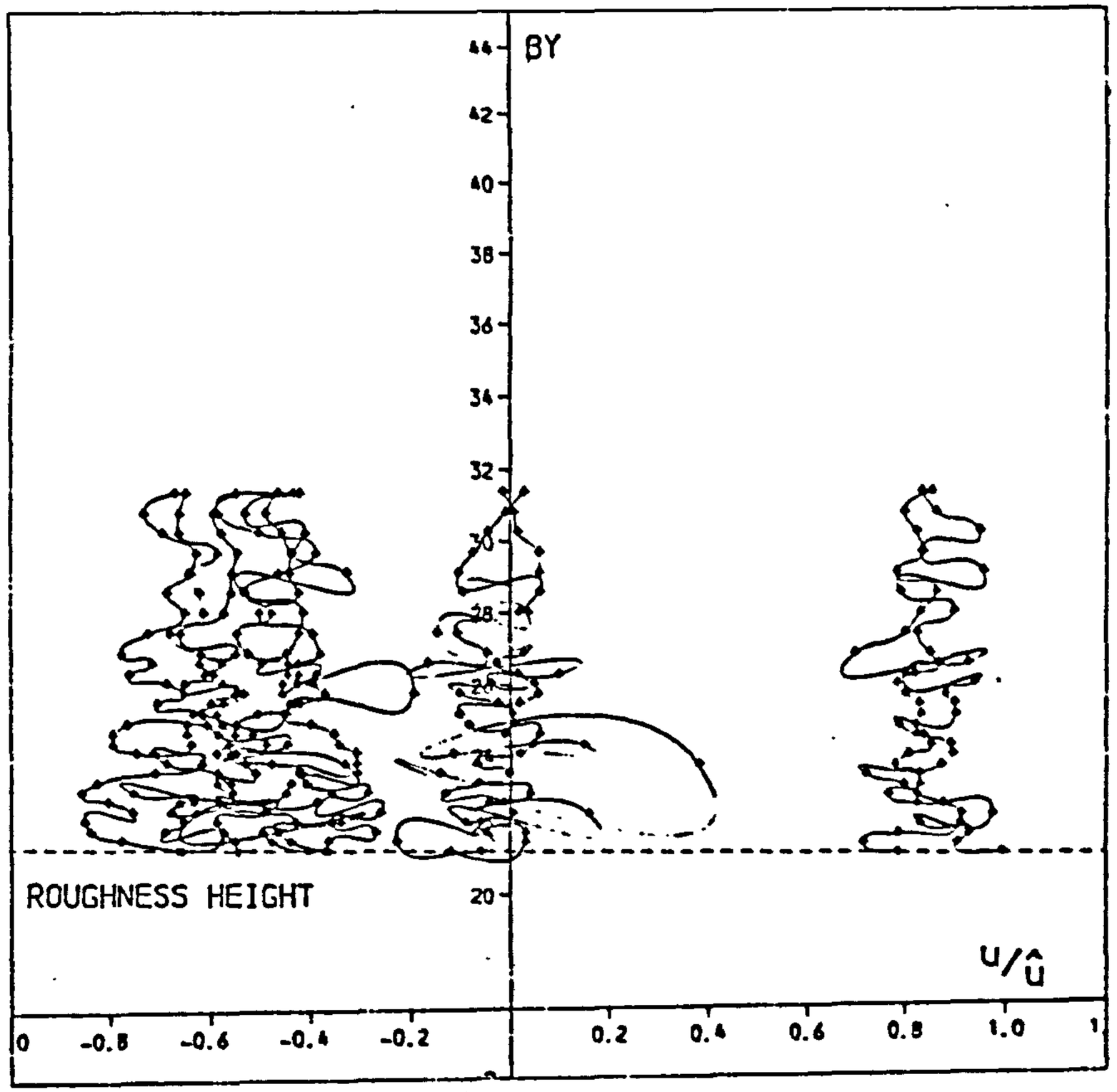

(b)

$\hat{u}$=159.0 mm/s

(iii) T=2.2s , position R

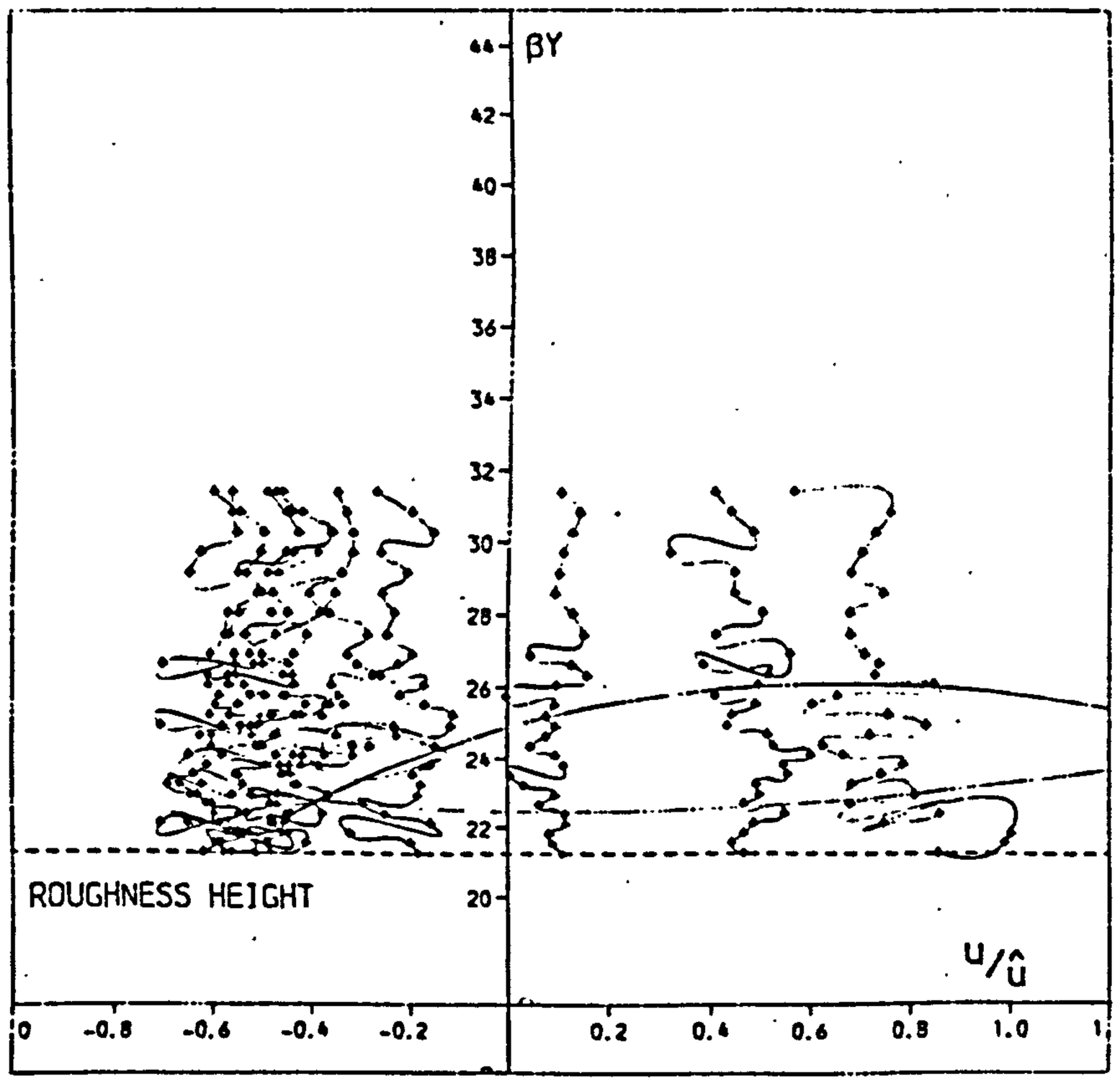

(a)

$\hat{u}$=219.0 mm/s

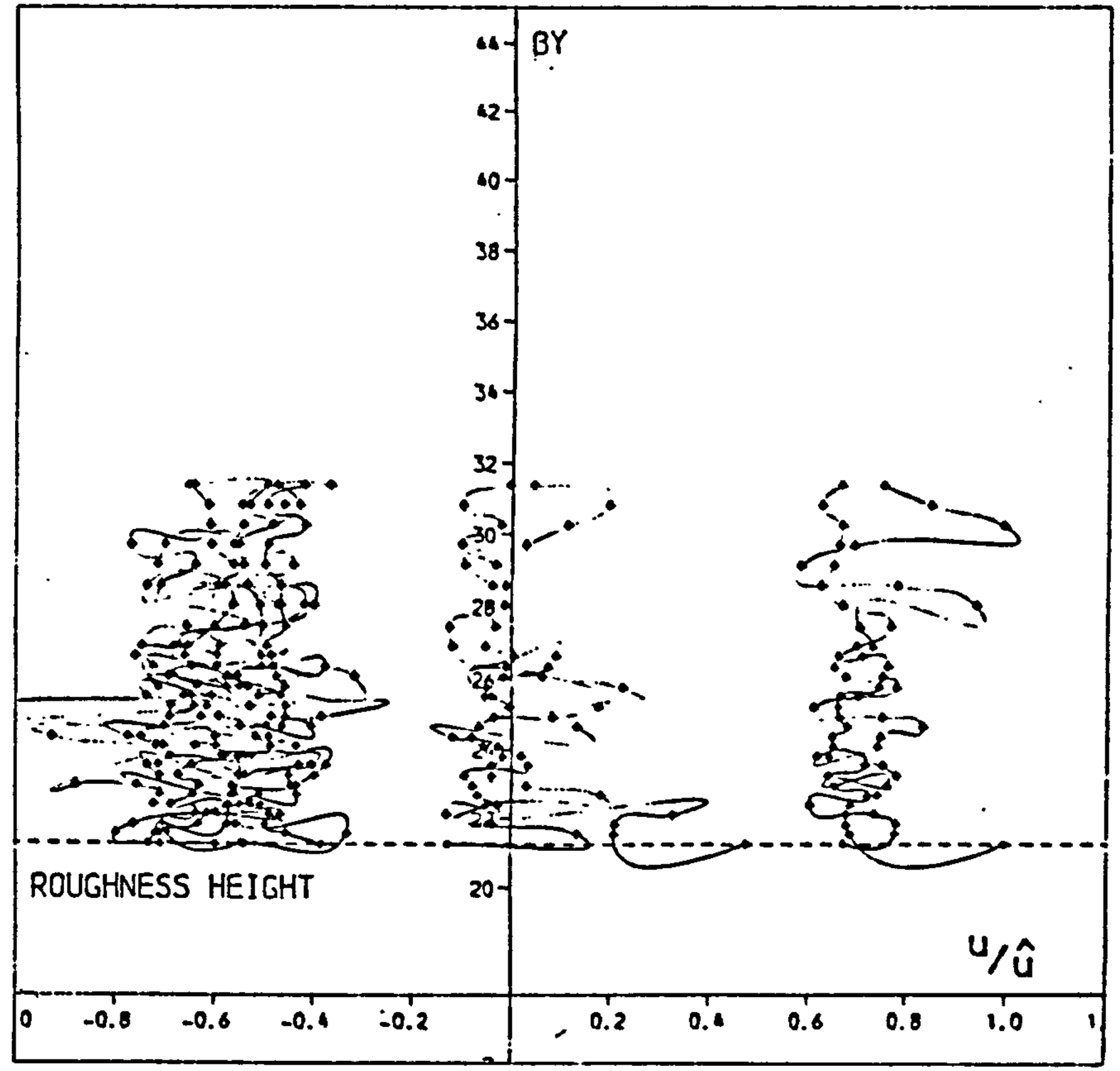

(b)

$\hat{u}$=139.0 mm/s

(iv) T=2.2s , position S

6.15(a) Trough - or - S position

6.15(b) Crest - or - R position

Fig. 6.15 Correlation Coefficient of Boundary Layer Velocity over 3-D rough bed at different heights.

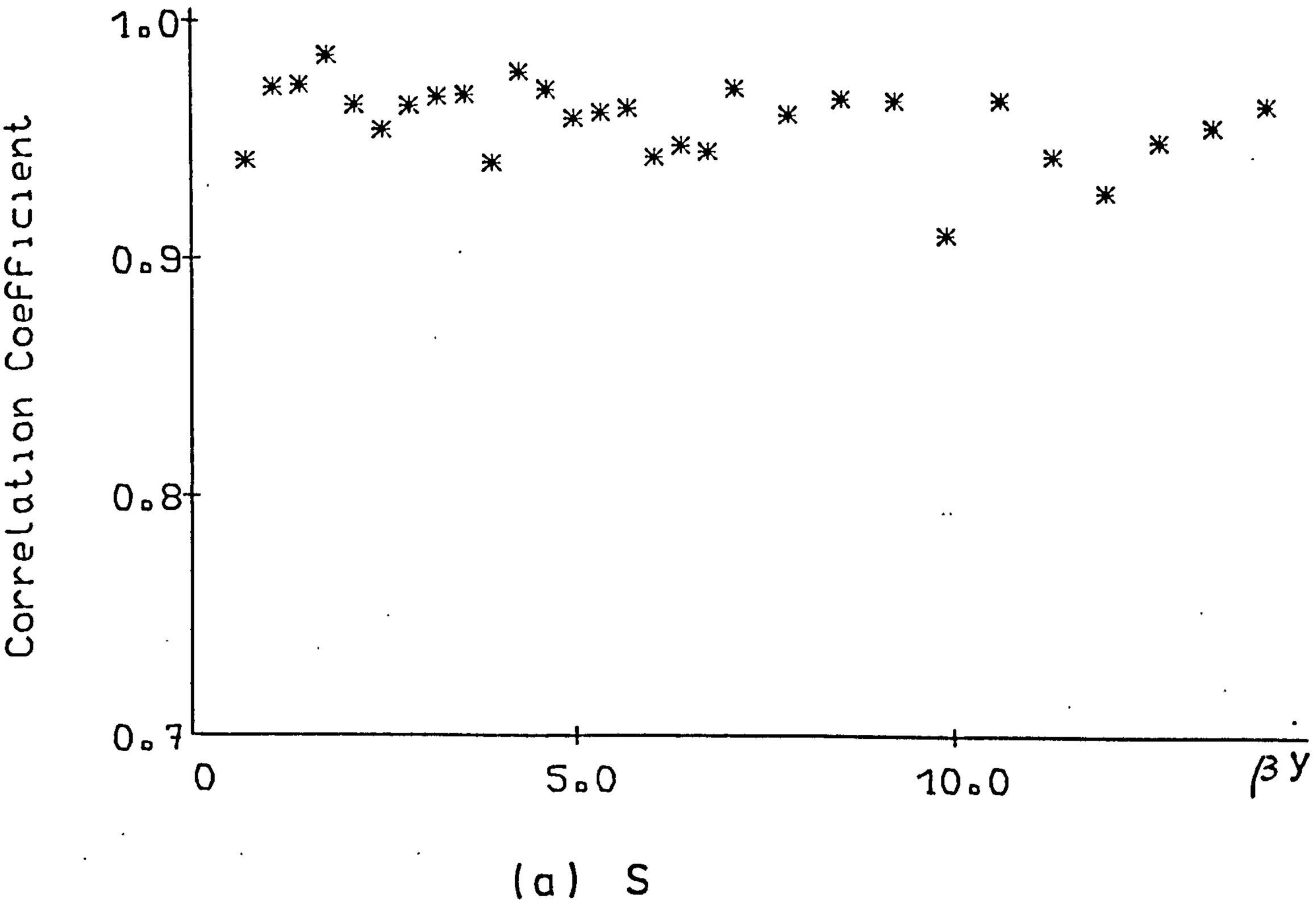
Correlation Coefficient
1.0
0.9
0.8
0.7
0
5.0
10.0
β y

(a) S

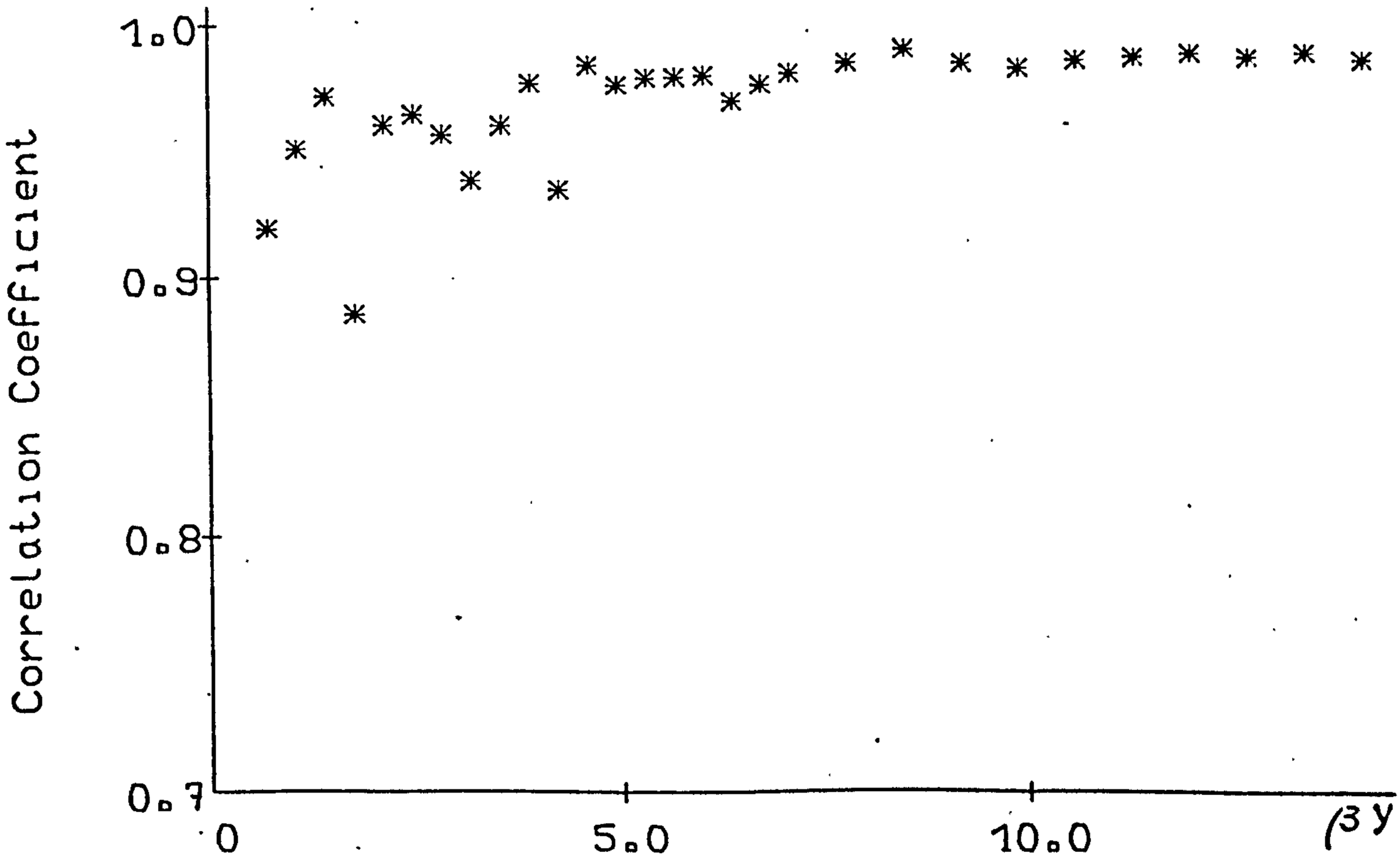
Correlation Coefficient
1.0
0.9
0.8
0.7
0
5.0
10.0
β y

(b) R

(i) T=1.4s

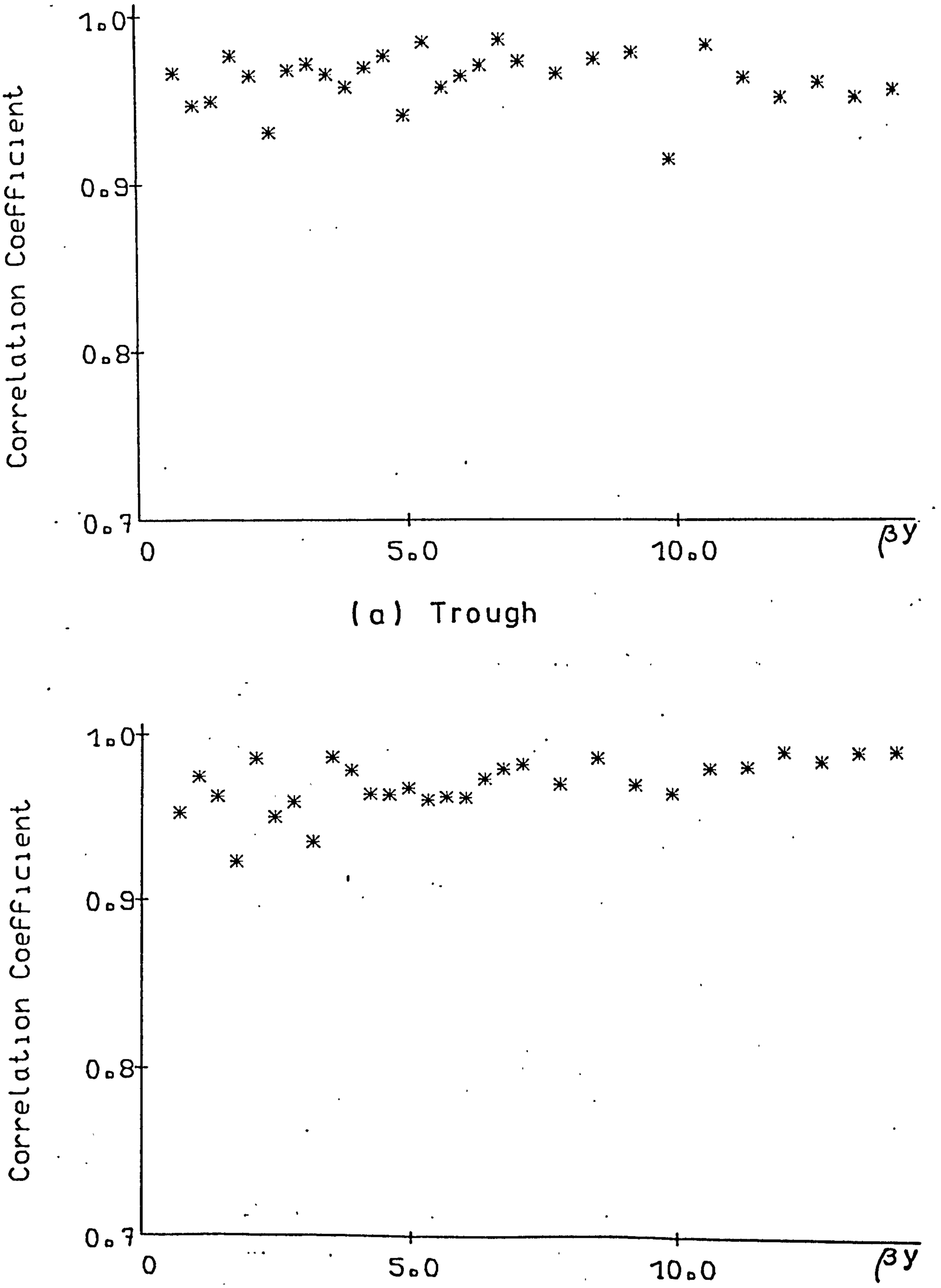

(a) Trough

(b) Crest

(ii) T=1.4 s

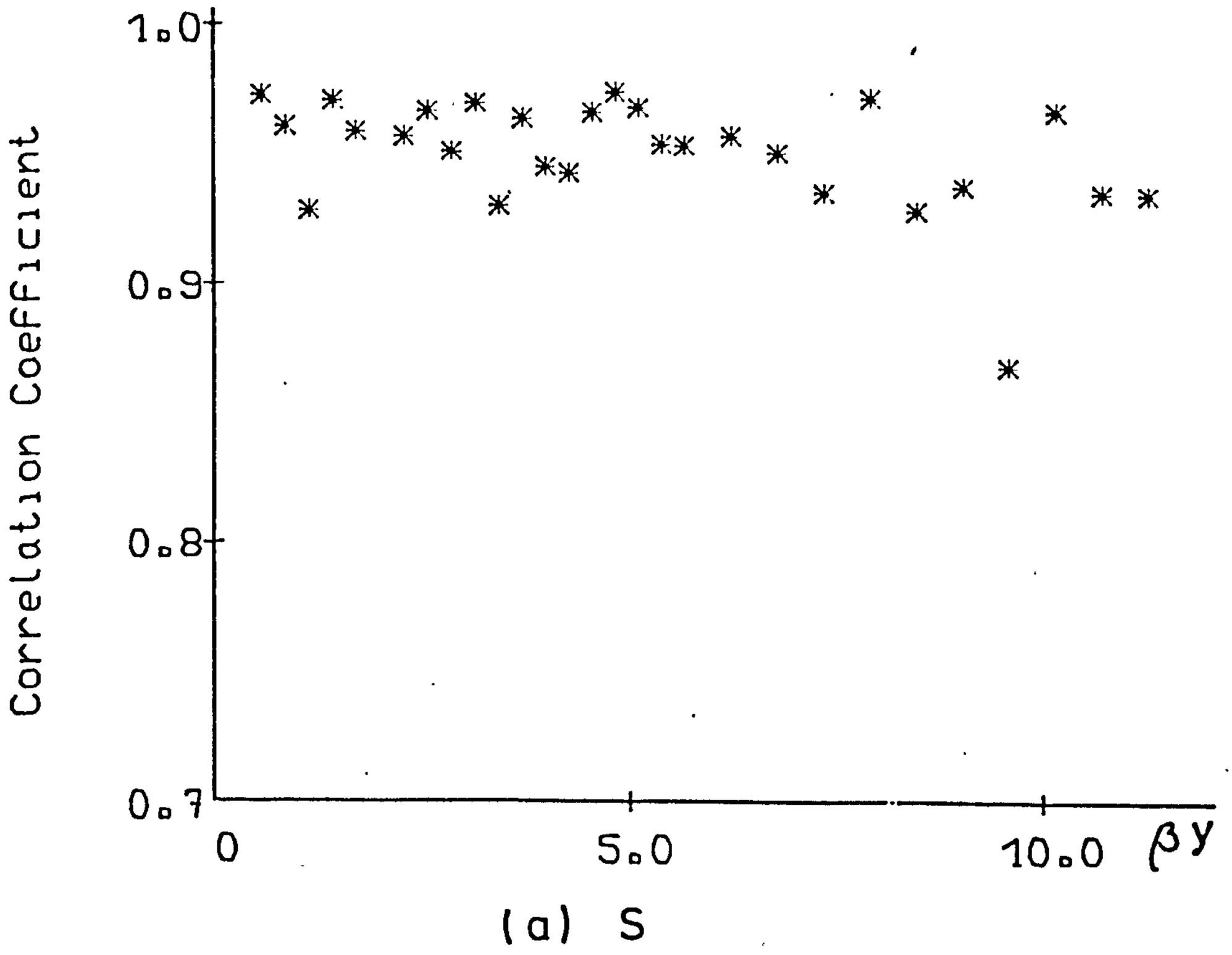

(a) S

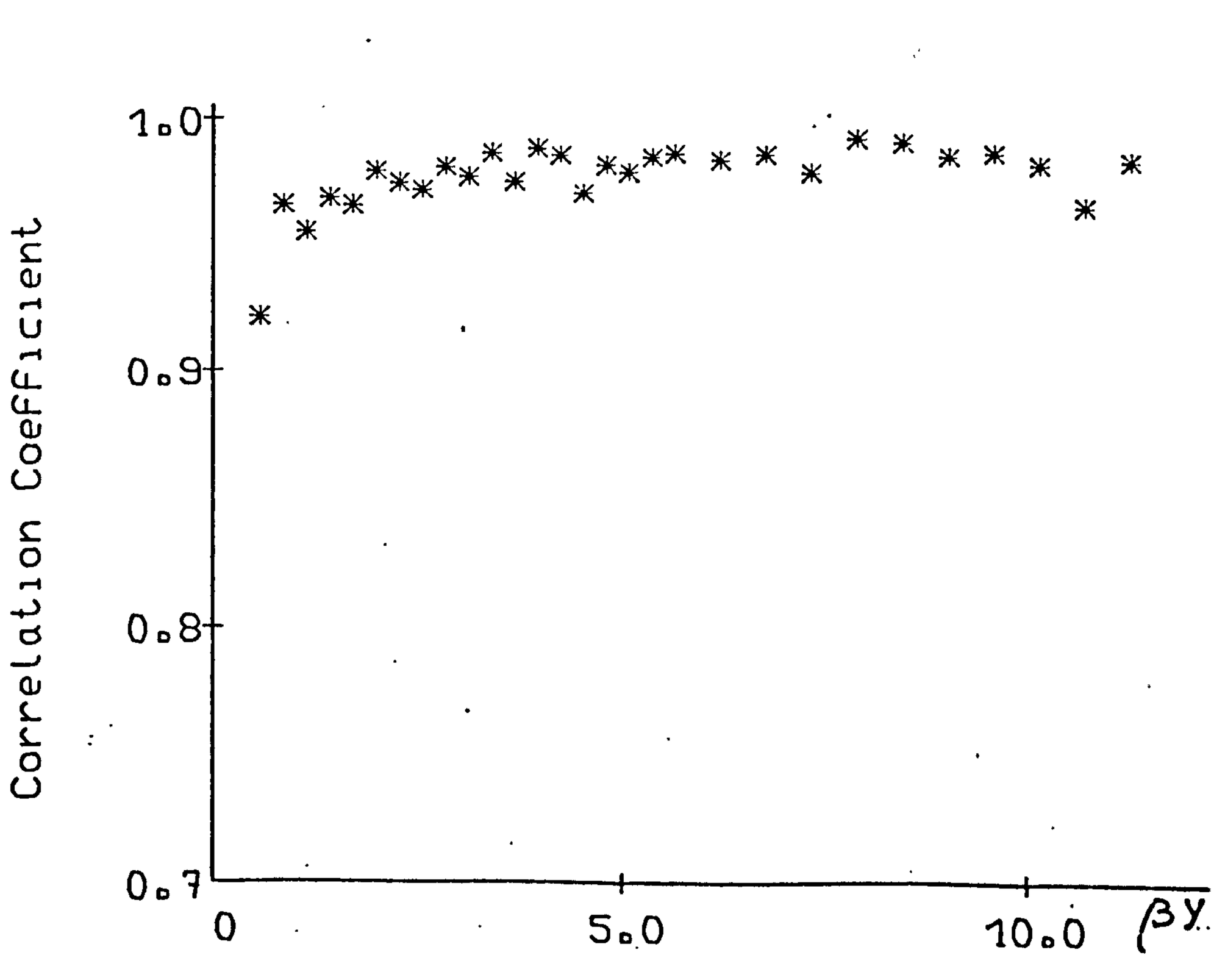

(b) R

(iii) T=2,2s

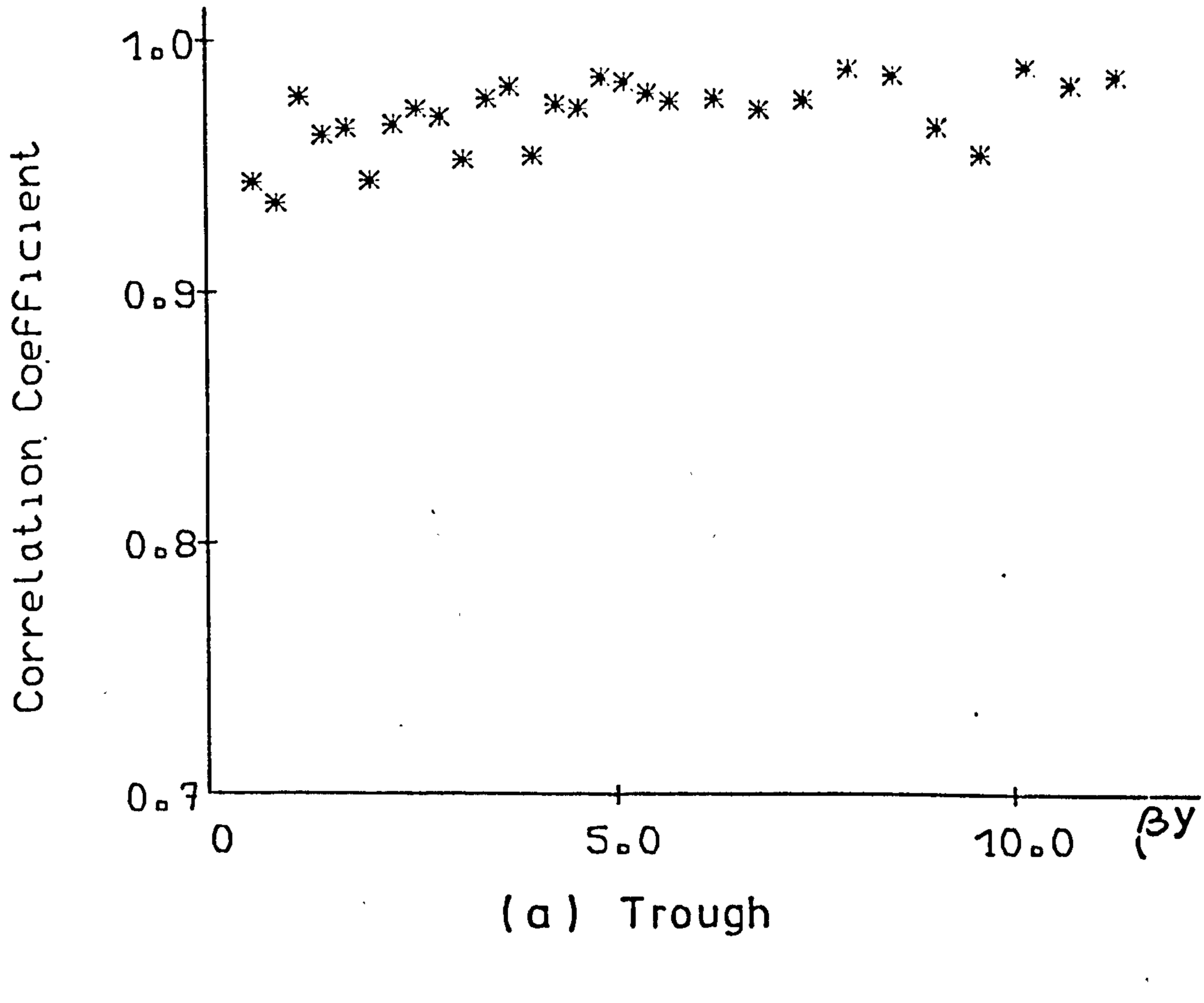

(a) Trough

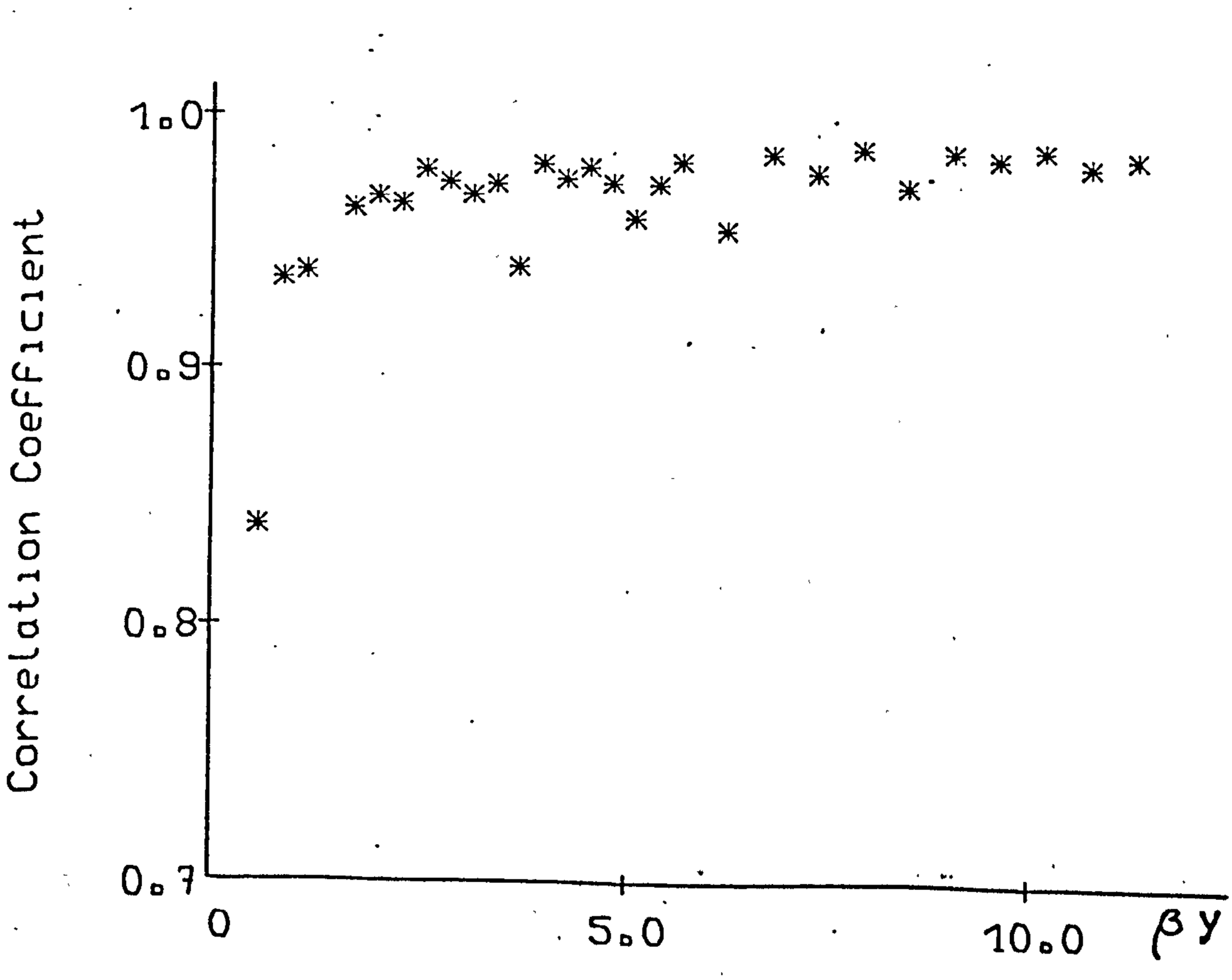

(b) Crest

(iv) T=2.2s

too). The results are more closely correlated, whilst for S it seems that the correlation coefficients up to the observed height varies and no indication of closing to high positive correlation.

However, since the same result was observed for the coefficient over troughs and crests, it is conclusive that the 3-DS trough is a highly turbulent area. This can be explained by a close look at this position on the bed (Fig. 6.16). While the other three positions on the bed

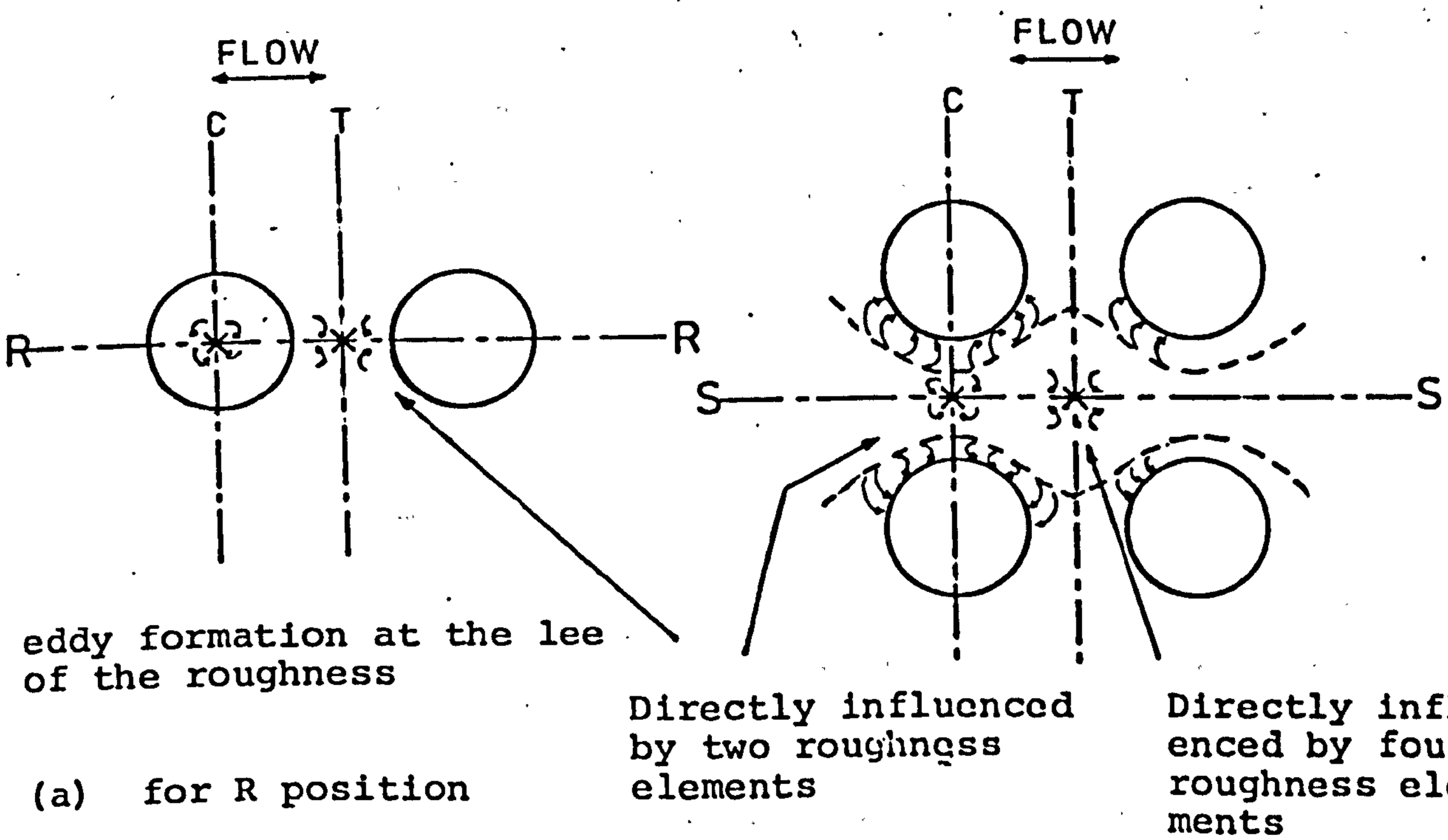

Figure 6.16 The Plan View of Eddy Formation at Different Points for the 3-D Rough Bed.

are influenced by one (3-DR over crest) or two roughness elements directly, the 3-DS trough is influenced by four roughness elements which affect the flow by eddies from all directions and make it more turbulent.

This effect, to some extent, is shown in Fig. 6.17 as well. The velocity distribution over 30 cycles at 1.5 mm and 5 mm above the roughness peaks shows two important features of the velocity distribution. The importance of these is that each phase (of the three arbitrary phases) the 30 points show a distribution more closely approaching a normal one than those for 2-D rough bed. Although the flow might be more turbulent, it is less random because of the smoothness of the roughness elements. (This problem was discussed for the 2-D rough bed and the result for 3-D rough bed makes the assumption valid).

Also since the standard deviation values for the two heights do not differ much, and indeed for some results the S.D. for the 5 mm location is greater than for the 1.5 mm location (unlike for the 2-D rough bed) this shows that the flow at the edge of the boundary layer is as turbulent as the flow inside the boundary layer thickness. Table 6.4 shows the turbulence intensity values are greater for S position than R position, and very little difference exists for values at different depths or even different periods (which was noticed for the 2-D rough bed results).

More about the influence of 3-D roughness on flow is

*	1.5 mm height over rough bed
o	5 mm height over rough bed
SD	Standard Deviation
O.O-1.O	The range of the data.

Fig. 6.17 The Velocity Distribution for 3 arbitrary phases (a, b, c) and mean velocity (d) over 30 cycles over 3-D rough bed.

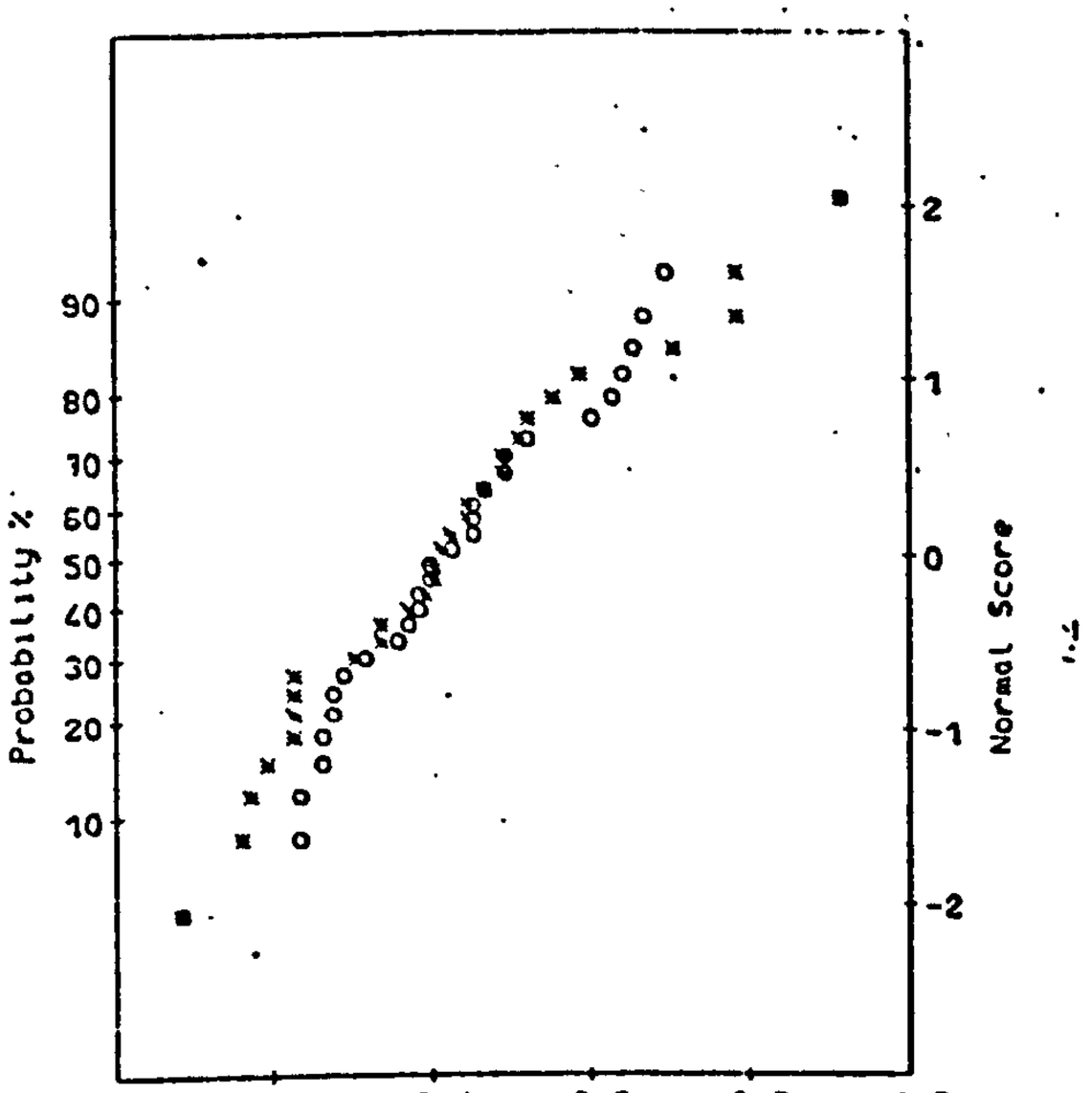

	SD	Mean	1.0	0.0
×	20.8	170.7	231.3	127.0
o	14.8	169.8	217.0	133.2

(a)

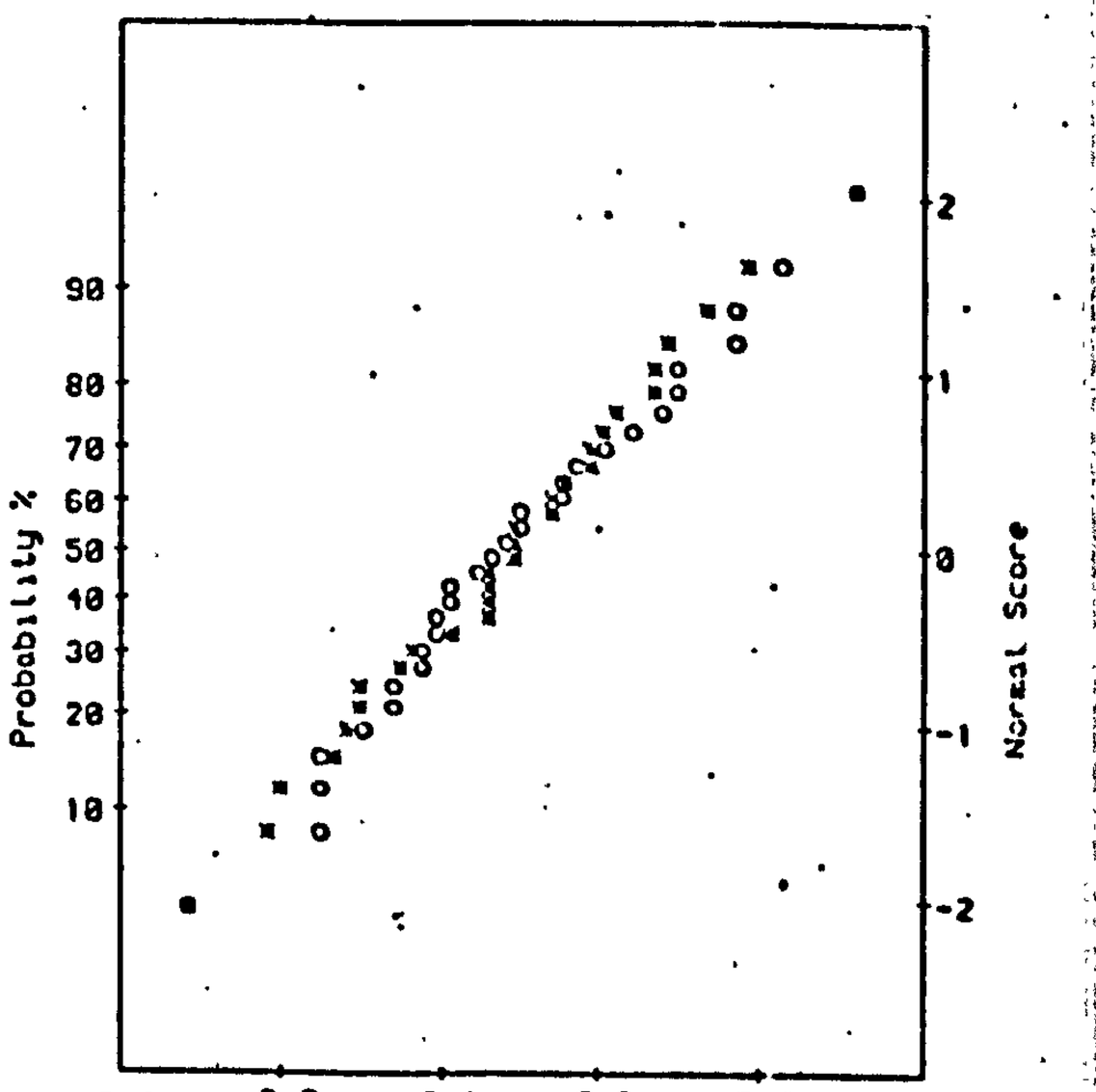

	SD	Mean	1.0	0.0
×	13.4	−164.6	−128.5	−198.5
o	12.4	−175.9	−143.9	−207.1

(b)

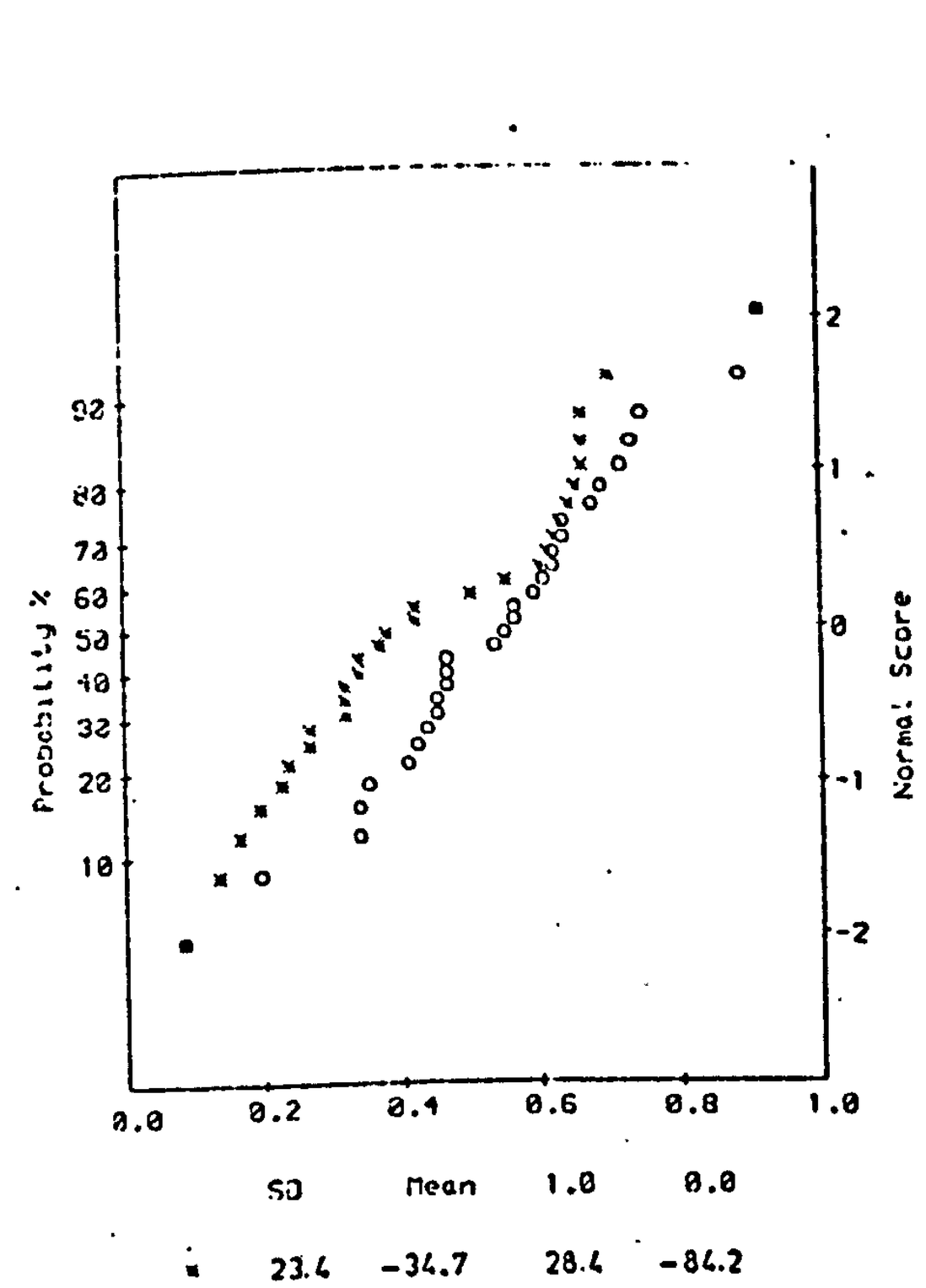

	SD	Mean	1.0	0.0
×	23.4	−34.7	28.4	−84.2
o	14.9	−48.3	−10.8	−91.9

(c)

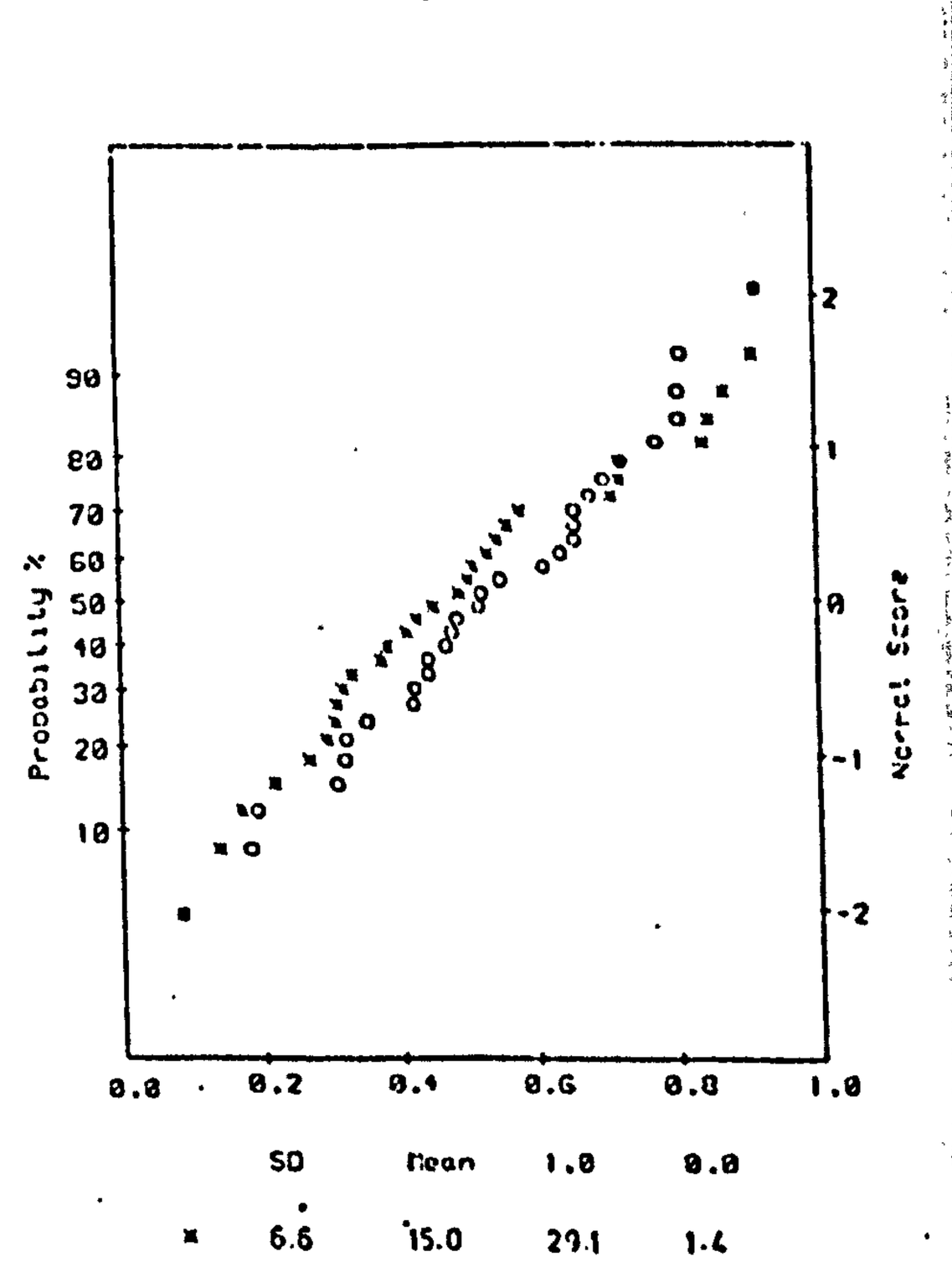

	SD	Mean	1.0	0.0
×	6.6	15.0	29.1	1.4
o	5.1	10.1	21.6	−2.9

(d)

(i) T = 1.4 s, R

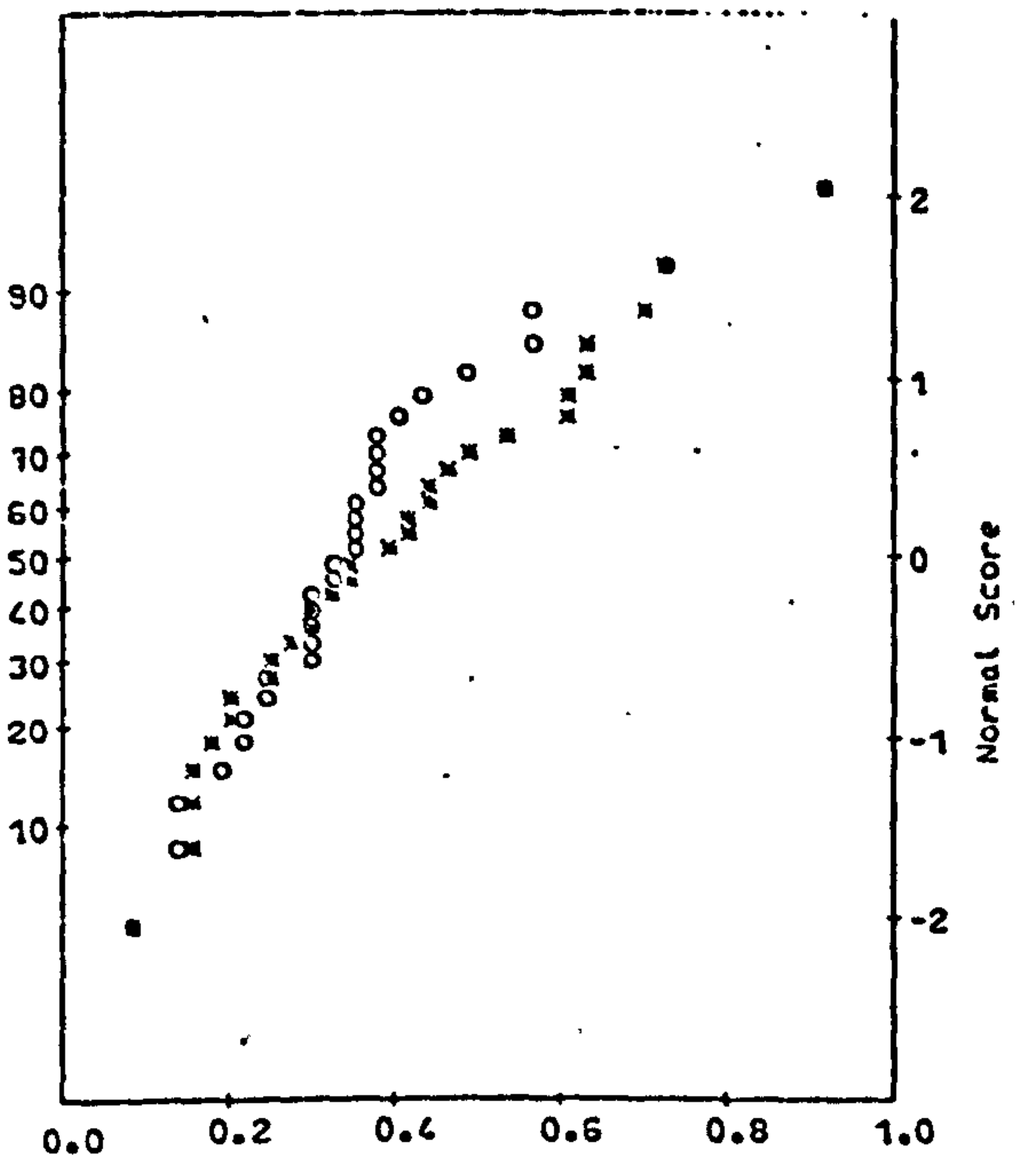

	SD	Mean	1.0	0.0
x	32.5	228.0	324.5	164.2
o	24.3	197.1	288.6	146.8

(a)

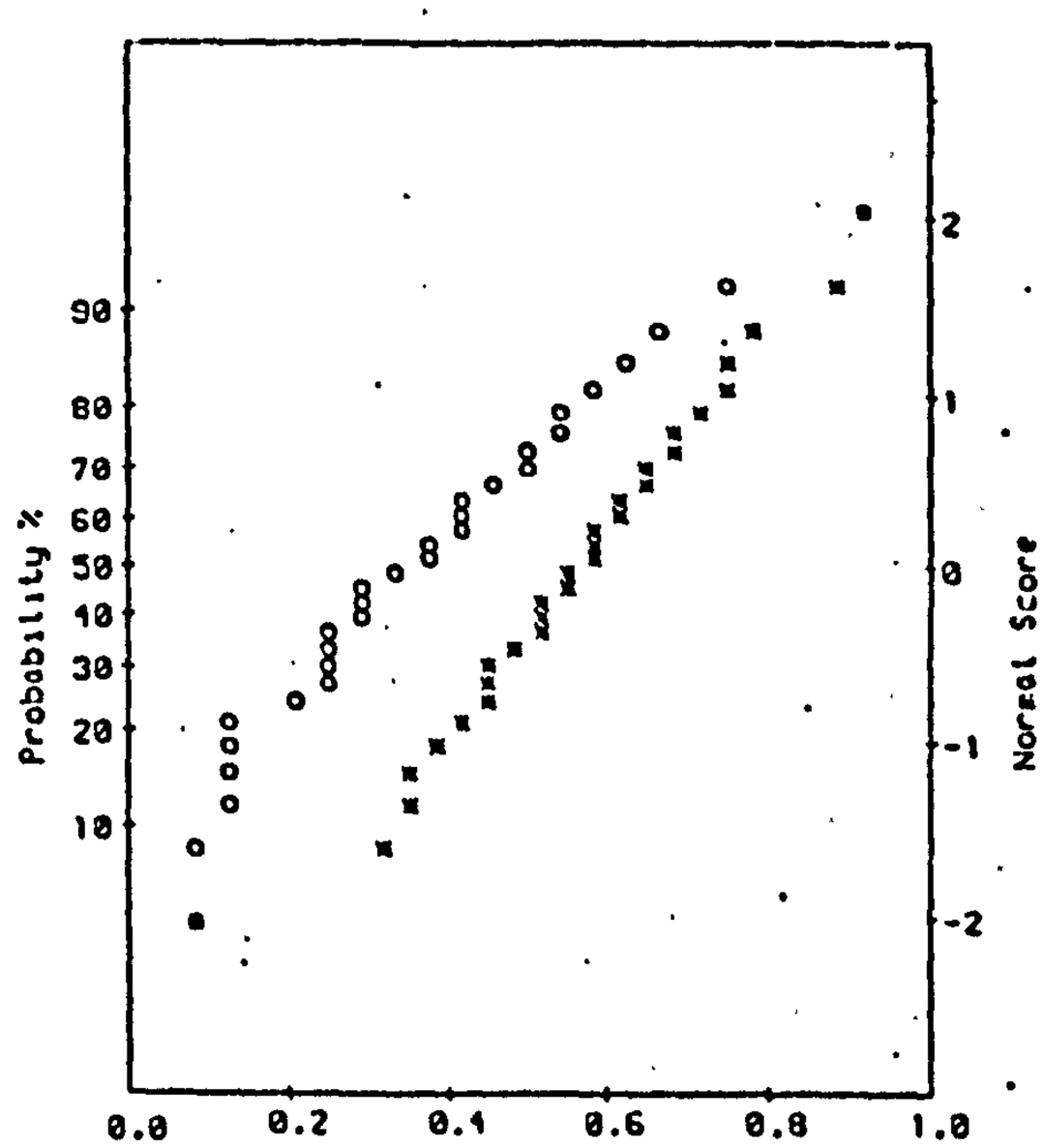

	SD	Mean	1.0	0.0
x	20.2	-191.0	-140.8	-255.2
o	19.1	-181.1	-123.7	-215.1

(b)

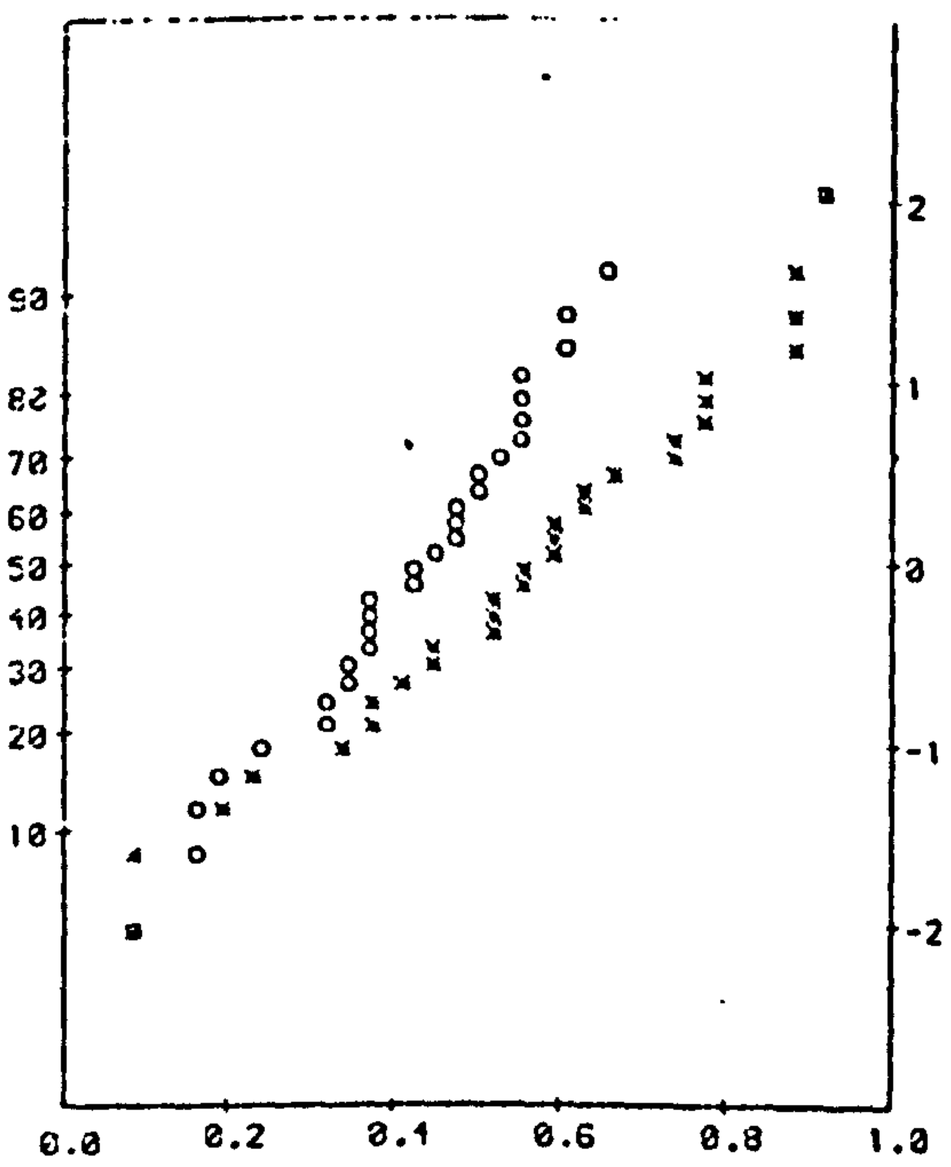

	SD	Mean	1.0	0.0
x	24.2	-112.1	-65.3	-170.6
o	25.0	-92.1	-8.5	-154.9

(c)

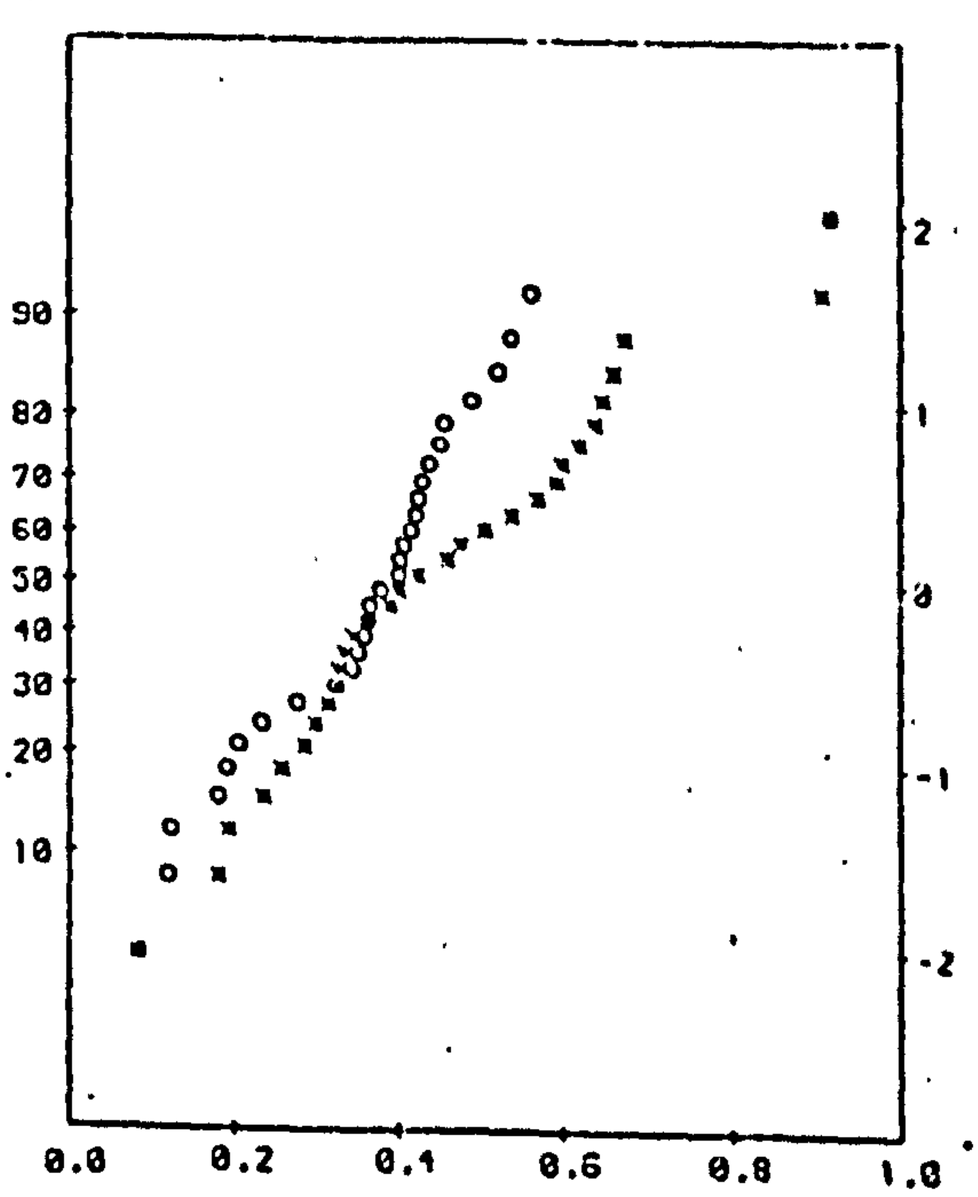

	SD	Mean	1.0	0.0
x	10.1	17.2	44.8	-5.3
o	9.5	14.2	51.1	-7.5

(d)

(ii) T = 1.4 s, S

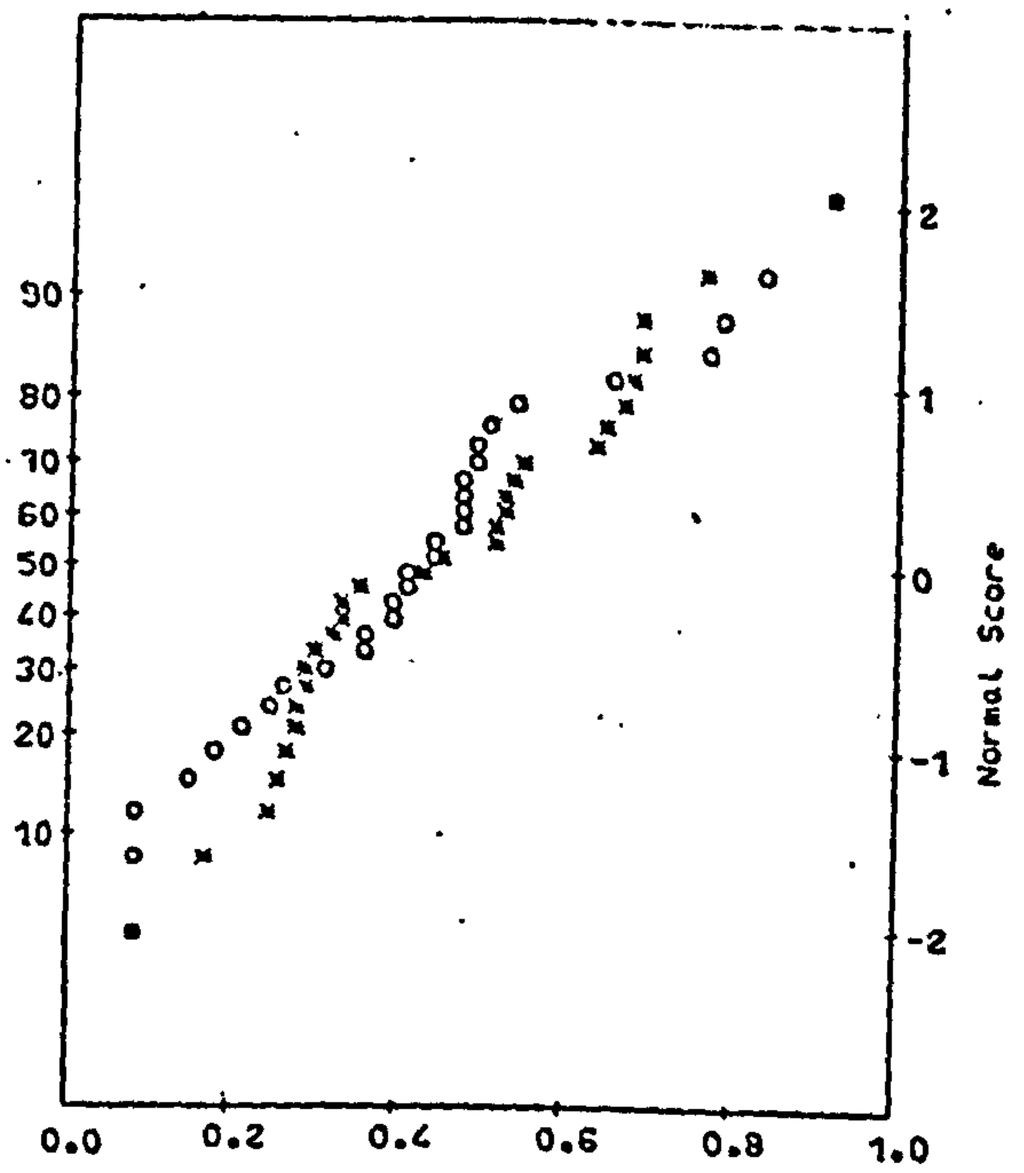

	SD	Mean	1.0	0.0
x	21.1	27.0	85.0	−20.7
o	15.2	15.4	55.7	−14.3

(a)

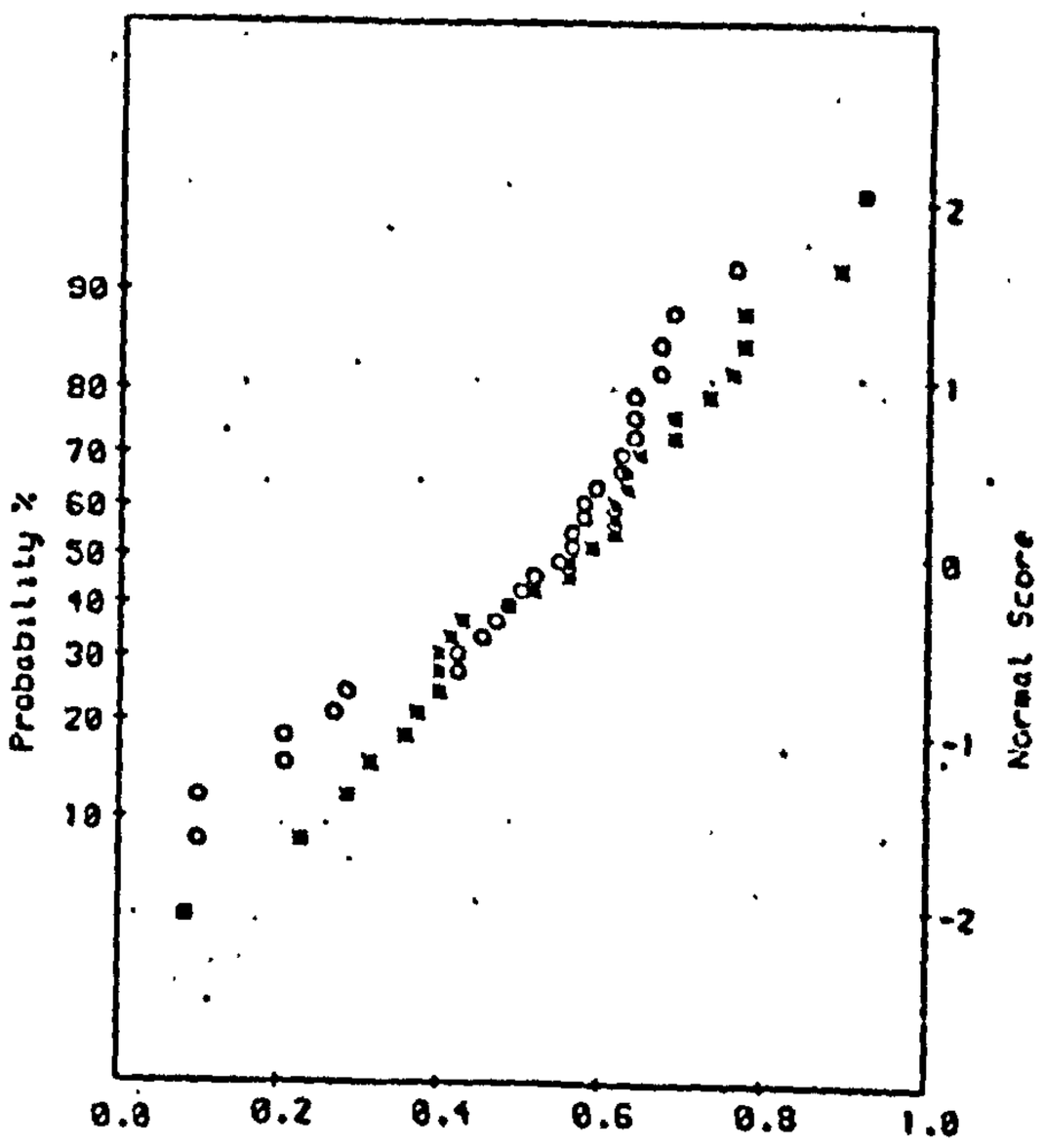

	SD	Mean	1.0	0.0
x	15.7	−125.1	−88.8	−168.4
o	15.3	−118.8	−81.2	−155.4

(b)

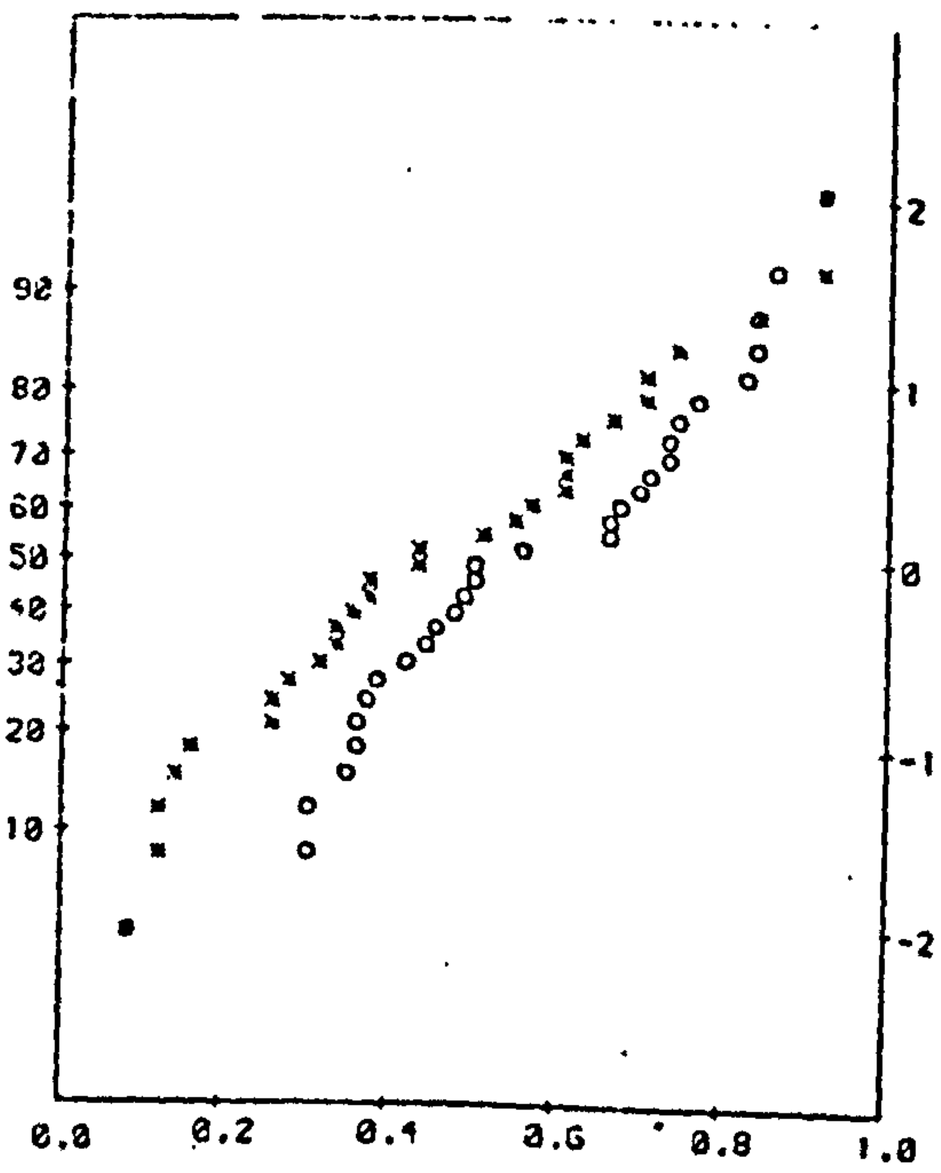

	SD	Mean	1.0	0.0
x	14.2	−130.1	−98.5	−157.5
o	20.6	−123.2	−80.4	−179.1

(c)

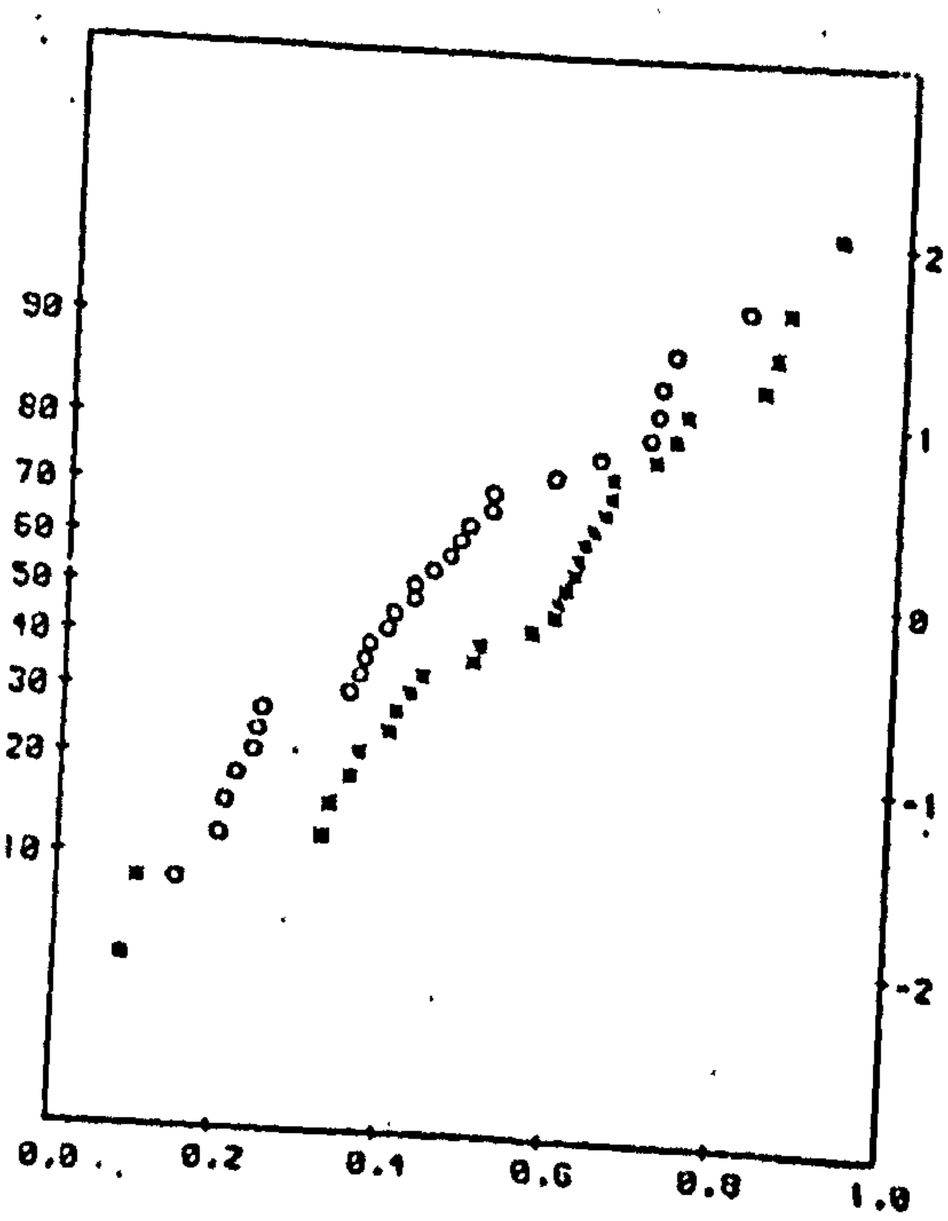

	SD	Mean	1.0	0.0
x	3.8	−43.0	−34.8	−53.1
o	6.1	−36.9	−22.8	−51.8

(d)

(iii) T = 2.2 s, S

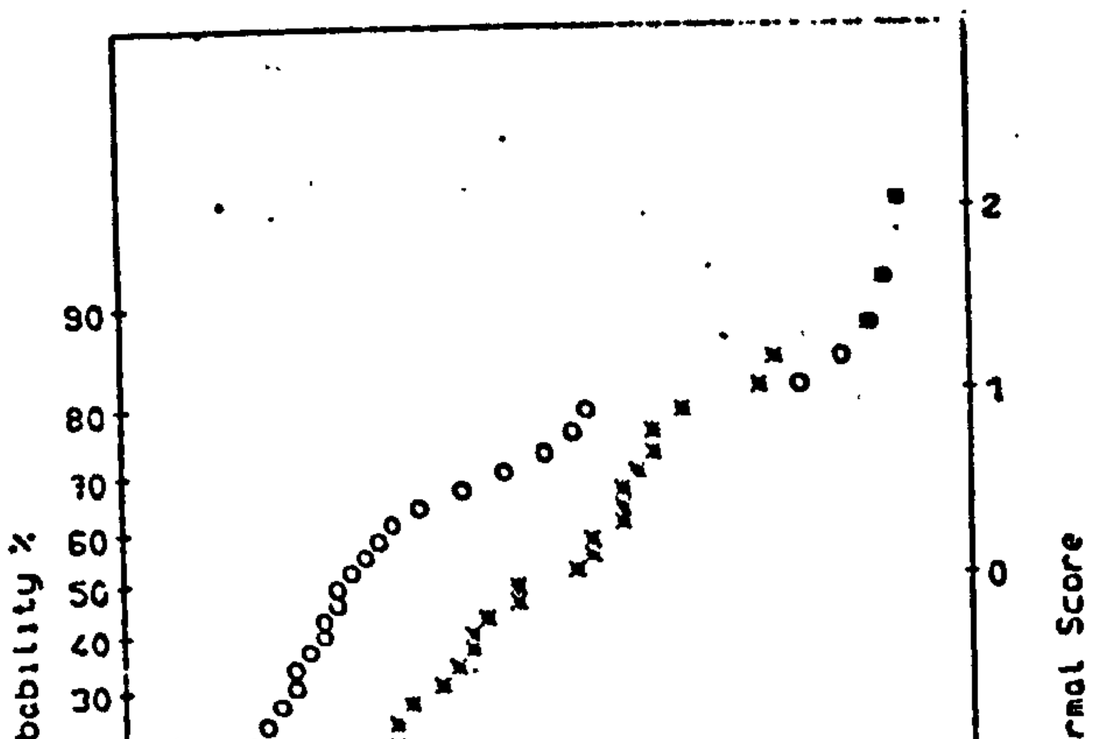

	SD	Mean	1.0	0.0
×	13.6	21.4	52.9	−10.4
o	17.9	25.7	69.3	0.7

(a)

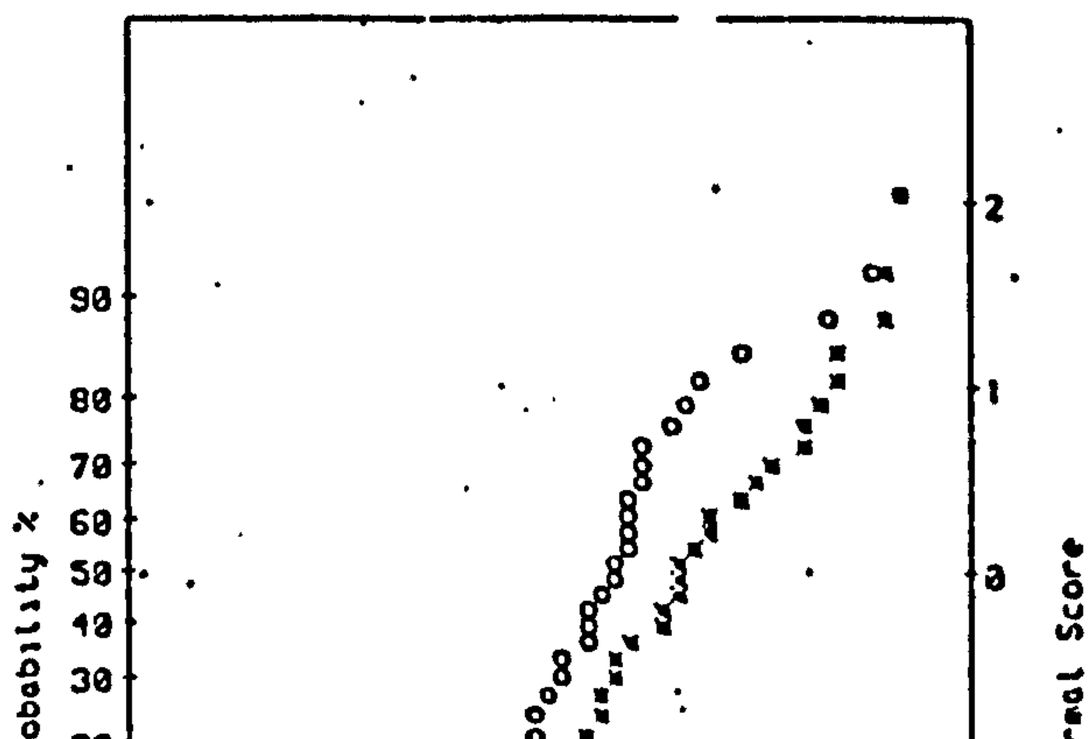

	SD	Mean	1.0	0.0
×	11.1	−85.1	−63.9	−125.8
o	12.0	−88.8	−58.9	−127.5

(b)

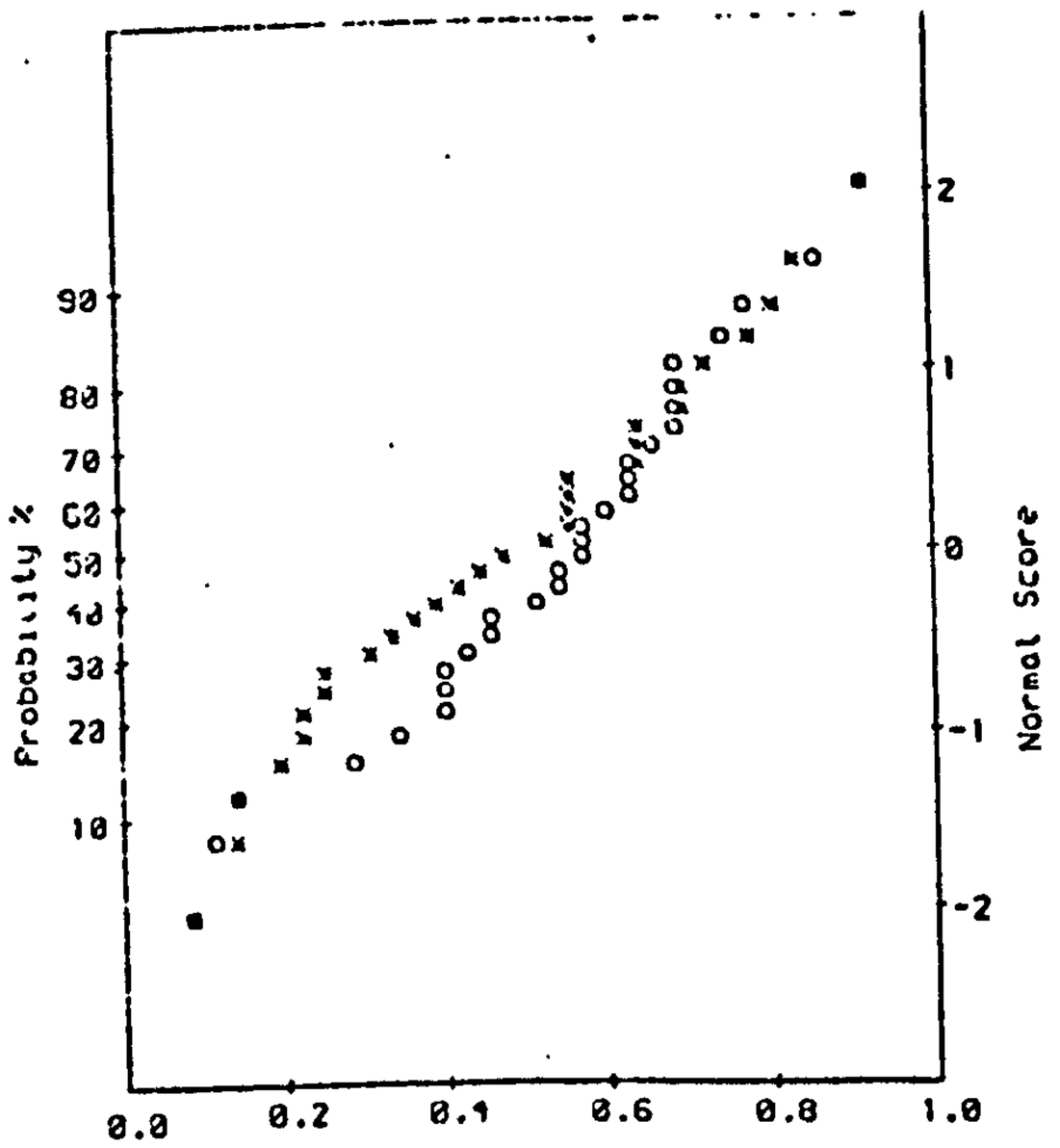

	SD	Mean	1.0	0.0
×	9.5	−84.9	−63.4	−104.6
o	8.1	−86.7	−68.1	−107.9

(c)

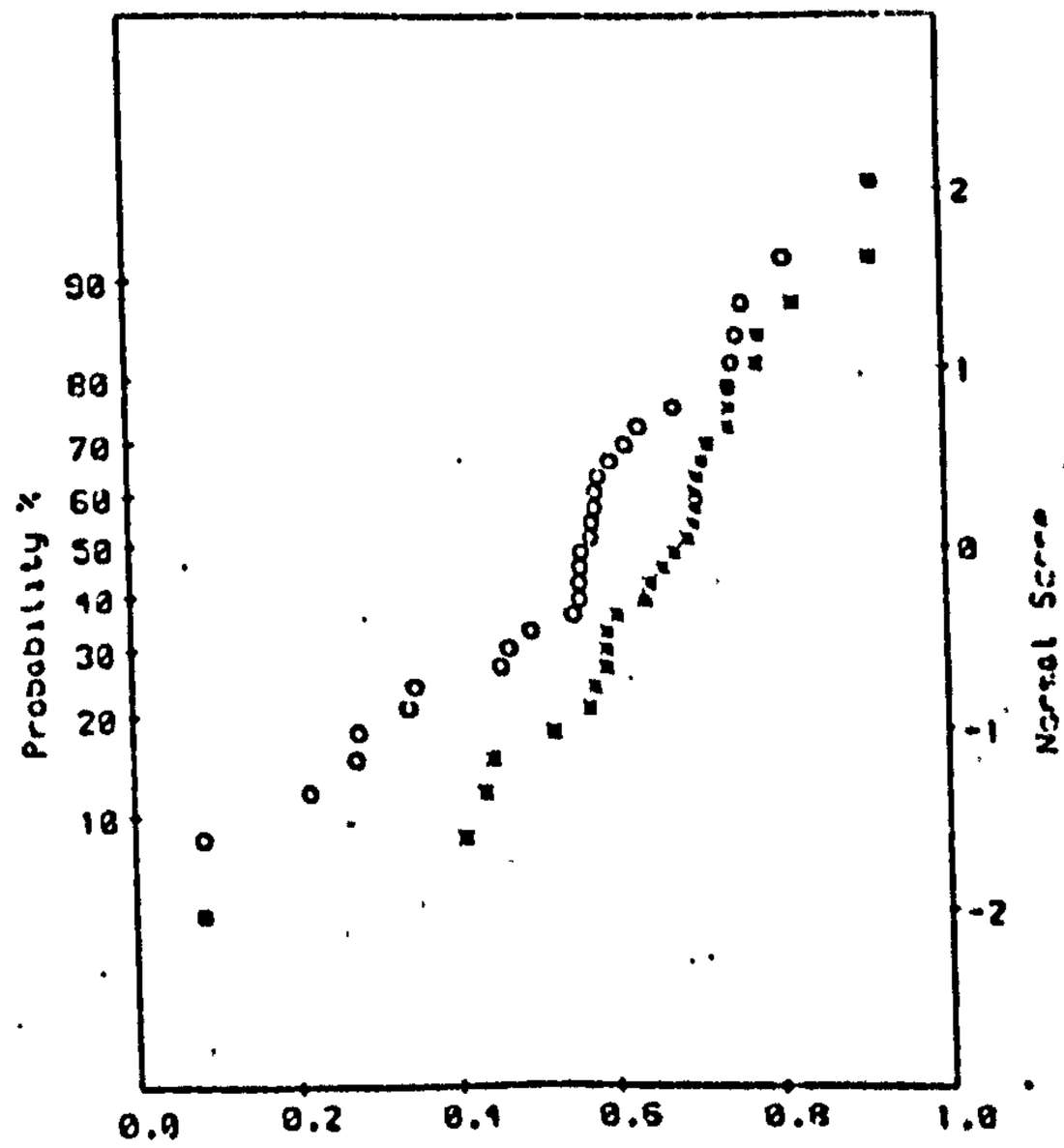

	SD	Mean	1.0	0.0
×	2.9	−13.7	−7.3	−25.3
o	3.0	−14.6	−7.8	−22.5

(d)

(iv) T = 2.2 s, R

T/sec	T.I. %				$Re = \frac{\hat{U}_\infty \kappa}{\nu}$
	R position		S position		
	1.5 mm	5 mm	1.5 mm	5 mm	
1.4	11	8	11	9	4683
2.2	9	11	15	15	3178

Table 6.4. Re and T.I. values for 3-D rough bed.

discussed in the next section when the flow is compared for smooth, 2D and 3-D rough beds.

6.4 The Influence of Roughness on Boundary Layer Velocity

The influence of roughness on the flow can only be studied when it is compared with the situation which is very close to the theoretical predictions and hence flow over smooth bed would be the basis for comparison.

Also for the rough beds results there is more than one choice, since the velocity profile over trough and crest at each period has been observed. But knowing the relationship between the two sets of results (and for 3-D rough bed, the 4 sets of results) from the correlation coefficient graphs, either of the profiles can be selected. Either choice has advantages and disadvantages, but probably the profile over the crest (and for 3-D rough bed at R) having a solid base makes a better choice, especially when the turbulent effect (in the case of 3-DR trough, and 3-DS trough and crest) has interfered with the flow to the extent that the laminar velocity profile is eliminated (Fig. 6.14).

Fig. 6.18 shows the velocity profile at each phase on individual graphs (10 graphs for each period). It illustrates the relationship and correlation which exist between the velocity profile for the three different types of bed. While the velocity over the 3-D rough bed is increased in modulus and is perturbed, relative to the smooth bed result, very little differences in the velocity values is observed for

6.18(a) $T = 1.4$ s, $\hat{U} = 320$ mm/s

✛ 3-D rough bed

✠ 2-D rough bed

♦ Smooth bed

6.18(b) $T = 2.2$ s, $\hat{U} = 220$ mm/s

Fig. 6.18 Boundary Layer Velocity Profile (10 phases in a cycle).

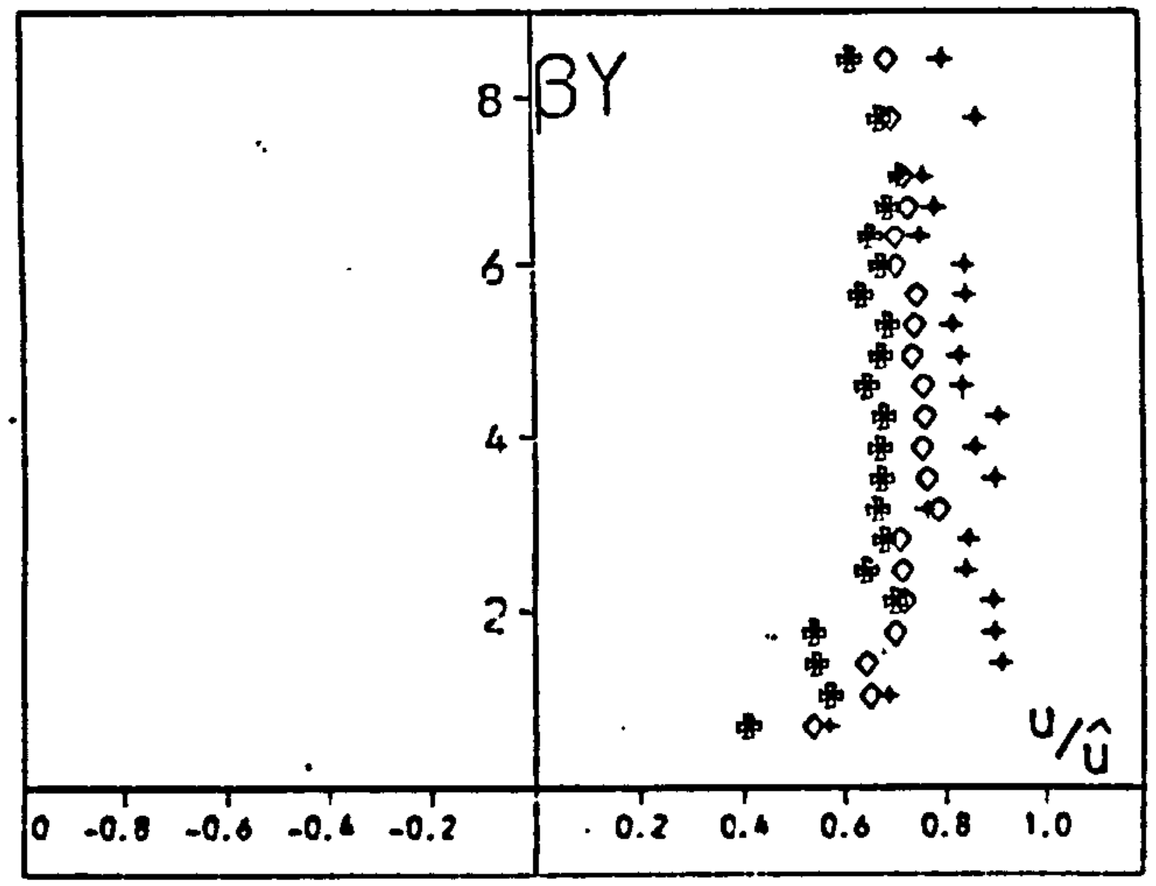

(a)

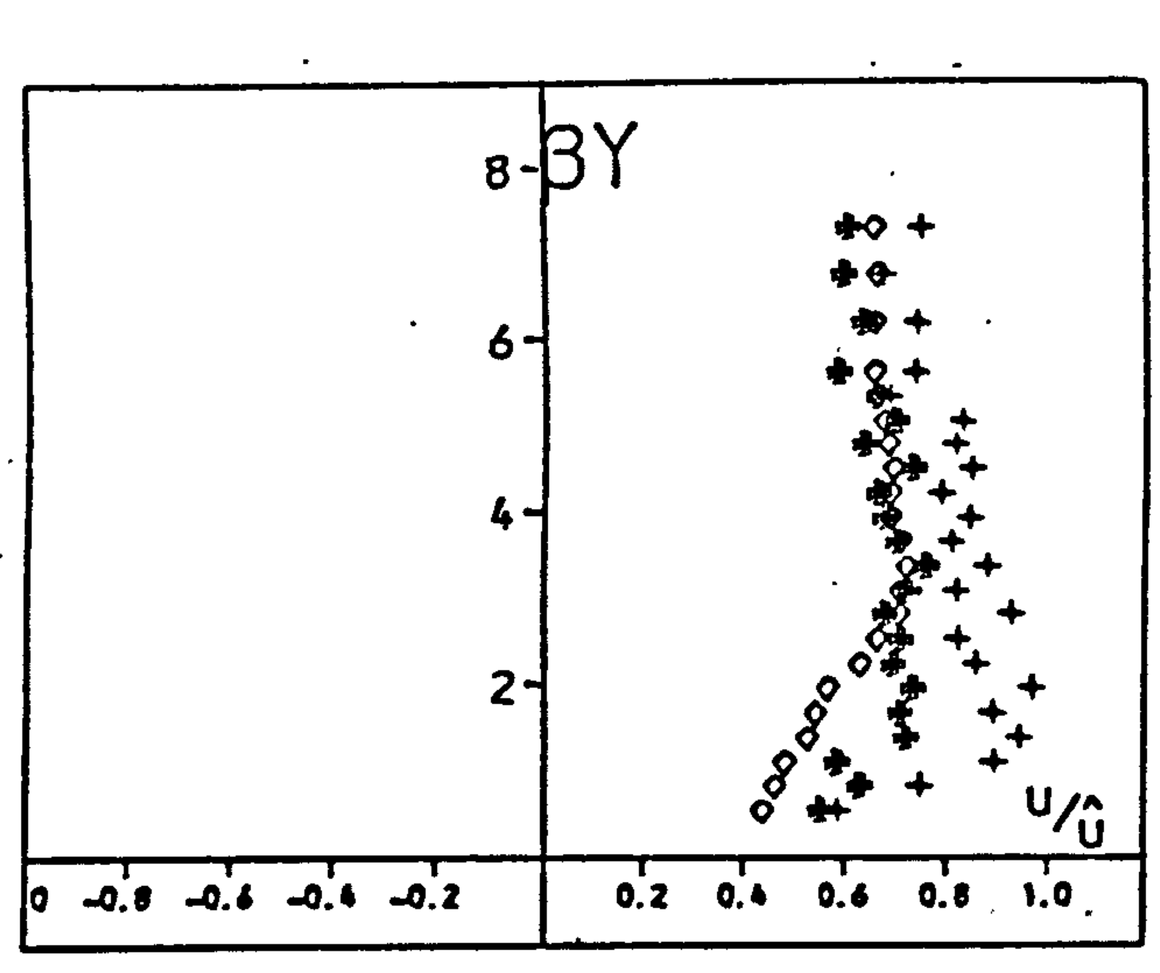

(b)

(i) t_1

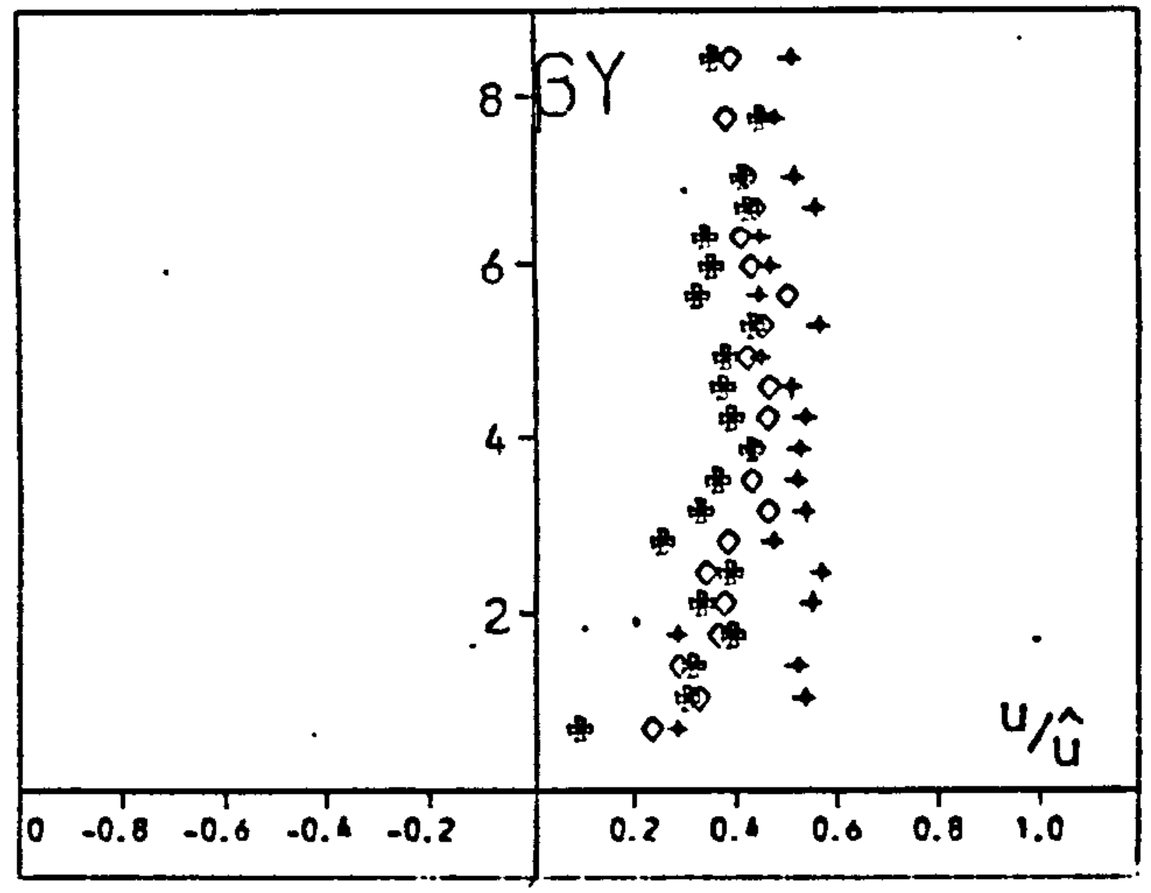

(a)

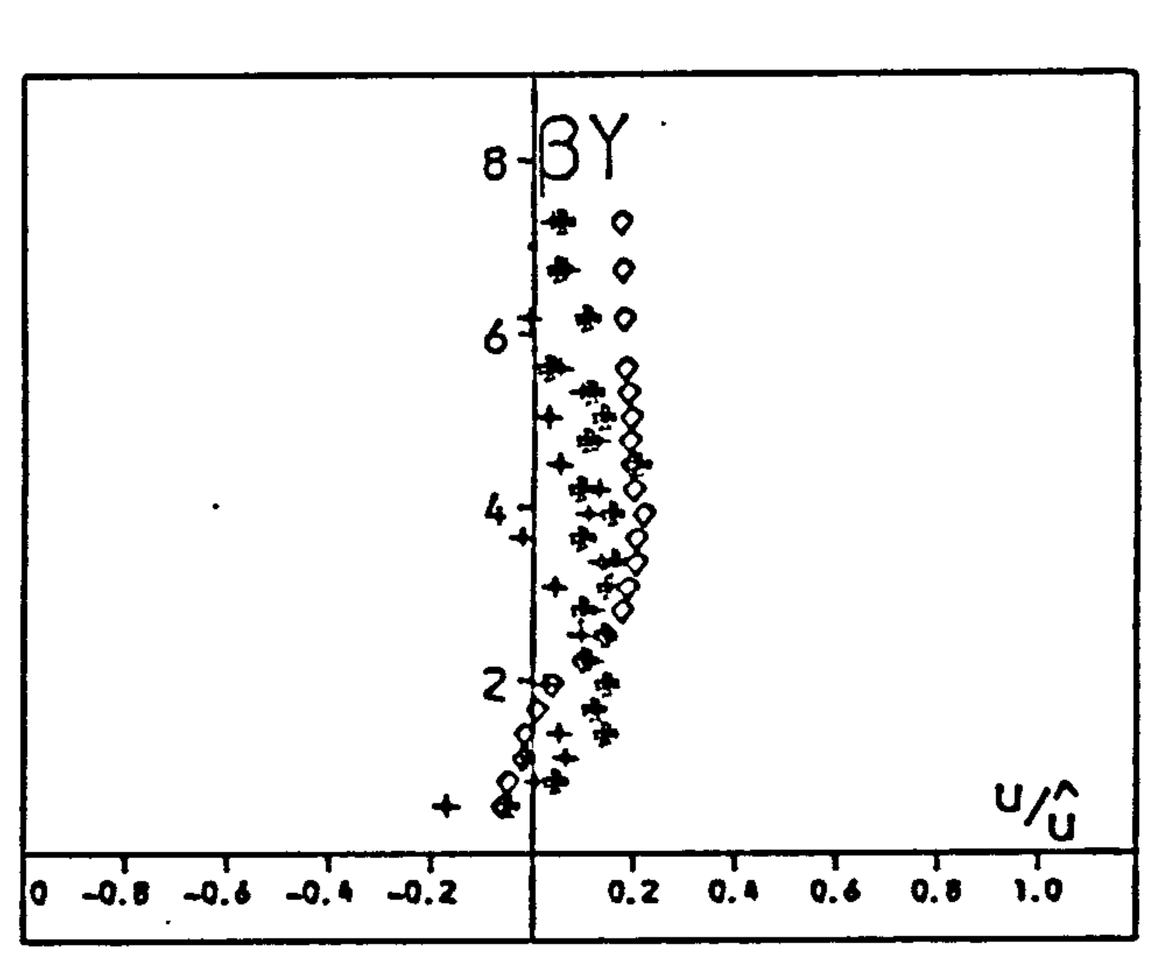

(b)

(ii) t_2

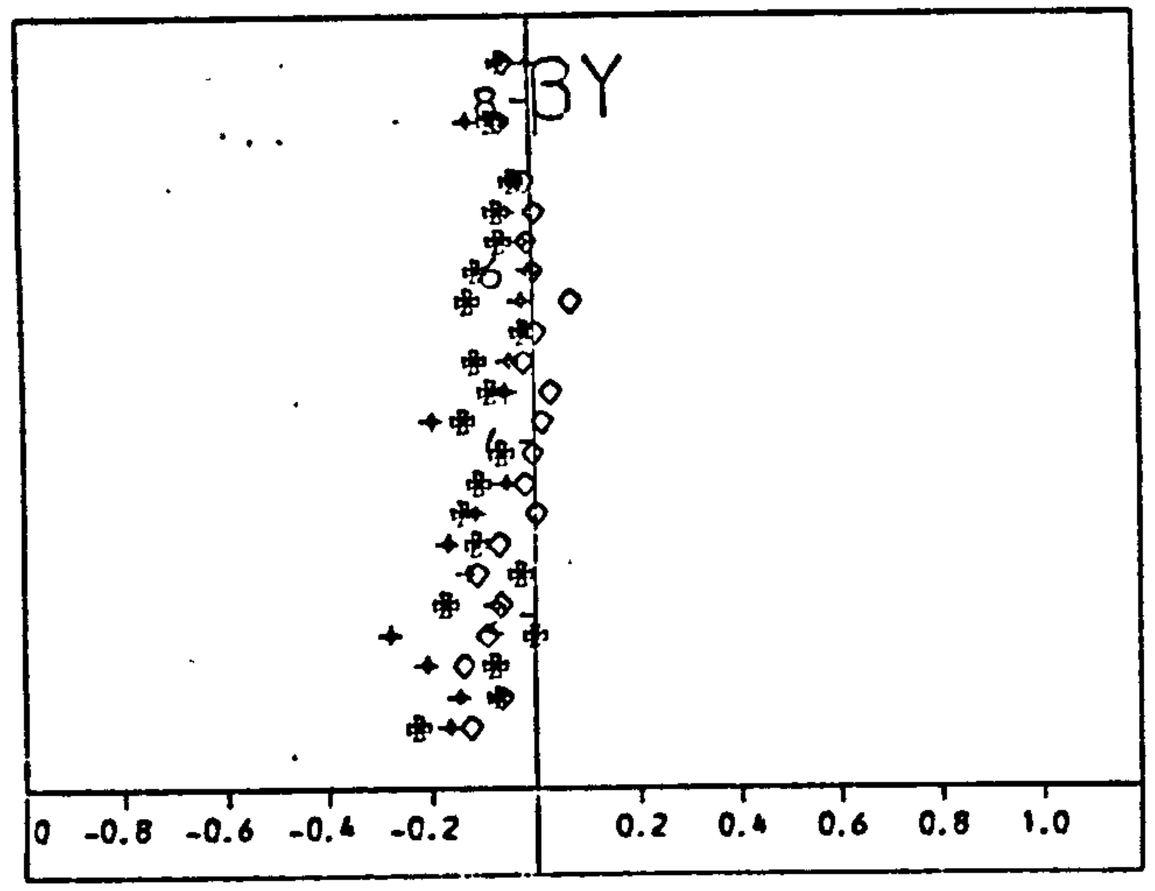

(a)

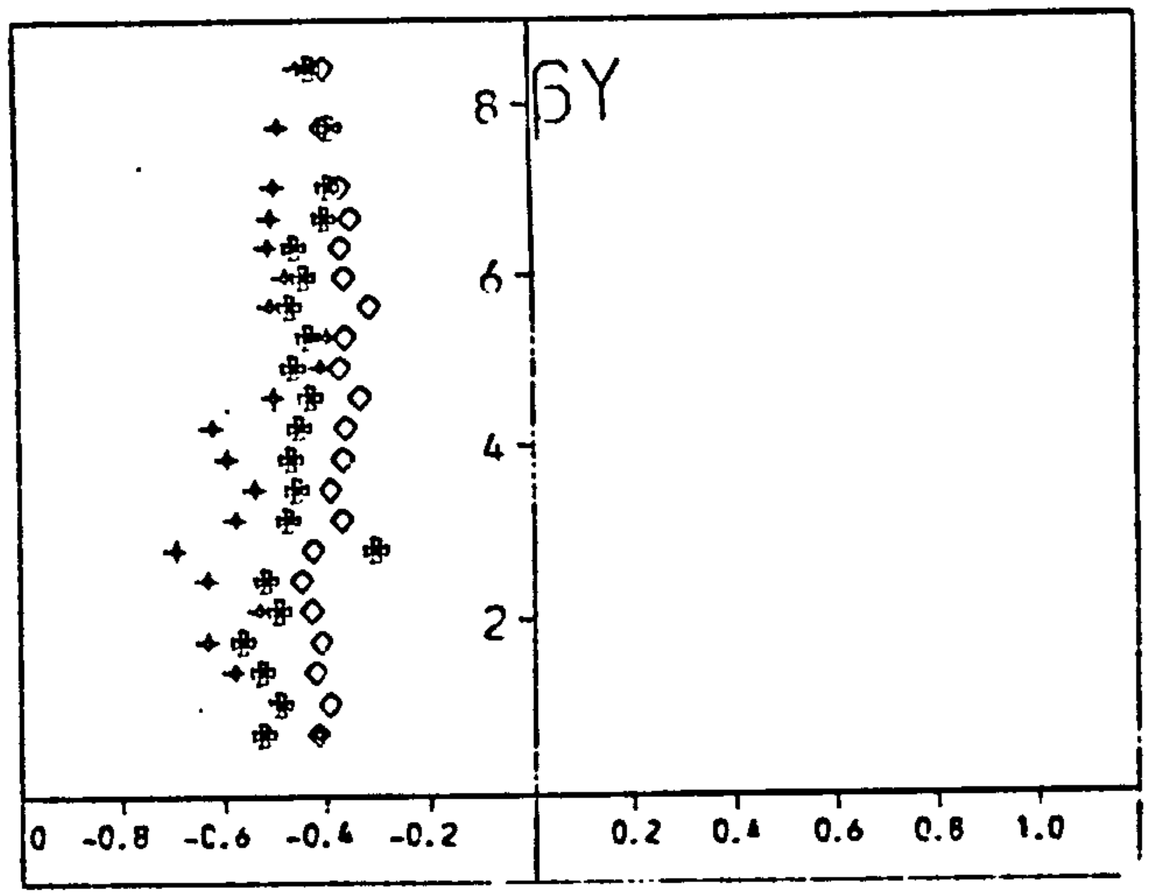

(a)

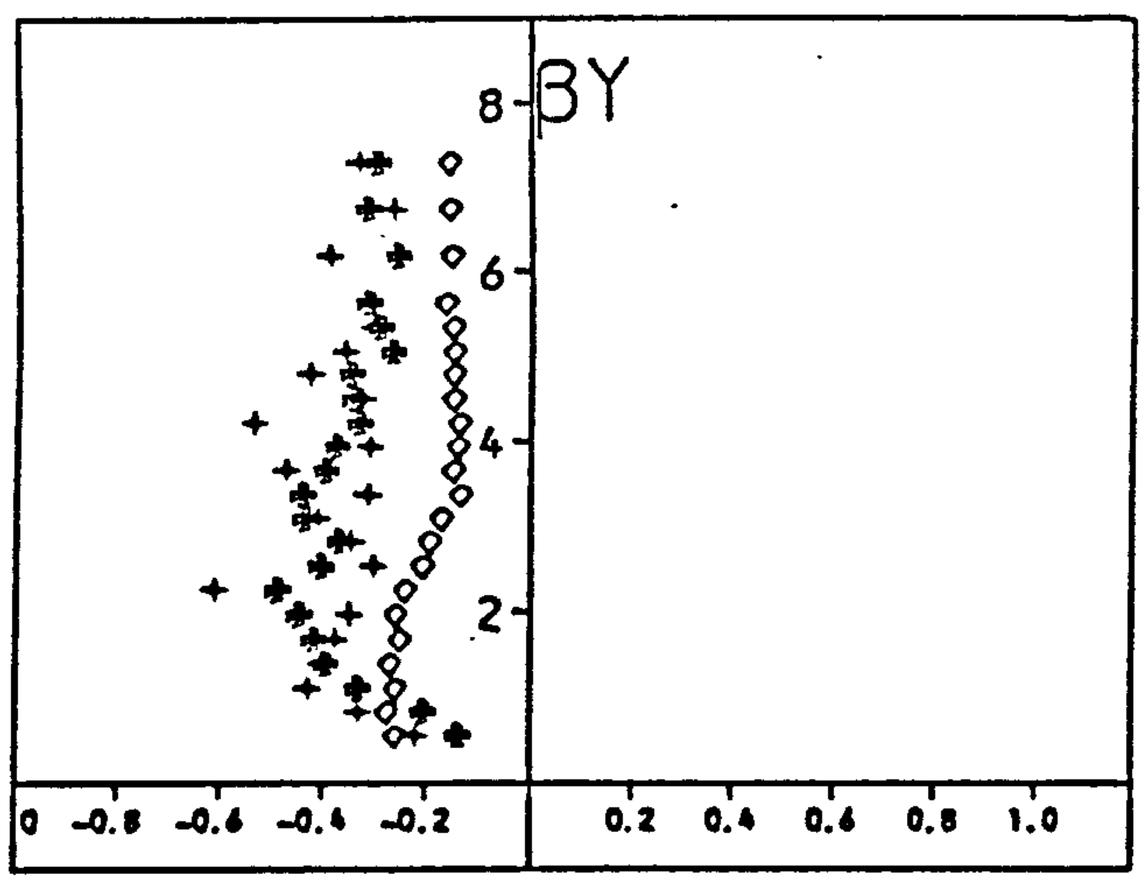

(b)

(iii) t_3

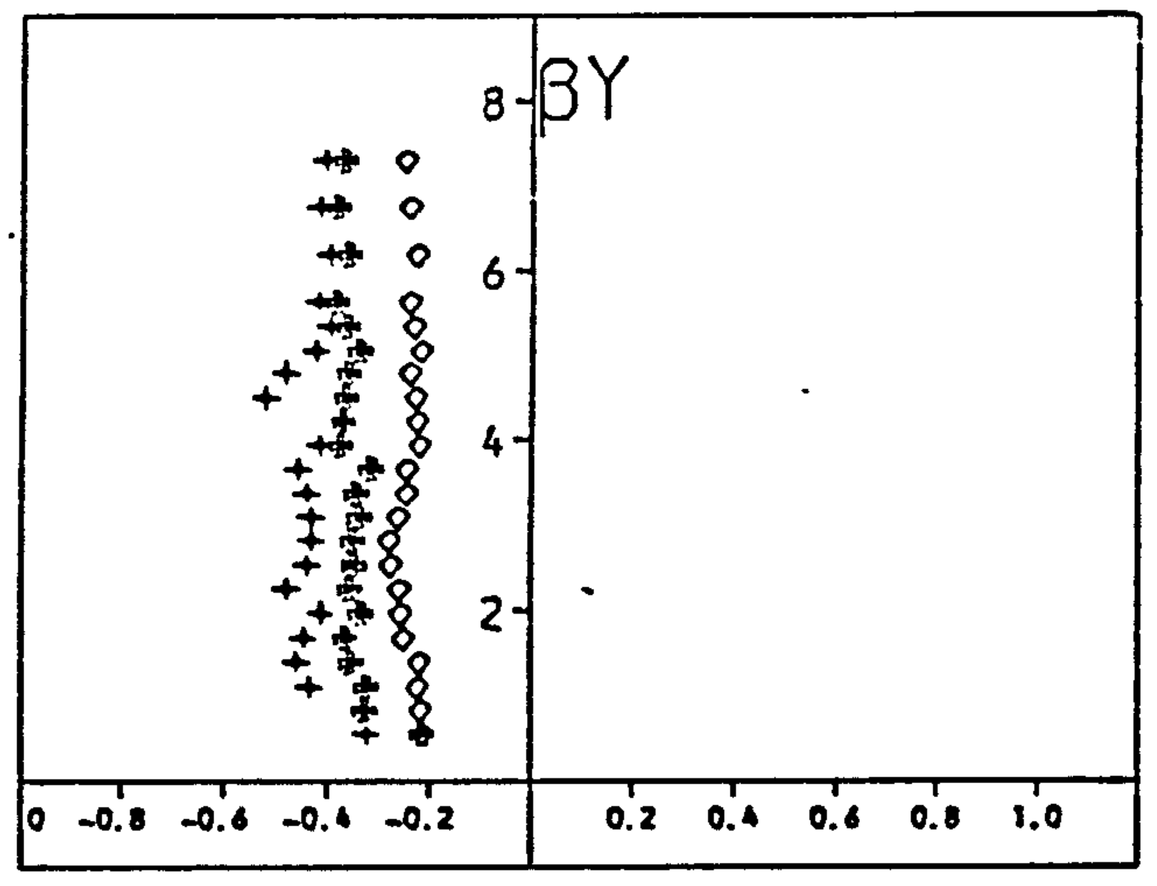

(b)

(iv) t_4

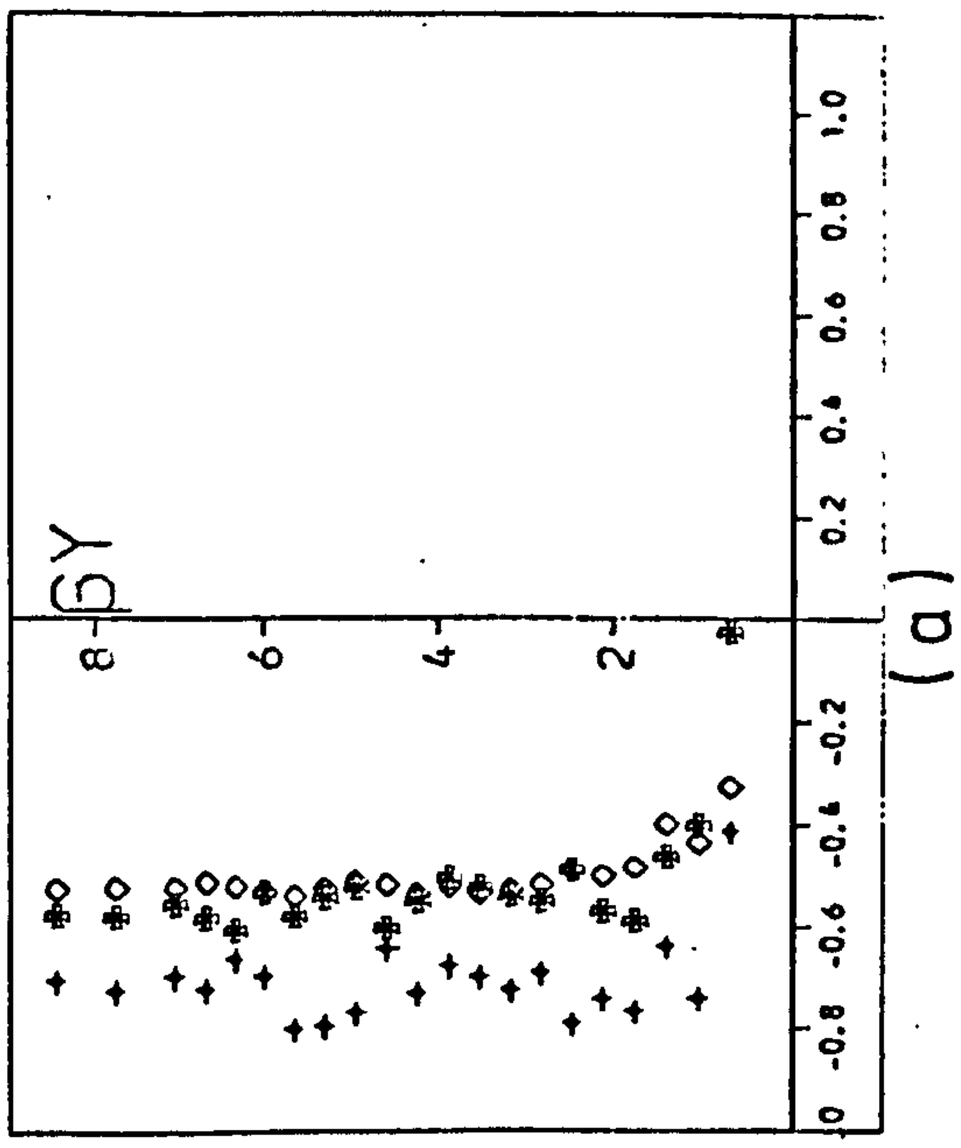

(a)

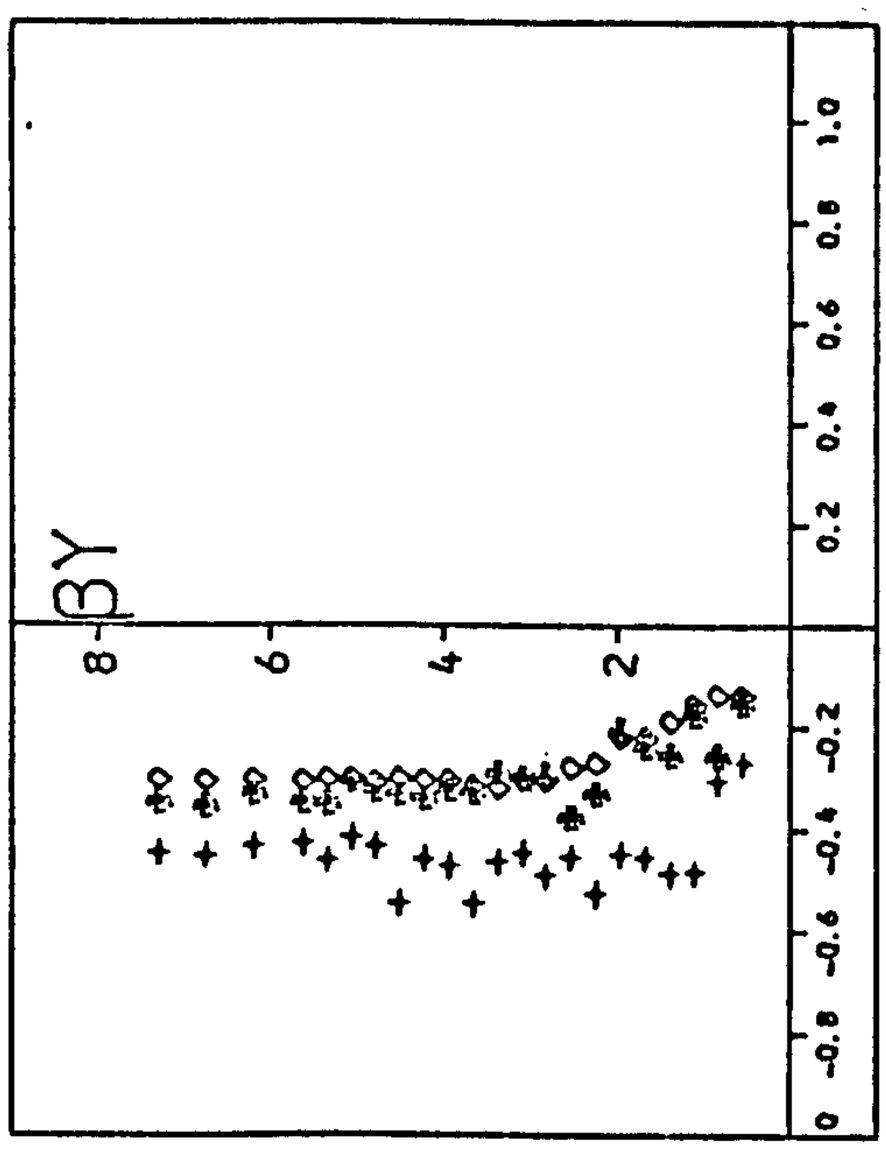

(b)

(vi) t_6

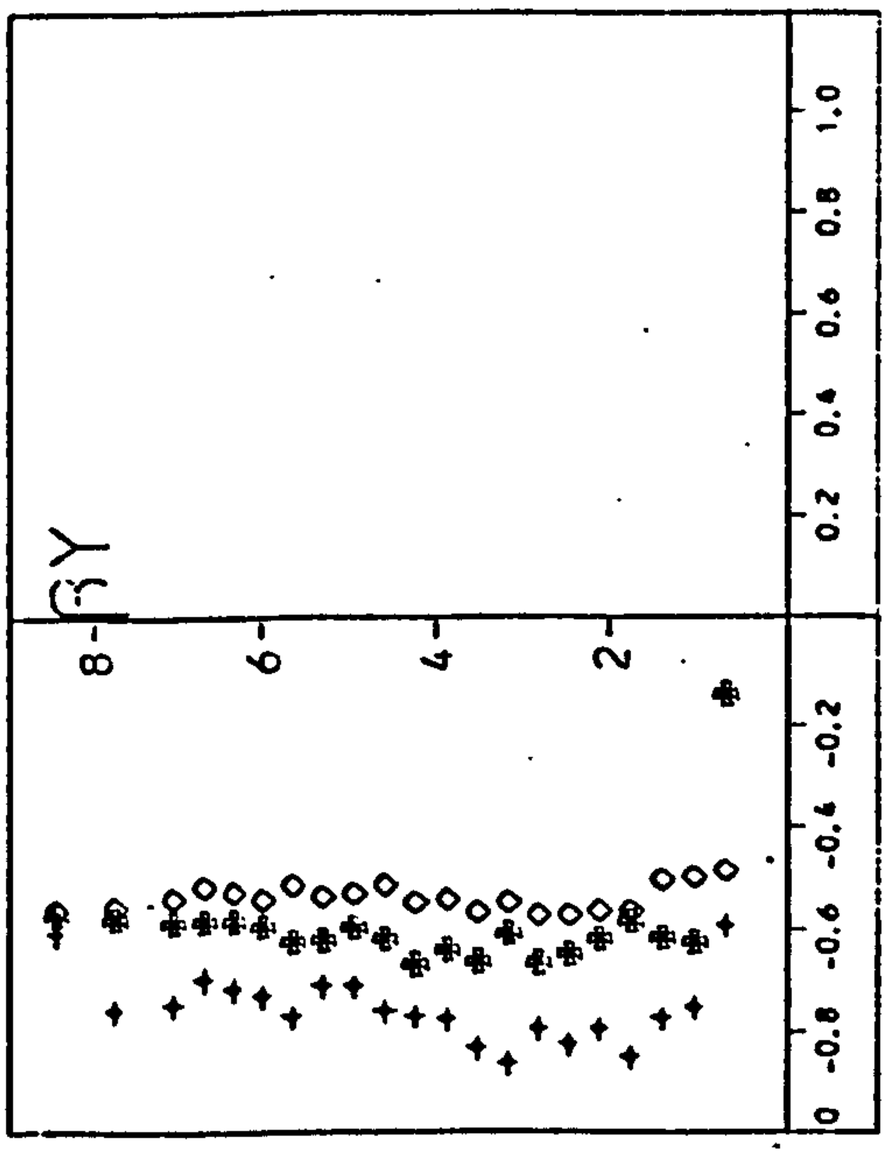

(a)

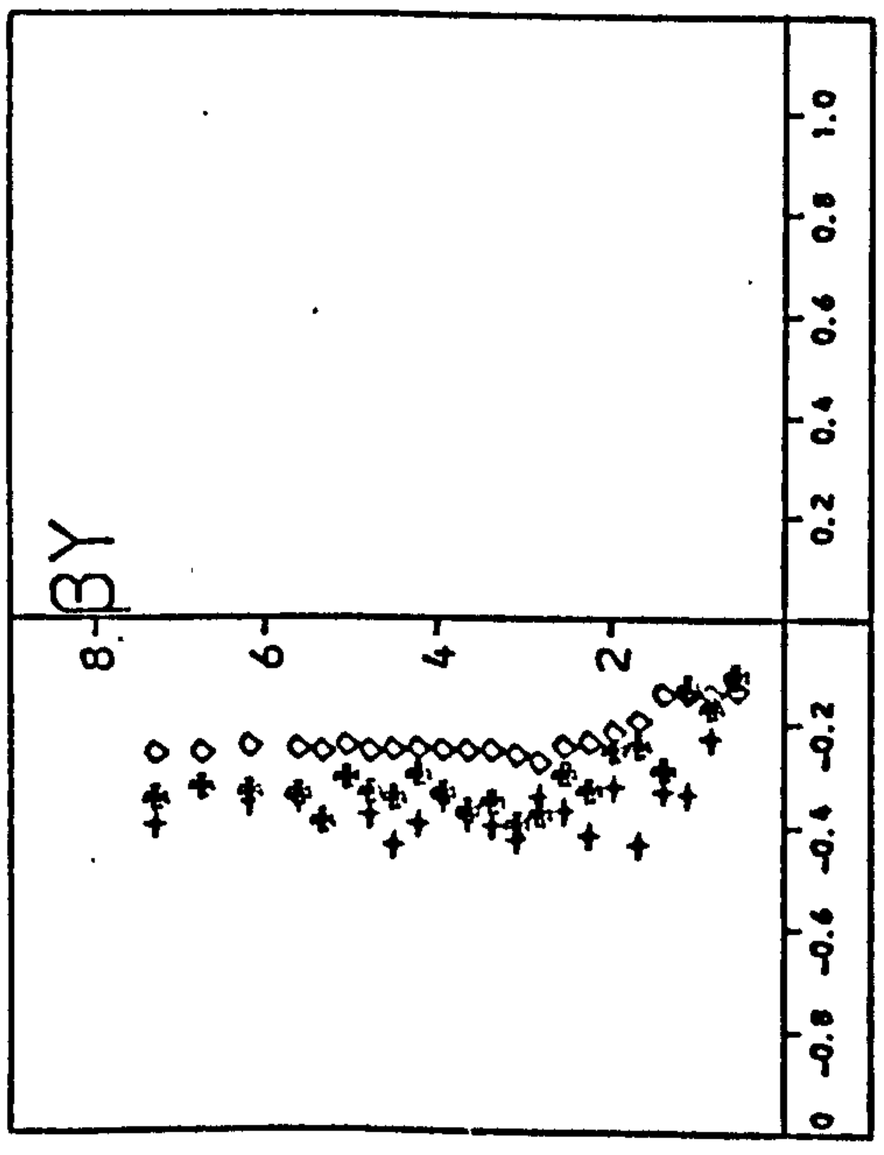

(b)

(v) t_5

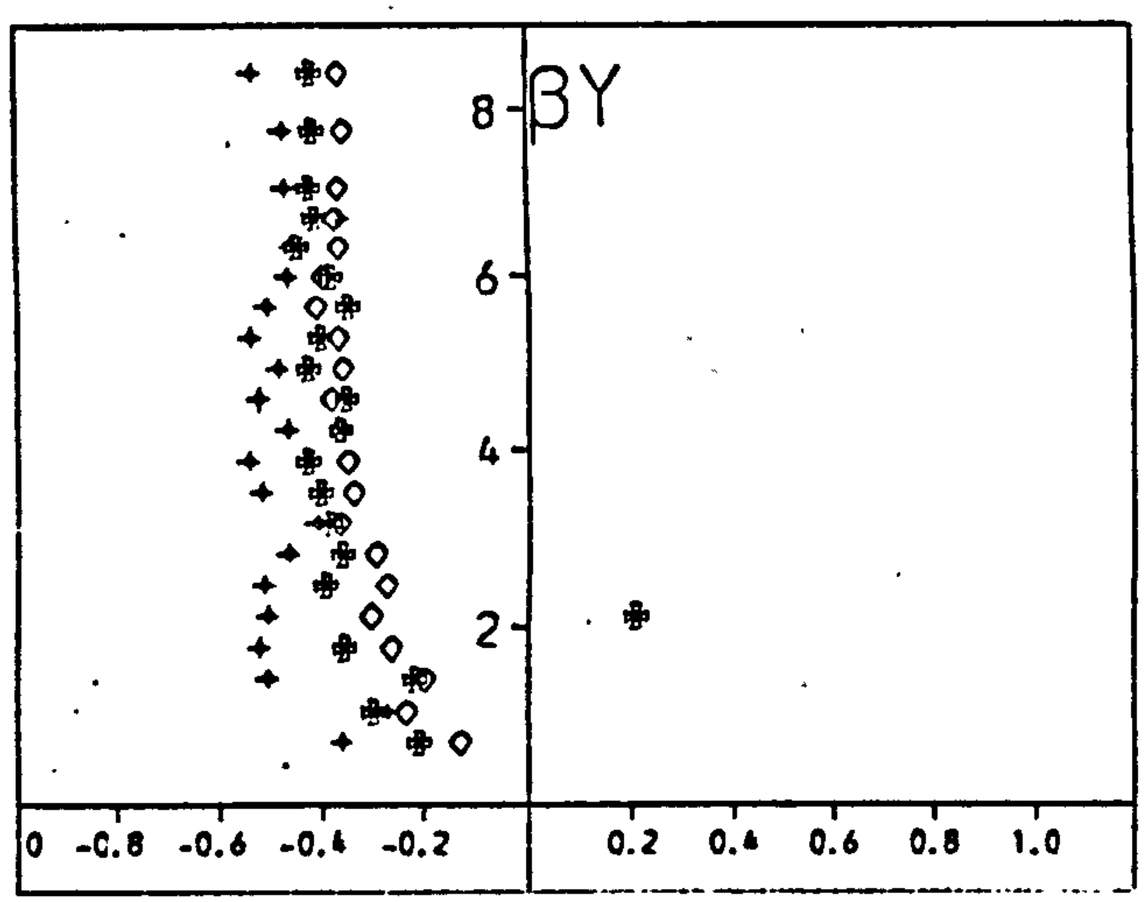

(a)

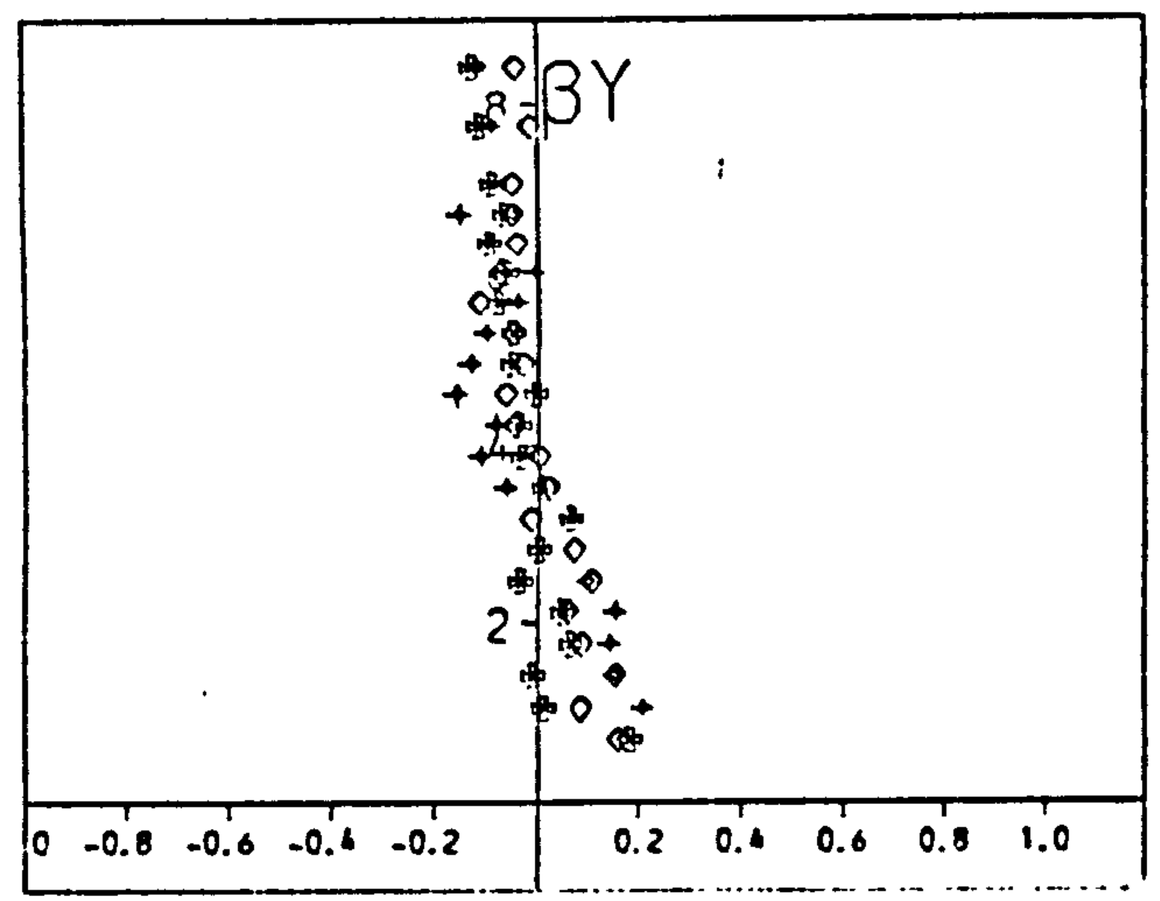

(a)

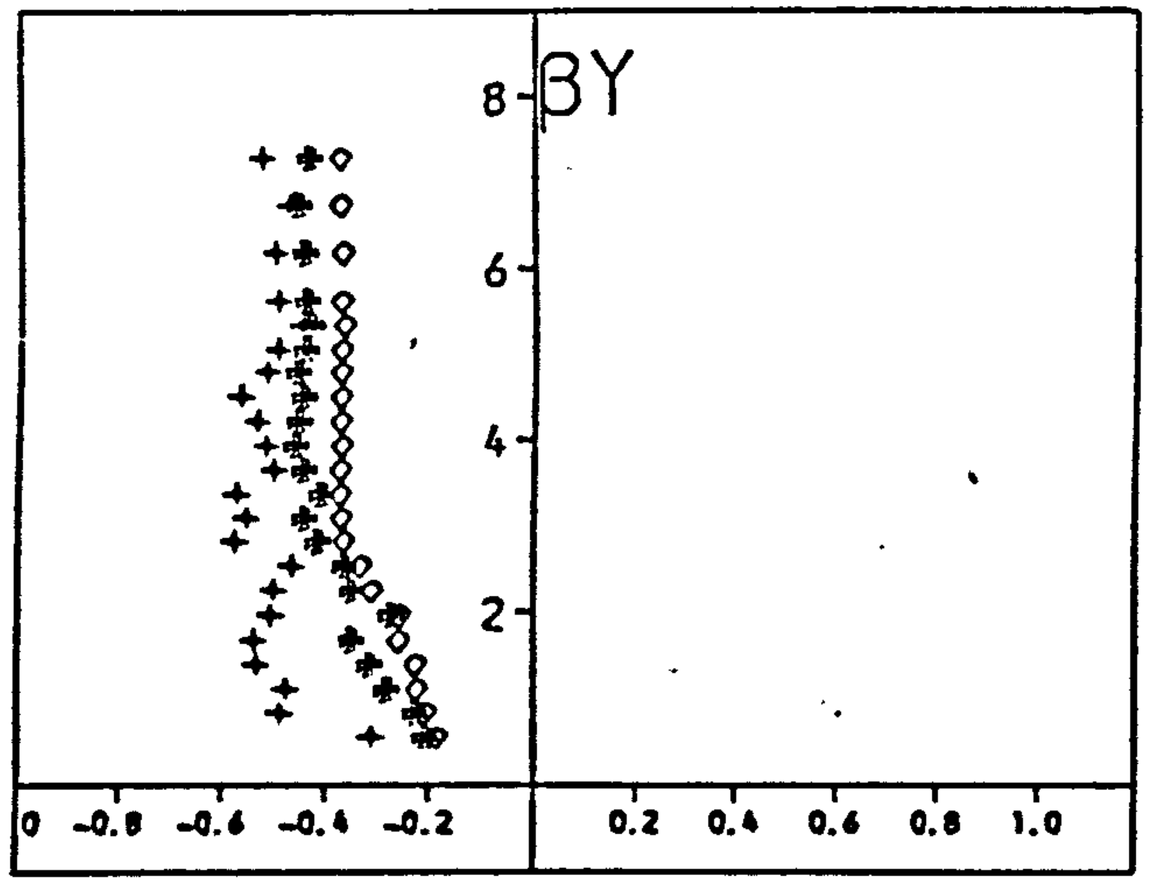

(b)

(vii) t_7

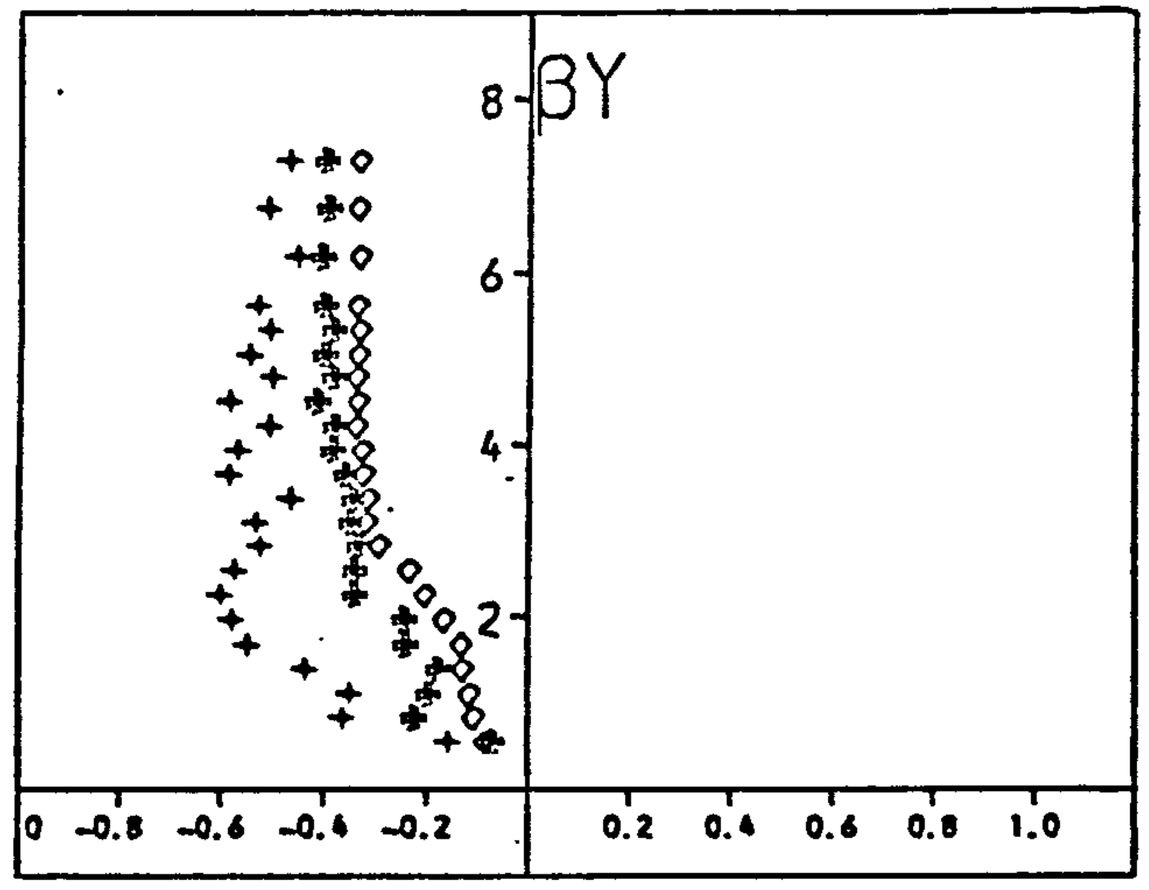

(b)

(viii) t_8

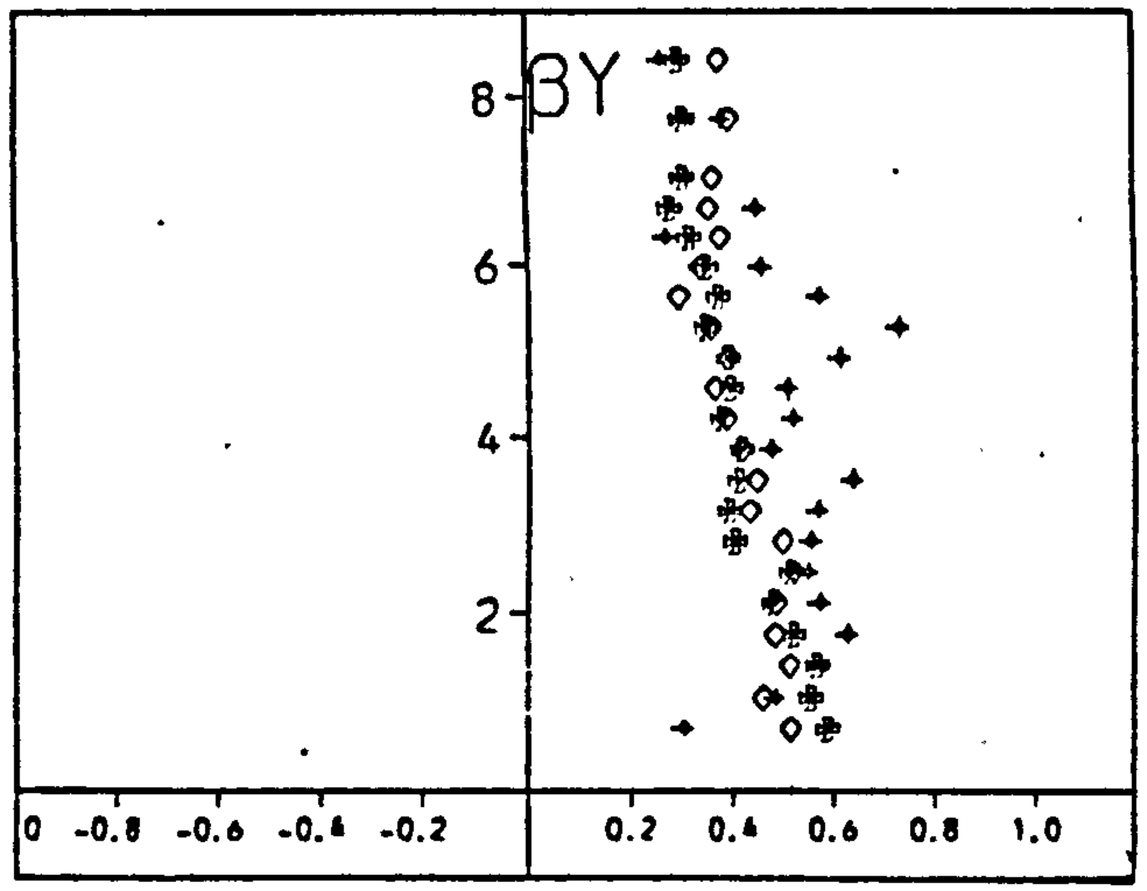

(a)

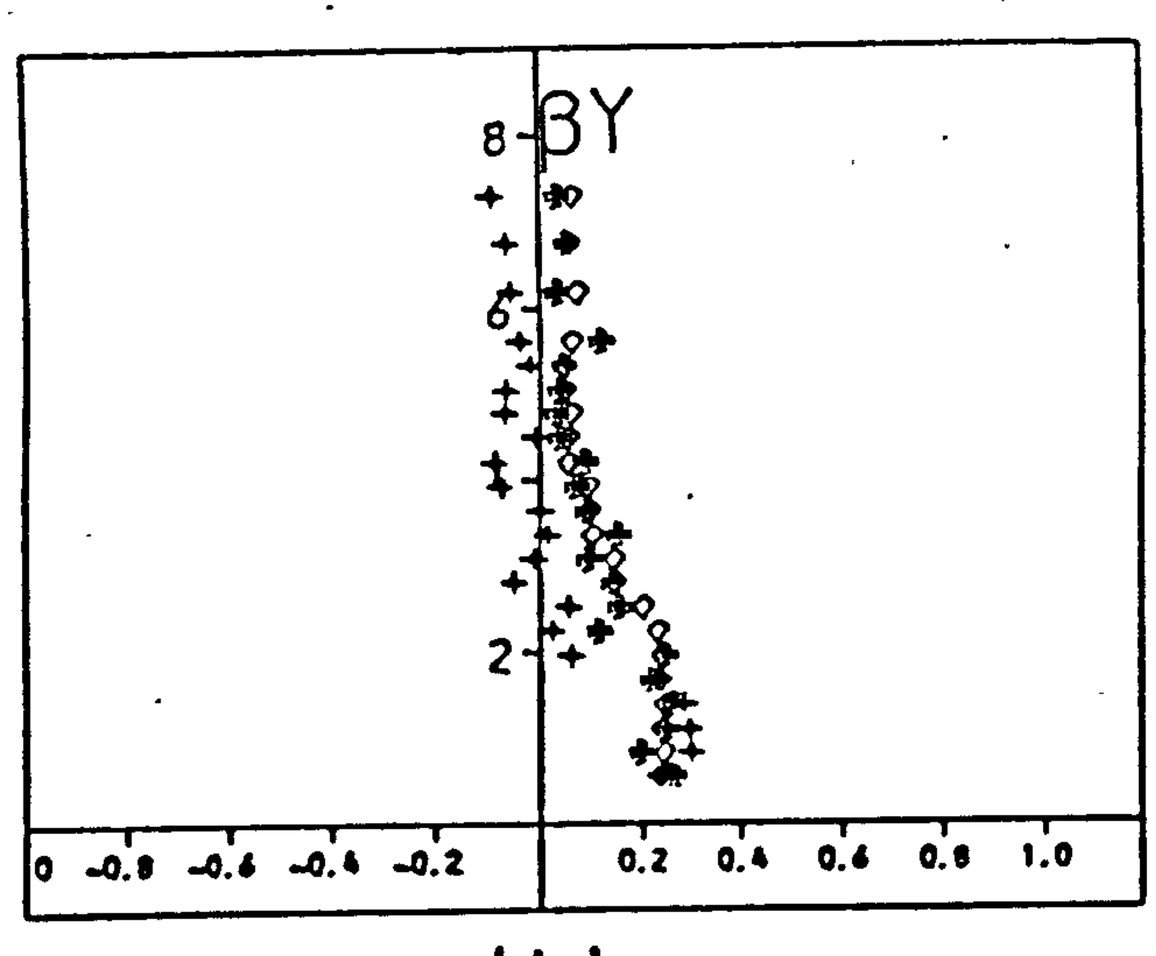

(b)

(ix) t_9

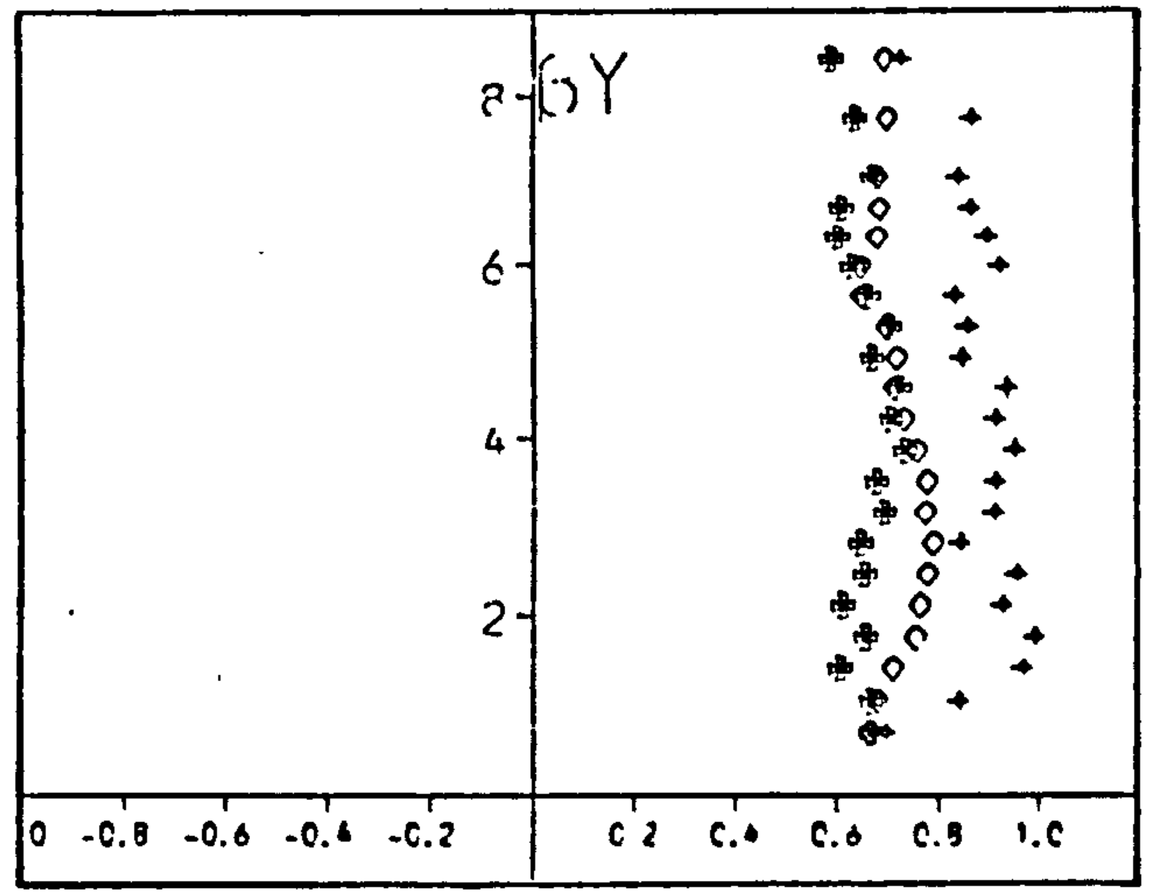

(a)

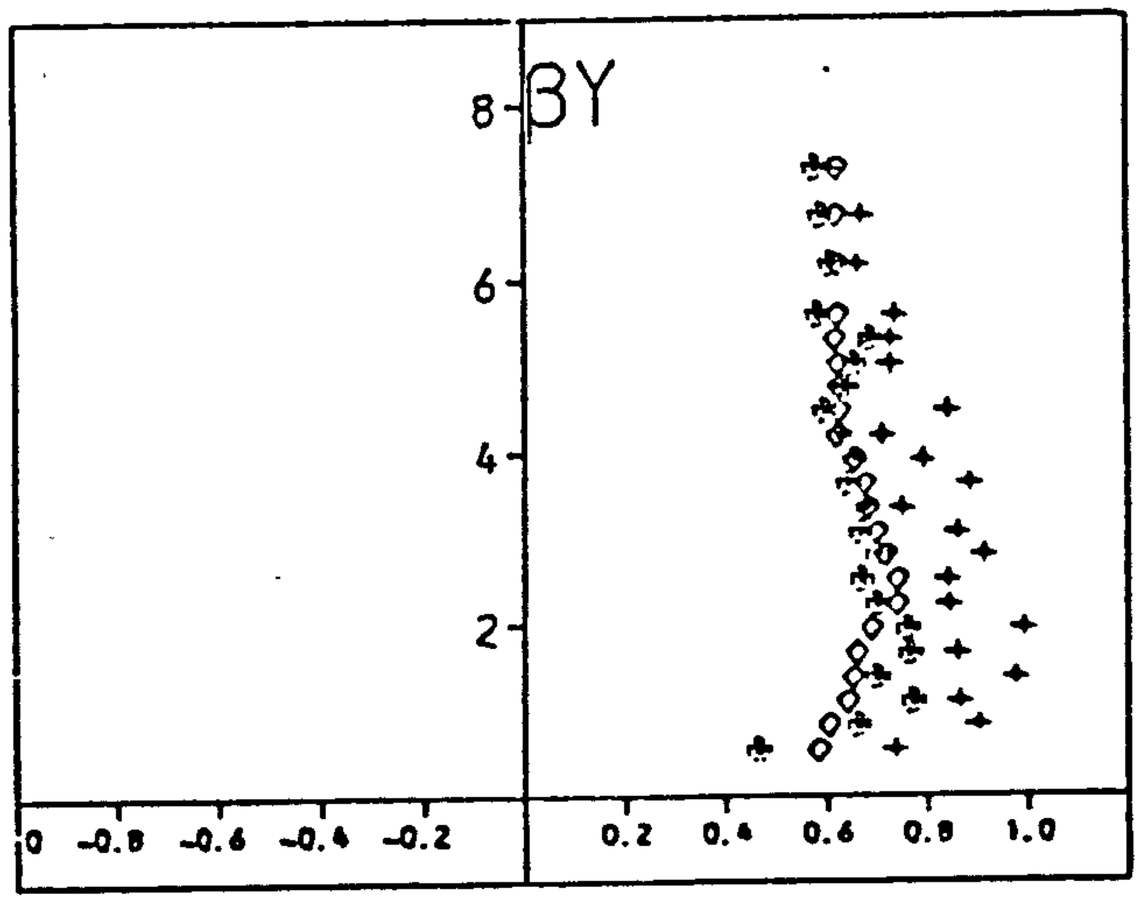

(b)

(x) t_{10}

2-D rough bed and very little fluctuation can be seen outside the boundary layer thickness. Fig. 6.19, which presents the correlation coefficients, does not show the increase in the value of velocity, but clearly proves the statement of fluctuation in flow.

A more interesting conclusion from Fig. 6.18 is that although the roughness elements introduce turbulence to the flow, shape of velocity profile is not changed and almost the same profile as for smooth bed, is observed for flow over rough beds. This makes it easier to compare the observed data for rough beds with the theoretical predictions.

It has been shown that the suitable equation for predicting velocity over a smooth bed is a second order of Lamb's equation with the velocity coefficients from equation 6.7, which yields equation 6.5. Although Sleath's and Kalkanis's equations (see 2.5.2.) are first order, the corrections which have been used by them, for rough beds, can be applied for the second order equation as well.

Since the modifications for turbulent flow from laminar flow equations concern the values of $f_1(y)$ and $f_2(y)$ (for second order $f_3(y)$ and $f_4(y)$ should be included as well, Eq. 6.5) in the equation;

$$U = \hat{U}_\infty [\text{Cos } \sigma t - f_1(y) \text{ Cos } (\sigma t - f_2(y))]$$

the general changes of the velocity profile can be studied by taking different values for the f's.

6.19(a) T = 1.4 s

6.19(b) T = 2.2 s

Fig. 6.19 Correlation Coefficient for Boundary layer velocities over smooth, 2-D and 3-D rough beds with each other at different depths.

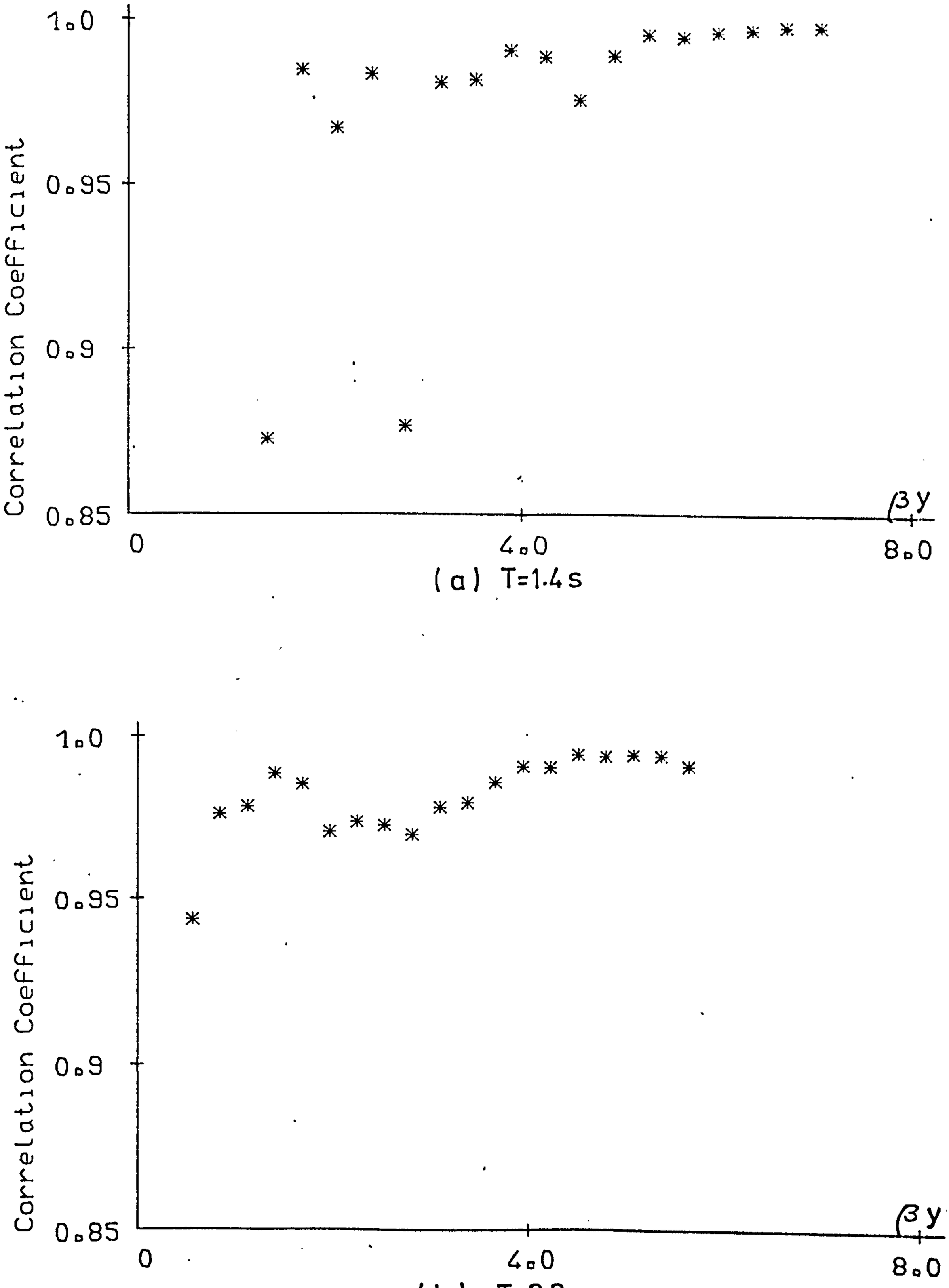

(i) Smooth and 2-D rough bed

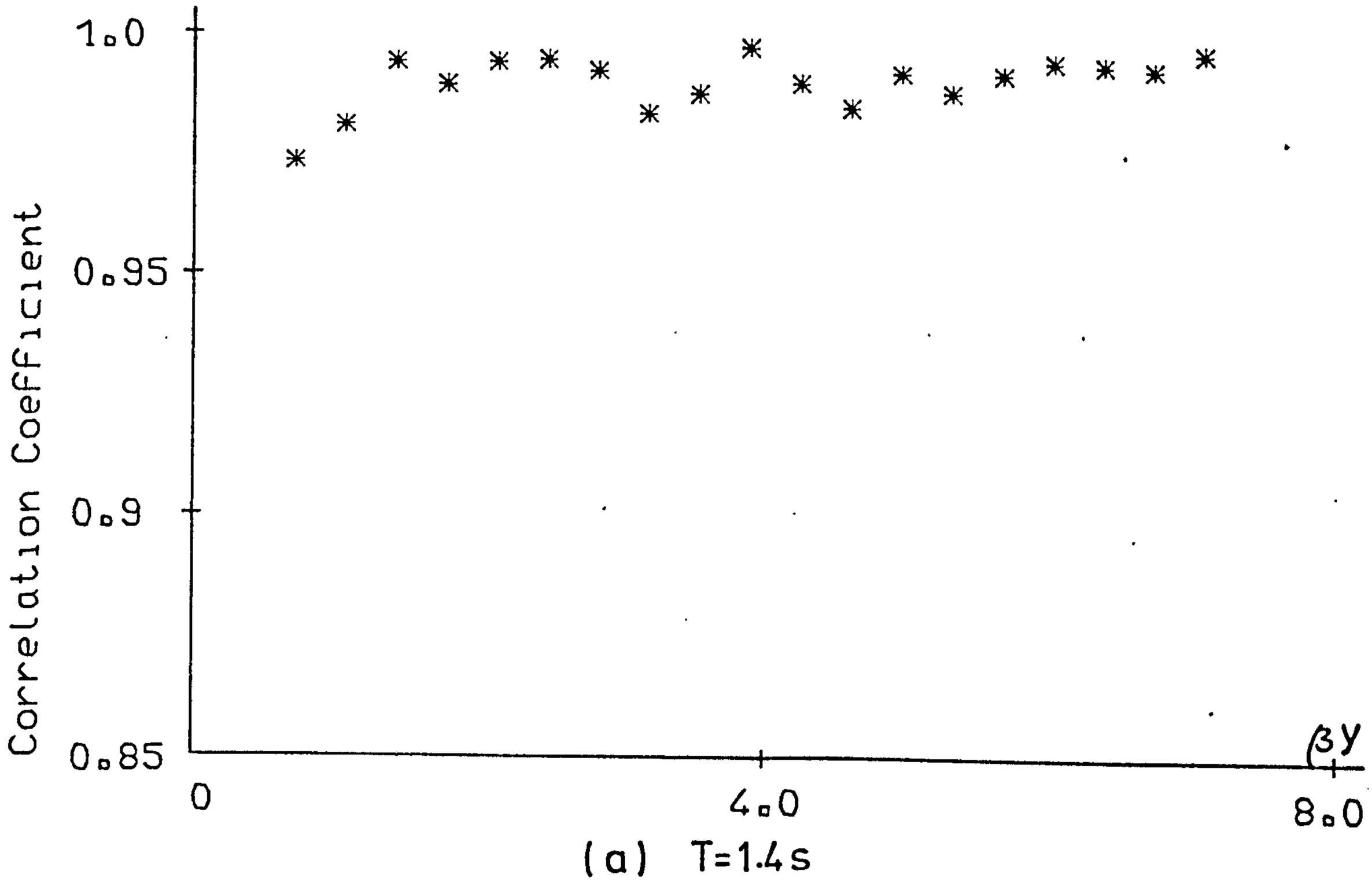

(a) T=1.4s

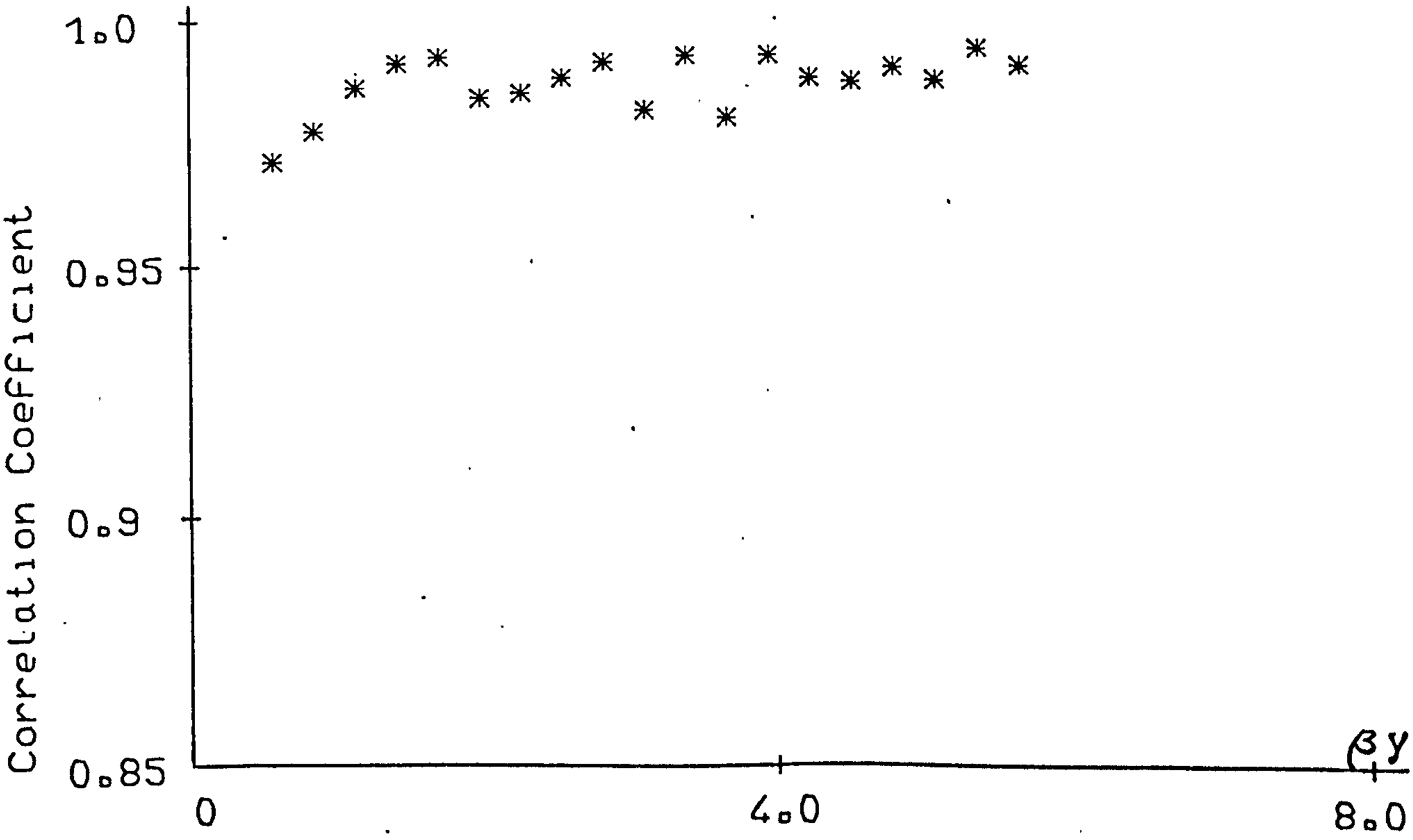

(b) T=2.2s

(ii) Smooth and 3-D rough bed

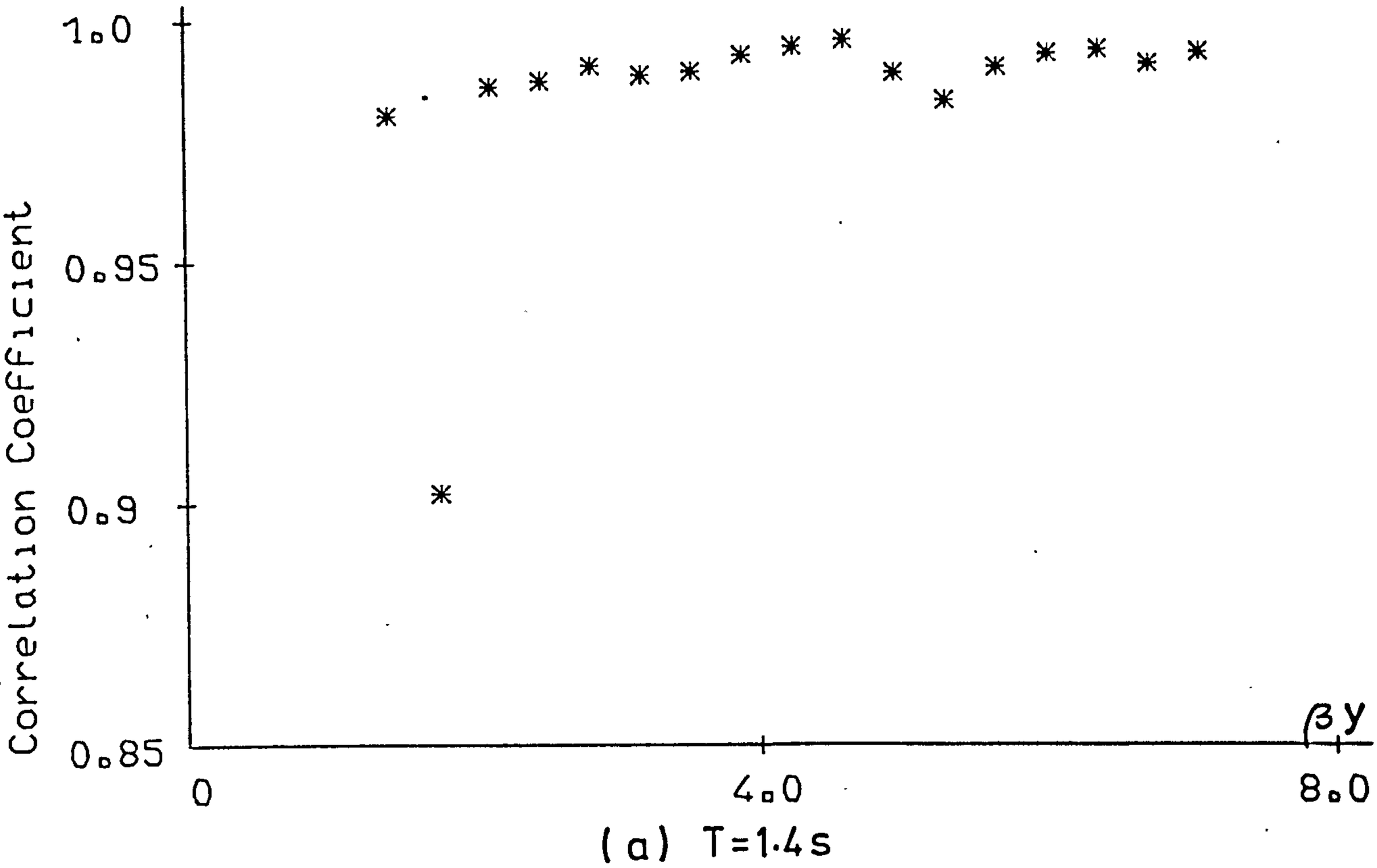

(a) T=1.4s

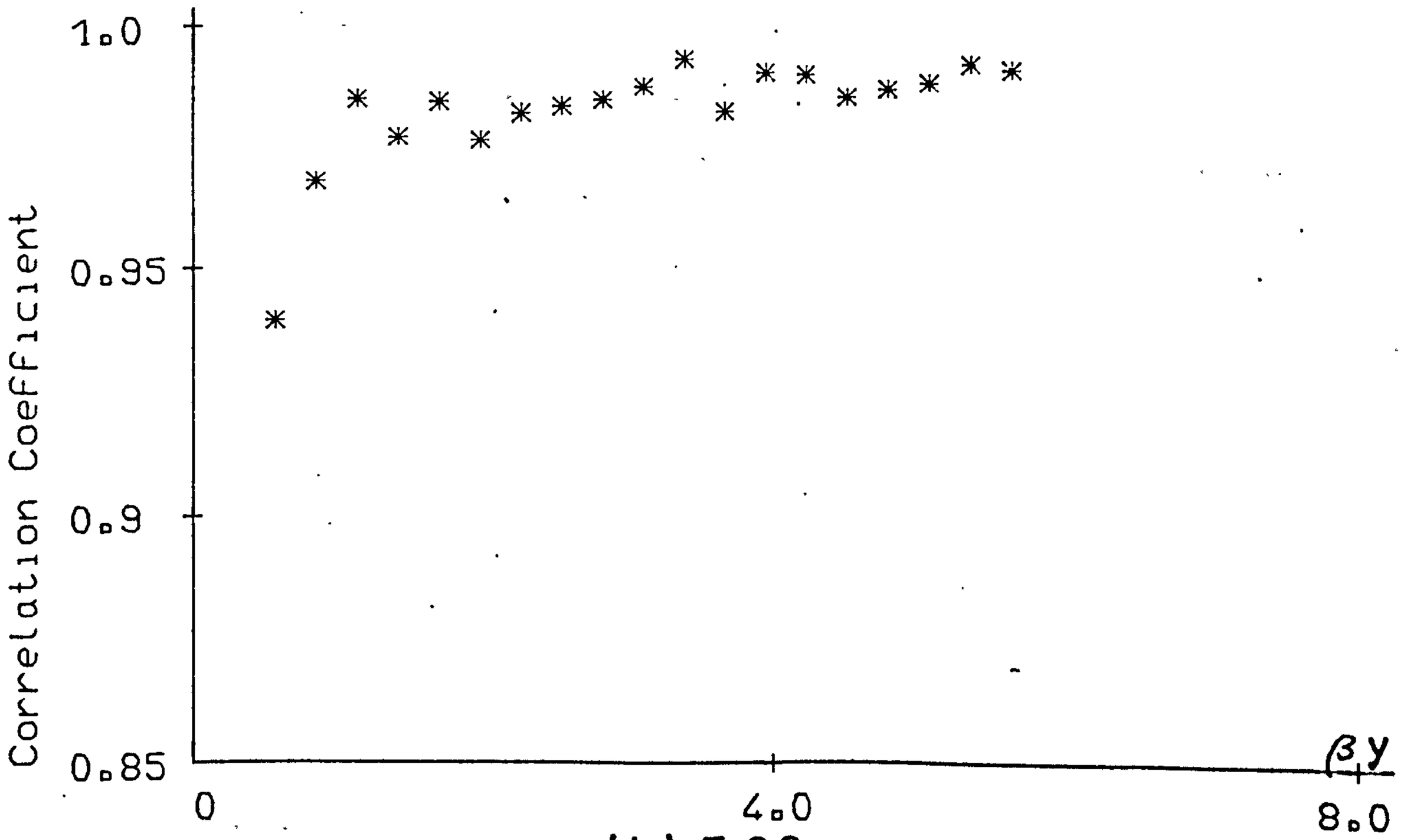

(b) T=2.2s

(iii) 2-D and 3-D rough beds

However, accepting the relationship between the four functions (Beech (1978)) as;

$$f_1(y) = e^{-\beta y}$$

$$f_3(y) = e^{-\sqrt{2}\beta y}$$

$$f_2(y) = \frac{f_4(y)}{\sqrt{2}} = \beta y$$

Fig. 6.20 shows the variation of the velocity profile for different values of the above functions (Fig. 6.20a is the equation without any alterations) as follows;

(i) When the f_1 and f_3 are divided by an integer (say 10), then the outcome of the profile (Fig. 6.20b) is an exaggerated peak for each phase.

(ii) On the other hand by multiplying f_1 and f_3 by the same integer, then the thickness of viscous boundary layer decreases rapidly (Fig. 6.20c).

(iii) If the functions f_2 and f_4 are divided by an integer, the peak for the velocity profile seems to vanish (Fig. 6.20d) and hence a normal boundary layer profile is introduced.

(iv) But by multiplying the f_2 and f_4 functions by an integer, causes many peaks for each profile; in this case the integer 10, produces 5 maximums and 5 minimums at each phase (Fig. 6.20e).

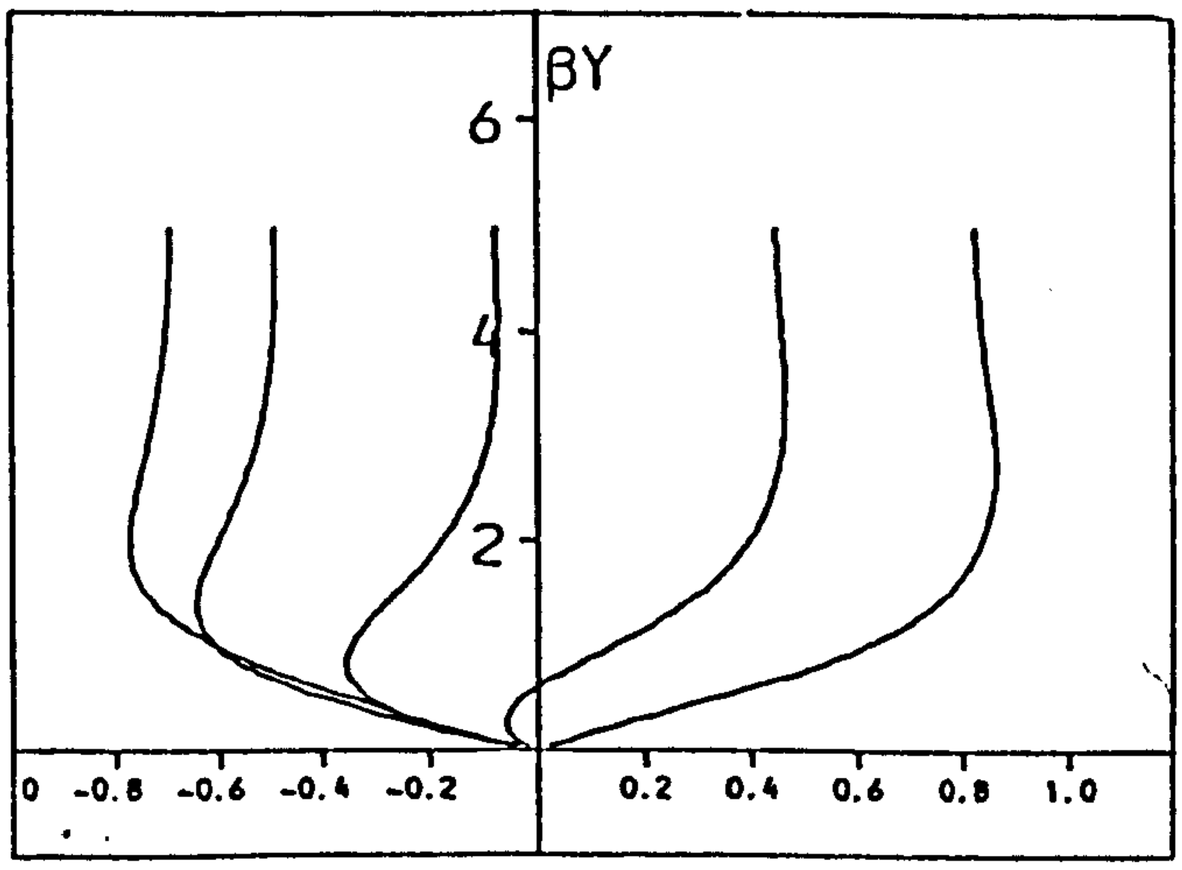

(a)

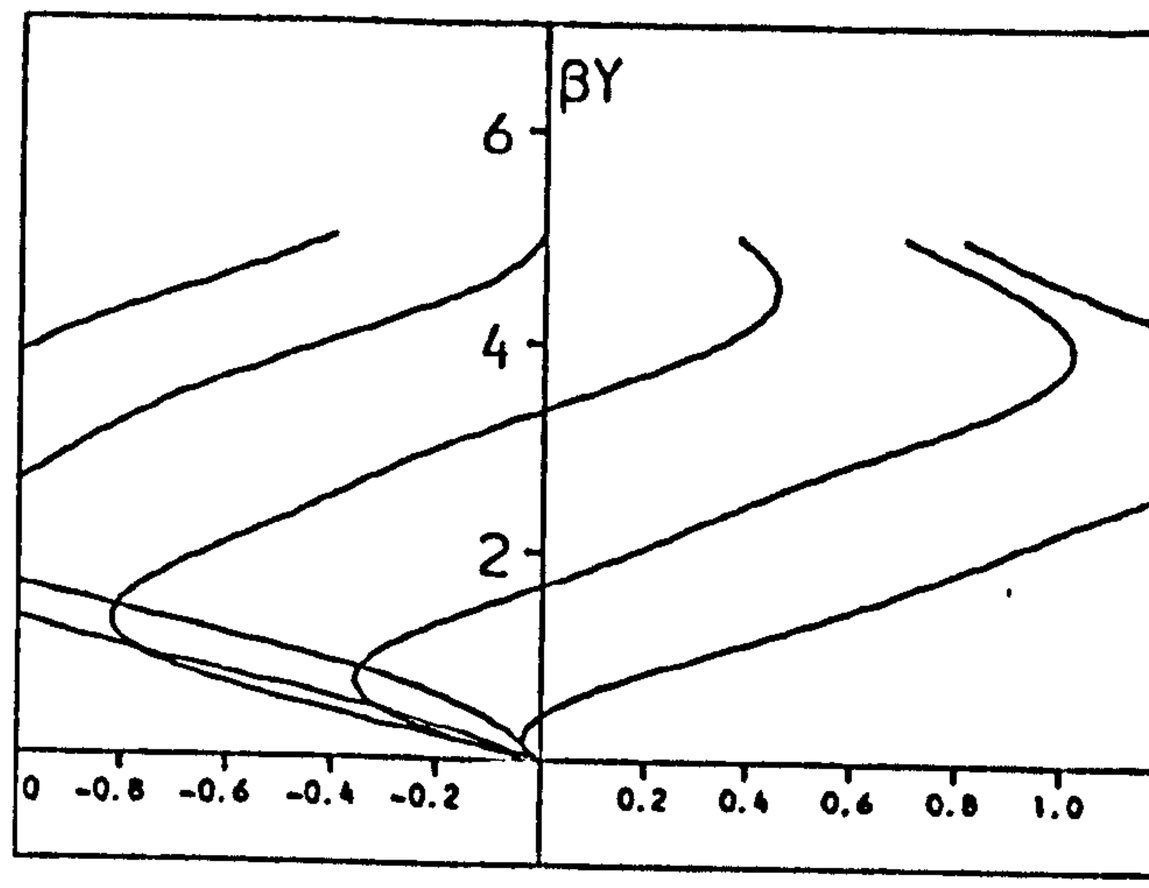

(b)

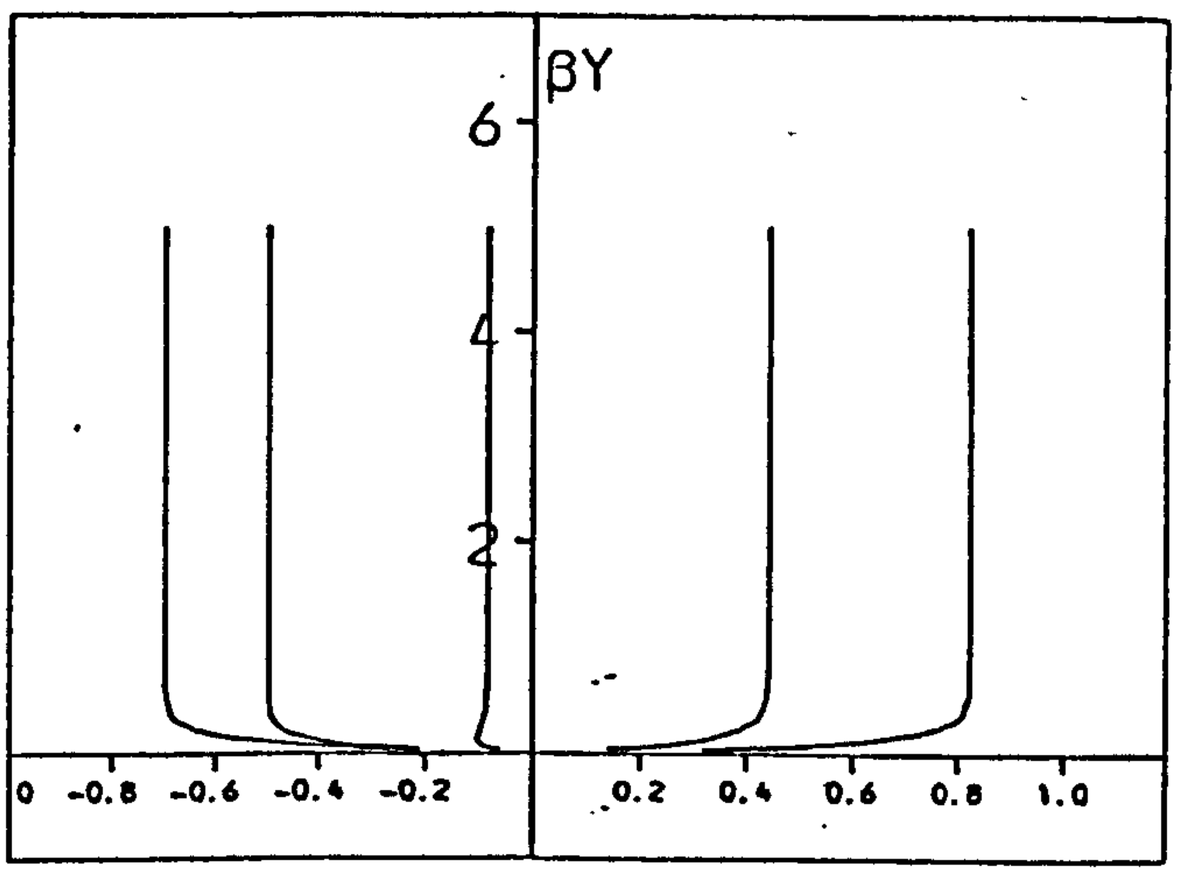

(c)

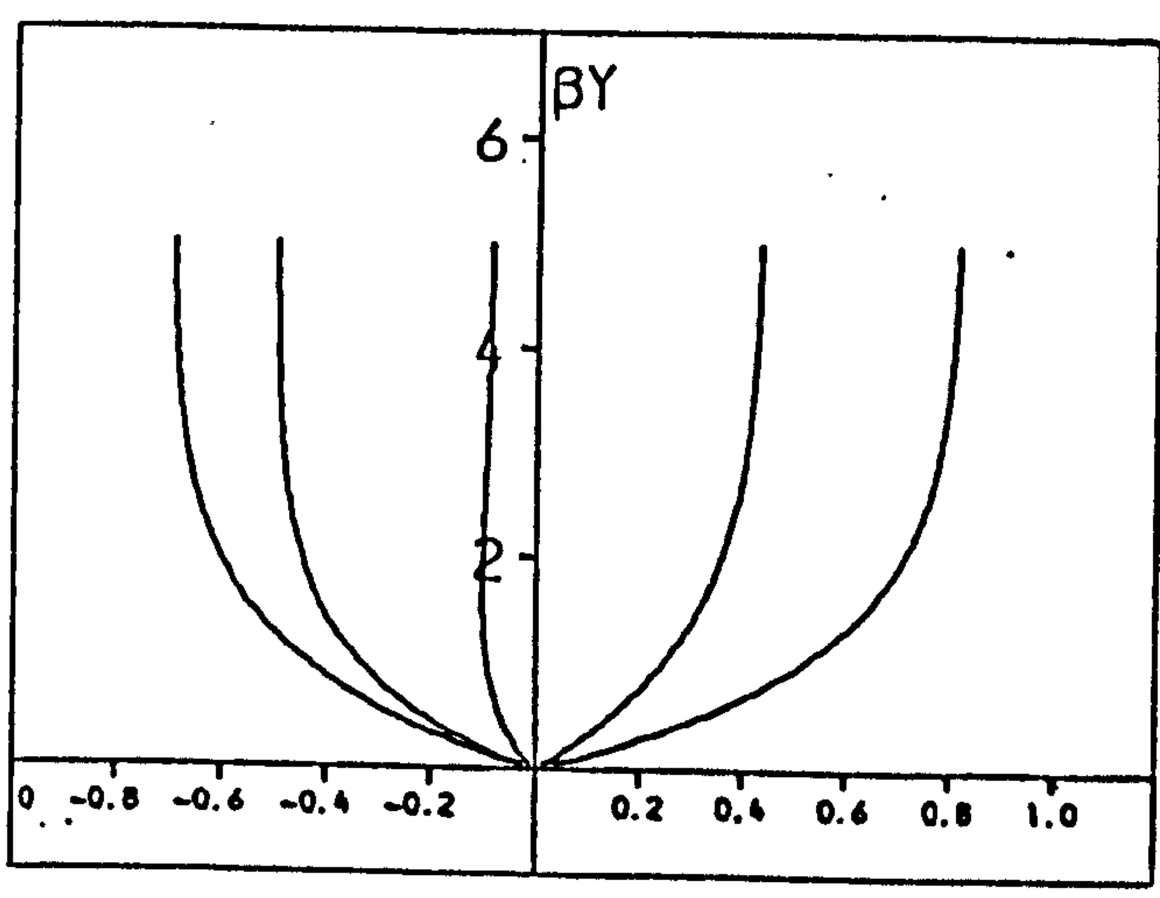

(d)

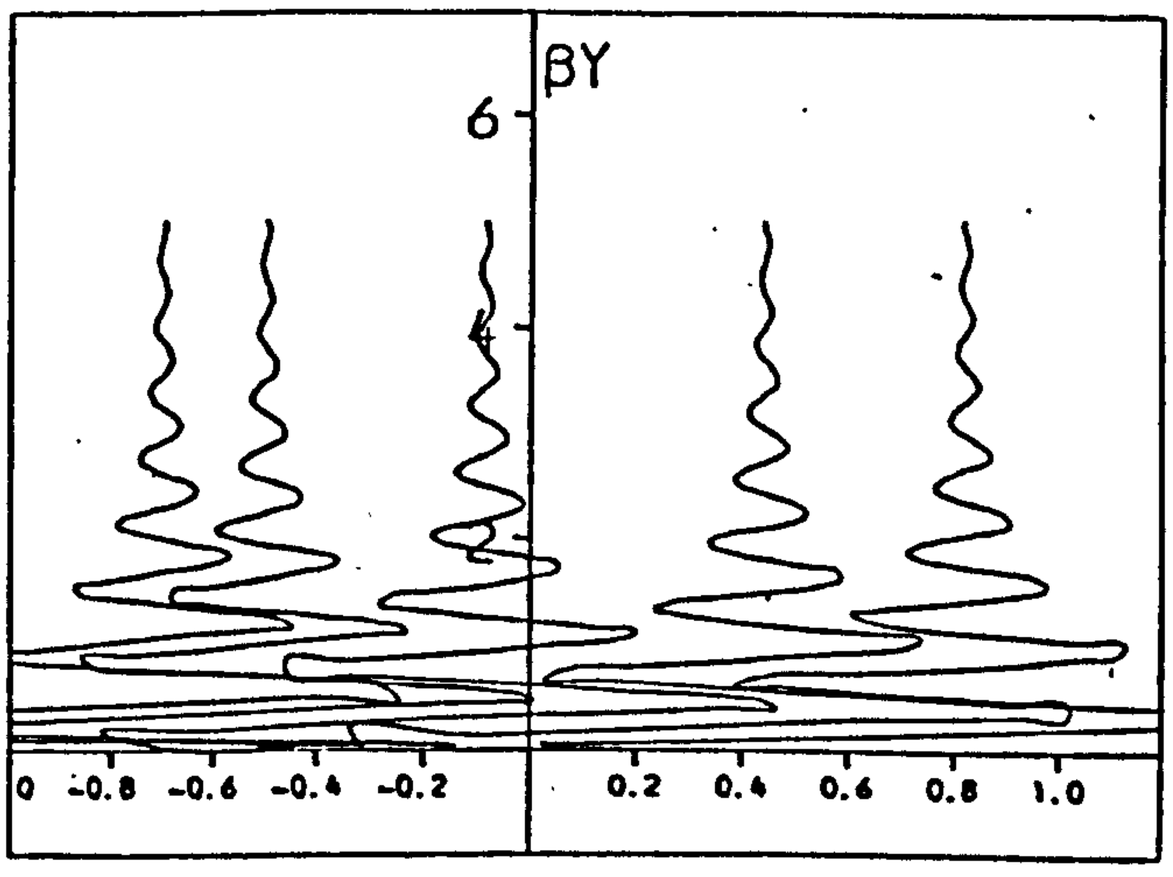

(e)

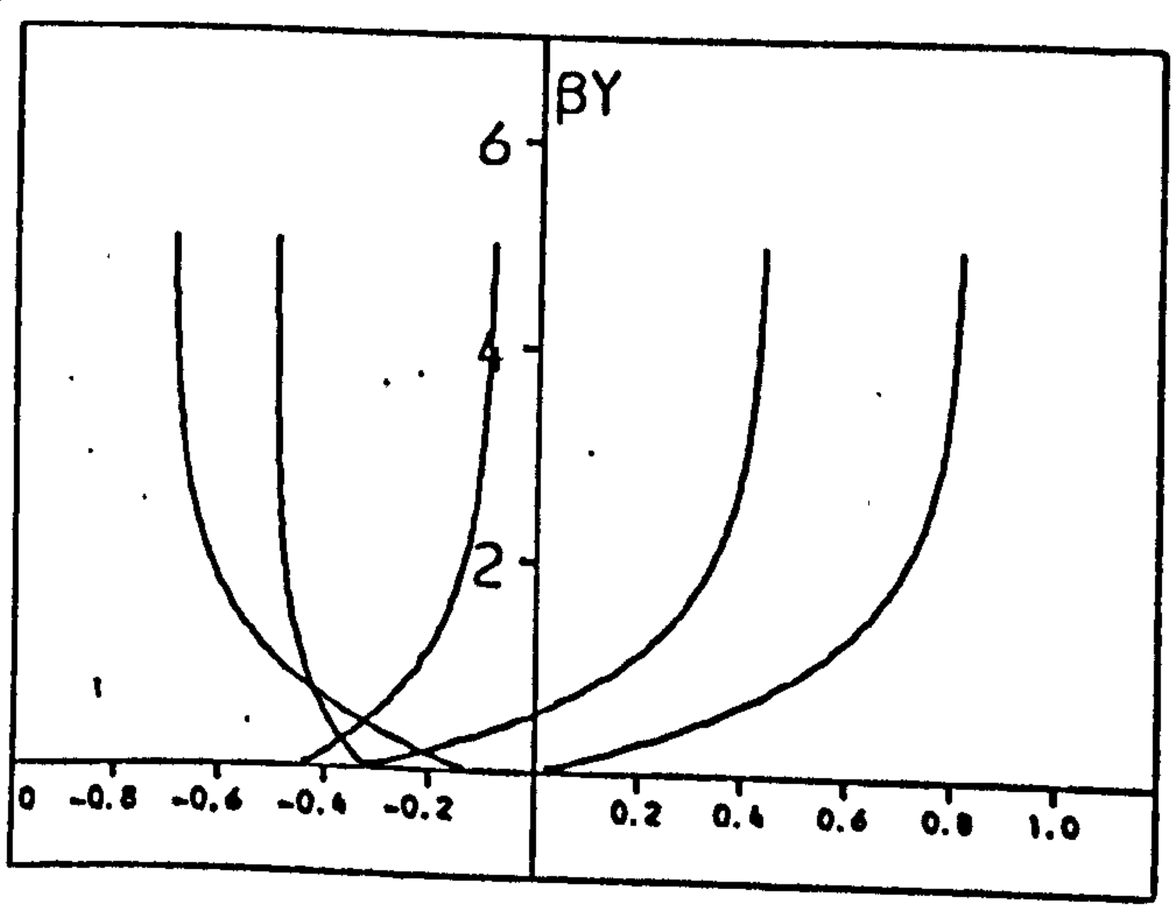

(f)

Fig. 6.20 The boundary layer profile, Eq. 6.5, for different f values.

(v) And finally the function suggested by Kalkanis ($0.5\ (\beta y)^{2/3}$) for f_2 and f_4, of which the outcome is shown in Fig. 6.19f.
(A factor weighted by the relative amplitude of the harmonics could have been used)

Almost all the profiles presented in Fig. 6.20 are not applicable for the prediction of data presented in Fig. 6.18. For example no separation at bed (or close to bed) is apparent from the data in the way Fig. 6.18f illustrates and this rules out the Kalkanis prediction. Since the profile presented in Fig. 6.20e has multiple peaks, and there is no sign of this effect for data, therefore choice (iv) cannot be taken. The corrections to functions f_1 and f_3 which result in graphs (b) and (c) also appear to be exaggerations of the real case, and hence, not suitable for use to predict the observed result. Also, since a peak can be seen in the velocity profile for the rough bed, the Sleath equation, graph (d+b), would not be a good prediction (which has no peaks).

Nevertheless most of the discrepancies between the measured results and the theories are due to the turbulent flow over the rough beds. The tabulated Reynolds number values for rough beds (Tables 6.3 and 6.4) indicate that the flow is well into the transition region from laminar to turbulent flow (Re_{crit} being 640 for 2-D and 104 for 3-D rough beds - Kalkanis (1964)), where Re values correspond to the velocity observed at the edge of smooth boundary flow ($\hat{U}_\infty$). This causes fluctuating velocity profiles and is more difficult to predict.

An important effect of roughness elements is in intensifying the velocity within the boundary layer which is not predicted by the theories, as well as the intensity of the perturbed flow. In almost all the graphs of Fig. 6.18 the velocity profile for 3-D rough bed has larger values than the velocity for smooth bed, while not much difference is noticeable between the intensity of flow for smooth and 2-D rough bed.

Hence if an equation in the form of smooth laminar (equation 6.5) prediction is going to be used, new values for ℓ_1 and ℓ_2 should be taken (since the ℓ_n values are calculated for the smooth laminar case - Eq. 6.7) or a correction factor be applied to the same ℓ_n values.

Also, with the turbulence intensity being significant, the perturbation velocity (U_p) should be taken into account. Because U_p exist through the cycle (Fig. 6.12), no sinusoidal function can represent the perturbation velocity, but instead it can be seen that the value of U_p and also the intensified velocity decrease exponentially by increasing βy, with a maximum value which occurs at the top of roughness for both velocities. Therefore a coefficient in the form of $e^{-\beta y/c}$ can be derived, where c is related to the roughness height ($c = \beta\kappa$, κ is the roughness height), and equation for rough boundary layer velocity can be written;

$$u_R = U + U\ (C_1 + C_2)e^{-y/\kappa} \qquad (6.9)$$

where U is the laminar boundary layer velocity from equation 6.5, C_1 is the percentage increase of velocity and C_2 is the percentage of maximum perturbed velocity $(\frac{U_p}{U} \times 100\%)$.

Also for present data, the values of X (Sleath's No. $= \beta\kappa/2\pi$) which are 4.24 and 3.31 for the 3-D rough bed and 1.04 and 0.81 for the 2-D rough bed can have some significance for the C constants (assuming that for X values less than one, a minimum of 1 should be taken for calculations).

For example the value of coefficient C_1 (by close inspection of Fig. 6.18), can be related to X. Since for 3-D rough bed the velocity is increased while for 2-D rough bed it is not, it is conclusive that C_1 is related to the value of X. However, because of the lack of rough bed variation results, proper relationships cannot be obtained except by assuming;

$$C_1 = f(X-1) \qquad (6.10)$$

The coefficient C_2 which is related to turbulence intensity is more a function of Reynolds number, the higher the value of Re, the more turbulent the flow is and hence higher value for turbulent intensity. Therefore;

$$C_2 = f(Re) \qquad (6.11)$$

Obtaining the values of C_1 and C_2 (Table 6.5) from the observed data, the profile represented by equation 6.9 for two phases for the rough beds (first and fifth phases) is

Rough Bed	C_1	C_2
2-D	20	-
3-D	20	40

Table 6.5 The Observed Values of C_1 and C_2 for Eq. 6.9 as a % of $\hat{U}_\infty$

represented in Fig. 6.21. The figure shows a better fit of the equation to the 3-D rough bed results than those obtained for 2-D rough bed. This is caused by the sharp edges of the roughness elements (for 2-D rough bed), which increase the random movement of the flow that is especially close to the top of the roughness as was discussed in Section 6.3.

Nevertheless the shortage of sets of data for various rough beds makes the confidence in the reliability of the equation 6.9 weak at this stage, and certainly opens an option of need for further work, and obtaining the relationships for equations 6.10 and 6.11.

From equation 6.9 it would be very difficult to calculate a velocity maximum and velocity maximum phase as for laminar flow (Figs. 6.2 and 6.7). The same conclusion is reached from the graphs presented in Fig. 6.12, that the flow is turbulent and a unique set of results does not exist. If, however, at each height a sample of the population of velocities is analysed, then the equation 6.9 will behave as for laminar flow and the same profiles as presented in Fig. 6.2b can be corresponded with the data.

The equation was found not to be a good theoretical means of predicting the reults of 3-Ds trough and crest and 3-DR trough. This is due to the high intensity eddies (caused by the roughness elements) which completely eliminate the laminar viscous boundary layer profile above the roughness

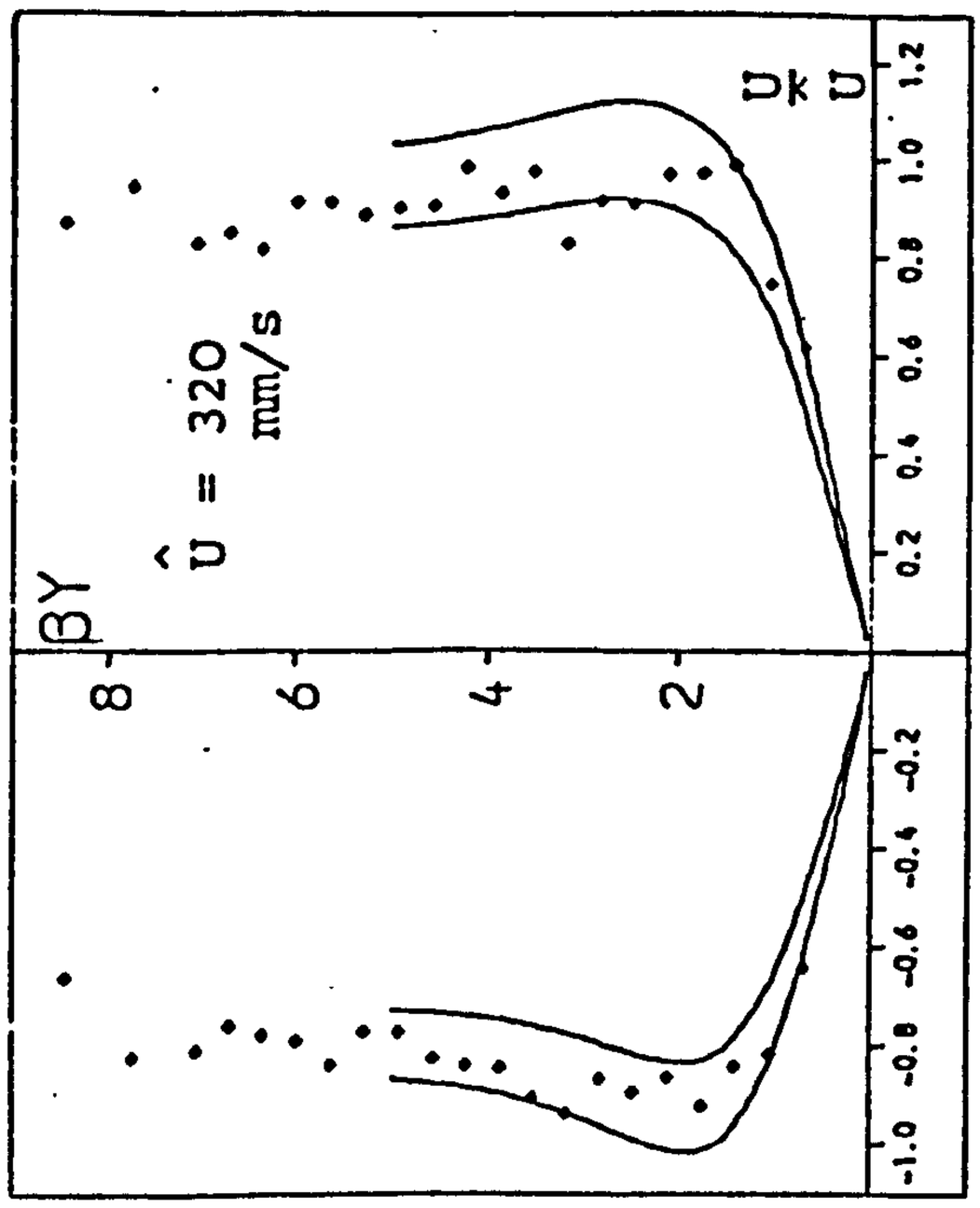

(a) T=1.4 s

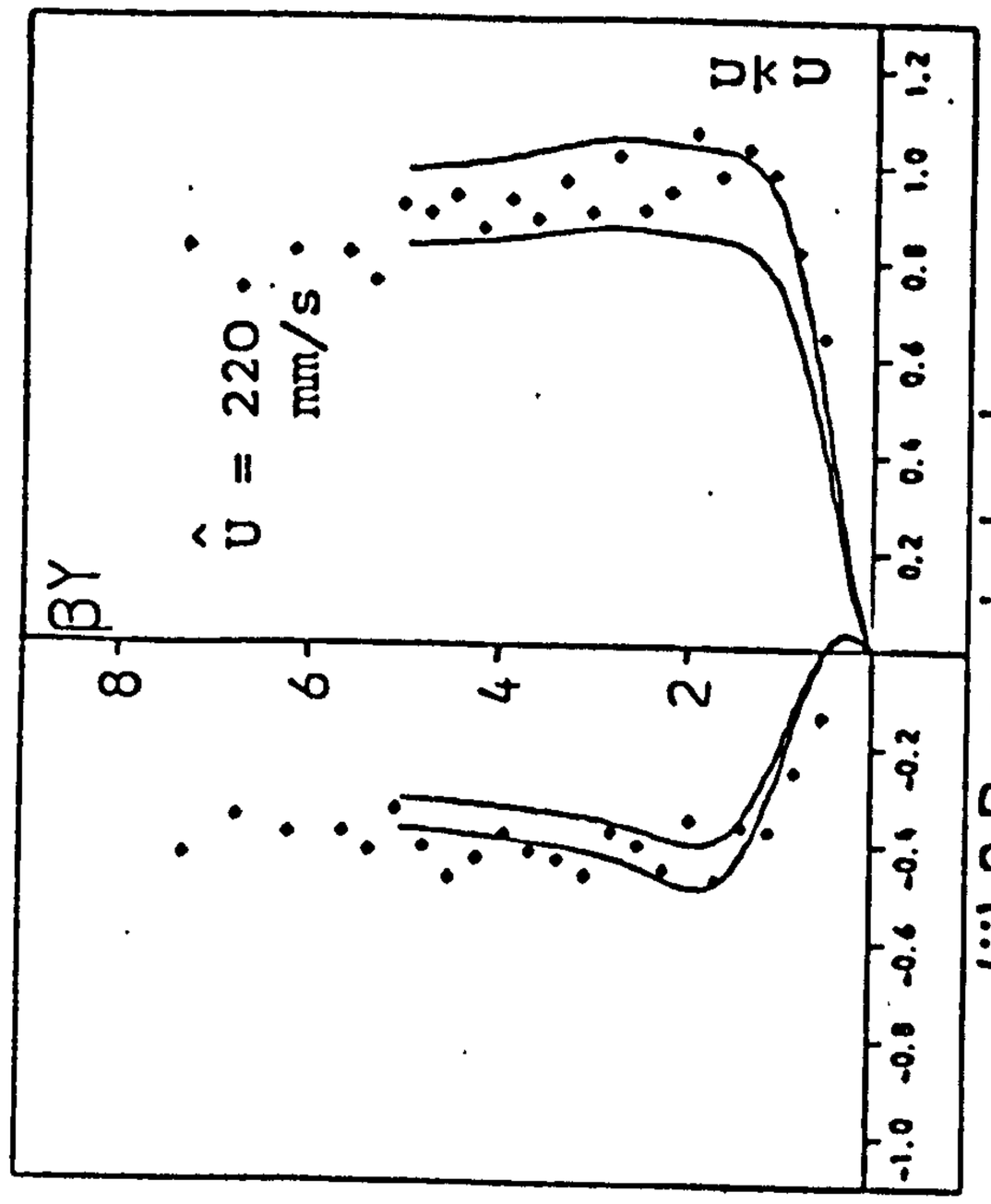

(ii) 3D rough bed

(b) T=2.2 s

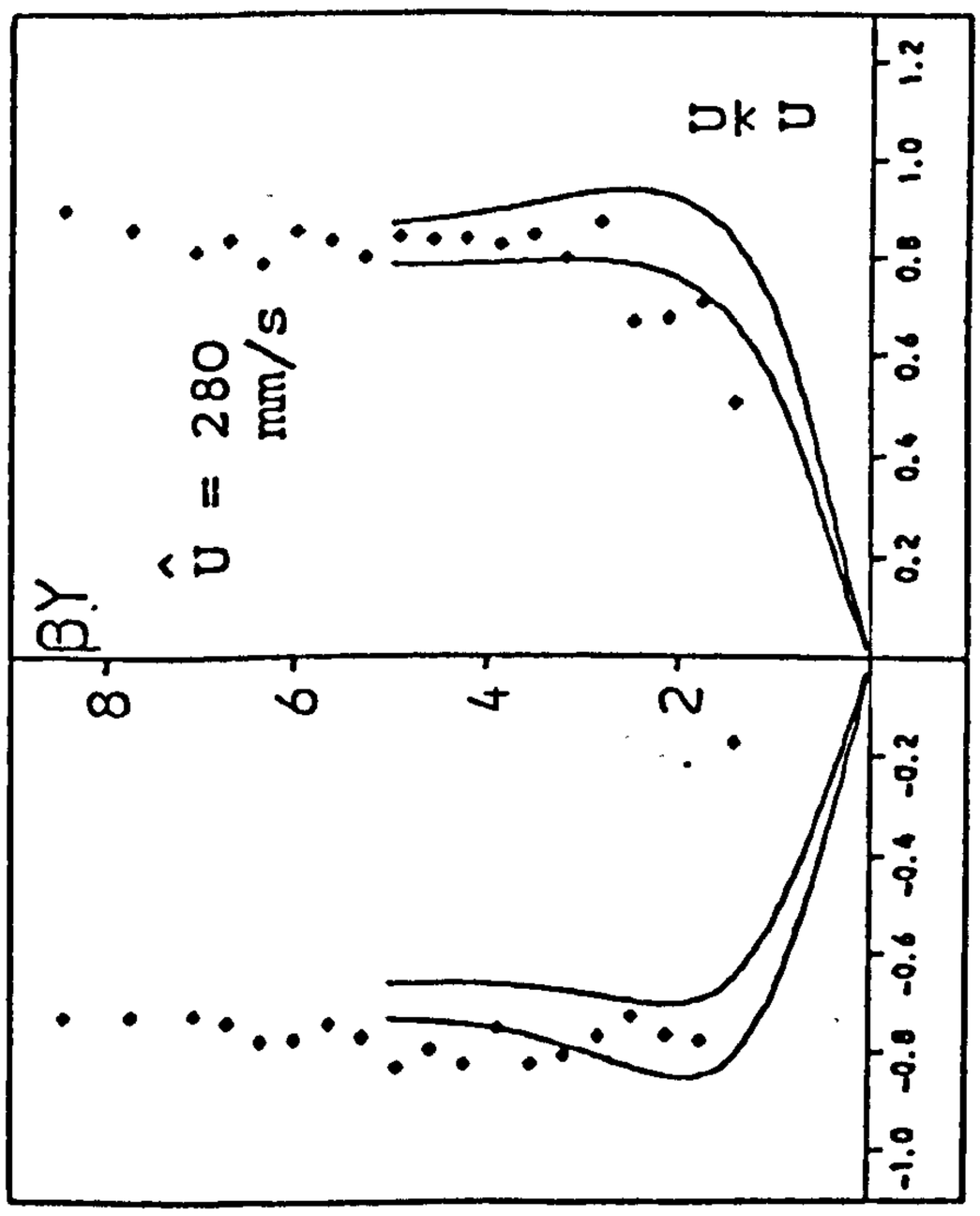

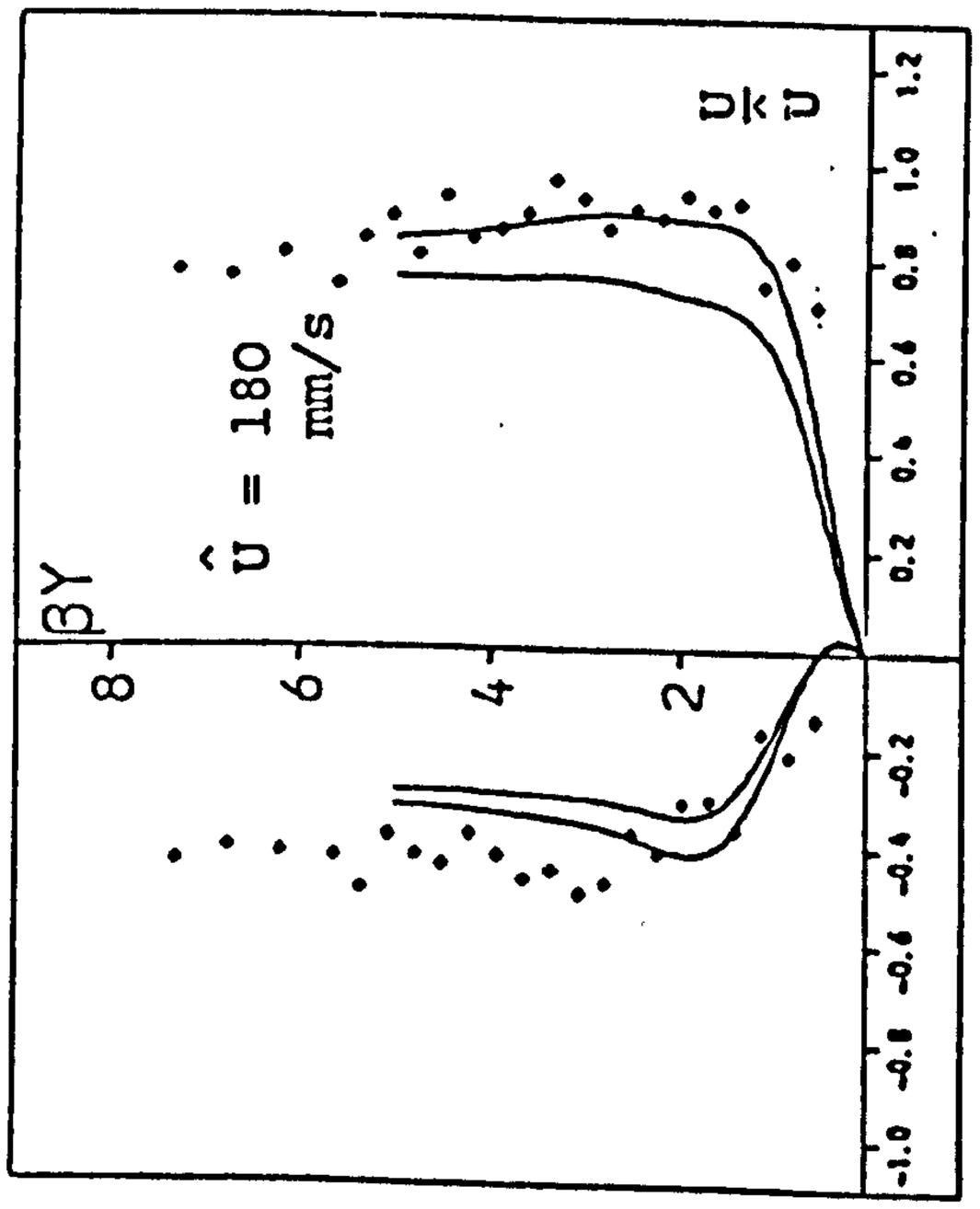

(i) 2D rough bed

FIG 6.21 THE VELOCITY PROFILE FROM EQ.6.9

level as was discussed earlier in this section (the results below the roughness level are discussed in Chapter Seven). While for 2-D rough bed results over trough, being in good agreement with the velocity profile over crest (Figs. 6.8 and 6.11), equation 6.9 is a good prediction. The difference between the two sets of results (for 2-D rough bed) is mainly due to the level of datum. In case of crest it is the roughness level, in contrast to trough which seemed to have a lower datum level.

The difference between the influence of 2-D and 3-D rough beds on the flow (from observed data) is not thoroughly due to the type of the roughness, but the values of Reynolds number. The larger the Re values the more turbulent the flow becomes and thus less predictable and the elimination of the entire laminar boundary layer thickness.

Although the obtained results are evidently a basis for discussion, lack of sufficient data for various rough beds limits our support for this hypothesis.

6.5 Roughness Effect on Mass Transport Velocity

It is now known that up to 20% turbulence and 40% increase in velocity is introduced by the rough beds to the flow within the boundary layer thickness.

A similar fluctuation occurs for the mean velocity as presented in Figs. 6.17(d) and 6.13(d), having a normally

distributed set of data, but the observed mean velocities fluctuate very little as shown by the standard deviations in the figures, considering that the position of sampling data has been one of the high turbulence areas. Beside small perturbation of the mean velocity, the turbulent flow has not increased the mean velocity much, but instead the corresponding eddies help to disturb the suspended material within the boundary layer even more, and within each half cycle when the velocity fluctuates from a maximum to zero the transport of the materials is at a larger rate because of these velocity changes.

Hence, the mean velocity is not changed much due to roughness elements and the increase in mass transport is due to the turbulence intensity which is a random movement. Except that when the wave period increases the materials due to a rough bed would move in the direction opposite to the wave progression (or shore in case of ocean waves), and the rougher the bed (or the larger the Reynolds number value), the greater would be the offshore velocity above the roughness.

6.6 Concluding Remarks

1. The velocity over smooth bed was always laminar,

2. The boundary layer velocity profile was well represented by the modified Stokes second order shear wave

equations (6.5 and 6.7) for intermediate water waves.

3. The mean velocity had lesser values than the Longuet-Higgins conduction solution (except for 1.4 s wave period), but of the same profile.

4. For 3-D rough bed with large size roughness elements, thus resulting greater Re values, the laminar boundary layer became highly perturbed and the profile was completely eliminated (except over the roughness element where only the flow was perturbed). conclusion was also reached due to a poor correlation existing between the velocities at different positions over the rough bed (R and S, crest and trough) throughout the boundary layer thickness.

5. As for 2-D rough bed the flow was disturbed close to the top of roughness crest but the laminar boundary layer profile re-appears close to the edge of the boundary layer thickness which also resulted in high correlation with increasing height.

6. For rough beds, the boundary layer velocity equation is in the form of equation 6.9 (depending on the Re values).

7. Due to the roughness elements the mean velocity was not changed much, just perturbed.

8. The influence of the 2-D and 3-D rough beds were similar except for the size of the roughness elements.

CHAPTER SEVEN

VELOCITY RESULTS AND ANALYSIS OF FLOW INSIDE THE ROUGHNESS ELEMENTS

7.1 INTRODUCTION

The understanding of the flow behaviour below the roughness element height (or around the roughness elements) is important for two major reasons;

(i) The changes in mass transport velocity due to the roughness element, and thus the movement of the bed material and exerted forces.

(ii) The mixing of the eddies, introduced by the roughnesses, into the boundary layer zone and beyond.

While the results for rough boundary layer velocity have been analysed and discussed in Chapter 6, and the velocity profile outside the boundary layer region is the subject of Chapter 5, this chapter contains the analysis of the flow inside (or between) the roughness elements.

7.2 THE RESULTS

Since the water velocity at levels below the roughness height fluctuates more than outside the roughness zone, the vertical profile of the velocity within the depth of the roughness and at different phases of wave cycle (as was done for the boundary layer velocity results) were seen to be

random. Instead the more useful characteristics of turbulence intensity and mean velocity within this depth, are analysed and discussed for the rough beds. (It is this data which is used for discussion in this chapter and not the 121 sample points data within each cycle).

7.2.1 Two Dimensional Rough Bed

The velocity was recorded over 5 cycles at 17 depths with equal intervals of 0.25 mm from just above the bottom of the bed (0.5 mm height) to just below the top of the roughness (4.5 mm, when the roughness height κ = 4.65 mm), for the five wave periods (1.4 to 2.2 sec.). Also at the two extreme heights, lowest and highest, the velocity was observed over 45 cycles.

The five-cycle mean velocity at each depth and the range of the five values of the one-cycle mean velocity at each depth are shown in Fig. 7.1. This figure also shows the 45-cycle mean velocity taken at the two particular levels, and the standard deviation about that mean of the 45 values of the one cycle mean velocity. Samples of the velocity profiles at the two heights (showing the range of velocity at twenty phases within a cycle span) are shown in Fig. 7.2. Fig. 7.3 illustrates the distribution of the velocity sampled at three arbitrary phase positions in each of the 45 cycles, together with the mean velocity distribution over the 45 cycles (Fig. 7.3d), in the form of a probability distribution

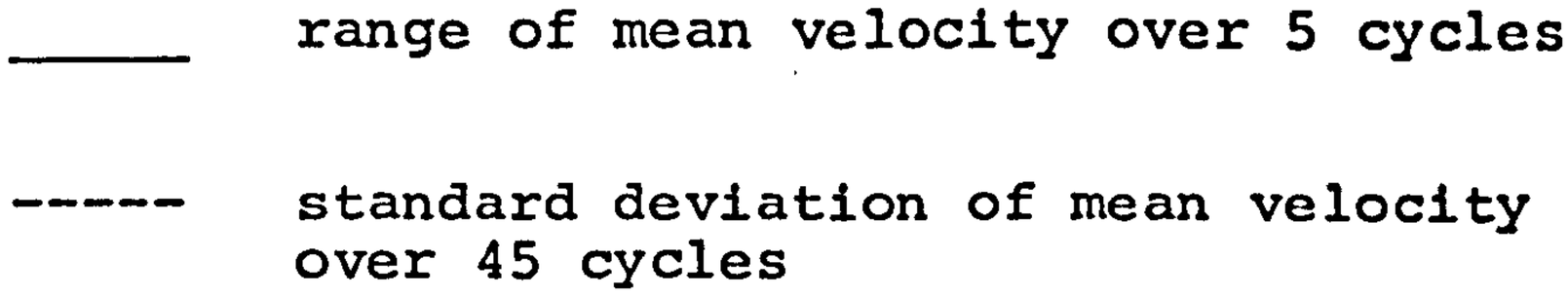

Figure 7.1 The Variation of the Mean Velocity Inside the Roughness Elements (2-D rough bed).

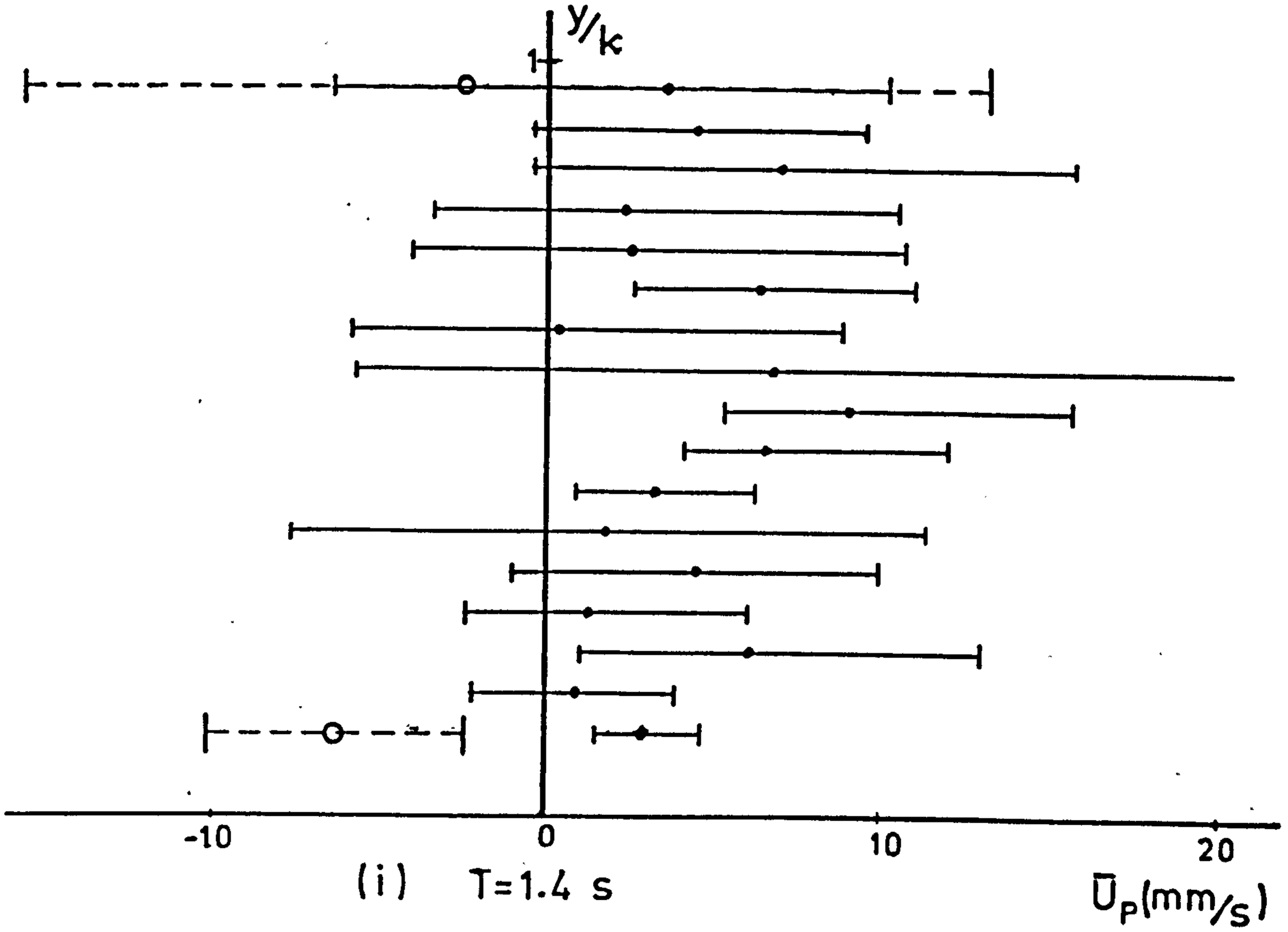
y/k
1
-10
0
10
20
(i) T=1.4 s
$\bar{U}_p$(mm/s)

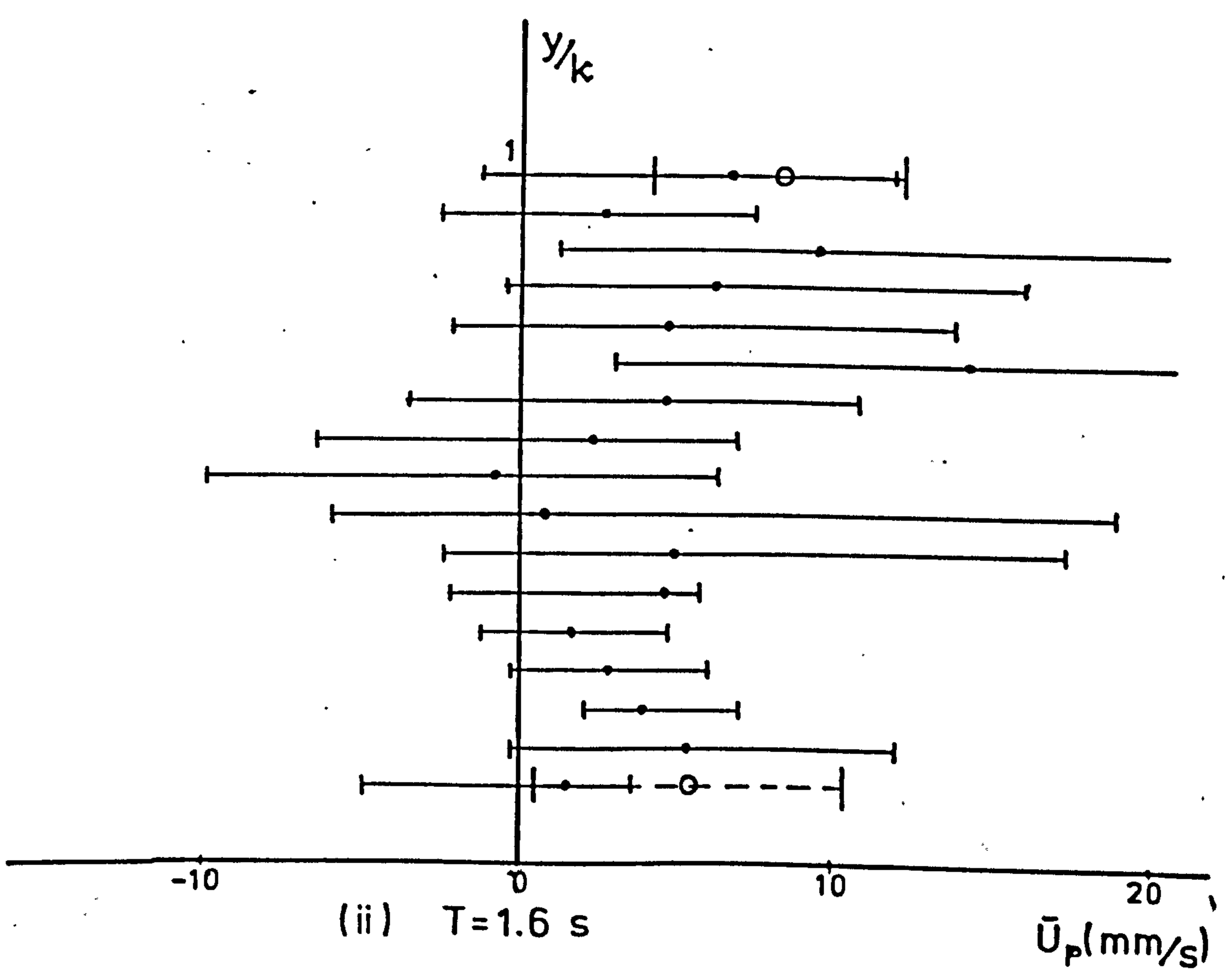
y/k
1
-10
0
10
20
(ii) T=1.6 s
$\bar{U}_p$(mm/s)

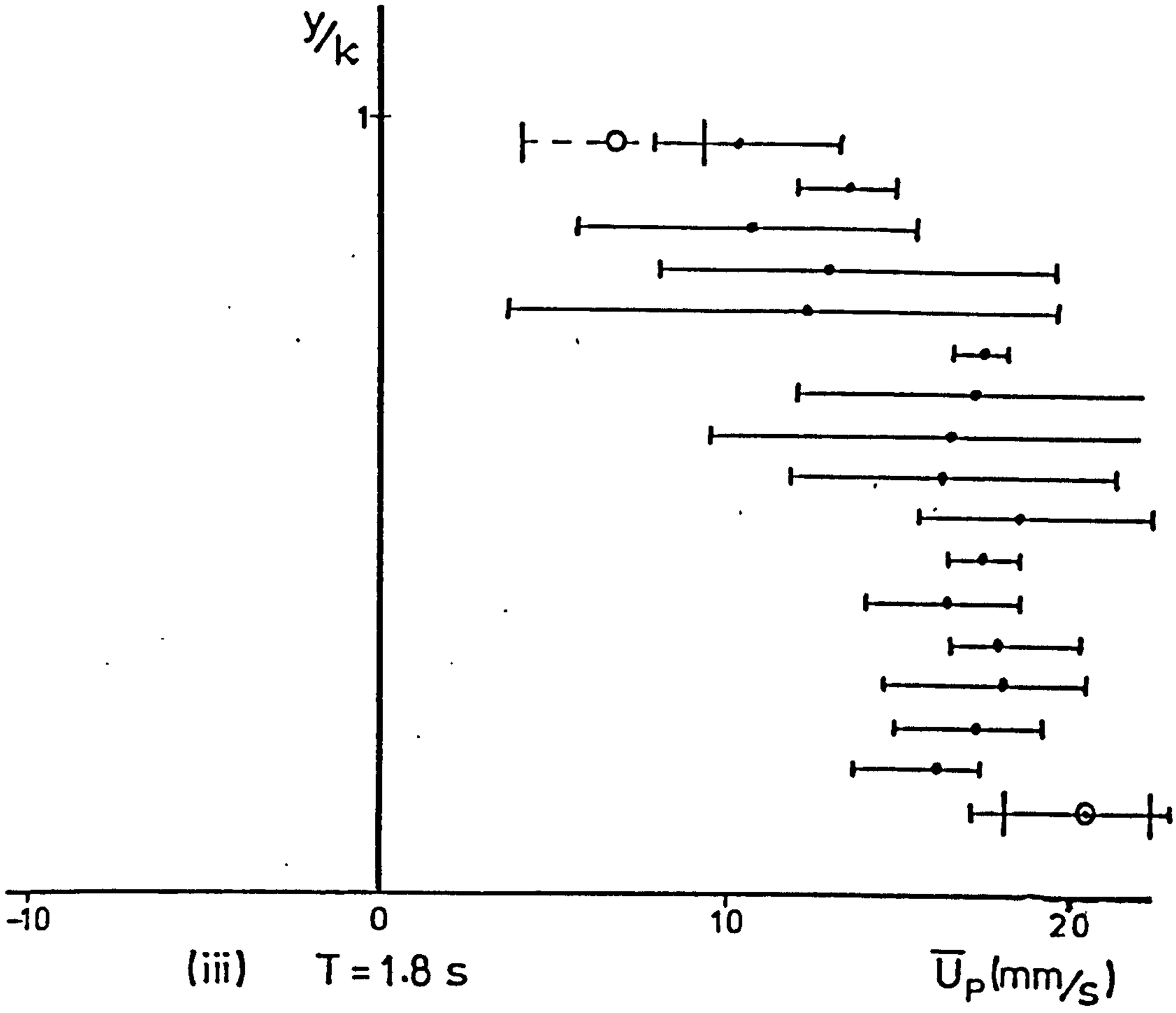

(iii) T = 1.8 s

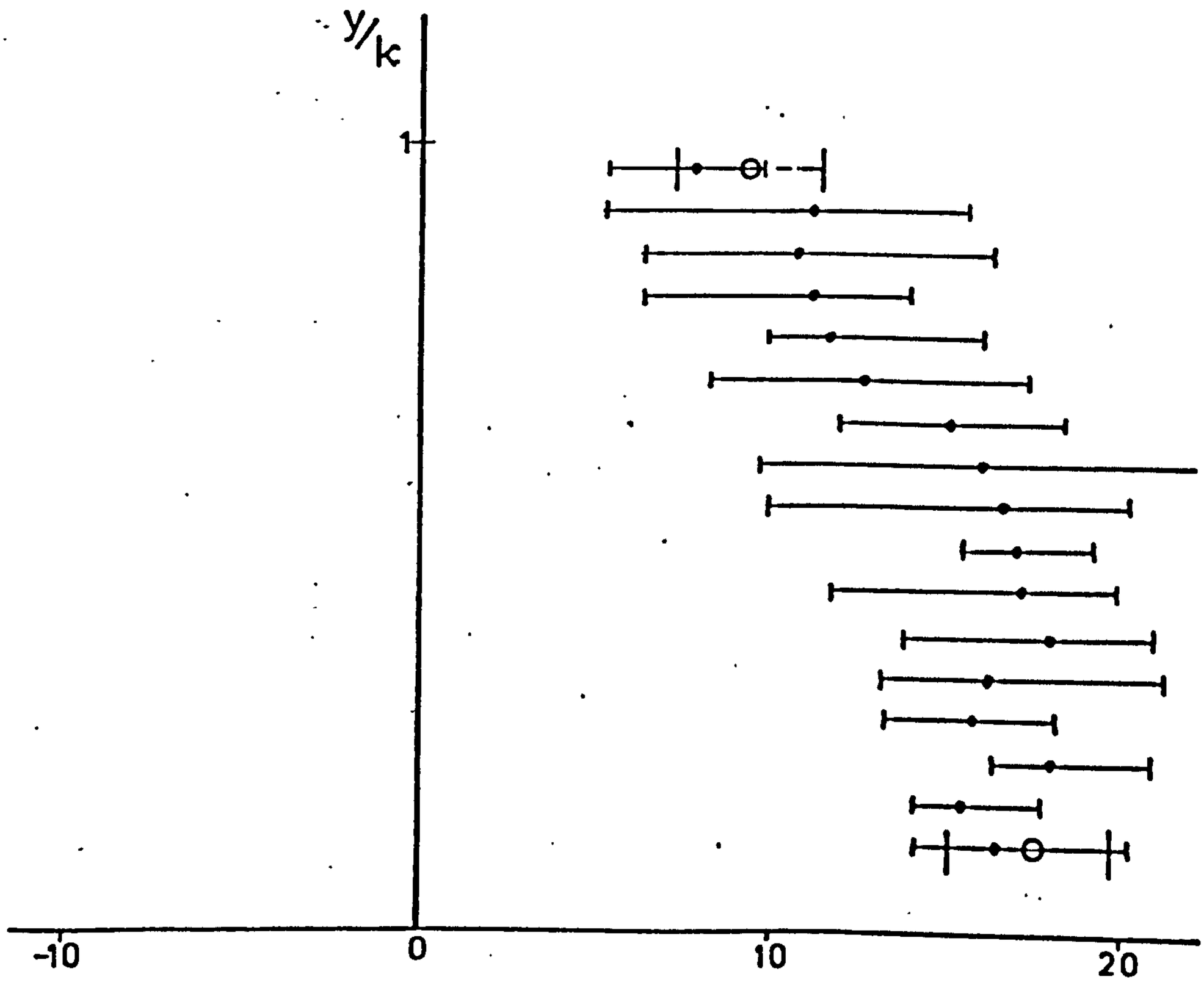

(iv) T = 2.0 s

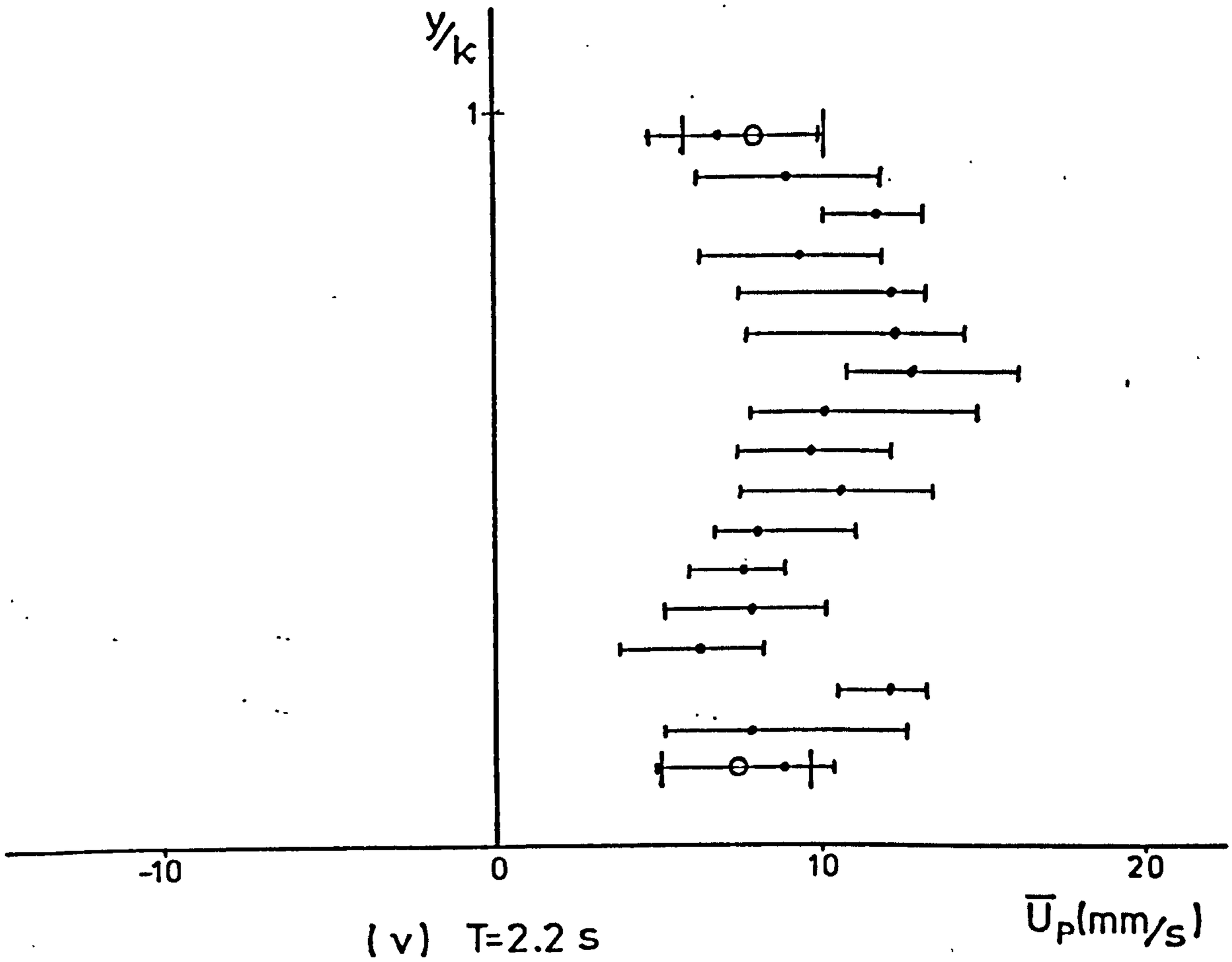

(v) T=2.2 s

(i)

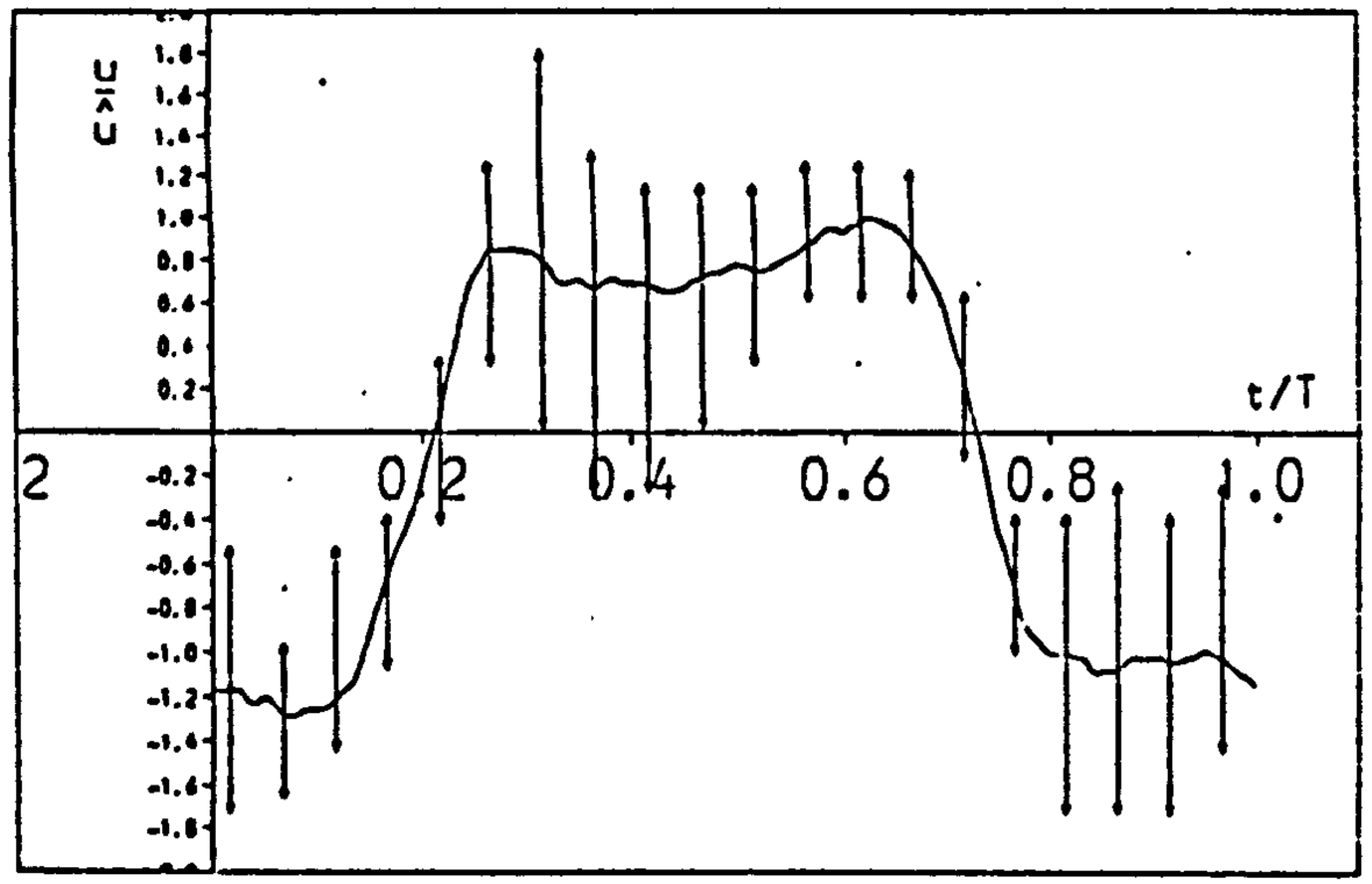

Y=0.5 MM T=1.4 SEC $\hat{U}$=62.7 mm/s

(a)

(ii)

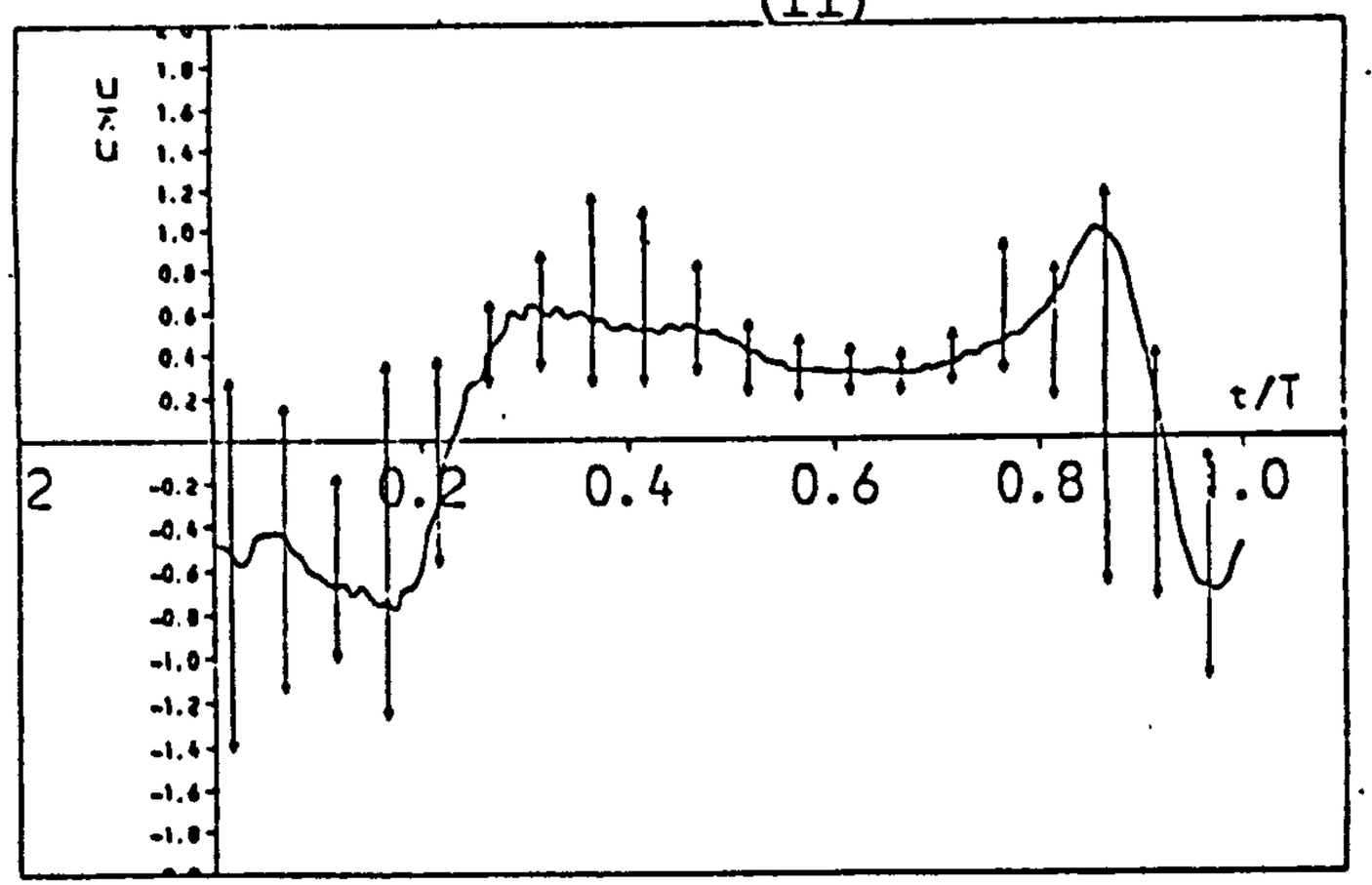

Y=0.5 MM T=2.2 SEC $\hat{U}$=48.0 mm/s

(a)

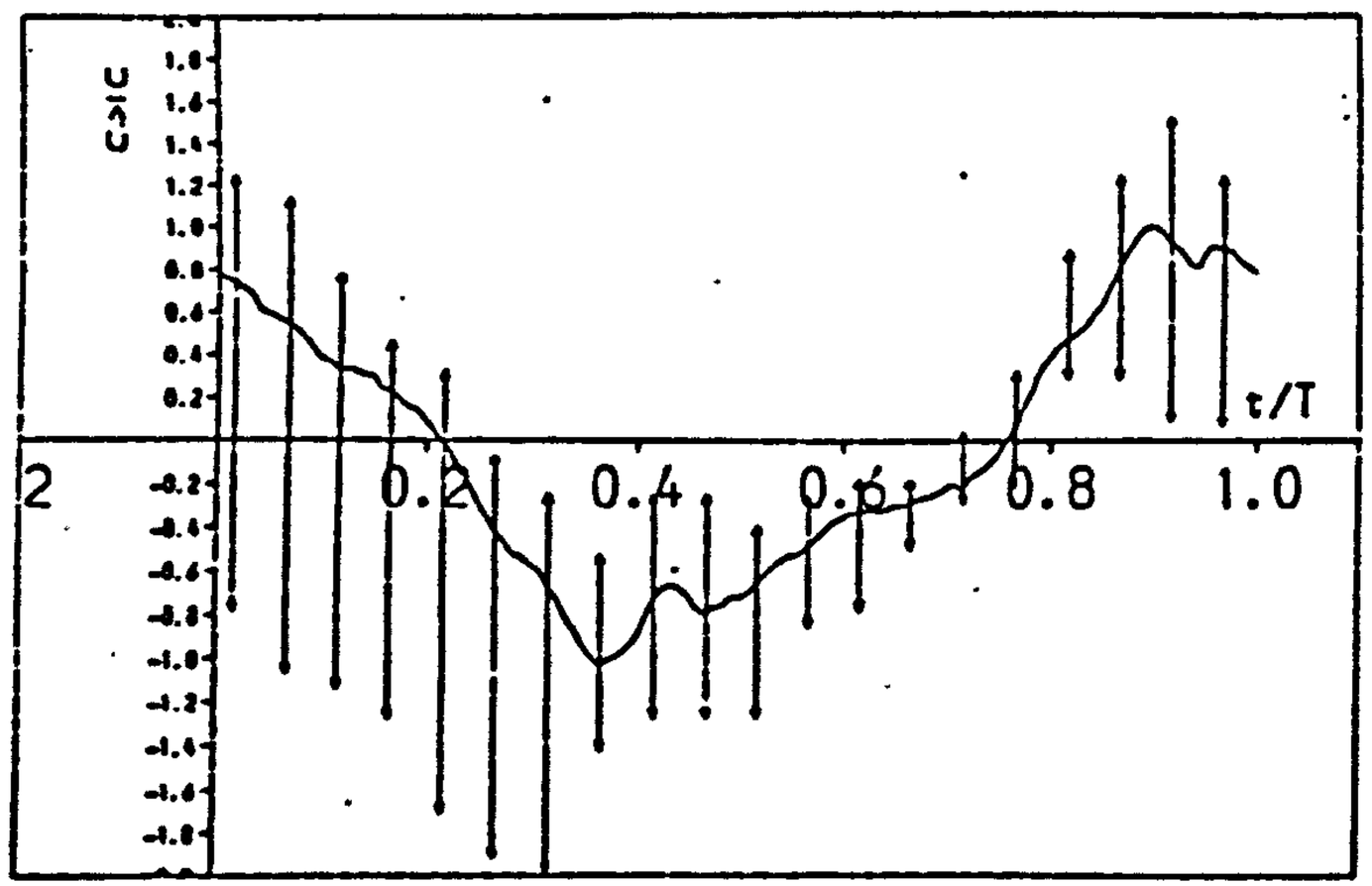

Y=4.5 MM T=1.4 SEC $\hat{U}$=128.9 mm/s

(b)

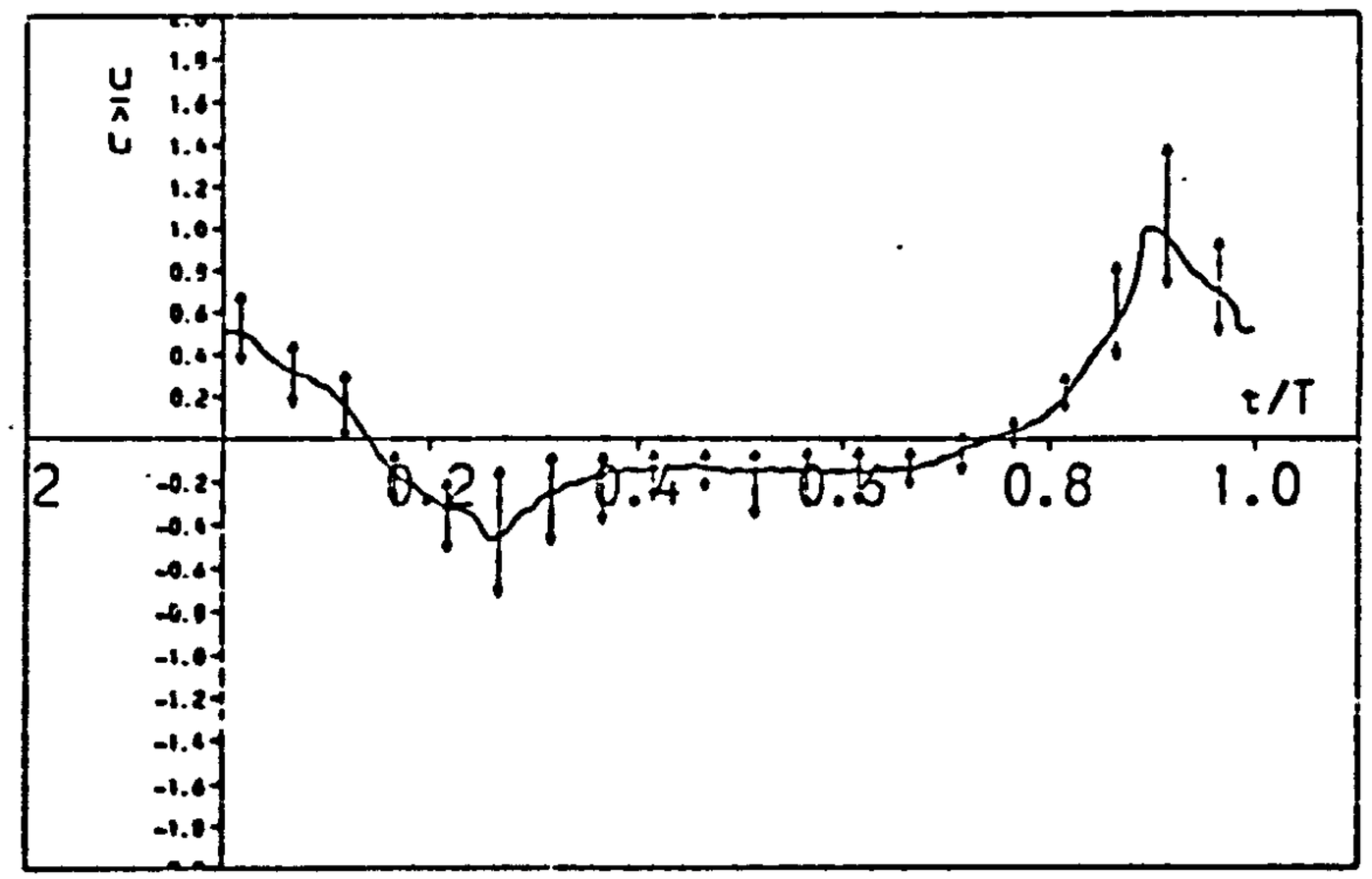

Y=4.5 MM T=2.2 SEC $\hat{U}$=124.6 mm/s

(b)

Fig. 7:2 The Mean Cyclic Variation of Velocity over 45 Waves at Two Heights Below Roughness

*	0.5 mm height over the bed
o	4.5 mm height over the bed
SD	Standard Deviation
0.0-1.0	The range of the data

Fig. 7.3 The Velocity Distribution for 3 arbitrary phases (a, b, c) and mean velocity (d) over 45 cycles inside 2-D rough bed.

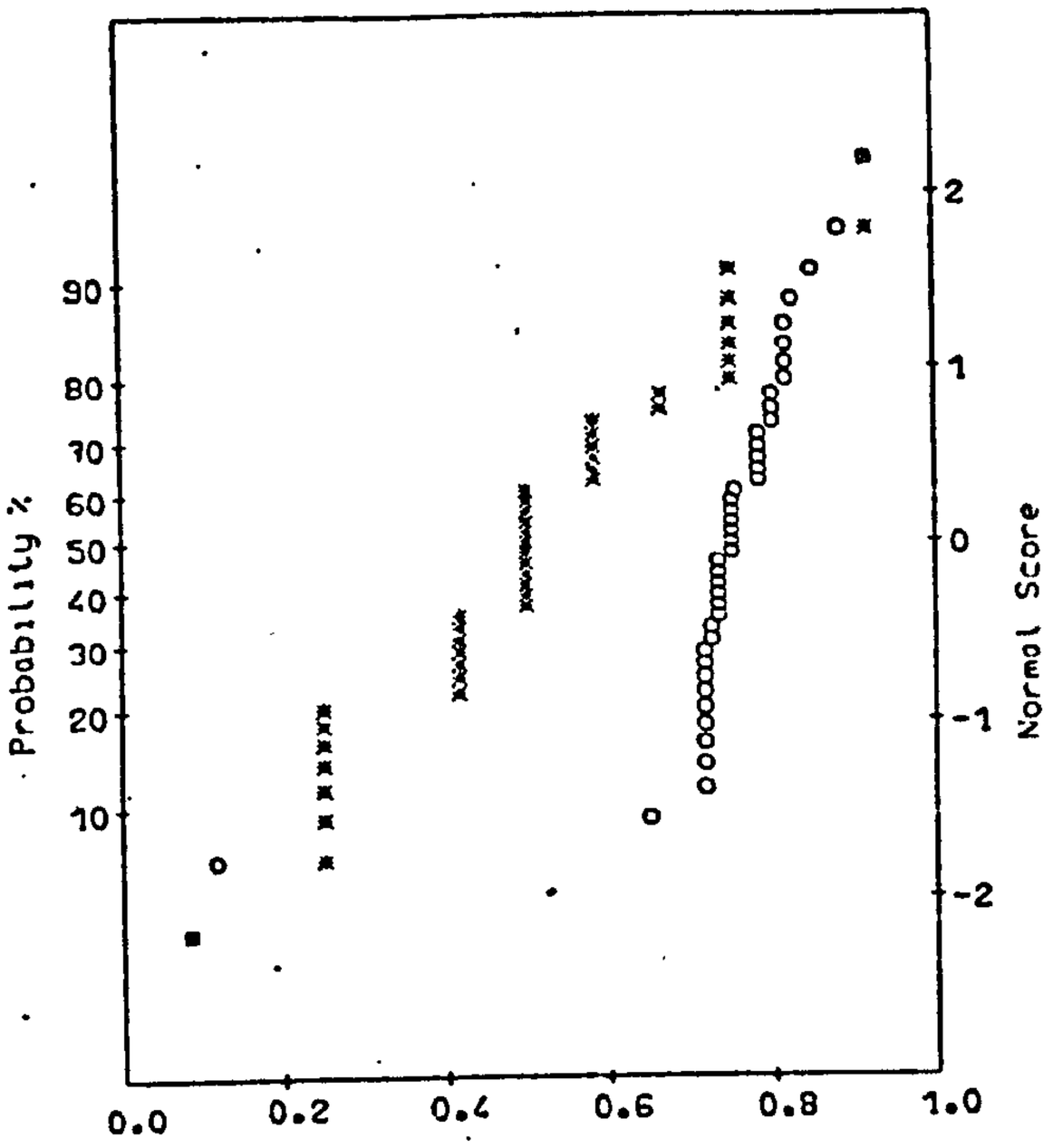

	SD	Mean	1.0	0.0
x	10.3	−74.6	−47.7	−102.6
o	41.2	43.4	117.1	−157.5

(a)

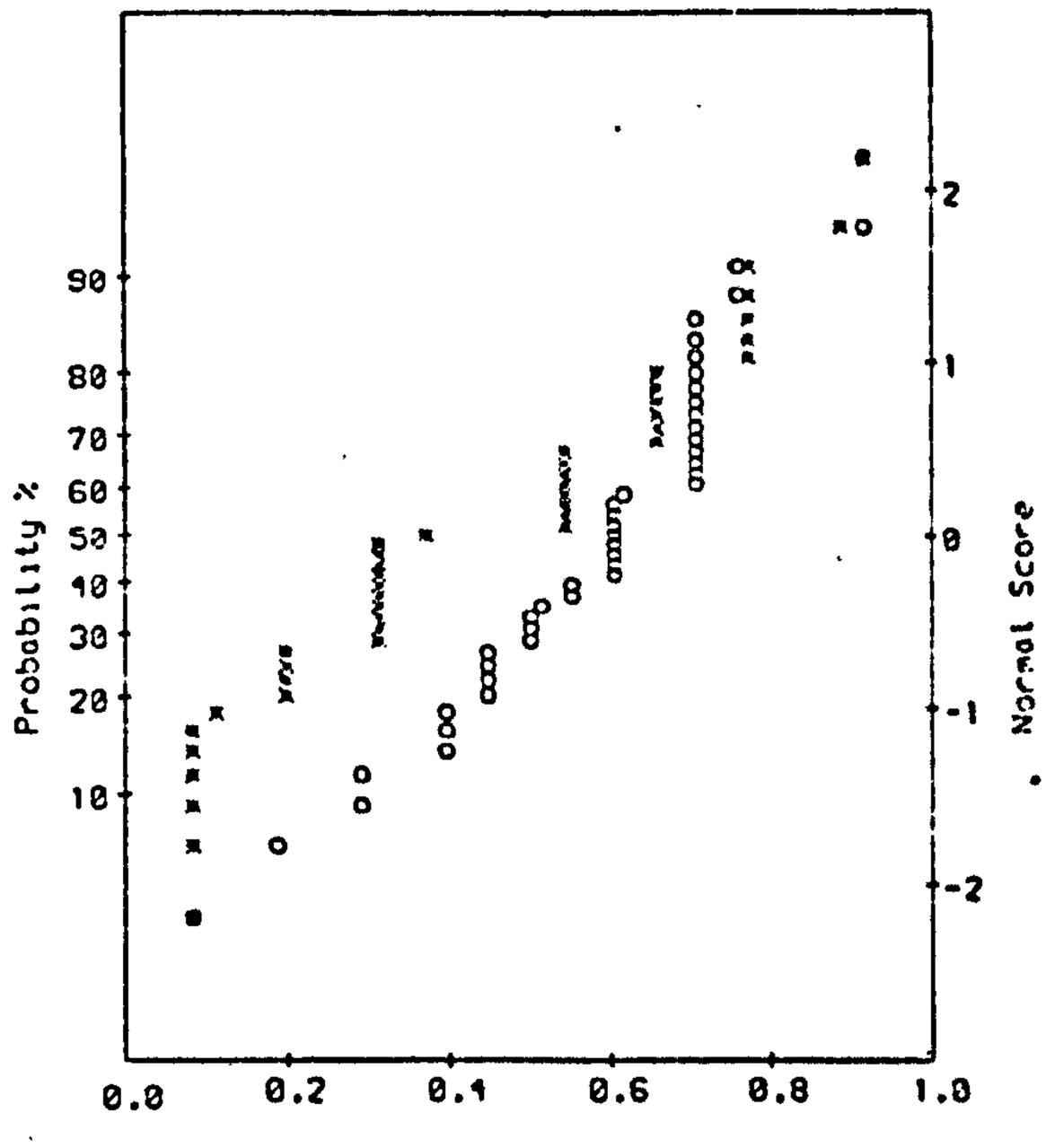

	SD	Mean	1.0	0.0
x	10.0	53.4	75.7	36.0
o	15.3	−63.5	−26.6	−114.5

(b)

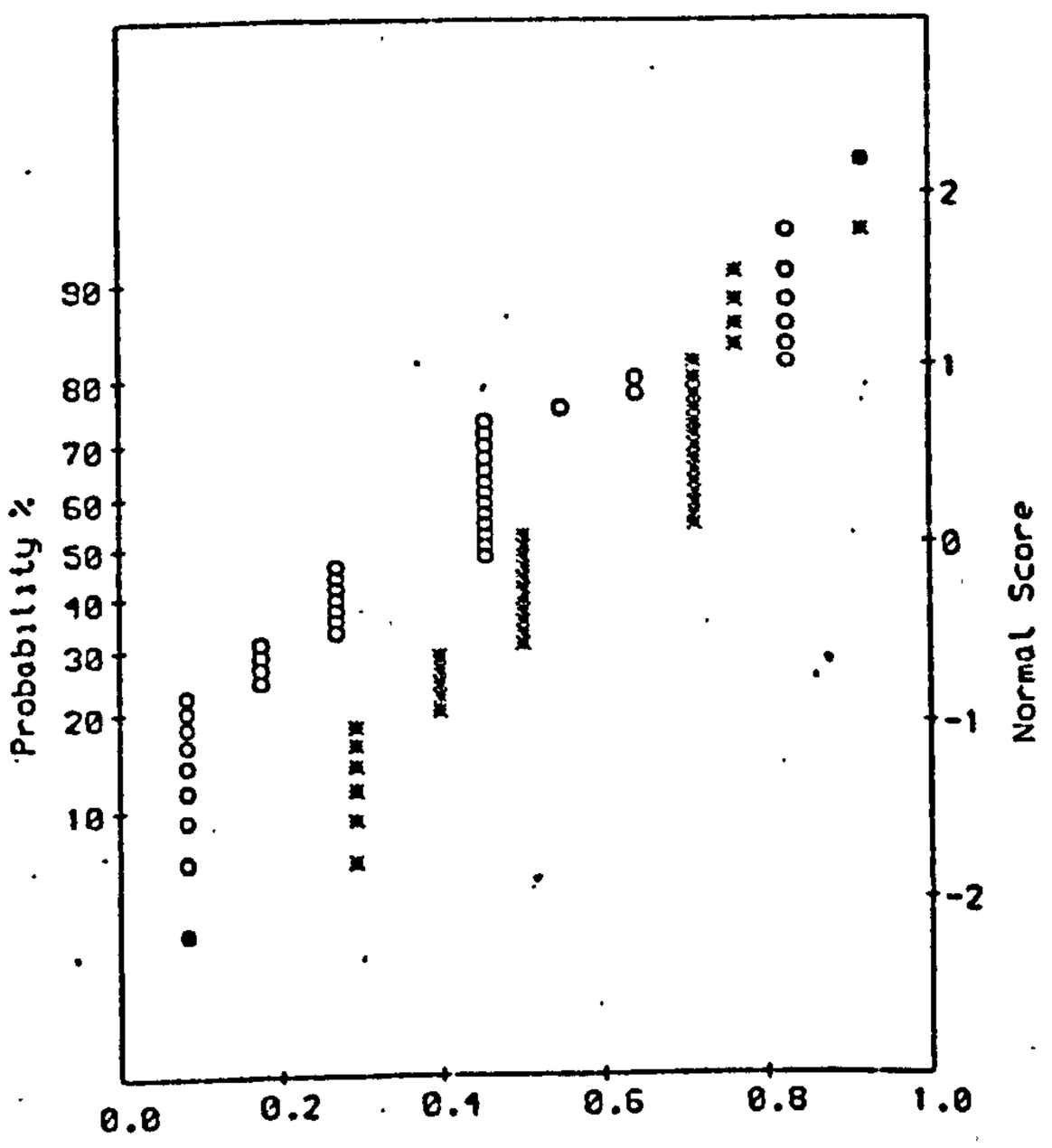

	SD	Mean	1.0	0.0
x	8.5	−3.7	15.5	−28.5
o	12.6	−18.6	11.3	−38.0

(c)

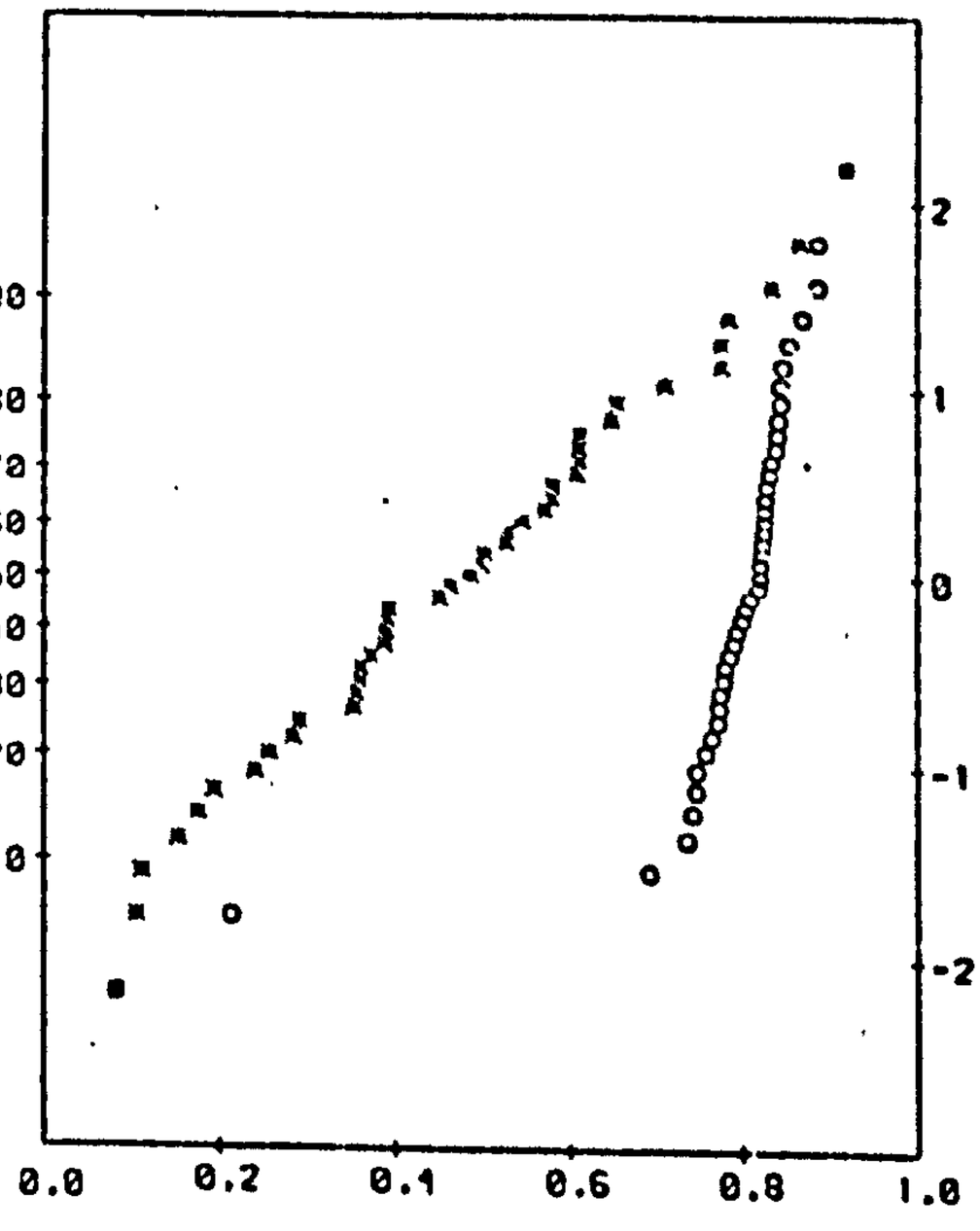

	SD	Mean	1.0	0.0
x	3.9	−6.3	3.2	−14.7
o	15.7	−2.5	21.2	−85.5

(d)

(i) T = 1.4 s

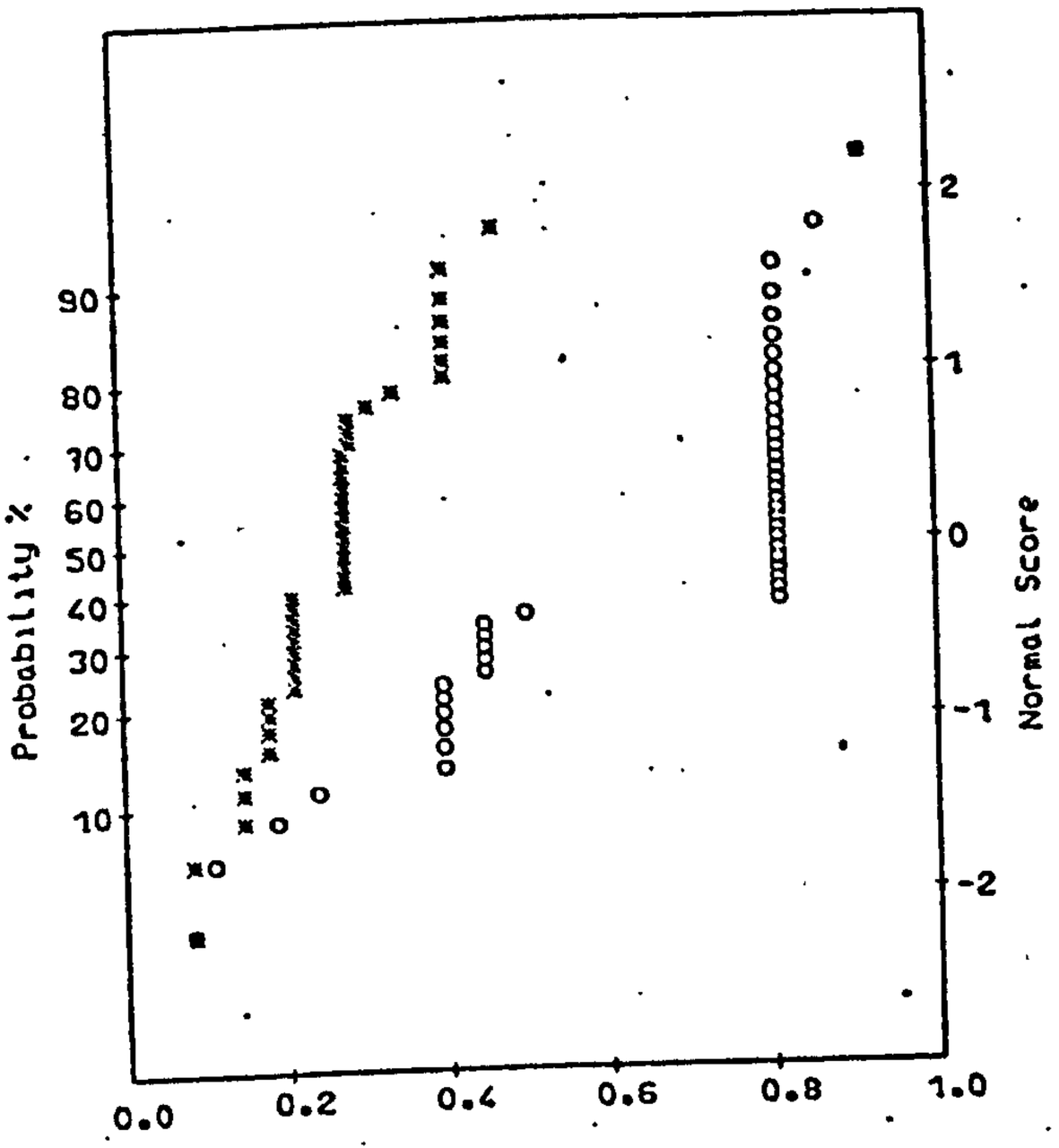

	SD	Mean	1.0	0.0
x	18.6	−52.3	51.2	−91.6
o	10.3	32.3	47.6	3.5

(a)

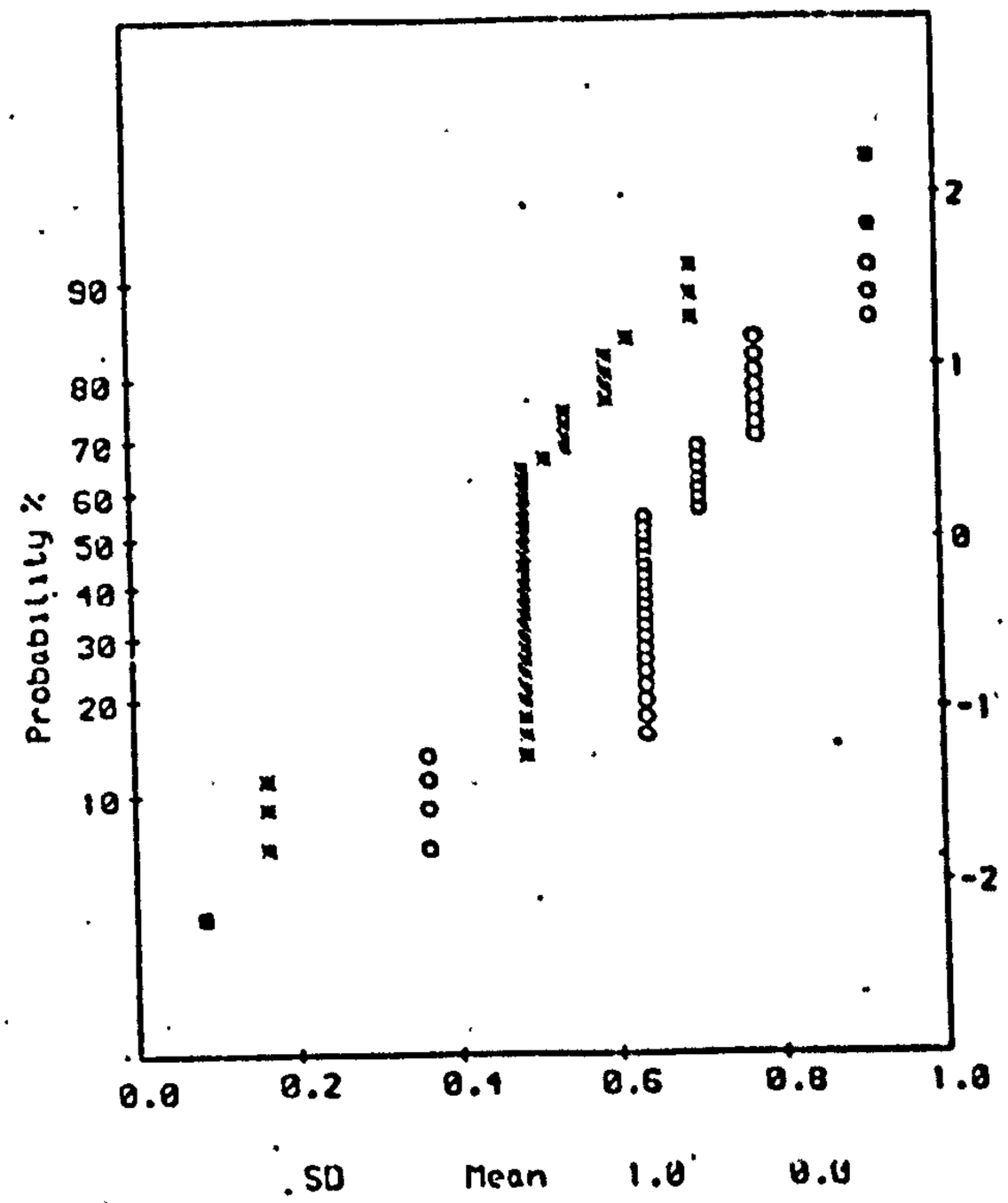

	SD	Mean	1.0	0.0
x	6.6	40.2	61.2	18.5
o	10.7	−32.0	−10.1	−76.1

(b)

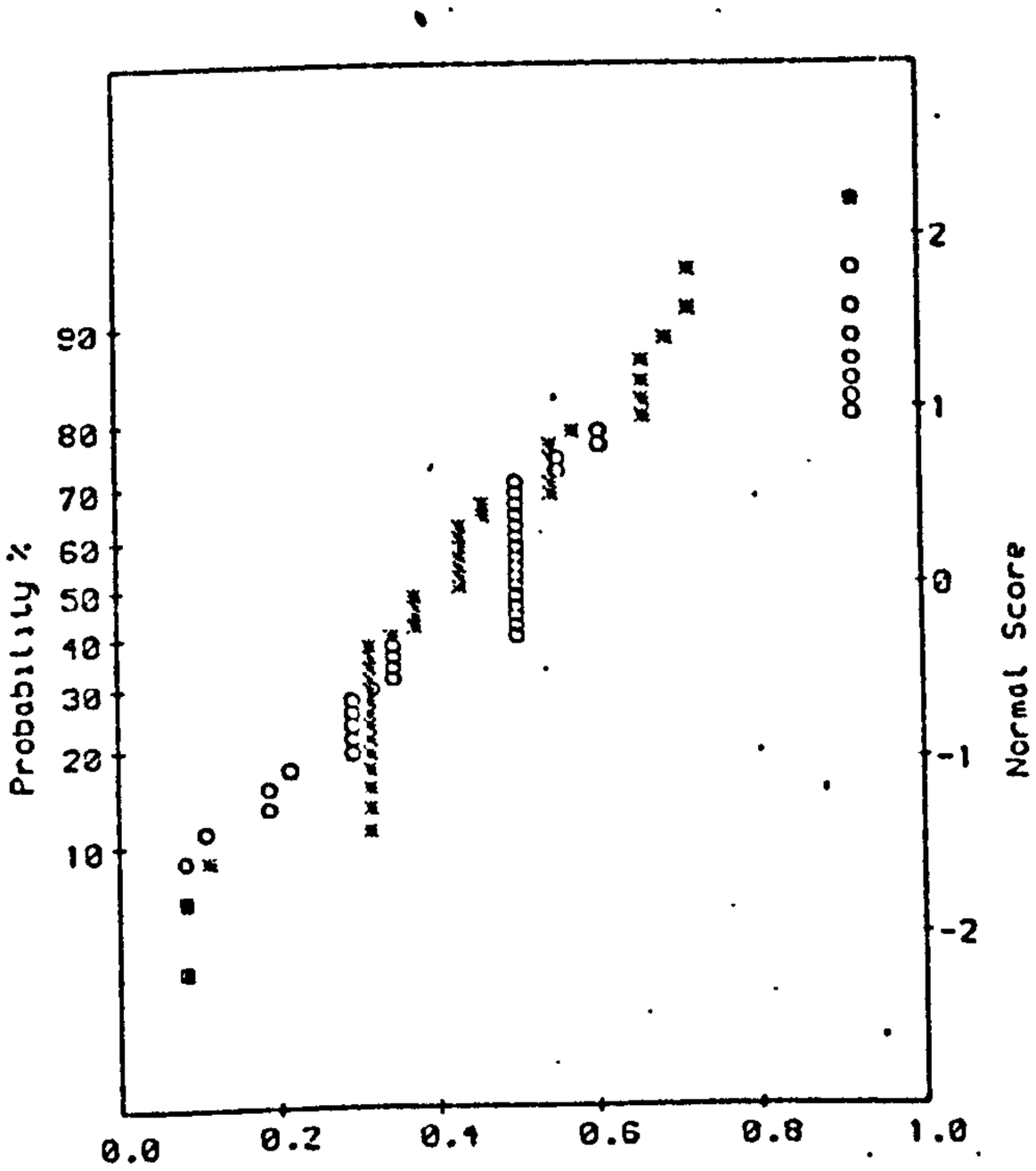

	SD	Mean	1.0	0.0
x	6.9	62.2	84.9	45.1
o	10.9	20.2	43.0	−1.0

(c)

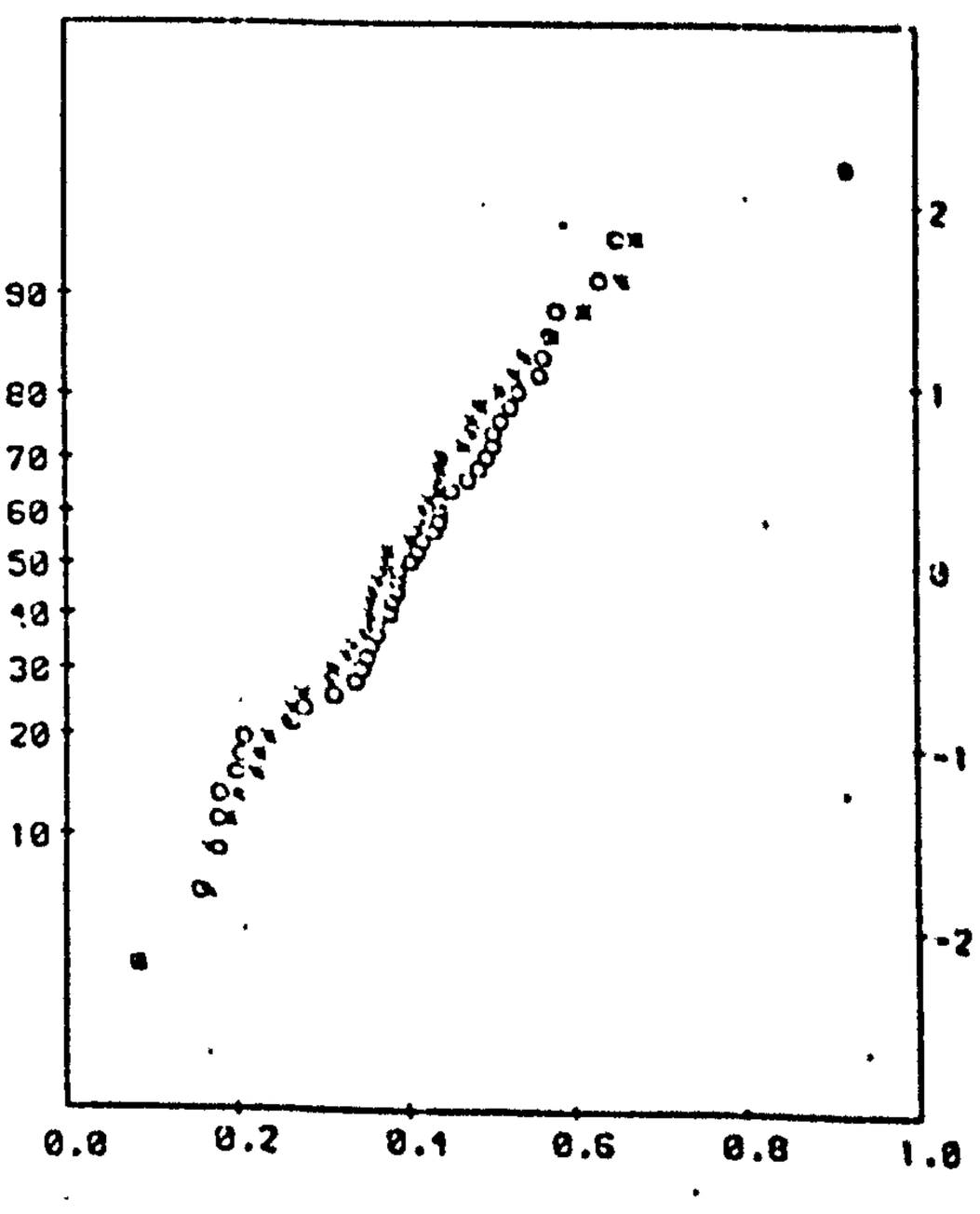

	SD	Mean	1.0	0.0
x	4.9	5.5	24.9	−7.0
o	4.0	8.2	23.6	−2.3

(d)

(ii) T = 1.6 s

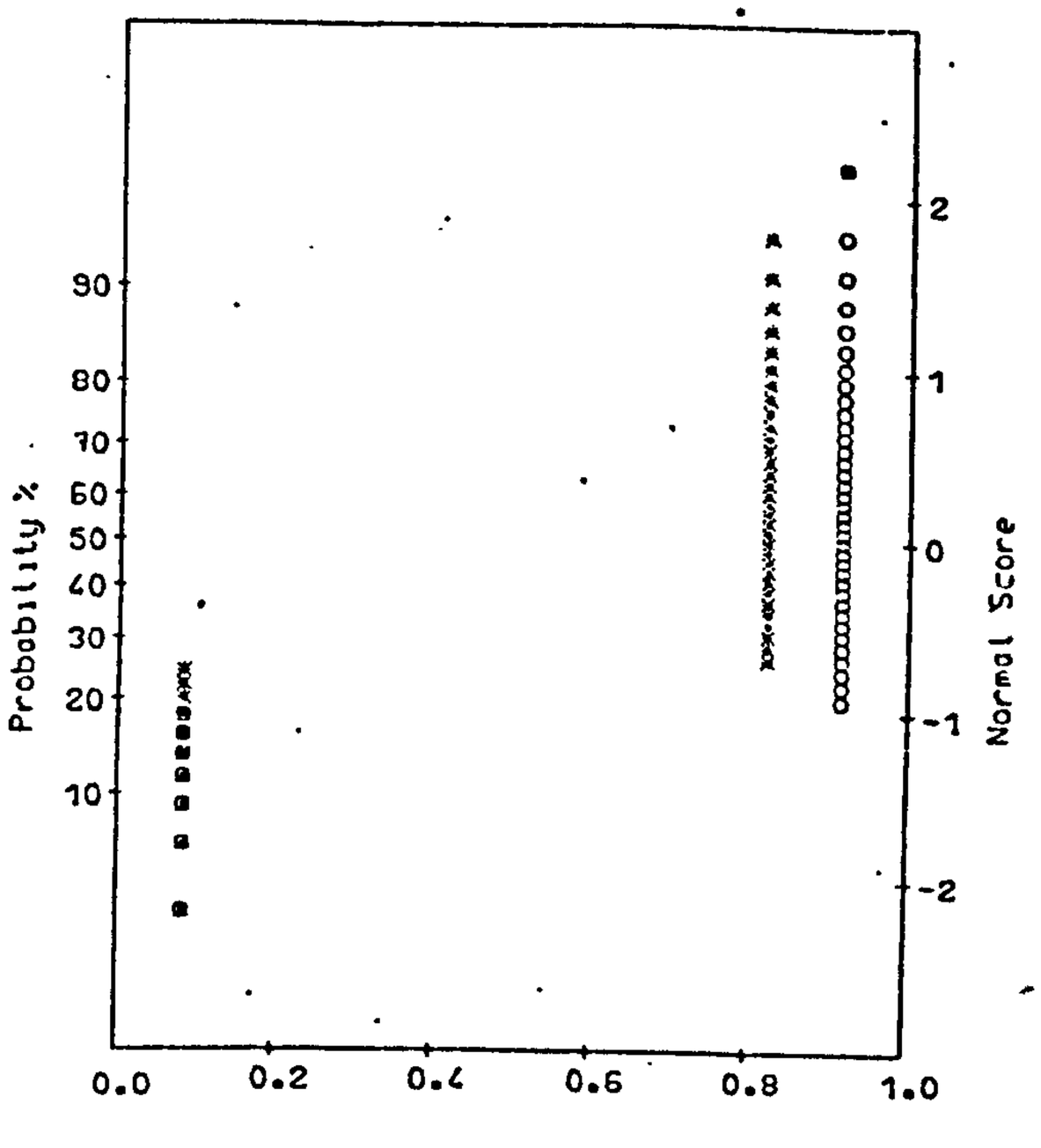

	SD	Mean	1.0	0.0
x	7.9	-1.5	7.1	-17.7
o	6.7	36.3	41.1	19.2

(a)

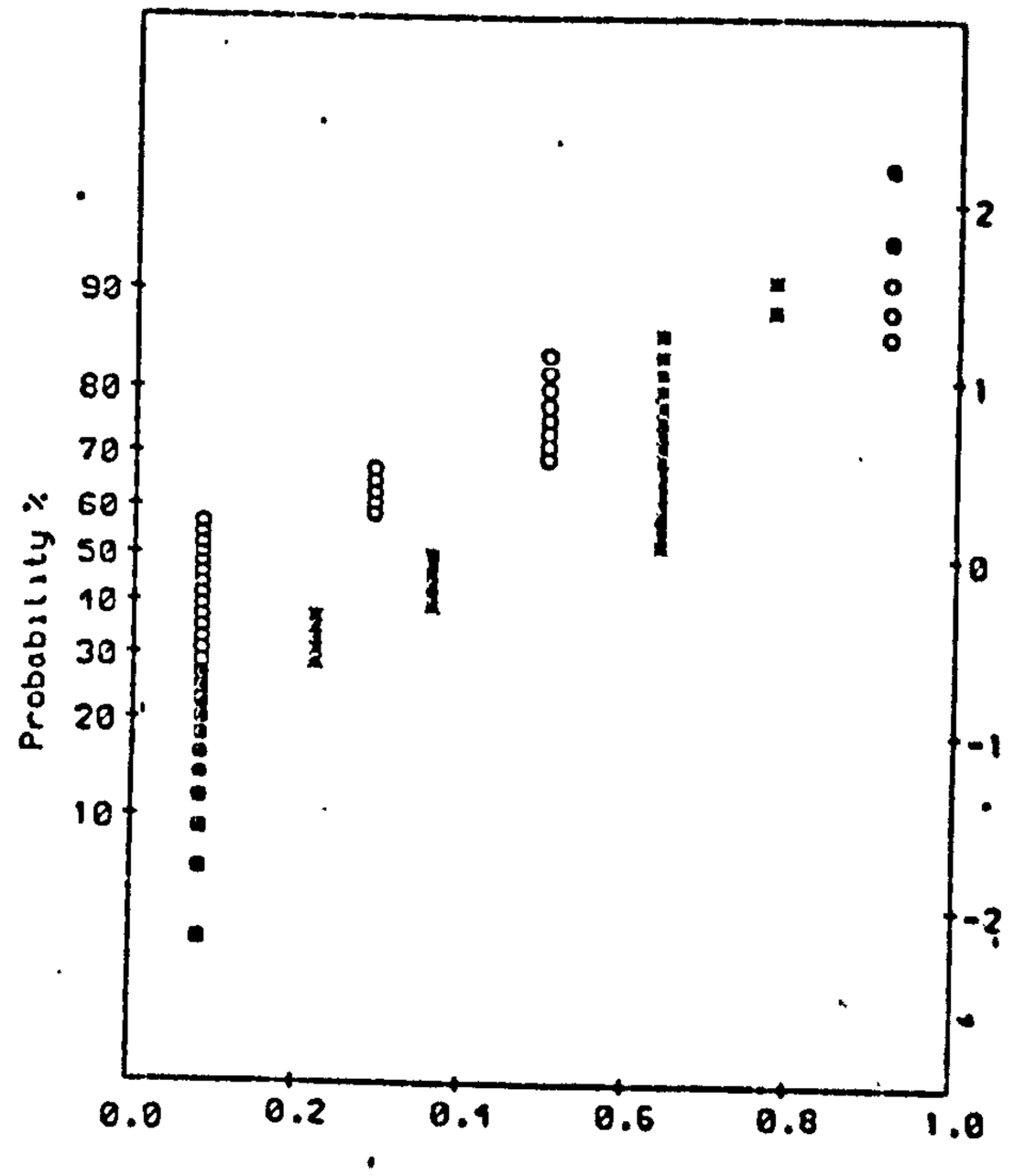

	SD	Mean	1.0	0.0
x	8.8	50.7	69.5	36.5
o	6.2	-29.6	-13.8	-35.7

(b)

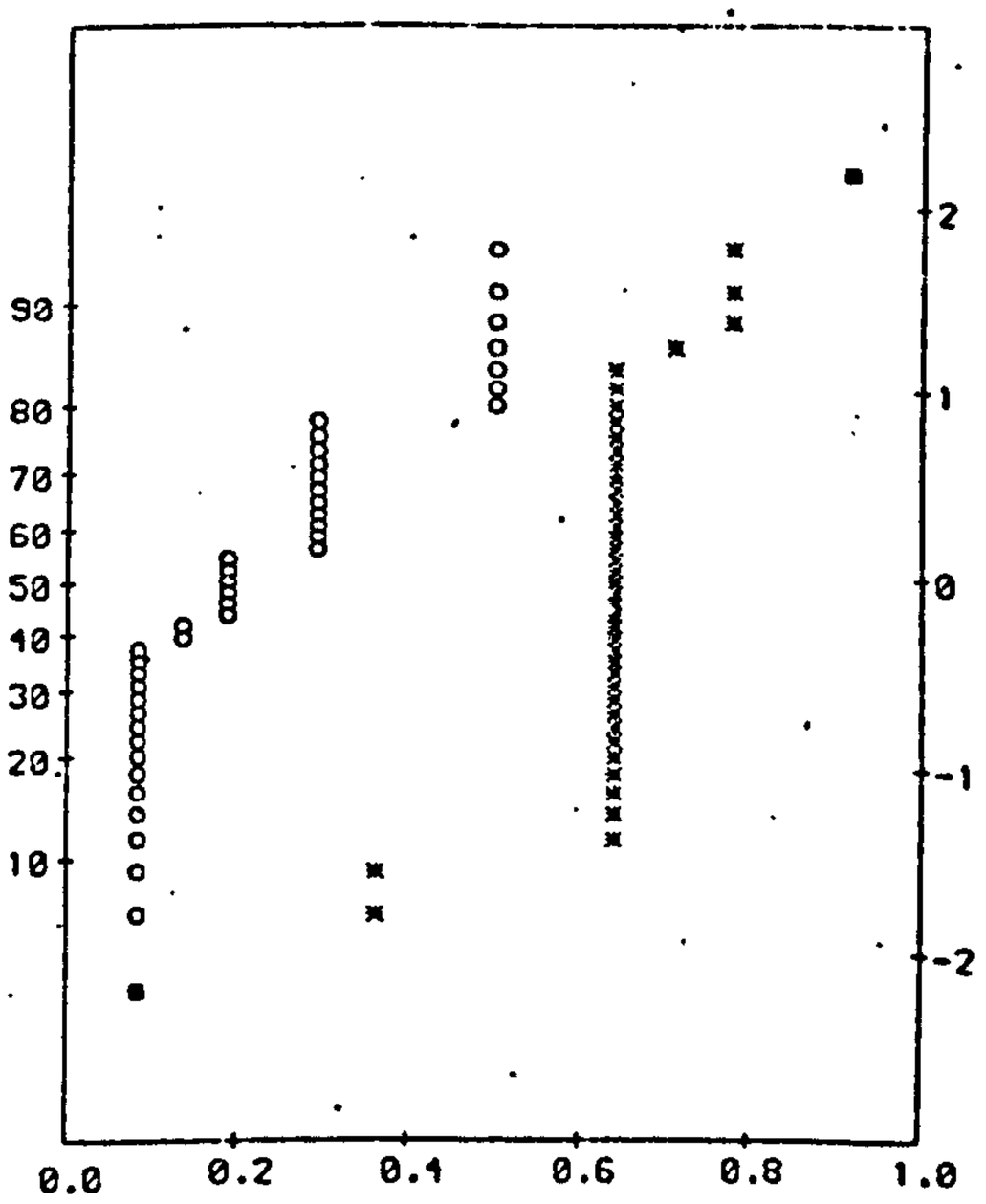

	SD	Mean	1.0	0.0
x	3.9	57.3	69.5	36.5
o	8.0	9.6	43.0	-1.0

(c)

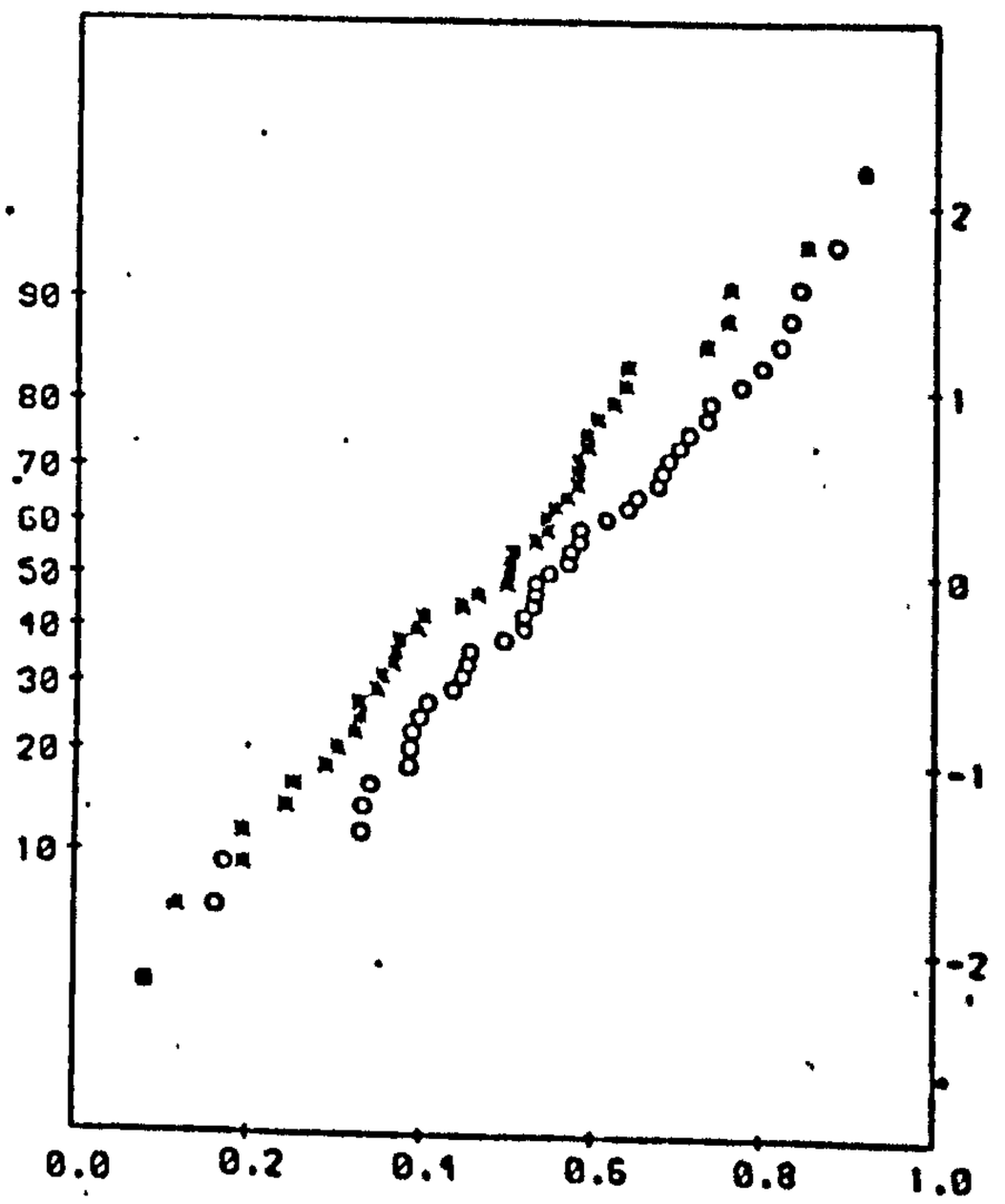

	SD	Mean	1.0	0.0
x	2.1	20.3	26.0	15.1
o	2.6	6.7	12.6	-0.6

(d)

(iii) T = 1.8 s

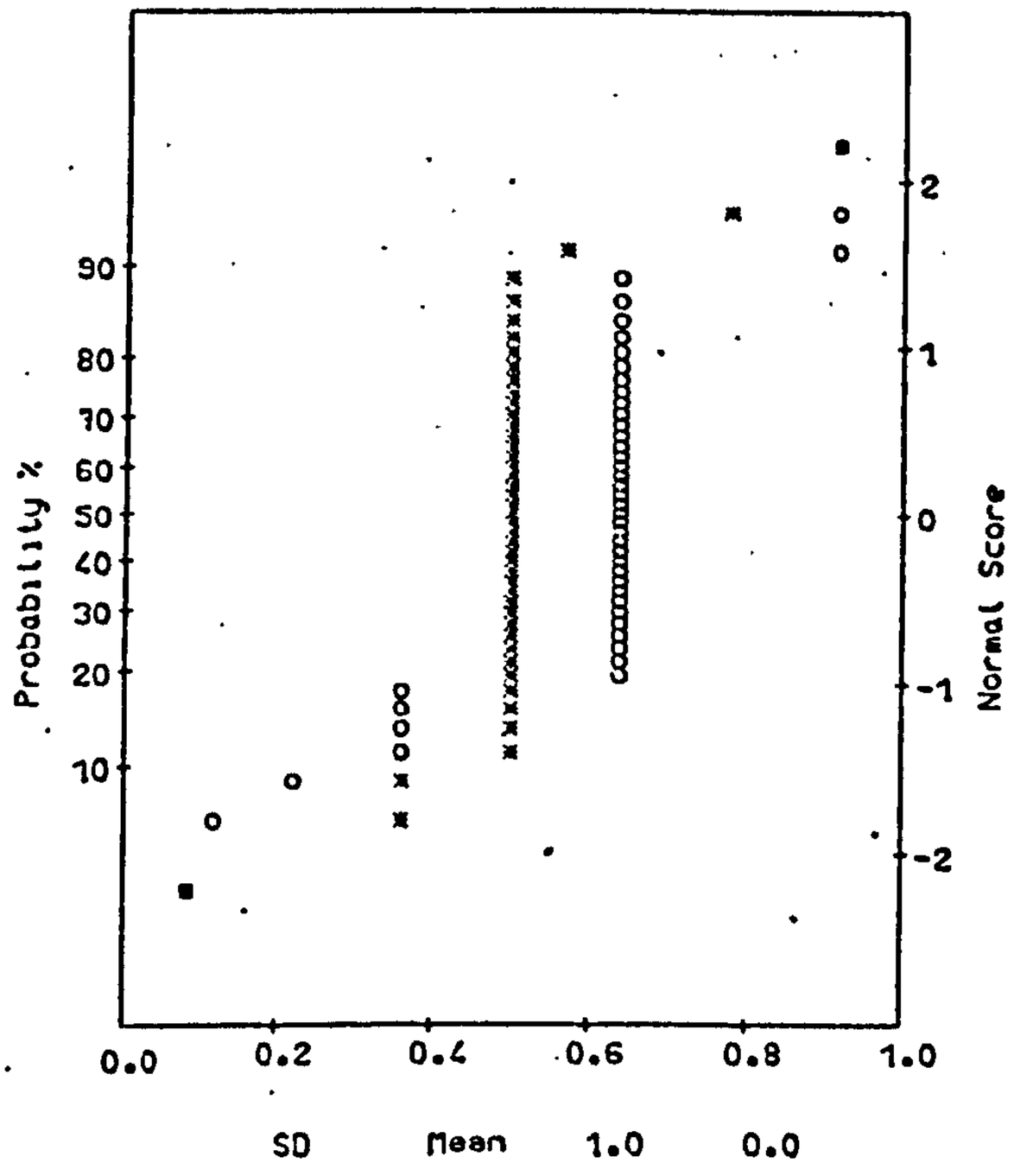
Probability %
90
80
70
60
50
40
30
20
10
2
1
0
-1
-2
Normal Score
0.0
0.2
0.4
0.6
0.8
1.0
SD Mean 1.0 0.0
× 13.6 -33.7 32.0 99.9
o 11.0 36,7 63.1 -2.8

(a)

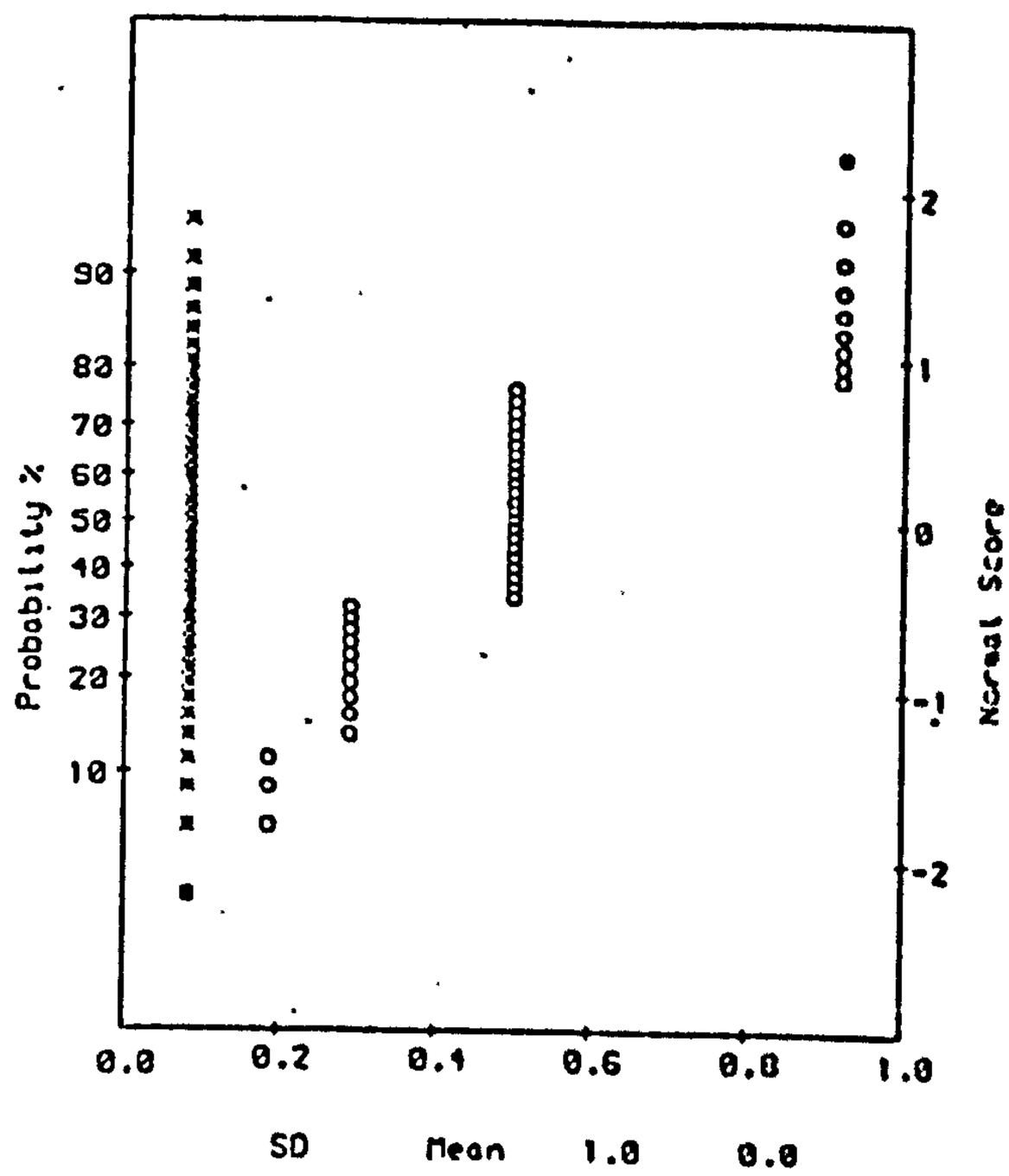
Probability %
90
80
70
60
50
40
30
20
10
2
1
0
-1
-2
Normal Score
0.0
0.2
0.4
0.6
0.8
1.0
SD Mean 1.0 0.0
× 0.3 39.3 41.8 39.1
o 10.4 -15.3 6.4 -37.6

(b)

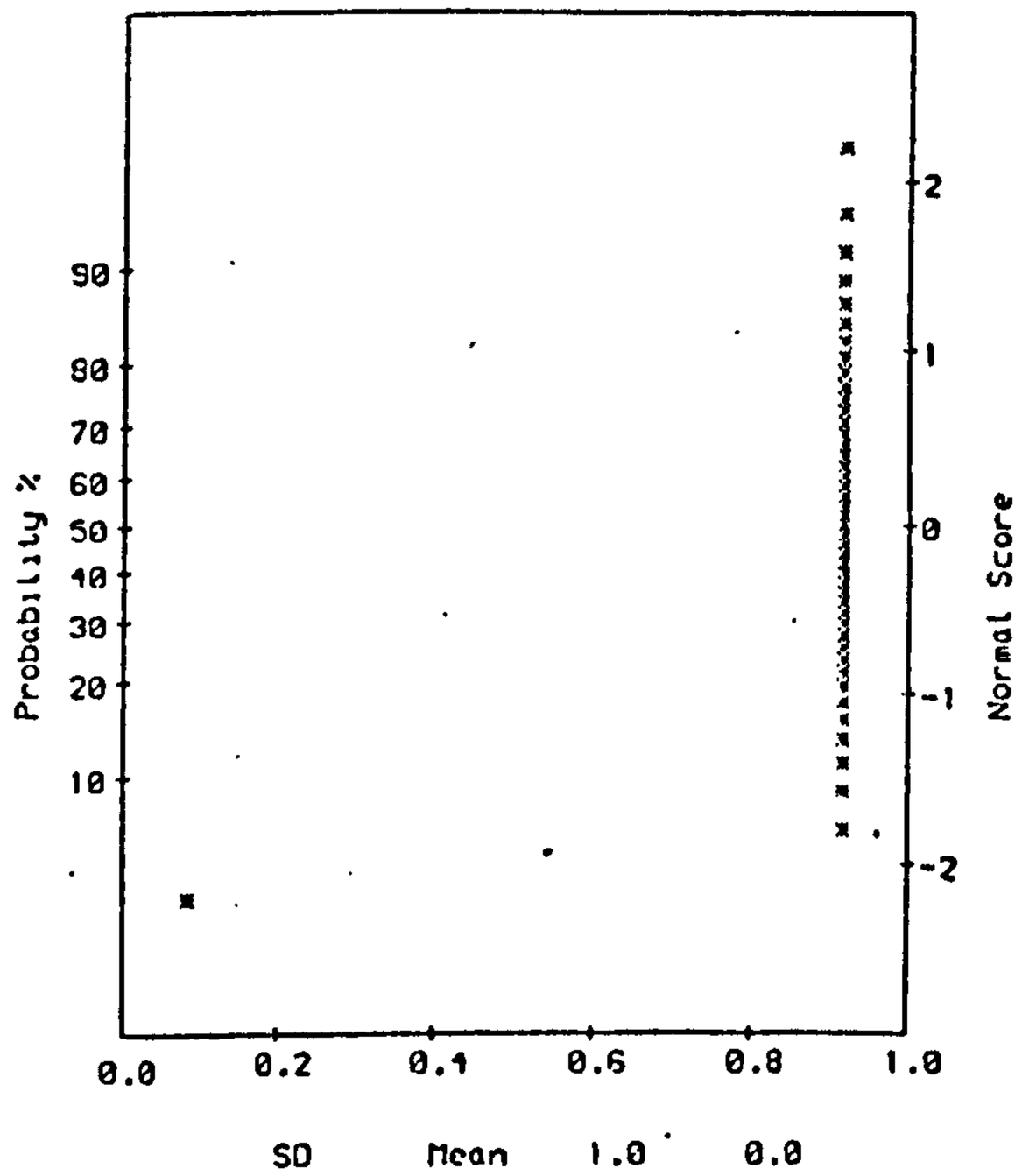
Probability %
90
80
70
60
50
40
30
20
10
2
1
0
-1
-2
Normal Score
0.0
0.2
0.4
0.6
0.8
1.0
SD Mean 1.0 0.0
× 2.7 38.9 41.1 19.2

(c)

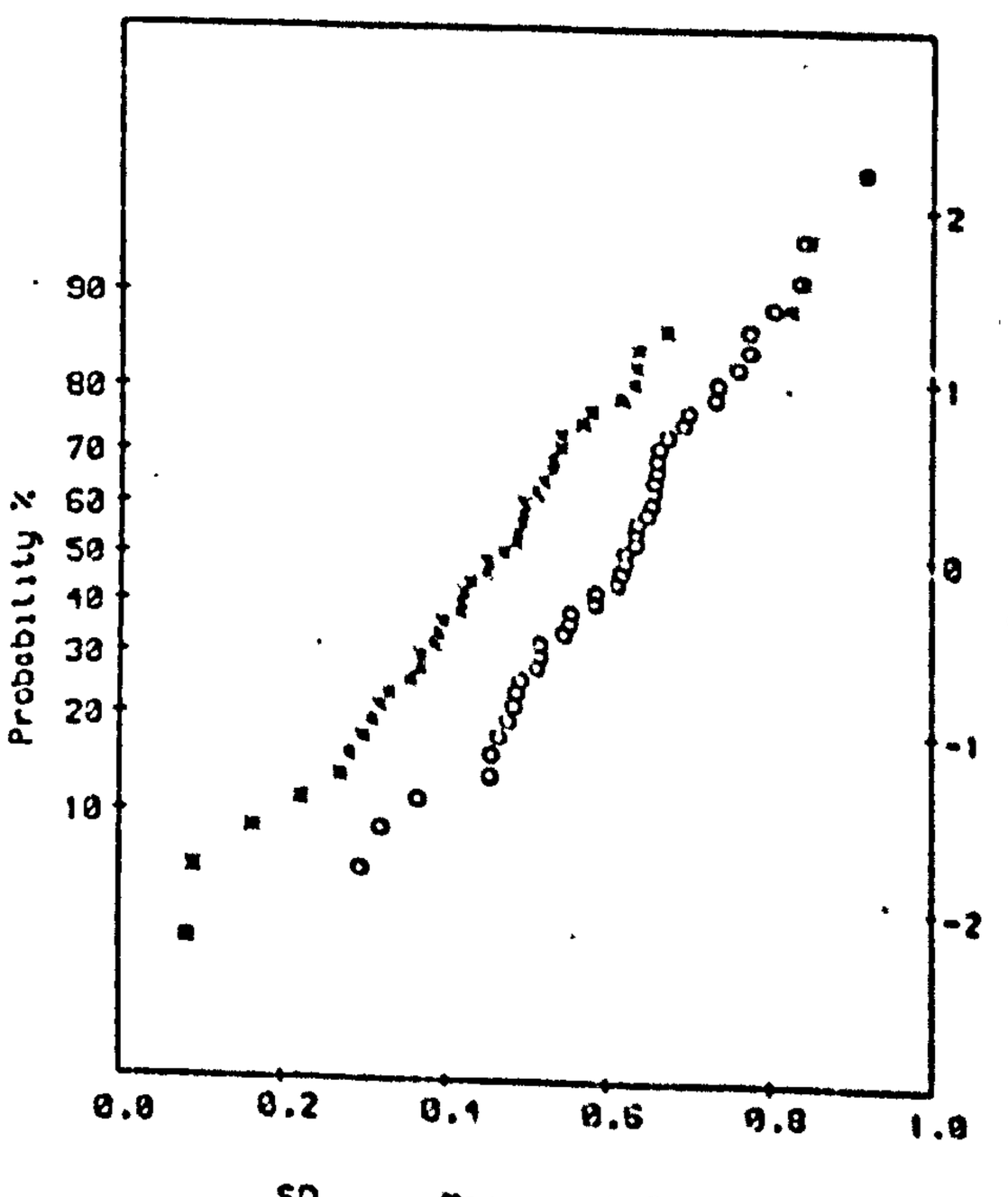
Probability %
90
80
70
60
50
40
30
20
10
2
1
0
-1
-2
Normal Score
0.0
0.2
0.4
0.6
0.8
1.0
SD Mean 1.0 0.0
× 2.3 17.5 24.3 11.5
o 2.1 9.3 14.9 0.8

(d)

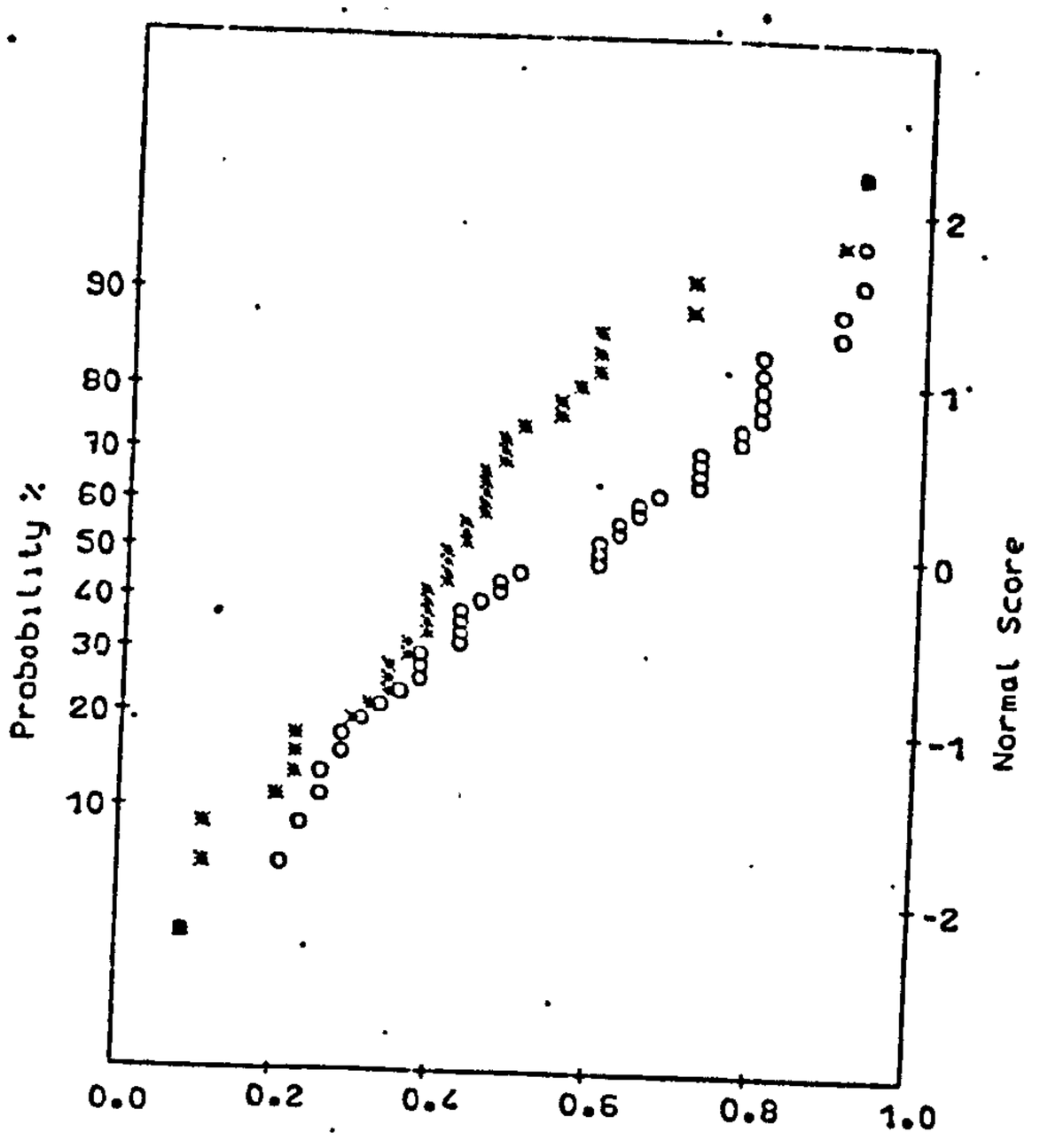

	SD	Mean	1.0	0.0
×	8.6	−31.6	3.3	−52.6
o	10.6	15.0	35.5	−11.3

(a)

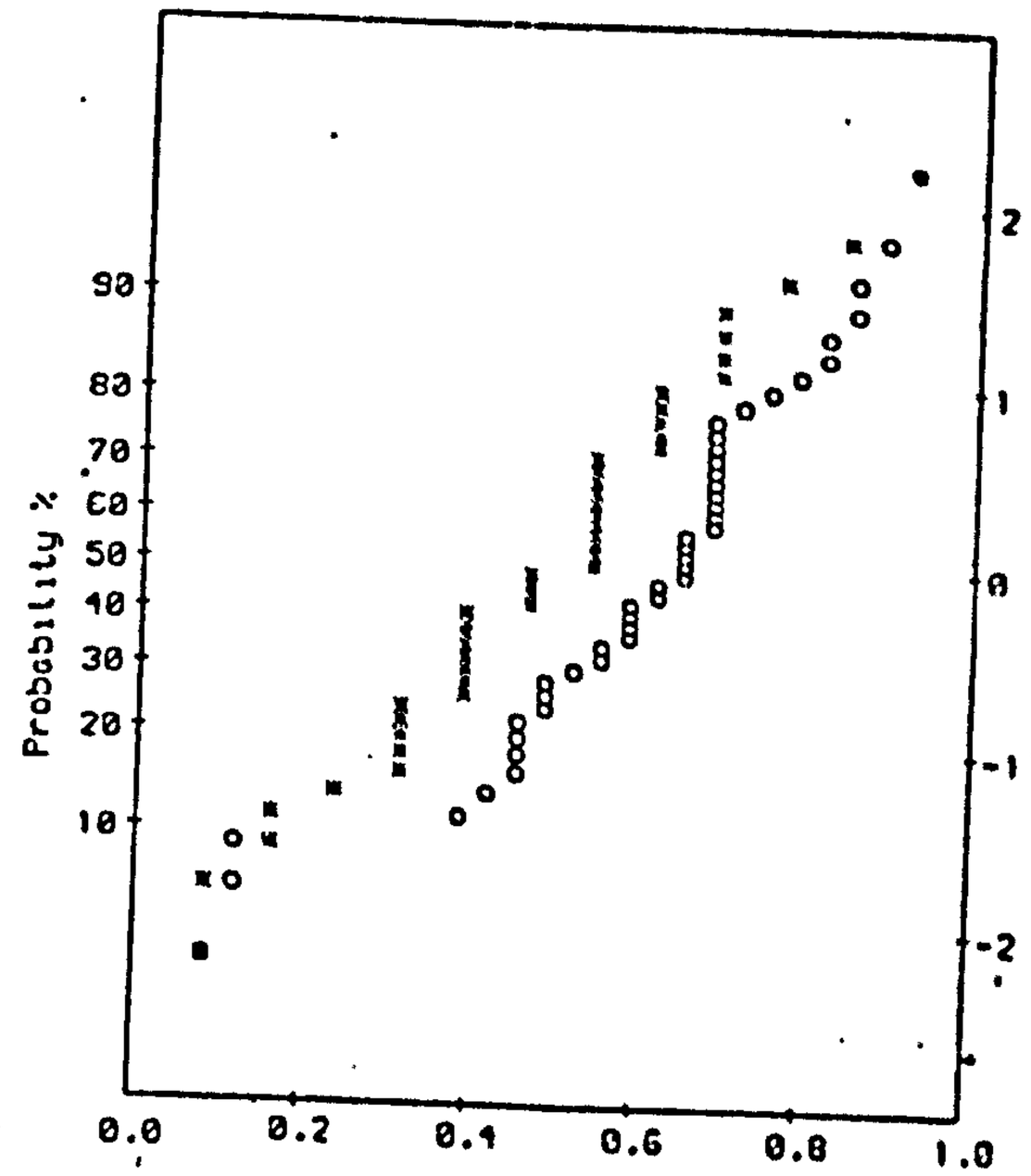

	SD	Mean	1.0	0.0
×	2.7	15.7	23.7	8.5
o	6.4	−18.2	−4.5	−38.9

(b)

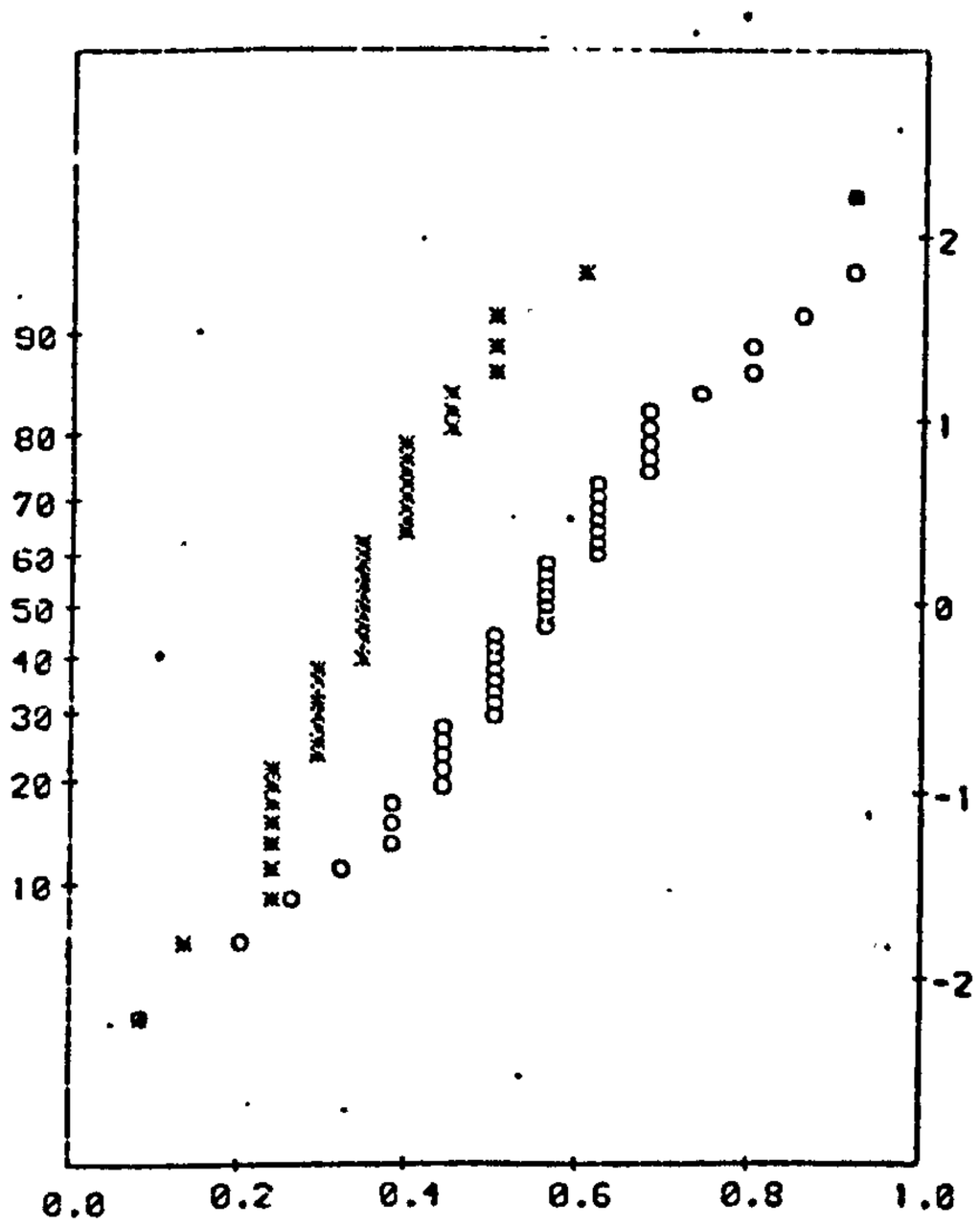

	SD	Mean	1.0	0.0
×	2.8	19.2	33.4	11.5
o	3.3	−2.9	5.7	−13.5

(c)

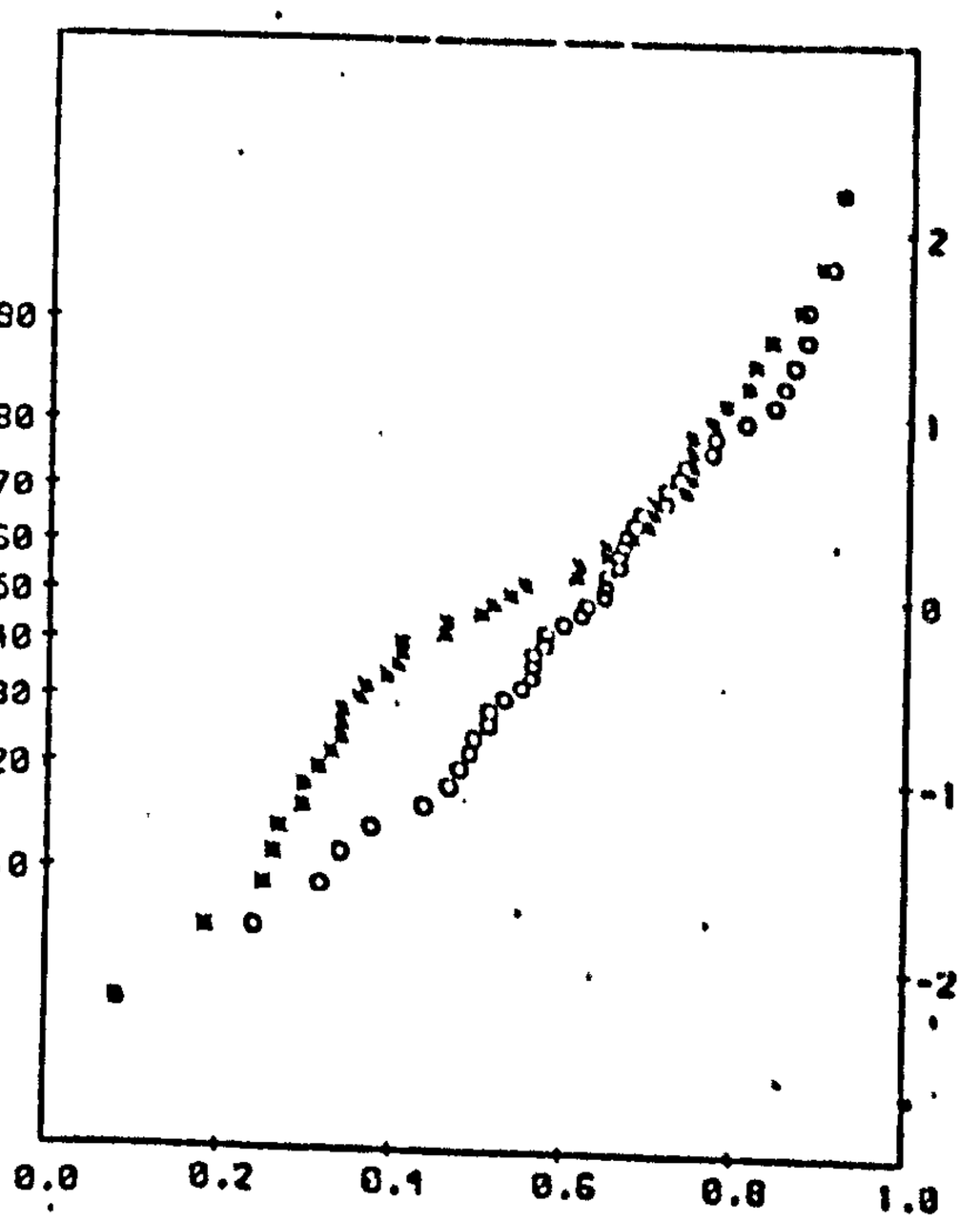

	SD	Mean	1.0	0.0
×	2.3	7.5	12.3	1.9
o	2.2	8.0	12.7	0.4

(d)

(v) T = 2.2 s

graph (same procedure as explained in Chapter 6).

The analytical relationship between the two sets of samples (5 cycles and 45 cycles) is discussed later in this chapter (see 7.3). Meanwhile Figs. 7.3a, b, c, clearly correspond to a non-normally distributed sample for all the periods, especially at the two periods of 1.8 and 2.0 sec. for which most of the data points are concentrated at one or two values (Fig. 7.3c (IV), shows that at 4.5 mm height no data points are shown in the figure, since all the 45 values have the same value).

Nevertheless, for the mean velocity (Fig. 7.3d) all of the distributions tend to be normal, which is an important result since the relevant normal distribution theories and equations, and hence discussions, can be applied (as will be seen = section 7.3). Also with the data being normally distributed, the mean of the 45 cycles shown in Fig. 7.1 and the corresponding range of one standard deviation can be taken as the basis for assumptions about general behaviour of the mean velocity.

Thus it is meaningful and sensible that Fig. 7.1 be analysed with respect to the sample mean velocity data. A first suggestion from the figure is that as the wave period increases the flow becomes less turbulent. Even though the range of values of mean velocity at each height does not represent the actual intensity of turbulence, since it is only the range of 5 data points, if a high range is observed

throughout the depth it cannot be merely coincidence and the flow must be turbulent. For 1.4 second wave period the velocity fluctuates in a large range and as the wave period increases the range of fluctuation decreases with the lowest value observed for 2.2 second wave.

Besides the figure, the tabulated values of observed turbulence intensity given in Table 7.1 yield the same conclusion. Also it shows that the turbulence is less at the height closer to the top of the roughness than closer to the bottom of the roughness (i.e., the turbulence intensity decreases with increasing height). This is not conclusive from the figure, since the turbulence values represent the velocity fluctuation and only the mean velocity fluctuations are shown in the figure.

However, Fig. 7.1 clearly illustrates that as the wave period increases and the fluctuations decrease, the mean velocity at all heights becomes positive (in the direction of wave progression) and its value decreases.

Fig. 7.2, which shows the velocity profile over 45 cycles, has two important features. The first is the shape of the profile close to the bed (y = 0.5 mm) which is more of a square wave than the usual sinusoid, as has been observed throughout the investigation. In fact the shape of the profile is somehow the same as the roughness profile itself, with a rapid change in the velocity direction and a longer

T/sec	2-D rough bed	
	0.5 mm	4.5 mm
1.4	30	32
1.6	29	8
1.8	15	9
2.0	26	9
2.2	18	9

Table 7.1. The observed values of turbulence intensity inside roughness at the two positions 0.5 and 4.5 mm for 2-D rough bed.

lasting peak value in that direction. There is no doubt that this is the effect of the roughness shape itself - that is the sharp edges of the roughness elements at the bed are responsible for this effect and as will be seen (Fig. 7.5) this is not observed for the 3-D rough bed which has a smoother shape. At a level further from the bed the velocity profile reverts to a sinusoidal shape (Fig. 7.2b).

The second and probably the more interesting conclusion to be drawn from Fig. 7.2 is the clear indication of phase shift of the cyclic motion as the bed is approached. Relative to the velocity outside the boundary layer the velocity at the bed is shifted by approximately 180 degrees. For the velocity profile close to the top of the roughness, the expected phase difference relative to the free surface water occurs which is a maximum value of about 30 degrees for the 1.4 second wave period presented in the figure. This result shows that at these two heights the velocity directions are nearly always opposite to each other, which means a very high intensity eddy occurs somewhere in that region. If a comprehensive logging of the velocity profile throughout the whole depth were carried out, and not only at the two depth positions as here, then the profile of the eddy could probably be exactly explained.

7.2.2 Three Dimensional Rough Bed

As for boundary layer velocity results, the velocity inside the roughness was observed at two sections on the

rough bed, R and S (see 4.2.3) and for two wave periods (1.4 and 2.2 seconds). Each set of data was recorded over 3 cycles at 19 levels with equal intervals of 1 mm, from 0.5 mm to 18.5 mm height (the roughness height was 18.95 mm). At the two extreme positions (0.5 mm and 18.5 mm height) the velocity was recorded over 30 cycles. A similar presentation of graphs, as for the 2-D rough bed, are shown for the 3-D rough bed in Figs. 7.4, 7.5, 7.6.

Fig. 7.4, which contains the range of the mean velocities at each depth plus one standard deviation of the mean velocity over 30 cycles at the two particular heights, shows a less perturbed set of results at R than at S. This effect shows up in the figure as a larger range of mean velocity for S than for R. The reason for this is discussed in section 6.3 (and Fig. 6.15). Also the values of Table 7.2, which are the turbulence intensity values, show a similar result - higher values from the data collected at the S position.

Although the velocity result for S is more perturbed, similar velocity profiles occur at R and S (samples of the velocity variations at the two particular levels for position S - for T = 1.4 s - and R - for T = 2.2 - are presented in Fig. 7.5). Also the velocity distributions for 30 cycles are similar for the two cases and can probably be taken as normal for both cases (Fig. 7.6).

———— range of mean velocity over 3 cycles

----- standard deviation of mean velocity over 30 cycles

Figure 7.4 The Variation of Mean Velocity Inside the Roughness Elements (3-D rough bed).

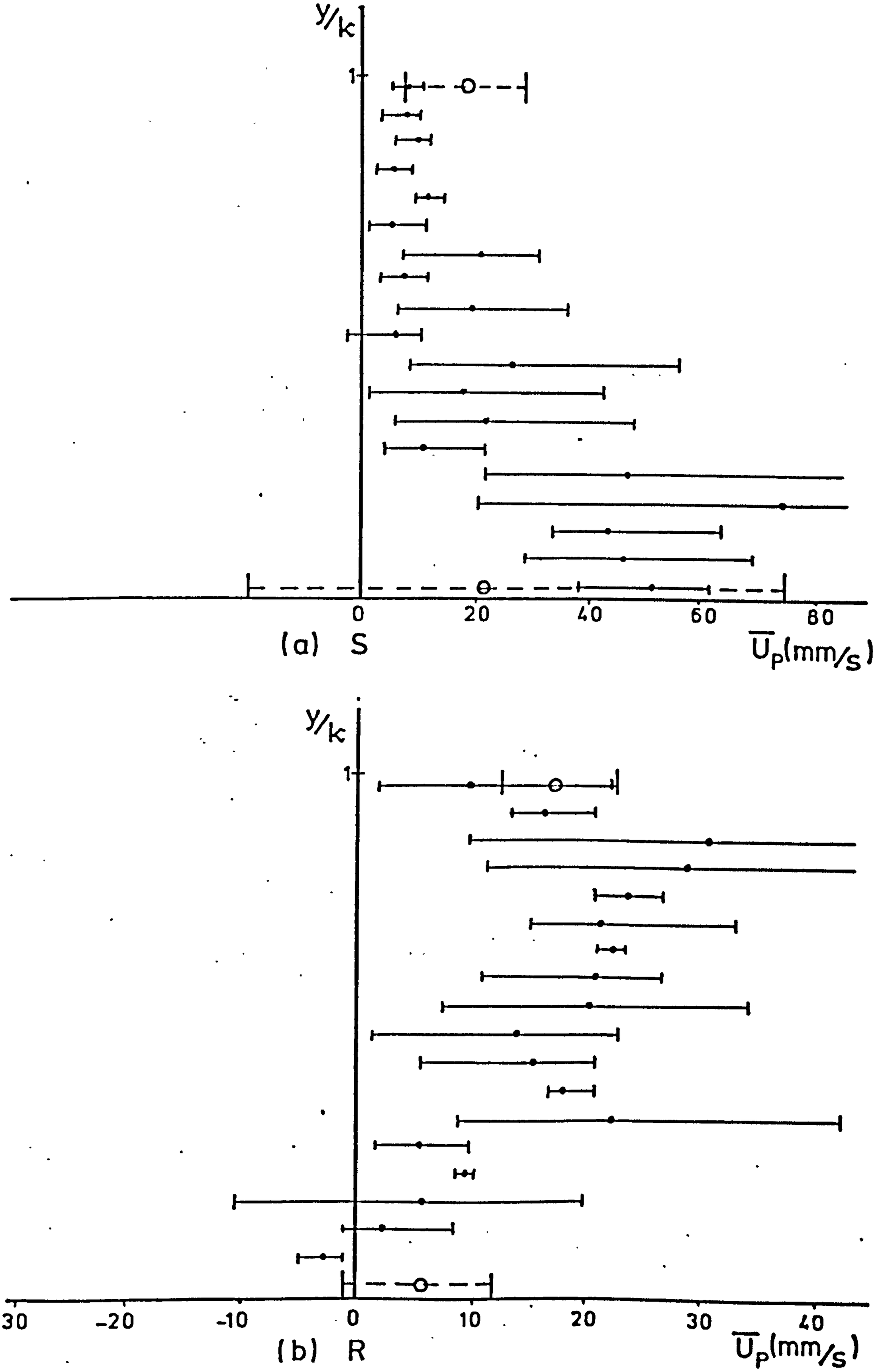
y/k
1
0
20
40
60
80
(a) S
$\overline{U}_p$(mm/s)
y/k
1
-30
-20
-10
0
10
20
30
40
(b) R
$\overline{U}_p$(mm/s)

(i) T=1.4 s

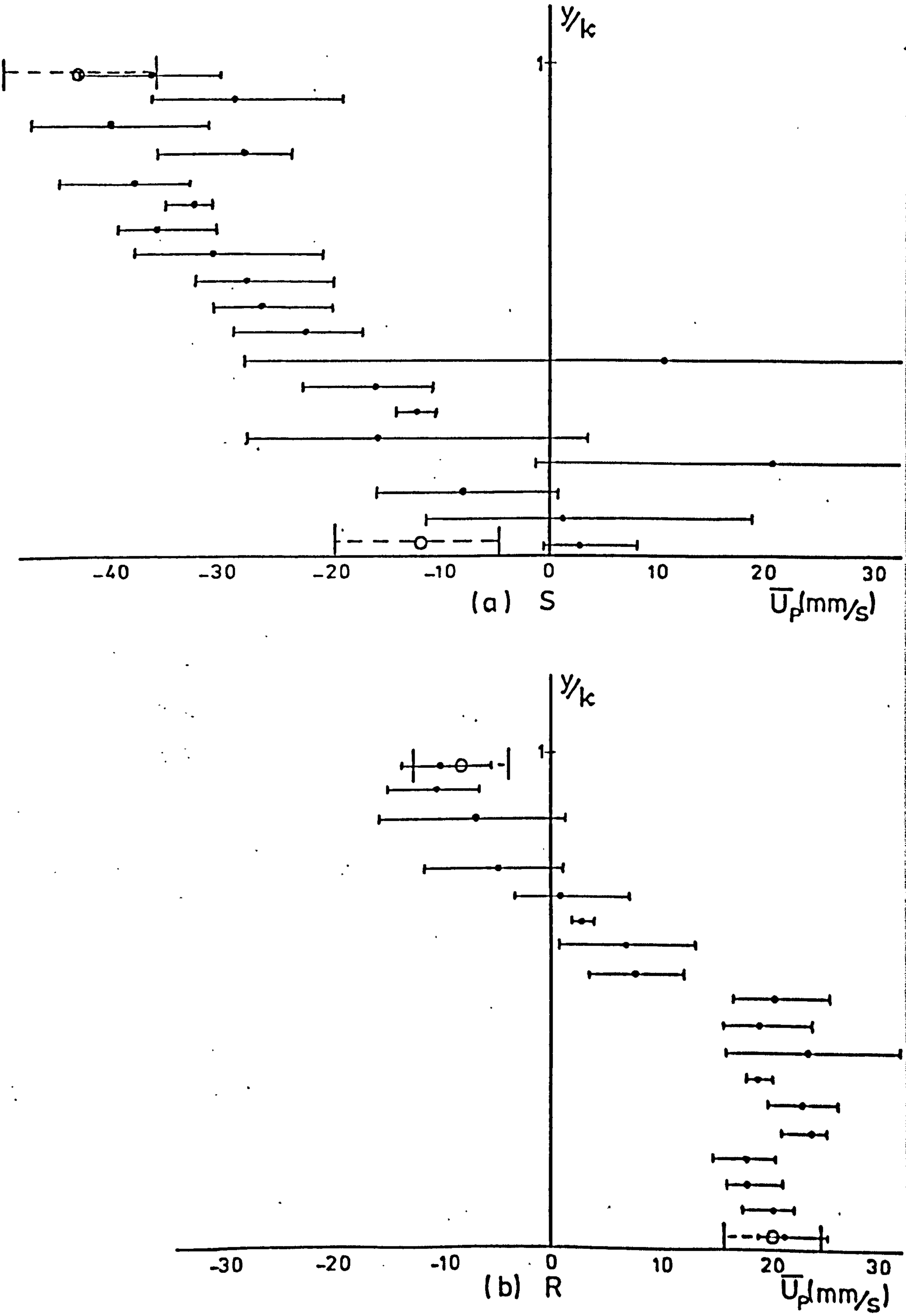
y/k
1
-40
-30
-20
-10
0
10
20
30
(a) S
$\overline{U}_p$(mm/s)
y/k
1
-30
-20
-10
0
10
20
30
(b) R
$\overline{U}_p$(mm/s)

(ii) T=2.2 s

(i)

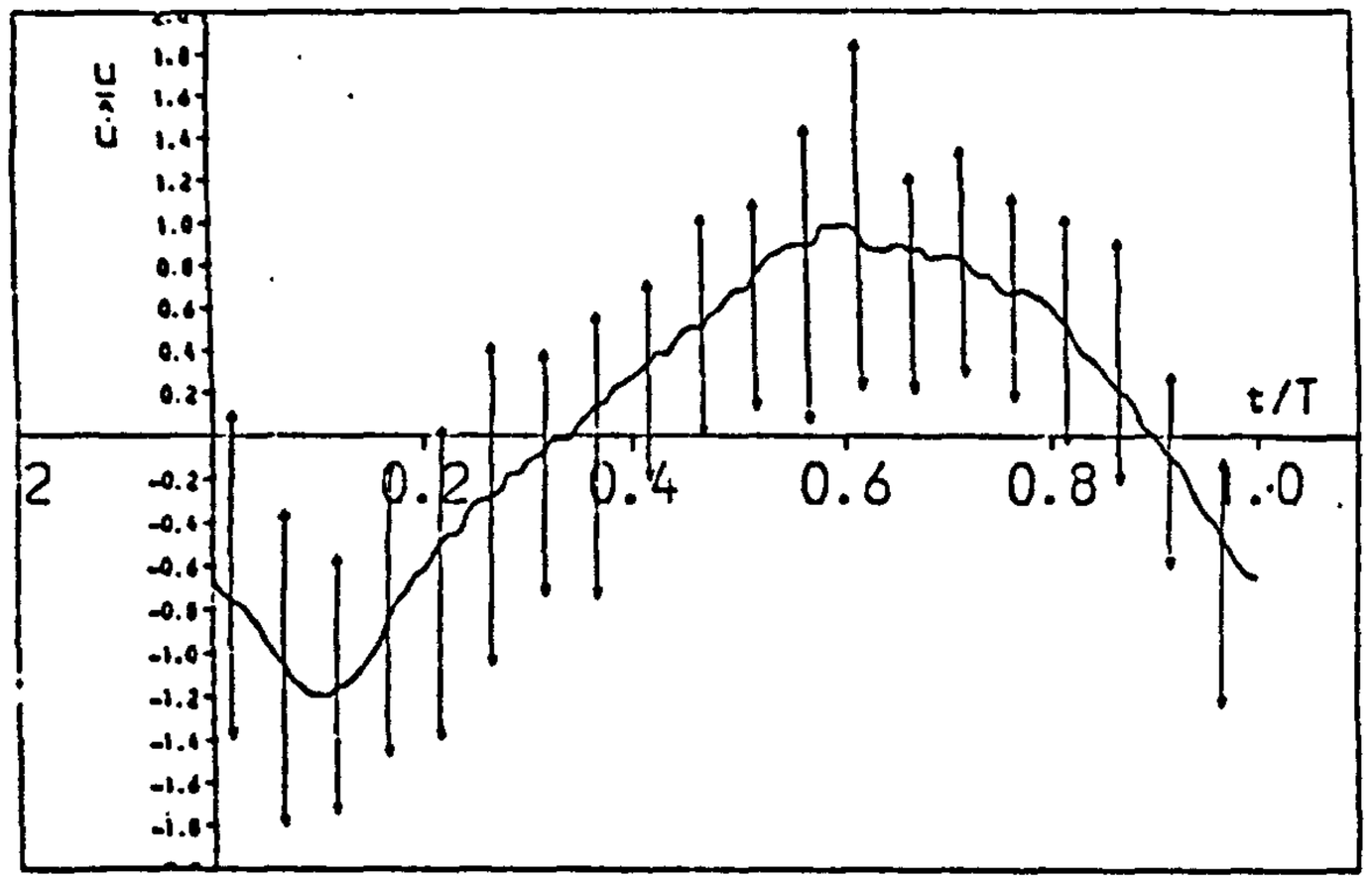

Y= 0.5 MM T=1.4 SEC $\hat{U}$=89.0 mm/s

(a)

(ii)

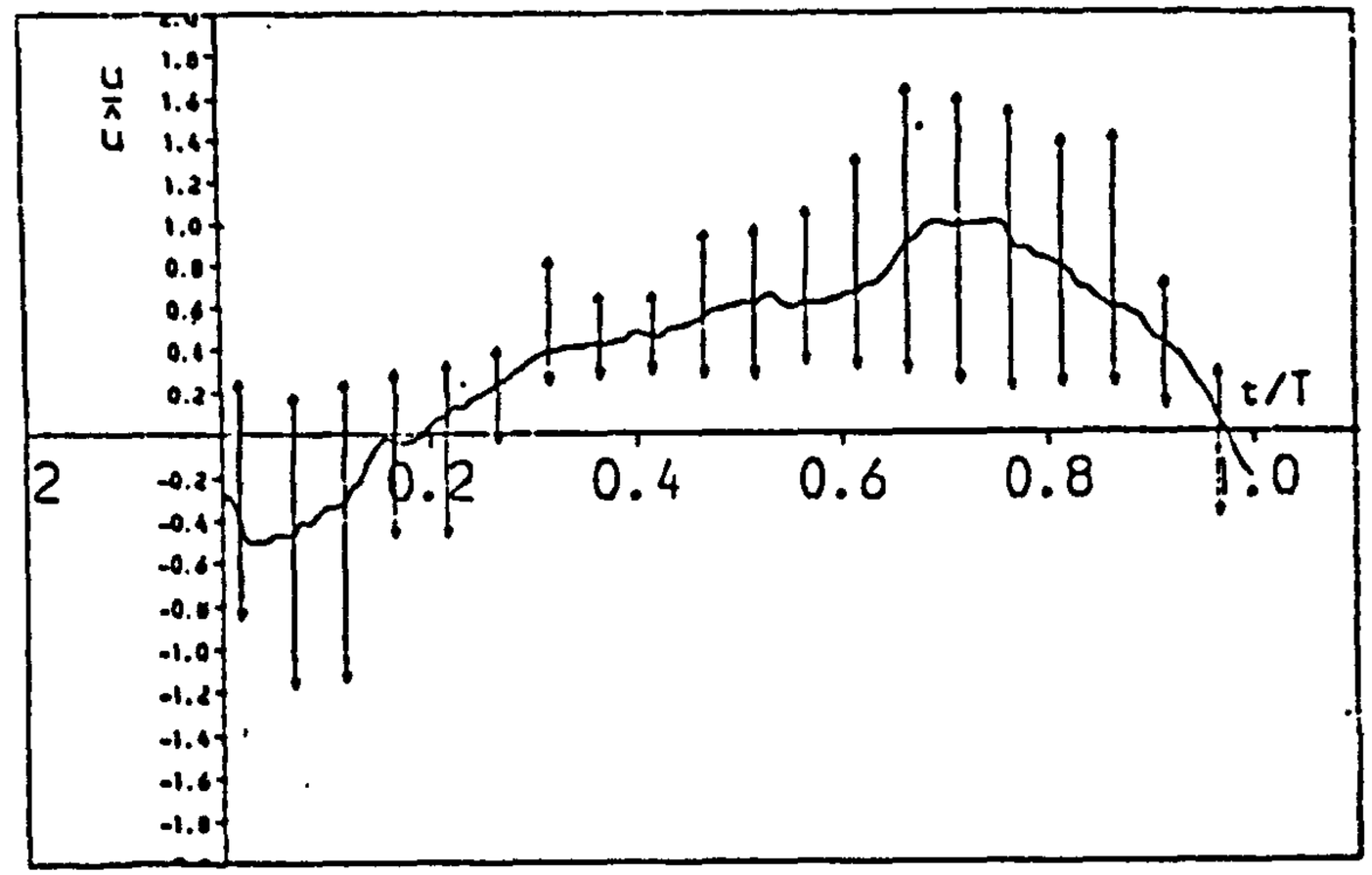

Y= 0.5 MM T=2.2 SEC $\hat{U}$=54.0 mm/s

(a)

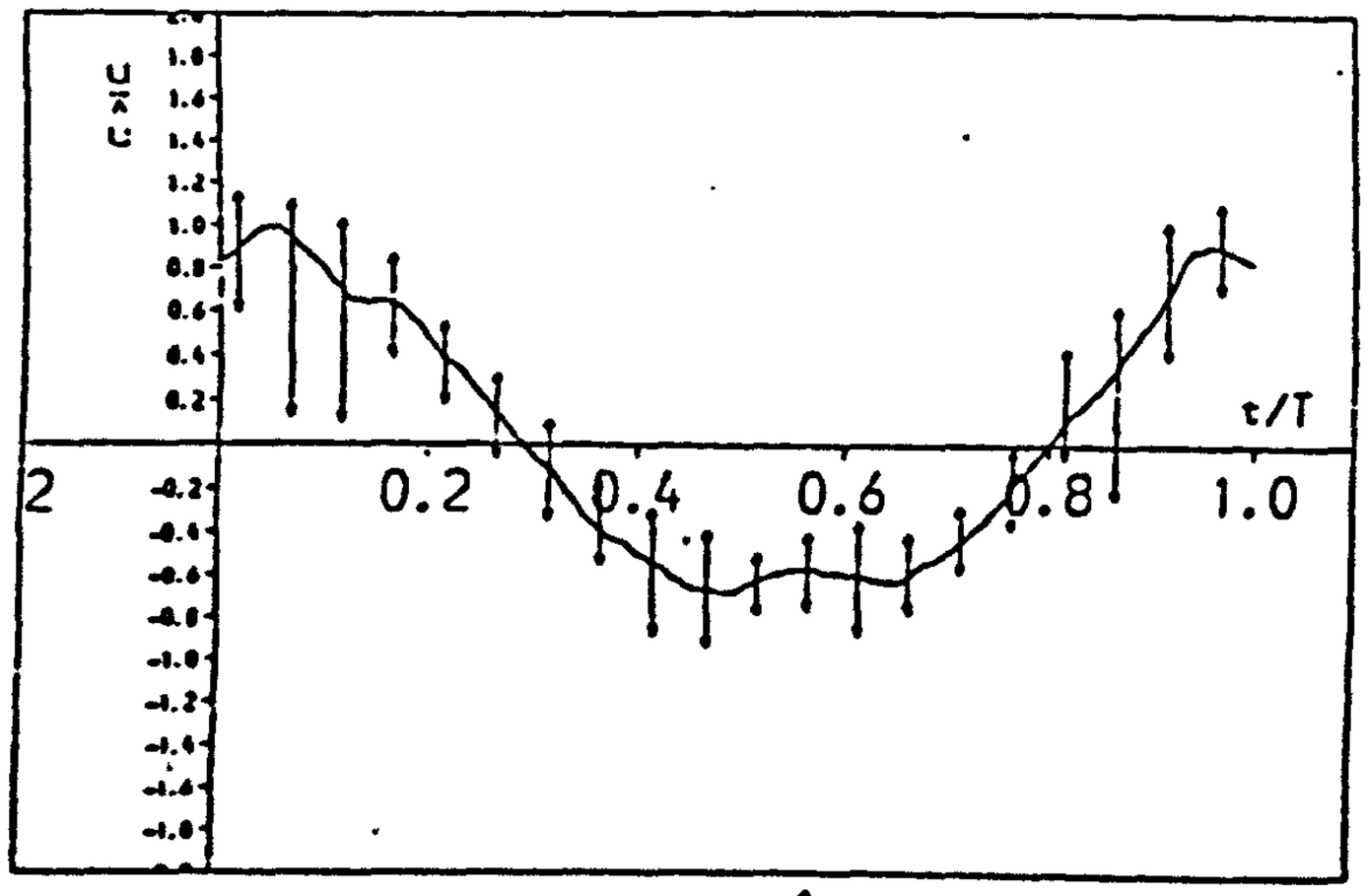

Y=18.5 MM T=1.4 SEC $\hat{U}$=316.0 mm/s

(b)

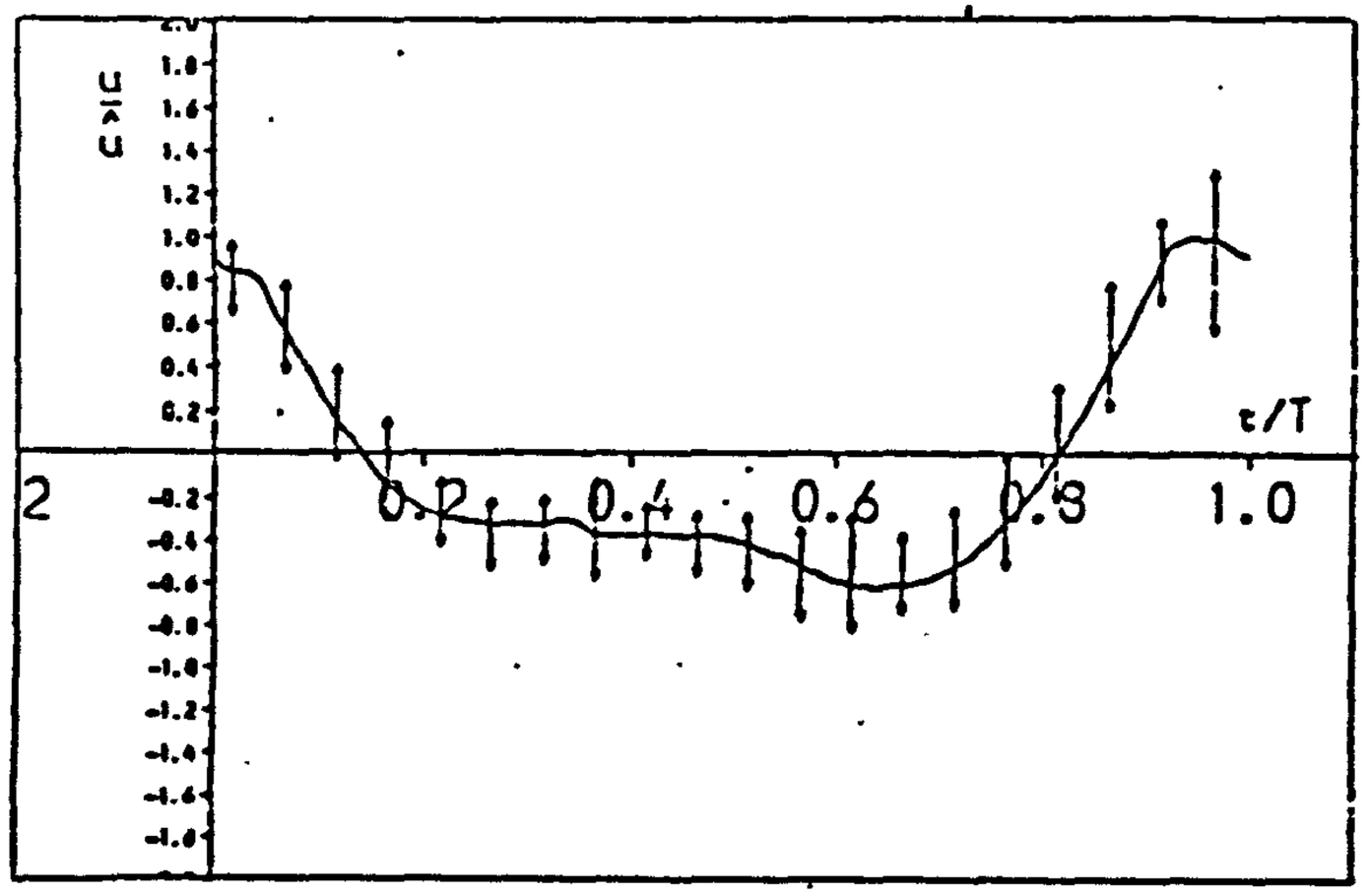

Y=18.0 MM T=2.2 SEC $\hat{U}$=157.9 mm/s

(b)

Fig. 7.5 The Mean Cyclic Variation of Velocity Over 30 Waves at Two Heights Below Roughness Height (3-D Bed).

*	0.5 mm height over the bed
o	18.5 mm height over the bed
SD	Standard Deviation
0.0-1.0	The range of the data

Fig. 7.6 The velocity distribution for 3 arbitrary phases (a, b, c) and mean velocity (d) over 30 cycles inside 3-D rough bed.

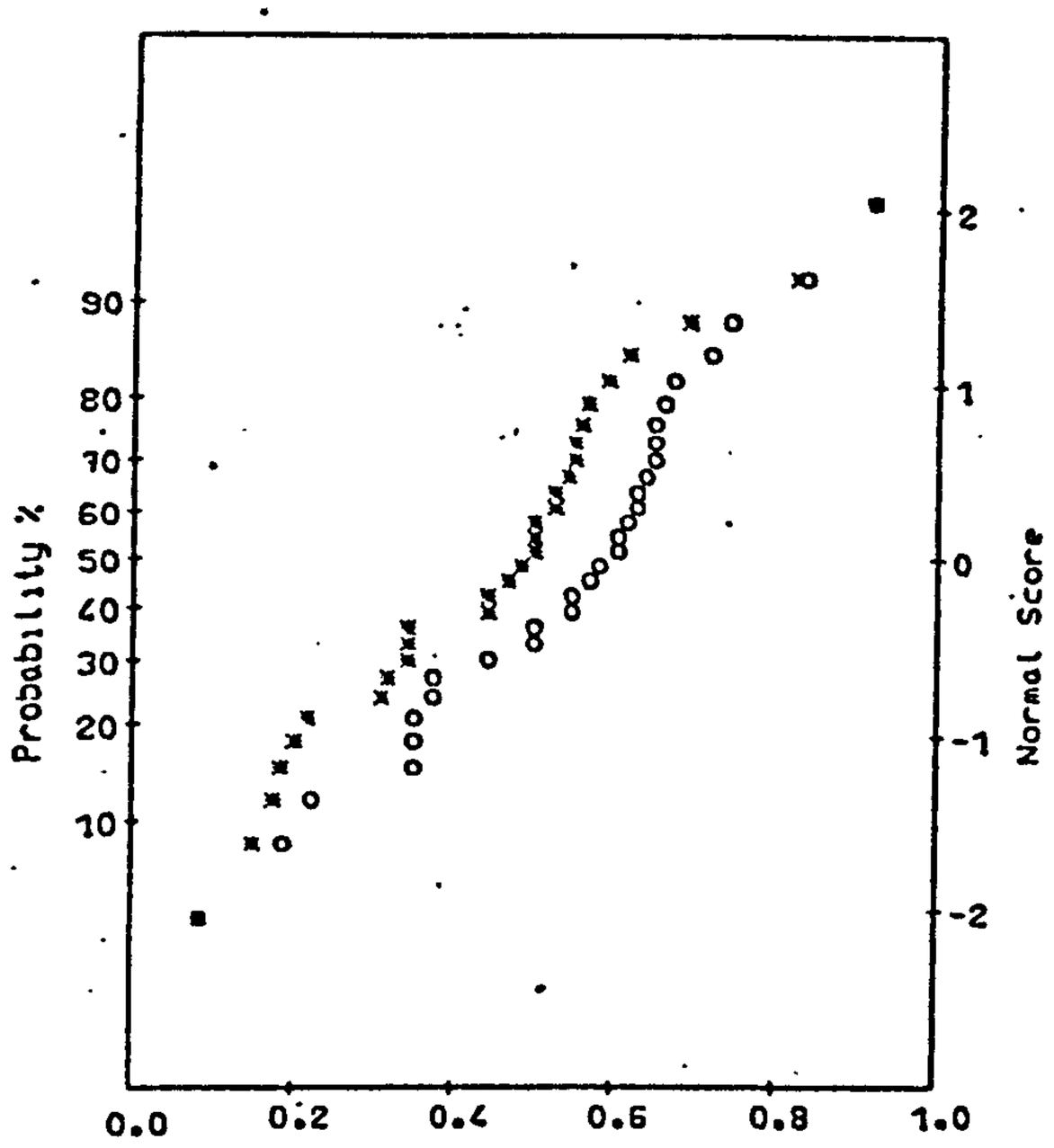

	SD	Mean	1.0	0.0
x	26.7	−93.4	−17.7	−154.9
o	18.6	159.0	204.5	122.1

(a)

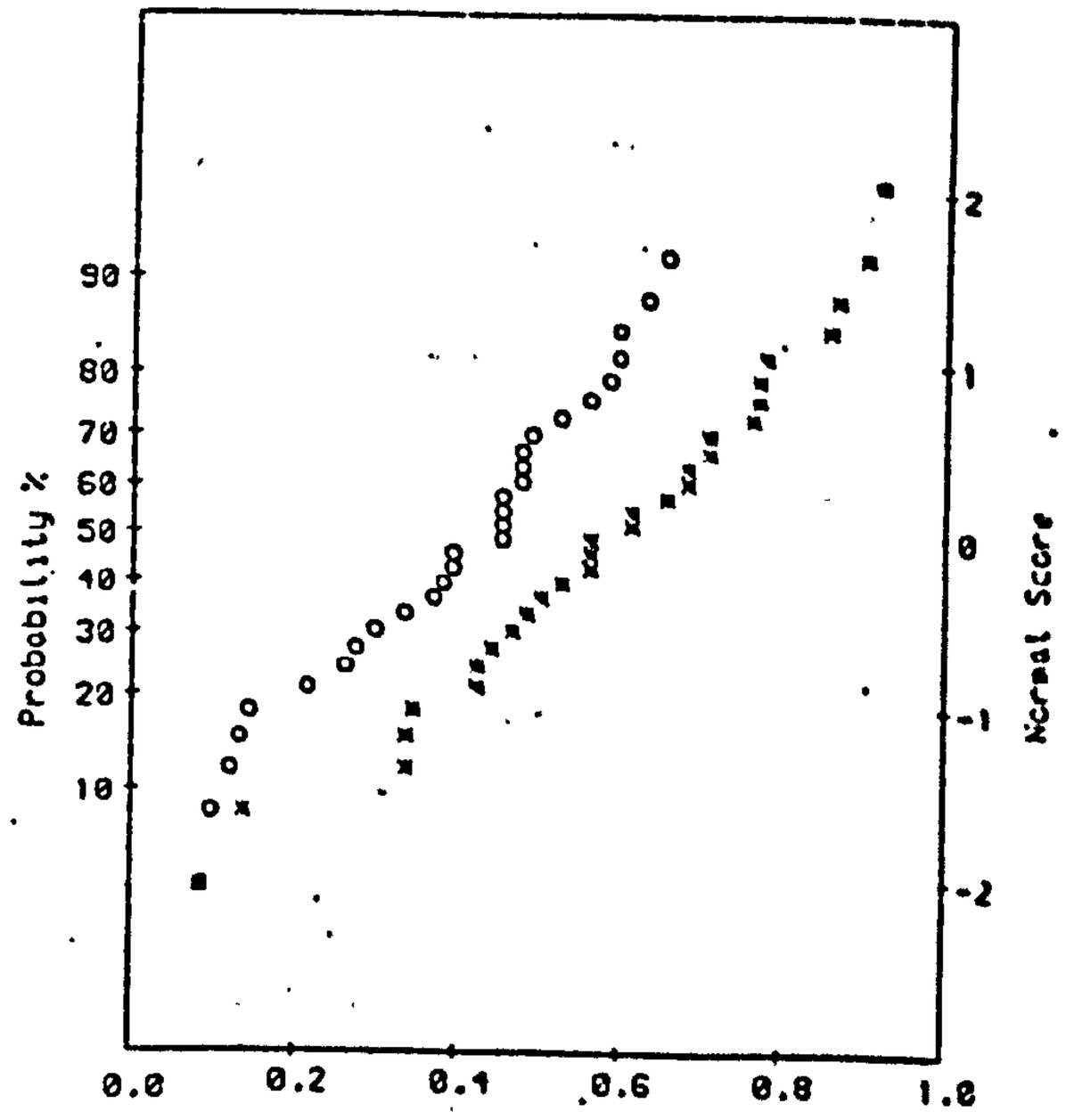

	SD	Mean	1.0	0.0
x	27.9	73.2	128.4	−3.5
o	18.4	−155.7	−98.9	−195.0

(b)

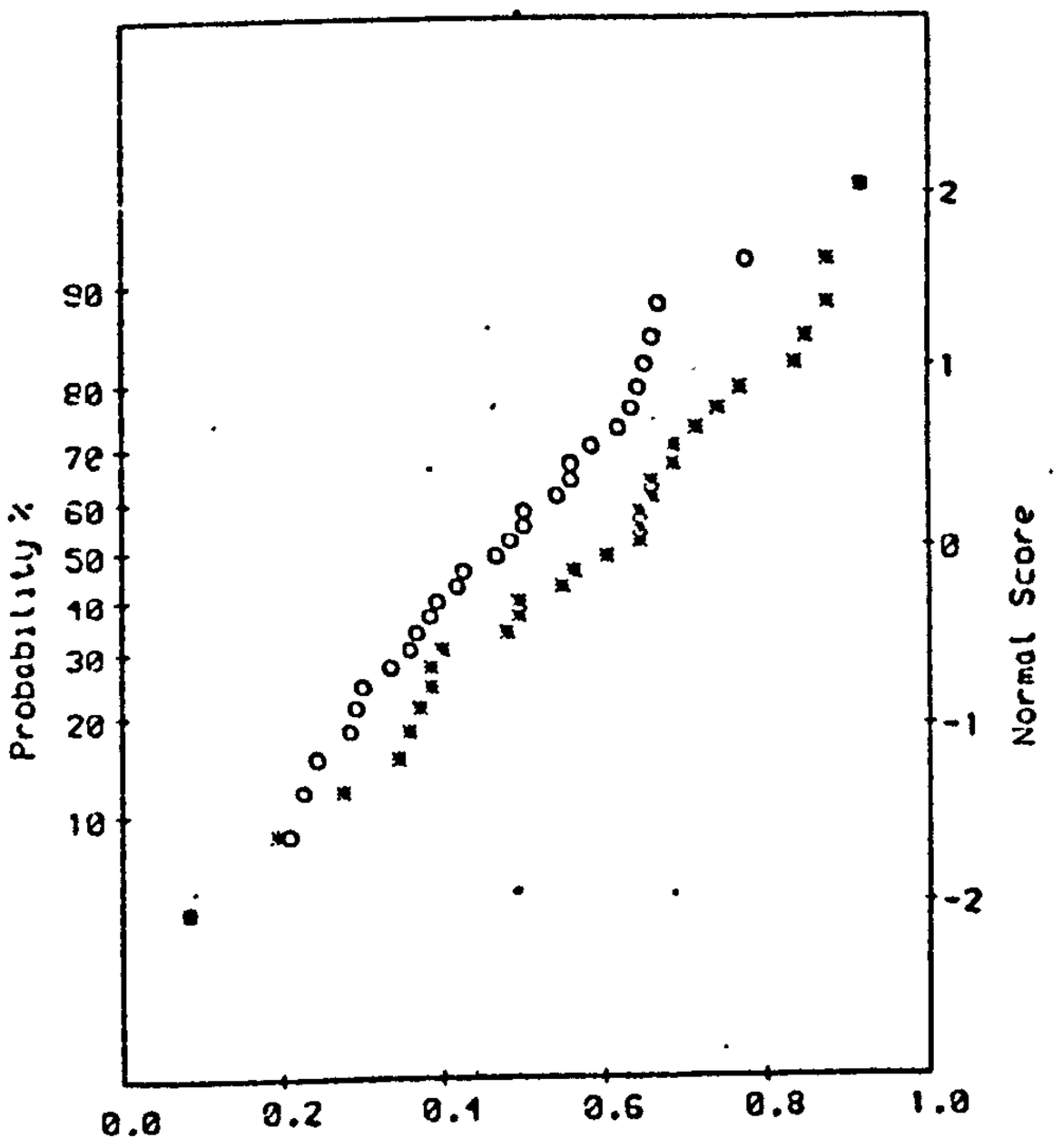

	SD	Mean	1.0	0.0
x	17.9	61.0	96.9	13.1
o	25.5	−18.5	54.4	−82.8

(c)

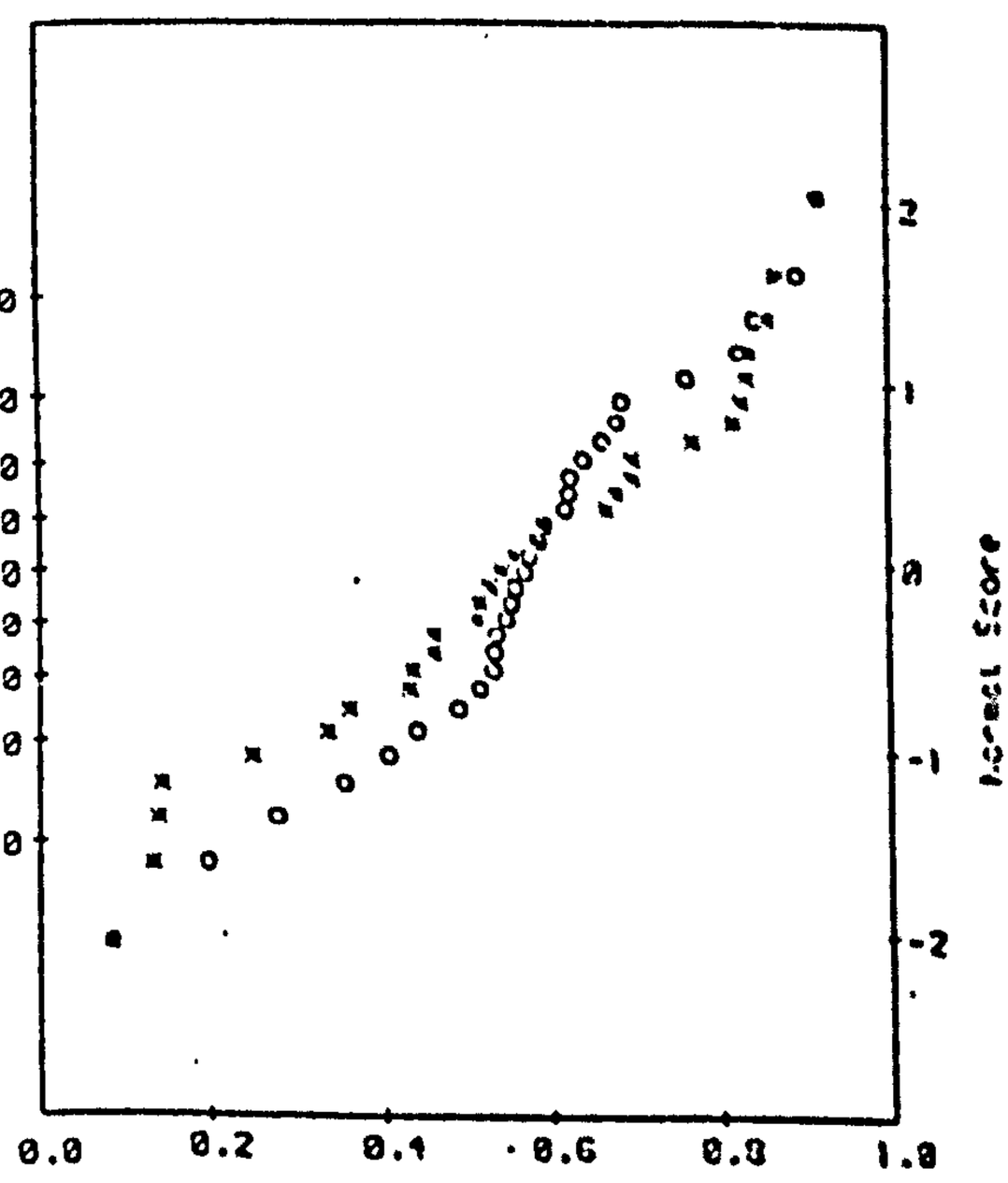

	SD	Mean	1.0	0.0
x	6.4	5.6	17.4	−8.9
o	5.7	17.3	30.5	−0.4

(d)

(i) T = 1.4 s, R

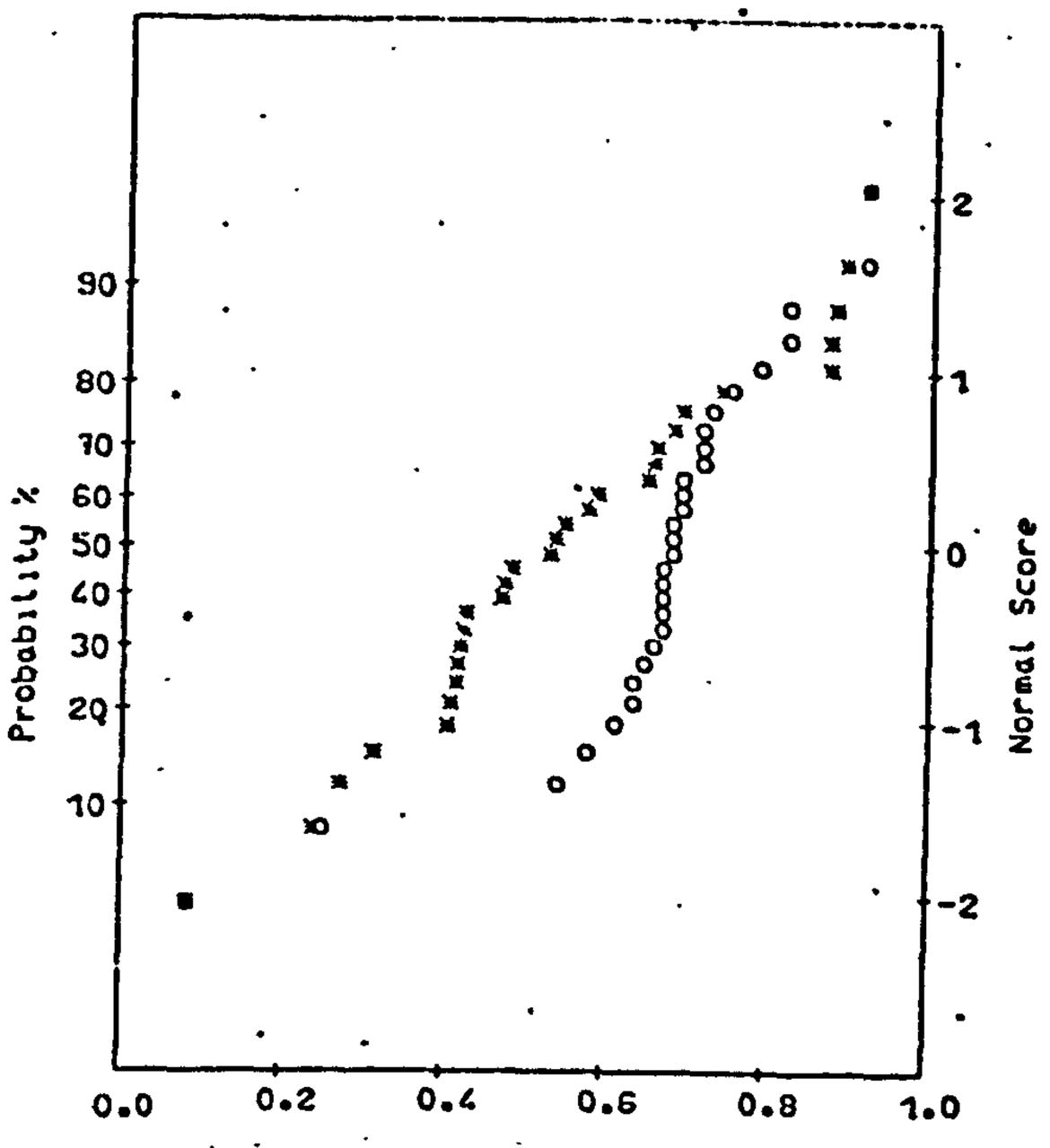

	SD	Mean	1.0	0.0
×	65.3	48.9	189.1	−122.6
o	52.4	207.1	315.3	−9.6

(a)

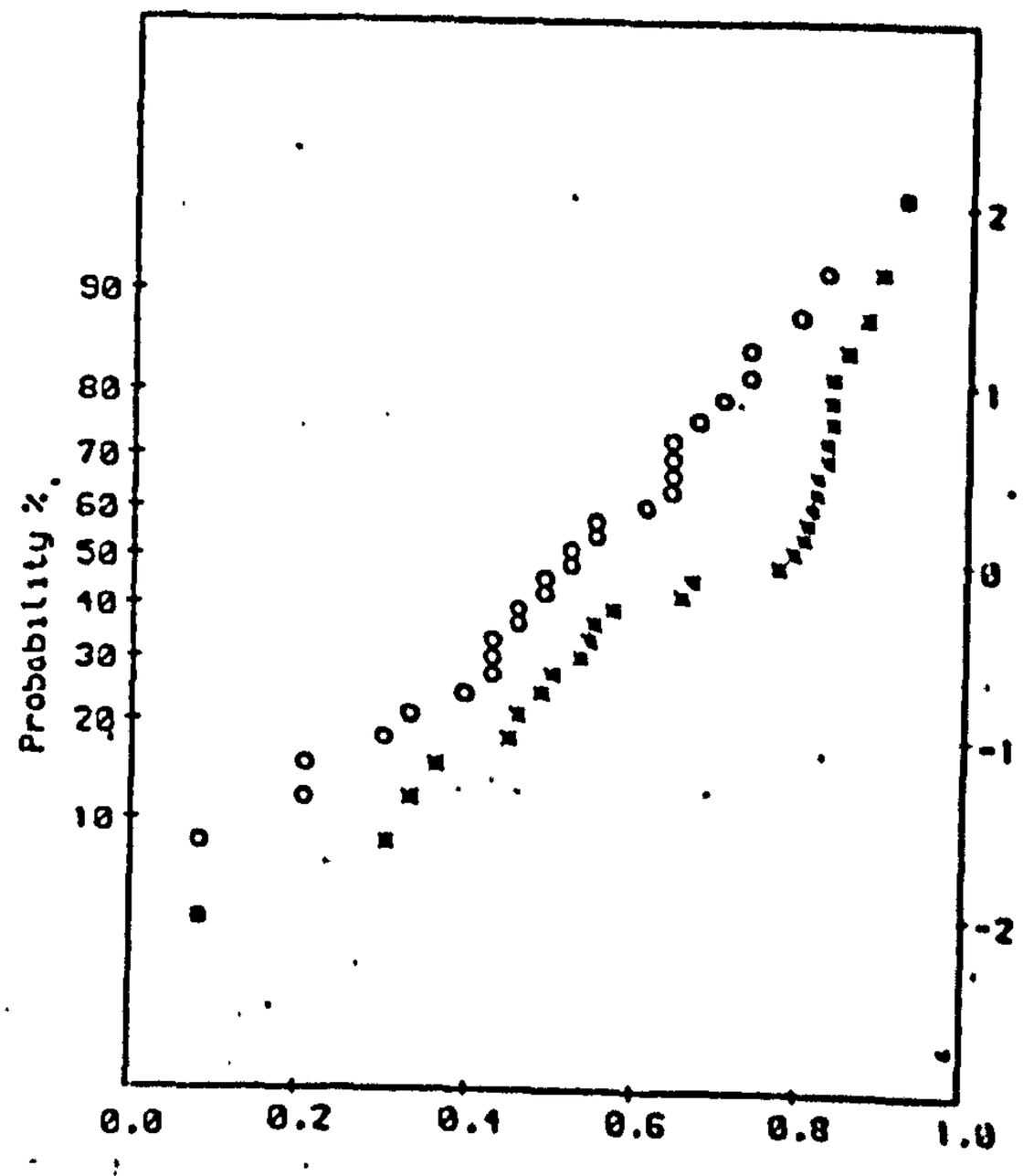

	SD	Mean	1.0	0.0
×	43.7	−31.4	38.2	−165.0
o	25.7	−181.1	−121.0	−244.5

(b)

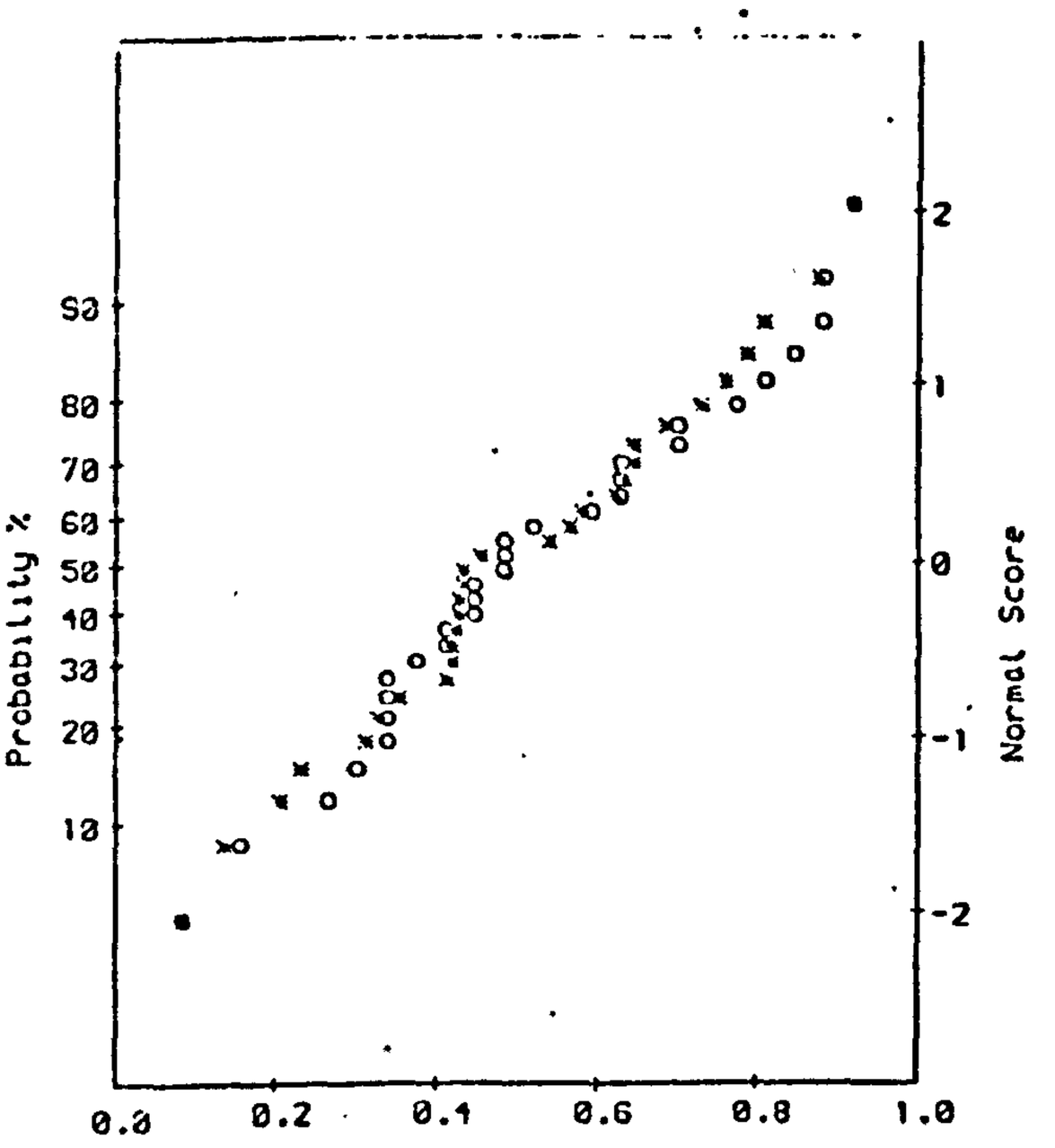

	SD	Mean	1.0	0.0
×	46.4	23.0	129.7	−87.2
o	23.2	−119.6	−69.1	−174.4

(c)

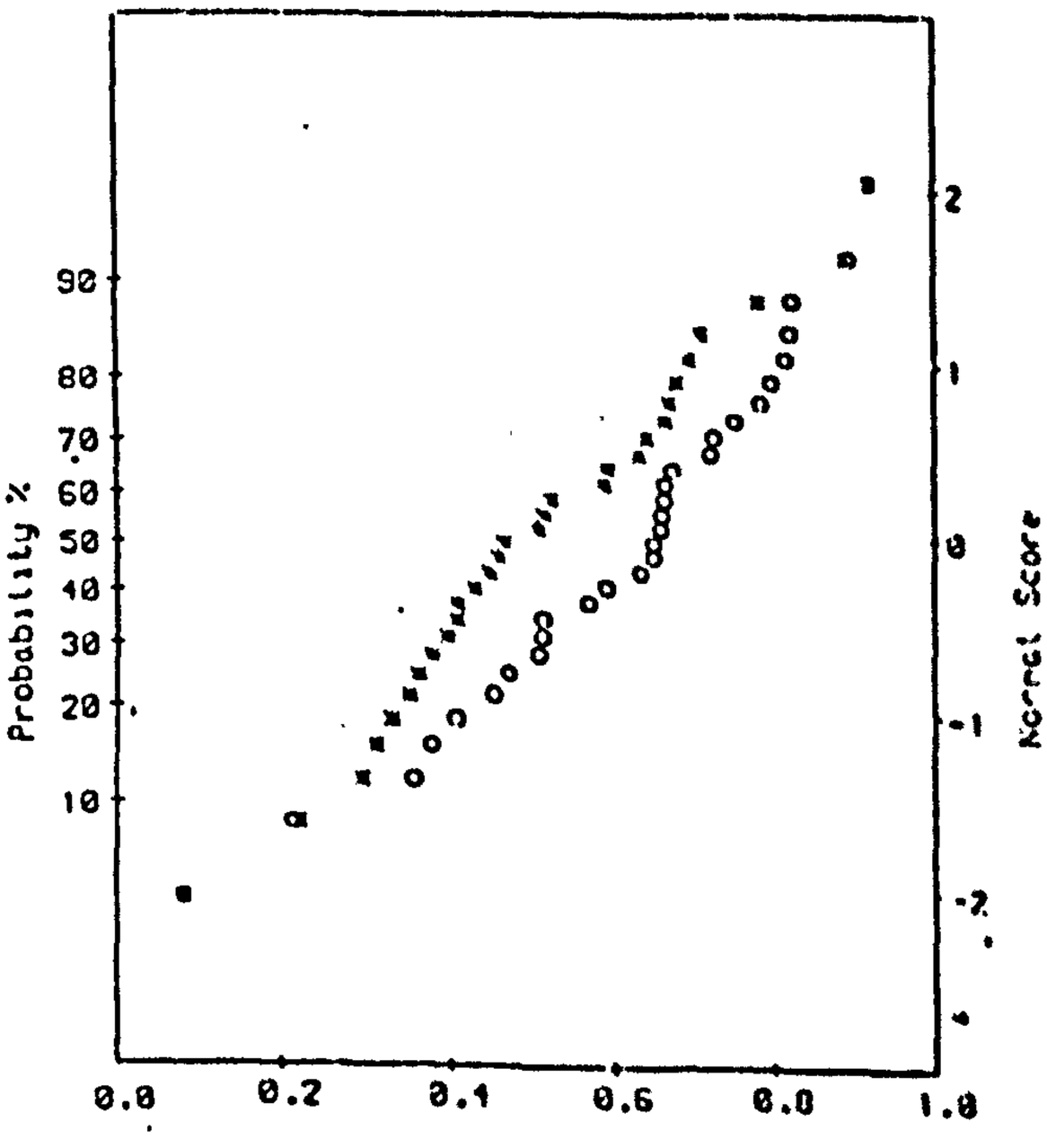

	SD	Mean	1.0	0.0
×	40.0	21.5	122.9	−85.2
o	10.4	18.1	38.7	−14.5

(d)

(ii) T = 1.4 s, S

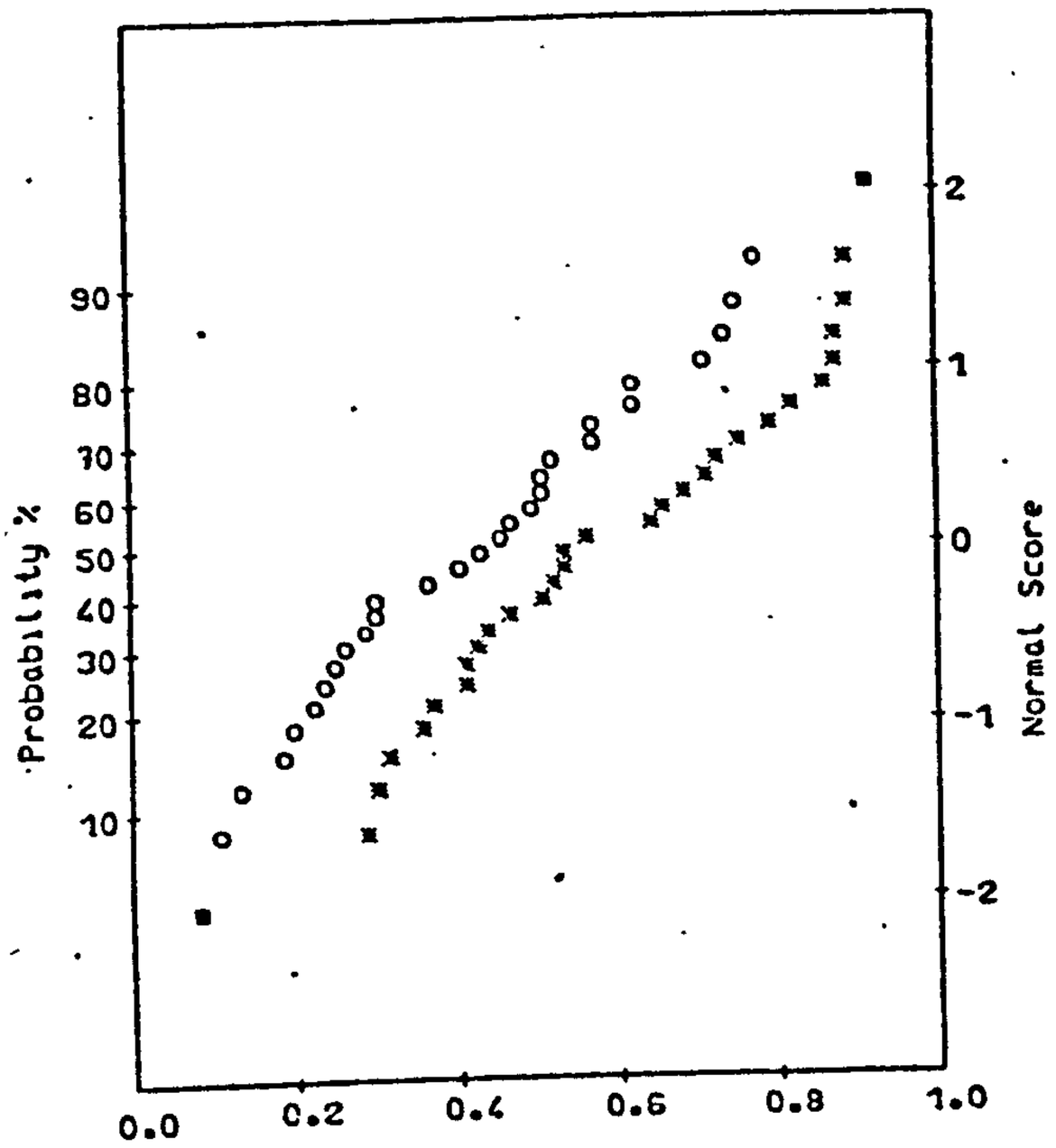

	SD	Mean	1.0	0.0
x	18.7	−13.2	21.4	−62.4
o	19.6	18.2	68.7	−20.5

(a)

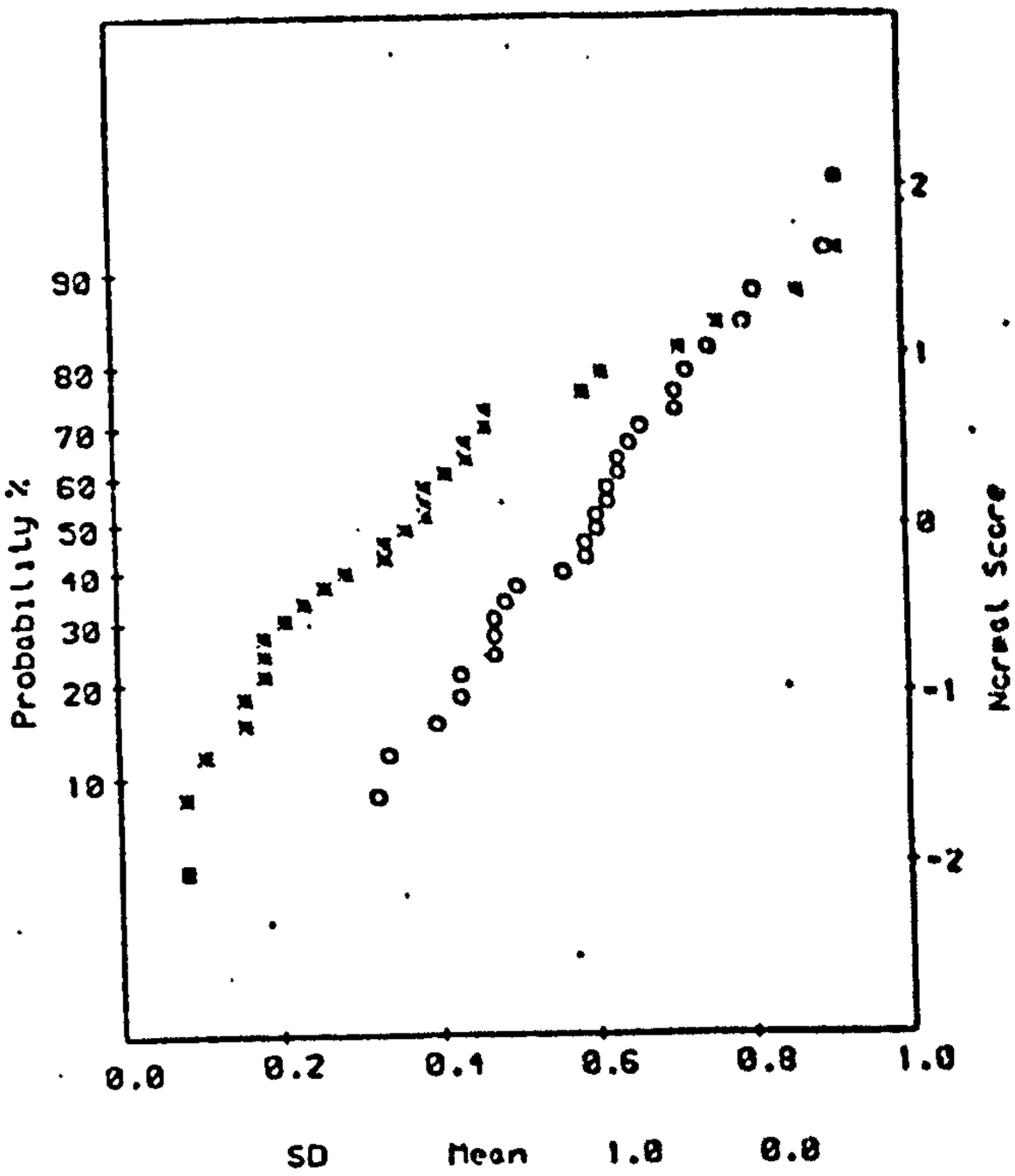

	SD	Mean	1.0	0.0
x	11.0	33.2	60.5	15.2
o	13.7	−80.0	−47.9	−124.7

(b)

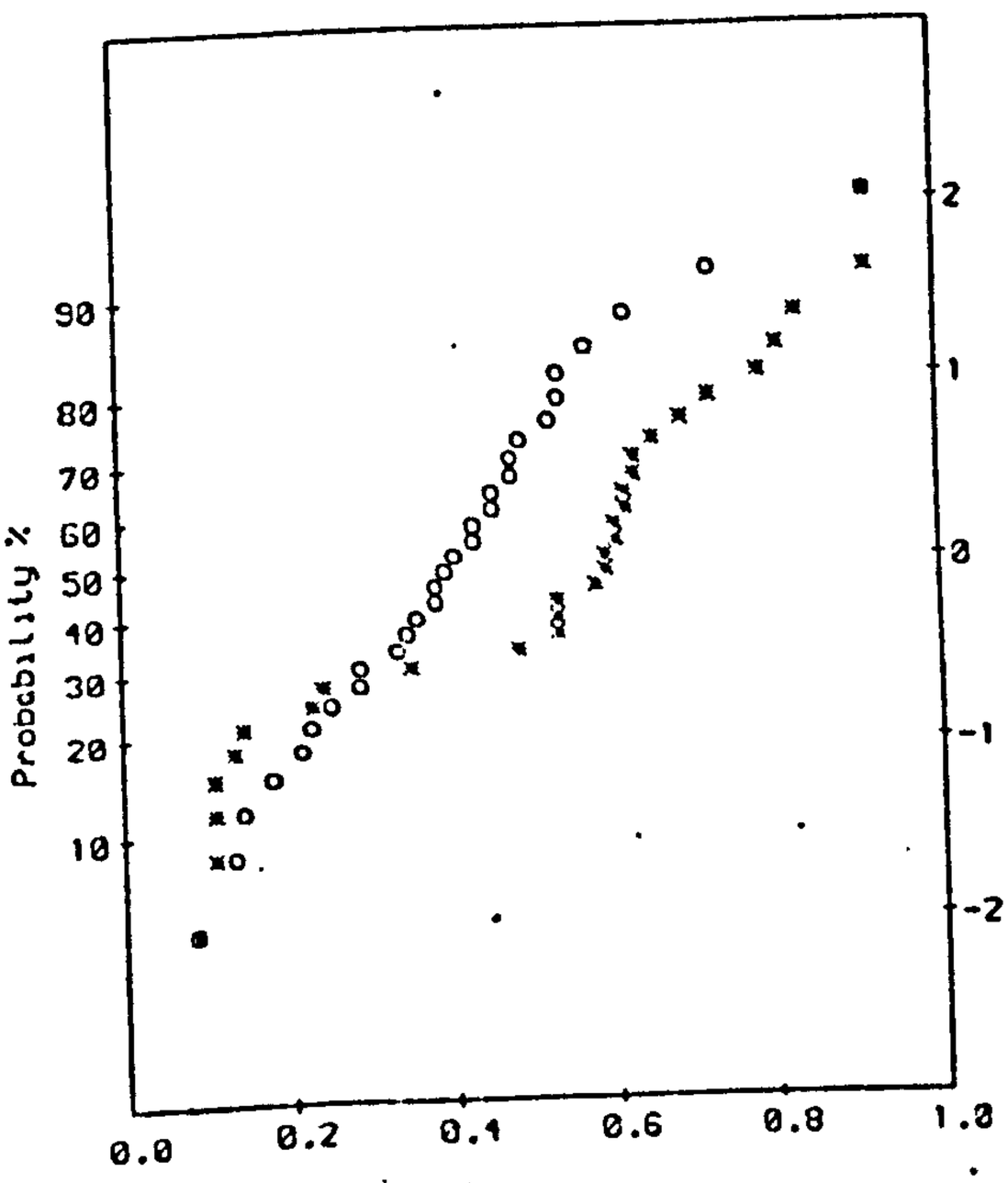

	SD	Mean	1.0	0.0
x	24.3	53.7	−100.1	5.4
o	17.3	−74.1	−16.5	−112.6

(c)

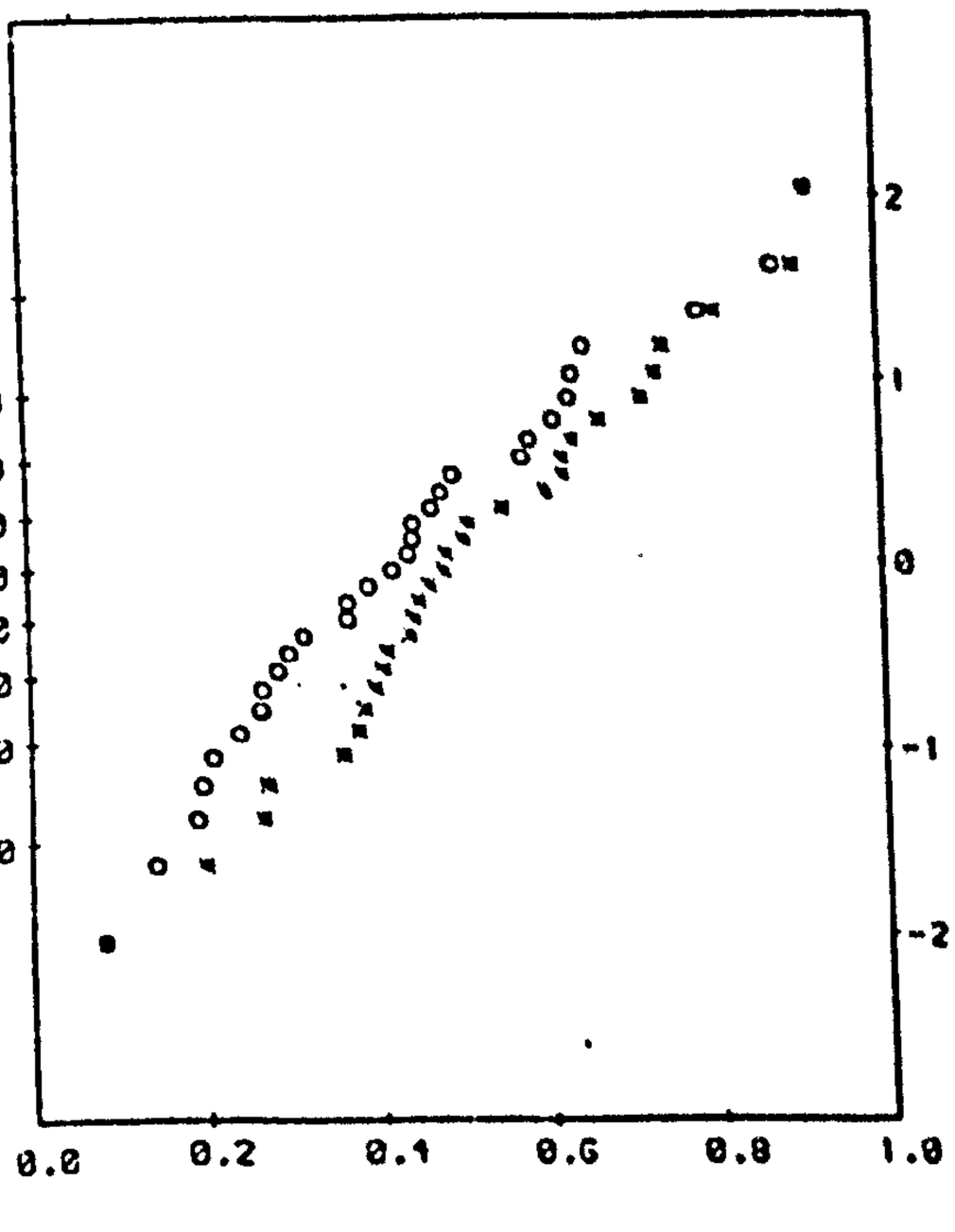

	SD	Mean	1.0	0.0
x	4.4	20.3	31.1	8.7
o	4.4	−8.5	3.2	−17.6

(d)

(iii) T = 2.2 s, S

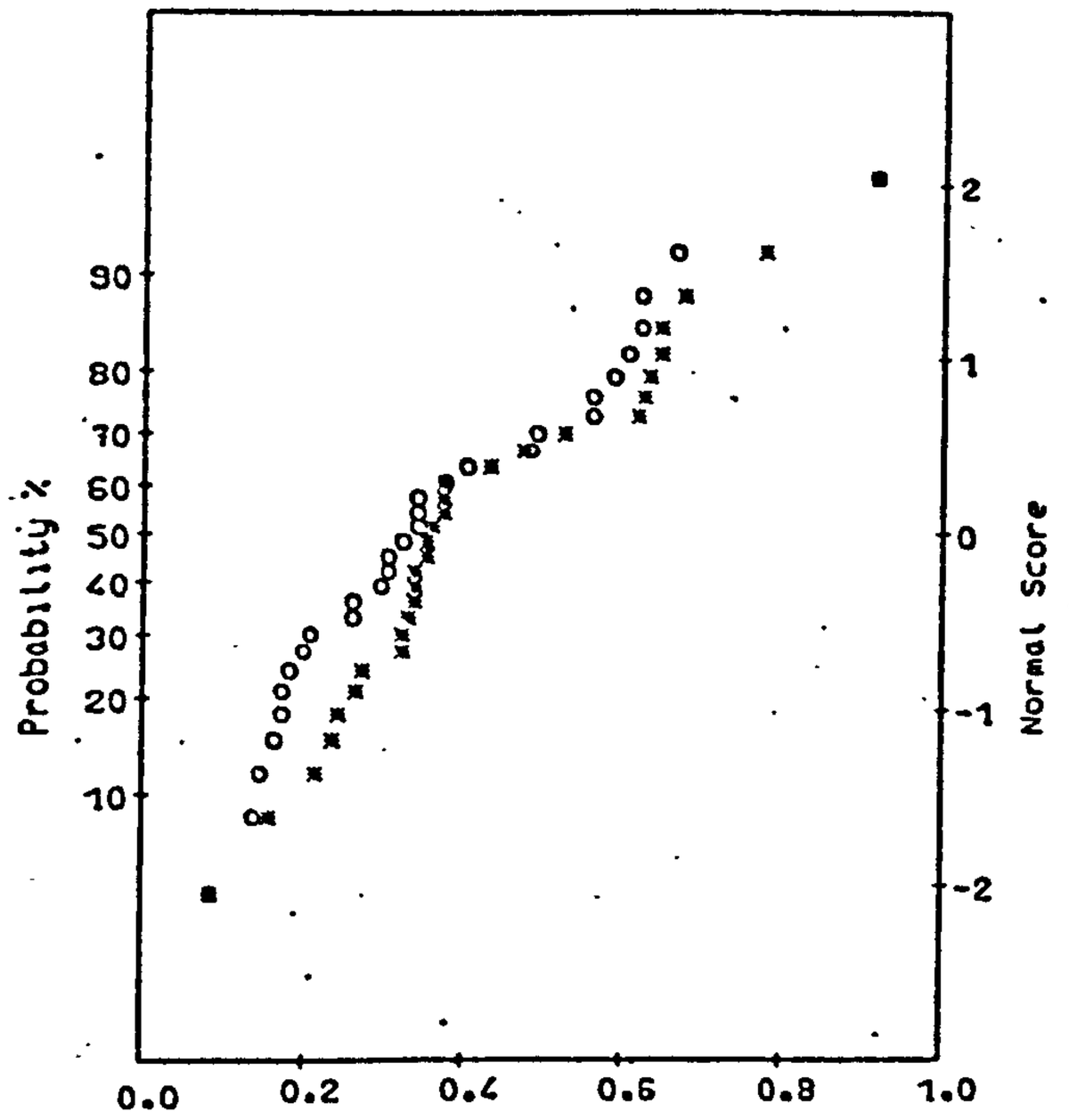

	SD	Mean	1.0	0.0
×	30.7	−73.1	18.4	−139.5
o	25.9	. 20.6	101.7	−27.3

(a)

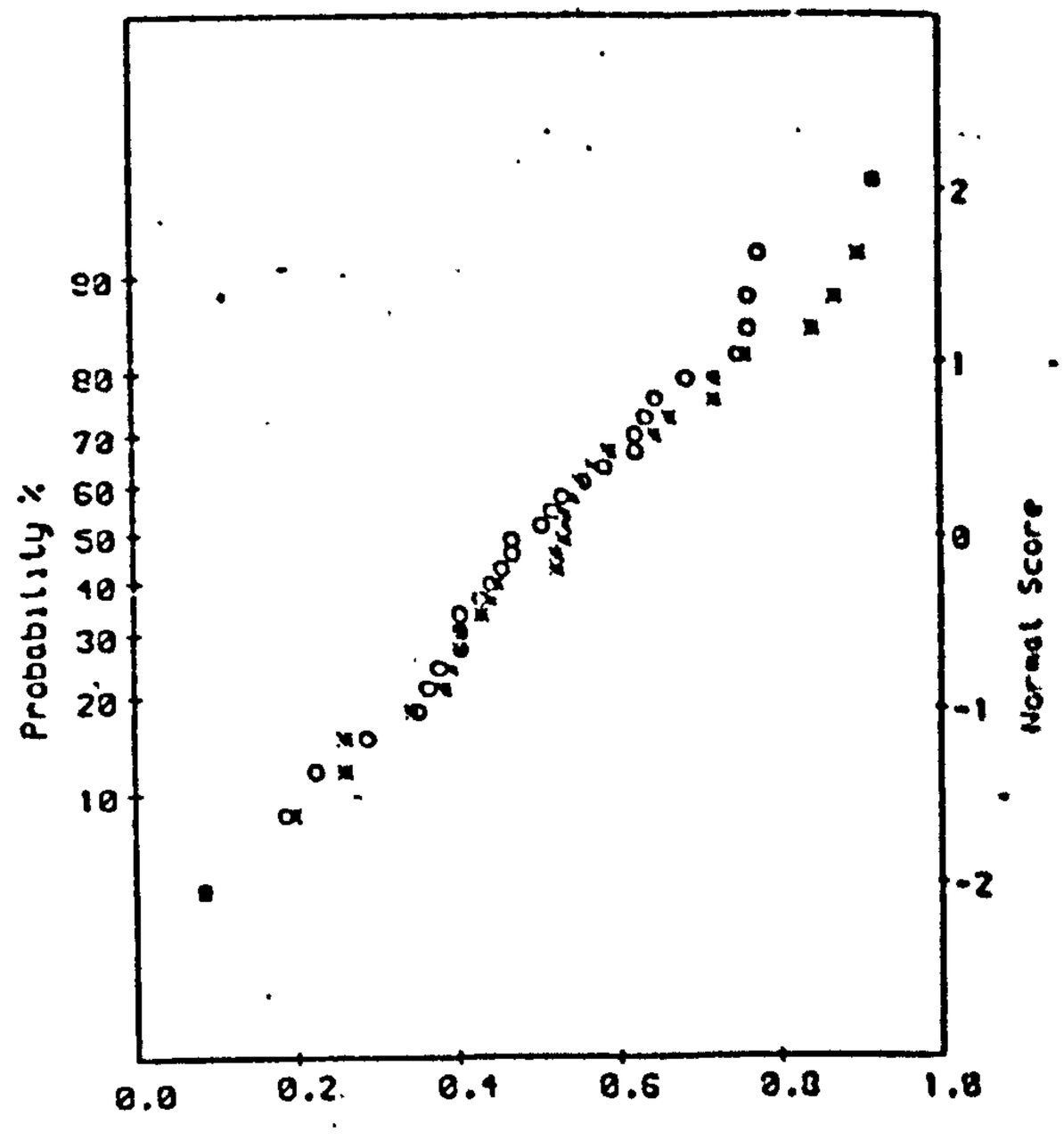

	SD	Mean	1.0	0.0
×	25.3	−45.1	12.0	−110.2
o	17.0	−130.8	−86.9	−176.1

(b)

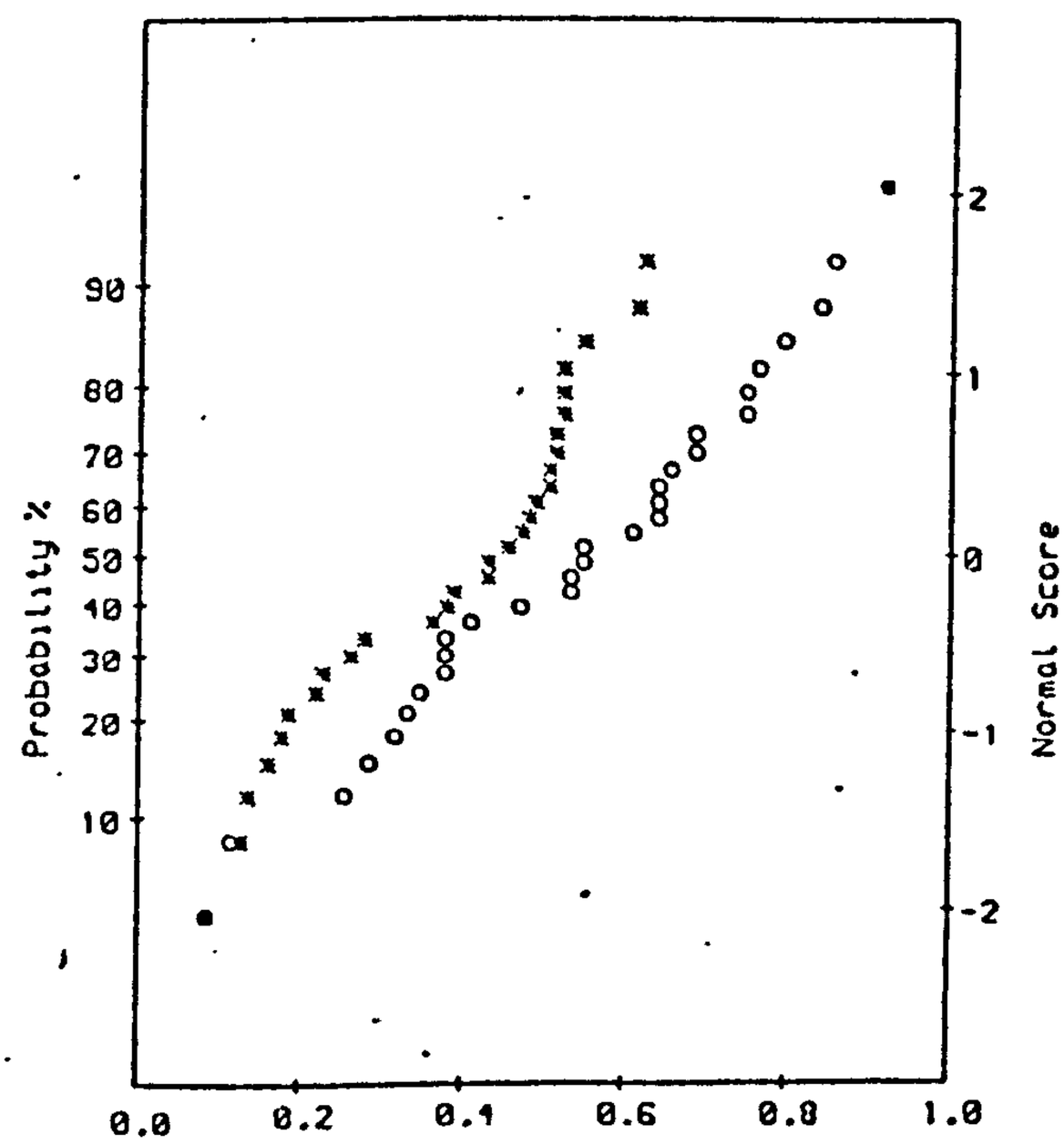

	SD	Mean	1.0	0.0
×	25.2	−6.6	74.9	−61.0
o	16.2	128.2	−93.7	−168.0

(c)

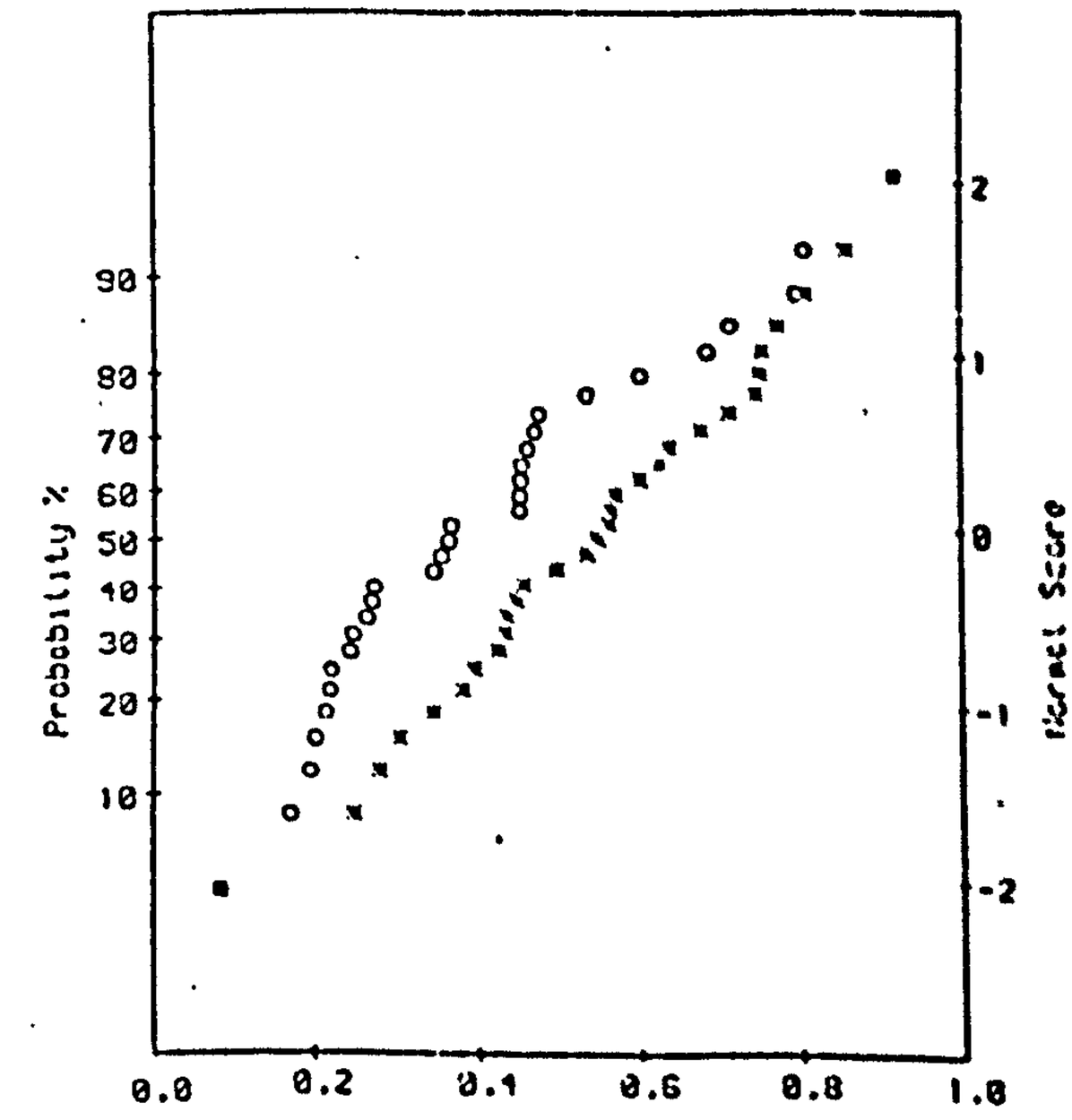

	SD	Mean	1.0	0.0
×	7.7	−12.1	5.8	−33.7
o	7.0	−43.2	−23.5	−56.9

(d)

(iv) T = 2.2 s, R

T/sec	R		S	
	0.5 mm	18.5 mm	0.5 mm	18.5 mm
1.4	34	11	73	17
2.2	45	12	27	18

Table 7.2. The observed values of turbulent intensity inside roughness at the two positions 0.5 and 18.5 mm for 3-D rough bed.

Comparison of Figs. 7.2 and 7.5 verifies the assumption about the shape of the velocity profile for the 2-D rough bed (Fig. 7.5a) since a sinusoidal profile results for the 3-D rough bed at a position close to the bed. Also the phase shift/depth relationship which shows trends in the two figures which closely correspond, indicates again the high intensity eddies as being introduced by the rough beds.

The turbulent flow inside the roughness element results in a very poor correlation between the data for R and S. As shown in Fig. 7.7, the correlation coefficients fluctuate wildly with height increase, and at each level, are three sets of data (velocity measurement) correlated. As the height approaches the level of the top of the roughness element the three values (at each height) get closer to a common value and this common value approaches unity, indicating a correlated set of results. It was also shown (Sec. 6.3) that for heights greater than the roughness elements the correlation coefficient approached unity asymptotically.

In Fig. 7.4, different profiles of mean velocity throughout depth are observed for R and S sections. For the former, the mean velocity values, for T = 2.2s, are positive up to half roughness height, while for the S results the mean velocity is always negative for these waves. When the wave period is 1.4 sec. similar velocity profiles occur for both positions but the velocity fluctuates more at S than at R.

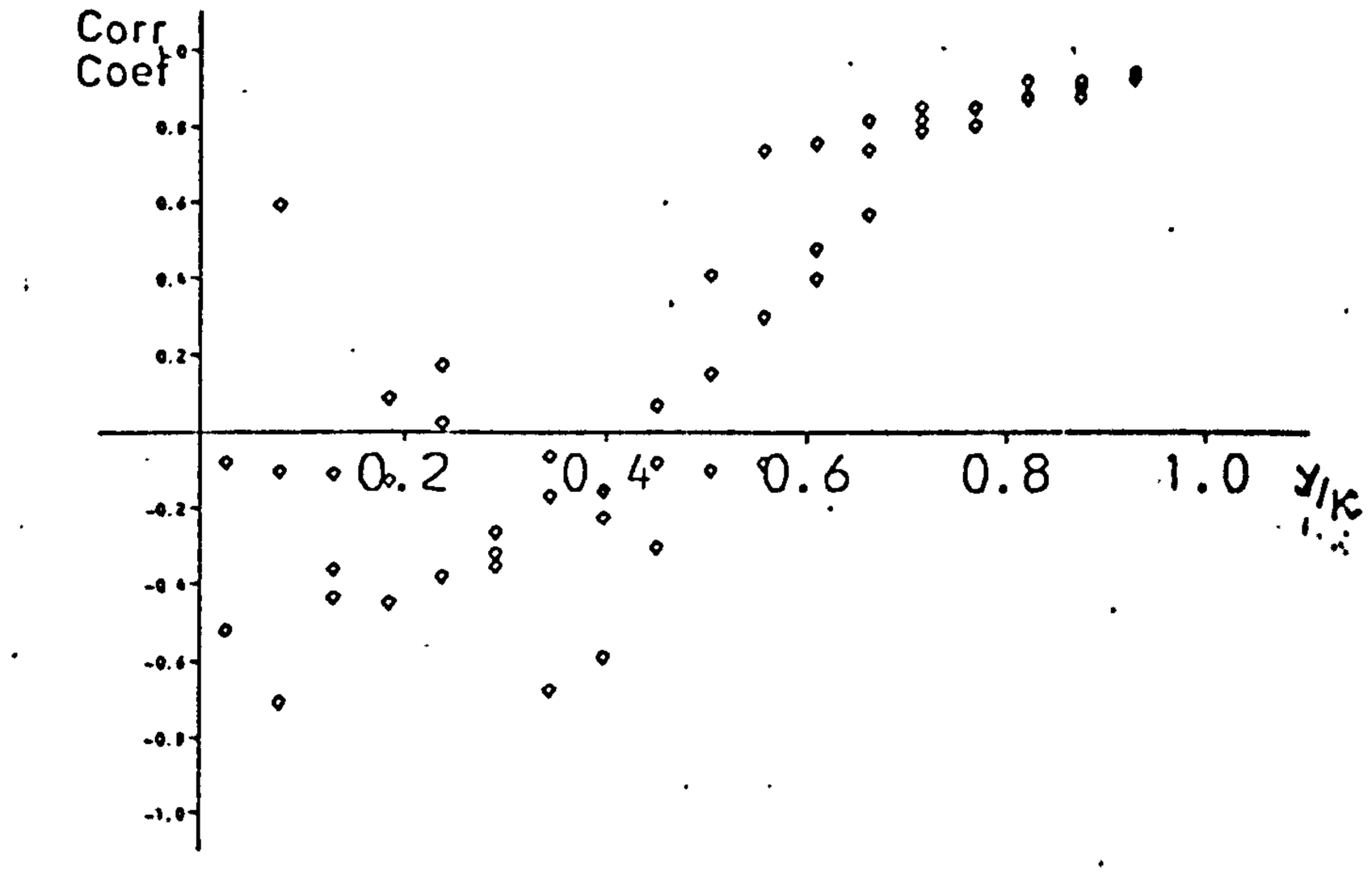

(a) T=1.4 s

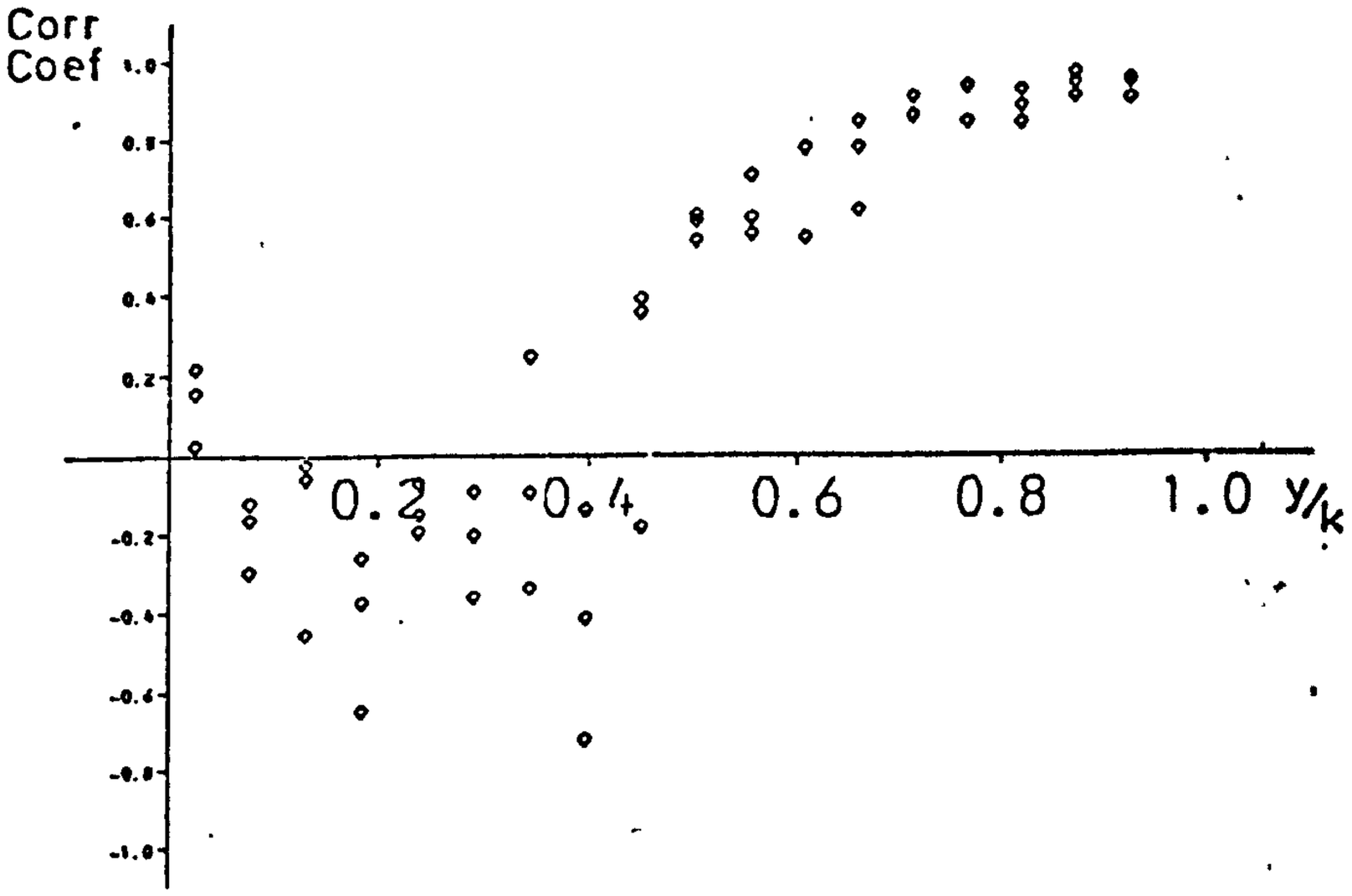

(b) T=2.2s

Figure 7.7 The Correlation Coefficient for Velocity Below Roughness Height (3-DR and 3DS).

However, if the height is expressed in mm (and not by the ratio y/κ) then very similar results occur for the R section and the 2-D rough bed (a positive velocity throughout the 4.5 mm depth). The only difference is that the mean velocity for the 2-D rough bed has smaller values (almost half) than those for 3-DR (comparison of Fig. 7.1 and Fig. 7.4 show this).

7.3 THE SIGNIFICANT 't' TESTS FOR THE 3 AND 5 CYCLES SAMPLE

Population

The statistical relationship between the two sets of samples (5 and 45 cycles for 2-D rough bed, 3 and 30 cycles for 3-D rough bed) could be tested by applying different significant tests (Appendix E). The most relevant test in this case is the 't' test for which the procedure is given in the appendix. Before applying the test and discussing the result of it, two assumptions have to be made;

(i) That the large samples (45 and 30 cycle samples) are representative of the population, in other words the mean velocity over the large number of cycles is the true mean.

(ii) The small samples (3 cycles or 5 cycles) can be subjected to the test since the population for each is normally distributed.

The t values from the tests for the small samples are

in Table 7.3, and by reference to statistical tables the significance of the tests can be found. The t values of two tailed distribution at 5 per cent level of significance having four and two degrees of freedom are 2.78 and 4.30 respectively. This means that any value greater than these become significant from the statistical view point and a difference between the two samples exists. And since the large sample is accepted to be the true sample of the total population, it is the small sample which is then not representative of the population. (4 and 2 degrees of freedom correspond 2-D and 3-D rough beds results respectively)

From the 't' tests values, for each wave period a possibility of one of three conditions can occur;

(a) If the t values at both depths are less than the significant level value then very likely all the observations throughout the depth can be taken as representative of the true values.

(b) If the t values at neither depth is less than the 5 per cent significant level then the conclusion is that the results for 5 or 3 cycle samples are not good representations of the mean population.

(c) And finally if one of the two depths has a t value outside the 5 per cent level it can be assumed that up to some depth the small samples are not significantly different from the true mean population.

T/s	2-D Bed		3-D Bed			
			R		S	
	0.5 mm	4.5 mm	0.5 mm	18.5 mm	0.5 mm	18.5 mm
1.4	14.6	.59	14.6	1.16	2.58	5.2
1.6	2.46	.63				
1.8	.11	3.98				
2.0	.90	1.88				
2.2	1.16	1.11	.68	1.26	5.71	1.93

Table 7.3. The t values for the small sample population at the two depths inside the roughness for rough bed.

None of the results shown in Table 7.3, fall into the condition (b), and most results (1.6, 2.0, 2.2 sec. wave period for 2-D bed and 2.2 sec. for 3-DR bed) satisfy (a). Thus the profiles of mean velocity shown in Fig. 7.1 can be assumed to be not significantly different from the true profiles. Again, the similarity between the t test results of 2-D rough bed and 3-DR rough bed shows that the R section of the 3-D rough bed very much influences the velocity as does the 2-D rough bed.

If the calculated t values greater than the 5 per cent probability t values, are also greater than the one per cent t values (4.60 and 9.93, for four and two degrees of freedom respectively), as are all the results for the 1.4 sec. wave period, then the conclusions based on the small sample throughout the depth will be very weak. But if the t values are less than the 1 per cent t values (1.8 sec. wave for 2-D bed, 2.2 sec. for 3-DS bed), then most of the small samples are not significantly different from the true values. However, these two last points should not be emphasised because they are based on small samples of observations and unless more results were available it would be difficult to make well-founded general comments.

7.4 CONCLUDING REMARKS

1. The t-tests show that most of the 3 and 5 cycles sample population represent the true population (i.e. except when wave period is 1.4 sec.).

2. The mean velocity for the 2-D rough bed is almost always positive, the exception being 1.4 second wave period.

3. The mean velocity for 3-DR rough bed is positive close to the bed and negative close to the top of roughness for the 2.2 sec. wave period, and is positive throughout the depth for the 1.4 sec. wave. The results for this position also behave very much like those for the 2-D rough bed.

4. The mean velocity for 3-DS rough bed is always negative for 2.2 sec. wave period and always positive for 1.4 sec. wave period. Also the results for 3-DS are more turbulent than the results for 3-DR or 2-D rough bed, especially close to the bed.

5. The roughness effect (for all rough beds) introduces high intensity eddies within the roughness elements, since the velocity at top of the roughness elements is almost in phase with the velocity at the free surface, whilst close to bed it is 180 degrees out of phase with the free surface velocity.

CHAPTER EIGHT

CONCLUSIONS

8.1 Introduction

In the last three chapters (5, 6 and 7) are the presentations of results and full discussion for this investigation. A summary of the advantages and disadvantages of the method of observation and analysis, the concluding remarks, and the scope for improvements and better understanding of the rough oscillatory boundary layer are presented and recommended in this chapter.

8.2 The Performance of the Wave Breaker

The objective of using a wave breaker was to absorb most of the incident wave energy and allow as little wave as possible to be reflected. The more wave reflected the less is the correlation between the collected and calculated wave characteristics. The most obvious wave factor effected by a reflected wave is the wave height, since theoretically with increasing wave period the wave height should decrease if the circumstances are not changed. Considering the shortness of the wave channel (having only 2 to 3 m of working section length) reduces the chance of carrying out many tests and a comparison of the present data and Beech's (1978 - using the same channel but a different wave breaker) showed (Appendix B) the improved dissipating efficiency of the incident waves by the present wave

breaker and hence a desirable and successful modification for the wave channel.

8.3 The Measuring Instruments

8.3.1 The Wave Surface Probe

The probe was proved to be a highly accurate piece of equipment for measuring the wave profile of the small period waves as shown by the present data and also by Beech's. However, if the time of running a test was long, then the probe output changed, and thus it was more accurate if from time to time during a test, the output was checked with the initial value, as well as 'curing' the probe over a long period (say half a day) before using it. The only disadvantage of using the probe was its insertion into the water and hence its disturbing the wave profile.

8.3.2 Wave Celerity Probes

The two probes and the control box for measuring the characteristics of a wave (wave length and period), were very efficient and accurate. The system was able to record down to 0.01 s with an accuracy of ±3%, which could be improved by recording the data over 10 or more wave passages. The only weakness of the instrument was that the wave celerity and hence the wave length was not measured at the working section but over one metre length, half metre length each side of it.

8.3.3 L.D.V.

The velocity was measured very accurately by the laser-doppler velocimeter system. The reaction of the equipment has been seen to be very fast in the detection of fluctuating or very low intensity (vertical velocity at the edge of boundary layer) velocity. The only inadequacy of the equipment for this investigation was the poor response of the photomultiplier to vertical velocity very close to the rough beds (or inside the roughness elements) due to the reflected light from the surface of the bed. Whether a high intensity laser or better optical units or system could give better response in these locations is questionable. Otherwise the L.D.V. was a highly reliable tool for velocity measurements up to a very close distance to the surface wave, as well as very close to the bed and inside the roughness elements.

8.4 The Method of Data Analysis

Considering the difficulties explained in Chapters 4, 5, 6 and 7, the procedure and method of analysis of the results were carried out with relatively good understanding of the flow behaviour as was required. Whilst a satisfactory method of analyses was carried out on the results observed for the smooth bed giving a comprehensive understanding of the laminar flow conditions, for a complete appraisal of the turbulent flow the method of analysis was not performed quickly enough, as a great amount of data needed to be analysed to get a good

picture of the rough bed oscillatory boundary layer. No doubt the fluctuating velocity could be more comprehensively understood if more information was available throughout the turbulent depth. As was seen with the full analysis of flow at four locations inside the perturbed-flow depth, the flow behaviour was analysed and discussed, and important conclusions reached; it would have been interesting to check some of these observations from the standpoint of greater confidence if more data could have been sampled and analysed.

Thus by using a faster analyses system (e.g. micro or PDP computers with fast analogue to digital convertor unit) the turbulent flow could be studied to a greater accuracy and in greater detail, as was shown in Chapters 6 and 7 by partially doing the analysis.

Collecting 120 data elements in each cycle resolved precise profiles of the orbital velocity and surface wave, but when more detailed characteristics of the flow, such as velocity maxima phase or turbulent intensity of the perturbed flow, were required the number of readings in each cycle had to be doubled or even tripled.

Hence, a combination of faster analyses and the collection of more data, can facilitate a comprehensive study of the turbulent flow behaviour.

8.5 Results and Stokes Second Order Theories

8.5.1 Surface Wave Profile

The relative depth values of 0.154 to 0.086 classify the waves as intermediate water waves. On the other hand, the Ursell parameter values of more than 20 which were calculated for waves above 2.0 sec. period, suggest that these are the shallow water waves, with the waves of 1.9 sec. period and less being in the intermediate region. Thus, beside the minor disagreement between the data and Stokes prediction, caused by the wave probe as explained earlier, the poor correlation between the results and theory for waves of longer period than 1.9 sec. arises because the Stokes second order is a means of prediction for the intermediate water waves. The high correlation for the rest of the results tends to confirm this.

8.5.2 Orbital Horizontal and Vertical Velocities Outside the Viscous Boundary Layer

Stokes second order equations gave orbital velocity values for intermediate waves in the bulk of fluid which correlated well with observed values except for the modulus, which always seemed to underestimate the actual maximum velocity, throughout the whole depth range. The ratio of the measured to calculated maximum velocity coefficients were similar to those of equation 6.7 to predict the profile and modulus of the velocity with little disagreement.

8.5.3 Viscous Boundary Layer Velocity

With Reynolds numbers of 580 to 820 and with the flow staying laminar, a second order prediction in the form of equation 6.5 with the coefficients to be found from equation 6.7, gave good agreement of prediction with the observed results (also results from Beech (1978)). Although the equations predictions correlated well with the data, it needs further tests with other channels for the adequacy of the equations to be proved. The data from a wave channel is essentially different to that from experimental rigs using oscillatory beds and U tubes.

8.5.4 Drift Velocity

Longuet-Higgins conduction solution well predicted the profile of the drift velocity, considering that the small values of data meant a possibility of a larger error percentage. The disagreement with the conduction solution is that except for boundary layer thickness, the mean velocity was always negative (in opposite direction to wave progression), while the theory showed positive velocity up to one third of the water depth from bed.

8.6 Effect of Rough Beds on the Flow

8.6.1 Outside the Boundary Layer

The effect of roughness elements above the bed, cause an exponential decrease of velocity fluctuation with height. Using artificial rough beds in two and three dimension, in this case with small roughness sizes, the formed eddies,

at a very small height from the bed, disappeared in the bulk of fluid and did not cause any significant effects above the boundary layer thickness.

8.6.2 Inside the Boundary Layer

The effect of rough beds on the laminar boundary layer flow can be concluded as two major points;

(a) The larger roughness elements, hence higher Reynolds number values, caused high intensity eddies which mixed into the boundary layer velocity and eliminated the laminar boundary layer profile completely. For small Re values, the profile was perturbed, but with increasing height the laminar profile reappeared.

(b) The larger roughness element increased the boundary layer velocity, which did not happen for smaller size roughness.

The results yield equation 6.9 for rough beds (2-D and 3-D). However observations on velocity fluctuations over a variety of rough beds are necessary for testing the general validity of the equation.

8.6.3 Inside the Roughness Elements

The knowledge of flow behaviour inside and around roughness elements has importance in the contribution it gives to the mass transport velocity as well as the eddy formation.

The significance tests proved that for turbulent flow more data points would be required to analyse the flow thoroughly, while for less turbulent flows the collected data resulted in the reliable conclusions of the presence of large intensity eddies inside the roughness elements (for 2-D and 3-D rough beds) and a positive mean velocity (for most conditions), though turbulent.

8.6.4 Roughness Effect on Mass Transport Velocity

The mass transport inside the roughness elements is nearly always positive, above the rough beds (inside the boundary layer thickness) its value was not increased but perturbed, which would help to suspend more material and hence enhance the transportation of mobile bed material.

8.7 The Dye Observation

Crystals of potassium permanganate were dropped into the working section to observe the flow for all conditions. Probably the only useful observation was the effect of mass transport throughout the depth, which clearly supported the measured results. Close to the bed, and especially with the rough beds, a diffuse cloud of dye was observed with random movements. The vortices trapped between the roughness elements travelled in no clear path and continuously mixed with each other.

The dye observation did not yield a confident method of

explaining the flow, except to facilitate flow visualisation of the mass transport in the bulk of fluid and of the existing eddies.

8.8 Author's Recommendations

The conclusions to this investigation open the scope for further study of the following points:-

1. The applicability of the laminar boundary layer equations (6.5 and 6.7), which proved to well represent the present results, could be further examined for more oscillatory boundary layer tests.

2. A variety of rough beds are advised to be used in order to achieve;

   (a) The validity of equation 6.9 and a full relationship for equations 6.10 and 6.11, for cases of rough bed oscillatory boundary layer.

   (b) Understanding of the detailed behaviour of eddy formations inside the roughness elements.

3. The application of the results of the aforementioned recommendations (1 and 2) for tests of the same nature on mobile beds.

APPENDIX A - A SUMMARY OF THE WAVE THEORIES

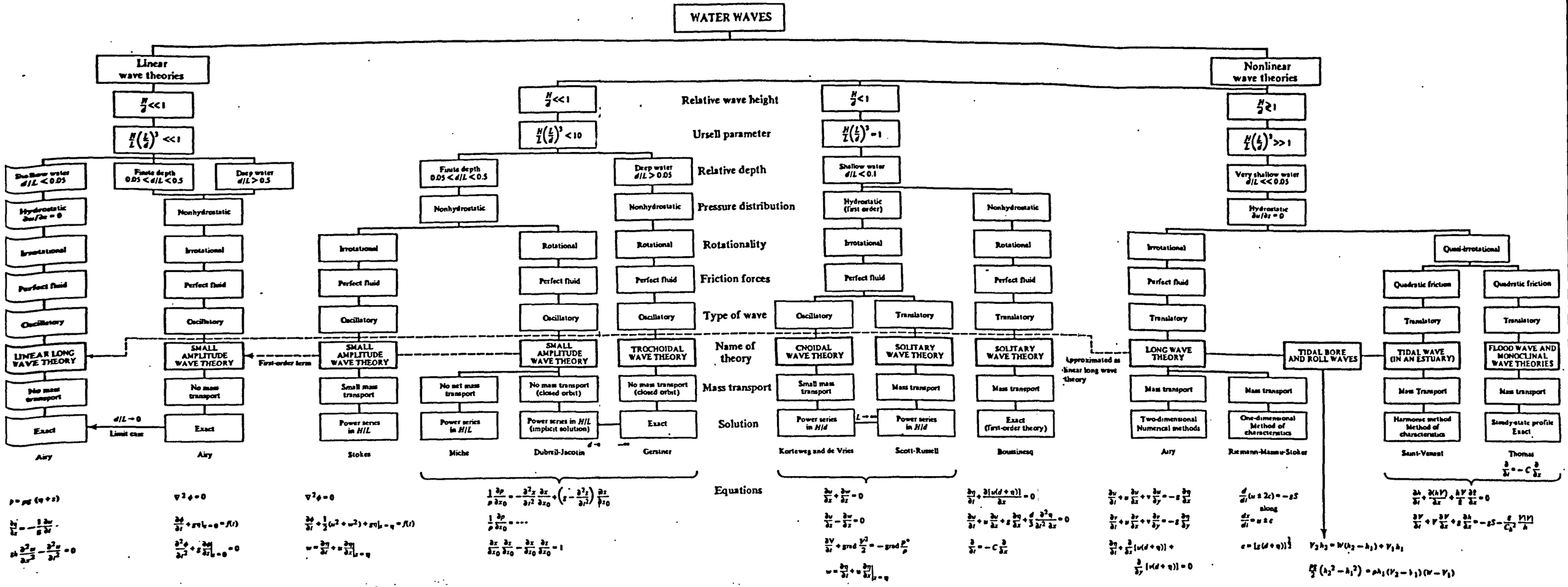

FIG A.1 SUMMARY OF THE WAVE THEORIES.

(AFTER LE MEHAUTE, 1976.)

APPENDIX B - RESULTS FOR WAVE BREAKER AND WORKING SECTION AREA

APPENDIX B

RESULTS FOR WAVE BREAKER AND WORKING SECTION AREA

B.1 The Working Section Area Tests

It was discussed in Chapter 3 that theoretically a further distance from the wave generator results in a more settled and hence more realistic wave profile. The observations at the two sections (mid-point of the wave channel and the working section about 1 m from the wave breaker) show little difference between the two profiles (Fig. B.1 illustrating the wave profiles for four wave periods). Thus the section which more favours the theory was chosen.

B.2 The Effect of the Wave Breaker on Wave Amplitude

A high absorbtion effect from the wave breaker, results in a smooth decrease for the wave height with decreasing the wave period considering the circumstances are not changed. Fig. B.2 shows the results of variations of H/d with wave periods for the two investigations (d = 0.3 m for the two cases). Having used the same instruments but different wave breakers, it is clear that the wave absorber used for this investigation was more effective in dissipating the wave energy.

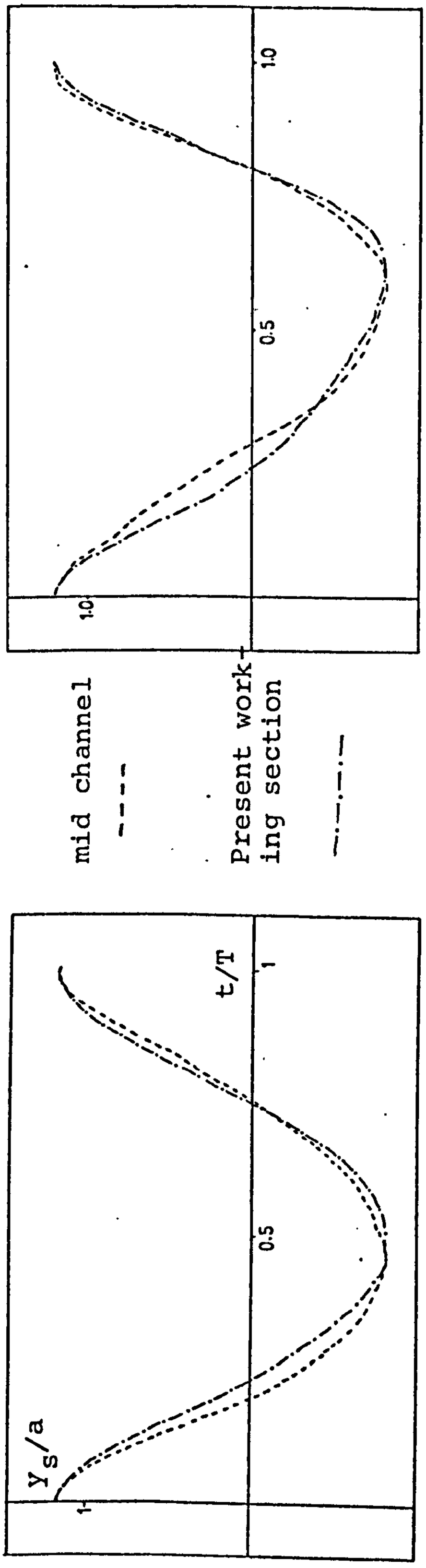

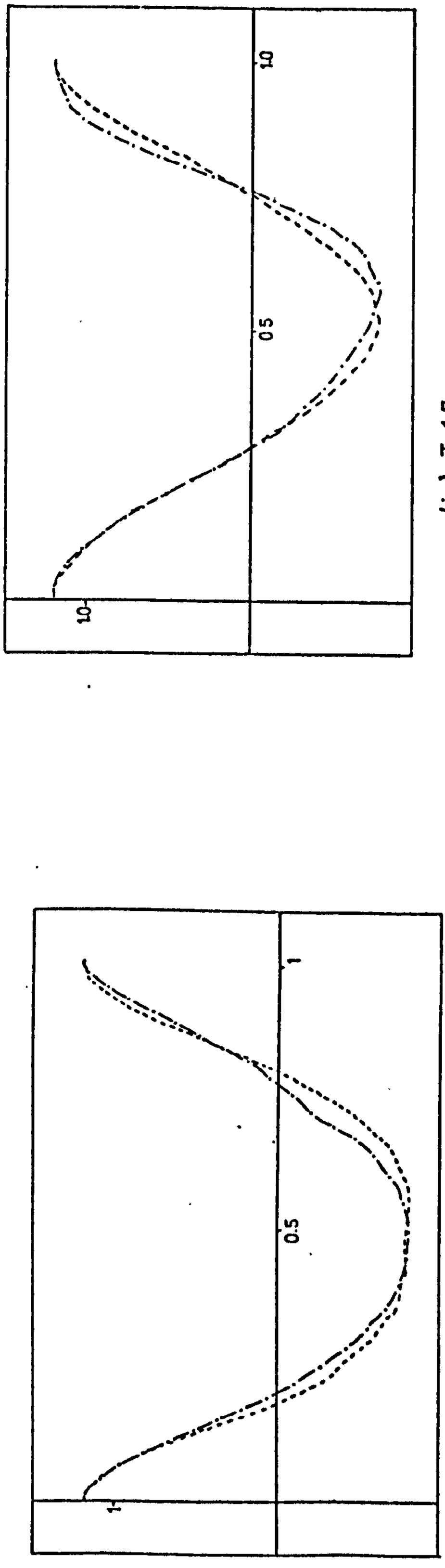

Fig. B.1 Surface Wave Profile at two Sections in the Channel.

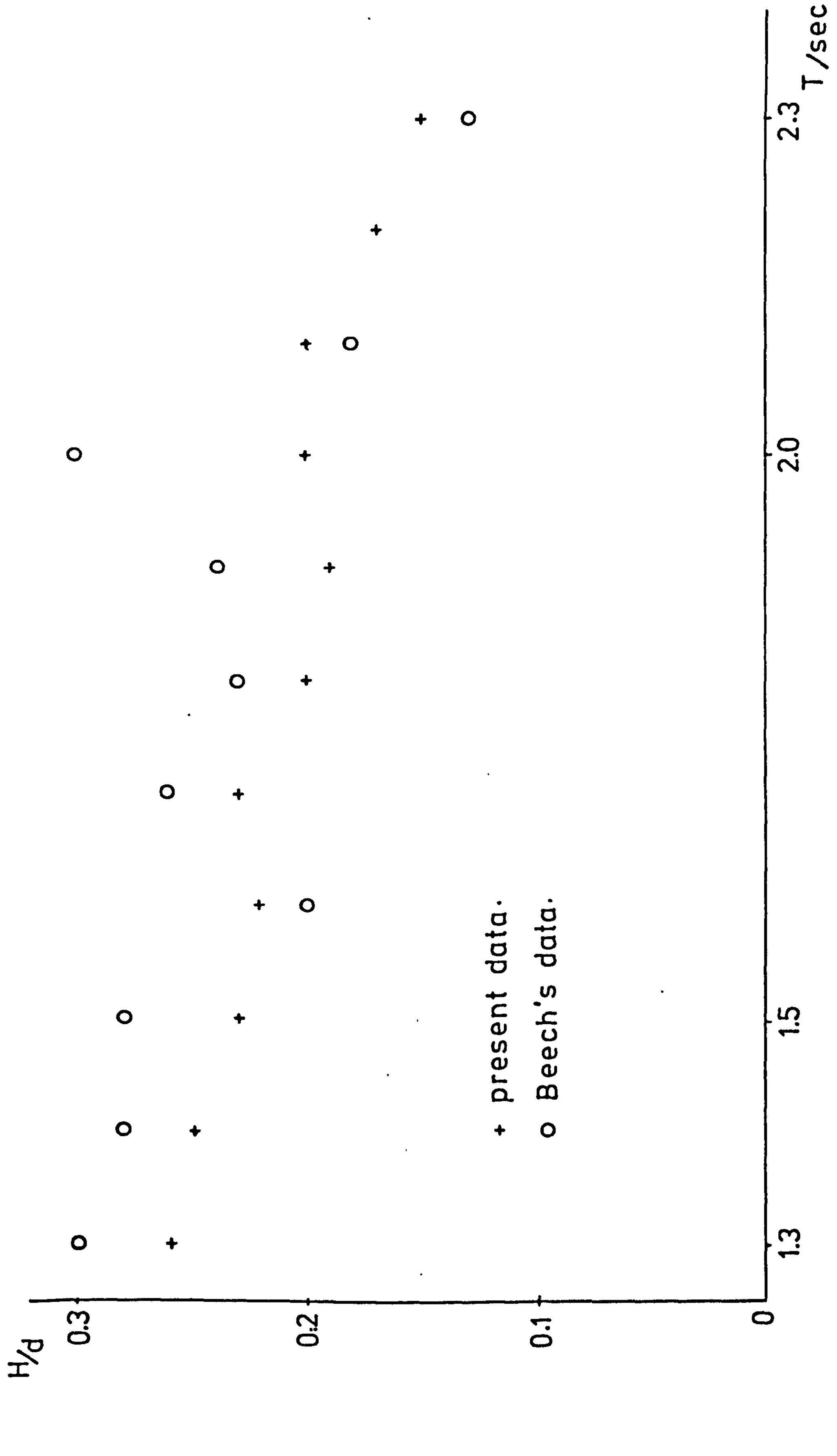

FIG B.2 THE VARIATION OF H/d WITH T.

APPENDIX C - SOME FORTRAN PROGRAMS

APPENDIX C

SOME FORTRAN PROGRAMS

A large number of Fortran programs and subroutines were used to analyse the data. It did not seem to fulfil any purpose by presenting all the programs, instead five of the more repetitive subroutines are presented in Figure C.1. as follows;

(i) Subroutine POSTN - was used for data shifting to be in phase with the Stokes predictions.

(ii) Subroutine MAXI - for evaluating the maximum value within data.

(iii) Subroutine PRIOR - to present the data in order.

(iv) Subroutine DRIFT - to evaluate mean velocity.

(v) Fig. C.1(v) - for calculating the Fourier series harmonics.

```
      SUBROUTINE POSTN(IS,DD,D)
      DIMENSION DD(121),D(121)
      INTEGER IS,IR
      J=0
      DO 501 I=1,121
      IF(I.GT.(121-IS))GOTO 502
      IR=I+IS
      GOTO 503
  502 J=J+1
      IR=J
  503 DD(I)=D(IR)
  501 CONTINUE
      RETURN
      END
```

(i)

```
      SUBROUTINE MAXI(X,XMAXI,XMINI,M)
      DIMENSION X(121,50),XMAXI(121),XMINI(121)
      DO 24 K=1,20
      I=(6*K)-5
      XMA=-1000.0
      XMI=1000.0
      DO 25 J=1,M
      IF(XMA.LT.X(I,J)) XMA=X(I,J)
      IF(XMI.GT.X(I,J)) XMI=X(I,J)
   25 CONTINUE
      XMAXI(I)=XMA
      XMINI(I)=XMI
   24 CONTINUE
      RETURN
      END
```

(ii)

```
      SUBROUTINE PRIOR(XZ,XZ1,XZ2,M)
      DIMENSION XZ(50)
      REAL XZ,XZ1,XZ2
      DO 1 J=1,M-1
      N=M-J
      DO 2 I=1,N
      XZ1=XZ(I)
      XZ2=XZ(I+1)
      IF(XZ1.LT.XZ2)GOTO 2
      XZ(I)=XZ2
      XZ(I+1)=XZ1
    2 CONTINUE
    1 CONTINUE
      RETURN
      END
```

(iii)

Figure C.1 Fortran Subroutines.

```
      SUBROUTINE DRIFT(Z,X,M,ZAVE)
      DIMENSION X(121,50)
      Z=0.0
      DO 110 J=1,M
      DO 210 I=1,121
      Z=Z+X(I,J)
  210 CONTINUE
  110 CONTINUE
      ZAVE=Z/(121.0*M)
      RETURN
      END
```

(iv)

```
      DIMENSION U(121),UX(100,10),BY(100),YD(22),D(22),
     1XX(22),VV(100),V(22,11)
      REAL P
      DO 100 I=1,121,11
      READ(9,200)(U(J),J=I,I+10)
  200 FORMAT(11F7.1)
  100 CONTINUE
      P=3.14159
      F=0.
      FS1=0.
      FS2=0.
      FC1=0.
      FC2=0.
      DO 300 I=1,120
      X=P*(I-1)/60
      F1S=U(I)*SIN(X)
      F2S=U(I)*SIN(2*X)
      F1C=U(I)*COS(X)
      F2C=U(I)*COS(2*X)
      F=U(I)+F
      FS1=FS1+F1S
      FS2=FS2+F2S
      FC1=FC1+F1C
      FC2=FC2+F2C
  300 CONTINUE
      A=F/60.
      A1=FC1/60.
      A2=FC2/60.
      B1=FS1/60.
      B2=FS2/60.
```

(v)

Figure C.1 ...

APPENDIX D - MASS TRANSPORT/MEAN VELOCITY RELATIONSHIP

APPENDIX D

MASS TRANSPORT/MEAN VELOCITY RELATIONSHIP

The average velocity of water particles at a fixed point over one period is called mean velocity and the average velocity of one water particle over a period is the mass transport velocity.

Considering the motion in Fig. D.1, when P is the point on the orbit and Q is the mean position of the orbit,

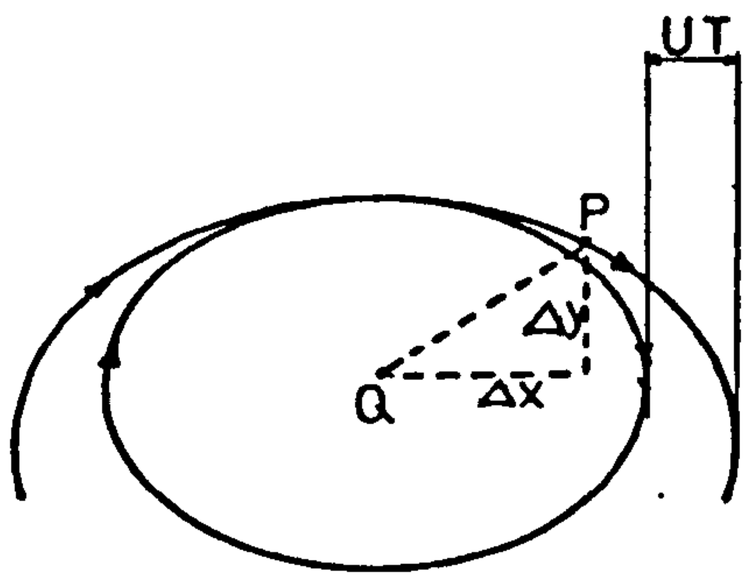

Fig. D.1 Mass Transport Velocity (P) Relative to the Mean Velocity of the Orbit (Q)

therefore the instantaneous velocity at P relative to Q is;

$$\Delta U = \frac{\partial u}{\partial x}\,\Delta x + \frac{\partial u}{\partial y}\,\Delta y \qquad (D.1)$$

where Δx and Δy are the horizontal displacements of P relative to Q and are;

$$\Delta x = \int u\,dt \quad , \quad \Delta y = \int v\,dt \qquad (D.2)$$

Therefore the relationship between mass transport (U) and mean ($\bar{u}$) velocity is;

$$U = \bar{u} + \Delta u = \bar{u} + \overline{\frac{\partial u}{\partial x} \int u dt} + \overline{\frac{\partial u}{\partial y} \int v dt} \qquad (D.3)$$

Equation D.3 can be used for conversion of mean to mass transport velocity when the second and third terms on the right hand side of the equation are evaluated. This is shown by Beech (1978);

$$\left.\begin{aligned} \overline{\frac{\partial u}{\partial x} \int u dt} &= \frac{u_1^2 + u_2^2}{2c} \\ \overline{\frac{\partial u}{\partial y} \int v dt} &= \frac{\hat{u}'\hat{v}}{2\sigma} \end{aligned}\right\} \qquad (D.4)$$

where u_1 and u_2 are the coefficients of first and second order term in the Stokes 2nd order equation and $\hat{u}'$ is the differential with respect to y.

APPENDIX E - STATISTICAL DEFINITIONS AND PROCEDURES

APPENDIX E

STATISTICAL DEFINITIONS AND PROCEDURES

E.1 Sample mean and dispersion

A set of n observations of a stochastic variable, x, has a mean value;

$$\bar{x} = \frac{\sum_{i=1}^{n} x_i}{n}$$

Dependent upon the size of n, the value of $\bar{x}$ may be different to the population mean value μ, which is the value of x for $n \to \infty$.

The variance of this set of n observations is given by:

$$\sigma_x^2 = \frac{\sum_{i=1}^{n} (x_i - \bar{x})^2}{n}$$

This is a fundamental measure of the dispersion of the sample.

The standard deviation of the sample observations from the sample mean is equal to the root mean square deviation:

$$\sigma_x = \sqrt{\frac{\sum_{i=1}^{n} (x_i - \bar{x})^2}{n}}$$

Using the sample observations and the sample mean, the best estimate which can be made of the population variance is:

$$s_x^2 = \frac{\sum_{i=1}^{n} (x_i - \bar{x})^2}{(n-1)}$$

Thus $$s_x^2 = \left(\frac{n}{n-1}\right) \sigma_x^2$$

(Calculation of the actual population variance would require prior knowledge of the population mean μ.)

(n-1) is the number of degrees of freedom remaining for the calculation of s^2 with the mean value $\bar{x}$ determined. The factor $[n/(n-1)]$ is known as Bessel's correction. For proof of this correction reference should be made to statistical texts.

E.2 Weighted mean

Suppose k samples are taken with mean values $\bar{x}_1$, $\bar{x}_2$, ... $\bar{x}_1$, ... $\bar{x}_k$ and population variance estimates s_1^2, s_2^2 ... s_i^2, ... s_k^2. If these samples are from a common population with mean value μ, the combination is made to give an unbiased estimate, $\bar{x}$, of μ with the least possible variance. The method of solution of this problem is dealt with in detail by Hald (1967).

The solution is the following:

$$\bar{x} = \frac{\sum_{i=1}^{n} w_i \bar{x}_i}{\sum_{i=1}^{k} w_i}$$

with minimum variance

$$\sigma^2 = \frac{1}{\sum_{i=1}^{k} w_i}$$

where

$$w_i = \frac{n_i}{s_i^2}$$

and n_i = No. of observations forming the i th sample.

E.3 The normal distribution

The normal probability distribution curve is represented by:

$$y = \frac{1}{\sigma\sqrt{(2\pi)}} \cdot e^{\frac{-(x-\mu)^2}{2\sigma^2}}$$

y is the probability density for observation x.

The area under this curve between two observation values, x_1 and x_2 is the probability of occurrence of an observation between these values. The area under the curve is normalised, so that the probability of occurrence of an observation from this population within the total population range is unity (or 100%).

Deviations of observations from the mean, expressed as multiples of the population standard deviation introduces the reduced nominal variate (R.N.V.)

$$\text{Reduced normal variate} = \frac{(x-\mu)}{\sigma}$$

The distribution of the area under the curve about the mean value, μ, is such that the following probability values occur for the ranges given:

Range of Observation	Range of R.N.V.	Probability of Occurrence
$\mu \pm \sigma$	1 to -1	68.1%
$\mu \pm 2\sigma$	2 to -2	95.5%
$\mu \pm 3\sigma$	3 to -3	99.7%

E.4 Significance Tests

A test statistic is a population distribution parameter which is used to assess the properties of a distribution, or the difference between two distributions.

A difference between two populations is said to be present if the test statistic value is significant - that is, if the test statistic value lies outside predetermined limits. These predetermined limits are set by the chosen significance level. For example, a 5% significance level indicates that the extent to which the hypothesis of no difference between two populations is to be verified is such that there will be a 5% probability of a judgement being made that the populations are not different when, in fact, they are different. From the statistical viewpoint, if the 5% significance level is reached, the differences are said to be probably significant. For the 1% level the difference

is statistically 'significant' and for the 0.1% the term used is 'highly significant'. It should be noted that the significance level is equally divided between the two ends of the normal distribution.

E.4.1 The 't' tests

This test is applied to assess the significance of the difference between two sample mean values. The test is applied to the hypothesis that there is no difference between the mean values and that they are derived from the same population. The fundamental process is to calculate the probability of the difference $|\bar{x}_1-\bar{x}_2|$ having a value as large as, or greater than, that observed.

Firstly the combined population variance, s^2, is estimated from the sum of the squares of both samples divided by the total number of degrees of freedom:

$$s^2 = \frac{\sum_{i=1}^{n_1}(x_{1i}-\bar{x}_1)^2 + \sum_{i=1}^{n_2}(x_{2i}-\bar{x}_2)^2}{(n_1-1) + (n_2-1)}$$

or

$$s^2 = \frac{s_1^2(n_1-1) + s_2^2(n_2-1)}{(n_1-1) + (n_2-1)}$$

Use is then made of the fact that the mean values of samples of n observations drawn from a normally distributed population are themselves normally distributed about the population mean, with variance of σ^2/n. The standard

deviations of the two means $\bar{x}_1$ and $\bar{x}_2$ are thus

$$\frac{s}{\sqrt{n_1}} \quad \text{and} \quad \frac{s}{\sqrt{n_2}}, \quad \text{respectively}$$

The standard deviation of the difference of the means is seen to be:

$$s_d = \sqrt{\left(\frac{s^2}{n_1} + \frac{s^2}{n_2}\right)}$$

$$= s \sqrt{\frac{(n_1 + n_2)}{n_1 n_2}}$$

The signifance of the difference between the means is measured by the ratio:

$$t = \left|\frac{\bar{x}_1 - \bar{x}_2}{s_d}\right|$$

Values of t for various significance levels and degrees of freedom are tabulated in statistical texts. If the calculated value of t is greater than the tabulated value at the chosen level of significance, then the hypothesis of no difference is rejected. It should be noted that this does not necessarily mean that it can be concluded that the mean values are definitely from the same population.

E.5 Least squares regression

The linear regression is of the form

$$y = (mx + c) + v$$

where

v = residual, or error, in actual y

from expected y.

The usual method in least squares linear regression is to vary m and c to produce minimum Σv^2. Two Normal Equations result:

$$\frac{\partial(\Sigma v^2)}{\partial m} = \frac{\partial(\Sigma v^2)}{\partial c} = 0$$

which give the values of m and c.

E.6 Covariance and correlation

The covariance of two variables x and y, which is a parameter which describes the relationship between them, is defined by:

$$s_{xy} = \frac{1}{(n-1)} \sum_{i=1}^{n} (x_1-\bar{x})(y_i-\bar{y}) \qquad \text{(best estimate)}$$

If the variables are independent, then s_{xy} will tend towards zero. For large values of y occurring with large values of x (and similarly small values) then s_{xy} will be positive and the variables are said to be positively correlated. The reverse holds true for negative correlation.

However, s_{xy} depends on the units in which x and y are measured. This is overcome by dividing the value of s_{xy} by the product of the standard deviations of x and y, to give the coefficient of correlation:

$$r_{xy} = \frac{s_{xy}}{s_x s_y}$$

It can be shown that (Hald (1967))

$$-1 \leq r_{xy} \leq 1$$

For $r_{xy} = 1$ or -1 there is a functional relationship between x and y with positive or negative correlation, respectively.

E.7 Cumulative probability plots

This subject is dealt with in detail by most texts on statistical analysis. The following précis is presented to facilitate an understanding of the adopted method of drawing the cumulative probability graphs in this thesis.

The data to be presented on a probability basis is the result of n tests on samples randomly taken from the population. The results are ordered from 1 to n, with the least value having order 1. The fractional cumulative probability of occurrence of a result less than a prticular ordered result, x_i, (of order i) is given by

$$P_i = \frac{i}{(n+1)}$$

Plotting P_i versus x_i (both on linear scales) gives a curve with a point of inflexion at the median value. For a normal distribution of the s_i a plot of P_i versus x_i on

normal probability coordinates linearizes this curve. It is the reduced normal variate which is plotted on a linear scale and the cumulative probability (represented by the area under the normal distribution curve) appears as a non-linear axis.

From the value of P_i, corresponding to an x_i, the value of the reduced normal variate can be read off from tables of areas of the normal curve. Hence the goodness of fit of the data to a normal distribution can be estimated by the correlation of reduced normal variate and test data.

APPENDIX F - REFERENCES

APPENDIX F

REFERENCES

AIRY (G.B.) (1845);
On Tides and Waves,
Encyclopedia Metropolitana, London.

BAGNOLD, R.A. (1946)
Motion of Waves in Shallow Water. Interactions Between Waves and Sand Bottoms,
Proc. Roy. Soc. Land series A, Vol. 187.

BAGNOLD, R.A. (1947)
Sand Movement by Waves; Some Small-Scale Experiments with Sand of Very Low Density.
J. of C. Eng. Vol. 27 p. 447.

B.E.B. (1942)
A Summary of the Theory of Oscillatory Waves,
Tech. Rep. No. 2, U.S. Government Printing Office.

BEECH, N. (1978)
Boundary Layers Due to Gravity Waves,
Ph.D. Thesis, University of Nottingham.

BLAKE, K.A. and JESPERSEN, K.I. (1972)
The Laser Velocimeter,
NEL Report. (National Engineering Lab.)

BLAKE, K.A. (1972)
Lecture given at the Colloquim,
(Imperial College) The NEL Laser Velocimeter.

BREBNER, A., J.I. COLLINS (1961)
The Effect on Mass-Transport of the Onset of Turbulence at the Bed under Periodic Gravity Waves.
Trans. of Eng. Inst. of Canada, Vol. 5.

BREBNER, A., ASKEW, J.A. and LAW, S.W., (1966)
The Effect of Roughness on the Mass-Transport of Progressive Gravity Waves,
10th Conf. of Coastal Eng.

CARSTENS, M.R. and NEILSON, F.M. (1976)
Evolution of a Dumed Bed under Oscillatory Flow,
J. Geoph. Res., Vol. 72, pp. 3053-3059.

CHAKRABARTI, S.K. (1980)
Laboratory Generated Waves and Wave Theories,
J. of the Waterway Port Coastal and Ocean Div. Vol. 106.

DEAN, R.G. (1970)
Relative Validity of Water Wave Theories,
Proc. ASCE, 96.

DE. S.C. (1955)
Contributions to the Theory of Stoke's Wave,
Proc. Camb. Phil. Soc., 51.

DRAIN, L.E. (1980)
Laser Doppler Technique,
Chichester, Wiley.

EAGLESON, P.S. (1959)
The Damping of Oscillatory Waves by Laminar Boundary Layers,
U.S. BEB Technical Memorandum No. 117.

EAGLESON, P.S. and DEAN, R.G. (1966)
Small Amplitude Wave Theory,
Proc. ASCE, Vol. 88, HY1O.

EINSTEIN, H.A. (1972)
A Basic Description of Sediment Transport on Beaches,
Conf. "Waves on Beaches", Ed. R.E. Meyer.

FISHLOCK, D. (1967)
A Guide to the Laser,
London, Macdonald.

GEORGE, C.G. and SLEATH, J.F.A. (1978)
Oscillatory Laminar Flow above a Rough Bed,
Proc. of 16th Conf. of Coastal Eng.

GERSTNER, F.A. (18O2)
Theories der Wellen,
Abhandlungen der Koniglichen bohmisehen gesellschaft der Wissenschaften, Prague.

GREATED, C. (1971)
A Review of Laser Flow Measuring Techniques
Meeting at the National Institute of Oceanography. (Current Measuring Techniques).

HALD, A. (1967)
Statistical Theory with Engineering Application,
7th edition, J. Wiley & Sons.

HEADING, J. (1970)
Mathematical Methods in Science and Engineering,
2nd Ed., Edward Arnold.

HORIKAWA, K. and WATANABE, A. (1969)
"Laboratory Study on Oscillatory Boundary Layer Flow",
Coastal Eng. in Japan, Vol. 11.

HUNT, J.N. (1953)
A Note on Gravity Waves of Finite Amplitude,
Quarte. J. Mech. App. Math. 6.

ISAACSON, M.Q. (1978)
Mass Transport in Shallow Water Waves,
J. of Waterway Port Coastal Div. Vol. 104.

JONSSON, I.G. (1963)
Measurement in the Turbulent Wave Boundary Layer,
10th Congress IAHR Lond. p. 85.

JONSSON, I.G. (1966)
Wave Boundary Layers and Friction Factors,
Proc. of the 10th Congress on Coastal Eng.

JONSSON, I.G. (1980)
A New Approach to Oscillatory Rough Turbulent Layer,
Proc. Ocean Eng. Vol. 7.

KAJIURA, K. (1968)
A Model of the Bottom Boundary Layer in Water Waves,
Bull. Earthquake Res. Inst. Vol. 46, p. 75.

KALKANIS, G. (1957)
Turbulent Flow Near an Oscillating Wall,
U.S., BEB Tech. Memo. No. 97.

KALKANIS, G. (1964)
Transportation of Bed Material due to Wave Action,
U.S., BEB Tech. Memo. No. 2.

KAMPHUIS, J.W. (1972)
Scale Selection for Wave Models,
C.E. Research. Report No. 71. Queen's University at Kingston, Ontario.

KAMPHUIS, J.W. (1975)
Friction Factor Under Oscillatory Waves,
J. of the Waterways, Harbour and Coastal Eng. Div. ASCE Vol. 110.

KELLER, J.B. (1948)
The Solitary Wave and Periodic Waves in Shallow Water,
Comm. Applied Maths.

KEILLER, D.C. and SLEATH, J.F.A. (1976)
Velocity Measurements Close to a Rough Plate Oscillating in its Own Plane,
J. Fluid Mech. Vol. 73, part 4.

KEULEGAN, G.H. (1950)
Wave Motion in Engineering Hydraulics,
Proc. of the Fourth Hydraulic Conference.

KINSMAN, B. (1965)
Wind Waves,
Prentice-Hall, Englewood Cliffs N.J.

KNIGHT, D. (1978)
Review of Oscillatory Boundary Layer Flow,
J. of the Hydraulic Div. Proc. of the A.S.O.C.E. Vol. 104.

KORTWEG, D.J. and DE VRIES, G. (1895)
On the Change of Form of Long Waves Advancing in a Rectangular Canal, and on a New Type of Long Stationary Waves,
Phil. Mag. fifth seq. 39.

LAITONE, E.V. (1960),
The Second Approximation to Cnoidal and Solitary Waves,
J. Fluid Mech. 9.

LAMB (1932)
Hydrodynamics,
6th Ed., Cambridge University Press.
a. Art. 229. b. Art. 228. c. Art. 345-347.

LE-MEHAUTE, B., DIVOKY, D. and LIN, A. (1968)
Shallow-Water Waves; A Comparison of Theories and Experiments,
Proc. A.S.C.E. (11th Conf. Coastal Eng.) 1, 86-107.

LE-MEHAUTE,B. (1976)
An Introduction to Hydrodynamic and Water Waves,
by Springer-Veilag, N.Y. Inc.

LHERMITTE, M.P. (1958)
Contribution 'a' l'etude de la couche limite des houles "mono chromatique",
La houille blanche, No. Special A, p. 366.

LI, H. (1954)
Stability of Oscillatory Laminar Flow Along a Wall,
U.S. BEB Tech. Memo. No. 48.

LIGHTHILL, M.J. (1978)
Waves in Fluid,
Cambridge U.P.

LENNET, A.E. (1972)
Laser Technology in Aerodynamic Measurements,
AGARD L.S. 49.

LONGUET-HIGGINS, M.S. (1953)
Mass Transport in Water Waves,
Phil. Trans. of the Royal Soc. of London, Vol. 245, (1952-53).

LONGUET-HIGGINS, M.S. (1958)
The Mechanics of the Boundary Layer near the Bottom in a Progressive Wave,
An Appendix to Russell and Osorio paper. An Experimental Investigation of Drift Profiles in a Closed Channel.

MANNING, R. (1973)
Laser Doppler Measurements on a Sloping Beach,
J. of Hyd. Res.

MANOHAR, M. (1955)
Mechanics of Bottom Sediment Movement Due to Wave Action,
U.S. BEB Tech. No. 75.

McCORMIC, M.E. (1973)
Ocean Engineering Wave Mechanics,
John Wiley and Sons.

RAUDKIVI, A.J. (1976)
Loose Boundary Hydraulics,
2nd edition, Pergamon Press.

RAYLEIGH, L. (1911)
Scientific Papers,
Cambridge U.P. Vol. VI.

REYNOLDS, O. (1883)
An Experimental Investigation of the Circumstances which Determine Whether the Motion of Water Shall Be Direct or Sinuous and of the Laws of Resistance,
Phil. Trans. Roy. Soc. London, Vol. 174, pt. 3.

RICHARDS, B.E. (1977)
Measurement of Unsteady Fluid Dynamic Phenomena,
Washington, Hemisphere.

RIEDEL, H.P. and KAMPHUIS, J.W. and BREBNER, A. (1972)
Measurement of Bed Shear Stress Under Waves,
Proc. 13th Conf. on Coastal Eng.

RUSSELL, R.C.H. and OSORIO J.D.C. (1958)
An Experimental Investigation of Drift Profiles in Closed Channels,
Proc. 6th Conf. Coastal Eng.

SCHLICHTING, H. (1968)
Boundary Layer Theory,
6th Edition, McGraw Hill.

SILVESTER, R. (1974)
Coastal Engineering 1,
Elsevier Scientific Publishing Company.

SKYELBREIA, L. (1959)
Gravity Waves, Stoke's Third Order Approximation;
Tables of Function,
Berkeley, Calif. The Engineering Foundation Council on Wave Research.

SLEATH, J.F.A. (1970)
Velocity Measurements Close to Bed in a Wave Tank,
J. of Fluid Mech. Vol. 42.

SLEATH, J.F.A. (1972)
A Second Approximation to Mass Transport,
J. of Marine Research.

SLEATH, J.F.A. (1973 a)
A Numerical Study of the Influence of Bottom Roughness on Mass Transport by Water Waves,
Proc. International Conf. Numerical Methods in Fluid Dynamics, Univ. Southampton, U.K., I.13.

SLEATH, J.F.A. (1974.b)
Mass Transport over a Rough Bed,
J. of Marine Research.

SLEATH, J.F.A. (1974.a)
Stability of Laminar Flow at Sea Bed,
J. of Waterways Harbour and Coastal Eng. Div.

SLEATH, J.F.A. (1974.b)
Velocities Above Rough Bed in Oscillatory Flow,
Proc. A.S.C.E. J. Waterways Harbours Coastal Eng. Div.

SLEATH, J.F.A. (1975)
Transition in Oscillatory Flow over Rippled Bed,
Proc. of the Inst. of Civil Eng., Vol. 59, part 2.

SORENSEN, R.M. (1978)
Basic Coastal Engineering,
New York, Wiley.

STOKES, G.G. (1847)
On the Theory of Oscillatory Waves,
Trans. Cambridge Philosophical Soc. Vol. (VIII).

STOKES, G.G. (1851)
Trans. Cambridge Philosophical Society, Vol. IX.

URSELL, F. (1953)
The Long Wave Paradox in the Theory of Gravity Waves,
Proc. Cambridge Phil. Soc. 49.

VINCENT, G.E. (1957)
Contribution to the Study of Sediment Transport on a Horizontal Bed due to Wave Action,
Proc. 6th Conf. Coastal Eng.

WATRASIESWICZ, B.M. and RUDD, M.J. (1976)
Laser Doppler Measurements,
Butterworth and Co.

WEHAUSEN, J.V. (1963)
Recent Development in Free Surface Flows,
Univ. of California, Berkeley Inst. Eng. Res. Tech. Rep.

WEIGEL, R.L. (1964)
Oceanographic Engineering,
Prentice-Hall Inc.

WILTON, J.R. (1914)
Deep Water Waves,
Phil. Mag. 6th Ser. 27.

WOOD, A.M. (1969)
Coastal Hydraulics,
Macmillan and Co. Ltd.

BOYER, M.C. (1955)

'Electrolytic Measurement of Low Velocities in Water'

Proc. of the 6th Hydraulic Conference

SHERCLIFF, J.A. (1962)

'The Theory of Electromagnetic Flowmeasurement'

Camb. Univ. Press